Università degli Studi di Cagliari

DOTTORATO DI RICERCA

SCIENZE E TECNOLOGIE CHIMICHE

Ciclo XXVI

NEUTRAL RECEPTORS FOR ANION RECOGNITION: SYNTHESIS, SELECTIVITY STUDIES AND TRANSPORT PROPERTIES

03/B1 Fondamenti delle scienze chimiche e sistemi inorganici

Presentata da:	Dott.ssa Martina Olivari
Coordinatore Dottorato	Prof. Mariano Casu
Tutor/Relatore	Dr. Claudia Caltagirone

Esame finale anno accademico 2012 – 2013

To my Grandmother

Ringraziamenti

Il mio più grande e sentito ringraziamento va alla Dr. Claudia Caltagirone per il supporto e la fiducia dimostratami, per avermi pazientemente aiutato, guidato e incoraggiato durante tutta la durata del mio dottorato, ma soprattutto per essere una persona splendida sia in ambito lavorativo che dal punto di vista umano. Non avrei mai potuto desiderare un capo migliore.

Un altro ringraziamento speciale è per il Dr. Riccardo Montis, nessun grazie sarà mai abbastanza per tutto quello che ha fatto per me in laboratorio e nella mia vita privata. Da collega è diventato uno dei miei amici più cari, senza il quale non avrei superato i momenti più difficili di questi ultimi anni e senza il quale questa tesi sarebbe stata decisamente meno bella! Grazie per essermi sempre stato vicino.

Ringrazio la Dott.ssa Alessandra Garau e la Dott.ssa Greta De Filippo Filippo sempre disponibili ad aiutarmi ogni volta che ne avevo bisogno.

Vorrei ringraziare il Prof. Francesco Isaia e il Prof. Vito Lippolis per il loro aiuto e la loro costante presenza.

Ringrazio la dott.ssa Romina Lai e la Dr. Anna Pintus (per me Romi e Annetta), da colleghe ad amiche inseperabili, per il loro supporto quotidiano durante l'ultimo anno e perchè senza le nostre 'mirabolanti avventure' le giornate sarebbero state sicuramente meno ricche di risate e divertimenti (soprattutto le nostre pause pranzo!!).

Ringrazio inoltre la dott.ssa Valeria Meli per la compagnia e le chiacchere in laboratorio e soprattutto per essere l'unica disposta a non dare mai buca alle uscite, anche se non siamo ancora riusciti a farne una!

Vorrei ringraziare dal più profondo del cuore anche tutti i 'miei ragazzini' che hanno svolto il loro tirocinio con noi. Grazie agli ormai Dottori Marco Mais, Arianna Casula, Giacomo Picci, Mattia Nieddu, Walter Cucchiara e Laura Pala; perchè mentre cercavo di insegnare loro i trucchi del mestiere, io ho imparato cose molto più importanti e mi sono affezionata ad ognuno di loro. Grazie per aver riempito le mie giornate con gioie, risate e merendine (i colpevoli dei miei chili di troppo sanno chi sono!).

Ringrazio il Sig. Antonio Sabeddu, il nostro 'usignolo' del laboratorio, per il suo quotidiano aiuto e per il suo buonumore.

Mille volte grazie a tutto il gruppo di ricerca per avermi fatto sentire ogni giorno a casa e perchè mi sono sentita parte di una piccola grande famiglia.

Vorrei ringraziare il Prof. Philip Gale e tutto il suo gruppo di ricerca per avermi permesso di lavorare presso i suoi laboratori all'Università di Southampton. Un ringraziamento particolare va a Louise Karaggiannidis per la sua simpatia ed allegria e per l'aiuto datomi nei vesicle test.

Un ringraziamento speciale va alla mia 'famiglia inglese', Clem, Boris, Emma, Marc, Thomas, e Fivi ma soprattutto grazie a Rossella, Mara e Laura che mi hanno aiutato dal primo giorno nella terra straniera ed hanno portato calore e colore nella fredda e grigia Inghilterra. Grazie a loro Southampton è diventata un posto meraviglioso!

Come non ringraziare poi tutti i miei amici, recenti e di lunga data, perchè riescono a sopportarmi anno dopo anno (e soprattutto durante la stesura di questa tesi) e perchè sono sempre la mia isola felice, anche quando tutto il resto va male, posso sempre contare su di loro.
Un grazie speciale va ad Andrea per avermi tranquillizzato e incoraggiato durante questi ultimi mesi, se sono riuscita a scrivere questa tesi senza impazzire è merito suo.
Infine vorrei ringraziare i miei genitori e tutta la mia famiglia per aver sempre creduto molto in me (anche se non hanno ancora capito su cosa lavoro) e per avermi aiutato in ogni momento della mia vita. Spero di averli resi orgogliosi.
Ringrazio tutte le persone che ho incontrato durante questo bel cammino perchè è grazie a loro che sono arrivata fino a qui.

ABSTRACT

This thesis reports the synthesis and studies of a new series of compounds containing urea groups that can function as selective anion receptors and efficient anion transmembrane transporters.

Two new asymmetric ureidic receptors **L^1** (1-(1H-indol-7-yl)-3- (quinolin-2-yl)urea) and **L^2** (1-(quinolin-2-yl)-3-(quinolin-8-yl)urea), shown in *Figure 1*, have been synthesised and their affinity towards different anions tested in DMSO-d_6. **L^1** adopts both in solution and in the solid state an (**E**,**Z**) conformation. A moderate affinity for acetate has been observed with **L^1** while no interaction has been observed with **L^2**. The different behaviour has been ascribed to the presence/absence of the indole group. In the case of **L^1** the indole group causes the formation of a peculiar supramolecular architecture with two molecules of the receptor binding the anions in (**E**,**Z**) conformation via H-bonds. **L^2** also adopts an (**E**,**Z**) conformation in the solid state. However, the absence of the indole in **L^2** hampers the formation of the supramolecular assembly with the participation of anionic species. The results are discussed in Chapter 2.

In Chapter 3 a new family of bis-ureidic receptors (**L^3**-**L^8**) is reported (*Figure 2*). The binding properties of **L^3**-**L^8** towards different anions (acetate, benzoate, glutarate, malonate, dihydrogen phosphate, hydrogen pyrophosphate, triphosphate, AMP and ADP) have been studied by means of ^{1}H-NMR, UV-Vis and fluorescence spectroscopies and a remarkable affinity for $HPpi^{3-}$ has been observed in the case **L^5** (in DMSO- d_6 and DMSO-d_6/5% H_2O) which also acts as fluorimetric chemosensor, even at naked eye, for this anion. Theoretical calculations helped us to explain the binding properties observed.

A series of bis-ureidic receptor **L^9**-**L^{14}** (*Figure 3*) was prepared and the studies of their transmembrane anion transport activity and anion binding properties are described in Chapter 4. Vesicle anion transport assays using ion selective electrodes demonstrate that these compounds function as efficient mobile carriers that are able to transport chloride through lipid bilayer predominantly *via* anion exchange mechanism including Cl^-/NO_3^- and Cl^-/HCO_3^- antiport. Compound **L^{14}** was found to be the most active transporter of the series. As anion receptors, we observed that compounds **L^{10}** and **L^{12}** demonstrate strong 1:1 binding with TBA fluoride (K_a >10^4 M^{-1}) and moderate 1:1 binding with TBA dihydrogenphosphate.

In Chapter 5, the anion transport efficiency of a series of trisureas **L^{15}**-**L^{20}** (*Figure 4*) was investigated. The compounds showed a potent transmembrane anion transport activity. The mechanism of transport was extensively investigated using a combination ion selective electrode and fluorescence techniques. It was found that compounds **L^{15}**-**L^{20}** mediate chloride transport *via* Cl^-/NO_3^- and Cl^-/HCO_3^- antiport and NaCl symport. The tris-urea **L^{15}** was found to be a remarkably potent anion carrier at low concentration.

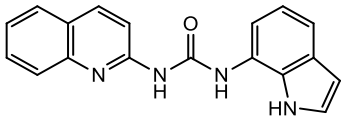

L^1

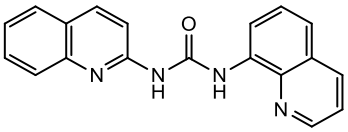

L^2

Figure 1. Summary of receptors synthesised and studied in Chapter 2.

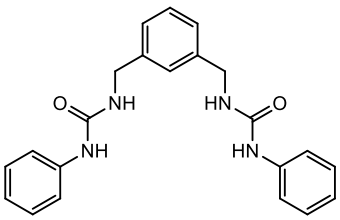

L^3

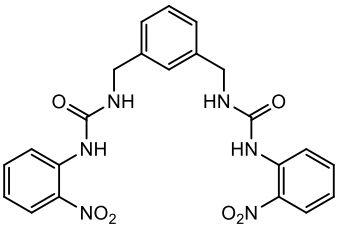

L^4

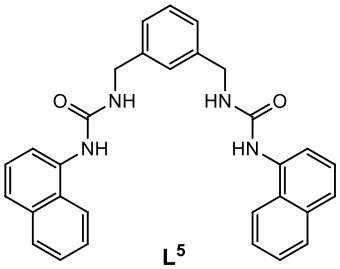

L^5

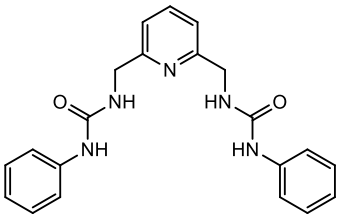

L^6

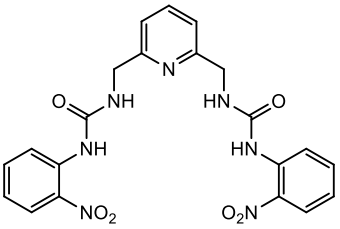

L^7

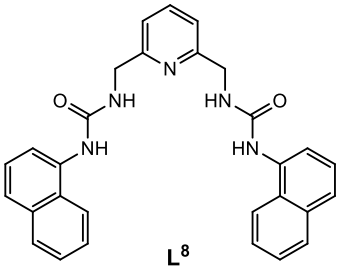

L^8

Figure 2. Summary of receptors synthesised and studied in Chapter 3.

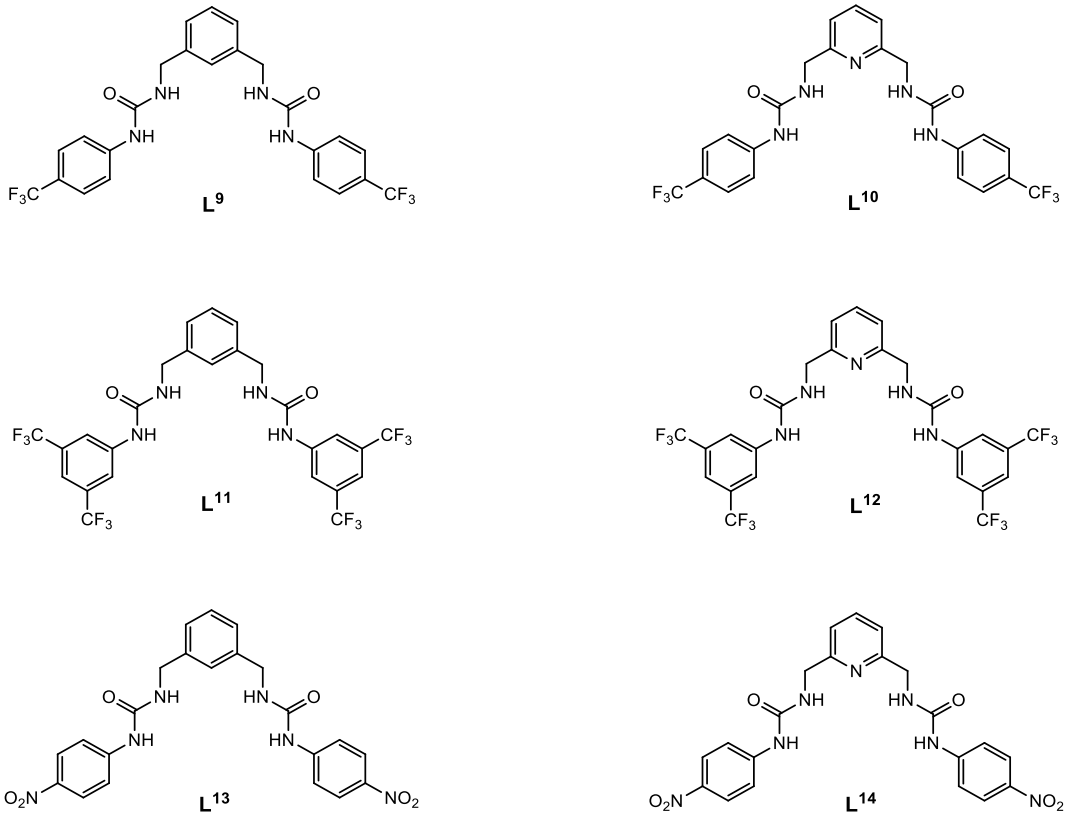

Figure 3. Summary of receptors synthesised and studied in Chapter 4.

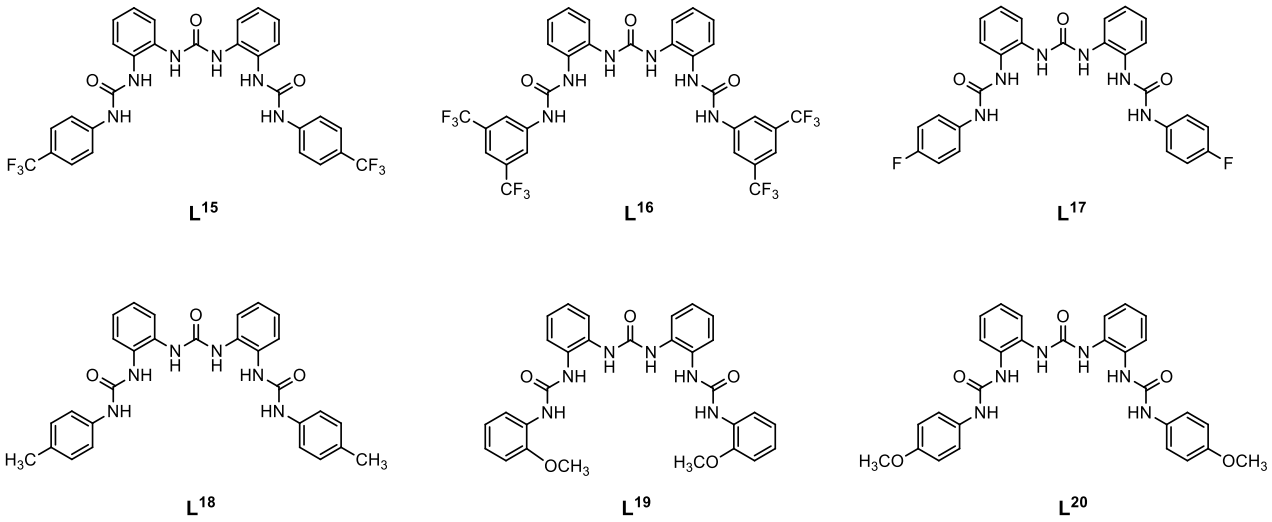

Figure 4. Summary of receptors synthesised and studied in Chapter 5

Contents

Chapter 1: Introduction

1.1 Supramolecular Chemistry

Supramolecular chemistry is an expanding area of research that was rapidly developed in the last decades. It is a multidisciplinary field between chemistry, physics and biology.
In 1987 J.M. Lehn, who won the Nobel Prize for his work in this area, defined supramolecular chemistry as "the chemistry of molecular assemblies and of intermolecular bond"[1], as "chemistry beyond the molecule, bearing on the organised entities of higher complexity that result from the association of two or more chemical species held together by intermolecular forces"[2] such as hydrogen-bonding, hydrophobic interactions, π-π stacking interactions, van der Waals forces and electrostatic effects. Therefore supramolecular chemistry examines the weaker and reversible non-covalent interactions between molecules instead the covalent bond as traditional chemistry.
The study of non-covalent interactions is crucial to understanding many biological processes that are often the inspiration for supramolecular research. Indeed, the development of supramolecular chemistry's philosophical roots began in 1894 when H. E. Fisher, trying to explain the high specificity of enzyme-substrate interactions, described the 'Lock and Key' principle, the basis of molecular recognition and host-guest chemistry. An enzyme can catalyse a single reaction with high or totally specifity because his size, shape and position are ideal for one specific substrate. In other words, they are exactly complementary as a key with the lock. One of the most important examples of the lock and key principle in biological system is the DNA double helix that is composed of two strands of purine and pyrimidine bases paired together by complementary specific hydrogen bonds in such a way that only adenine-thymine and guanine- cytosine base pairs can be formed.
The result of the specific and selective non-covalent interaction between an appropriate receptor and a substrate is a compound characterised by new structural and new physical-chemical properties named *supramolecule*. (*Figure 1.1*)

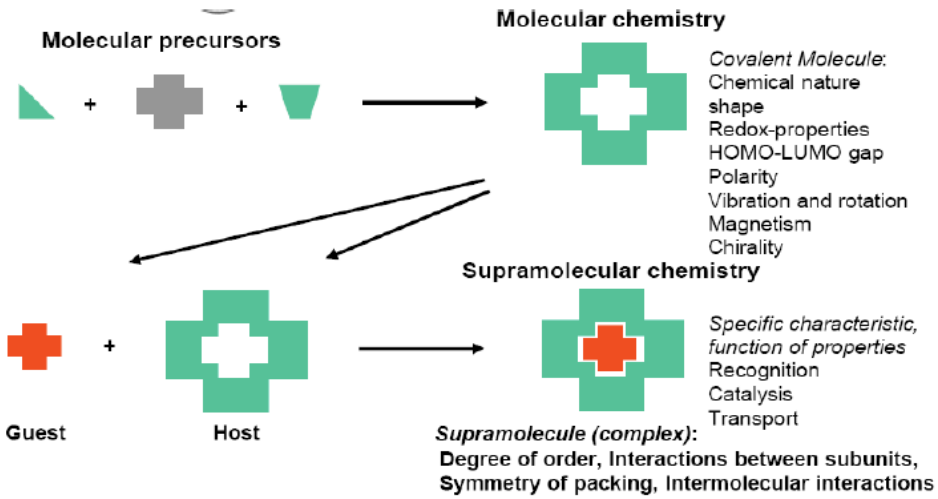

Figure 1.1. Comparison between the scope of molecular and supramolecular chemistry

There must be a molecular recognition between receptor and substrate which is, along with the intramolecular non-covalent interactions, the key concept in all fields of development in supramolecular chemistry:

1. *Host-guest complexation* involves the interaction between a molecule (host) and a second molecule (guest) through weak non-covalent bonds (therefore the formation of the complex is reversible). *Host* is generally a large molecule which has convergent binding sites (hydrogen bonds donors, Lewis bases) and a cavity or pseudo-cavity that can accommodate a smaller *guest* molecule that presents divergent binding sites (hydrogen bond acceptors, Lewis acids) and that must have a structural geometry complementary to that of the host molecule.

2. *Molecular self-assembling and self-organization* are the spontaneous and reversible association of molecules through non-covalent interactions without guidance or management from an outside source to give a new ordered structure. Self-assembly may be subdivided into intermolecular self-assembly (to form a supramolecular assembly), and intramolecular self-assembly (or folding as demonstrated by foldamers and polypeptides). Molecular self-assembly also allows the construction of larger structures such as micelles, membranes, vesicles, liquid crystals, and is important for crystal engineering.

3. *Crystal engineering* is "the understanding of intermolecular interactions in the context of crystal packing and in the utilisation of such understanding in the design of new solids with desired physical and chemical properties".[3,4]

4. *Supramolecular transport* is the transport of a substrate across the lipid bilayer of a membrane by a receptor with suitable size and lipophilicity that can function as a mobile carrier or may form a channel. This is a relatively new and expanding field of supramolecular chemistry and can found application in biology and medicine.

5. *Supramolecular sensors* are systems consisting of a receptor, a possible spacer and an active unit that is able to change its physical and chemical properties following the specific interaction between receptor and substrate. Therefore the molecular sensors can translate the complexation in detectable analytical signal (changes in pH, fluorescence, colour or electronic distribution).

1.2 Anions recognition

The design of anion receptors is a rich research area of supramolecular chemistry that has developed much more recently than the coordination chemistry of cations, It initiated in the 1960s by work of Shriver and Biallas[5] and Park and Simmons[6] but started to develop in the 1990s and particularly in the last decade moving from simple anions receptors in organic solvents to receptors which complex anions in water, systems able to bind anions *in vivo*, compounds capable of transporting anions across cell membranes, and so on.

Anion recognition is an area of intense interest since the anions are ubiquitous in the Nature and are involved in many chemical and biological processes.

They are essential for life, their recognition, transport or transformation is important for almost every biochemical process. Anions participate in the formation of most of the enzyme-substrate or enzyme-cofactor complexes. ATP, the free energy source of life, DNA or RNA, the genetic material, are polyanions at physiological pH. The regulation of cellular anion concentrations is fundamental to many biological processes such as regulating osmotic pressure, activating signal transduction pathways, maintaining cell volume, and in the production of electrical signals. The malfunction of anion transport is a cause of numerous diseases. Cystic fibrosis, one of the best known of these disorders, is linked to misregulation of chloride and bicarbonate caused by a genetic modification of the CFTR (Cystic Fibrosis Transmembrane Conductance Regulator) present in the membrane of epithelial cells.[7]

Many anionic species are also the cause of serious environmental problems. Inorganic anions such as pertechnetate, chromate, arsenate, nitrate, perchlorate, phosphate, sulfate and sulfide are included in the "Priority pollutant list" of the European Community for the problems of pollution they create. Nitrates and phosphates, used as fertilizer, can be the cause of eutrophication of rivers and lakes. Many organic phosphates found in pesticides can cause water poisoning. Pertechnetate, produced by the nuclear fuel reprocessing, is a toxic and radioactive anion.

It is not surprising, therefore, that the need to develop receptors for anions in complex media such as blood, cells, soil, water etc. has become of great importance.

However, the design of anion receptors is more challenging in comparison to the design of receptors for cation due to some of their properties:

- *Size*: anions are larger than their isoelectronic cations therefore the receptor must have an appropriate cavity for complexation. (see *Table 1.1*)

Table 1.1 A comparison of the radii of isoelectronic cations and anions.

Cation	Radius Å	Anion	Radius Å
Na^+	1.16	F^-	1.19
K^+	1.52	Cl^-	1.67
Rb^+	1.66	Br^-	1.82
Cs^+	1.81	I^-	2.06

- *Charge*: they have a lower charge to radius ratio hence they can only form electrostatic interactions less efficient than covalent bonds established with the cations

- *Geometry*: anions have a wide range of geometries *(Figure1.2)* and it's more difficult to design receptors whit a high level of complementarity to complex an anion guest selectively.

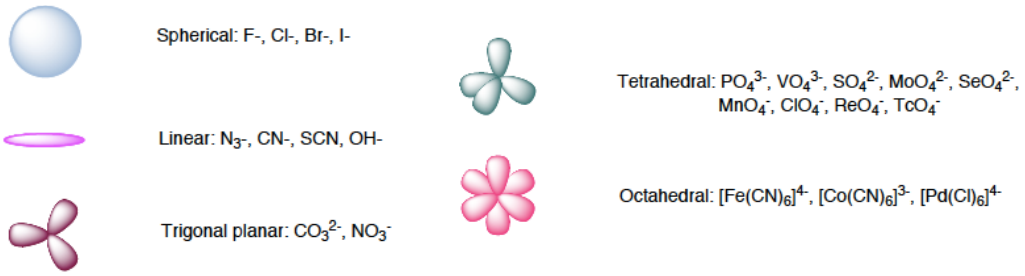

Figure 1.2. Geometries of anions

- *pH dependence*: at low pH anions can become protonated and lose their negative charge. Thus it's necessary that the receptors function within the pH range of anions target, this is particular important if the receptor is protonated because its protonation window must also be taken into account.

- *Solvent*: the solvent is another important parameter to consider. Anion recognition is based on electrostatic interactions that can be established also between the solvent and the anion, for example, protic solvents can form strong hydrogen bonds with the anions therefore the receptor must compete effectively with the solvent for the bond with the anion and take his place. Moreover the receptor must also compete with the counter cation of the anionic guest.

- *Hydrophobicity*: hydrophobicity can also influence the interaction between a receptor and an anion guest. The Hofmeister series shows increasing hydrophobicity of anions, and consequently their decrease of aqueous solvation. Hydrophobic anions are generally bound more strongly in hydrophobic binding sites. (*Figure 1.3*)

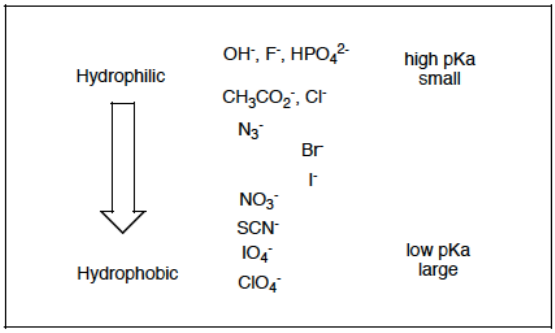

Figure 1.3. The Hofmeister Series.

In order to design an effective and selective anion receptor, over all these factors mentioned, must also take into account the types of noncovalent interaction used to complex the anionic guest. These include electrostatic interactions, hydrogen bonding, Lewis acids, and combinations of these interactions working together.

The easiest way to bind an anion is to introduce positive charges in the receptor to form strong ***electrostatic interaction***. The more charged groups are present the more these interactions should be effective. However, this may cause problems in the design because the positive charges tend to repel one another. This problem can be overcome by building receptors rigid or cyclic, which can also create binding cavities for the anions.

Another way to complex anions is to use ***hydrogen bond interactions***. Anions can be considered as electron pair donors and they are able to interact with an electron pair acceptors such as an electropositive hydrogen atom to form a hydrogen bond. A wide variety of anion receptors are neutral and contain groups capable of giving this kind of interaction as N-H or O-H. It is, therefore, possible to design receptors with the hydrogen atoms correctly oriented in a convergent manner in order to bind selectively an anion with a specific geometry. These receptors include alcohols, amides, ureas, pyrroles or indoles.

Finally, another way to bind anions is to use metal ions, which act as ***Lewis acids***. Alike hydrogen bonds donor groups also electron-deficient Lewis acids can bind anions as they can accept electron pairs from anionic guest into their vacant orbitals.

All this type of interactions can be used together to produce very effective receptors for anions.

1.3 Classification of anion receptors

On the basis of this type of interactions mentioned, anion receptors can be classified into:

- Charged anion receptors: Ammonium based receptors
  Guanidinium based receptors
  Imidazolium and triazolium based receptors

- Neutral anion receptors: Amide based anion receptor
  Urea and thiourea based anion receptor
  Indole and pyrrole based anion receptors
  Alcohol based anion receptor

- Metal and Lewis acid anion receptors

1.3.1 Charged anion receptor

The employment of positively charged groups is the most intuitive and easy way to bind anions and was the earliest synthetic approaches to the construction of anion receptor systems. The charged receptors can contain ammonium, guanidinium or imidazolium groups.

Ammonium based anion receptor

The ammonium groups have been largely use in the anion recognition chemistry, they can be generated by protonation of amines and show a strong tendency to bind anions in organic and aqueous solvent thank to the ability to form both strong electrostatic and hydrogen bonds interactions.

The first examples of a synthetic anion receptors were reported in 1968 by Simmons and Park and consist in a series of macrobicyclic ammonium bridged receptor which can complex anions through electrostatic interactions and hydrogen bonds.[6] The receptor **1**, with 9 methylene group in length, showed the highest affinity for chloride with K_a=4 M^{-1} in 50% TFA solution. The crystal structure of this complex reported by Marsh and co-workers in 1975 showed that both ammonium hydrogen atoms pointed into the interior of the cavity when the chloride is present suggesting that the anion was bound within the cavity of the receptor.[8]

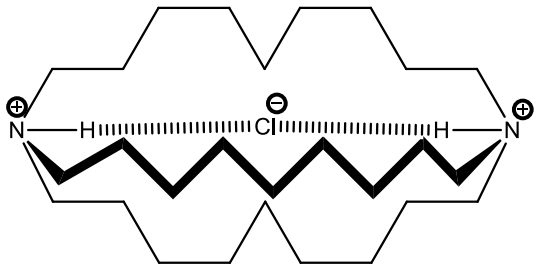

1

Bencini, Lippolis and co-workers have recently investigated the effect of the aromatic linker between two [9]aneN_3 ammonium units in receptors **2**–**4.**[9] In aqueous solutions the two [9]aneN_3 units are protonated and can bind anions via hydrogen bonding and electrostatic interactions. Using potentiometric, ^{1}H-NMR and ^{31}P-NMR measurements it was found that **2** selectively binds triphosphate, while **3** selectively binds diphosphate and **4** monophosphate in aqueous solutions over a wide pH range, these binding properties of the receptors were influenced by the distance between the two [9]aneN_3 imposed by the different spacer separating the two macrocyclic units.

Furthermore, **2** and **3** are also able to interact selectively with the nucleotides ATP (adenosine triphosphate) and ADP (adenosine diphosphate) over inorganic phosphate

species. The receptor **2** showed the highest associations with ATP and ADP, this could be attributed to the highest ability of phenantroline to establish stabilizing π stacking and hydrophobic interactions with the adenine units of the guests.

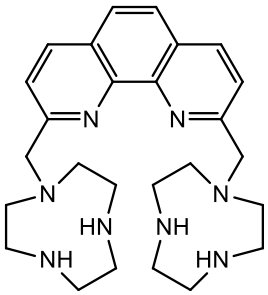

2

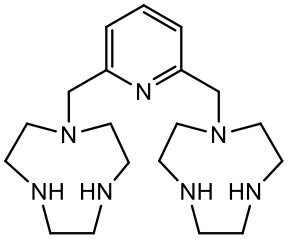

3

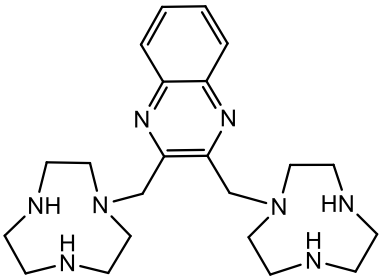

4

Subsequently the groups of Bencini and Lippolis have studied the anion binding properties of terpyridine analogue **5**.[10] Potentiometric titrations, ^{1}H-NMR and fluorescence spectra in water showed that receptor **5** is only able to selectively bind and sense diphosphate over mono- and triphosphate, after the addition of Zn^{2+} the metal ion causes a conformational change from trans–trans to cis–cis to create a convergent binding site that has optimal dimensional fitting for diphosphate (*Scheme 1*).

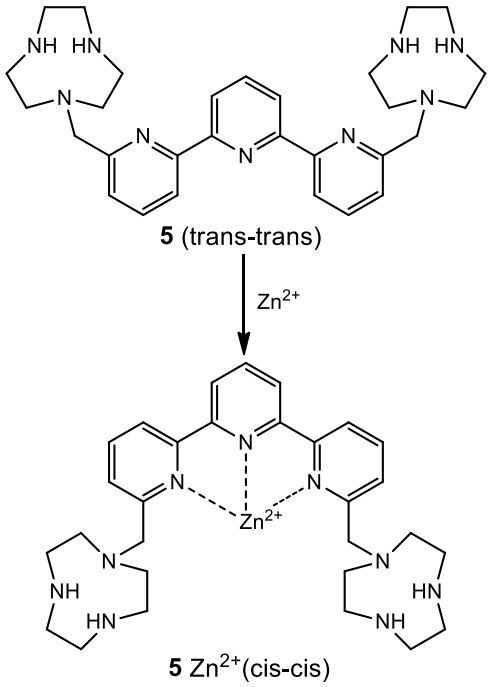

Scheme 1.1 Zn^{2+} induced conformational change of the terpyridine unit in receptor **5**

Guanidinium based anion receptor

The guanidinium group has a high basicity, hence it has the advantage of remaining protonated over a wide pH range (pK_a 13.6). The hydrogen bond donors are pointed in the same direction and therefore the guanidinium-based receptors often show a high affinity and selectivity for oxyanion substrates.

Schmuck and co workers have reported five guanidiniocarbonyl pyrrole based receptors **6**-**10** containing also a primary ammonium attached by flexible chain linkers.[11] The anion binding properties were investigated by UV-Vis titrations in buffered water at pH 6 containing 10% DMSO with some N-acetyl amino acid carboxylates (Ala, Phe, Val, Glu, Asp) and sulfate and acetate. A minimum linker length of four carbons was found to be necessary to allow efficient anion binding by both positive charges. In fact, the two shortest bis-cations **6** and **7** shown only weak binding of substrates while increasing length of the linkers, an increase of the complex stability is observed. The highest complex stability is showed by the receptor **9** with Phe (K_a = 4700 M^{-1}).

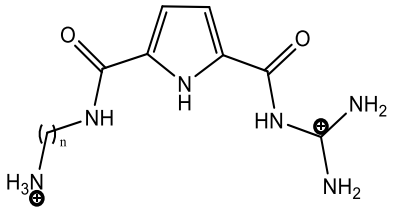

6 n = 2 **8** n = 4
7 n = 3 **9** n = 5

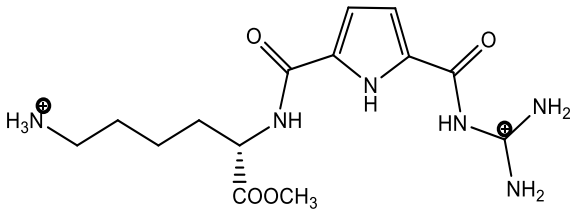

10

Imidazolium based anion receptor

The imidazolium groups possess acidic CH moieties and are able to complex anions by a combination of electrostatic interactions and $^{+}$CH--A^{-} hydrogen bond instead the most commonly $^{+}$NH--A^{-} hydrogen bond. This has the advantage of being independent of the pH.

Kim and co-authors have synthesise a new water-soluble and fluorescent imidazolium-anthracene cyclophane **11**.[12] Fluorescence spectroscopy studied in 100% aqueous solution at pH 7.4 with 100 equivalents of the TBA anion salts showed the high selectivity of **11** for iodide and a range of phosphates, most significantly GTP, with the observation of chelation-enhanced fluorescence quenching (CHEQ) of excimer emission. The affinity constants were 1.1 x 10^3/2.1 x 10^6 M^{-1} and 1.3 x 10^4 M^{-1} for GTP and I^- respectively.

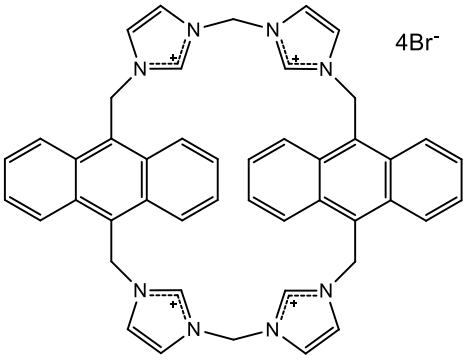

11

GTP and I^- display different binding modes for receptor **11** (1:2 and 1:1, respectively). ^{1}H-NMR titration experiments and DFT calculations suggest that this altered binding mode is due to GTP being bound by two receptors through imidazolium $CH^{+}\cdots O$ interactions and there is no interaction between anthracene moieties and guanine of GTP, while I^- is bound within the cavity through both imidazolium $CH^{+}\cdots$anion and anthracene $CH\cdots$anion interactions. In both examples there is a separation of the face-to-face contact of anthracene units, which is a source of excimer formation, and this is the cause of quenching of the excimer fluorescence.

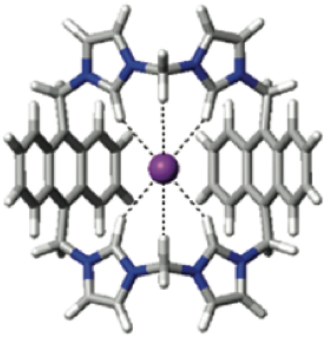

11-I^-

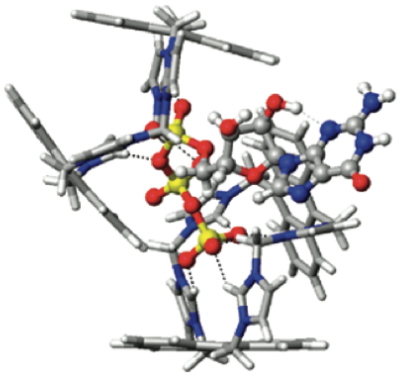

11-GTP

Figure 1.4.The X-ray structure of the complex of receptor **11** with iodide and GTP.

Flood and co-workers have reported the anion binding properties of aryl-triazole containing receptors such as **12**. These triazolophanes displayed high binding affinity for Cl^- (> 10^6 M^{-1} in CH_2Cl_2), due to pre-organisation (macrocyclic effect), the presence of CH hydrogen bond donor groups and size complementarity of the receptor and chloride.[13,14] In order to investigate the importance of structural rigidity of the triazolophanes as a pre-organisation factor to explain the high affinity for chloride, Flood and his group compared the Cl- binding affinity of three triazolophanes, a ‘‘strongly’’ preorganised macrocycle **12**, a ‘‘partially’’ preorganised macrocycle **13** and a ‘‘poorly’’ preorganised macrocycle **14**.[15] Computational studies and ^{1}H-NMR titrations showed that high rigidity (in combination with the macrocyclic effect) prevents the relaxation of close $H\cdots H$ contacts and retains the preorganised nature of the CH triazole hydrogen bond donors in **12** to maximise the strength of the interactions between the receptor and chloride.

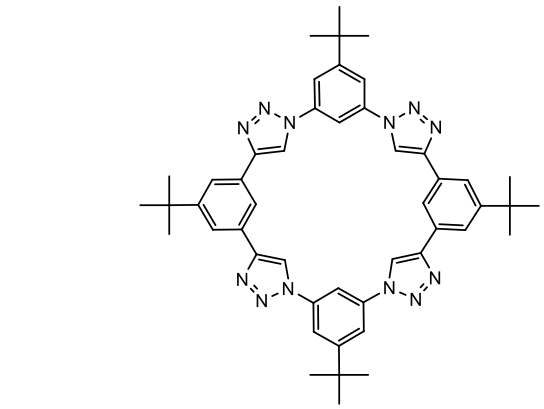

12

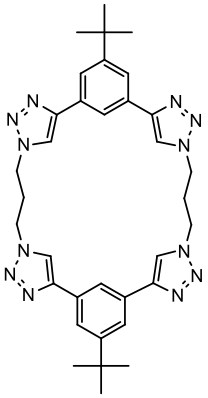

13

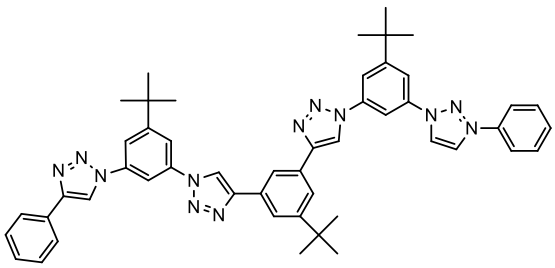

14 (unfolded)

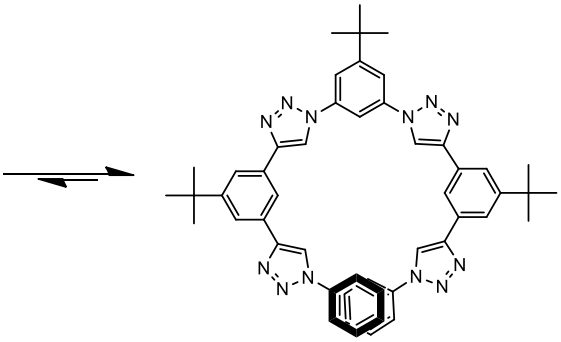

14 (folded)

1.3.2 Neutral anion receptor

Amides based anion receptor

The amide group contain both hydrogen bond acceptors (oxygen lone pairs) and hydrogen bond donors (NH). There are many examples in Nature of anion binding by proteins by neutral amide functions and for this reason it has aroused great interest in the anion recognition chemistry. A wide variety of amide-containing anion receptors have been employed to bind anionic species.

The first example of a synthetic anion receptor containing secondary amides was reported by Pascal and co-workers in 1986.[16] The system has three amide groups orientate within the cavity when the anions are present. ^{1}H-NMR titration showed that the receptor can bind fluoride anions in DMSO-d_6.

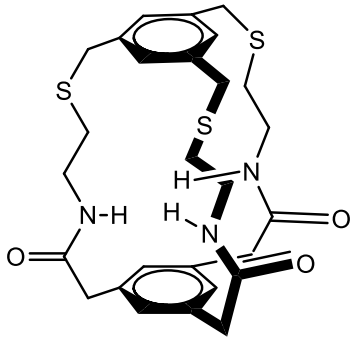

15

Recently, Yatsimirsky *et al.* have studied a series of isomeric N,N'-bis(pyridyl)-2,6-pyridine-dicarboxamides **16-18**.[17] The anion binding properties were examined by ^{1}H NMR titrations in CD_3CN with chloride and acetate. It was found that the m-isomer **16** was able to form 1:1 and 1:2 (receptor:anion) complexes with both anions (chloride: log K_a=1.8, log β_{21}=4.23; acetate: log K_a = 2.6, log β_{21}=4.7), the p-isomer **17** was able to form 1:1 complex with chloride (log K_a=2.85) and both 1:1 and 1:2 complexes with acetate (log K=3.48, log β_{21}=6.5) while no interaction and weak binding were observed for the o-isomer **18** with chloride and acetate log K = 0.7) respectively.

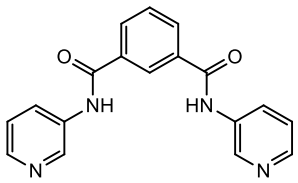

16

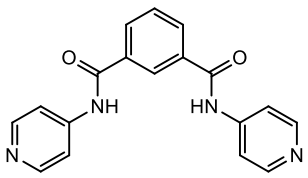

17

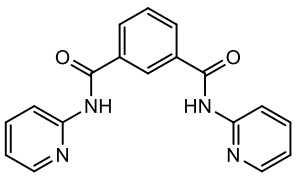

18

Urea and thiourea based anion receptor

The urea and thiourea functions are the most widely employed groups in the design of neutral anion receptor. They are easy to synthesise and contain two NH donor group oriented in the same direction, in a bidentate manner, suitable for interacting with Y-shaped anions such as carboxylate, phosphate, sulfate and nitrate.

Fabbrizzi and co-workers have reported the anion binding affinities of the simple 1,3-bis(4-nitrophenil)urea receptor **19** with a variety of anions.[18] UV-Vis titrations in CH_3CN, using the TBA salts of anions, displayed the preference of this receptor for oxoanions with the formation of 1:1 complex with acetate and benzoate anions with high constants (log K_a = 6.61 and 6.62 respectively). In the case of fluoride, the first equivalent of the anion formed the most stable complex with the receptor with the highest binding constant (log K_a =7.38) and then the addition of a second equivalent of fluoride caused the deprotonation of the receptor due to formation of HF_2^-. The crystal X-ray structure of the complex of **19** with acetate showed the formation of two N−H···O hydrogen bonds of moderate strength between the urea group and the two oxygen atoms of the oxoanion.

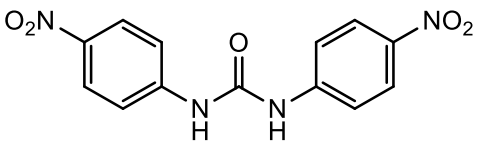

19

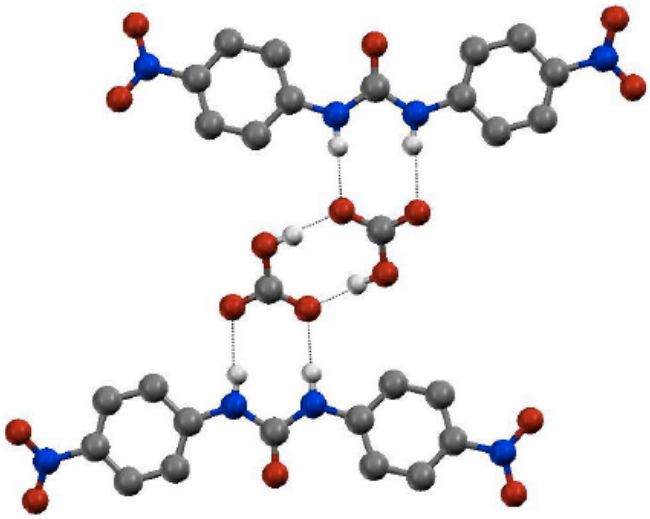

Figure 1.5. Complex with receptor **19** and bicarbonate crystallised by Fabbrizzi and co-workers

Gale *et al.* have investigated the carboxylate complexation by a family of ortho-phenylenediamine based bis-ureas receptor.[19,20] They first synthetize and studied the anion binding properties of compound **20** using ^{1}H-NMR titration in DMSO-d_6/0.5% water. This compound proved to be selective for carboxylate anions binding acetate with a stability constant of 3210 M^{-1} and benzoate with a stability constant of 1330 M^{-1}. The crystal structure of the benzoate complex of **20** showed the formation of four hydrogen bonds between the receptor and carboxylate anion in the solid state.

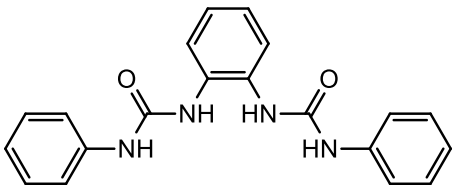

20

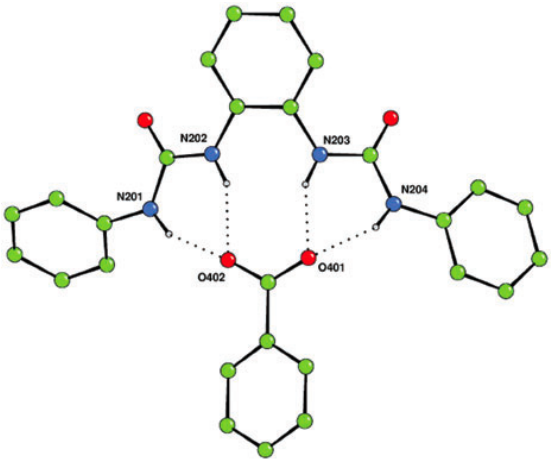

Figure 1.6. The structure of the benzoate complex of receptor **20**

Considering the high affinity for carboxylates of receptor **20** Gale and his group decided to synthesise the compounds **21** and **22** by introducing electron-withdrawing substituents in the bis-urea skeleton in order to enhance the selectivity for anions. [21] Compounds **21** and **22** showed significantly increase of anions affinity compared to compound **20**, binding acetate with a stability constant of 8080 M^{-1} and 4018 M^{-1} respectively in DMSO-d_6/0.5% water solution. The most interesting result was the higher stability constant showed by receptor **21** for dihydrogen phosphate (k_a = 4724 M^{-1} compared to 732 M^{-1} of compound **20**) probably due to dihydrogen phosphate interact strongly with the central urea hydrogen atoms that are more acidic in compound **21**.

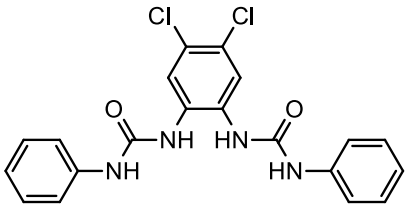

21

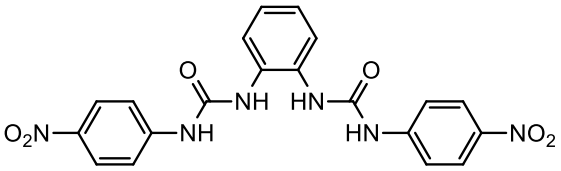

22

The same research group has also studied the anion binding properties of a new hybrid amide–urea macrocycles, compound **23** containing a 2,6-dicarboxamidopyridine group and compound **24** containing an isophthalamide group.[22,23] The macrocycle **23** possesses high selectivity for carboxylates over dihydrogen phosphate and chloride, it binds acetate approximately 100 times more strongly than dihydrogen phosphate both in DMSO-d6/0.5% water and in DMSO-d6/5% water solution. Instead, macrocycle **24** displayed a low affinity and selectivity for carboxylates and appeared to be not stable in DMSO-d_6/0.5% water undergoing hydrolysis. This instability is due to compound **24** with the isophtalamide group adopts a twisted conformation that is subject to hydrolyse. In macrocycle **23**, in contrast, the pyridine group is able to form intramolecular hydrogen bonds with the amide groups stabilising the macrocycle to a more planar conformation.

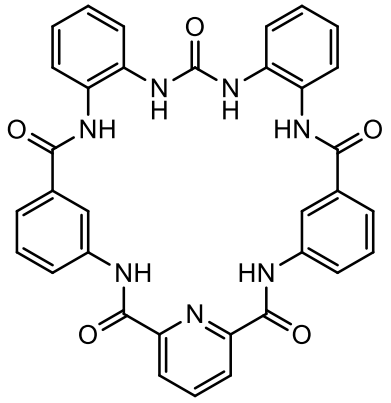

23

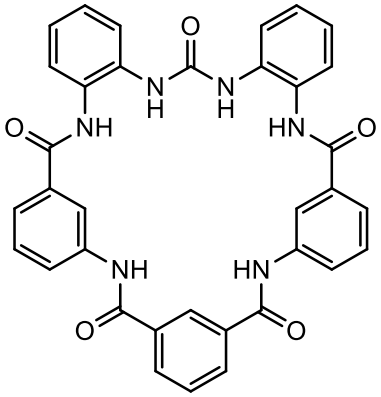

24

Martínez-Máñez, and co-workers, in collaboration with Rurack have investigated the anion complexation properties of two azo dye derivatives **25** and **26** containing a urea and a thiourea group, respectively.[24] Both compounds displayed an intense yellow absorption band at 375-400 nm in acetonitrile due to a charge-transfer process from the electron donor groups (urea and thiourea moieties) to the electron acceptor nitro group. The UV-Vis titration showed two different chromogenic responses toward anions in acetonitrile solution: a bathochromic shift of ca. 40 nm corresponding to a colour change from yellow to pale orange due to anion recognition with AcO^-, BzO^-, $H_2PO_4^-$ and Cl^-, and a strong red shift of ca. 200 nm with the appearance of a new band at 580 nm and a colour change to blue attributed to the deprotonation in the presence of fluoride. The high binding affinities were observed in accord with the intrinsic acidity of the protons of the binding site and the basicity of the anions as reported by the stability constants of the receptors shown in *Table 1.2*.

Table 1.2 Stability constants (K_a/M^{-1}) of compounds **25** and **26** in CH_3CN measured by UV-Vis titration

Anions	25	26
Cl^-	370 ± 110	1250 ± 50
CH_3COO^-	27100 ± 600	60000 ± 4000
$C_6H_5COO^-$	13200 ± 200	41000 ± 2000
$H_2PO_4^-$	3900 ± 300	7400 ± 600

Furthermore, Compound **26** may be used to sense carbon dioxide. The blue solution of the deprotonated receptor **26** with fluoride turns yellow when is left open to the air, due to dissolution of carbon dioxide in the solution. Proton NMR studies of the **26**/F^-/CO_2 system in CD_3CN showed the formation of a complex in which the thiourea moiety is hydrogen-bonding HCO_3^- formed through a reaction between traces of water and carbon dioxide in the presence of basic fluoride.

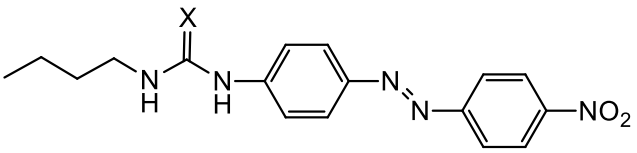

25 X = O
26 X = S

Ghosh and his research group have designed a series of TREN-based tris ureas receptors **27**-**29**.[25] Binding constants were determined by ^{1}H-NMR titration in DMSO-d_6 for **27** and **28** and by fluorescence titrations for **29** due to the presence of the fluorescent anthracene group. All three receptors showed selectivity for dihydrogen phosphate over the other anions taken into account, with association constant of log K_a= 5.52 M^{-1} for **27**, 4.04 M^{-1} for **28** and 4.60 M^{-1} for **29**. The receptor **27** binds dihydrogen phosphate more strongly than the other receptor due to the electron-withdrawing effects of the $–C_6F_5$ moieties that enhance the acidity of the NH bond donors groups. In the solid state receptor **27** form a pseudo-dimeric cage where a dihydrogen phosphate is encapsulated (*Fig. 1.7*). The cage formed by two receptor moieties is held together by π-π stacking interactions and the $H_2PO_4^-$ dimer is bound in the centre of the cage *via* numerous hydrogen bonding.

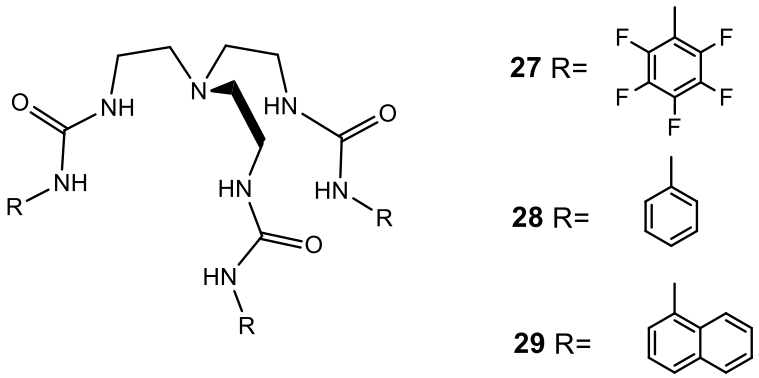

27 R=
28 R=
29 R=

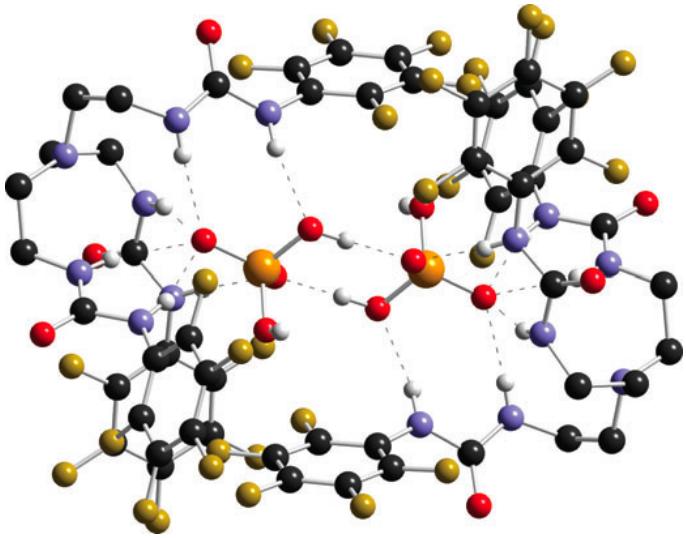

Figure 1.7. A $H_2PO_4^-$ dimer inside the pseudo cage formed by receptor **28** in the solid state.

The same group, more recently, has reported the first example of the recognition of tetrabutylammonium sulfate by the pentafluorophenyl tripodal receptor **30** *via* strong ion pair interactions both in solution and in solid state.[26] The X-ray structure (Fig. 1.8) showed that the SO_4^{2-} was completely encapsulated in the centre of the cavity formed by the three arms of the tripodal receptor via N–H···O hydrogen bonding interactions to all six –NH protons of the three urea groups. While both of tetrabutylammonium counterion were bound by five C-H···O interactions on the exposed side of the anion acting as a cap of the sulfate-bowl. 2-dimensional diffusion ordered spectroscopy (2D-DOSY) and ^{1}H-NMR studies showed the presence of the ion pair complex also in solution of DMSO-d_6 at 298 K. The affinity of **30** for different anions was evaluated by ^{1}H-NMR titration in DMSO-d_6 displaying the strong binding of sulfate (log K_a = 5.74) over dihydrogen phosphate (log K_a = 4.39), acetate (log K_a = 3.41) and chloride (log K_a = 3.38) in 1:1 binding stoichiometry.

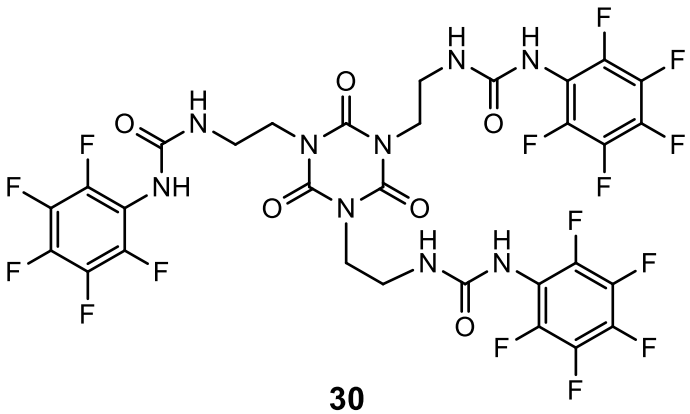

30

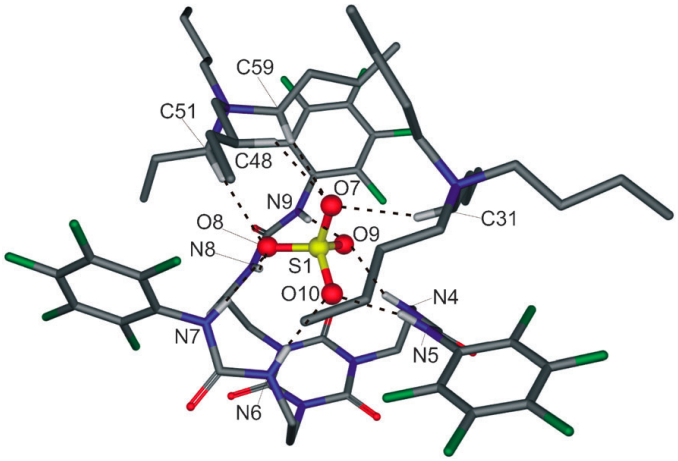

Figure 1.8. The X-ray structure of receptor **30** and tetrabutylammonium sulfate.

Wu and co-workers have reported the anion binding and extracting properties of tripodal hexaurea **31**.[27] The crystal structure showed that **31** encapsulate a single sulfate anion by 12 hydrogen bonds to the six urea groups forming a tetrahedral cage with each of the three terminal arms folded along an edge of the bottom triangular face and each urea group chelating an edge of the tetrahedron (*Fig. 1.9*). Compound **31** is the only receptor reported to date that displayed saturated coordination of a sulfate ion by a single host. The binding studies carried out by 1H-NMR titration showed high selectivity for sulfate, over other anion, with $K_a > 10^4$ M^{-1} for 1:1 binding stoichiometry also in competitive DMSO-d_6/25% water solution. As **31** is water-tolerant and selective for sulfate the extracting studies were performed using NMR techniques. The receptor **31** demonstrated to be also able to efficiently extract sulfate anions from aqueous $NaNO_3/Na_2SO_4$ solutions into $CDCl_3$.

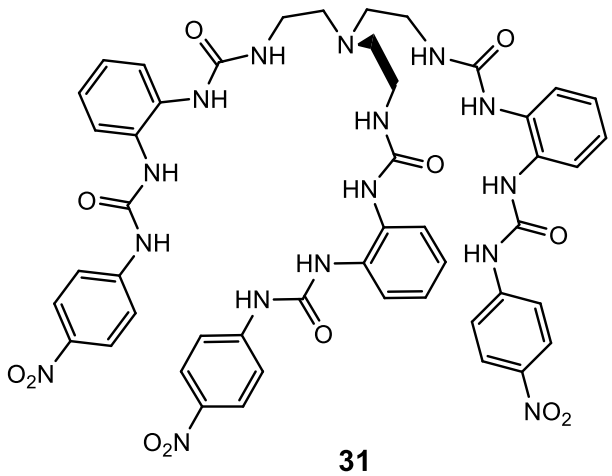

31

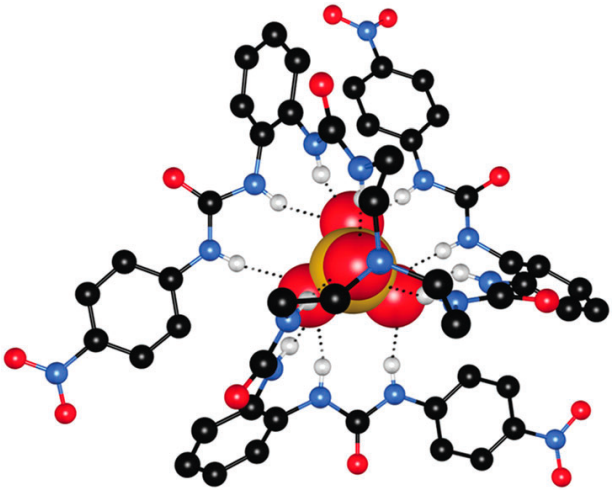

Figure 1.9. Crystal structure of the sulfate complex of receptor **31**

Gunnlaugsson and co-workers have developed a series of simple diarylureas **32**-**34**[28] and thioureas **35**-**37**[29] functionalised with a single acetamide moieties in the para-, meta- and ortho-position on one of the aryl groups and an electron withdrawing CF_3 group on the other. The anion binding affinities were investigated by both UV/Vis titrations in CH_3CN and ^{1}H-NMR techniques in DMSO-d_6. The compounds were found to interact strongly with AcO^-, $H_2PO_4^-$, $H_2P_2O_7^{2-}$ and F^- in CH_3CN, as determined by the changes in their respective absorption spectra. Compound **34** is the only receptor that formed complexes with 1:1 stoichiometry in which all three of the NH hydrogen bond donor groups bind to the anionic guest. While for all other receptors the dominant species was a 1:2 (receptor:anion) complex. The complexation of one equivalent of the anions by the urea or thiourea groups was leaded to activation of the amide moiety that was able to complex a second equivalent of anion as a consequence of positive allosteric effects in these structures. In general the ligands bind acetate more strongly than other anions taken into account. Compared to their urea counterparts, the thioureas **35** and **36** showed a higher anion affinity than **32** and **33**.

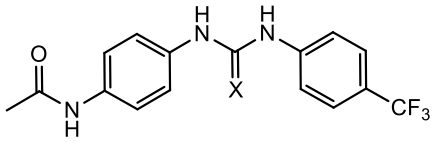

32 X = O
35 X = S

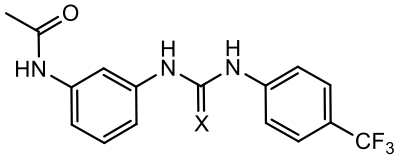

33 X = O
36 X = S

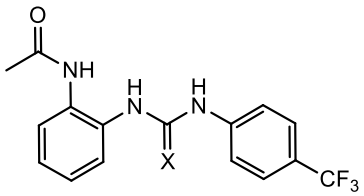

34 X = O
37 X = S

Lodeiro and co-workers have recently designed and synthesized two novel nitrophenilyurea and nitrophenylthiourea colorimetric sensors **38** and **39**.[30] The anion binding properties were investigated by UV-Vis spectroscopy in DMSO. Upon addition of OH^- and F^- to a solution of **38** and **39**, the absorption maxima at 345 and 375 nm decreased gradually, and a new band at 463 and 496 nm increased, respectively. A red shift is observed due to a perturbation in the internal charge transfer (ICT) character of the sensors linked to the deprotonation of the receptors by the anions. Both receptors followed the binding selectivity $H_2PO_4^- > F^- > OH^- > CN^- > CH_3COO^-$ and allowed naked-eye detection of these anions, while no interaction occurred with NO_3^-, ClO_4^-, Cl^-, Br^-, and I^- anions. Strongest interaction with anions and more intense colours were observed for compound **39**, though compound **38** was able to discriminate between F^-, OH^-, CN^- ,CH_3COO^- and $H_2PO_4^-$ giving different response and colour changes with these anions, therefore it showed better chemosensing properties than compound **39**.

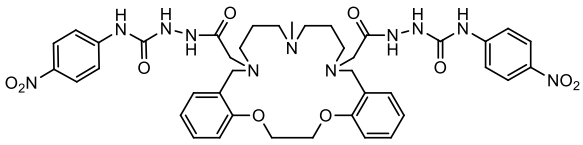

38

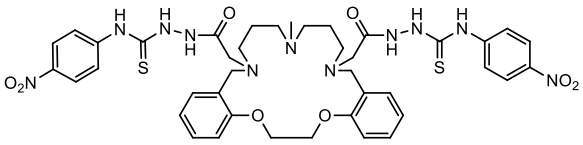

39

Indole and Pyrrole based anion receptor

Indole and pyrrole both contain a single hydrogen bond donor group and have no hydrogen bond acceptors like amides or ureas that may involve in intramolecular competition due to NH···O hydrogen bonding interactions. Sessler and co-workers have pioneered the use of pyrrole in anion complexation in the early 1990s establishing pyrrole as an excellent anion receptor group, whilst the anion complexation chemistry of indole has been slowly to begun and it is still an area to explore. The indole group is important in biological systems, is contained in the aminoacid tryptophan and is found to have some activity as a catalytic residue in enzymes. For example, bisindolylmaleimides and indolocarbazoles function as potent protein kinase C inhibitors.[31,32]

Jeong and colleagues have synthesised and studied a biindolyl based receptor **40** and **41**.[33] The receptor **40** possesses two indole NHs and two amide NHs, while **41** contains two indole NHs and four urea NHs. These receptors are able to bind axoanions in a polar solvent mixture (DMSO/0.1-0.2% water) with binding affinities strongly dependent on the number of hydrogen bond donors present on the molecule. Binding studies were carried out by UV-Vis spectroscopy and showed that the binding selectivity for both receptors was $HP_2O_7^{3-} > H_2PO_4^- > AcO^-$ with compound **41** showing higher binding affinity for pyrophosphate ($K_a > 5x10^6$) than **40** ($K_a > 5.2x10^5$).

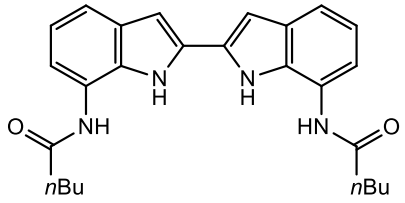

40

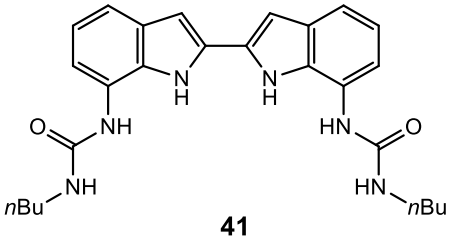

41

Caltagirone and co-workers have reported the anion complexation properties of a bipyridyl receptor functionalised with two amidoindole pendant arms **42a** and its neutral Pt(II) complex **42b**.[34]

The binding studies conducted in DMSO-d_6/0.5% water solution showed that the complex **42b** possessed a stability constant with dihydrogen phosphate of 3640 M^{-1} higher than that showed by receptor **42a** (90 M^{-1}). This result is attributed to the presence of Pt (II) that is able to induce a pre-organisation of the receptor resulting in an enhanced affinity for anions.

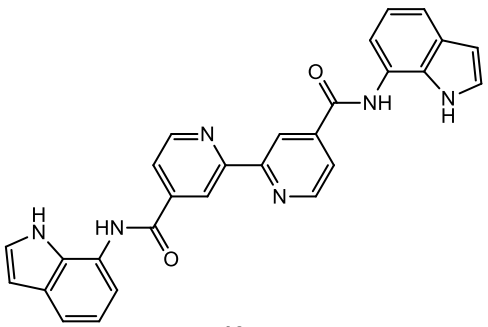

42a

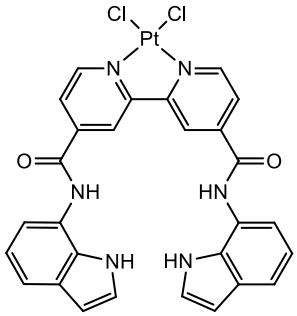

42b

Mani and his group have studied the anion recognition ability of macrocyclic **43** and open chain dipyrrolylmethane receptor **44** by proton NMR titrations techniques in acetone-d_6.[35] Compound **43** was found to bind strongly fluoride anion with a stability constant >10^4 M^{-1} in a 1:1 binding mode over other halide. Comparable result in stability constant (log K_a > 4) was obtained for receptor **44** in $CDCl_3$ in a 1:2 stoichiometry. The crystal structure of both receptors with HSO_4^- revealed the formation of the 1:1 complexes of SO_4^{2-} and the protonated receptors.

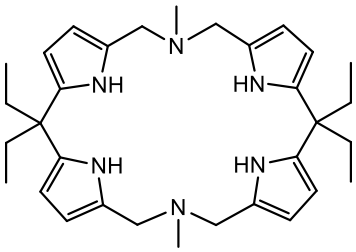

43

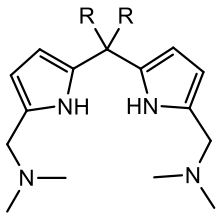

R = Ph

44

The same group have investigated the anion affinity of the azatripyrrolic **45** and azatetrapyrrolic **46** macrocycles.[36] Binding constants for the halide anion complexes were

obtained by ^{1}H NMR titrations in acetone-d_6 and they showed different binding modes. Compound **45** was found to form 1:1 fluoride complex with a stability constant of 1138 M^{-1}. Whilst for Cl^- and Br^- showed a 2:1 (receptor:anion) binding mode with stability constant of 3182 M^{-1} and 243 M^{-1}. The macrocycle **46** bind Cl^- and Br^- more strongly than **45** with a 1:1 stoichiometry with stability constant of 13586 M^{-1} for Cl^- and 1181 M^{-1} for Br^-.

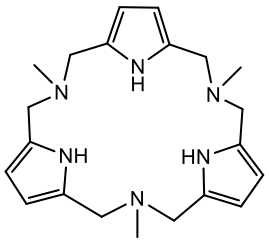

45

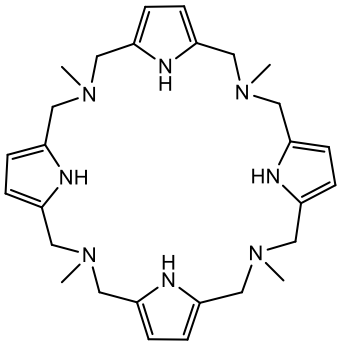

46

Alcohol based anion receptor

Hydroxyl groups are among the best known of all hydrogen-bonding donor groups and they are involved in many natural recognition processes. Nonetheless, They have been rarely used in the design of anion receptors due to their tendency to deprotonate in the presence of basic anions in organic solutions. However, in the literature there are efficient systems containing hydroxyl groups.

Kondo *et al.* studied the anion complexation properties of two D-ribose based epimers **47** and **48** by ^{1}H NMR titration experiments in $CDCl_3$ and CD_3CN.[37] For both receptor was obtained a higher affinity constant with AcO^- over $H_2PO_4^-$, Cl^- and Br^- in CD_3CN and compound **48** showed to have a better anion binding ability than compound **47**, probably due to electrostatic and/or steric repulsion between the anomeric O atom in **47** and the anions.

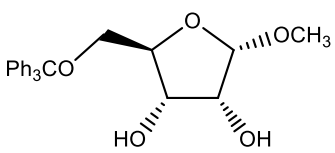

47

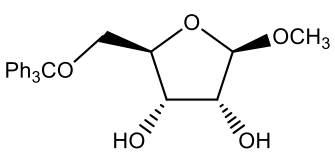

48

1.3.3 Lewis acids based anion receptor

The first example of this type of interaction was the simple chelating boron-based receptor **49** reported in 1967 by Shriver and Biallas[5]. It can form a strong complex with methoxide anions. Later Kats also produced a boron-based receptor **50** with two boron atoms rigidly held on an aromatic framework that is able to bind hard anions such as hydride or fluoride.

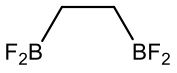

49

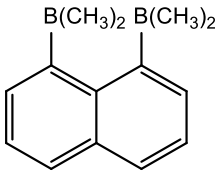

50

Caltagirone and Lippolis have reported the anion binding properties of the copper(II) complex of receptor **51** previously reported as a fluorescent sensor for zinc (II) ions.[38,39] This receptor was able to form a coordinative unsatured complex with copper (II) and therefore was suitable for anion complexation. The binding ability were determined by UV/Vis titration in CH_3CN and H_2O and showed that only addition of CN^- and I^- gave a significant response. The stability constant with I^- was found to be of log K_a = 4.8 in CH_3CN and 2.4 in H_2O with a 1:1 stoichiometry and the formation of this complex is accompanied by a colour change of the solution from cyan to green. The interaction with CN^- was found to form both 1:1 and 2:1 (anion:receptor) complexes evident by the colour change from cyan to dark blue and pink respectively. While in water the receptor formed a stable complex with 1:1 binding mode (log K_a >7) with CN^- manifested by colour change from cyan to dark blue.

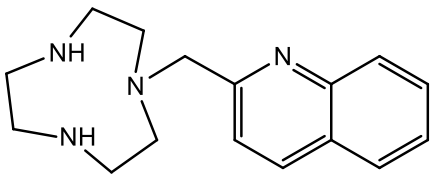

51

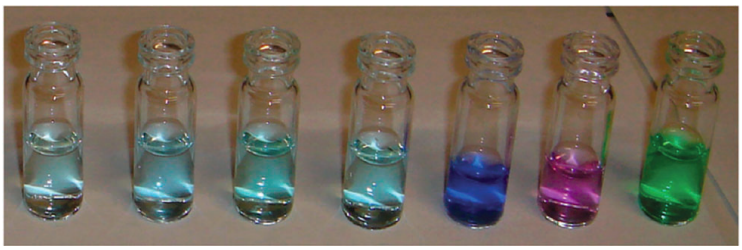

Figure 1.13. Colour change of **51** (10^-3 M) after addition of different anions in CH_3CN. From left to right: free receptor; +1 eq. F^-; +1 eq. Cl^-; +1 eq. Br^-; +1 eq. CN^-; +2 eq. CN^-; +1 eq. I^-.

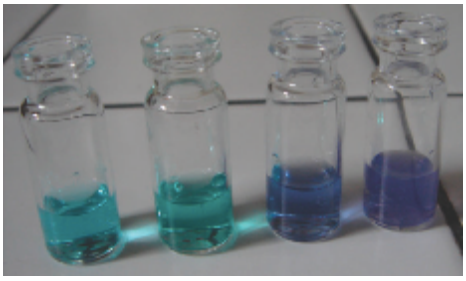

Figure 1.14. Colour change of **51** (1.72 x $10^{-}3$ M) after addition of I^- and CN^- in H2O. From left to right: free receptor; +1eq. of I^-; +1eq. of CN^-; + 2 eq. of CN^-.

1.4 Molecular sensors

A chemical sensor is a device that transforms chemical information, ranging from the concentration of a specific sample to total composition analysis into an analytically useful signal (change in pH, light emission or electronic distribution).[40]
These devices to be defined as chemical sensors, must possess peculiar properties:

- the receptor should be specific and selective to one substrate, or at least to a small group of them.
- The interaction between the receptor and the analyte should be rapidly and reversible.
- The sensor should have a good chemical stability and maintain its activity over a long time period.
- The sensor should be easy to synthesise and cheap.

A very useful approach recently followed by chemists for the design of new efficient chemical sensors takes advantage of the principles of supramolecular chemistry.[41,42,43] This "bottom-up" approach starts the design of a device from a molecular level, ensuring a resolution unachievable with a classic "top-down" approach. The resulting supramolecular species are usually called molecular sensors or chemosensor to distinguish them from chemical sensors, which are macroscopic devices.[44,45,46] A molecular sensor consists essentially of a receptor, able to bind the substrate, and an active unit, able to change its physical properties after the interaction between the receptor and the substrate, generally separated by a spacer.

The sensors are classified according to the principles of signal transduction in:

- Optical sensors
- Electrochemical sensors
- Electrical sensors
- Magnetic sensors
- Thermometric sensors

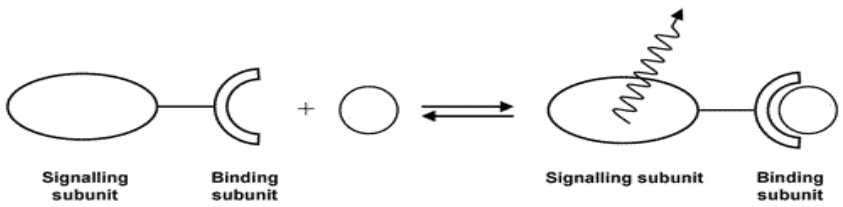

Figure 1.15. General scheme of a molecular sensor.

1.4.1 Optical anion sensors

Molecular sensors that change their photophysical properties following the recognition of a substrate are defined optical sensors. They can be divided into *fluorescent sensors*, if the active unit is a fluorophore and change their fluorescence properties, and *colorimetric sensors*, if the active unit is a cromophore and change their absorption properties.

1.4.1.1 Fluorescent chemosensor

Among the optical sensors, the fluorescent systems offer many advantages: fluorescence measurements are usually very sensitive, low cost, easily performed, and versatile, offering subnanometer spatial resolution with submicron visualization and submillisecond temporal resolution.
Fluorescent sensors can be classified in two classes: *intrinsic* chemosensor in which the fluorophore functions as both binding and signalling unit or *conjucted* chemosensors in which binding and signalling moieties are separated by a spacer.
Fluorescence of a fluorophore unit can be switched between "ON-OFF" and "OFF-ON" states by interaction of the substrate with the receptor unit, hence a chelation enhancement of fluorescence (CHEF) or a chelation enhancement of quenching of fluorescence (CHEQ) can occur upon the host-guest recognition.
Different photoinduced mechanisms are responsible for the CHEF and CHEQ effects such as photoinduced electron transfer (PET), electron energy transfer (EET), excited state proton transfer (ESPT), Fluorescence Resonance Energy Transfer (FRET) and monomer-excimer formation.

Photoinduced Electron Transfer (PET)
Weller explained the photoinduced electron transfer in the 1960s.[47] Generally, fluorescence is observed when an excited electron passes from the excited state to the ground state by releasing the excess of energy radioactively. Fluorescent sensor may work with PET mechanism when the fluorophore and the receptor are connected by a spacer that keeps the two units together but separated. This photoinduced process depends on the relative energies of the molecular orbital of the fluorophore and the receptor. The HOMO of the receptor ($HOMO_R$) must be energetically between the HOMO and the LUMO of the fluorophore ($HOMO_F$ and $LUMO_F$). As a result of excitation, a series of photoinduced electron transfer occur: the first take place from $HOMO_{R\ of}$ the receptor to the $SOMO\text{-}1_{F*}$ of the excited fluorophore followed by an electron transfer from the $SOMO_{F*}$ of the fluorophore to the so formed $SOMO_R$ of the receptor. The transition from the excited to the ground state of the fluorophore occurs *via* a non-radiative relaxation thus the system is in an OFF state. While if the energy of the $HOMO_R$ of the receptor, or receptor-substrate, is lower than that of the $HOMO_F$ and $LUMO_F$ of the fluorophore, PET

can not take place and the de-excitation occurs radiatively, therefore the system is in an ON state.

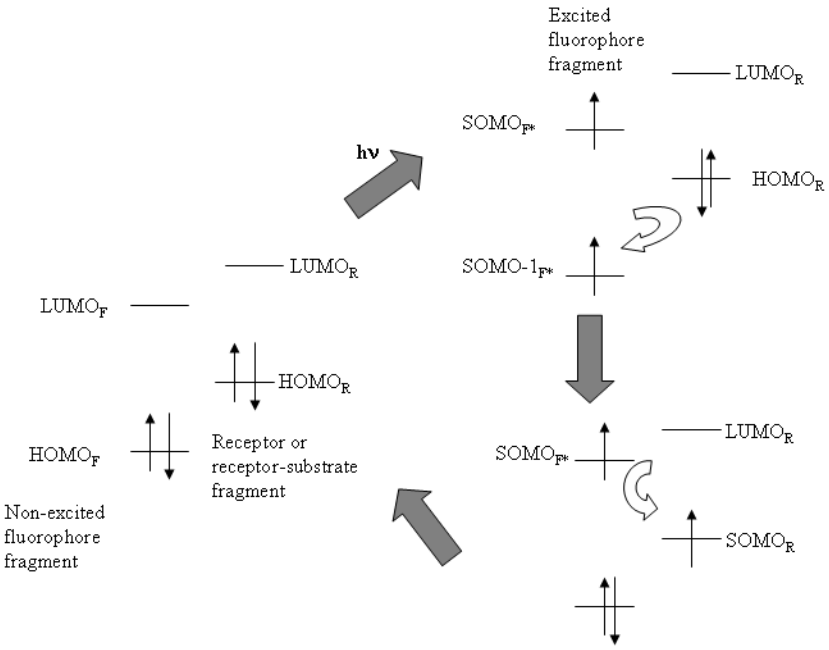

Figure 1.16. Simplified PET process with the participation of the $HOMO_F$ and $LUMO_F$ of the non-excited fluorophore fragment and the $HOMO_R$ of the receptor or receptor-substrate moiety.

A similar process can happen when the $LUMO_R$ of the receptor has an energy between the $HOMO_F$ and the $LUMO_F$. A photoinduced electron transfer from $SOMO_{F*}$ of the excited fluorophore to the $LUMO_R$ of the receptor can take place followed by a further PET from the so formed $SOMO_R$ to the $SOMO\text{-}1_{F*}$ of the fluorophore. Also in this case de-excitation is a non radiative process and the system is in an OFF state.

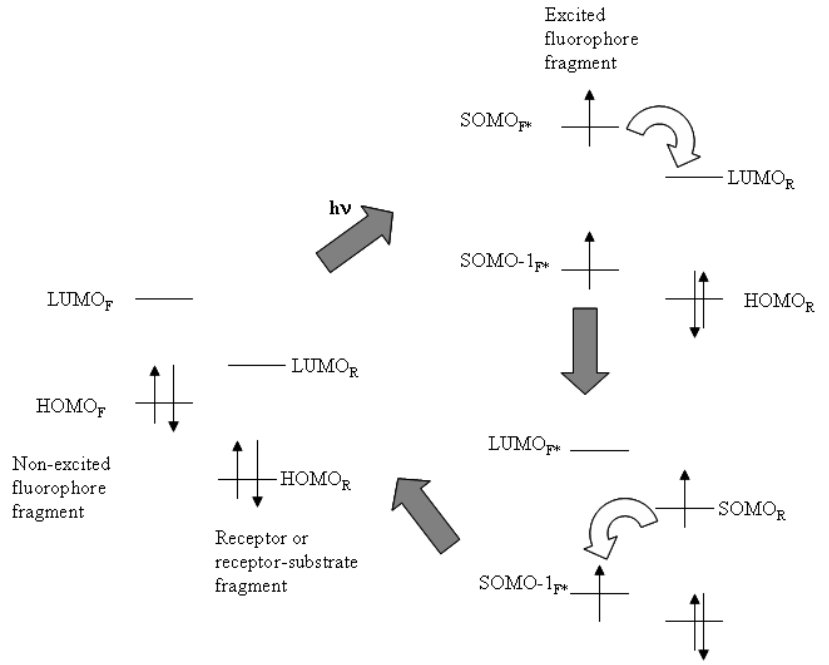

Figure 1.17. Simplified PET process with the participation of the $HOMO_F$ and $LUMO_F$ of the non-excited fluorophore fragment and the $LUMO_R$ of the receptor or receptor-substrate moiety.

The first example of PET sensor for the anion recognition was developed by Czarnick and co-workers. The receptor **52** behaves as OFF-ON fluorescent sensor for phosphate at pH 6 in H_2O. When the anthracene groups is in its excited state a photoinduced electron transfer can take place from the unprotonated amine resulting in a quenching of anthracene fluorescence, thus the receptor is in a OFF state. However, when the complex with hydrogen phosphate occurs the amine can be protonated by the anion, therefore the lone pair of electron of the amine is not available to induce the PET mechanism and the anthracene fluorescence switches ON.

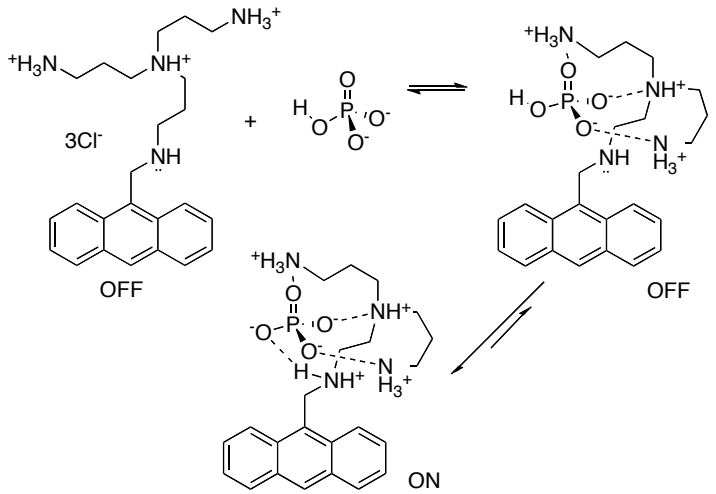

Figure 1.18 OFF-ON behaviour of tricationic **52** upon interaction with hydrogen phosphate

Gunnlaugsson and co-workers have reported a series of thioureas based 4-amino-1,8-naphthalimide moiety developed as photoinduced electron transfer (PET) fluorescent anion sensors.[48] These molecules were designed on the fluorophore–spacer–receptor model where the receptors, the thiourea moieties, were connected to the fluorophore (the naphthalimide ring) *via* the 4-amino group for **53**-**55**, and *via* the imide site for **56** and **57**. The fluorescence of the compounds could be quenched upon addition of anionic guests such as AcO^-, $H_2PO_4^-$ and F^- in DMSO solution whilst no changes were observed in their absorption spectra, demonstrating the receptors function as PET sensors. In these naphtalimide based receptors the PET sensing can occur bi-directionally.

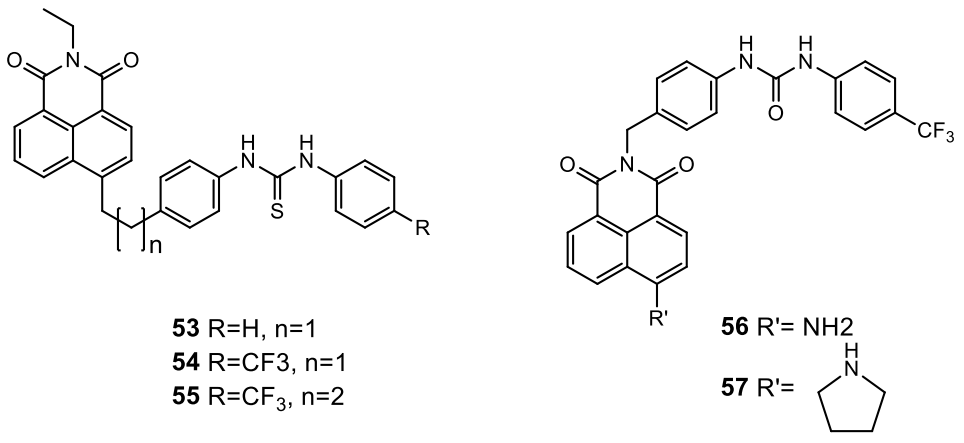

53 R=H, n=1
54 R=CF3, n=1
55 R=CF_3, n=2

56 R'= NH2
57 R'=

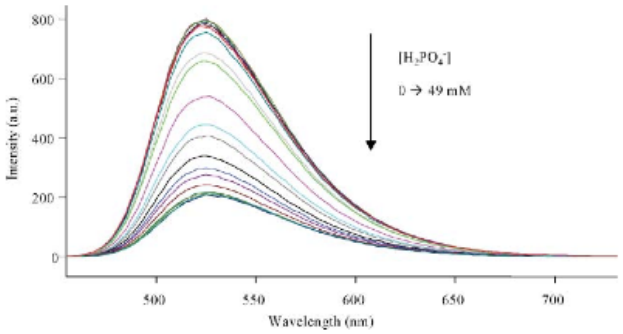

Figure 1.19. Quenching of fluorescence of 60 upon addition of H2PO4-

Electron Energy Transfer (EET)

The electron energy transfer (EET) causes a CHEQ effects. This mechanism is possible when both $LUMO_R$ and $HOMO_R$ of the receptor are energetically between the $HOMO_F$ and the $LUMO_F$ of the fluorophore. After the excitation, a simultaneous exchange of two electrons from the $SOMO_{F*}$ and from the $HOMO_R$ to the $LUMO_R$ and the $SOMO\text{-}1_{F*}$ respectively followed by electron transfer from $SOMO_{R*}$ to $SOMO\text{-}1_{R*}$ of the receptor can take place. This decay occurs in a non-radiative way so the process resulting in a fluorescence quenching and the system is in an OFF state. (*Figure 1.20*)

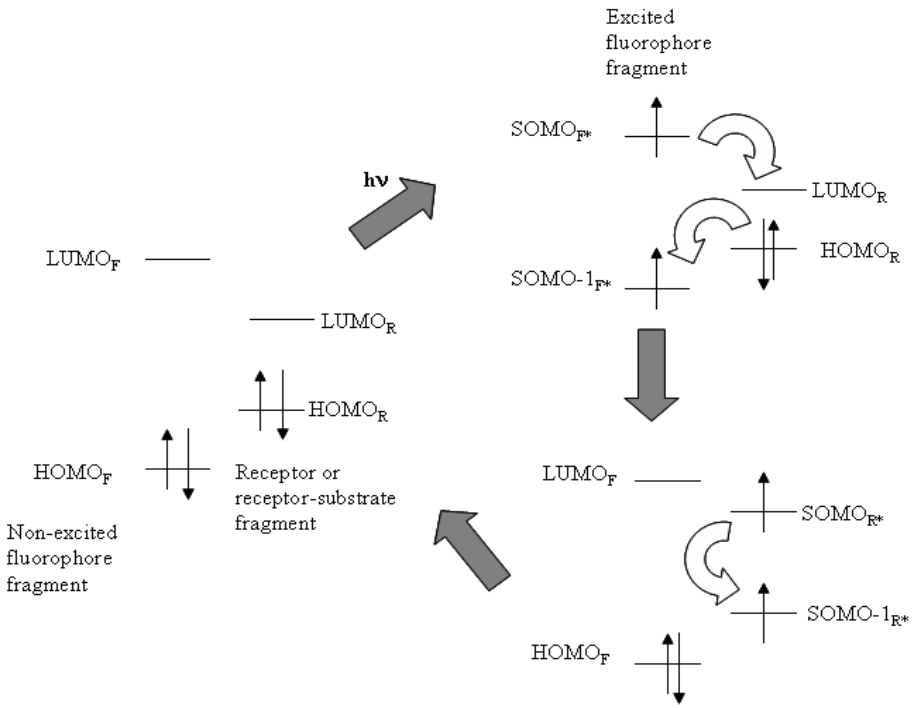

Figure 1.20. Simplified EET process with the participation of the $HOMO_F$ and $LUMO_F$ of the non-excited fluorophore and both $LUMO_R$ and $HOMO_R$ of the receptor or receptor-substrate moiety

Excited State Proton Transfer (ESPT)

According to this further signalling mechanism ESPT, the unit receptor-anion close to the fluorophore group can stabilize the positive charge of the latter in the excited state (which has an emission energy hv_1) and may promote an intermolecular proton transfer to the anion, accompanied by a new fluorescent emission hv_2.

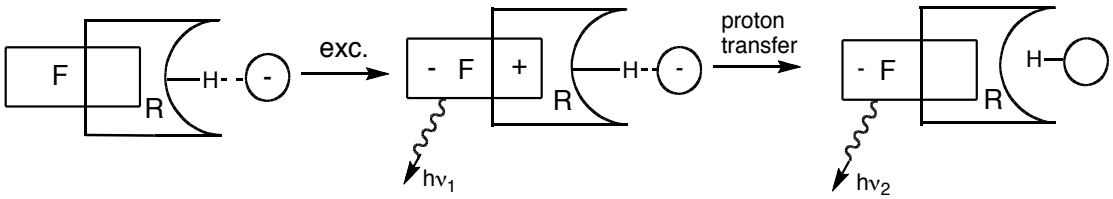

Figure 1.21. Mechanism of Excited State Proton Transfer.

Choi and Hamilton have reported the macrocycle **58** containing an aminocoumarin fluorophore as a sensor for dihydrogen phosphate based on the ESPT principle.[49] The receptor showed the formation of a new fluorescent band at longer λ value (around 550 nm) by addition of dihydrogen phosphate. Whilst this no occurs with compound **59** (used as a model) that does not present the cumarin moiety. The addition of the most basic $H_2PO_4^-$ anion is linked to the highest intensity change of the maximum of the second band while in the presence of $PhPO_3H^-$ it is modest, and absent with the less basic *p*-TsO^-. This correlation of the second emission band with bound anion basicity suggested that proton transfer from the fluorophore excited state was occurring.

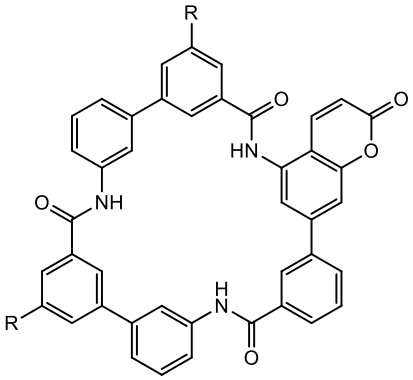

58 R = NHBoc

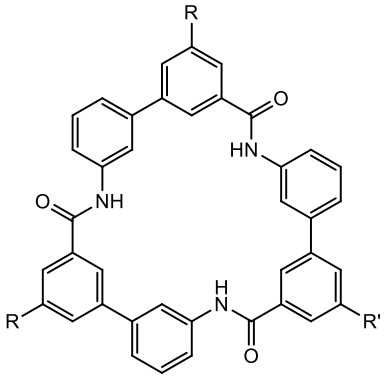

59 R = NHBoc

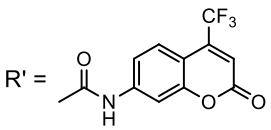

Fluorescence Resonance Energy Transfer (FRET)

Another sensing mechanism that has been widely adopted in for analyte detection is binding-induced modulation of fluorescence resonance energy transfer (FRET). FRET is basically a non radiative transfer of excitation energy between a donor and an acceptor

unit and it can occur if the emission spectrum of the donor overlaps the absorption spectrum of the acceptor, so that several vibronic transitions have the same energy as the corresponding transitions of the acceptor.[50,51]

Anzenbacher and his research group developed receptor **60** based on central 2,3-di(1H-2-pyrroyl) quinoxaline (DPQ) molecule substituted by two ethylenpyrene groups.[52] The amplification of the signal of the sensor **60** is determined by RET from the pyrene (donor) moieties to the DPQ (acceptor) moiety as confirmed by time-resolved fluorescence spectroscopy and a quantum yield measurement. The fluorescence of pyrene (29.0 ns in air-saturated CH_2Cl_2) is quenched, while the lifetime of the DPQ acceptor is extended to 2.2 ns. As shown in *Figure 1.22* only the addition of fluoride and pyrophosphate in dichloromethane causes the fluorescence emission quenching of **60** over other anions studied.

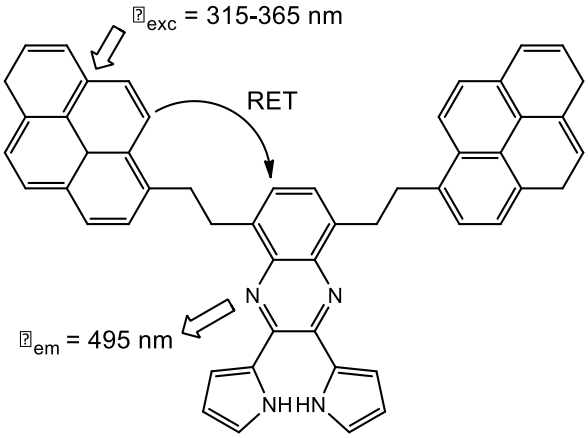

60

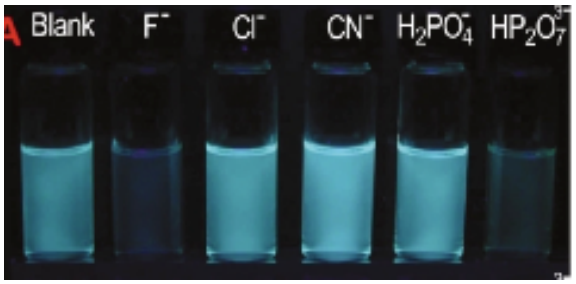

Figure 1.22 Anion-induced changes in fluorescence intensity of 10 mM in DCM solutions of sensor **60.** The anions (*ca.* 100 mmol) were added in the form of their tetrabutylammonium salts.

Monomer-excimer formation

The formation of excimer is possible in fluorescent sensors that contain more then one fluorogenic unit characterised by a high π delocalisation such as pyrene or anthracene groups. An excimer is a complex formed by interaction of a fluorophore in the excited state with a fluorophore of the same structure in the ground state. If they are connected by a flexible receptor the complexation with the anion may cause changes in the structural conformation of the system and bring the fluorophores in close proximity. This

may cause the formation of the excimer and the excimer emission, in addition to monomer emission, can be observed. Normally the excimer band is red-shifted with the respect to that of monomer.

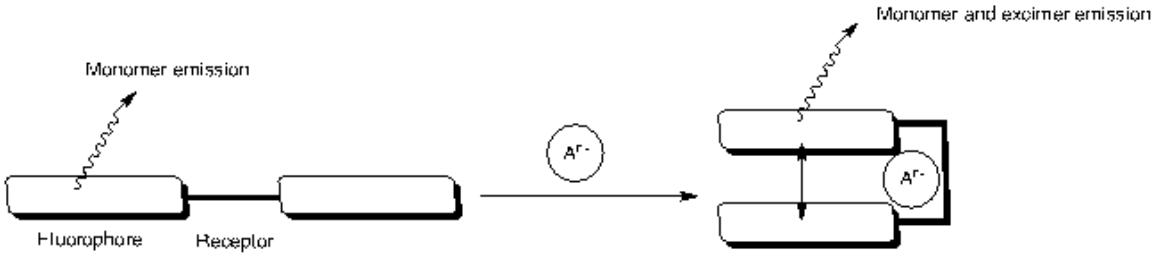

Figure 1.23. Chemosensors composed of a flexible coordinating subunit and two "flat" fluorophores. Coordination with a substrate induces spatial proximity between the fluorophore moieties and dual emission from the monomer and the excimer.

Teramae *et al.* have synthetized a pyrene-functionalized mono-guanidinium sensor **61** that was found to form a 2:1 (receptor:anion) pyrophosphate complex with high selectivity in methanol.[53] The receptor showed a structured emission band at 370-450 nm, which was assigned to a pyrene monomer emission. Upon addition of Ppi, a structureless band with an emission maximum at 476 nm appeared, while the monomer emission was quenched. The new broad band observed at 476 nm can be assigned to the formation of an intramolecular excimer in the 2:1 complex of **61** with Ppi, where Ppi functions as a spacer linking two host molecules.

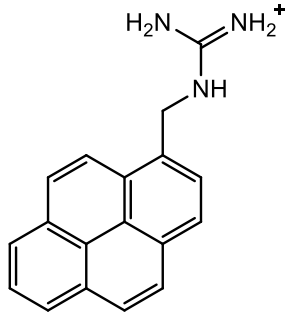

61

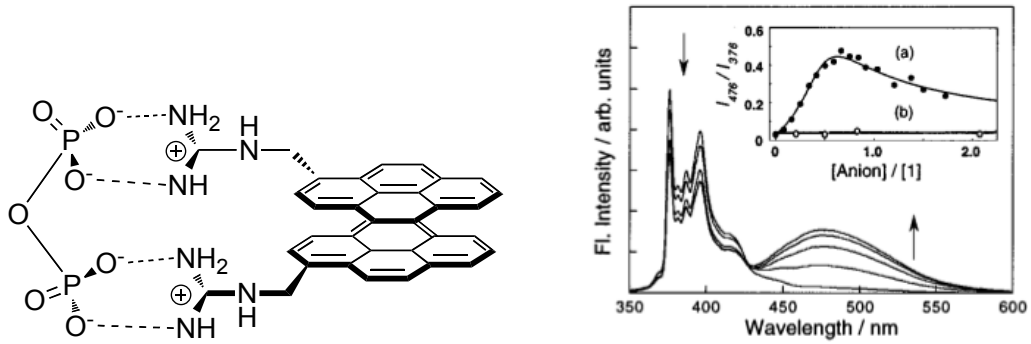

Figure 1.24.Formation of complex $[(P_2O_7)(\mathbf{61})_2]^{2-}$ and fluorescence spectra of 68 upon addition of pyrophosphate in methanol.

1.4.1.2 Colorimetric sensors

The colorimetric sensors respond to occurred complexation of the substrate with a change in their absorption properties that can be qualitatively detected even to the naked eye. The anion recognition by a colorimetric sensor causes the variation in relative energy between the HOMO and the LUMO orbitals that is manifested by a change of colour of the cromophore. The colour changes of the solution of the receptor caused by the addition of the anions may be due to the formation of a complex or the deprotonation of the receptor by an anion sufficiently basic.

Tucker and his group have reported a ferrocene-based ditopic chromoionophore **62** containing a urea and a benzocrown ether moieties as binding site for anions and cations, respectively.[54] The binding properties were evaluated by UV-Vis spectroscopy in acetonitrile. Upon addition of 10 equivalents of F^- the absorption band of the nitrobenzene moiety at 304 and 332 nm became two clearly separated bands at 288 and 356 nm and, at the same time, a new absorbance appears at 472 nm corresponding to a change of colour from colourless to yellow (*Fig. 1.25a* green). The binding constant was found to be K_a = 9340 M^{-1} for a 1:1 complex between **62** and fluoride. Whilst, the further addition of K^+ reversed the chromogenic process, upon addition of 10 equivalents of K^+ the band at 472 nm disappeared and the colour of the solution turned to colourless (*Fig. 1.25a* blue). The binding constant for the complex with K^+ in the presence of 10 equivalents of F^- was K_a = 1460 M^{-1}. The experiment was repeated by reversing the order of the guest addition to a solution of **62**. The addition of K^+ induced a small change in absorption intensity and the solution remained colourless. By addition of F^- no colour change was observed thus, the presence of K^+ inhibits the chromogenic response of the system to F^- anions. The NMR studies in CD_3CN showed that K^+, bound by the benzocrown unit, also interact with the urea moiety of the receptor making the hydrogen bonding interactions between **62** and F^- weaker and therefore causing the colour quenching process.

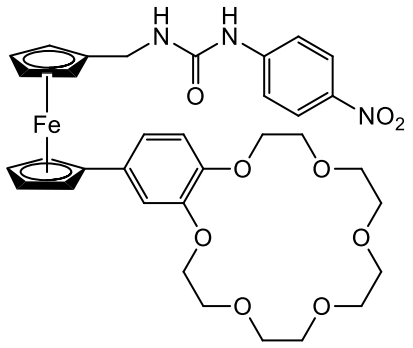

62

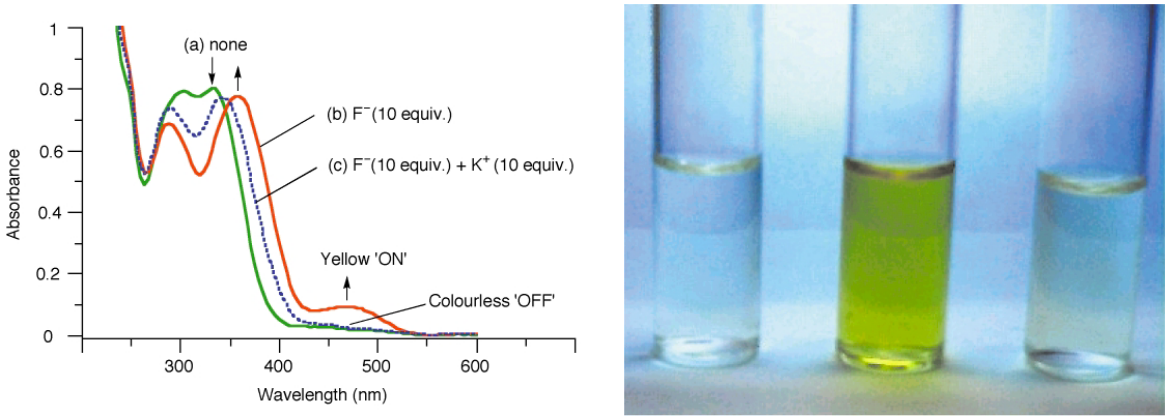

a) b)

Figure 1.25 a) UV-vis spectrum of **62** in CH_3CN (5 x 10^{-5} M) (a) in its free form (b) in the presence of 10 mol. equiv. of F^- (c) in the presence of 10 mol. equiv. of F^- and 10 mol equiv. of K^+. ***b)*** Photograph showing the colour changes of **62** in CH_3CN (2.5 x 10^{-4}M). Left to right: In the absence of ions, in the presence of 10 mol. equiv. of F^-, in the presence of 10 mol. equiv. of F^- and 10 mol. equiv. of K^+.

Xie and co-workers have designed two oligopyrrole–hemiquinone compounds **63** and **64** as colorimetric sensors for fluoride via deprotonation of the receptor.[55] The UV/Vis measurements were conducted in DMSO and showed that the addition of fluoride to **63** caused the decrease of the band at 496 nm and a new band at 568 nm appeared (*Fig. 1.26a*), inducing a colour change from dark orange to blue (*Fig. 1.26b*) due to internal charge transfer (ICT) originated from the deprotonation of the NH moiety, and the formation of HF_2^-. While, the initial addition of < 40 eq. of different anions to **64** resulted in a decrease of the bands at 459 and 571 nm and an increase of a new band at 740 nm, resulting in a colour change from wine-red to grey due to a deprotonation of the sensor. Upon further addition (>40 eq.) of anions only F- induced the decrease of the band at 740 nm and the development of a new band at 624 nm. A further colour change of the solution from grey to green occurred (*Fig. 1.27c*), which can be ascribed to the second deprotonation process. The double deprotonation of **64** is made possible by the presence of the additional hemiquinone electron-withdrawing group that increases the acidity of the NH groups.

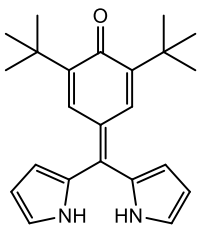

63

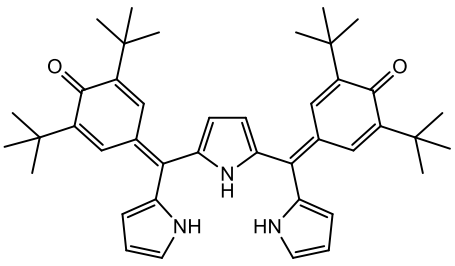

64

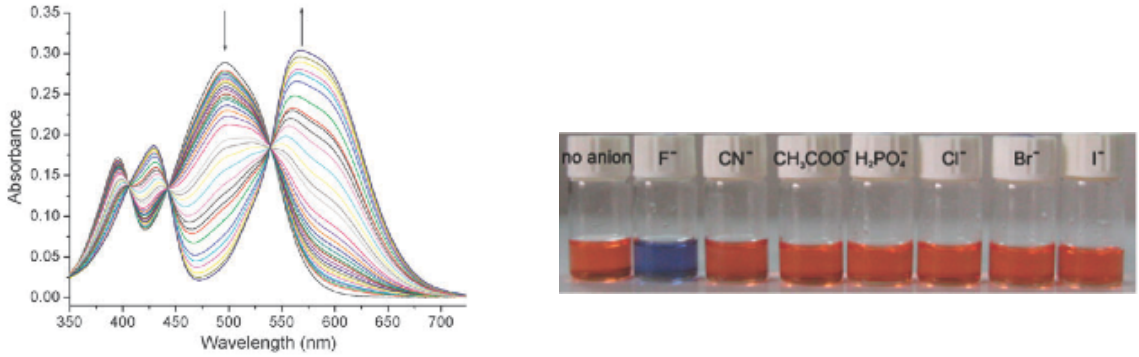

a) **b)**

Figure 1.26. a) UV-vis spectral changes of **63** (10 mM in DMSO) observed upon the addition of 0–180 eq. F- (TBA salt) in DMSO. ***b)*** A photograph showing the colour change of **63** (25 mM) in DMSO upon addition of 40 eq. of various anions.

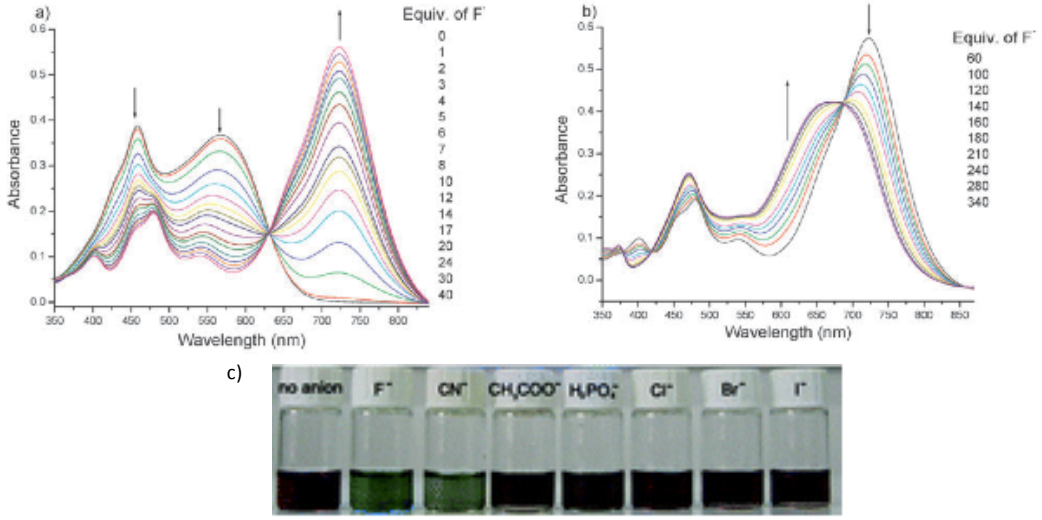

Figure 1.27. ***a)*** UV-vis spectral changes of **64** (10 mM in DMSO) observed upon addition of <40 eq of F^- (TBA salt) and ***b)*** >40 eq. of F^- in DMSO. ***c)*** A photograph showing the colour change of **64** (25 mM) in DMSO upon addition of >40 eq. of various anions.

1.5 Anion transporters

The anion recognition chemistry, as stated above, has undergone rapid growth over the last 20 years.[56] An important and relatively new application of this field is the development of compounds that can bind and transport anions across lipid bilayer membranes.[57,58,59,60]

The anion transport is crucial in many cellular processes such as regulation of pH value, maintenance of osmotic balance, production of electrical signals, transport of nutrients into cells and regulation of secretions across epithelial layers. In biological systems the transport of ions is facilitated by molecules that act either as carriers or channels. (*Figure 1.27*)

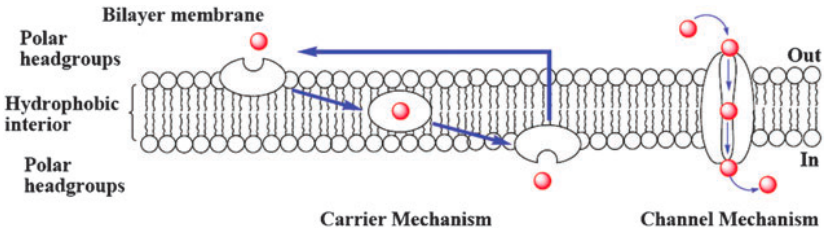

Figure 1.27. The mechanism of transmembrane ion transport involves ion carriers or ion channels.

Carriers are mobile and can diffuse across the hydrophobic membrane to transport the anions from one side of the membrane to the other side, whereas ion channels are usually proteins fixed within the bilayer and typically span the membrane providing a hydrophilic pathway for ions.

The transport mechanisms are uniport or co-transport, which can be divided in symport or antiport (*Figure 1.28*). Uniport process occurs when a single type of ion is transported at time. Co-transport involves the transport of two species in the same direction (symport) or in opposite directions (antiport).

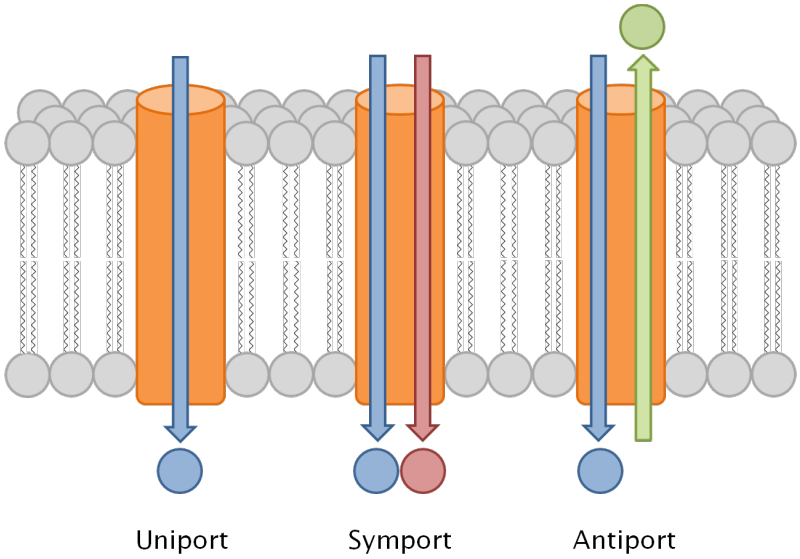

Figure 1.28 transmembrane transport by uniport, symport and antiport processes

The misregulation of anion transport proteins is linked to a variety of diseases known as channelopathies [7] such as Beast disease (form of macular degeneration leading to vision loss), myotonia (muscle stiffness), nephrolithiasis (kidney stones), Bartter's syndrome (renal salt loss), osteopetrosis (bone disease) and most notably cystic fibrosis (CF).

Cystic fibrosis is a genetic disorder caused by a mutation in the gene for CFTR (cystic fibrosis transmembrane conductance regulator) which is a transmembrane protein found in the apical membrane of epithelial cells of the airways, pancreas, intestine, sweat gland, salivary gland and the vas deferens. The CFTR mediates the excretion of Cl^- from the cell in a process coupled to the action of Cl^-/ HCO_3^- anion exchange protein, causing HCO_3^- efflux (*Figure 1.29*).

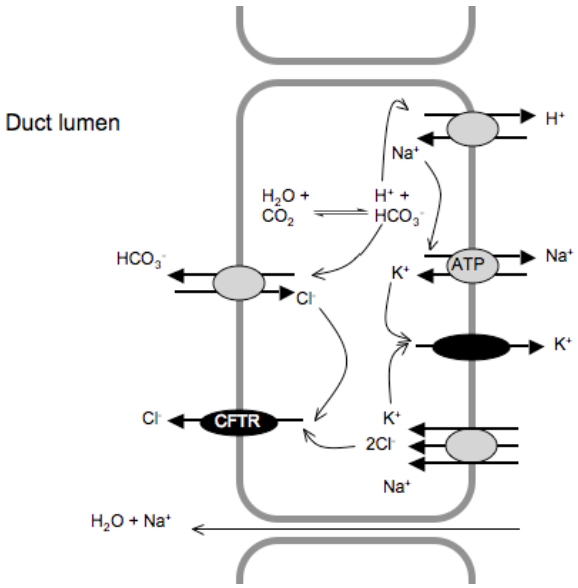

Figure 1.29. A representation of the ion transport processes in the epithelial cells of the pancreatic duct.

The malfunction of this protein causes an alteration of the secretion of chloride ions and a consequent greater reabsorption of sodium and water and an accumulation of HCO_3^- in the cell membrane of the glands of external secretion. Consequently, these glands secrete a thick, sticky mucus that clogs the main ducts, causing the clinical manifestations of the disease, such as appearance of recurrent pulmonary infections, pancreatic insufficiency, steatorrhea, states of malnutrition, cirrhosis of the liver, intestinal obstruction and male infertility. Quinton has hypothesized that the abnormal production of viscous mucus, in addition to the secretion of less water, is associated with reduced transport of HCO_3^-.[61] Cystic fibrosis is the most common fatal inherited disease in the Caucasian population, currently there is no cure for CF and the average life expectancy of the patients is around 30 years.

It is no surprising, therefore, the recent interest in developing synthetic transporters for Cl^- and HCO_3^- that can may have a pharmaceutical applications in the treatment of these type of disease.

1.5.1 Natural anion transporters

The design of synthetic anion transporters can take inspiration from natural products able to mediate anion transport in biological system. There are only a few examples of naturally occurring anion transporters, the most studied are the family of prodigiosins, red pigments produced by microorganisms such as *Streptomyces* and *Serratia*.[62] Prodigiosin **65**, tripyrrolic alkaloid belonging to a family of prodiginines, is able to bind H^+/Cl^- by a combination of electrostatic interactions and hydrogen bonding, Parr *et al.* have reported its crystal structure of hydrochloride salt that shows the chloride coordinated by three hydrogen- bond from the protonated tripyrrolic scaffold.[63] Prodigiosin **65** has also been found to mediate Cl^-/ HCO_3^- antiport (*Figure 1.30*).[64,65]

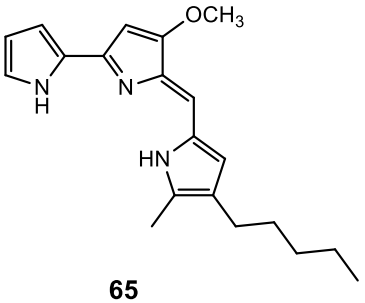

65

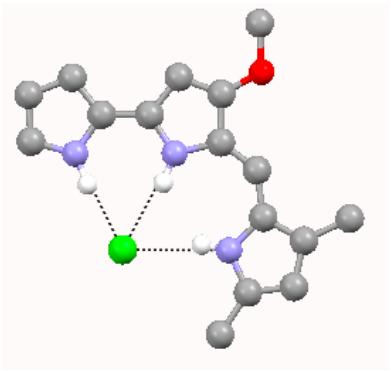

Figure 1.30. The crystal structure of the HCl salt of compound **71**

The Prodigiosin have also a range of potentially pharmacological properties, including immunosuppression, anticancer and antibiotic effects. Various mechanisms responsible for these activities have been proposed. Among them there is evidence that the anticancer activity is linked to anion transport. The HCl co-transport decreases the pH value inside the cancer cells triggering apoptosis.[66]

Sessler and co-worker have explored the Cl^- transporter ability and the anticancer activity of a series of synthetic prodigiosin analogues such as tripyrrolic and dipyrrolic system **66-70**.[67]

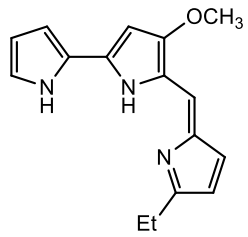

66

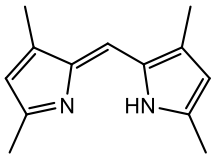

67

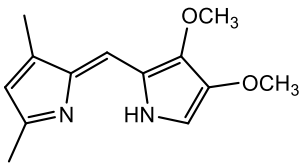

68

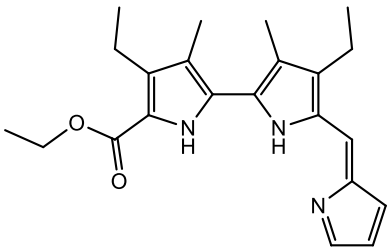

69

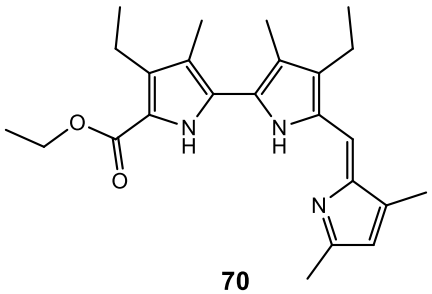

70

The chloride transport properties of these compounds through vesicle assays were investigated. The mechanism of transport was H^+/Cl^- symport and the order of activity was **66**>>**69**≈**67**>**68**>>**70**. The compound **66**, the most prodigiosin-like, was found to be the most effective carrier among the analogues. The anticancer properties of the compounds were studied in human lung and prostate cancer cell lines and it was found that the antitumor activity follows the same order observed for the anion transport. Generally, the most potent anion transporter has the highest anticancer activity. This suggests that the anion transport is directly linked to anticancer effect; hence the anion transporters may have a potential future application in the therapies of both cystic fibrosis and cancer.

The tambjamine alkaloids are other family of natural products structurally related to prodigiosin with anticancer and antimicrobial properties that was investigated by Quesada and co-workers.[68] They studied four naturally occurring tamjamines **71**-**74** and two synthetic analogues **75** and **76**.

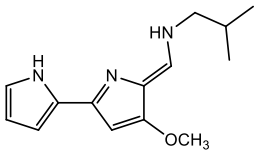

71

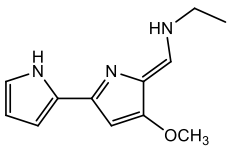

72

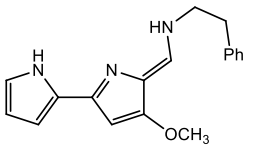

73

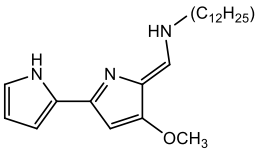

74

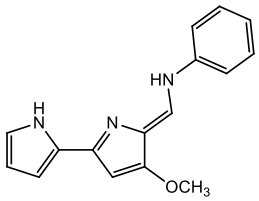

75

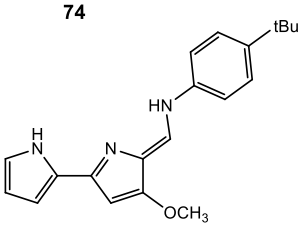

76

The vesicle test assays shown that these compounds were a potent anion transporter *via* a Cl^-/HCO_3^- antiport mechanism. The synthetic tambjamine **76** shown the highest transport activity promoting >90% chloride efflux with a carrier loading of 0.2 mol% with respect to lipid, while the compound **72** is the worst transporter of the series, presumably because its low lipophilicity. These compounds are a poor HCl cotransporter probably due to their relative high basicity, i.e. at physiological pH they do not deprotonate.
The anticancer activity was explored using GLC4 cells and it was found that the tambjamine derivatives can deacidify the acidic organelles in these cells except the compound **72** that is inactive.

Recently, Davis and co-workers have reported the chloride transport activity of the sphingolipid C2-ceramide, another example of naturally occurring transmembrane anion transporters that can function both as anion carriers and anion channels.[69] The ceramide is known to form spanning pore in the membrane for anion transport at high concentrations (above 10 mol% to lipid), thereby the release of pro apoptotic proteins from mitochondria is triggered.[70] Davis and co-workers demonstrated that compound **77** is still able to give a Cl^-/HCO_3^- and a Cl^-/NO_3^- antiport even at low concentrations (1 mol% to lipid). This suggests that at lower concentrations the compound functions *via* a mobile carrier mechanism. The ^{1}H-NMR titration with TBACl in CD_2Cl_2 shown that the two OH groups and NH group were involved in hydrogen-bond interactions with Cl^-.

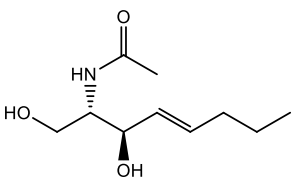

77

Davis *et al.* have also reported the Cl^-/NO_3^- antiport activity of the natural product monoacylglycerols **78** and **79** that are able to bind the anions by $OH^{-\cdots}A^-$ hydrogen bond interactions. In the synthetic analogues **80** and **81** is introduced a further hydrogen bonds donor group and, in the case of **81**, also a perfluorinated chain which allows a higher anion transport activity than the natural compound **78**.[71]

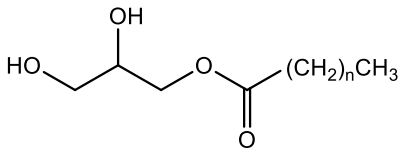

78 n = 6
79 n = 16

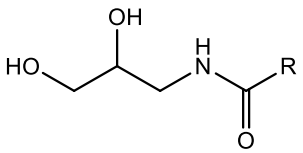

80 R = $(CH_2)_6CH_3$
81 R = $(CF_2)_6CF_3$

1.5.2 Synthetic anion transporters

In order to design synthetic anion transporters, both mobile carriers and anion channels, the most intuitive method is mimic the naturally occurring compounds such as the prodigiosins or the chloride channels proteins (ClC) family. An other approach is to draw inspiration from the anion receptor chemistry, thus using the common strategies for complexing anions such as hydrogen bond and electrostatic interactions. Therefore the transporter compounds must have sufficient water solubility for delivery but also must be sufficiently lipophilic for insertion within the lipid bilayer and the synthetic anion channel must also be large enough to span the membrane. It could also be useful to follow a rule of thumb, such as "Lipinski's rules of five" to improve the ADME properties (Absorption, Distribution, Metabolism, and Excretion). These include having a molecular weight of less than 500, not more than five hydrogen-bond donors, not more than ten hydrogen-bond acceptors and a log*P* (octanol-water partition coefficient) of not greater than five.

Anion carriers

In 2011 Quesada and co-workers investigated the anion transport ability of obatoclax **83**, a synthetic prodiginine containing an indole group that is currently in clinical trials as an anticancer drug. [72,73] The analogues **84**-**88** have been also synthesized and studied. The anion transport experiments shown that the compound **83**-**87** are able to transport chloride and bicarbonate by an antiport mechanism according to the order of activity **84**>**83**>**85**>**86**>>**87**. Therefore the compound **84** has proved to be the most potent anion carrier of the series, while the BODIPY analogue **88** was found to be inactive. The cytotoxicity was investigated on the small cell lung cancer cell line GLC4 and has been found that the anticancer activity reflects the anion transporter ability. This is further evidence that the anticancer activity is correlated to the ability of these compounds to

decrease the pH value by anion transport process within the tumour cell triggering apoptosis.

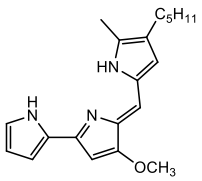

82 Prodigiosin

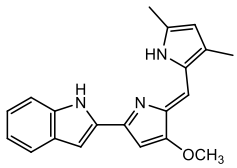

83 Obatoclax

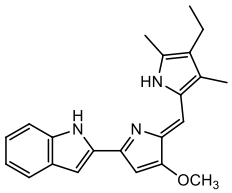

84

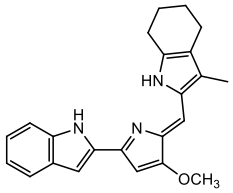

85

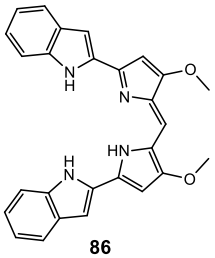

86

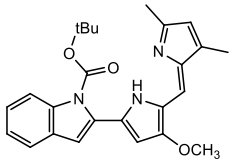

87

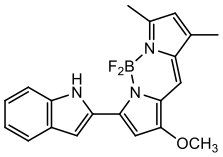

88

Some of the earliest and most effective anion transporters are the series of cholapods reported by A. P. Davis *et al*. These systems are based on a cholic acid scaffold containing pendant urea and thiourea for anion complexation combined with a lipophilic steroid skeleton. The anion binding studies of cholapods **88**-**93** shown that these compound form a complex with chloride with a high affinity constant. Moreover the anion transport experiments were performed. These molecules promote a Cl^-/NO_3^- anion exchange and among them the most effective transporter was the cholapod **89** that showed the strongest binding of Cl^- and NO_3^-.[74]

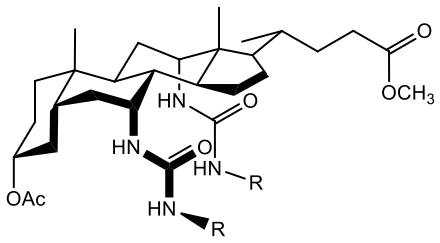

89 R = p-nitrophenyl
90 R = 4-methoxyphenyl
91 R = 3-methoxyphenyl
92 R = 4-methylphenyl
93 R = Ph

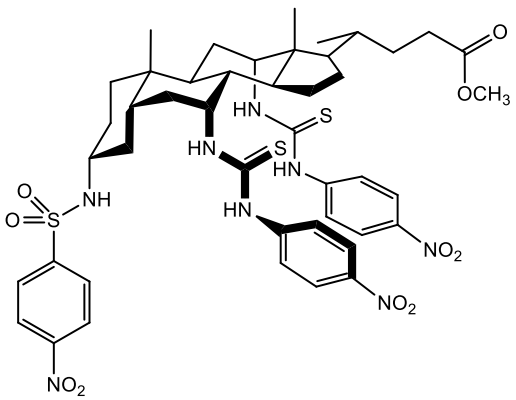

94

More recently the same authors demonstrate how the anion transport properties could be increased varying the substituents on the cholapods skeleton by structure-activity relationship study.[75] They found that thioureas have a better ability to bind anions than the ureas, due to the higher acidity of the NH, and consequently a better anion transport activity. The compound **94** shows a chloride affinity 200 times greater than **90** and also shows a Cl^-/NO_3^- antiport more efficient. Furthermore it is possible to increase the activity

placing electron-withdrawing groups in the aromatic urea substituents and manipulating the group at steroidal C3.

Davis and co-workers have also developed the cholaphanes by cyclization of the cholapod scaffold such as **95**.[76] These compounds possess a better ability to transport anions than their acyclic analogues due to a more enclosed binding site for facilitate the transport of the anion through the apolar lipid bilayer.

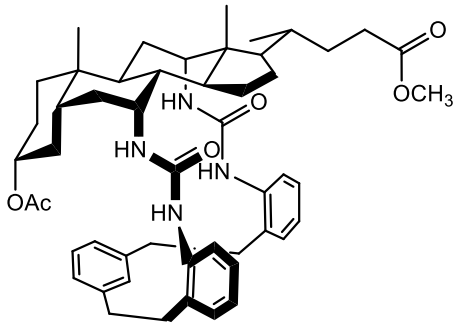

95

Gale and co-workers have investigated the transport ability of a series of tren-based ureas and thioureas **96**-**99**.[77] The ureidic compounds have been shown to be inactive (**96**) or to have only a moderate Cl^-/NO_3^- antiport activity (**97**), whereas the thioureas compounds were a very efficient Cl^-/NO_3^- and Cl^-/HCO_3^- antiporters. Therefore the thioureas possess greater activity as membrane transporters in comparison to analogous ureas and generally are capable of binding anions more strongly. In this case, however, the ureidic receptors possess affinity constants for chloride higher than those shown by thioureas compounds. Hence the best ability to transport anions of the thioureas molecules is more probably due to their greater lipophilicity rather than the anion binding properties.

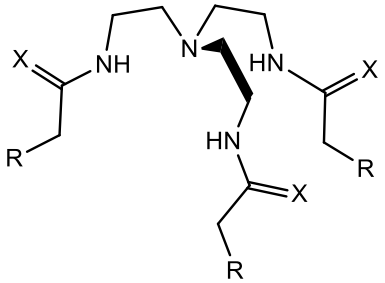

96 R = Bu, X = O
97 R = Ph, X = O
98 R = Bu, X = S
99 R = Ph, X = S

The same group have more recently developed a series of simple molecules containing single thioureas and ureas groups (**100**-**105**).[78] Their anion transporter activity have been studied and it was found that, while the ureas compounds were inactive, the thiourea

compounds were capable of Cl^-/HCO_3^- antiport with compound **105**, which contains an indole group, was the most efficient among this series.

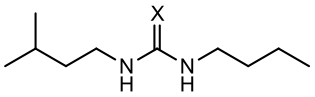

100 X = O
101 X = S

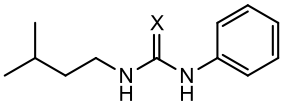

102 X = O
103 X = S

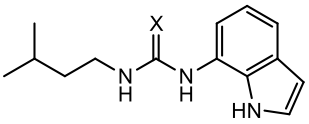

104 X = O
105 X = S

Accordingly to these results, Gale and co-workers decided to study the ability to facilitate anion transporters of a series of similar compounds containing indole group and, in some case, a trifluoromethyl group in order to enhance the lipophilicity of the transporters.[79]

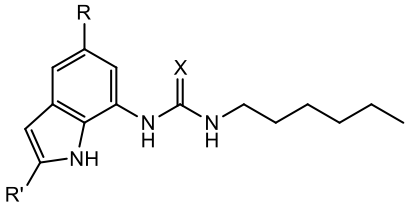

106 X = O, R = H, R' = H
107 X = S, R = H, R' = H
108 X = O, R = CF_3, R' = *n*Bu
109 X = S, R = CF_3, R' = *n*Bu

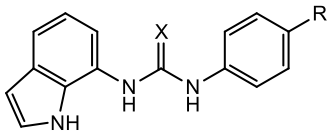

110 X = O, R = H
111 X = S, R = H
112 X = O, R = CF_3
113 X = S, R = CF_3

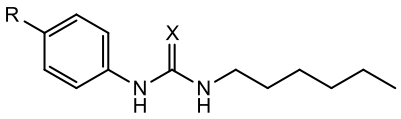

114 X = O, R = H
115 X = S, R = H
116 X = O, R = CF_3
117 X = S, R = CF_3

They found that the trifluoromethyl functionalised compounds were better anion transporters than the unfluorinated analogues, corresponding to an increase of lipophilicity, and ones again thioureas shown a greater transport activity than ureas. The compound 4 proved to be the most effective transporter of the series.
Furthermore, the in vitro cytotoxic assays of compounds **106**-**117** on several cancer cell lines indicated that compounds **108**, **109**, **112**, **116** and **117** had significant cytotoxicity and were able to trigger apoptosis especially in GLC4 and A375 cells.

Anion channels

Also in this case, the easier approach to design efficient anion channels is based on natural product, thus mimicking naturally occurring chloride transport proteins.

The first examples of anion channel was reported by Tomich and colleagues who synthesised a short peptides M2GlyR based on natural anion channels, the brain glycine receptor (GlyR).[80] The anion transport properties of the segment of this protein were tested and the channel activity was ascribed to tetrameric and pentameric aggregates. The group have subsequently tested over 200 peptides based on variation of M2GlyR in order to increase the transport ability, the water solubility and decrease the aggregation.[81] The sequence C-K_4-M2GlyR prepared by the addition of lysine residues to the N- or C-terminus of the **119** is one of the most efficient (*Figure 1.31*). [82]

M2GlyR **118**	H_2N-PARVG LGITT VLTMT TQSSG SRA-COOH
C-K_4-M2GlyR **119**	H_2N-PARVG LGITT VLTMT TQSSG SRAKK KK-COOH

Figure 1.31. The structure of M2GlyR **118** and the synthetic analogue C-K_4-M2GlyR **119**.

Gokel et al. have also reported a synthetic peptides for chloride transport based on naturally occurring amino acid sequence found in the ClC proteins family. The prototype was the amphiphilic heptapeptide SCMTR that is able to cause a rapid efflux of chloride from vesicle systems by an antiport mechanism.[83] It also transport carboxyfluorescein, hence the channel is large enough to allows the passage of this fluorescent dye (diameter about 1nm). The SCMTR peptide forms a dimer that defines the ion-conducting pore (*Figure 1.32*).

SCMTR 120 (C18H37)2NCOCH2OCH2CO-GGPGGG-OCH2Ph

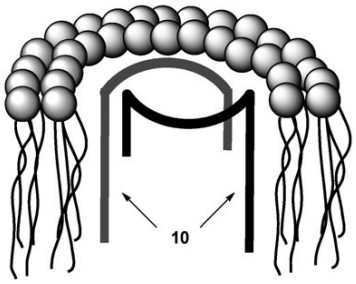

Figure 1.32.The structure of SCMTR **120**.

Matile and his group have proposed compounds that use anion-π interactions to facilitate the anion transport across the membrane such as oligo-(p-phenylene)-N,N-naphtalenediimide (O-NDI) **121** which forms a rigid π rod that span the lipid bilayer membrane.[84] The HPTS pH assays in EYPC vesicles revealed that these compound mediate anion selective transport with a rare halide selectivity sequence ($Cl^- > F^- > Br^- > I^-$) by OH^-/A^- exchange mechanism.

More recently the same group investigated the membrane transport activity of oligo(p-phenylene)-N,N-perylenediimide (O-PDI) rods **122**.[85] These species were found to

facilitate Cl^-/OH^- exchange, to mediate the antiport of anions and electrons and to have photosynthetic activity (see *Figure 1.33*).

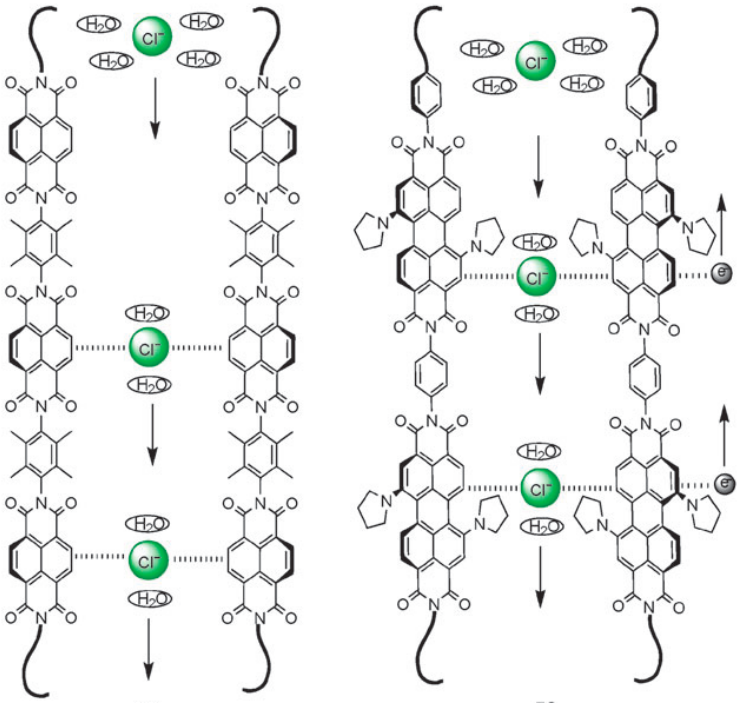

Figure 1.33. Representation of anion- π slides **121** and **122** developed by Matile and colleagues. Left oligo-naphthalenediimide rod; right oligo-perylenediimide rod showing the anion/electron antiport needed for photosynthetic activity.

The group of J.T.Davis reported the anion transport properties of a series of calix[4]arene amides locked in a partial cone or cone conformation.[86] Vesicle test using intravesicular lucigenin have shown that **123** and **124** were good Cl^-/NO_3^- antiporters. The compound **126** containing an ester group instead of an amide group was found to be much less active while the triamide compound **125** was more active compared to the tetramide compounds **126** and **124**, furthermore its anion transport ability could be modulated as function of the pH. Increasing the pH of the system, the Cl^- transport was significantly reduced as a consequence of the deprotonation of the phenolic OH group.

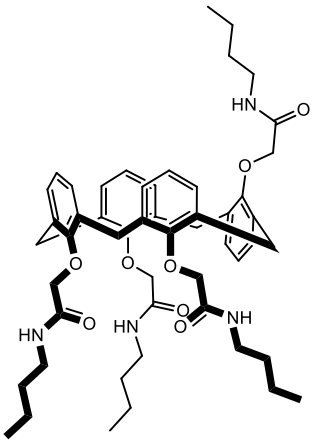

123

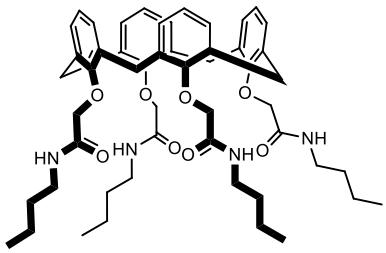

124

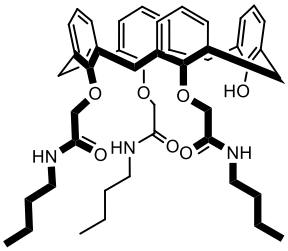

125

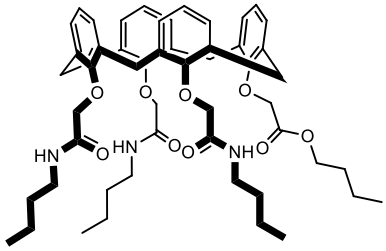

126

1.6 Aim of the thesis

The receptors that will be discussed in the next chapters are reported in *Figure 1.34*. The importance of supramolecular chemistry regarding anion recognition and anion transport across lipid membranes has been introduced in the previous pages. As shown in the previous paragraphs, there is a wide range of compounds developed in the last years that have been used for these purposes. From the examples reported above we have demonstrated that hydrogen bond donors have a great importance in synthesis of compounds that can be used to selectively bind anions and for the development of efficient mobile carriers. Many functional groups are able to form hydrogen bond with anionic substrates. Among them the urea moiety is the most largely employed due to its facile synthesis, its NH acidity and its strong tendency to bind oxo-anions, moreover it contain two NH hydrogen bond donor groups.

The work in this thesis focused on the design and synthesis of a new series of compounds containing urea groups that can function both as selective anion receptors and efficient anion transmembrane transporters. The anion binding properties have been studied *via* solid state, where possible, ^{1}H-NMR titration experiments and UV/Vis and fluorescence spectroscopy, in order to also investigate their properties as colorimetric and fluorescent sensors. The anion transport ability has been studied using vesicle-based methods.

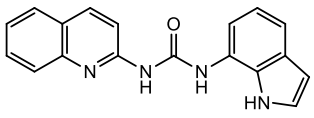

L^{1}

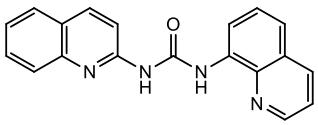

L^{2}

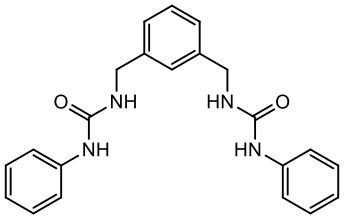

L^{3}

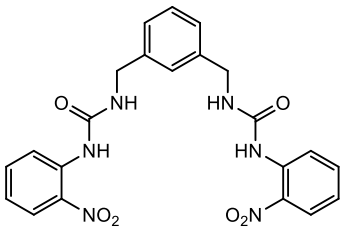

L^{4}

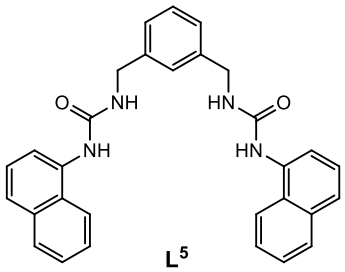

L^{5}

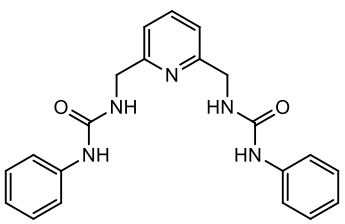

L^{6}

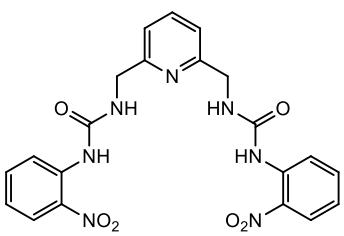

L^{7}

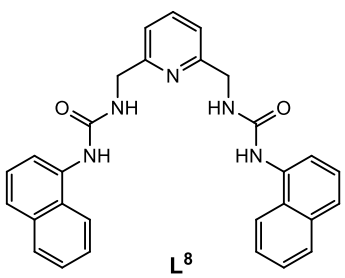

L^{8}

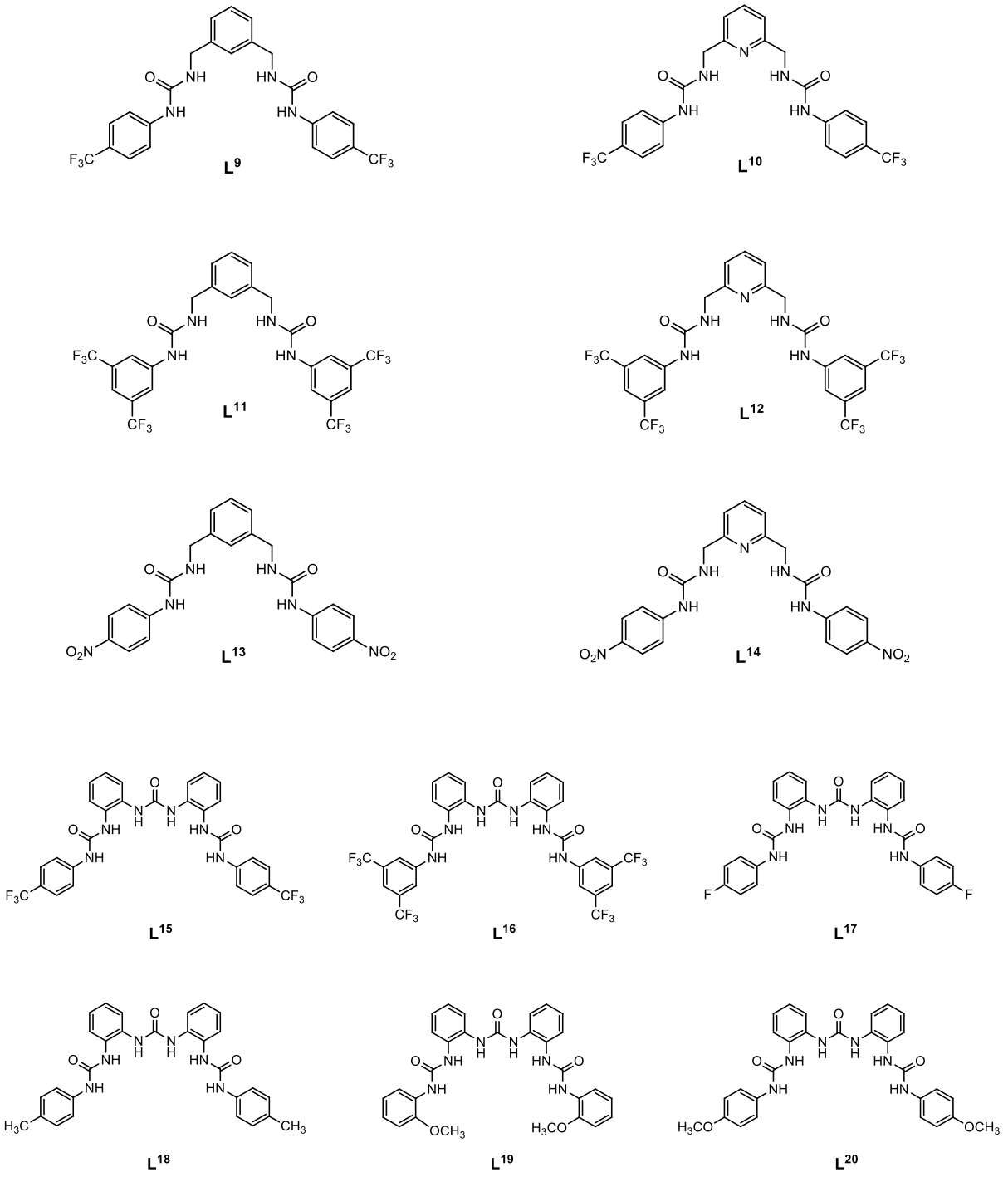

Figure 1.34. Receptors discussed in the thesis.

References

1. Lehn, J. M. Cryptates: inclusion complexes of macropolycyclic receptor molecules. *Pure Appl. Chem.* **50,** 871–892 (1978).

2. Lehn, J. -M. Supramolecular Chemistry—Scope and Perspectives Molecules, Supermolecules, and Molecular Devices (Nobel Lecture). *Angew. Chemie Int. Ed. English* **27,** 89–112 (1988).

3. Desiraju, G. R. Crystal engineering: a holistic view. *Angew. Chem. Int. Ed. Engl.* **46,** 8342–56 (2007).

4. Desiraju, G. R. *Crystal engineering : the design of organic solids by G. R. Desiraju*. *J. Appl. Crystallogr.* **24,** (International Union of Crystallography, 1989).

5. Shriver, D. F. & Biallas, M. J. Observation of the Chelate Effect with a Bidentate Lewis Acid, F2BCH2CH2BF2. *J. Am. Chem. Soc.* **89,** 1078–1081 (1967).

6. Park, C. H. & Simmons, H. E. Macrobicyclic amines. III. Encapsulation of halide ions by in,in-1,(k + 2)-diazabicyclo[k.l.m.]alkane ammonium ions. *J. Am. Chem. Soc.* **90,** 2431–2432 (1968).

7. Ashcroft, F. M. *Ion Channels and Disease: Channelopathies*. (2000).

8. Bell, R. A., Christoph, G. G., Fronczek, F. R. & Marsh, R. E. The Cation H13O6+: A Short, Symmetric Hydrogen Bond. *Science (80-.).* **190,** 151–152 (1975).

9. Bazzicalupi, C. *et al.* Exploring the binding ability of polyammonium hosts for anionic substrates: selective size-dependent recognition of different phosphate anions by bis-macrocyclic receptors. *Inorg. Chem.* **50,** 7202–16 (2011).

10. Bazzicalupi, C. *et al.* Selective binding and fluorescence sensing of diphosphate in H2O via Zn(2+)-induced allosteric regulation of the receptor structure. *Chem. Commun. (Camb).* **48,** 139–41 (2012).

11. Schmuck, C. & Bickert, V. Oxoanion binding by flexible guanidiniocarbonyl pyrrole-ammonium bis-cations in water. *J. Org. Chem.* **72,** 6832–9 (2007).

12. Ahmed, N., Shirinfar, B., Geronimo, I. & Kim, K. S. Fluorescent imidazolium-based cyclophane for detection of guanosine-5'-triphosphate and I(-) in aqueous solution of physiological pH. *Org. Lett.* **13,** 5476–9 (2011).

13. Li, Y. & Flood, A. H. Pure C H Hydrogen Bonding to Chloride Ions: A Preorganized and Rigid Macrocyclic Receptor. *Angew. Chemie* **120,** 2689–2692 (2008).

14. McDonald, K. P., Hua, Y., Lee, S. & Flood, A. H. Shape persistence delivers lock-and-key chloride binding in triazolophanes. *Chem. Commun. (Camb).* **48,** 5065–75 (2012).

15. Hua, Y., Ramabhadran, R. O., Karty, J. A., Raghavachari, K. & Flood, A. H. Two levels of conformational pre-organization consolidate strong CH hydrogen bonds in chloride-triazolophane complexes. *Chem. Commun. (Camb).* **47,** 5979–81 (2011).

16. Pascal, R. A., Spergel, J. & Engen, D. Van. No Title. *tetrahedron Lett.* **27,** 4099 (1986).

17. Dorazco-González, A., Höpfl, H., Medrano, F. & Yatsimirsky, A. K. Recognition of anions and neutral guests by dicationic pyridine-2,6-dicarboxamide receptors. *J. Org. Chem.* **75,** 2259–73 (2010).

18. Boiocchi, M. *et al.* Nature of urea-fluoride interaction: incipient and definitive proton transfer. *J. Am. Chem. Soc.* **126,** 16507–14 (2004).

19. Brooks, S. J., Gale, P. A. & Light, M. E. Carboxylate complexation by 1,1'-(1,2-phenylene)bis(3-phenylurea) in solution and the solid state. *Chem. Commun. (Camb).* 4696–8 (2005). doi:10.1039/b508144k

20. Brooks, S. J., Gale, P. A. & Light, M. E. ortho-Phenylenediamine bis-urea–carboxylate: a new reliable supramolecular synthon. *CrystEngComm* **7,** 586 (2005).

21. Brooks, S. J., Edwards, P. R., Gale, P. A. & Light, M. E. Carboxylate complexation by a family of easy-to-make ortho-phenylenediamine based bis-ureas: studies in solution and the solid state. *New J. Chem.* **30,** 65 (2006).

22. Brooks, S. J., Gale, P. A. & Light, M. E. Anion-binding modes in a macrocyclic amidourea. *Chem. Commun. (Camb).* 4344–6 (2006). doi:10.1039/b610938a

23. Brooks, S. J., García-Garrido, S. E., Light, M. E., Cole, P. A. & Gale, P. A. Conformational control of selectivity and stability in hybrid amide/urea macrocycles. *Chemistry* **13,** 3320–9 (2007).

24. Ros-Lis, J. V. *et al.* Signalling Mechanisms in Anion-Responsive Push-Pull Chromophores: The Hydrogen-Bonding, Deprotonation and Anion-Exchange Chemistry of Functionalized Azo Dyes. *European J. Org. Chem.* **2007,** 2449–2458 (2007).

25. Lakshminarayanan, P. S., Ravikumar, I., Suresh, E. & Ghosh, P. Trapped inorganic phosphate dimer. *Chem. Commun. (Camb).* 5214–6 (2007). doi:10.1039/b713365k

26. Ravikumar, I. & Ghosh, P. Unusual recognition of (n-Bu4N)2SO4 by a cyanuric acid based host via contact ion-pair interactions. *Chem. Commun. (Camb).* **46,** 6741–3 (2010).

27. Jia, C. *et al.* Highly efficient extraction of sulfate ions with a tripodal hexaurea receptor. *Angew. Chem. Int. Ed. Engl.* **50,** 486–90 (2011).

28. Dos Santos, C. M. G., McCabe, T., Watson, G. W., Kruger, P. E. & Gunnlaugsson, T. The recognition and sensing of anions through "positive allosteric effects" using simple urea-amide receptors. *J. Org. Chem.* **73,** 9235–44 (2008).

29. Boyle, E. M., McCabe, T. & Gunnlaugsson, T. Synthesis, photophysical and NMR evaluations of thiourea-based anion receptors possessing an acetamide moiety. *Supramol. Chem.* **22,** 586–597 (2010).

30. Aldrey, A. *et al.* Colorimetric macrocyclic anion probes bearing nitrophenylurea and nitrophenylthiourea binding groups. *Tetrahedron* **69,** 4578–4585 (2013).

31. Qatsha, K. A., Rudolph, C., Marme, D., Schachtele, C. & May, W. S. Go 6976, a selective inhibitor of protein kinase C, is a potent antagonist of human immunodeficiency virus 1 induction from latent/low-level-producing reservoir cells in vitro. *Proc. Natl. Acad. Sci.* **90,** 4674–4678 (1993).

32. Toullec, D. *et al.* The bisindolylmaleimide GF 109203X is a potent and selective inhibitor of protein kinase C. *J. Biol. Chem.* **266,** 15771–81 (1991).

33. Lee, J.-Y., Lee, M.-H. & Jeong, K.-S. Synthesis and Binding Properties of Anion Receptors Containing Multiple Hydrogen Bond Donors. *Supramol. Chem.* **19,** 257–263 (2007).

34. Caltagirone, C. *et al.* Metal-induced pre-organisation for anion recognition in a neutral platinum-containing receptor. *Chem. Commun. (Camb).* 6279–81 (2009). doi:10.1039/b912942a

35. Mani, G., Guchhait, T., Kumar, R. & Kumar, S. Macrocyclic and acyclic molecules synthesized from dipyrrolylmethanes: receptors for anions. *Org. Lett.* **12,** 3910–3 (2010).

36. Mani, G., Jana, D., Kumar, R. & Ghorai, D. Azatripyrrolic and azatetrapyrrolic macrocycles from the Mannich reaction of pyrrole: receptors for anions. *Org. Lett.* **12,** 3212–5 (2010).

37. Kondo, S., Kobayashi, Y. & Unno, M. Anion recognition by d-ribose-based receptors. *Tetrahedron Lett.* **51,** 2512–2514 (2010).

38. Aguado Tetilla, M. *et al.* Colorimetric response to anions by a "robust" copper(II) complex of a [9]aneN3 pendant arm derivative: CN- and I- selective sensing. *Chem. Commun. (Camb).* **47,** 3805–7 (2011).

39. Mameli, M. *et al.* Synthesis and coordination properties of quinoline pendant arm derivatives of [9]aneN(3) and [9]aneN(2)S as fluorescent zinc sensors. *Inorg. Chem.* **48,** 9236–49 (2009).

40. Hulanicki, A., Glab, S. & Ingman, F. Chemical sensors: definitions and classification. *Pure Appl. Chem.* **63,** 1247–1250 (1991).

41. Pinalli, R., Nachtigall, F., Ugozzoli, F. & Dalcanale, E. Supramolecular Sensors for the Detection of Alcohols. *Angew. Chem. Int. Ed. Engl.* **38,** 2377–2380 (1999).

42. F.C.J.M. van Veggel; Mass Sensors, in "Comprehensive Supramolecular Chemistry', J.-M. Lehn (Ed. in chief), Pergamon Oxford 1996, vol. 10, chapter 7, p 171-185.

43. guest editor Fabbrizzi L. special issue on luminescent sensors. *Coord. Chem. Rev.* **205,** 1–232 (2000).

44. Janata, J., Josowicz, M., Vanýsek, P. & DeVaney, D. M. Chemical Sensors. *Anal. Chem.* **70,** (1998).

45. Bakker, E., Bühlmann, P. & Pretsch, E. Carrier-based ion-selective electrodes and bulk optodes. 1. General characteristics. *Chem. Rev.* **97,** 3083–3132 (1997).

46. Bühlmann, P., Pretsch, E. & Bakker, E. Carrier-based ion-selective electrodes and bulk optodes. 2. Ionophores for potentiometric and optical sensors. *Chem. Rev.* **98,** 1593–1687 (1998).

47. Weller, A. Electron-transfer and complex formation in the excited state. *Pure Appl. Chem.* **16,** 115–124 (1968).

48. Veale, E. B., Tocci, G. M., Pfeffer, F. M., Kruger, P. E. & Gunnlaugsson, T. Demonstration of bidirectional photoinduced electron transfer (PET) sensing in 4-amino-1,8-naphthalimide based thiourea anion sensors. *Org. Biomol. Chem.* **7,** 3447–54 (2009).

49. Choi, K. & Hamilton, A. D. A Dual Channel Fluorescence Chemosensor for Anions Involving Intermolecular Excited State Proton Transfer We thank the National Institutes of Health for financial support of this work. *Angew. Chem. Int. Ed. Engl.* **40,** 3912–3915 (2001).

50. Valeur, B. & Berberan-Santos, M. N. *Molecular Fluorescence: Principles and Applications*. (2012).

51. Lakowicz, J. R. *Principles of Fluorescence Spectroscopy*. (2007). 3rd ed. Springer: New York, (2006).

52. Pohl, R. *et al.* Strategies toward improving the performance of fluorescence-based sensors for inorganic anions. *Chem. Commun. (Camb).* 1282–3 (2004). doi:10.1039/b315268e

53. Nishizawa, S., Kato, Y. & Teramae, N. Fluorescence Sensing of Anions via Intramolecular Excimer Formation in a Pyrophosphate-Induced Self-Assembly of a Pyrene-Functionalized Guanidinium Receptor. *J. Am. Chem. Soc.* **121,** 9463–9464 (1999).

54. Miyaji, H., Collinson, S. R., Prokeŝ, I. & Tucker, J. H. R. A ditopic ferrocene receptor for anions and cations that functions as a chromogenic molecular switch. *Chem. Commun. (Camb).* **2,** 64–5 (2003).

55. Wang, Q., Xie, Y., Ding, Y., Li, X. & Zhu, W. Colorimetric fluoride sensors based on deprotonation of pyrrole-hemiquinone compounds. *Chem. Commun. (Camb).* **46,** 3669–71 (2010).

56. Gale, P. a, Busschaert, N., Haynes, C. J. E., Karagiannidis, L. E. & Kirby, I. L. Anion receptor chemistry: highlights from 2011 and 2012. *Chem. Soc. Rev.* (2013). doi:10.1039/c3cs60316d

57. Davis, A. P., Sheppard, D. N. & Smith, B. D. Development of synthetic membrane transporters for anions. *Chem. Soc. Rev.* **36,** 348–57 (2007).

58. Davis, J. T., Okunola, O. & Quesada, R. Recent advances in the transmembrane transport of anions. *Chem. Soc. Rev.* **39,** 3843–62 (2010).

59. Busschaert, N. & Gale, P. a. Small-molecule lipid-bilayer anion transporters for biological applications. *Angew. Chem. Int. Ed. Engl.* **52,** 1374–82 (2013).

60. Gale, P. a, Pérez-Tomás, R. & Quesada, R. Anion Transporters and Biological Systems. *Acc. Chem. Res.* **XXX,** (2013).

61. Quinton, P. M. Cystic fibrosis: impaired bicarbonate secretion and mucoviscidosis. *Lancet* **372,** 415–7 (2008).

62. Fürstner, A. Chemistry and biology of roseophilin and the prodigiosin alkaloids: a survey of the last 2500 years. *Angew. Chem. Int. Ed. Engl.* **42,** 3582–603 (2003).

63. Jenkins, S., Incarvito, C. D., Parr, J. & Wasserman, H. H. Structural studies of C-ring substituted unnatural analogues of prodigiosin. *CrystEngComm* **11,** 242 (2009).

64. Seganish, J. L. & Davis, J. T. Prodigiosin is a chloride carrier that can function as an anion exchanger. *Chem. Commun. (Camb).* 5781–3 (2005). doi:10.1039/b511847f

65. Davis, J. T. *et al.* Using small molecules to facilitate exchange of bicarbonate and chloride anions across liposomal membranes. *Nat. Chem.* **1,** 138–44 (2009).

66. Chen, Y. A Mechanism for Tamoxifen-mediated Inhibition of Acidification. *J. Biol. Chem.* **274,** 18364–18373 (1999).

67. Sessler, J. L. *et al.* Synthesis, Anion-Binding Properties, and In Vitro Anticancer Activity of Prodigiosin Analogues. *Angew. Chemie* **117,** 6143–6146 (2005).

68. Iglesias Hernández, P. *et al.* Tambjamine alkaloids and related synthetic analogs: efficient transmembrane anion transporters. *Chem. Commun. (Camb).* **48,** 1556–8 (2012).

69. Harrell, W. A., Bergmeyer, M. L., Zavalij, P. Y. & Davis, J. T. Ceramide-mediated transport of chloride and bicarbonate across phospholipid membranes. *Chem. Commun. (Camb).* **46,** 3950–2 (2010).

70. Siskind, L. J. & Colombini, M. The lipids C2- and C16-ceramide form large stable channels. Implications for apoptosis. *J. Biol. Chem.* **275,** 38640–4 (2000).

71. Bahmanjah, S., Zhang, N. & Davis, J. T. Monoacylglycerols as transmembrane Cl- anion transporters. *Chem. Commun. (Camb).* **48,** 4432–4 (2012).

72. Díaz de Greñu, B. *et al.* Synthetic prodiginine obatoclax (GX15-070) and related analogues: anion binding, transmembrane transport, and cytotoxicity properties. *Chemistry* **17,** 14074–83 (2011).

73. Nguyen, M. *et al.* Small molecule obatoclax (GX15-070) antagonizes MCL-1 and overcomes MCL-1-mediated resistance to apoptosis. *Proc. Natl. Acad. Sci. U. S. A.* **104,** 19512–7 (2007).

74. Koulov, A. V *et al.* Chloride transport across vesicle and cell membranes by steroid-based receptors. *Angew. Chem. Int. Ed. Engl.* **42,** 4931–3 (2003).

75. McNally, B. A. *et al.* Structure-activity relationships in cholapod anion carriers: enhanced transmembrane chloride transport through substituent tuning. *Chemistry* **14,** 9599–606 (2008).

76. Judd, L. W. & Davis, A. P. From cholapod to cholaphane transmembrane anion carriers: accelerated transport through binding site enclosure. *Chem. Commun. (Camb).* **46,** 2227–9 (2010).

77. Busschaert, N. *et al.* Tripodal transmembrane transporters for bicarbonate. *Chem. Commun. (Camb).* **46,** 6252–4 (2010).

78. Andrews, N. J. *et al.* Structurally simple lipid bilayer transport agents for chloride and bicarbonate. *Chem. Sci.* **2,** 256 (2011).

79. Moore, S. J. *et al.* Towards "drug-like" indole-based transmembrane anion transporters. *Chem. Sci.* **3,** 2501 (2012).

80. Reddy, G. L., Iwamoto, T., Tomich, J. M. & Montal, M. Synthetic peptides and four-helix bundle proteins as model systems for the pore-forming structure of channel proteins. II. Transmembrane segment M2 of the brain glycine receptor is a plausible candidate for the pore-lining structure. *J. Biol. Chem.* **268,** 14608–15 (1993).

81. Shank, L. P. *et al.* Redesigning channel-forming peptides: amino acid substitutions that enhance rates of supramolecular self-assembly and raise ion transport activity. *Biophys. J.* **90,** 2138–50 (2006).

82. Tomich, J. M. *et al.* Aqueous solubilization of transmembrane peptide sequences with retention of membrane insertion and function. *Biophys. J.* **74,** 256–67 (1998).

83. Schlesinger, P. H. *et al.* SCMTR: a chloride-selective, membrane-anchored peptide channel that exhibits voltage gating. *J. Am. Chem. Soc.* **124,** 1848–9 (2002).

84. Gorteau, V., Bollot, G., Mareda, J., Perez-Velasco, A. & Matile, S. Rigid oligonaphthalenediimide rods as transmembrane anion-pi slides. *J. Am. Chem. Soc.* **128,** 14788–9 (2006).

85. Perez-Velasco, A., Gorteau, V. & Matile, S. Rigid oligoperylenediimide rods: anion-pi slides with photosynthetic activity. *Angew. Chem. Int. Ed. Engl.* **47,** 921–3 (2008).

86. Harrowfield, J. *et al.* Membrane-active calixarenes: toward "gating" transmembrane anion transport. *Tetrahedron* **63,** 10743–10750 (2007).

Chapter 2: Non-symmetric substituted ureas locked in (E,Z) conformation

Chapter 2: Non-symmetric substituted ureas locked in (E,Z) conformation

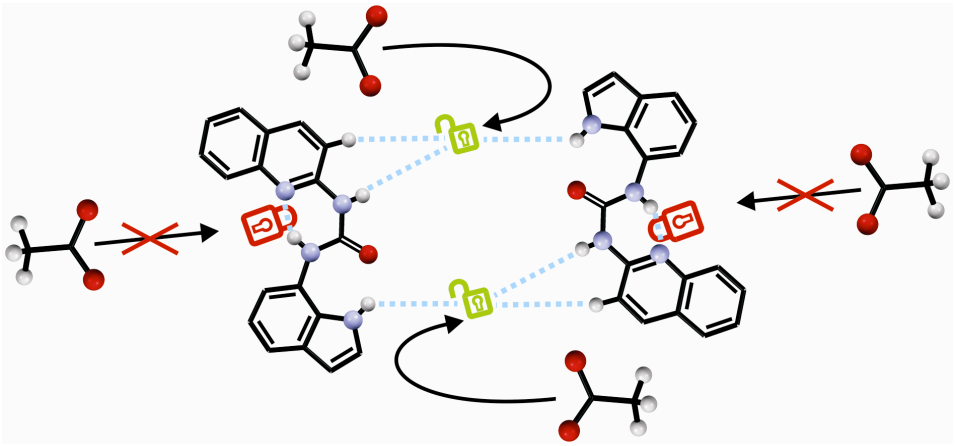

2.1 Introduction

A popular area of supramolecular chemistry in which hydrogen bonds play a key role is anion recognition performed by neutral receptors containing ureidic, amidic, indolic etc. NH groups able to act as hydrogen bond donors towards anionic substrates.[1,2,3,4] Moreover, in biological systems, the integrity of a huge number of biomolecular structures, information storage and transfer processes, replication and catalysis are strongly dependent on the formation of specific patterns of complementary inter- and intramolecular hydrogen bonds.[5,6,7] For this reason designing, developing and understanding new systems able to self-assemble only by means of hydrogen bonds formation is one of the challenges of modern supramolecular chemistry.[8] When designing an anion receptor many factors must be taken into account such as the number and typology of the hydrogen bond donor groups, the complementarity in shape and dimension between the binding domain of the receptor and the anionic substrate, and the nature of the receptors in terms of formation of intra- or inter-molecular hydrogen bonds (that could prevent the availability of the donor groups for anion coordination).

As shown in the previous chapter, indoles are efficient hydrogen bond donating groups in anion recognition, and recently have been largely employed in synthetic anion receptor systems from the group of Gale. They have reported, first, compound **127** that showed to bind carboxylate and dihydrogen phosphate with high affinity constants (see *Table 2.1*). However, NMR studies revealed that the oxoanions interact strongly with ureidic and indolic groups and much more weakly with the amide group. Thus, in order to improve the anion binding properties, Gale and co-workers designed the symmetric diindolylurea compounds **128** and **129** by elimination of the amidic moiety and introduction of a second indole.[9,10]

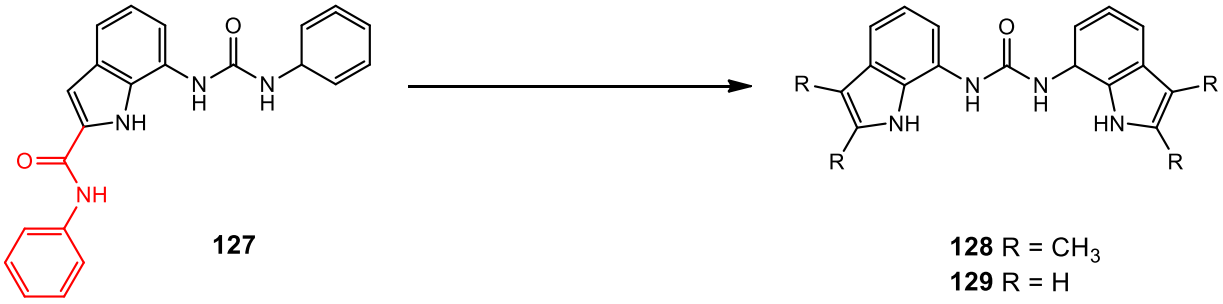

Scheme 2.1. Design of the receptors **128** and **129**, starting from receptor **127**

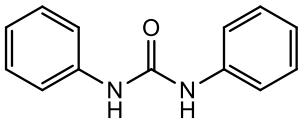

130

Both these compound were shown to bind strongly AcO^-, BzO^- and $H_2PO_4^-$ with stability constants greater than 10^4 M^{-1} in DMSO-d_6/0.5% water mixtures by ^1H NMR titration techniques. 1,3-diphenylurea **130**, used as a model compound, binds anions significantly less strongly than compound **128** (see *Table 2.1*). Binding studies were also conducted in 10% water demonstrating that receptors **128** and **129** showed selectivity for dihydrogen phosphate with stability constants of 4790 and 5170 M^{-1} respectively (see *Table 2.1*). While increasing the amounts of water to 25% only compound **129** was found to bind dihydrogen phosphate with a stability constant of 160 M^{-1} and acetate with stability constant of 20 M^{-1}. The ability to bind selectively and strongly $H_2PO_4^-$ in this polar and competitive solvent mixture of a neutral receptor is very notable.

Table 2.1 Equilibrium constants (K_a/M^{-1}) of compound **127**, **128** and **130** in DMSO-d_6/0.5% water and of compound **128** in DMSO-d_6/10% water at 298 K with the tetrabutylammonium anion salts considered. In all cases 1:1 receptor:anion stoichiometry was observed. Errors estimated to be no more than ≤10%

Anions	**127** in DMSO-d_6 /0.5% water	**128** in DMSO-d_6 /0.5% water	**130** in DMSO-d_6 /0.5% water	**128** in DMSO-d_6 /10% water
Cl^-	38	128	31	16
$CH_3CO_2^-$	10^4	$>10^4$	1260	567
$C_6H_5CO_2^-$	4460	$>10^4$	674	736
$H_2PO_4^-$	4950	$>10^4$	523	4790

Crystals of the phosphate complex of **129** were obtained from DMSO/water solution. The X-ray structure showed that dihydrogen phosphate undergone deprotonation and three equivalents of the receptor bound PO_4^{3-} by twelve hydrogen bonds (*Fig. 2.1*). A similar behaviour was revealed by the crystals of bicarbonate complex of **128**, the deprotonated anion CO_3^{2-} was bound *via* eight hydrogen bond by two molecules of **128** (*Fig. 2.2*), while

the structure of the crystals of the benzoate complex revealed that benzoate was bond in 1:1 stoichiometry *via* four hydrogen bond (*Fig 2.3*).

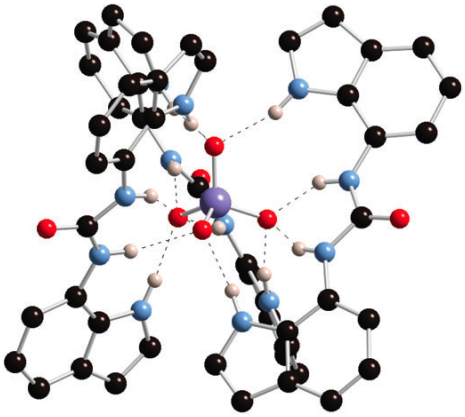

Figure 2.1. The phosphate complex of compound **129**

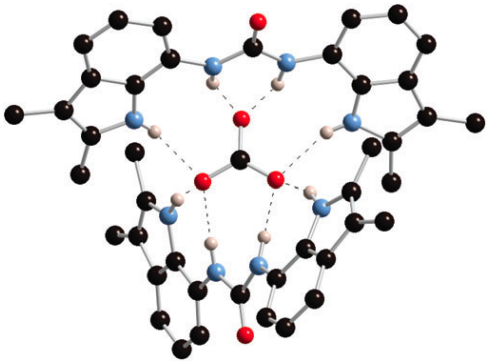

Figure 2.2. The carbonate complex of compound **128**

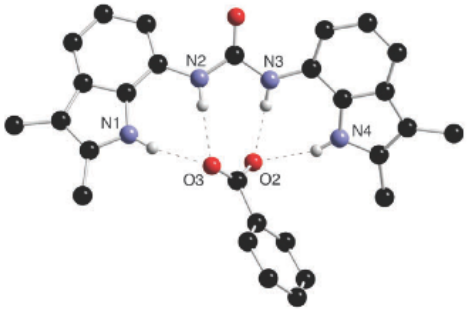

Figure 2.3. The benzoate complex of compound **128**

Gale and co-workers have also studied the oxoanions binding affinities of the amide functionalized diindolylureas **131**-**134**.[11,12] Crystals of the benzoate complex of **131** revealed that receptor bound three equivalents of benzoate in the solid state. One benzoate anion was bound via four hydrogen bonds by the central diindolylurea group, whereas the two pendant amidoindole moieties, oriented out of the cavity, bound other two equivalent of benzoate *via* two or three hydrogen bonds. The crystal structure of the complex with sulfate and monophosphate anions, instead, showed that compound **131** bound SO_4^{2-} and HPO_4^{2-} *via* eight and nine hydrogen bond respectively in a 1:1 stoichiometry.

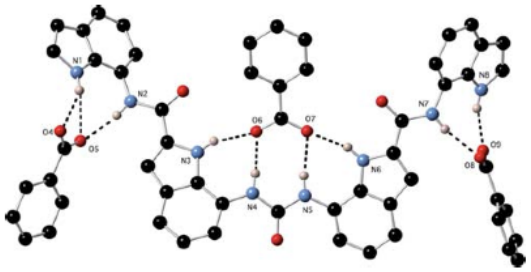

Figure 2.4 Crystal structure of the benzoate complex of compound **131**

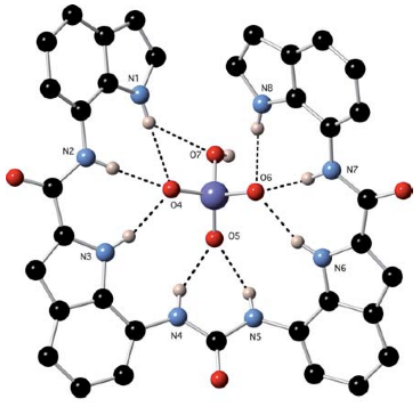

Figure 2.5 Crystal structure of the phosphate complex of compound **131**

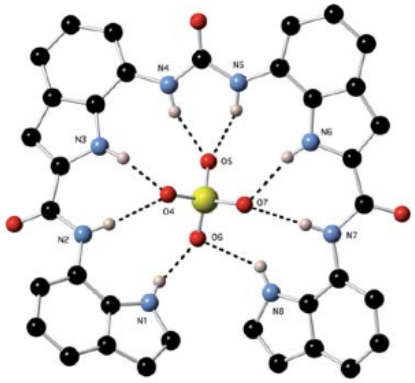

Figure 2.6 Crystal structure of the sulfate complex of compound **131**

The anion binding properties were also studied by ^{1}H-NMR titrations in DMSO-d_6/water solvent mixtures. All compounds bound sulfate strongly in DMSO-d_6/0.5% water. Compound **134** formed a 1:1 sulfate complex with stability constant greater than 10^4 whilst compound **131** and **132** also formed 1:1 complex but upon addition of higher concentration of sulfate there were multiple equilibria present. By changing the solvent conditions in DMSO-d_6/10% water, the complexity of the equilibria was reduced and the formation of 1:1 complex was predominant. Under this competitive solvent mixtures compound **132** has shown a stability constant of >10^4. The authors also found that upon addition of dihydrogen phosphate to compound **131**-**133** in DMSO- d_6/0.5% water solution, new peaks appear in the NMR spectrum when more than one equivalents of the anion was added due to deprotonation of the bound anion and the corresponding formation of monohydrogen phosphate complex. The pK_a of the bound dihydrogen phosphate is reduced by the receptor that forms six hydrogen bonds to it such and the addition of further aliquots of $H_2PO_4^-$ results in deprotonation of the bound anion.

Following our interest in anion recognition involving indole as hydrogen bond donor group[13,14] we designed and successfully synthesised two new ureidic asymmetric

derivatives: **L**[1] which contains a quinoline and an indole moiety, and **L**[2] featuring two quinoline moieties.

L[1]

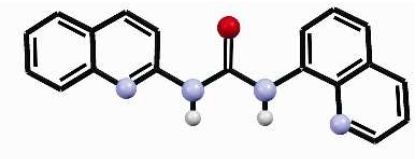

L[2]

2.2 Synthesis

AS shown in Scheme 2.2, Both receptor **L**[1] and **L**[2] were synthesised starting from 2-isocyanatoquinoline obtained by Curtius rearrangement from quinoline-carbonyl azide[15] and 7-aminoindole, prepared by reduction of 7-nitroindole, and 8-aminoquinoline, respectively, in dry toluene. In the case of **L**[1] the resulting precipitate was washed with DCM and then with MeOH to get the pure product in 29% yield. In the case of **L**[2] the pure product was simply obtained by filtration from the reaction mixture as a white solid in 63% yield.

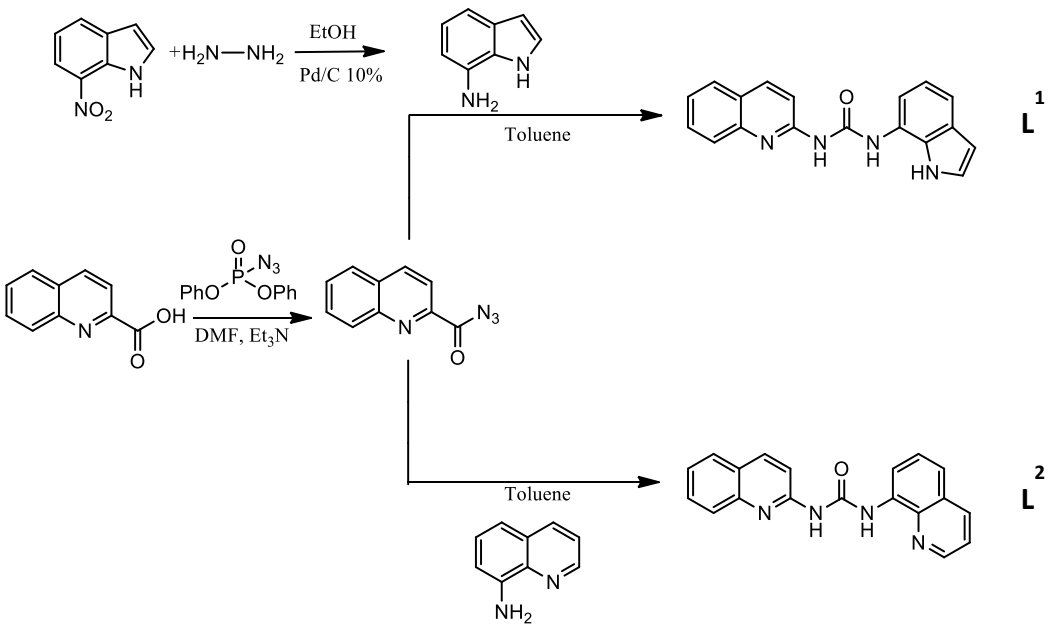

Scheme 2.2 Synthesis of **L**[1] and **L**[2]

2.3 Solid state studies

Crystals suitable for X-ray diffraction analysis were obtained for both substituted urea derivatives **L**[1] and **L**[2]. **L**[1] was crystallised by slow evaporation from a 1:1 (v/v) mixture of

DCM and MeOH resulting in a solvate phase (**L^{1}α**)[a]. A further crystallization experiment from MeOH/THF 2:1 (v/v) in the presence of tetrabutylammonium acetate, resulted in a second phase of the receptor **L^1** (**L^{1}β**)[a]. Crystals of **L^2** were grown by slow evaporation from DMSO.

The two phases **L^{1}α** (trigonal, *R*-3, Z' = 1) and **L^{1}β** (orthorombic, *Pna*2$_1$, Z' = 2), adopt an (*E*,*Z*) conformation (*Fig. 2.7a*) with the formation of an intramolecular hydrogen bond between one of the NHs of the urea moiety and the nitrogen of the quinoline group (N(3)···N(1) distances, are 2.658(4) Å for **L^{1}α** and respectively 2.653(6) Å and 2.682(6) Å for **L^{1}β**) in agreement with the literature data on solid state regarding pyridyl urea derivatives.[16,17,18] Moreover, the presence of the indole group allows the formation of an additional intramolecular hydrogen bond between the NH of the indole and the ureidic carbonyl group (N4···O1 distances are 2.686(4) Å for **L^{1}α** and respectively 2.687(5) Å and 2.703(5) Å for **L^{1}β**).

Similarly to the two phases **L^{1}α** and **L^{1}β**, the crystal structure of **L^2** (monoclinic, *P2$_1$/c*, Z' = 2) shows an intramolecular hydrogen bond involving one of the ureidic NH group and the nitrogen of the quinoline group (N(4)···N(2) and (N(6)···N(8) distances are respectively 2.697(2) Å and 2.694(2) Å), resulting in an (*E*,*Z*) conformation (*Fig. 2.7b*).

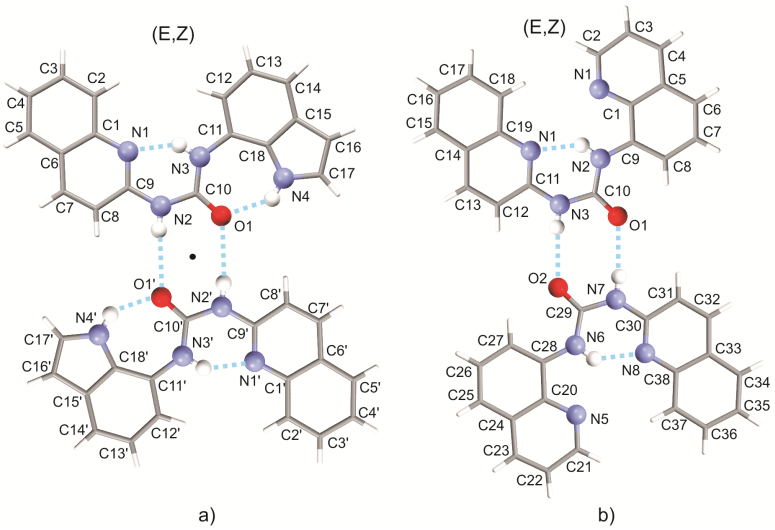

Figure 2.7 Ureidic dimer and relevant intra and inter-molecular interactions for **L^{1}α** (a) as representative for the pair (**L^{1}α** and **L^{1}β)** and **L^2**(b) in the (*E,Z*) conformation. The numbering scheme is also reported. Centre of inversion is indicated as • (symmetry code: -x+5/3, -y+1/3, -z-2/3).

A further common feature in the three structures is represented by the adoption of a similar supramolecular synthon[19] (*Fig 2.7a* and *b*) consisting of a dimer (centrosymmetric for **L^{1}α** and pseudo-centrosymmetric for **L^{1}β** and **L^2**) connected via hydrogen bonds involving the donor ureidic carbonyl group of one molecule and the ureidic NH group not involved into intramolecular hydrogen bonds of an adjacent molecule (N(2)···O(1) distances are 2.845(4) Å for **L^{1}α**, N(102)···O(201) and N(202)···O(101) distances are

[a] The notation **α** and **β** is based on order of discovery and does not refer to any stability order, nor any melting temperature order. **L^{1}α** is solvate, the exact nature is unlcear, but an assumed 3 MeOH molecules were treated using squeeze

respectively 2.997(5) Å and 2.848 (5) Å for **L^{1}β** and N(3)···O(2) and N(7)···O(1) distances are 2.830(2) and 2.888(2) Å for **L^2**). This is not surprising if the similar shape/conformation and the common set of hydrogen bond donor and acceptor are taken into account.
A crystal packing comparison of the three structures **L^{1}α**, **L^{1}β** and **L^2**, carried out using the XPac program[20,21,22], reveals that this common supramolecular synthon is precursor of a higher dimensional common molecular arrangement.

The analysis reveals a 1-D similarity[21] defined as Supramolecular Construct[20] (SC A). This consists of a row of ureidic dimers, which respectively propagates along the *001* direction for **L^{1}α** (lattice vector = 7.098 Å), the *0-10* direction for **L^{1}β** (lattice vector = 7.131 Å) and the 100 direction for **L^2** (lattice vector = 8.041 Å). Apart the N-H···O dimers discussed above, no significant interactions are involved in connecting the SC A (*Fig. 2.8*) which is mainly the result of the close packing. The only exception is represented by **L^{1}β,** in which π-π interactions respectively involving the ureidic and quinolinic moieties of adjacent dimers, contribute in connecting this molecular arrangement (the shortest Cen-Cen distances are respectively 3.63 Å and 3.80 Å).

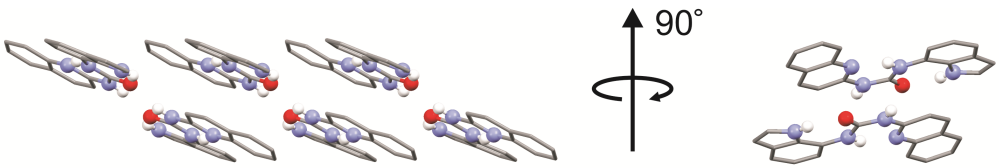

Figure 2.8 Representation of the SC A along its direction of propagation viewed along two perpendicular direction.

The SCs A are then differently assembled in the three structures, generating major departures in the resulting crystal packing (*Fig. 2.9*).

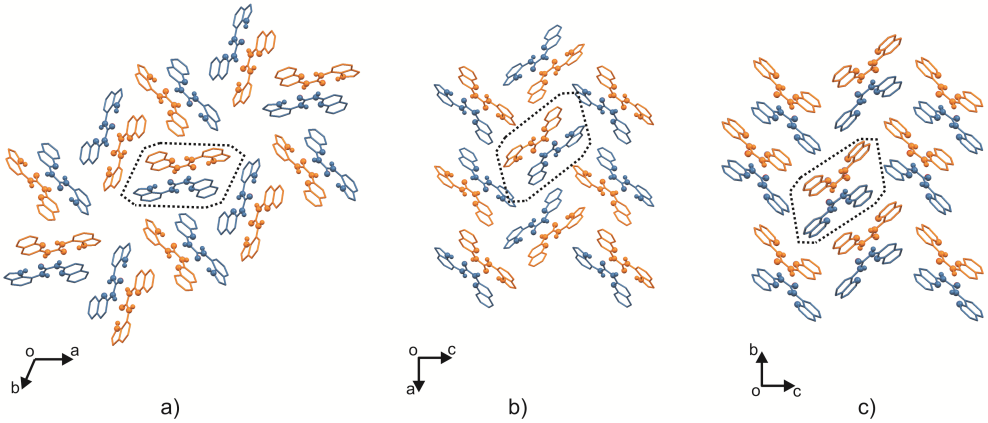

Figure 2.9 Crystal packing representation of the three structures **L^{1}α**, **L^{1}β** and **L^2**. a) **L^{1}α** viewed along the *001* direction; b) **L^{1}β** viewed along the *010* direction; c) **L^2** viewed along the *100* direction. The molecules are colour coded according to the orientation of the ureidic C-O vector: blue pointing towards the viewer, orange pointing away from the viewer. An instance of the SC A viewed along its direction of propagation is also indicated by black dashed lines.

Furthermore, the analysis of the crystal packing of **L^{1}α** viewed along the *001* direction reveals the presence of 1-D channels built by indolic units which have not any potential strong hydrogen bond donor or acceptor (*Fig 2.10* and *2.11*).

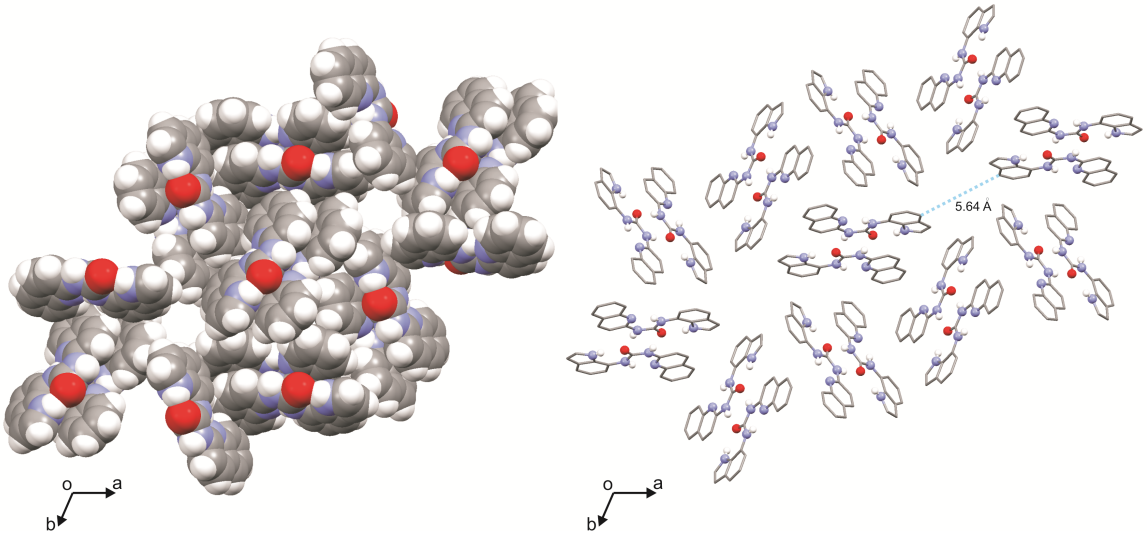

Figure 2.10 1-D channels for **L^{1}α** viewed along the *001* direction: spacefill representation (left), capped sticks representation (right). An estimation of the diameter (Å) measured as (quin)H-(quin)H distances is also reported.

A calculation of the solvent accessible void for **L^{1}α** (probe radius 1.2 Å)[23,24] gives a value of 101.4 Å^3 for each channel.

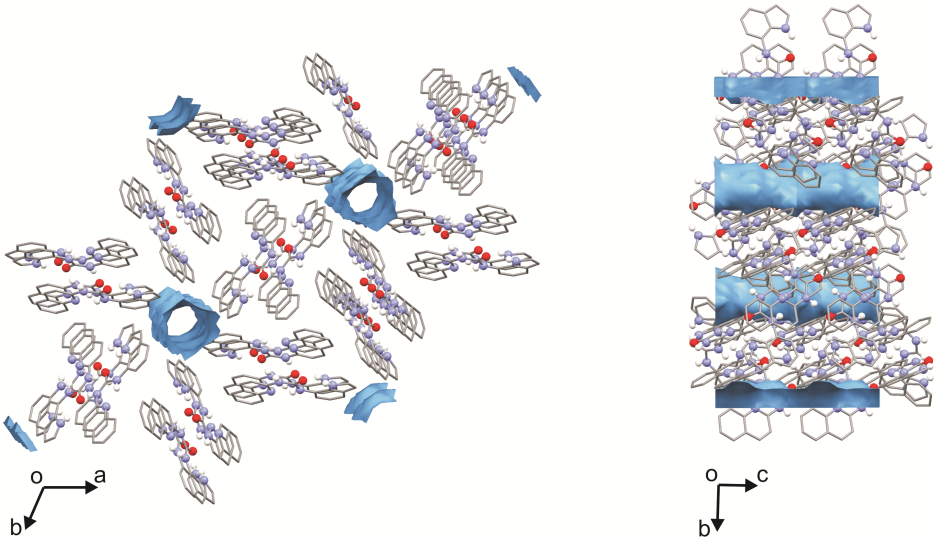

Figure 2.11 Solvent accessible surface (probe radius 1.2 Å) calculated for **L1α**, respectively viewed along the *001* direction (left) and the *100* direction (right).

This value is consistent with the expected volume for solvent molecules such as H_2O (40 Å^3) and generally small molecules (100-300 Å^3). At this stage it is not possible to discriminate which solvent, MeOH or DCM, initially co-crystallised with, but from volume and electron density considerations (methanol has an electron count of 18; squeeze suggests an electron count of 47 per cell which would give 3 molecules of this solvent per unit cell) methanol is assumed the most likely. This is also confirmed by elemental analysis.

2.4 Solution studies

We investigated whether the two receptors could assume in solution the same conformation observed in the solid state and which was their behaviour in the presence of anionic substrates.

In $CDCl_3$ solution **L[1]** adopts the same (*E*,*Z*) conformation observed in the solid state as confirmed by ^{1}H-NMR chemical shift assigned by ^{1}H-^{1}H TOCSY experiments. In particular the N3–H3A signal, involved in a strong intramolecular hydrogen bond, is observed at 12.97 ppm, the N4–H4A signal is observed at 10.20 ppm and the N2–H2A one is observed at 7.86 ppm. The chemical shift of the N2–H2A signal is concentration dependent in the concentration range of 20-0.25 mM (see Figure 2.12) in agreement with its involvement in an intermolecular hydrogen bond forming a duplex as observed in the solid state, while the N3–H3A and the N4–H4A signals are concentration independent being locked by intramolecular hydrogen bonds. A nonlinear regression analysis[25,26] of the ^{1}H-NMR data yielded to a dimerization constant of 430± 37 M^{-1}.

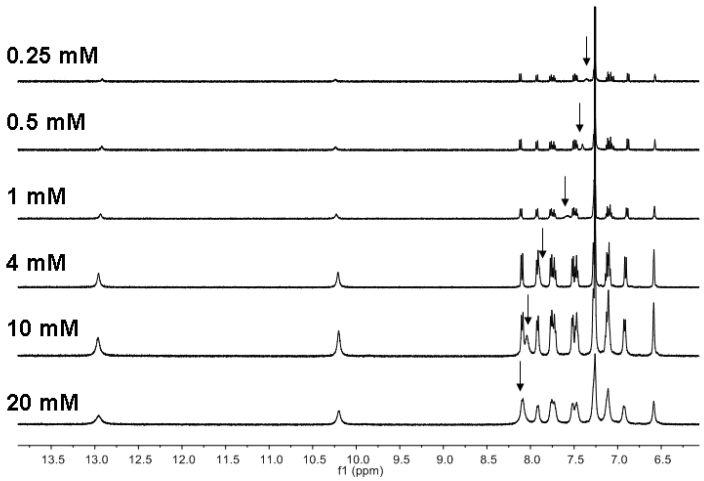

Figure 2.12 ^{1}H-NMR stack plot of solutions of **L[1]** in $CDCl_3$ at 298 K at decreasing concentrations. The arrows indicate the N2–H2A signal moving towards higher fields upon dilution.

Moreover, variable temperature ^{1}H-NMR experiments (see *Figure 2.13*) confirmed the presence of a duplex in solution in these experimental conditions as, once again, the N2–H2A signal moves upfield by increasing the temperature ($1.50\cdot10^{-2}$ ppm K^{-1}) while the signal of N3–H3A involved in an intramolecular hydrogen bond shows a much lower shift with temperature ($5.27\cdot10^{-2}$ ppm K^{-1}); in the range 294-321 K;[27,28] the N4–H4A signal resulted unaffected.

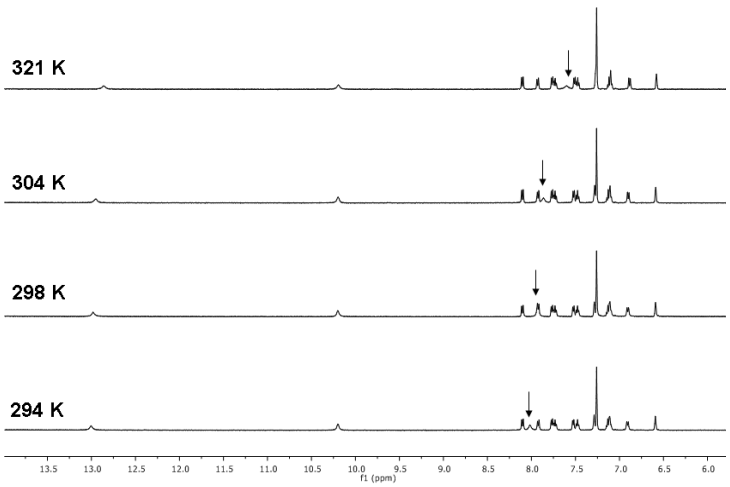

Figure 2.13 ^{1}H-NMR stack plot of solutions of **L^{1}** in $CDCl_3$ at 298 K at variable temperature. The arrows indicate the N2–H2A signal moving upfield upon increasing the temperature.

Anion binding studies were performed by means of ^{1}H-NMR titrations in $CDCl_3$ in the presence of acetate, benzoate and chloride (as their tetrabutylammonium salts). Interestingly, upon addition of 0.4 equivalents of acetate or benzoate all the NH signals broaden and the C8–H8A signal starts to move downfield. In particular, in the presence of an excess of acetate (around 3 equivalents) the NH signals can be observed again as sharp signals as shown in the stack plot in *Figure 2.14*.

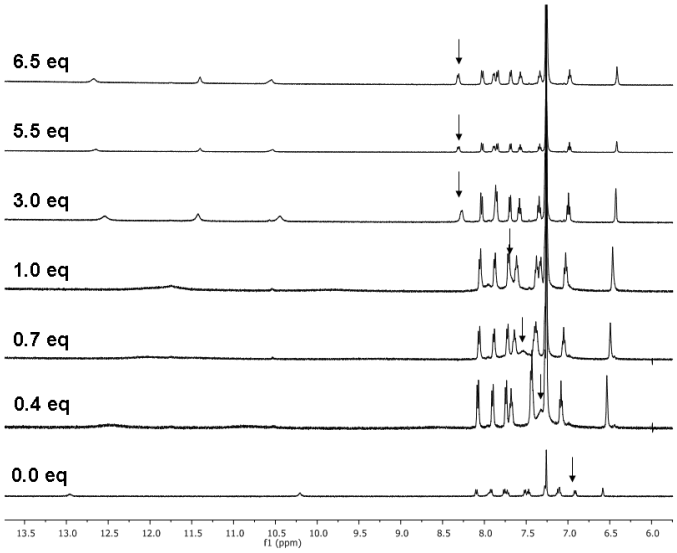

Figure 2.14 ^{1}H-NMR stack plot of a $CDCl_3$ solution of L^{1} (0.005 M) upon addition of tetrabutylammonium acetate (0.075 M) in $CDCl_3$ at 298 K. The arrows indicate the C8–H8A signal.

In particular the signal for N3–H3A is not affected by the presence of the anionic substrate, indicating that this proton is still involved in the intramolecular hydrogen bond N3–H3A···N1, while the N2–H2A, N4–H4A, and C8–H8A signals move downfield (about 1.5 ppm, 2.7 ppm, and 1.4 ppm, respectively). These results suggest that upon addition of acetate the duplex is no longer present in solution and the anion is bound to each

monomer by means of three hydrogen bonds, two from the NH moieties (one ureidic and one indolic) and one from the CH group of the quinoline.
A similar behaviour was observed in the presence of benzoate while in the case of chloride the broaden of the NH signals was less dramatic (*Figure 2.15*).

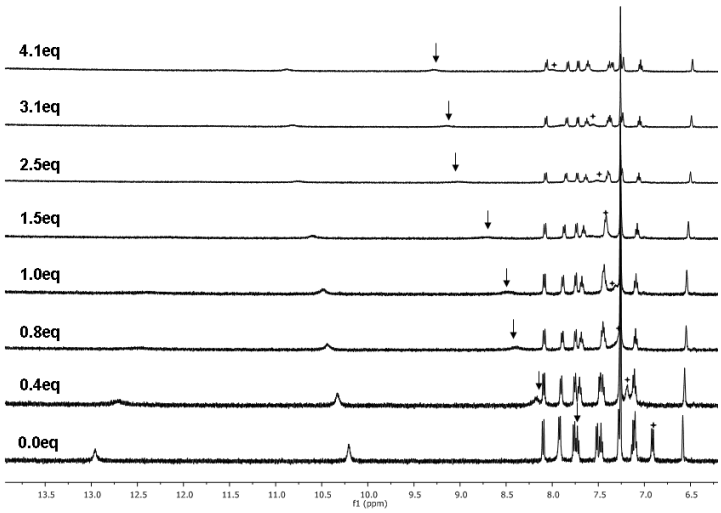

Figure 2.15 ^{1}H-NMR stack plot of a $CDCl_3$ solution of L^1 (0.005 M) upon addition of tetrabutylammonium chloride (0.075 M) in $CDCl_3$. The arrows indicate the C8–H8A (upfield) and the N2–H2A (downfield) signals.

The broadening of the NH signals prevented us from determining the affinity constants of **L^1** for the anionic substrates. For this reason we moved to DMSO-d_6, a solvent more suitable for these type of studies.
In DMSO-d_6, probably because of its higher solvating power, the formation of the duplex was not observed as confirmed by dilution and variable temperature experiments. However, on the basis of the ^{1}H chemical shift values observed (10.12(N2−H2A), 10.89 (N4−H4A) and 11.67 (N3−H3A) ppm) in comparison with those observed for the two ureidic and the indolic N-H groups in the symmetric 1,3-bis(1H-indol-7-yl)urea,[9,29] (8.63 and 10.77 ppm, respectively) the presence of the two aforementioned intramolecular H-bonds, namely, N3−H3A···N1 and N4−H4A···O1, can be inferred. This conclusion is further supported by both two-dimensional NOESY[30] and selective one-dimensional DPFGSE-noesy1d[31] experiments (200 ms mixing time). On the basis of the NOESY cross-peaks relative intensity, an upper limit of 2.7 Å has been applied to restrain the corresponding inter-proton distances together with the gromos-53a6 force field[32] parameters. One hundred structures were independently calculated using a simulated annealing protocol[2] with the software Dynamo [3] Additional inter-atomic distance restraints were also introduced to simulate the two mentioned intramolecular H-bonds. Violations from the

[b] Structure calculations were performed using the simulated annealing molecular dynamics algorithm implemented in DYNAMO (http://spin.niddk.nih.gov/NMRPipe/dynamo). The temperature was increased to 4000 K in 1000 initialization steps, then kept constant for 4000 steps, and finally slowly decreased to 0 K during the 20000 steps cooling stage. Experimental NOESY crossd peaks were classified on the basis of their relative intensity as strong, medium or weak, and an upper separation boundary of 2.7, 3.3 and 5.0 Å respectively was applied to restrain the distance between the corresponding protons

[3] Dynamo: the NMR molecular dynamics and analysis system http://spin.niddk.nih.gov/NMRPipe/dynamo.

experimental NOEs have never been observed. The 20 structures with the lowest potential energy were then selected and used for the analysis. Figure 2.16 shows the average structure together with the quantitative estimation of the different NOE enhancements (obtained analysing the one-dimensional noesy results with the so-called PANIC method).[33] It is interesting to note that N2−H2A and N4−H4A protons resulted to have almost the same distance from N3−H3A, as reflected by comparable NOE enhancements. However, N2−H2A provided a relatively higher NOE-enhancement to C8−H8A, as well as N3−H3A to C12−H12A. In the resulting molecular structure the two aromatic rings do not lie on the same plane but are differently tilted with respect to the carbonyl group, and N2−H2A and N4−H4A are located on opposite sides of the molecule. Overall, the statistical analysis showed that the most populated conformer is characterized by the two dihedral angles N1−N2−C10−O1 and N4−N3−C10−O1 equal to -106° and +15°, respectively. The (*E*,*Z*) conformation of the free receptor is thus maintained in solution both in $CDCl_3$ and in DMSO-d_6.

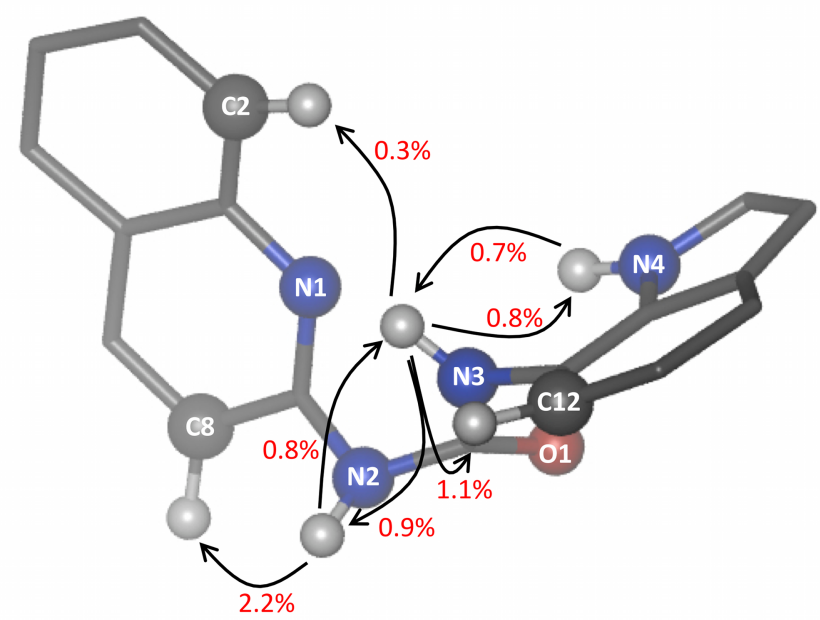

Figure 2.16 The most populated conformation adopted in solution by **L**[1] calculated on the basis of the experimental NOEs in DMSO-d_6 is reported together with the quantitative estimation of the NOE enhancements. The protons not mentioned in the discussion are omitted for clarity.

Anion-binding studies were performed by means of ^{1}H-NMR titrations in DMSO-d_6. In these experimental conditions no broadening of the NH signals was observed, as expected. The EQNMR program[34] was used to calculate stability constants from the ^{1}H-NMR titration curves obtained fitting the data to a 1:1 binding model. As shown in *Table 2.2* moderately high stability constants were observed for the adducts formation between **L**[1] and the anions considered with the highest value of K_a = 1203 M^{-1} for acetate. However, the affinity of **L**[1] towards anions is lower than that observed with symmetric bis-indolylureas[9] and symmetric and asymmetric carbazolylureas.[14]

This is probably due to the fact that only two of the three NHs available in **L**^{1} are effectively interacting with the anionic substrate. During ^{1}H-NMR titrations, in fact, we noticed that of the three NH groups of **L**^{1} only two (namely the N2–H2 and the N4–H4A) were shifted downfield upon addition of anions as shown in *Figure 2.17* in the case of acetate.

Table 2.2 Equilibrium constants (K_a/M^{-1}) for the reactions of **L**^{1} and **L**^{2} with the tetrabutylammonium anion salts considered (HCO_3^- was used as tetraethylammonium salt) in DMSO-d_6 at 300 K. All errors estimated to be ≤10% (except for chloride for which the error is estimated to be 21%)

Anion	L^{1}	L^{2}
F^-	deprot.	deprot.
Cl^-	12	no interaction
CH_3COO^-	1203	no interaction
$C_6H_5COO^-$	634	no interaction
HCO_3^-	282	no interaction
$H_2PO_4^-$	n.d	no interaction

The N3–H3A resulted unaffected by the addition of all the anions considered, indicating its involvement in the intramolecular hydrogen bond with N1. As observed in $CDCl_3$, also in DMSO-d_6 the C8–H8A is also affected by the presence of anions.

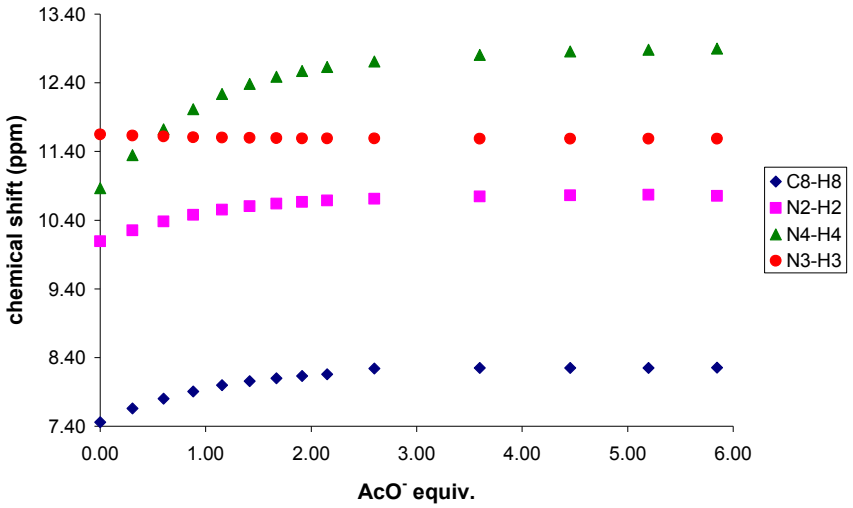

Figure 2.17 ^{1}H-NMR titration curves of **L**^{1} (0.005 M) with tetrabutylammonium acetate (0.075 M) in DMSO-d_6.

As we observed the most interesting results with acetate we decided to perform a detailed NMR study of **L**^{1} in the presence of this anion in order to understand the conformational changes experienced by the receptor and the nature of the complex.

Following the same procedure adopted in the absence of the anion, the most populated conformer for **L**^{1} in the presence of one equivalent of acetate was computed on the basis of the ^{1}H-NMR noesy experiments. It is interesting to note that the 2D-NOESY cross-peaks pattern resulted to be comparable to that obtained in the absence of acetate, indicating that the conformational changes induced by the anion are not dramatic. Violations of the

experimental NOEs have never been observed in all of these three cases and the N3−H3A···N1 intramolecular H-bond was always present. In particular, three different possible complexes have been hypothesised, all of which are, at least in principle, compatible with the 1:1 binding model derived from the titration curves (Figure 2.18). First, one acetate molecule might coordinate to the N2**–**H2A, the N4**–**H4A and the C8−H8A hydrogens of the same **L**^{1} molecule (*Figure 2.18a*). Second, two acetate molecules could coordinate to two **L**^{1}s, thus forming a duplex, by bridging analogous N-H groups, i.e. one of the acetates coordinating both the N2**–**H2As and the C8−H8As, while the other both the N4**–**H4As (*Figure 2.18b*). Lastly, the duplex could be formed by two acetate molecules coordinating different N-H groups from two **L**^{1}s (*Figure 2.18c*).

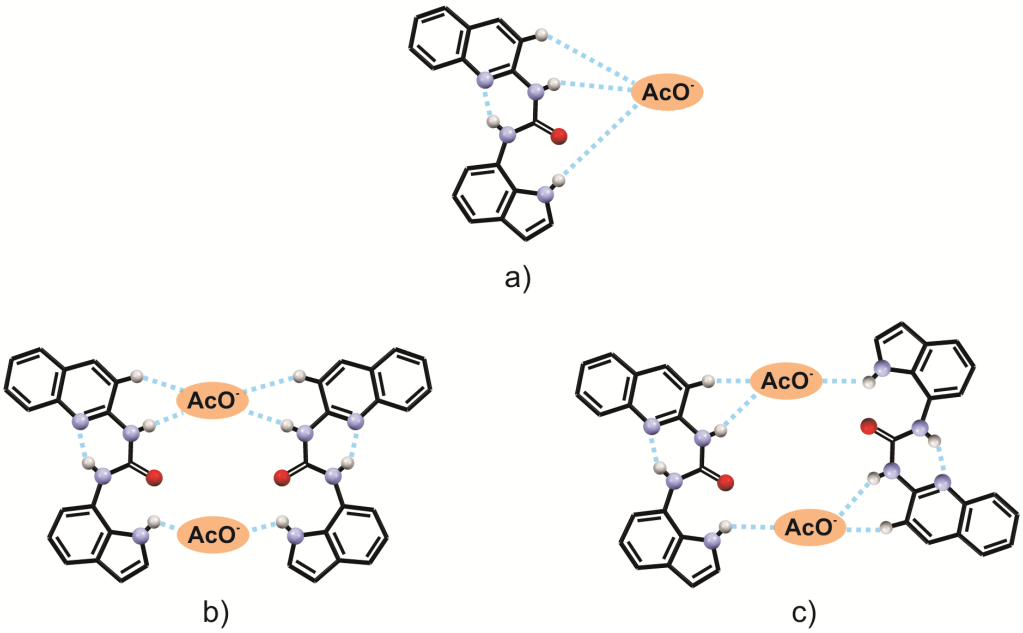

Figure 2.18 Proposed coordination modes of **L**^{1} with acetate.

Correspondingly, the most populated conformer obtained in each of the cases showed the same values for the N1−N2−C10−O1 and N4−N3−C10−O1 dihedral angles, ca. -136° and -67°, respectively. Thus, compared to the conformer obtained in the absence of anion (see *Figure 2.17*), while the tilt angle of the quinoline moiety remains almost comparable (due to the presence of the aforementioned intramolecular H**–**bond), that of the indole changes dramatically. *Figure 2.19* shows the average structure of **L**^{1} in the presence of one equivalent of acetate together with the quantitative estimation of the different NOE enhancements.

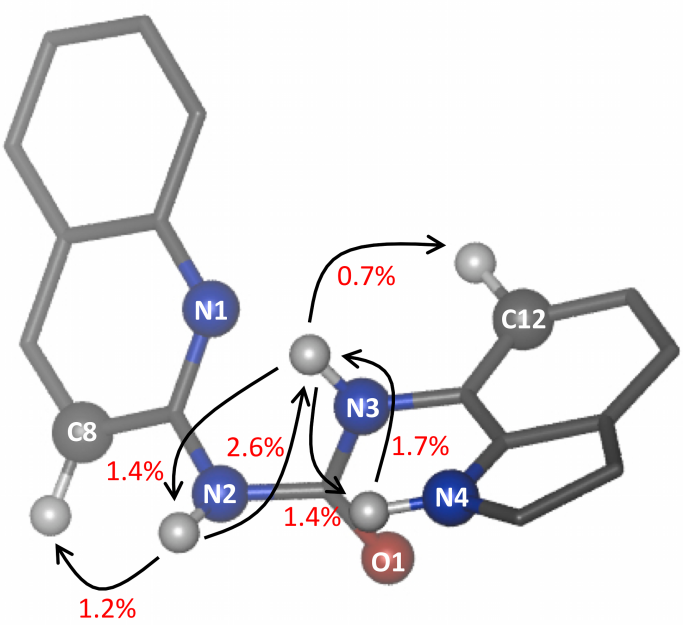

Figure 2.19 The most populated conformation adopted in solution by $\mathbf{L^1}$ in the presence of acetate calculated on the basis of the experimental NOEs in DMSO-d_6 is reported together with the quantitative estimation of the NOE enhancements. The protons not mentioned in the discussion are omitted for clarity.

Similarly to what was observed in the absence of the acetate, N2–H2A and N4–H4A have almost the same distance from N3–H3A. However, in the presence of acetate, the inter–HN NOE enhancements are higher than the H2A–H8A and the H3A–H12A ones. These observations further confirmed the structural change induced by the presence of the acetate, which, as shown in Figure 2.19, resulted in all the three HNs being located on the same side of the molecule. Finally, a deeper analysis of the ^{1}H chemical shift values obtained in the absence and in the presence of the acetate, allowed for discriminating between the three proposed binding possibilities. Indeed, not only the chemical shift of the N2–H2A, N4–H4A and C8–H8A protons changed, as said, but the C5–H5A, C7–H7A resonances also slightly shifted, while all the other signals remained unaffected. First, this is clearly not compatible with the model of one acetate molecule coordinating a unique $\mathbf{L^1}$. The formation of a supramolecular assembly like those in *Fig. 2.18b* and *Fig. 2.18c*, on the other hand, provides a valid explanation. Infact, while the shifts for N2–H2A, N4–H4A and C8–H8A can be explained considering the coordination of the anion, only the approaching of a second molecule of $\mathbf{L^1}$ involved in the supramolecular assembly, might affect the chemical shift of the C5–H5A and C7–H7A protons. The radial distribution functions were computed for all of the aromatic ring hydrogens of one $\mathbf{L^1}$ molecule with respect to all the carbons of the other.

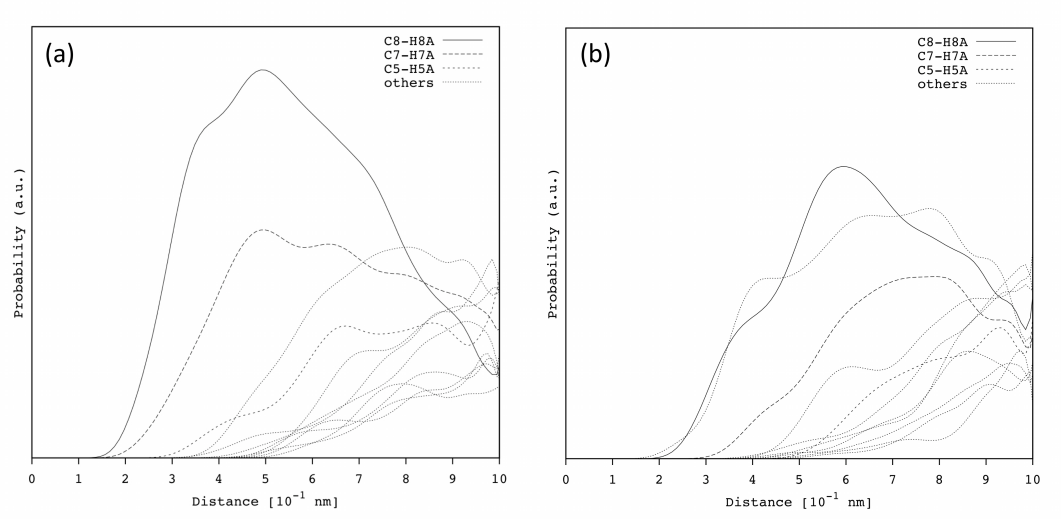

Figure 2.20 Radial distribution function for all the aromatic ring hydrogens for **L^1** in the antisymmetric (Fig. 2.19c) (a) and symmetric (Fig. 2.19b) (b) duplexes. All the distribution functions have been smoothed with a Bézier spline.

Definitely, among the two assemblies tentatively simulated, only the second one (see Fig. 2.18c) resulted to have the C5–H5A and C7–H7A protons as the closest atoms to the second **L^1** molecule. For the sake of clarity, *Figure 2.21* shows the most representative calculated configuration for this supramolecular assembly.

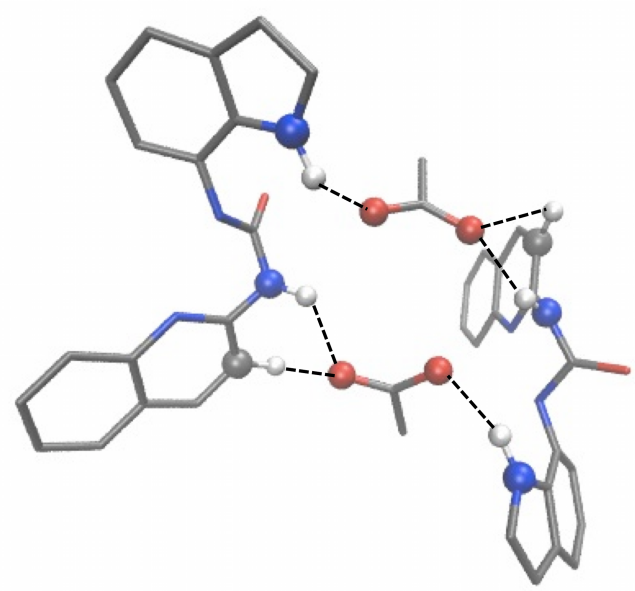

Figure 2.21 The most representative calculated configuration for two **L^1** and two interacting acetate molecules in the assembly formed in DMSO-d_6.

The proposed binding mode has never been observed, to the best of our knowledge, in indole containing ureas, both symmetric and asymmetric, with anions.

As shown in *Table 2.2* fluoride causes deprotonation of the receptor with a colour change in the solution from colourless to yellow and a change in the fluorescence emission with the formation of a new luminescence band in the visible region (see *Fig. 2.22*). The addition of dihydrogenphosphate causes the loss of the signal of the N2-H2A in the ^{1}H-NMR titration: this could be ascribed to a deprotonation or to a strong

binding. However, the interaction with this anion is not accompanied by a change of the photophysical properties of the system.

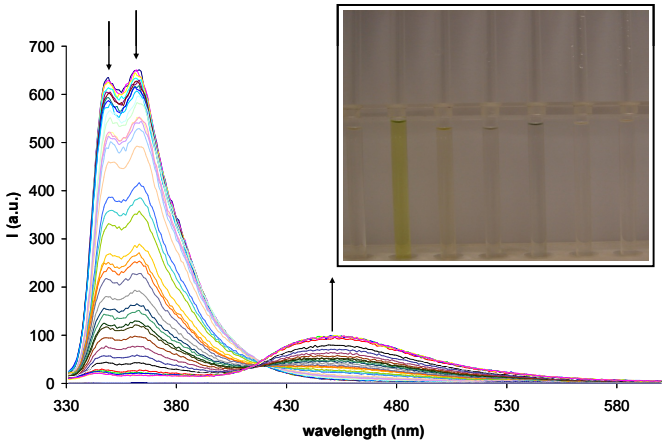

Figure 2.22 Changes in the fluorescence spectra of **L**^{1} ($1.27 \cdot 10^{-5}$ M) upon addition of increasing amounts of TBAF (2.5 x 10^{-2} M) in DMSO. Inset: Colour change of **L**^{1} (0.005 M) upon addition of five anion equivs. (0.075 M) in DMSO. From left to right: **L**^{1}, F^-, AcO^-, Cl^-, BzO^-, HCO_3^- and $H_2PO_4^-$.

Experimental evidence suggests that **L**^{2} adopts a (*E*,*Z*) conformation in solution, too. Infact, we observed negligible changes (see Fig. 2.24) in the ^{1}H-NMR spectrum of **L**^{2} in DMSO-d_6 upon addition of anions (except for fluoride that causes deprotonation without any change, however, in the absorption or emission properties of the system).

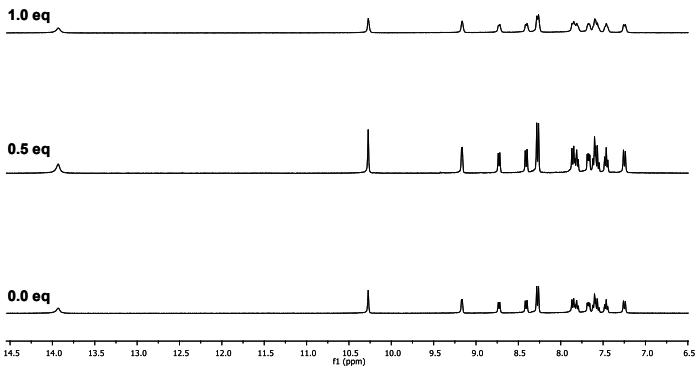

Figure 2.23 ^{1}H-NMR stack plot of a DMSO-d_6 solution of **L**^{2} (0.005 M) upon addition of tetrabutylammonium acetate (0.075 M) in DMSO-d_6 at 298 K.

Interestingly, the signal of one of the two ureidic NHs of the free **L**^{2} is far downfield (13.93 ppm) compared to the analogous **L**^{1} that falls at 11.64 ppm, and to the analogous symmetric bis-indolylurea that falls at 8.63 ppm[7c] suggesting that this NH is involved into an even stronger intramolecular hydrogen bond in solution compared to that observed for **L**^{1}; moreover, its chemical shift is concentration independent as observed in the compound *N*,*N*′-2,di-pyridilurea (for this compound the urea NH signal falls at 12.80 ppm in $CDCl_3$; we could not perform a ^{1}H-NMR experiment on **L**^{2} in $CDCl_3$ due to the very low solubility of the molecule in this solvent).[35] All this is consistent with **L**^{2} assuming an (*E*,*Z*) conformation in solution with one ureidic NH being strongly intramolecularly hydrogen

bonded as observed for **L[1]**. However, in this case, the absence of the indole group as hydrogen bond donor does not allow the interaction with anions as there would be only one hydrogen able to bind the guests via hydrogen bond.

2.5 Conclusion

In conclusion we have shown that when designing an anion receptor it is fundamental to consider the possibility of intra-molecular hydrogen bonds formation.
The indole moiety has demonstrated to be very useful for anion binding for the presence of the NH group that can act as an efficient hydrogen bond donor towards anionic substrates. In the case of **L[1]**, where an indole group has been replaced by a quinoline, the presence of an AD couple strongly stabilises the *anti* (*E,Z*) conformation even in the presence of anions. This favours the formation of a supramolecular architecture in solution in which two molecules of **L[1]** cooperate to bind anions in an unusual fashion compared to that observed in similar symmetric and asymmetric indole-containing ureas. In contrast, **L[2]** in which the indole moieties were replaced by quinolines, no interaction with anions is observed, thus confirming the crucial role played by indoles in designing neutral receptors for anion recognition.

2.6 Experimental

All reactions were performed in oven-dried glassware under a slight positive pressure of nitrogen. 2-quinolinecarbonyl azide,[1] and 7-aminoindole[2] were synthesised following a literature procedure. ^{1}H-NMR (400 MHz) and ^{13}C NMR (100 MHz, 126 MHz) spectra were determined on a Varian INOVA-400 spectrometer, and Varian INOVA-500 spectrometer. Chemical shifts for ^{1}H NMR are reported in parts per million (ppm), calibrated to the residual solvent peak set, with coupling constants reported in Hertz (Hz). The following abbreviations are used for spin multiplicity: s = singlet, d = doublet, t = triplet, m = multiplet. Chemical shifts for ^{13}C NMR are reported in ppm, relative to the central line of a septet at δ = 39.52 ppm for deutero-dimethylsulfoxide. Infrared (IR) spectra were recorded on a NICOLET 5700 FT-IR spectrophotometer and reported in wavenumbers (cm^{-1}). Microanalytical data were obtained using a Fisons EA CHNS-O instrument (*T* = 1000 °C). Fluorescence spectra were recorded on a Cary Eclypse spectrofluorimeter. All solvents and starting materials were purchased from commercial sources where available.
^{1}H spectra were acquired using a 6.7 μs pulse (90°), 1 s delay time, 1 s acquisition time and a spectral width of 5 kHz. ^{1}H-^{1}H correlation TOCSY experiments were recorded over the same spectral window as ^{1}H one-dimensional spectra, using 2048 complex points and

sampling each of the 512 increments with 64 scans with 250 ms spin-lock using the MLEV-17 mixing scheme. The same acquisition parameters have been applied for the acquisition of the NOESY experiments with 200 ms mixing time. Selective DPFGSE (Double Pulse Field Gradient Spin-Echo) one-dimensional noesy[3] has been performed with the same acquisition parameters as for simple ^{1}H spectra with 512 scans and 200 ms mixing time. In order to correct for sources of relaxation other than the dipolar one giving the noe enhancement, the so-called PANIC (Peak Amplitude Normalization for Improved Cross-relaxation) method was applied.[4] The intensity of each noe peak was divided by that of the inverted resonance in the same spectrum, thus providing a normalized noe enhancement. Generally speaking, this kind of transient NOE experiments, on the whole, usually give smaller NOE enhancements than are normally observed in the steady-state like experiments. However, this was the method of choice since it has been shown how the artefacts typically generated by difference NMR spectroscopy are eliminated, and how it is possible to measure NOE enhancements of as little as 0.02%.
Proton NMR titrations were performed by adding aliquots of the putative anionic guest (as the TBA salt, 0.075 M) in a solution of the receptor (0.005M) in DMSO-d_6/0.5% water to a solution of the receptor (0.005M).
Structure calculations were performed using the simulated annealing molecular dynamics algorithm implemented in DYNAMO (http://spin.niddk.nih.gov/NMRPipe/dynamo). The temperature was increased to 4000 K in 1000 initialization steps, then kept constant for 4000 steps, and finally slowly decreased to 0 K during the 20000 steps cooling stage. Gromos-53a6 force field parameters were obtained through the ProDrg server (http://davapc1.bioch.dundee.ac.uk/prodrg/).
The radial distribution functions have been computed through the software VMD[5] by selecting each of the aromatic ring protons of one **L^1** molecule involved in the duplex, on one hand, and all of the aromatic carbons of the other molecule, on the other. Results for the two proposed supramolecular assemblies (Fig. 2.18b and 2.18c) are shown in Figure 2.20.

2.6.1 Synthetic procedure

Synthesis of 1-(1H-indol-7-yl)-3-(quinolin-2-yl)urea (L^1)

A solution of 2-quinolinecarbonyl azide (0.1 g, 0.505 mmol) in anhydrous toluene (20 ml) was refluxed under N_2 for 4h to induce rearrangement into isocyanate. 7-aminoindole (0.06 g, 0.454 mmol) was then added and the resulting mixture was refluxed for 24h. A grey precipitate was formed, filtered and was left stirring in CH_2Cl_2 overnight. The solution was then filtered and the filtrate was concentrated in vacuum to give a light brown solid, which was washed with MeOH to give the desired compound as a white solid. Yield 29% (0.04g, 0.132 mmol) M.p.: 220°C; ^{1}H-NMR (400 MHz, DMSO-d_6, 298 K): δH 6.47-6.49 (m, 1H); 7.01 (t, J=7.6 Hz, 1H); 7.20 (d, J = 7.2, 1H); 7.30-7.50 (m, 4H); 7.70 (t, J = 7.6 Hz, 1H); 7.84 (d, J= 8.4 Hz, 1H); 7.89 (d, J=8 Hz, 1H);8.32 (d, J=8.8 Hz, 1H); 10.12 (s,

1H, NH); 10.89 (s, 1H, NH); 11.67(s, 1H, NH). ^{13}C-NMR (100 MHz, DMSO-d_6, 298 K) δC 101.65, 113.60, 115.14, 116.84, 119.06, 122.73, 124.39, 124.51, 125.63, 126.51, 127.76, 129.49, 129.73, 130.20, 138.73, 144.98, 152.46, 152.89. IR (KBr, cm^{-1}) ν = 3382 (br, NH indole stretching), 3255 (br, NH urea stretching),1649 (s, CO stretching). Crystals suitable for X-ray diffraction analysis were obtained by slow evaporation from a 1:1 mixture of DCM and MeOH resulting in a solvate phase (**L^1**α). Elemental analysis found (calculated for $C_{21}H_{26}N_4O_4$): C 63.45 (63.30); H 6.52 (6.58); N 14.11 (14.06). A further crystallization experiment carried out in the presence of tetrabutylammonium acetate from MeOH/THF 2:1 resulted in a non-solvated phase of the free receptor **L^1** (**L^1**β).
Elemental analysis found (calculated for $C_{18}H_{14}N_4O$): C 71.49 (71.51); H 4.66 (4.67); N 18.55 (18.53).

Synthesis of (1-(quinolin-2-yl)-3-(quinolin-8-yl)urea) (L^2)

A solution of 2-quinolinecarbonyl azide (0.1 g, 0.505 mmol) in toluene anhydrous (20 ml) was refluxed under N_2 for 4h to induce rearrangement into isocyanate. 8-aminoquinoline (0.65 g, 0.454 mmol) was then added and was refluxed overnight. The reaction mixture was filtered to give the desired product as a white solid. Yield 63% (0.09g, 0.286 mmol). M.p. <250°C; ^{1}H-NMR (400 MHz, DMSO-d_6, 298 K): δH 7.29 (d, J= 8.8 Hz, 1H); 7.50 (t, J=7.2 Hz, 1H); 7.58-7.72 (m, 3H); 7.83-7.90 (m, 2H); 8.31 (d, J=8.4 Hz, 2H); 8.44 (d, J= 8.4 Hz, 1H); 8.76 (d, J= 6.8 Hz, 1H); 9.18-9.21 (m, 1H); 10.30 (s, 1H, NH); 13.96 (s, 1H, NH). ^{3}C-NMR (126 MHz, DMSO-d_6, 298 K) δC 113.29, 115.80, 120.80, 122.03, 124.25, 124.48, 126.43, 127.17, 127.70, 128.06, 130.35, 136.29, 136.50, 138.53, 138.67, 145.13, 148.71, 151.97, 152.47. IR (KBr, cm^{-1}) ν = 3358 (br, NH indole stretching), 3220 (br, NH urea stretching), 1685 (s, CO stretching).
Crystals suitable for X-ray diffraction analysis were obtained by slow evaporation from DMSO. Elemental analysis: found (calculated for $C_{19}H_{14}N_4O$): C 72.59 (72.60); H 4.51 (4.49); N 17.81 (17.77).

2.6.2. Crystallographic Data

$L^1\alpha$

Diffractometer: *Nonius KappaCCD* area detector (ϕ scans and ω scans to fill *asymmetric unit*). Cell determination: DirAx[5] **Data collection:** Collect[6]. **Data reduction and cell refinement:** *Denzo*[7]. Absorption correction: Sheldrick, G. M. SADABS - Bruker Nonius area detector scaling and absorption correction - V2.10 **Structure solution:** *SHELXS97*[8]. **Structure refinement:** *SHELXL97* (G. M. Sheldrick (1997), University of Göttingen, Germany).

Special details: Hydrogens were located in the difference map and then placed in idealised positions and refined using a riding model. PLAT601_ALERT_2_B Structure Contains Solvent Accessible VOIDS of 101 A^3. Electron density peaks centred around the 3-fold axes could not be sensible modelled as solvent and the SQUEEZE algorithm was applied[9] from within the platon software[10]. The solvents used for crystallisation were DCM and MeOH.

$L^1\beta$ and L^2

Diffractometer: *Rigaku AFC12* goniometer equipped with an enhanced sensitivity (HG) *Saturn724+* detector mounted at the window of an *FR-E+ SuperBright* molybdenum rotating anode generator with HF *Varimax* optics (100µm focus). **Cell determination, Data collection, Data reduction and cell refinement & Absorption correction**: CrystalClear-SM Expert 2.0 r7 (Rigaku, 2011) , **Structure solution**: SHELXS97[8]. S**tructure refinement**: SHELXL97 (G. M. Sheldrick (1997), University of Göttingen, Germany).

Special details: All hydrogen atoms were placed in idealised positions and refined using a riding model.

Table 2.3. Crystal data and structure refinement details.

	$L^1\alpha$	$L^1\beta$	L^2
Empirical formula	$C_{21}H_{26}N_4O_4$	$C_{18}H_{14}N_4O$	$C_{19}H_{14}N_4O$
Moiety formula	$C_{18}H_{14}N_4O$,3(CH_3OH)	$C_{18}H_{14}N_4O$	$C_{19}H_{14}N_4O$
Formula weight	302.33	302.33	314.34
Crystal system	Trigonal	Orthorhombic	Monoclinic
Space group	*R*–3	$Pna2_1$	$P2_1/c$
a /Å	32.989(7)	22.003(4)	8.0410(17)
b /Å	32.989(7)	7.1308(14)	19.459(4)
c /Å	7.098(2)	18.677(4)	18.998(4)
α / º	90.00	90.00	90.00
β / º	90.00	90.00	94.696(3)
γ / º	90.00	90.00	90.00
V /Å^3	6689(3)	2930.5(9)	2962.6(11)
T / K	100(2)	100(2)	100(2)
Crystal shape	Needle	Slab	Plate
Crystal size / m^3	0.20 × 0.03 × 0.02	0.22 × 0.10 × 0.03	0.12 × 0.10 × 0.04
Colour	colourless	colourless	colourless
Z	18	8 (Z' = 2)	8 (Z' = 2)
θ range for data collection	2.96 – 25.02°	3.00 – 25.03°	2.54 – 31.28
Index ranges	$-38 \le h \le 18$, $0 \le k \le 39$, $0 \le l \le 8$	$-19 \le h \le 26$, $-5 \le k \le 8$, $-22 \le l \le 21$	$-11 \le h \le 11$, $-27 \le k \le 27$, $-13 \le l \le 27$
Reflections collected	2613	12023	16289
Independent reflections	2613 [R_{int} = 0.0000]	2677 [R_{int} = 0.1016]	8526 [R_{int}=0.0333]
Completeness	99.6 % (θ = 25.02°)	99.7 % (θ = 25.03°)	99.0 % (θ = 27.50°)
Absorption correction	Semi–empirical from equivalents	Semi–empirical from equivalents	Semi–empirical from equivalents
Max. and min. transmission	0.9982 and 0.9826	0.9973 and 0.9806	0.9964 and 0.9891
Refinement method	Full-matrix least-squares on F^2	Full-matrix least-squares on F^2	Full-matrix least-squares on F^2
Data / restraints / parameters	2613 / 0 / 208	2677 / 1 / 415	8526 / 0 / 433
Goodness-of-fit on F^2	1.164	1.044	1.119
Final *R* indices [$F^2 > 2\sigma(F^2)$]	*R1* = 0.0712, *wR2* = 0.1314	*R1* = 0.0624, *wR2* = 0.1016	*R1 = 0.0793, wR2 = 0.1604*
***R* indices (all data)**	*R1* = 0.0990, *wR2* = 0.1421	*R1* = 0.0859, *wR2* = 0.1085	*R1 = 0.1121, wR2 = 0.1788*
Largest diff. peak and hole	0.256 and –0.227 e Å^{-3}	0.239 and –0.302 e Å^{-3}	0.294 and –0.243 e Å^{-3}

Table 2.4 Hydrogen bonds [Å and °].

Phase	*D*–H···*A*	*d*(*D*–H)	*d*(H···*A*)	*d*(*D*···*A*)	∠(*DHA*)
	N2–H2A···O1^{i}	0.88	1.98	2.845(3)	169
$L^1\alpha$	N3–H3A···N1	0.88	1.90	2.657(3)	143
	N4–H4A···O1	0.88	1.98	2.686(3)	136
	N102–H102···O201	0.88	2.13	2.997(5)	169
	N103–H103···N101	0.88	1.90	2.654(6)	142
$L^1\beta$	N104–H104···O101	0.88	1.97	2.687(5)	137
	N202–H202···O101	0.88	1.97	2.848(5)	172
	N203–H203···N201	0.88	1.92	2.682(6)	143
	N204–H204···O201	0.88	2.00	2.703(5)	137
	N2–H902...N4	0.88	1.98	2.697(2)	138
L^2	N3–H903...O2	0.88	1.95	2.830(2)	175
	N6–H906...N8	0.88	1.98	2.694(3)	137
	N7–H907...O1	0.88	2.03	2.888(2)	166

i (-x+5/3, -y+1/3, -z- 2/3)

2.6.3 XPac procedure

The XPac methodology[11] enables the comparison of structures of related molecules. The analysis is carried out by using the XPac software, which allow the identification of any geometrically similar assemblies of molecules occurring in two or more structures. These common molecular arrangements are referred to as Supramolecular Constructs (SCs), and may have different dimensions: 0-D (discrete molecular assemblies), 1-D (similar stacks or rows of molecules), 2-D (similar sheets, packed differently) and 3-D (isostructurality, isomorphism and pseudo-isostructurality).

The analysis was carried out using all the atoms of the quinoline substituted group as Corresponding Ordered Set of Points (COSP) (see Figure 2.24), and medium filter parameters (a:10, p:14, d:1.5). For each similarity identified the software provide a dissimilarity index (χ)[12] (see table 2.4).

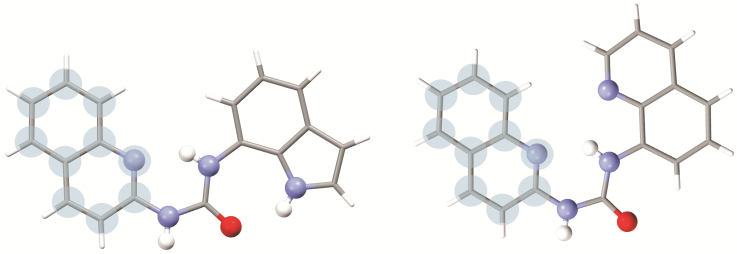

a) b)

Figure 2.24 Corresponding Ordered Set of Points (COSP) chosen for the analysis and represented for L^1(a) and L^2 (b).

Table 2.4. Dissimilarity index (χ) for the three comparisons $L^1\alpha$- $L^1\beta$, $L^1\alpha$- L^2 and $L^1\beta$- L^2.

	$L^1\alpha$	$L^1\beta$	L^2
$L^1\alpha$	-	1D χ = 8.9	1D χ = 8.3
$L^1\beta$	-	-	1D χ = 12.7

2.6.4. L^1 Dimerization constant determination by ^1H dilution experiment and variable temperature experiments in $CDCl_3$

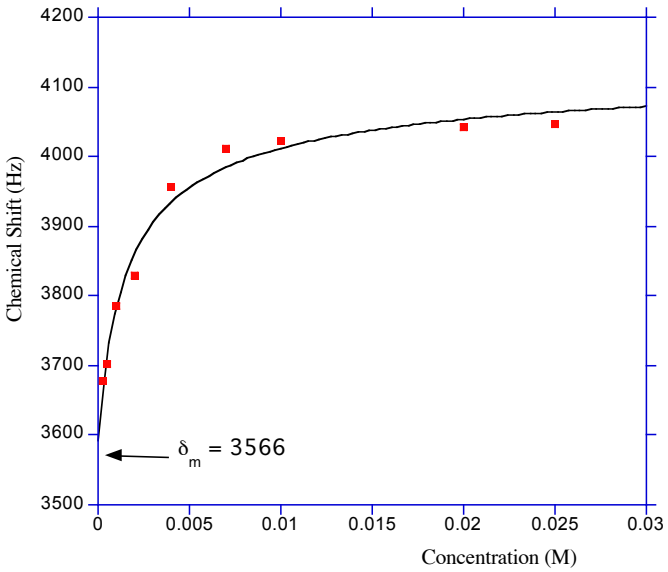

Figure 2.25. Determination of the dimerization constant (K_{dim}) of **L^1** in $CDCl_3$ at 298 K, experimental data square points. Standard nonlinear least-squares regression analysis of the concentration-dependent chemical shift changes of proton N2-H2A The equation used for fitting the data had the form $d_{obsd} = d_m + (d_{dim} - d_m)\,[1 + 8K_{dim}[A_0]]^{½} - 1] / [1 + 8K_{dim}[A_0]]^{½} + 1]$ where $[A_0]$ is the total concentration, d_{obsd} , d_m , d_{dim}, are the observed, monomer, and dimer chemical shift, respectively.[15]

K_{dim} = 430 ± 37 M^{-1} R = 0.9892

2.6.5. Proton NMR titration fitting

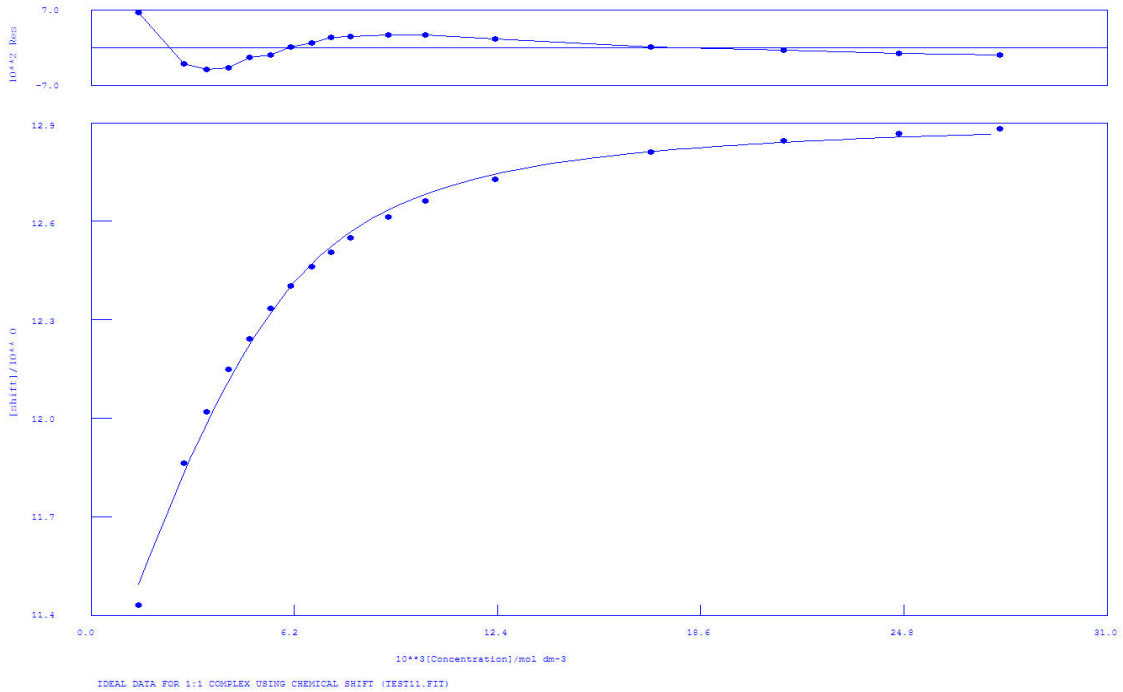

Calculations by WinEQNMR Version 1.20 by Michael J. Hynes
Program run at 09:48:53 on 06/07/2011
IDEAL DATA FOR 1:1 COMPLEX USING CHEMICAL SHIFT (TEST11.FIT)
Reaction: M + L = ML
FILE: TEST11.FIT
IDEAL DATA: K1 = 63.091; DELTA M = 20.0; DELTA ML = 120.0
File prepared by M. J. Hynes, October 22 2000

NO.	A	PARAMETER	DELTA	ERROR	CONDITION	DESCRIPTION
1	1	1.20340E+03	2.000E-01	1.244E+02	7.581E+00	K1
2	1	1.10926E+01	2.000E-01	3.048E-02	2.313E+00	SHIFT M
3	1	1.29822E+01	1.000E+00	2.099E-02	5.323E+00	SHIFT ML

Figure 2.26. ^{1}H-NMR of **L^{1}** with TBAAcO in DMSO-d_6/0.5%H_2O. The fitting has been obtained following the indolic NH.

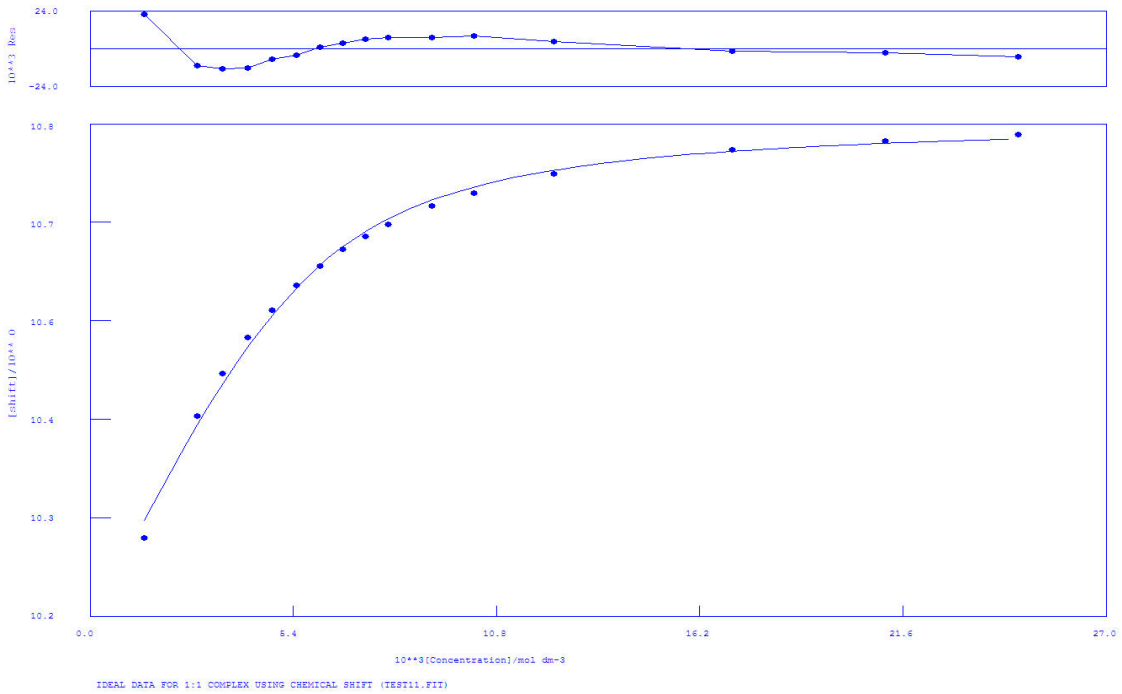

Calculations by WinEQNMR Version 1.20 by Michael J. Hynes
Program run at 09:08:59 on 06/13/2011

IDEAL DATA FOR 1:1 COMPLEX USING CHEMICAL SHIFT (TEST11.FIT)
Reaction: M + L = ML
FILE: TEST11.FIT
IDEAL DATA: K1 = 63.091; DELTA M = 20.0; DELTA ML = 120.0
File prepared by M. J. Hynes, October 22 2000

NO.	A	PARAMETER	DELTA	ERROR	CONDITION	DESCRIPTION
1	1	1.21636E+03	2.000E-01	1.394E+02	8.514E+00	K1
2	1	1.01842E+01	2.000E-01	1.034E-02	2.195E+00	SHIFT M
3	1	1.08061E+01	1.000E+00	8.433E-03	6.451E+00	SHIFT ML

Figure 2.27. ^{1}H-NMR of **L^{1}** with TBAAcO in DMSO-d_6/0.5%H_2O. The fitting has been obtained following the ureidic NH adjacent to the indole group.

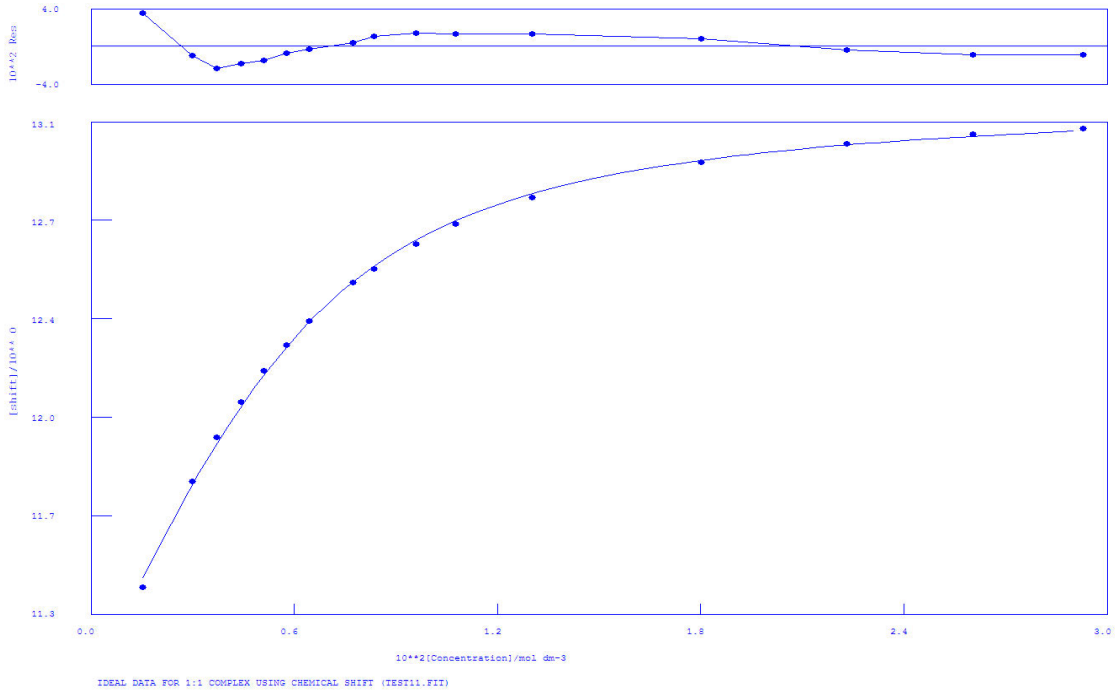

Calculations by WinEQNMR Version 1.20 by Michael J. Hynes
Program run at 10:40:20 on 06/07/2011

IDEAL DATA FOR 1:1 COMPLEX USING CHEMICAL SHIFT (TEST11.FIT)
Reaction: M + L = ML
FILE: TEST11.FIT
IDEAL DATA: K1 = 63.091; DELTA M = 20.0; DELTA ML = 120.0
File prepared by M. J. Hynes, October 22 2000

NO.	A	PARAMETER	DELTA	ERROR	CONDITION	DESCRIPTION
1	1	6.34266E+02	2.000E-01	3.280E+01	1.035E+01	K1
2	1	1.10338E+01	2.000E-01	1.708E-02	2.872E+00	SHIFT M
3	1	1.32032E+01	1.000E+00	1.518E-02	6.663E+00	SHIFT ML

Figure 2.28. ^{1}H-NMR of **L^{1}** with TBABzO in DMSO-d_6/0.5%H_2O. The fitting has been obtained following the indolic NH.

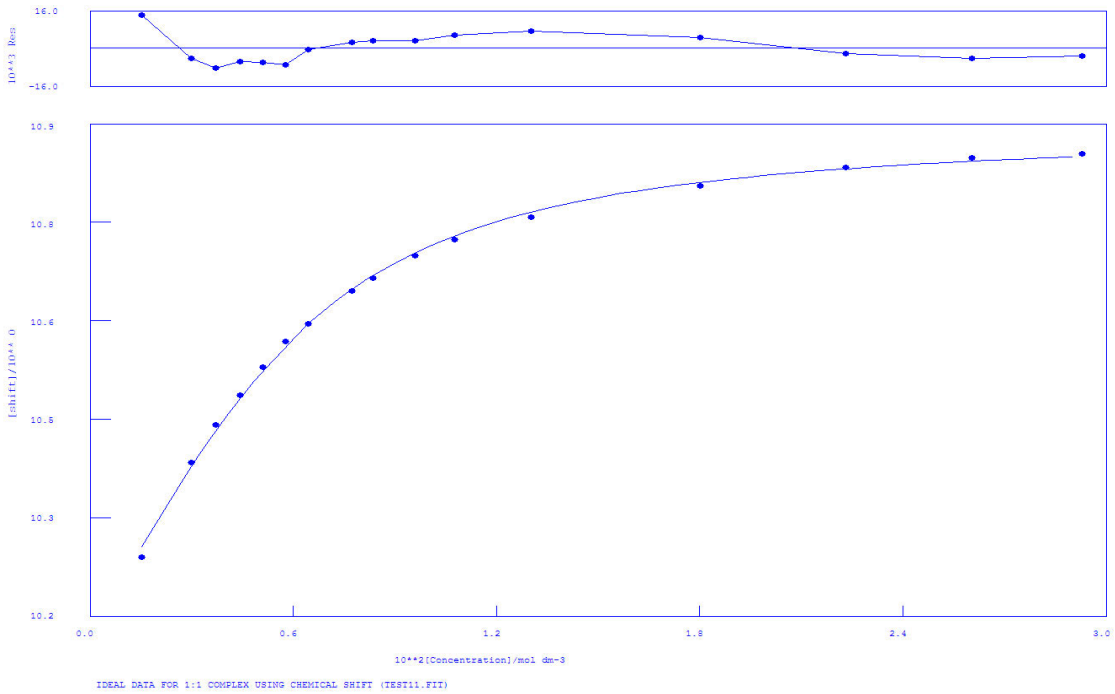

Calculations by WinEQNMR Version 1.20 by Michael J. Hynes
Program run at 12:39:37 on 06/14/2011

IDEAL DATA FOR 1:1 COMPLEX USING CHEMICAL SHIFT (TEST11.FIT)
Reaction: M + L = ML
FILE: TEST11.FIT
IDEAL DATA: K1 = 63.091; DELTA M = 20.0; DELTA ML = 120.0
File prepared by M. J. Hynes, October 22 2000

NO.	A	PARAMETER	DELTA	ERROR	CONDITION	DESCRIPTION
1	1	6.19952E+02	2.000E-01	3.787E+01	1.048E+01	K1
2	1	1.01636E+01	2.000E-01	6.813E-03	2.816E+00	SHIFT M
3	1	1.09005E+01	1.000E+00	6.267E-03	6.870E+00	SHIFT ML

Figure 2.29. ^{1}H-NMR of **L^{1}** with TBABzO in DMSO-d_6/0.5%H_2O. The fitting has been obtained following the ureidic NH adjacent to the indole group.

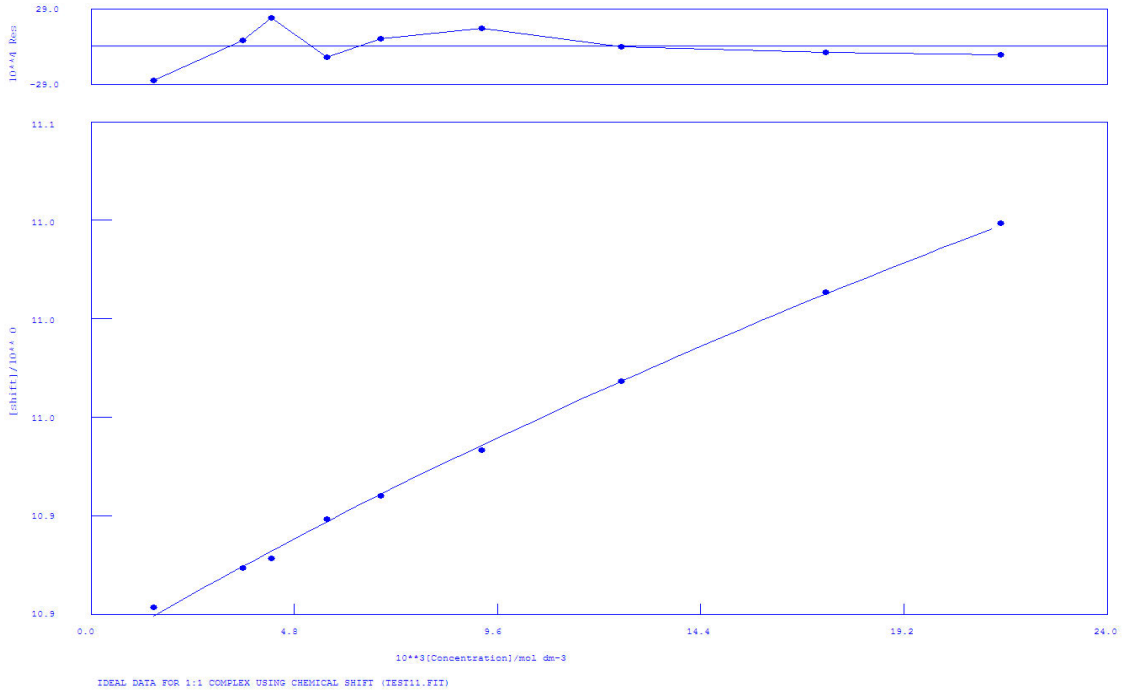

IDEAL DATA FOR 1:1 COMPLEX USING CHEMICAL SHIFT (TEST11.FIT)
Reaction: M + L = ML
FILE: TEST11.FIT
IDEAL DATA: K1 = 63.091; DELTA M = 20.0; DELTA ML = 120.0
File prepared by M. J. Hynes, October 22 2000

NO.	A	PARAMETER	DELTA	ERROR	CONDITION	DESCRIPTION
1	1	1.20095E+01	2.000E-01	2.574E+00	5.177E+02	K1
2	1	1.08884E+01	2.000E-01	1.301E-03	4.901E+00	SHIFT M
3	1	1.15419E+01	1.000E+00	1.080E-01	4.682E+02	SHIFT ML

Figure 2.30. ^{1}H-NMR of **L^{1}** with TBACl in DMSO-d_6/0.5%H_2O. The fitting has been obtained following the indolic NH.

References

1. Sessler, J. L., Gale, P. & Cho, W.-S. *Anion Receptor Chemistry*. (Royal Society of Chemistry, 2006). doi:10.1039/9781847552471

2. Gale, P. a. & Gunnlaugsson, T. Supramolecular chemistry of anionic species themed issue. *Chem. Soc. Rev.* **39,** 3595 (2010).

3. Caltagirone, C. & Gale, P. A. Anion receptor chemistry: highlights from 2007. *Chem. Soc. Rev.* **38,** 520–63 (2009).

4. Gale, P. A., García-Garrido, S. E. & Garric, J. Anion receptors based on organic frameworks: highlights from 2005 and 2006. *Chem. Soc. Rev.* **37,** 151–90 (2008).

5. Jeffrey, G. A. & Saenger, W. *Hydrogen Bonding in Biological Structures*. (Springer Berlin Heidelberg, 1991). doi:10.1007/978-3-642-85135-3

6. Sessler, J. L. & Jayawickramarajah, J. Functionalized base-pairs: versatile scaffolds for self-assembly. *Chem. Commun. (Camb).* 1939–49 (2005). doi:10.1039/b418526a

7. Mateos-Timoneda, M. A., Crego-Calama, M. & Reinhoudt, D. N. Supramolecular chirality of self-assembled systems in solution. *Chem. Soc. Rev.* **33,** 363–72 (2004).

8. Cooke, G. & Rotello, V. M. Methods of modulating hydrogen bonded interactions in synthetic host-guest systems. *Chem. Soc. Rev.* **31,** 275–286 (2002).

9. Caltagirone, C. *et al.* 1,3-Diindolylureas: high affinity dihydrogen phosphate receptors. *Chem. Commun. (Camb).* 3007–9 (2008). doi:10.1039/b806238b

10. Caltagirone, C., Hiscock, J. R., Hursthouse, M. B., Light, M. E. & Gale, P. A. 1,3-diindolylureas and 1,3-diindolylthioureas: anion complexation studies in solution and the solid state. *Chemistry* **14,** 10236–43 (2008).

11. Gale, P. A. *et al.* Anion-anion proton transfer in hydrogen bonded complexes. *Chem. Asian J.* **5,** 555–61 (2010).

12. Gale, P. A., Hiscock, J. R., Jie, C. Z., Hursthouse, M. B. & Light, M. E. Acyclic indole and carbazole-based sulfate receptors. *Chem. Sci.* **1,** 215 (2010).

13. Caltagirone, C. *et al.* Metal-induced pre-organisation for anion recognition in a neutral platinum-containing receptor. *Chem. Commun. (Camb).* 6279–81 (2009). doi:10.1039/b912942a

14. Hiscock, J. R., Caltagirone, C., Light, M. E., Hursthouse, M. B. & Gale, P. A. Fluorescent carbazolylurea anion receptors. *Org. Biomol. Chem.* **7,** 1781–3 (2009).

15. SAIKACHI, H., KITAGAWA, T., NASU, A. & SASAKI, H. Synthesis of Furan Derivatives. LXXXVII. Kinetic Studies of the Thermal Curtius Rearrangement of 2-Benzofuroyl Azide and Related Compounds. *Chem. Pharm. Bull. (Tokyo).* **29,** 237–244 (1981).

16. Chien, C.-H. *et al.* Substituent effects on pyrid-2-yl ureas toward intramolecular hydrogen bonding and cytosine complexation. *J. Org. Chem.* **69,** 1866–71 (2004).

17. McGhee, A. M., Kilner, C. & Wilson, A. J. Conformer independent heterodimerisation of linear arrays using three hydrogen bonds. *Chem. Commun.* 344 (2008). doi:10.1039/b712603d

18. Singha, N. C. & Sathyanarayana, D. N. 1H and 13C NMR spectra of some unsymmetric N,N'-dipyridyl ureas: spectral assignments and molecular conformation. *J. Chem. Soc. Perkin Trans. 2* 157–162 (1997). doi:10.1039/a606800f

19. Desiraju, G. R. Supramolecular Synthons in Crystal Engineering—A New Organic Synthesis. *Angew. Chemie Int. Ed. English* **34,** 2311–2327 (1995).

20. Gelbrich, T. & Hursthouse, M. B. A versatile procedure for the identification, description and quantification of structural similarity in molecular crystals. *CrystEngComm* **7,** 324 (2005).

21. Gelbrich, T., Threlfall, T. L. & Hursthouse, M. B. XPac dissimilarity parameters as quantitative descriptors of isostructurality: the case of fourteen 4,5'-substituted benzenesulfonamido-2-pyridines obtained by substituent interchange involving CF3/I/Br/Cl/F/Me/H. *CrystEngComm* **14,** 5454 (2012).

22. Hursthouse, M. B., Montis, R. & Tizzard, G. J. Intriguing relationships and associations in the crystal structures of a family of substituted aspirin molecules. *CrystEngComm* **12,** 953 (2010). b) Montis, R. & Hursthouse, M. B. Surprisingly complex supramolecular behaviour in the crystal structures of a family of mono-substituted salicylic acids. *CrystEngComm* **14,** 5242 (2012).c) Montis, R. & Hursthouse, M. B. Crystalline adducts of some substituted salicylic acids with 4-aminopyridine, including hydrates and solvates: contact and separated ionic complexes with diverse supramolecular synthons. *CrystEngComm* **14,** 7466 (2012).d) Montis, R. & Hursthouse, M. B. Surprisingly complex supramolecular behaviour in the crystal structures of a family of mono-substituted salicylic acids. *CrystEngComm* **14,** 5242 (2012).

23. Spek, A. L. Platon/PLUTON. *Acta Crystallogr. Sect. A Found. Crystallogr.* **A46, C34,** (1990).

24. Van der Sluis, P. & Spek, A. L. BYPASS: an effective method for the refinement of crystal structures containing disordered solvent regions. *Acta Crystallogr. Sect. A Found. Crystallogr.* **46,** 194–201 (1990).

25. Gutowsky, H. S. & Saika, A. Dissociation, Chemical Exchange, and the Proton Magnetic Resonance in Some Aqueous Electrolytes. *J. Chem. Phys.* **21,** 1688 (1953).

26. Schneider, H.-J. & Dürr, H. *Frontiers in supramolecular organic chemistry and photochemistry*. (1991). The dimerization constant was obtained by fitting the 1H-NMR data into a modified dimerization equation with the program Kaleidagraph.

27. Kessler, H. Conformation and Biological Activity of Cyclic Peptides. *Angew. Chemie Int. Ed. English* **21,** 512–523 (1982).

28. Hamuro, Y., Geib, S. J. & Hamilton, A. D. Oligoanthranilamides. Non-Peptide Subunits That Show Formation of Specific Secondary Structure. *J. Am. Chem. Soc.* **118,** 7529–7541 (1996).

29. Makuc, D., Hiscock, J. R., Light, M. E., Gale, P. A. & Plavec, J. NMR studies of anion-induced conformational changes in diindolylureas and diindolylthioureas. *Beilstein J. Org. Chem.* **7,** 1205–14 (2011).

30. Macura, S., Huang, Y., Suter, D. & Ernst, R. . Two-dimensional chemical exchange and cross-relaxation spectroscopy of coupled nuclear spins. *J. Magn. Reson.* **43,** 259–281 (1981).

31. Stott, K., Stonehouse, J., Keeler, J., Hwang, T.-L. & Shaka, A. J. Excitation Sculpting in High-Resolution Nuclear Magnetic Resonance Spectroscopy: Application to Selective NOE Experiments. *J. Am. Chem. Soc.* **117,** 4199–4200 (1995).

32. Oostenbrink, C., Villa, A., Mark, A. E. & van Gunsteren, W. F. A biomolecular force field based on the free enthalpy of hydration and solvation: the GROMOS force-field parameter sets 53A5 and 53A6. *J. Comput. Chem.* **25,** 1656–76 (2004).

33. Hu, H. & Krishnamurthy, K. Revisiting the initial rate approximation in kinetic NOE measurements. *J. Magn. Reson.* **182,** 173–7 (2006).

34. Hynes, M. J. EQNMR: a computer program for the calculation of stability constants from nuclear magnetic resonance chemical shift data. *J. Chem. Soc. Dalt. Trans.* 311 (1993). doi:10.1039/dt9930000311

35. Corbin, P. S., Zimmerman, S. C., Thiessen, P. A., Hawryluk, N. A. & Murray, T. J. Complexation-induced unfolding of heterocyclic ureas. Simple foldamers equilibrate with multiply hydrogen-bonded sheetlike structures. *J. Am. Chem. Soc.* **123,** 10475–88 (2001).

Chapter 3 : A new family of bis-ureidic receptors

Chapter 3: A new family of bis-ureidic receptors

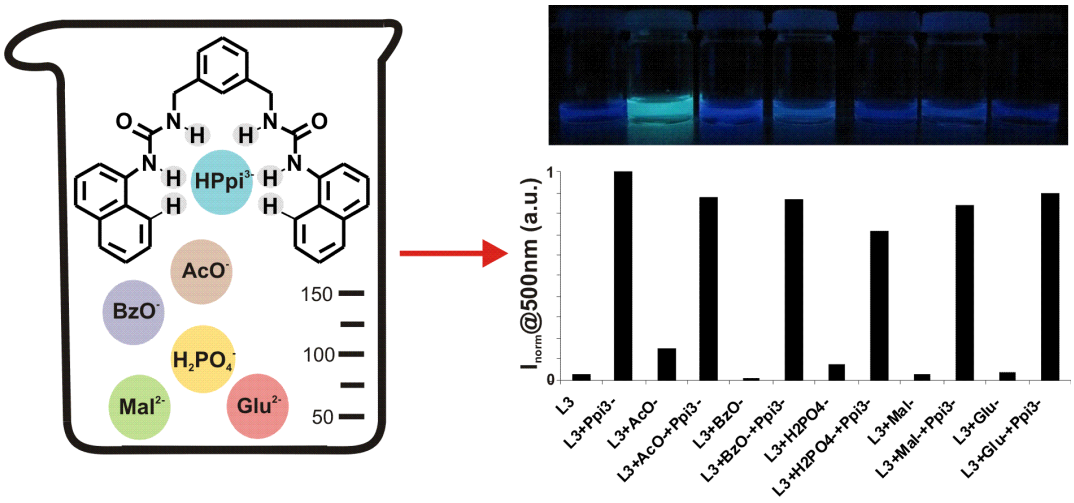

3.1 introduction

The anion recognition and sensing has recently received considerable attention because of the central role played by anions in biological, industrial, and environmental processes.[1, 2,3,4,5]

Colorimetric chemosensors for anions are of particular interest because they can allow a naked eye recognition and sensing, while fluorescent chemosensors offer many advantages over other types of chemosensors in terms of sensitivity, response time, and cost. Among anions, pyrophosphate (Ppi, this acronyms with omitted charges will be used throughout this paper when referring to pyrophosphate independently of its protonation degree) is a biologically important target because it is the product of ATP hydrolysis under cellular conditions.[6,7] Moreover, the detection of pyrophosphate has become important in cancer research as telomerase (a biomarker for cancer diagnosis) activity is measured by evaluating the amount of Ppi generated in the PCR amplification of the telomerase elongation product.[8] Furthermore, the high level of Ppi in synovial fluids is correlated to calcium pyrophosphate dehydrate disease (CPPD), a rheumatologic disorder.[9,10] For these reasons the detection and discrimination of pyrophosphate, especially by means of fluorescent chemosensors, has attracted the attention of chemists over the last 20 years.[11]

One of the first examples has been reported by Czarnick in 1994.[12] Czarnick's system **1** is based on an anthracene derivative bearing polyamine pendant arms and it is able to bind Ppi^{2-} in water at pH 7 and to discriminate pyrophosphate over phosphate. The chemosensor **135** binds pyrophosphate with fluorescence enhancement, and 1:1 complexation occurred with K_d = 2.9 µM at pH 7. This chemosensor shows a 2200-fold increase in pyrophosphate/phosphate discrimination. The fluorescent chemosensor **135**

was also used for a real-time assays of pyrophosphate hydrolysis catalyzed by inorganic pyrophosphatase.

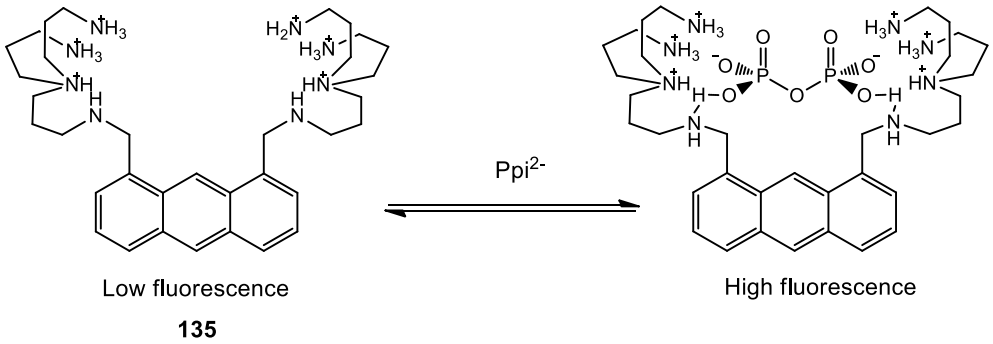

135

Scheme 3.1 Fluorescent chemosensor **135** with Ppi^{2-}.

Different strategies can be used to design chemosensors for anions (and Ppi, in particular) involving, for example excimer formation,[13,6] and displacement approach.[14,15,16] In particular, different systems containing metal ion complexes,[17,18,19] or guanidinium[20,21] or imidazolium[22,23,24] based platforms have been synthesised and studied. Also neutral receptors containing pyrroles able to recognise pyrophosphate both in aqueous[25,26] and non-aqueous environments[27] have been successfully developed. However, less examples of urea/thiourea containing receptors for pyrophosphate recognition have been reported in the literature so far.[28,29] In this contest we decided to synthesise and study a new family of bis-ureidic receptors based on 1,3-bis(aminomethyl)benzene and 2,6-bis(aminomethyl)pyridine. In 1995 Umezawa and co-workers[30,31] reported a series of bis-urea and bis-thiourea receptors **136**-**138** obtained by reaction of 1,3-bis(aminomethyl)benzene with butyl isocyanate, butyl isothiocyanate and phenyl isothiocyanate which showed a high dihydrogenphosphate selectively over other anions ($H_2PO_4^-$ > CH_3COO^- > Cl^- > HSO_4^- > NO_3^- > ClO_4^-).[30] Binding studies were carried out by ^{1}H-NMR titration in DMSO-d_6 and the highest association constant was found for receptor **138** (K_a=4600 M^{-1}). It was also found that the bis-thiourea **137** can bind dihydrogenphosphate more strongly than its bis-urea analogue **136** (K_a =820 and 110 M^{-1} respectively) probably due to the higher acidity of the thiourea groups than the ureas, making the thioureas a much stronger hydrogen bond donor. The binding selectivity was explained in terms of the complex geometry and the basicity of the guest anions.

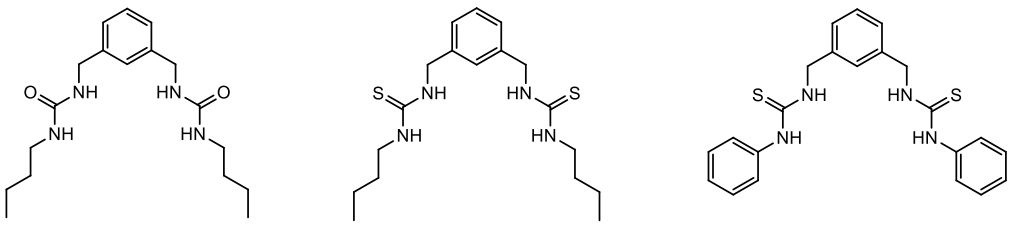

136 **137** **138**

The same group also studied the application of the phenyl-substituted thiourea **138** as ionophore for an anion selective electrode with remarkable sulfate selectivity.

More recently Sellergren and co-workers studied the recognition of tyrosine phosphorilated peptides by the vinylphenyl urea derivative of 1,3-bis(aminomethyl)benzene.[32]

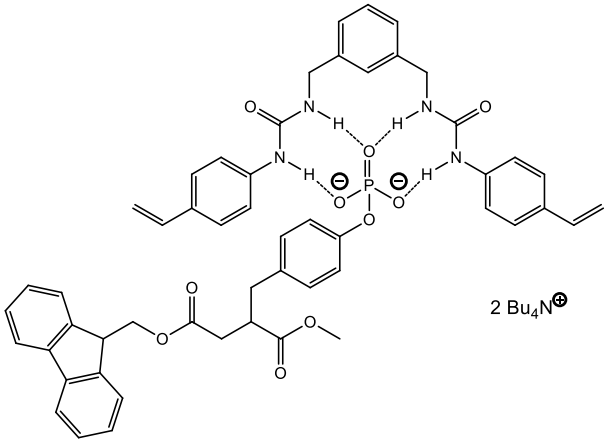

139

Scheme 3.2 complex formed between receptor **139** and Fmoc-pTyrOMe

However, to the best of our knowledge, examples of colorimetric and fluorimetric chemosensors based on 1,3-bis(aminomethyl)benzene or 2,6-bis(aminomethyl)pyridine platforms have never been reported so far.

3.2 Synthesis

We designed and successfully synthesised **L^3**-**L^8** using the reaction scheme shown on *Scheme 3.3* and *3.4*. In the case of **L^3**-**L^5** the commercially available 1,3-bis(aminomethyl)benzene reacted with the suitable isocyanate (phenyl isocyanate, 2-nitrophenyl isocyanate and 1-naphtyl isocyanate) in dichloromethane at room temperature under nitrogen to give the three receptors in 70-80% yield.

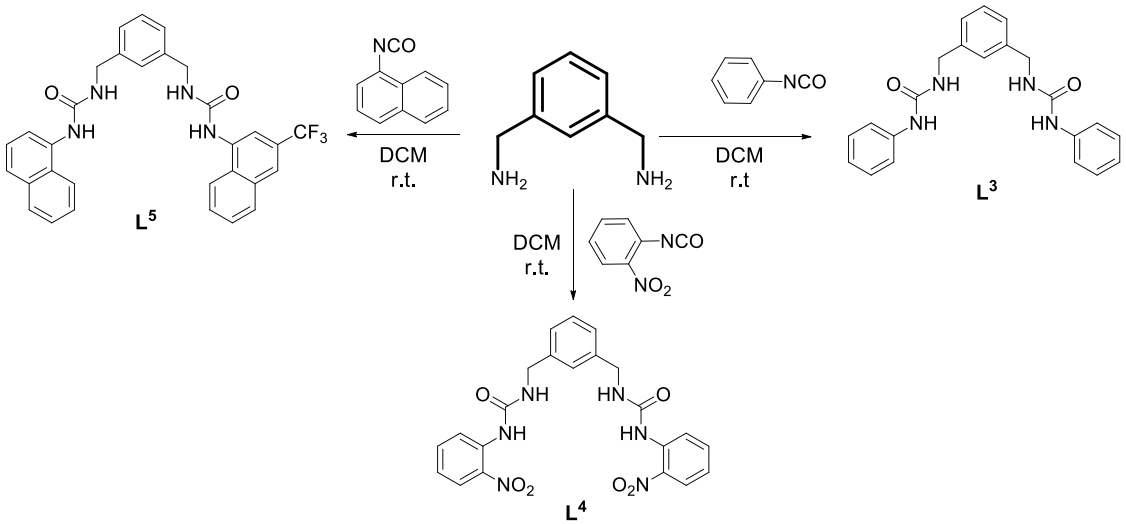

Scheme 3.3 Synthesis of compounds **L^3**-**L^5**

In the case of **L**^{6}-**L**^{8} we first synthesised the 2,6-bis(aminomethyl)pyridine hydrochloridric salt by a Delepine reaction on 2,6-bis(bromomethyl)pyridine obtained from 2,6-bis(hydroxymethyl)pyridine by bromination with HBr and PBr_3.[33] 1,3-bis(aminomethyl)pyridine hydrochloridric salt was reacted with the suitable isocyanate (phenyl isocyanate, 2-nitrophenyl isocyanate and 1-naphtyl isocyanate) in refluxing dichloromethane in the presence of triethylamine to obtain **L**^{6}-**L**^{8} in 40-50% yield.

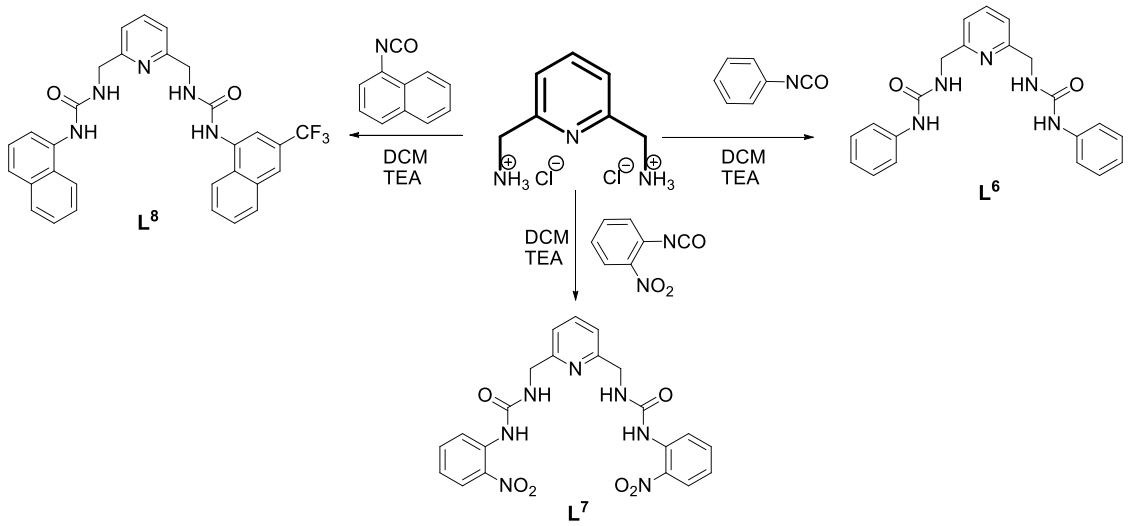

Scheme 3.4 Synthesis of compounds **L**^{6}-**L**^{8}.

In this way we built up a family of ligands comprising two virtually "optically innocent" receptors (**L**^{3} and **L**^{6}), two potential colorimetric sensors (**L**^{4} and **L**^{7}), and two potential fluorimetric sensors (**L**^{5} and **L**^{8}).

3.3 ^{1}H-NMR titrations

Firstly, we performed anion-binding studies by means of ^{1}H-NMR titrations in DMSO-d_6. The EQNMR program[34] was used to calculate stability constants from the ^{1}H-NMR titration curves obtained fitting the data to a 1:1 binding model as shown in *Table 3.1*.

Table 3.1 Equilibrium constants (K_a/M^{-1}) for the reactions of **L**^{3}-**L**^{8} with the tetrabutylammonium salts of the anion considered in DMSO-d_6 at 300 K. All errors estimated to be ≤13%.

Anion	L^{3}	L^{4}	L^{5}	L^{6}	L^{7}	L^{8}
CH_3COO^-	119	88	137	197	121	299
$C_6H_5COO^-$	65	109	78	106	60	88
Glutarate	43	10	20	77	15	30
Malonate	11	<10	<10	<10	<10	<10
$H_2PO_4^-$	484	181	435	698	167	273
HPpi^{3-}	5480	parz. deprot.	>10^{4}	deprot.	deprot.	deprot.

As shown in *Table 3.1* the six receptors showed a medium-low affinity for all the anions considered except for dihydrogen phosphate (in the case of **L**^{6}) and hydrogenpyrophosphate in the case of **L**^{3} and **L**^{5}.
In particular, **L**^{6}-**L**^{8} immediately deprotonated (both ureidic NHs) after the addition of 0.3 equivalents of HPpi^{3-}. **L**^{4}, on the other hand, underwent to a partial deprotonation of the ureidic NHs adjacent to the nitro group (in green in *Figure 3.1*) in the presence of 0.3 equivalents of anion. The signals of the other NHs (red) and of the phenyl CH (orange) progressively shifted downfield until one equiv.of HPpi^{3-}anion was added. Beyond this point also the signal of the ureidic protons adjacent to the aromatic ring disappeared (*Figure 3.1*).

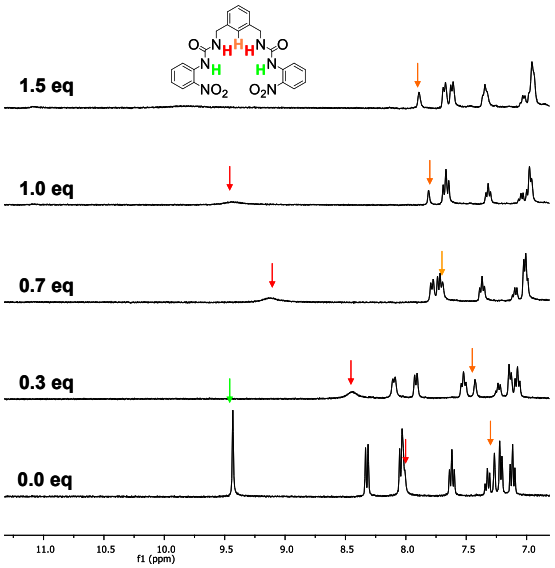

Figure 3.1 ^{1}H-NMR stack plot of a DMSO-d_6 solution of **L**^{4} (0.005 M) upon addition of tetrabutylammonium hydrogenpyrophosphate (0.075 M) in DMSO-d_6.

In the case of **L**^{3} it was possible to follow the downfield shift of the two NHs signals (green and red in *Figure 3.2*) and of the CH phenyl signal (orange) up to the addition of two equivalents of anion. A further excess of anion caused the disappearance of the two NHs signals.

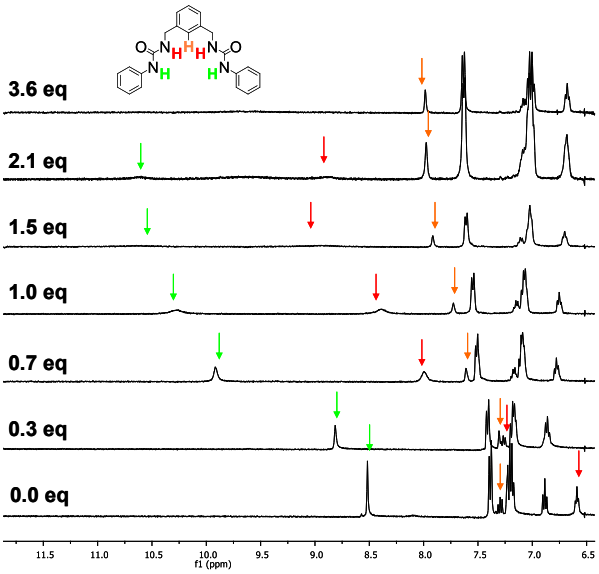

Figure 3.2 ^{1}H-NMR stack plot of a DMSO-d_6 solution of **L^{3}** (0.005 M) upon addition of tetrabutylammonium hydrogenpyrophosphate (0.075 M) in DMSO-d_6.

L^{5} showed a different behaviour compared to **L^{3}** and **L^{4}**. In fact, after addition of 0.3 equivalents of $HPpi^{3-}$ we observed the broadening and the downfield shift of the peak attributed to the NHs adjacent to the naphtilic group (green in *Figure 3.3*); however this signal could be followed until the end of the titration experiment (over five equivalents of anion added). The signal of the other ureidic NHs (red in *Figure 3.3*) also shifted upon addition of the anion without broadening. Differently to what observed with **L^{3}** and **L^{4}**, in the case of **L^{5}** we could not observe a shift of the phenyl CH singlet. Instead, a doublet attributed by ^{1}H-COSY to the napthilic CH pointing towards the pseudo-cavity of the receptor (blue in *Figure 3.3*) considerably shifted downfield upon addition of the anion.

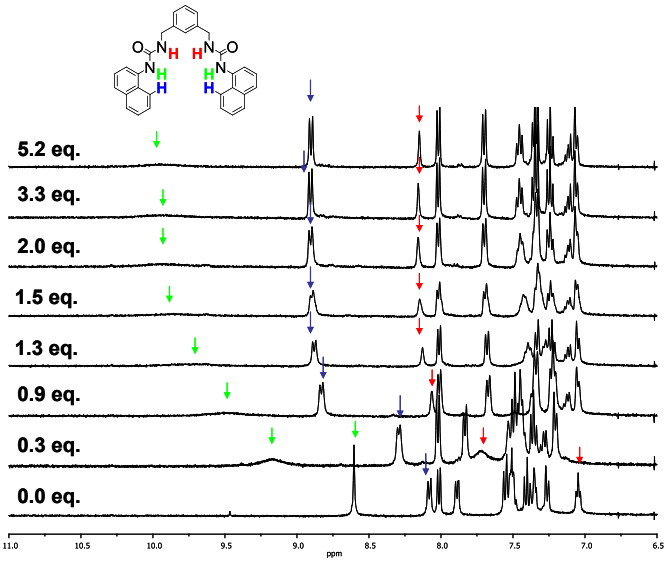

Figure 3.3 ^{1}H-NMR stack plot of a DMSO-d_6 solution of **L^{5}** (0.005 M) upon addition of tetrabutylammonium hydrogenpyrophosphate (0.075 M) in DMSO-d_6.

We also performed titrations of **L^{5}** in the presence of triphospate anion ($P_3O_{10}^{5-}$), AMP^{-} and ADP^{-} (as their sodium salts).

Table 3.2 Equilibrium constants (K_a/M^{-1}) for the reactions of $\mathbf{L^5}$ with tetrabutylammonium salts of hydrogenpyrophosphate, dihydrogen phosphate, acetate and benzoate and the sodium salt of AMP in DMSO-d_6 and DMSO-d_6/0.5%H_2O at 300 K. All errors estimated to be ≤14%

	$HPpi^{3-}$	AMP^-	$H_2PO_4^-$	AcO^-	BzO^-
$\mathbf{L^5}$ **(DMSO-d_6)**	$>10^4$	369	698	137	78
$\mathbf{L^5}$ **(DMSO-d_6/5%H_2O)**	570	35	21	15	11

Only with AMP^- we observed significant interactions (K_a = 369 M^{-1}) while with triphosphate and ADP^- the changes in the ^{1}H-NMR spectrum of $\mathbf{L^5}$ were negligible. The affinity of $\mathbf{L^5}$ for pyrophosphate was also tested in a more competitive solvent mixture i.e. DMSO-d_6/5%H_2O: in these experimental conditions the stability constant calculated for the formation of the 1:1 adduct of $\mathbf{L^5}$ with $HPpi^{3-}$ was 570 M^{-1}. This value is however higher than those calculated for the formation constants of the 1:1 adducts of $\mathbf{L^5}$ with the other anions considered in the same experimental conditions. This interesting behaviour of $\mathbf{L^5}$ could be explained considering the important contribution given by the naphtilic CH in assisting the interaction of the receptor with $HPpi^{3-}$.

An additional proof of the intervention of this proton in anion binding was brought by the X-ray crystal structure obtained for the 1:2 $\mathbf{L^8}$/BzO^- adduct obtained from $\mathbf{L^8}$ in the presence of an excess of tetrabutylammonium benzoate by slow evaporation of ethyl acetate (*Figure 3.4*). In contrast to what observed in solution (see Table 3.1) a complex with a 1:2 stoichiometry was isolated in the solid state where each anion interacts with the receptor via two hydrogen bonds (N1–H901···O3 2.816(4); N2–H902···O4 2.809(4); N4–H904···O5 2.831(4); N5–H905···O6 2.760(4) Å) and via a weaker interaction with the naphtylic CH (C28–H28···O6 3.164 and C2–H2···O3 3.136 Å).

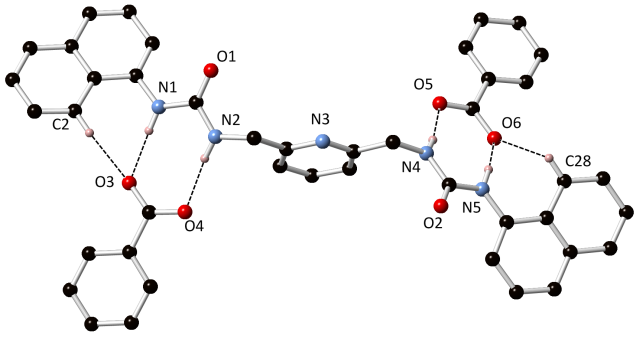

Figure 3.4 X-Ray crystal structure of the $[\mathbf{L^8}(BzO)_2]^{2-}$ adduct showing the main interactions with the numbering scheme adopted. Hydrogen atoms except those involved in hydrogen bonds and tetrabutylammonium counter ions have been omitted for clarity.

3.4 Theoretical calculations

In order to better understand the interactions between pyrophosphate and **L**^{5}, theoretical calculations were carried out. Molecular modelling investigations on the adducts formed by **L**^{3} and **L**^{5} with $HPpi^{3-}$, and by **L**^{5} with $H_2PO_4^-$ and $P_3O_{10}^{5-}$ in 1:1 ligand-to-anion molar ratio have been performed by means of an empirical force field method (AMBER3),[4] evaluating the atomic partial charges at the PM3 semi empirical level of theory[35,36] and using an implicit simulation of solvent environment (ε = 47 Fm^{-1}). Potential energy surface of all the systems has been explored by means of simulated annealing (T = 600 K, equilibration time = 10 ps, run time = 10 ps and cooling time = 10 ps, time step = 1.0 fs). For each studied system, 80 conformations have been sampled.

Two main results can be derived from our molecular modelling investigations: first of all, the binding between the **L**^{5} ligand and the studied substrates is not only due to H-bond interactions. Actually, the number of H-bonds established by the receptors grows with the number of acceptor groups of the anions and with their charge, so that the triphosphate anion gives rise to the same or even higher number of H-bonds with respect to the $HPpi^{3-}$ anion, which forms the most stable adduct with both **L**^{3} and **L**^{5} (see *Figure 3.5*).

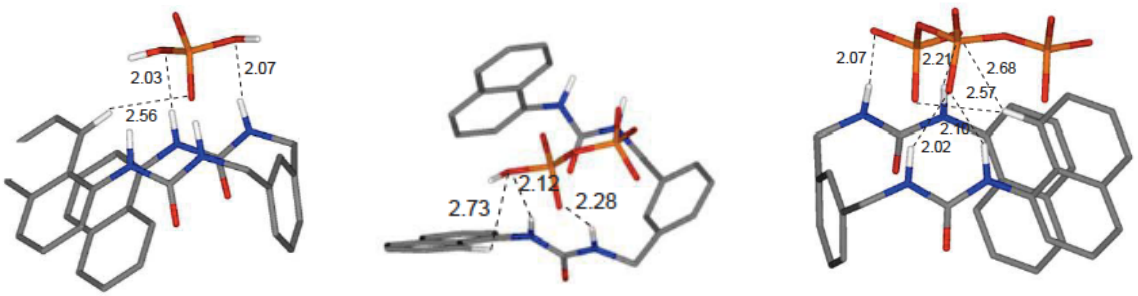

a) b) c)

Figure 5 Lowest energy conformers for **L**^{5} in adduct with a) $H_2PO_4^-$, b) $HPpi_3^-$ and c) $P_3O_{10}^{5-}$.

On the other hand, differently from $P_3O_{10}^{5-}$ and $H_2PO_4^-$, only the $HPpi^{3-}$ ion is capable of fitting into the pseudo cavity defined by the lateral arms of the receptor. As a consequence, entropic effects due to desolvation upon host-guest interactions are supposed to play an important role in determining the observed stability trend.

The second significant result is relative to the comparison of the low energy conformers calculated for the $HPpi^{3-}$/**L**^{3} adduct with those calculated for the $HPpi^{3-}$/**L**^{3} adduct. Actually, in all the conformations calculated for $HPpi^{3-}$/**L**^{3} (*Figure 3.6*) the phenyl groups are oriented in such a way that no interactions are observed between the aromatic protons and the oxygen of pyrophosphate, while in the case of $HPpi^{3-}$/**L**^{5} adduct a CH···O interaction is formed in all low energy conformations calculated (*Figure 3.7*).

[4] Hyperchem release 7.51 for Windows MM System, Hypercube, Inc., Gainesville, FL, 2002

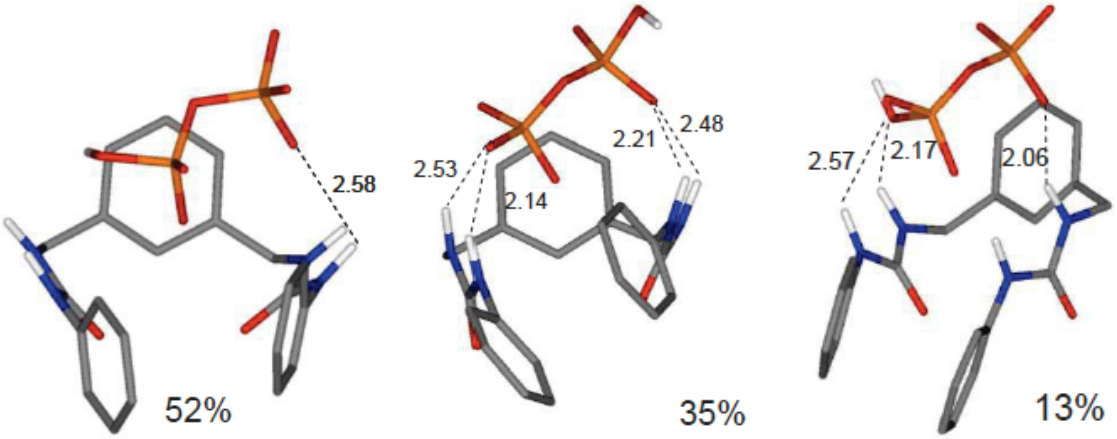

Figure 3.6 Conformers found for $\mathbf{L^3}$ in adduct with $HPpi^{3-}$ with their relative abundances.

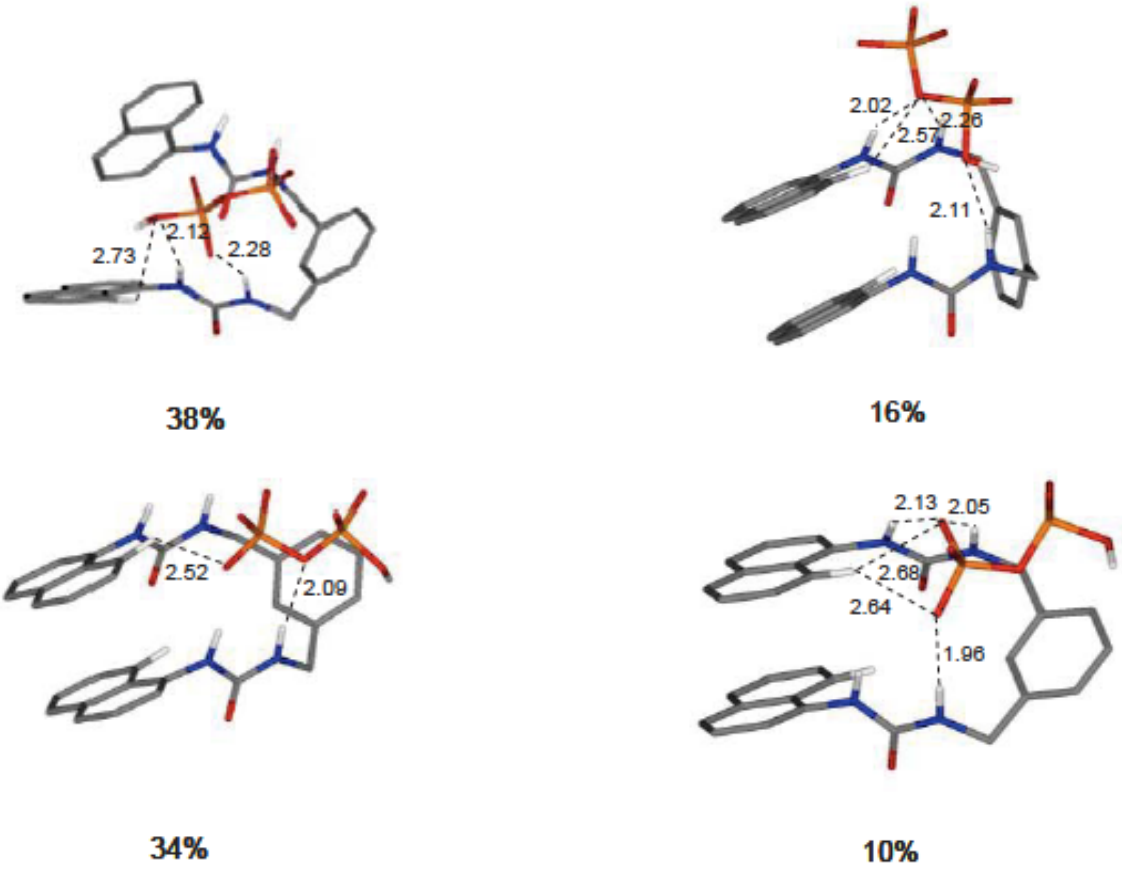

Figure 3.7 Conformers found for $\mathbf{L^5}$ in adduct with $HPpi^{3-}$ with their relative abundances

3.5 UV-Vis spectroscopy

A UV-Vis spectroscopy study was performed in DMSO in order to evaluate the potential application of $\mathbf{L^4}$ and $\mathbf{L^7}$, both containing two nitrophenyl units, as colorimetric sensors for anion recognition. In DMSO $\mathbf{L^4}$ as a free receptor showed an intense band in the UV region at 277 nm (ε = 11760 mol^{-1} cm^{-1} L^{-1}) and one less intense in the visible region at 380 nm (ε = 7260 mol^{-1} cm^{-1} L^{-1}) No significant changes in the UV-Vis spectrum of $\mathbf{L^4}$ were

observed upon addition of acetate, benzoate, glutarate, malonate and dihydrogen phosphate. Only in the case of $HPpi^{3-}$ we observed some remarkable changes. As shown in *Figure 3.8a* upon addition of increasing amounts of the anion we observed the disappearance of the band at 277 nm and the decrease of the band at 380 nm with a concomitant hypsochromic shift of 25 nm, that could be attributed either to the partial deprotonation observed in the ^{1}H-NMR titration or to an interaction via hydrogen bonding. In fact, as it has been recently reported by Gunnlaugsson and co-workers,[37] high concentrations (as those employed during ^{1}H-NMR titrations) could lead to a deprotonation while in more diluted conditions an effective anion binding could be observed. Receptor **L^7** showed only one absorption band at 345 nm (ε = 4460 mol^{-1} cm^{-1} L^{-1}). The addition of $HPpi^{3-}$ caused the formation of two new bands, one intense at 284 nm (ε = 25580 mol^{-1} cm^{-1} L^{-1}) and the other at 490 nm (ε = 5220 mol^{-1} cm^{-1} L^{-1}), as shown in *Figure 3.8b*. This latter could be probably attributed to the full deprotonation of the receptor.[38] In both cases the interaction with $HPpi^{3-}$ could be detected by naked eye with a colour change from yellow (free receptors) to red-orange (receptors in the presence of 1 equivalent of $HPpi^{3-}$) as shown in the inset in *Figures 3.8a* and *3.8b* for **L^4** and **L^7**, respectively.

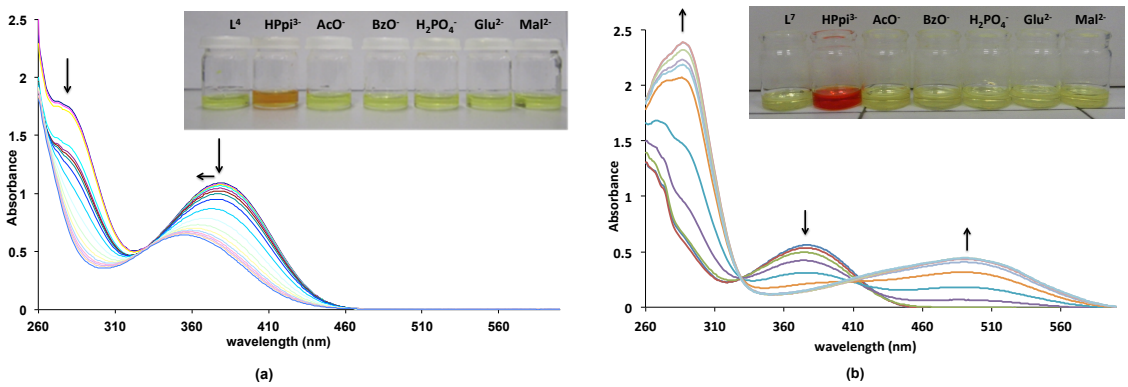

Figure 3.8 Changes in the fluorescence spectra of **L^4** (a) ($1.50\cdot10^{-4}$ M) and **L^7** (b) ($8.5\cdot10^{-5}$ M) upon addition of increasing amounts of $(TBA)_3HPpi$ ($2.5\cdot 10^{-2}$ M) in DMSO. Inset: Colour change of **L^4** (a) and **L^7** (b) (both 0.005 M) upon addition of five anion equivs. (0.075 M) in DMSO. From left to right: **L^4** (a) or **L^7** (b), $HPpi^{3-}$, AcO^-, BzO^-,$H_2PO_4^-$, Glu^{2-}, and Mal^{2-}.

The behaviour of **L^5** and **L^8** towards the chosen set of anions was studied by spectrofluorimetric titrations in DMSO. **L^5** shows an emission band at 380 nm (Φ = 0.46) when excited at 345 nm. This band can be attributed to the emission of a single fragment urea substituted naphthalene according to the data reported in the literature.[39] No significant changes were observed in the presence of all anions except hydrogen pyrophosphate.

Indeed, as shown in Figure 3.10a in the case of **L^5** upon addition of increasing amounts of $HPpi^{3-}$ a quenching of the emission band of the receptor was accompanied by the formation of a new band at 500 nm. This new band could probably originate from the intramolecular interaction in the excited state of two naphthalene moieties. This interaction could be favoured by the presence of the coordinated anion as also suggested by theoretical calculations (see *Figure 3.7*). Competitive studies confirmed

the selectivity of **L**^{5} for HPpi^{3-}.

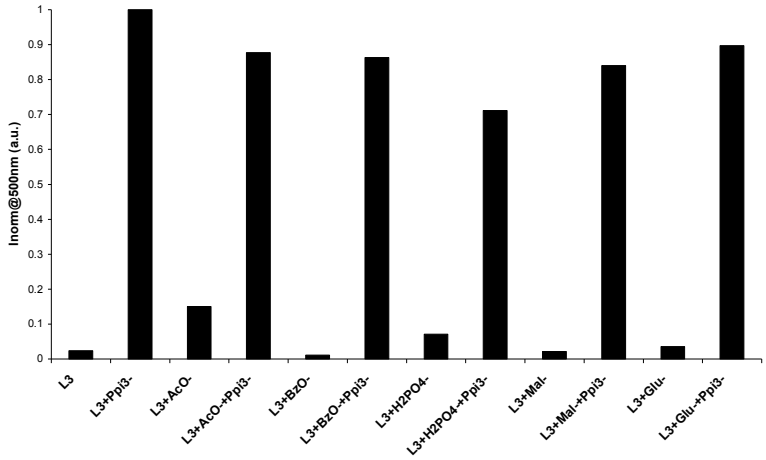

Figure 3.9 Changes in the intensity emission of **L**^{3} ($1.50\cdot10^{-4}$ M) at 500 nm after addition of 10 equivalents of HPpi^{3-} and 20 equivalents of the other anions in DMSO.

A similar behaviour was observed in the case of **L**^{8}. This receptor when excited at 345 nm showed an emission band at 375 nm (Φ = 0.56). Upon addition of HPPi^{3-} we observed the decrease of the band relative to the free receptor and the formation of a band at 495 nm. Also in this case, although the ^{1}H-NMR suggested a deprotonation event, the changes in the fluorescence spectrum of **L**^{8} could be attributed to the binding event (Figure 10b).

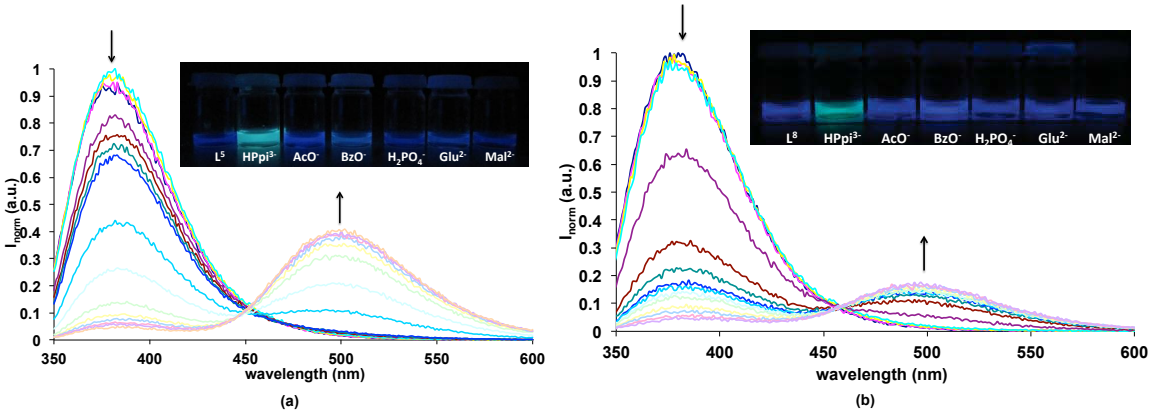

Figure 10 Changes in the fluorescence spectra of **L**^{5} (a) ($1.50\cdot10^{-4}$ M) and **L**^{8} (b) ($8.5\cdot10^{-5}$ M) upon addition of increasing amounts of $(TBA)_3HPpi$ ($2.5\cdot 10^{-2}$ M) in DMSO. Inset: Emission change of **L**^{5} (a) and **L**^{8} (b) (both 0.005 M) upon addition of five anion equivs. (0.075 M) in DMSO. From left to right: **L**^{5} (a) or **L**^{8} (b), HPpi^{3-}, AcO^{-}, BzO^{-},$H_2PO_4^{-}$, Glu^{2-}, and Mal^{2-}.

A further experimental evidence of the binding event *vs.* deprotonation was provided by recording the emission spectra of a 1:1 solution of **L**^{5} and **L**^{8} and TBAOH in DMSO in which we did not observed any emission at around 500 nm (see *Figure 3.11*).

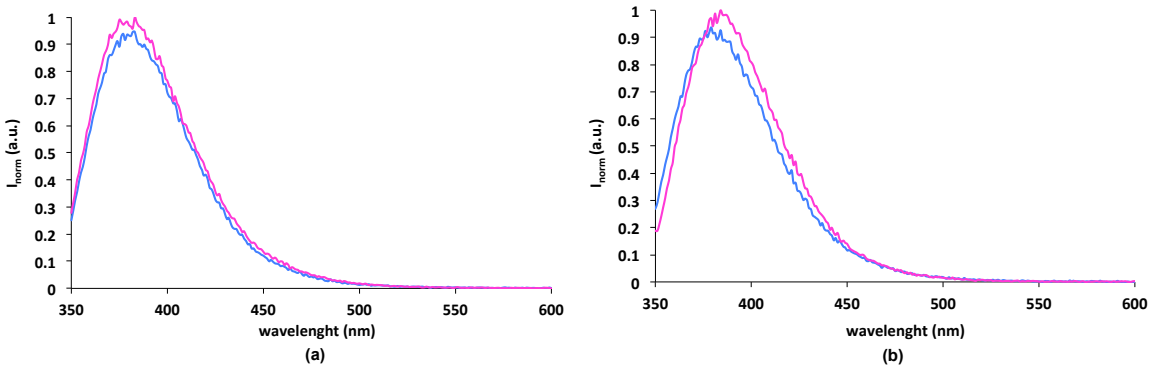

Figure 3.11 a) Emission spectra of $\mathbf{L^5}$ ($1.50\cdot10^{-4}$ M) (pink line) and of $\mathbf{L^5}$ in the presence of 1 equivalent of TBAOH (blue line) in DMSO. b) Emission spectra of $\mathbf{L^8}$ ($8.5\cdot10^{-5}$ M) (pink line) and of $\mathbf{L^8}$ in the presence of 1 equivalent of TBAOH (blue line) in DMSO.

3.6 Conclusion

In conclusion we synthesised a new family of bis-ureidic anion receptors based on the two 1,3-bis(aminomethyl)benzene and 2,6-bis(aminomethyl)pyridine platforms. We have demonstrated that by simply changing the substituents in the pendant ureidic moieties both a colorimetric and a fluorimetric selective sensing of hydrogen pyrophosphate, even at naked eye, can be achieved in DMSO. In particular, in the case of the receptors bearing naphtyl groups pendant arms, both binding and optical fluorimetric selectivity is achieved thanks to the uncommon interaction of an aromatic CH from the fluorophore with the $HPpi^{3-}$ guest.

3.7 Experimental methods

All reactions were performed in oven-dried glassware under a slight positive pressure of nitrogen. ^{1}H-NMR (400 MHz, 500MHz) and ^{13}C NMR (100 MHz, 125MHz) spectra were determined on a Varian INOVA-400 spectrometer, and Varian INOVA-500 spectrometer. Chemical shifts for ^{1}H NMR are reported in parts per million (ppm), calibrated to the residual solvent peak set, with coupling constants reported in Hertz (Hz). The following abbreviations are used for spin multiplicity: s = singlet, d = doublet, t = triplet, m = multiplet . Chemical shifts for ^{13}C NMR are reported in ppm, relative to the central line of a septet at δ = 39.52 ppm for deuterio-dimethylsulfoxide. Infrared (IR) spectra were recorded on a NICOLET 5700 FT-IR spectrophotometer and reported in wavenumbers (cm^{-1}). Microanalytical data were obtained using a Fisons EA CHNS-O instrument (*T* = 1000 °C). Fluorescence spectra were recorded on a Cary Eclypse spectrofluorimeter. All solvents and starting materials were purchased from commercial sources where available. Proton NMR titrations were performed by adding aliquots of the putative anionic guest (as the TBA salt, 0.075 M) in a solution of the receptor (0.005M) in DMSO-d_6/0.5% water to a solution of the receptor (0.005M).

The synthesis of pyridine-2,6-diyldimethanaminium chloride has already been reported in literature.

3.7.1 Synthetic procedure

Synthesis of 1,1'-(1,3-phenylenebis(methylene))bis(3-phenylurea) L^3

A solution of phenyl isocyanate (0.3595g, 3.02mmol) in DCM (10 ml) was added dropwise to the solution of phenyl-1,3- dimethylamine (0.222g, 1.63 mmol) in DCM (20 ml) and was left stirring at ambient temperature under a N_2 atmosphere for 24h. The precipitate was collected by filtration, washed with diethyl ether and dried under reduced pressure to give the desired product as a white solid.

Yield: 80.14**%** (g 0.49g, 1 mmol); M.p.:222-225°C; ^{1}H NMR(400 MHz, DMSO-*d_6*, 298K) δH:4.25 (d, J=5.6 Hz, 4 H); 6.56 (t, J=5.6 Hz, NH, 2H); 6.84 (t, J=7.6 Hz, ArH, 2H); 7.13-7.20(m, ArH, 7H); 7.26 (t, J=7.6 Hz,ArH, 1H); 7.35 (d, J=8 Hz, 4H); 8.49(s, NH, 2H); ^{13}C-NMR(100 MHz, DMSO-*d_6*, 298 K) δ_C 42.77; δ_{ArH} 117.7, 121.1, 125.6, 126.0, 128.3, 128.7, 140.5; δCO 155.21

Synthesis of 1,1'-(1,3-phenylenebis(methylene))bis(3-(2-nitrophenyl)urea) L^4

A solution of 2-nitrophenyl isocyanate (0.4825 g, 2.94 mmol) in 10 ml of DCM was added dropwise to the solution of phenyl-1,3-dimethylamine (0.235 g, 1.47 mmol) in 20 ml of DCM and was stirred at room temperature under a N_2 atmosphere for 24h. The yellow solid formed was isolated by filtration, washed with diethyl ether and dried under vacuum.

Yield: 77.64% (0.53g, 1.1mmol); M.p.:236-240°C; ^{1}H NMR(400 MHz, DMSO-*d6*, 298K) δH:4.32 (d, J=6 Hz, 4 H); 7.12 (t, J=8, ArH, 2H); 7.21 (d, J=7.2, ArH, 2H); 7.27 (s, ArH, 1H); 7.33 (t, J=7.2, ArH, 1H); 7.62 (t, J=8.4, ArH,2H); 8.00-8.06 (m, ArH, NH, 4H); 8.32 (d, J=8.4, 2H); 9.43 (s, NH, 2H); ^{13}C-NMR (100MHz, DMSO-*d6* , 298 K) δ_C 42.94; δ_{ArC} 121.4, 122.4, 125.3, 125.9, 126.2, 128.4, 134.9,135.8,136.8, 139.8; δ_{CO} 154.28.

Synthesis of 1,1'-(1,3-phenylenebis(methylene))bis(3-(naphthalen-1-yl)urea) L^5

1-naphthyl isocyanate (0.5084 g 3.00 mmol) dissolved in DCM (10 ml) was added dropwise to a solution of phenyl-1,3-dimethylamine (0.233g, 1.63mmol) in 20 ml of DCM. The mixture of reaction was allowed to stir for 24h under a N_2 atmosphere at room temperature. The resulting white precipitate was removed by filtration, washed with diethyl ether and dried under vacuum.

Yield: 67.22% (0.52 g, 1.1 mmol); M.p.: 245-248°C; ^{1}H NMR (500 MHz, DMSO-*d_6*, 298K) δ_{CH} 4.38 (d, J=6 Hz, 4 H); δ_{ArH} 7.04 (t, J=6 Hz, NH, 2H); 7.33-742 (m, ArH, 4H); 7.48-7.58 (m, ArH, 6H); 7.88 (d, J=7.5 Hz, ArH, 2H); 8.01 (d, J=7.5 Hz, ArH, 2H); 8.08 (d, J=8 Hz, ArH, 2H); 8.59 (s, NH, 2H) ^{13}C-NMR (100 MHz, DMSO-*d_6* , 298 K) δ_C 42.97; δ_{ArC} 116.4, 121.2, 122.1, 125.5,125.6, 125.7, 125.8,128.3, 133.7, 135.1, 140.7 δ_{CO} 155.6.

Synthesis of 1,1'-(pyridine-2,6-diylbis(methylene))bis(3-phenylurea) L^6

A solution of phenyl isocyanate (0.170 g; 1.42 mmol) in DCM (10 ml) was added dropwise to the suspension of pyridine-2.6-diyldimethanamine dihydrocloride (0.150g, 0.714

mmol) and TEA (1 ml) in DCM (20ml). The reaction mixture was refluxed for 24h under a N_2 atmosphere and the precipitate thus obtained was filtered off, washed with H_2O and dried over vacuum to give the product as a white solid.
Yield 53% (0.180 g; 0.378mmol); M.p. 225-226°C; ^{1}H NMR (500 MHz, DMSO-d_6, 298K) δCH 4.40 (d, J=5 Hz, 4 H); δ_{ArH} 6.73 (t, J=6 Hz, NH, 2H); 6.90 (t, 7Hz, ArH, 2H); 7.21-7.24 (m, ArH, 6H); 7.40 (d, J=8, ArH, 4H); 7.75 (t, J=8, ArH, 1H); 8.72 (s, NH, 2H); ^{13}C-NMR (125 MHz, DMSO-d_6 , 298 K) δ_C 45.17; δ_{ArC} 118.19, 119.52, 121.61, 129.11, 137.84, 140.9, 155.7, δ_{CO}159.04.

Synthesis of 1,1'-(pyridine-2,6-diylbis(methylene))bis(3-(2nitrophenyl)urea) L^7

A solution of 2-nitrophenyl isocyanate (0.468 g; 2.85 mmol) in 15 ml of DCM was added dropwise to a stirred suspension of pyridine-2.6-diyldimethanamine dihydrocloride and TEA (1 ml) in 20 ml of DCM. The reaction was refluxed under N_2 atmosphere overnight. The resulting precipitate was then filtered, washed with water and then whit MeOH, dried under reduced pressure and isolated as a yellow solid.
Yield: 51% (0.340g, 0.73 mmol); M.p. 234°C; ^{1}H NMR (500 MHz, DMSO-d_6, 298K) δCH 4.41 (d, J=6 Hz, 4 H); δ_{ArH} 7.14 (t, J=7 Hz, ArH, 2H); 7.25 (d, J=7.5Hz, ArH, 2H); 7.64 (t, J=7 ArH, 2H); 7.78 (t, J=8, ArH, 1H); 8.03-8.10 (m, 4H); 8.27 (d, J=8.5, ArH, 2H) 9.50 (s, NH, 2H) ^{13}C-NMR(125 MHz, DMSO-d_6 , 298 K) δ_C 44.91; δ_{ArC} 119.22, 121.60, 122.20, 125.24, 134.82, 135.53, 137.25, 137.47, 154.41; δ_{CO} 158.25

Synthesis of 1,1'-(pyridine-2,6-diylbis(methylene))bis(3-(naphthalen1-yl)urea) L^8

A solution of 1-naphthyl isocyanate (0.320 g; 1.90 mmol) in DCM (15 ml) was added dropwise to a stirred suspension of pyridine-2.6-diyldimethanamine dihydrocloride (0.200 g; 0.95 mmol) and TEA (1 ml) in DCM (15 ml). After refluxing under N_2 atmosphere overnight the white solid was isolated by filtration, washed with water and dried under reduced pressure.
Yield 59.7% (0.270 g; 0.57mmol); M.p. >250°C; ^{1}H NMR (500 MHz, DMSO-d_6, 298K) δCH 4.5 (d, J=6 Hz, 4 H); δ_{ArH} 7.20 (t, J=6 NH, 2H); 7.30 (d, J=8Hz, ArH, 2H); 7.43 (t, J=7.5 ArH, 2H); 7.49-7.59 (m, ArH, 6H); 7.80 (t, J=7.5, ArH, 1H); 7.90 (d, J=8, ArH, 2H); 8.00 (d, J=8, ArH, 2H); 8.14 (d, J=8, ArH, 2H); 8.77 (s, NH, 2H); ^{13}C-NMR (125 MHz, DMSO-d_6, 298 K) δ_C 44.89, δ_{ArC} 116.77, 119.14, 121.45, 122.24, 125.39, 125.71, 125.86, 128.28, 133.69, 135.03, 137.48, 155.65, δ_{CO} 158.61.

3.7.2. Proton NMR titration fitting

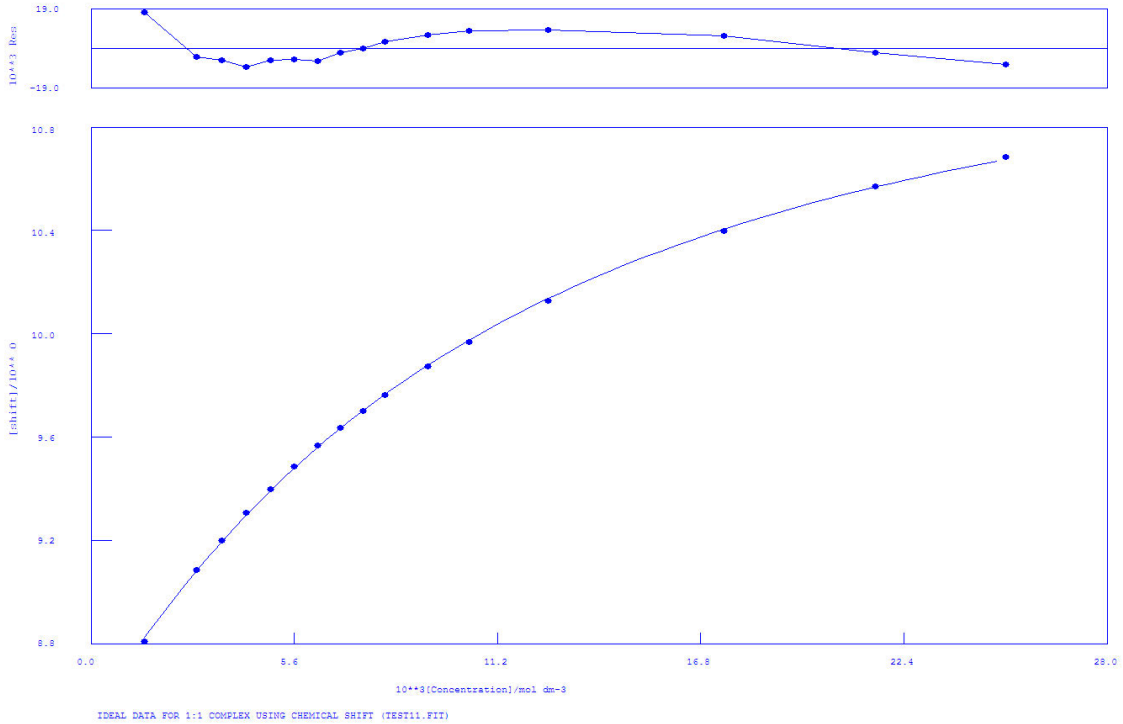

Calculations by WinEQNMR Version 1.20 by Michael J. Hynes
Program run at 12:50:07 on 12/30/2011

IDEAL DATA FOR 1:1 COMPLEX USING CHEMICAL SHIFT (TEST11.FIT)
Reaction: M + L = ML
FILE: TEST11.FIT
IDEAL DATA: K1 = 63.091; DELTA M = 20.0; DELTA ML = 120.0
File prepared by M. J. Hynes, October 22 2000

NO.	A	PARAMETER	DELTA	ERROR	CONDITION	DESCRIPTION
1	1	1.19274E+02	2.000E-01	3.364E+00	5.740E+01	K1
2	1	8.51926E+00	2.000E-01	9.384E-03	8.464E+00	SHIFT M
3	1	1.15161E+01	1.000E+00	2.614E-02	3.230E+01	SHIFT ML

0RMS ERROR = 8.03E-03 MAX ERROR = 1.73E-02 AT OBS.NO. 1
RESIDUALS SQUARED = 8.39E-04
RFACTOR = 0.0744 PERCENT

Figure 3.12 ^{1}H-NMR titration of **L^{3}** with TBAAcO in DMSO-d_6.

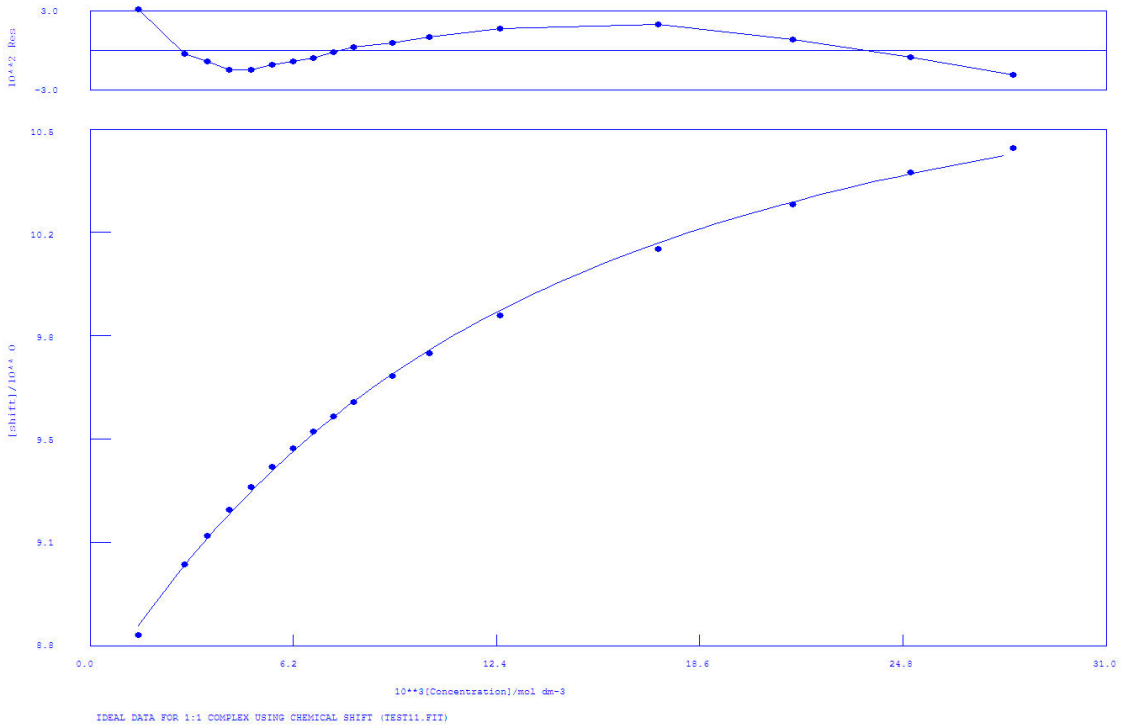

Calculations by WinEQNMR Version 1.20 by Michael J. Hynes
Program run at 14:59:54 on 01/04/2012

IDEAL DATA FOR 1:1 COMPLEX USING CHEMICAL SHIFT (TEST11.FIT)
Reaction: M + L = ML
FILE: TEST11.FIT
IDEAL DATA: K1 = 63.091; DELTA M = 20.0; DELTA ML = 120.0
File prepared by M. J. Hynes, October 22 2000

NO.	A	PARAMETER	DELTA	ERROR	CONDITION	DESCRIPTION
1	1	1.08941E+02	2.000E-01	5.928E+00	4.741E+01	K1
2	1	8.62882E+00	2.000E-01	1.547E-02	7.546E+00	SHIFT M
3	1	1.10901E+01	1.000E+00	4.079E-02	2.653E+01	SHIFT ML

0RMS ERROR = 1.45E-02 MAX ERROR = 3.11E-02 AT OBS.NO. 1
RESIDUALS SQUARED = 2.93E-03
RFACTOR = 0.1363 PERCENT

Figure 3.13 ^{1}H-NMR titration of **L^{1}** with TBABzO in DMSO-d_6.

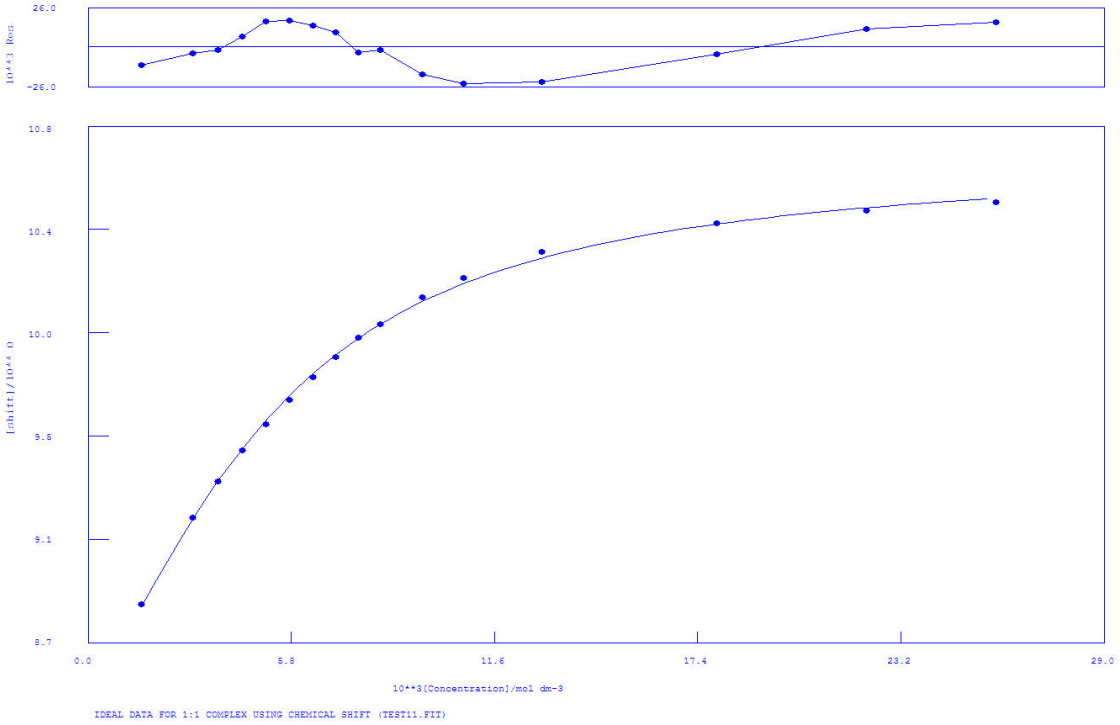

Calculations by WinEQNMR Version 1.20 by Michael J. Hynes
Program run at 11:06:06 on 12/29/2011

IDEAL DATA FOR 1:1 COMPLEX USING CHEMICAL SHIFT (TEST11.FIT)
Reaction: M + L = ML
FILE: TEST11.FIT
IDEAL DATA: K1 = 63.091; DELTA M = 20.0; DELTA ML = 120.0
File prepared by M. J. Hynes, October 22 2000

NO.	A	PARAMETER	DELTA	ERROR	CONDITION	DESCRIPTION
1	1	4.83740E+02	2.000E-01	2.235E+01	1.596E+01	K1
2	1	8.40857E+00	2.000E-01	1.770E-02	3.921E+00	SHIFT M
3	1	1.07129E+01	1.000E+00	1.774E-02	9.549E+00	SHIFT ML

0RMS ERROR = 1.51E-02 MAX ERROR = 2.38E-02 AT OBS.NO. 12
RESIDUALS SQUARED = 2.97E-03
RFACTOR = 0.1380 PERCENT

Figure 3.14 ^{1}H-NMR titration of **L^{1}** with $TBAH_2PO_4$ in DMSO-d_6.

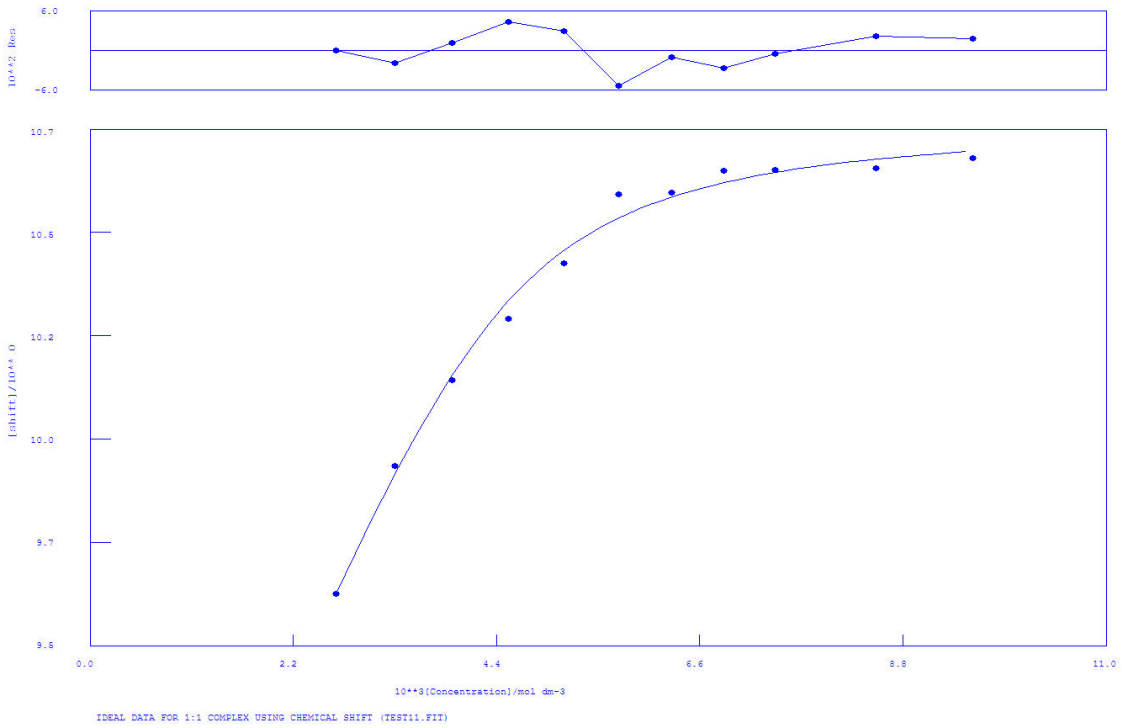

Calculations by WinEQNMR Version 1.20 by Michael J. Hynes
Program run at 12:59:10 on 02/08/2012

IDEAL DATA FOR 1:1 COMPLEX USING CHEMICAL SHIFT (TEST11.FIT)
Reaction: M + L = ML
FILE: TEST11.FIT
IDEAL DATA: K1 = 63.091; DELTA M = 20.0; DELTA ML = 120.0
File prepared by M. J. Hynes, October 22 2000

NO.	A	PARAMETER	DELTA	ERROR	CONDITION	DESCRIPTION
1	1	5.48167E+03	2.000E-01	1.185E+03	1.181E+01	K1
2	1	8.27172E+00	2.000E-01	7.242E-02	2.434E+00	SHIFT M
3	1	1.07303E+01	1.000E+00	3.290E-02	9.007E+00	SHIFT ML

0RMS ERROR = 3.11E-02 MAX ERROR = 5.49E-02 AT OBS.NO. 6
RESIDUALS SQUARED = 7.74E-03
RFACTOR = 0.2562 PERCENT

Figure 3.15 ^{1}H-NMR titration of **L^{1}** with $(TBA)_3HPpi$ in DMSO-d_6.

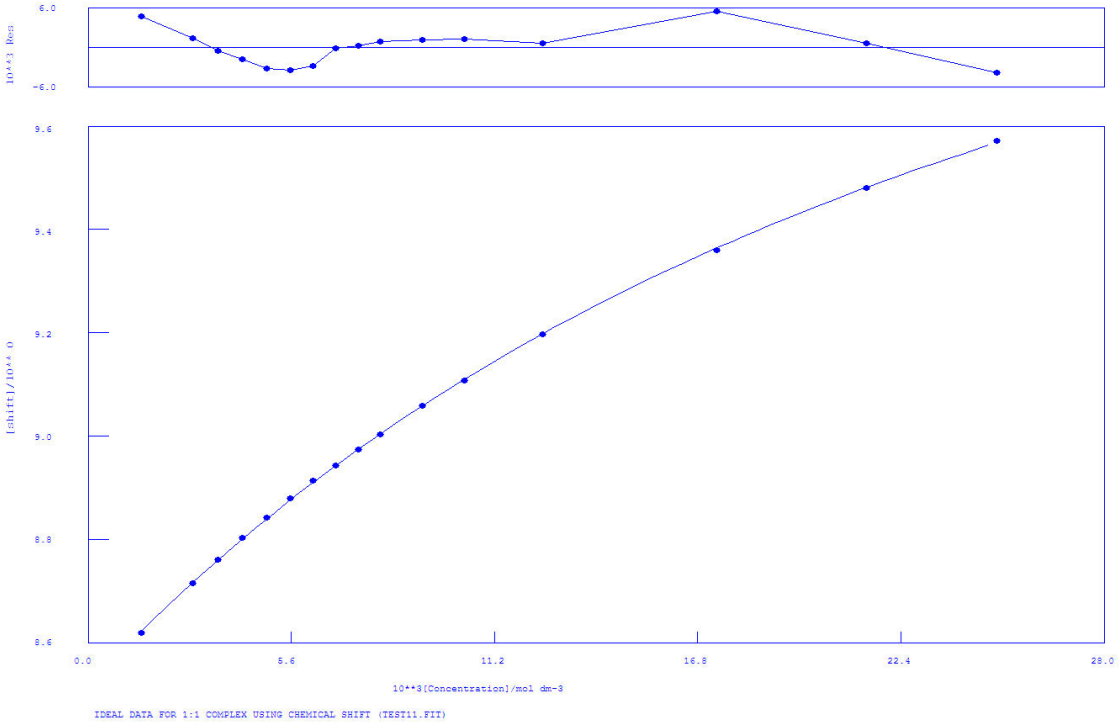

Calculations by WinEQNMR Version 1.20 by Michael J. Hynes
Program run at 10:40:22 on 01/27/2012

IDEAL DATA FOR 1:1 COMPLEX USING CHEMICAL SHIFT (TEST11.FIT)
Reaction: M + L = ML
FILE: TEST11.FIT
IDEAL DATA: K1 = 63.091; DELTA M = 20.0; DELTA ML = 120.0
File prepared by M. J. Hynes, October 22 2000

NO.	A	PARAMETER	DELTA	ERROR	CONDITION	DESCRIPTION
1	1	4.34068E+01	2.000E-01	1.224E+00	1.688E+02	K1
2	1	8.51709E+00	2.000E-01	2.894E-03	9.815E+00	SHIFT M
3	1	1.06512E+01	1.000E+00	2.964E-02	1.179E+02	SHIFT ML

0RMS ERROR = 2.87E-03 MAX ERROR = 5.48E-03 AT OBS.NO. 14
RESIDUALS SQUARED = 1.07E-04
RFACTOR = 0.0287 PERCENT

Figure 3.16 ^{1}H-NMR titration of **L^{1}** with $(TBA)_2Glu$ in DMSO-d_6.

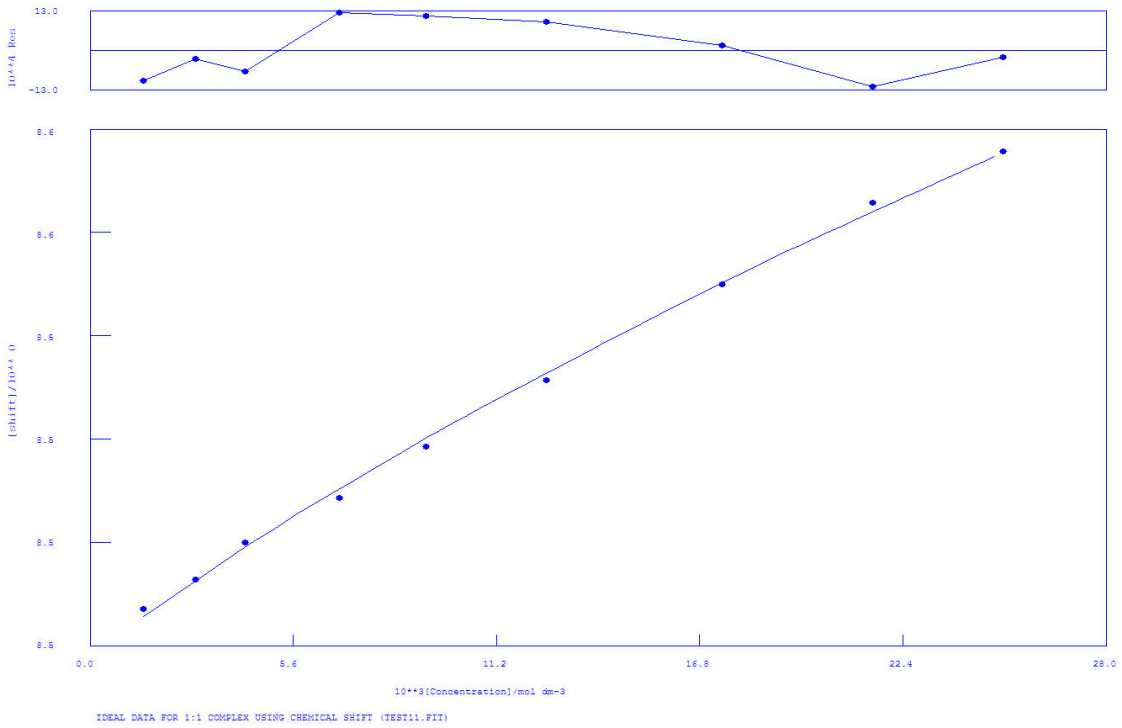

Calculations by WinEQNMR Version 1.20 by Michael J. Hynes
Program run at 10:50:01 on 01/27/2012

IDEAL DATA FOR 1:1 COMPLEX USING CHEMICAL SHIFT (TEST11.FIT)
Reaction: M + L = ML
FILE: TEST11.FIT
IDEAL DATA: K1 = 63.091; DELTA M = 20.0; DELTA ML = 120.0
File prepared by M. J. Hynes, October 22 2000

NO.	A	PARAMETER	DELTA	ERROR	CONDITION	DESCRIPTION
1	1	1.12687E+01	2.000E-01	3.822E+00	9.005E+02	K1
2	1	8.49895E+00	2.000E-01	1.054E-03	7.199E+00	SHIFT M
3	1	8.81263E+00	1.000E+00	8.114E-02	8.025E+02	SHIFT ML

0RMS ERROR = 1.06E-03 MAX ERROR = 1.22E-03 AT OBS.NO. 4
RESIDUALS SQUARED = 6.74E-06
RFACTOR = 0.0101 PERCENT

Figure 3.17 ^{1}H-NMR titration of **L^{1}** with $(TBA)_2Mal$ in DMSO-d_6.

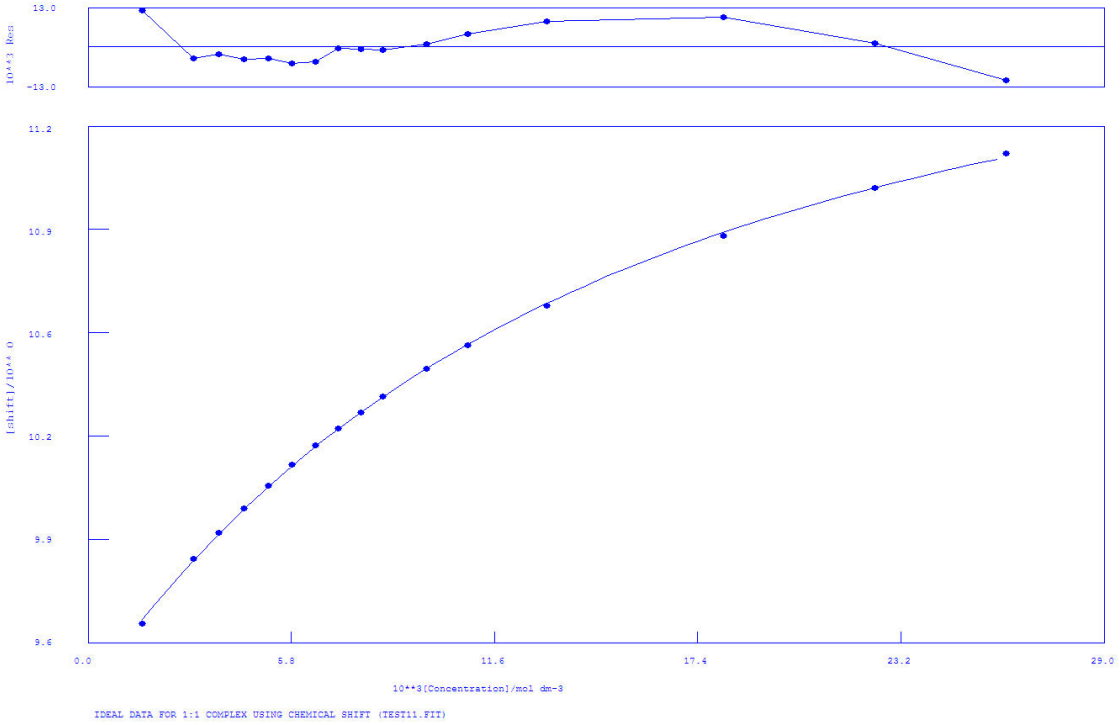

Calculations by WinEQNMR Version 1.20 by Michael J. Hynes
Program run at 15:23:03 on 12/16/2011

IDEAL DATA FOR 1:1 COMPLEX USING CHEMICAL SHIFT (TEST11.FIT)
Reaction: M + L = ML
FILE: TEST11.FIT
IDEAL DATA: K1 = 63.091; DELTA M = 20.0; DELTA ML = 120.0
File prepared by M. J. Hynes, October 22 2000

NO.	A	PARAMETER	DELTA	ERROR	CONDITION	DESCRIPTION
1	1	8.83907E+01	2.000E-01	2.582E+00	6.315E+01	K1
2	1	9.45328E+00	2.000E-01	7.234E-03	8.584E+00	SHIFT M
3	1	1.19201E+01	1.000E+00	2.498E-02	3.644E+01	SHIFT ML

0RMS ERROR = 6.52E-03 MAX ERROR = 1.21E-02 AT OBS.NO. 1
RESIDUALS SQUARED = 5.53E-04
RFACTOR = 0.0568 PERCENT

Figure 3.18 ^{1}H-NMR titration of **L^{2}** with TBAAcO in DMSO-d_6.

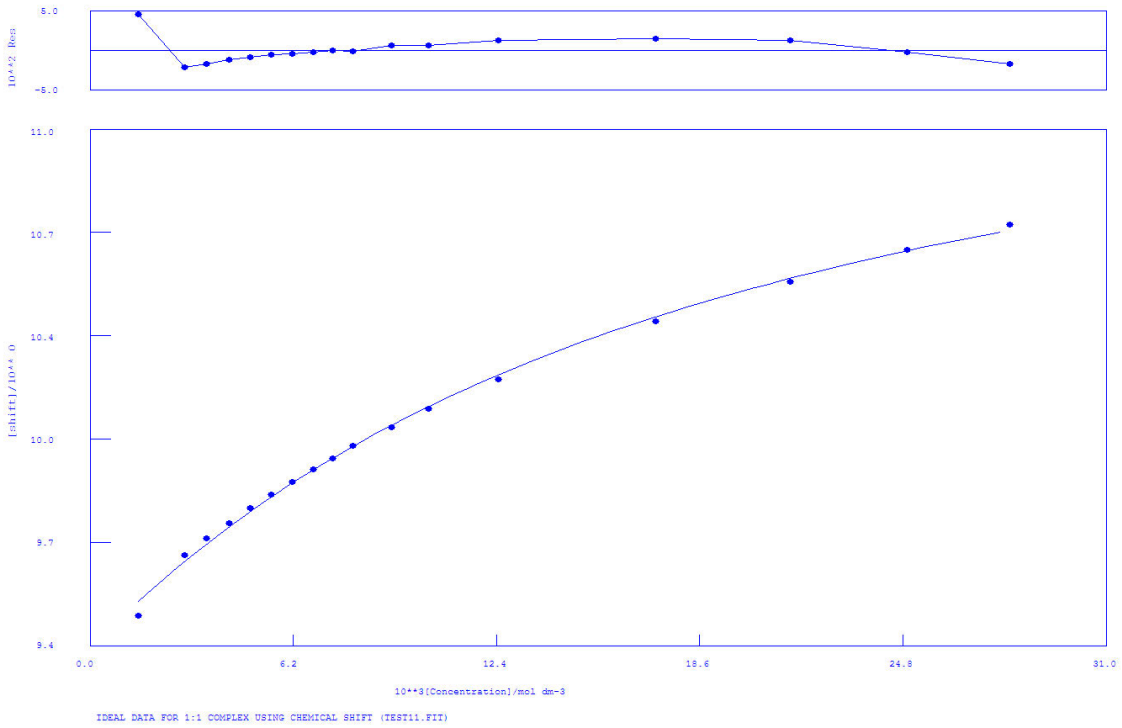

Calculations by WinEQNMR Version 1.20 by Michael J. Hynes
Program run at 15:52:48 on 12/16/2011

IDEAL DATA FOR 1:1 COMPLEX USING CHEMICAL SHIFT (TEST11.FIT)
Reaction: M + L = ML
FILE: TEST11.FIT
IDEAL DATA: K1 = 63.091; DELTA M = 20.0; DELTA ML = 120.0
File prepared by M. J. Hynes, October 22 2000

NO.	A	PARAMETER	DELTA	ERROR	CONDITION	DESCRIPTION
1	1	6.47549E+01	2.000E-01	6.441E+00	7.977E+01	K1
2	1	9.39505E+00	2.000E-01	1.697E-02	8.514E+00	SHIFT M
3	1	1.14835E+01	1.000E+00	8.118E-02	4.923E+01	SHIFT ML

0RMS ERROR = 1.69E-02 MAX ERROR = 4.48E-02 AT OBS.NO. 1
RESIDUALS SQUARED = 3.98E-03
RFACTOR = 0.1521 PERCENT

Figure 3.19 ^{1}H-NMR titration of **L²** with TBABzO in DMSO-d_6.

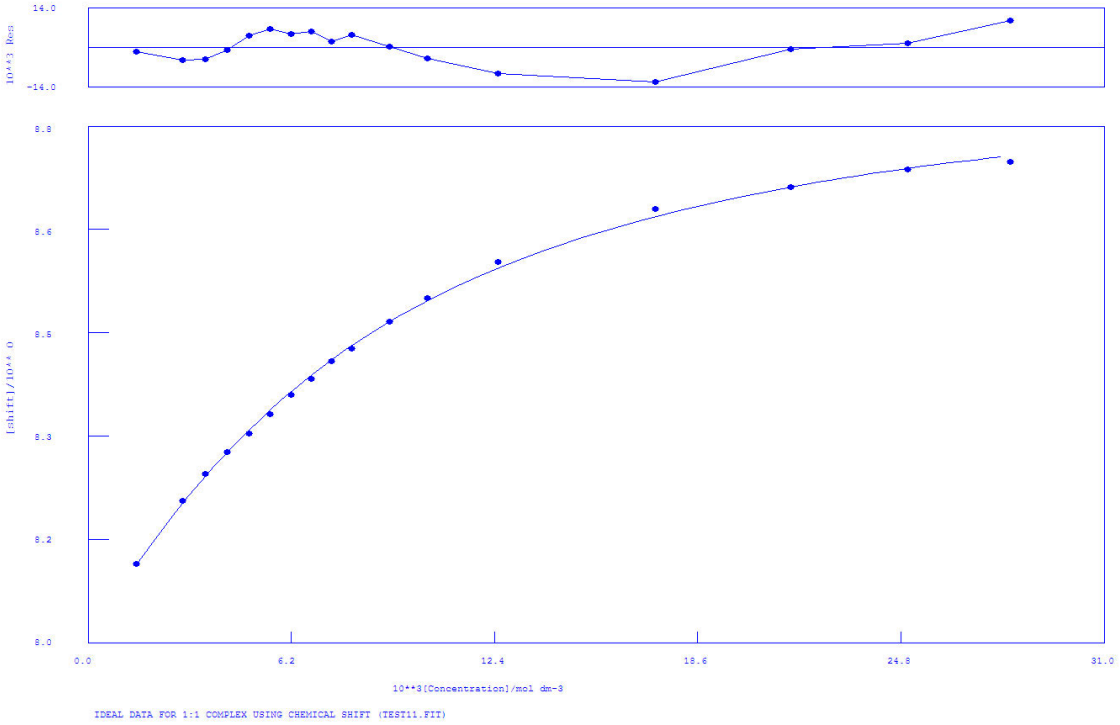

Calculations by WinEQNMR Version 1.20 by Michael J. Hynes
Program run at 16:15:07 on 12/16/2011

IDEAL DATA FOR 1:1 COMPLEX USING CHEMICAL SHIFT (TEST11.FIT)
Reaction: M + L = ML
FILE: TEST11.FIT
IDEAL DATA: K1 = 63.091; DELTA M = 20.0; DELTA ML = 120.0
File prepared by M. J. Hynes, October 22 2000

NO.	A	PARAMETER	DELTA	ERROR	CONDITION	DESCRIPTION
1	1	1.80508E+02	2.000E-01	9.117E+00	2.953E+01	K1
2	1	8.00609E+00	2.000E-01	6.519E-03	5.914E+00	SHIFT M
3	1	8.92857E+00	1.000E+00	1.136E-02	1.626E+01	SHIFT ML

0RMS ERROR = 6.08E-03 MAX ERROR = 1.23E-02 AT OBS.NO. 14
RESIDUALS SQUARED = 5.18E-04
RFACTOR = 0.0653 PERCENT

Figure 3.20 ^{1}H-NMR titration of **L^{2}** with $TBAH_2PO_4$ in DMSO-d_6.

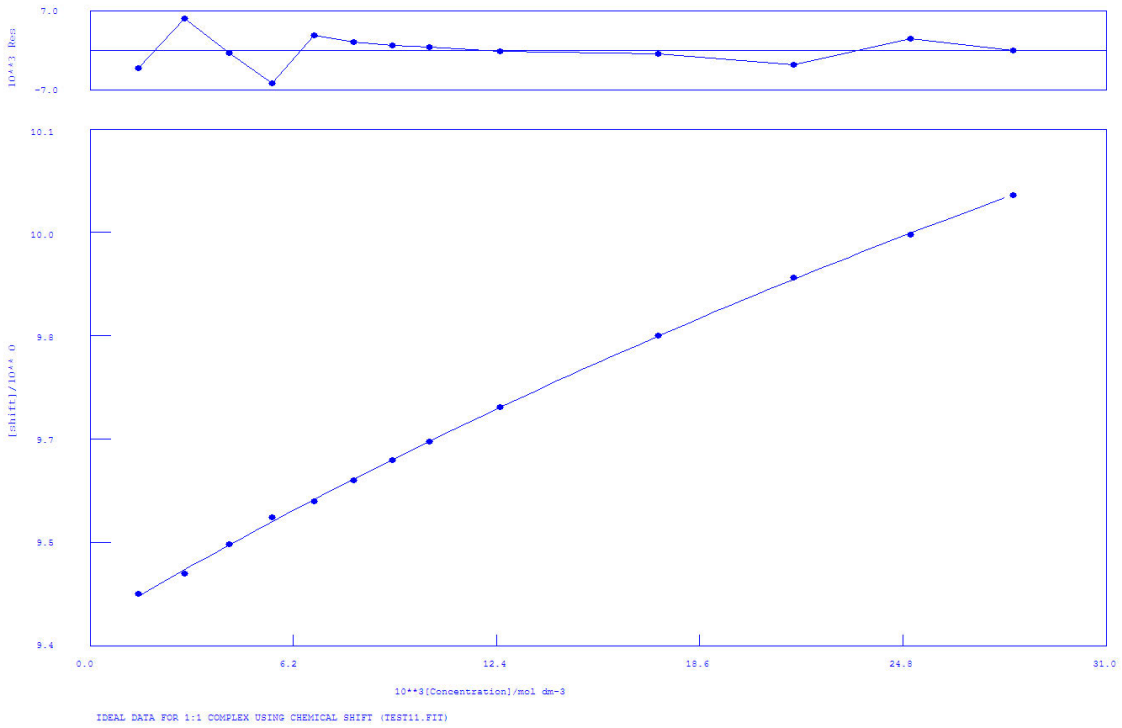

Calculations by WinEQNMR Version 1.20 by Michael J. Hynes
Program run at 11:40:12 on 01/27/2012

IDEAL DATA FOR 1:1 COMPLEX USING CHEMICAL SHIFT (TEST11.FIT)
Reaction: M + L = ML
FILE: TEST11.FIT
IDEAL DATA: K1 = 63.091; DELTA M = 20.0; DELTA ML = 120.0
File prepared by M. J. Hynes, October 22 2000

NO.	A	PARAMETER	DELTA	ERROR	CONDITION	DESCRIPTION
1	1	1.04984E+01	2.000E-01	1.028E+00	8.119E+02	K1
2	1	9.42859E+00	2.000E-01	2.719E-03	7.974E+00	SHIFT M
3	1	1.20573E+01	1.000E+00	1.932E-01	7.114E+02	SHIFT ML

0RMS ERROR = 3.13E-03 MAX ERROR = 5.92E-03 AT OBS.NO. 4
RESIDUALS SQUARED = 9.79E-05
RFACTOR = 0.0283 PERCENT

Figure 3.21 ^{1}H-NMR titration of **L^{2}** with $(TBA)_2Glu$ in DMSO-d_6.

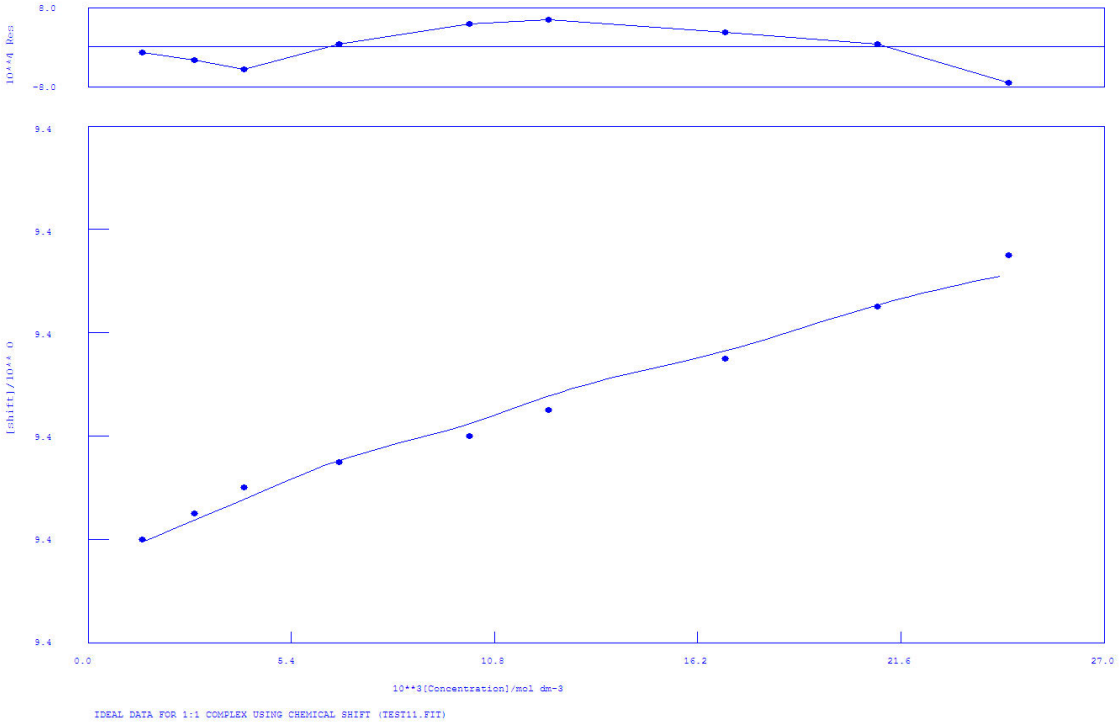

Calculations by WinEQNMR Version 1.20 by Michael J. Hynes
Program run at 11:49:43 on 01/27/2012

IDEAL DATA FOR 1:1 COMPLEX USING CHEMICAL SHIFT (TEST11.FIT)
Reaction: M + L = ML
FILE: TEST11.FIT
IDEAL DATA: K1 = 63.091; DELTA M = 20.0; DELTA ML = 120.0
File prepared by M. J. Hynes, October 22 2000

NO.	A	PARAMETER	DELTA	ERROR	CONDITION	DESCRIPTION
1	1	7.58123E+00	2.000E-01	7.427E-01	9.636E+00	K1
2	1	9.42298E+00	2.000E-01	2.983E-04	2.867E+00	SHIFT M
3	1	9.49195E+00	1.000E+00	6.581E-03	1.229E+01	SHIFT ML

0RMS ERROR = 4.91E-04 MAX ERROR = 7.30E-04 AT OBS.NO. 9
RESIDUALS SQUARED = 1.44E-06
RFACTOR = 0.0042 PERCENT

Figure 3.22 ^{1}H-NMR titration of **L^{2}** with con $(TBA)_2Mal$ in DMSO-d_6.

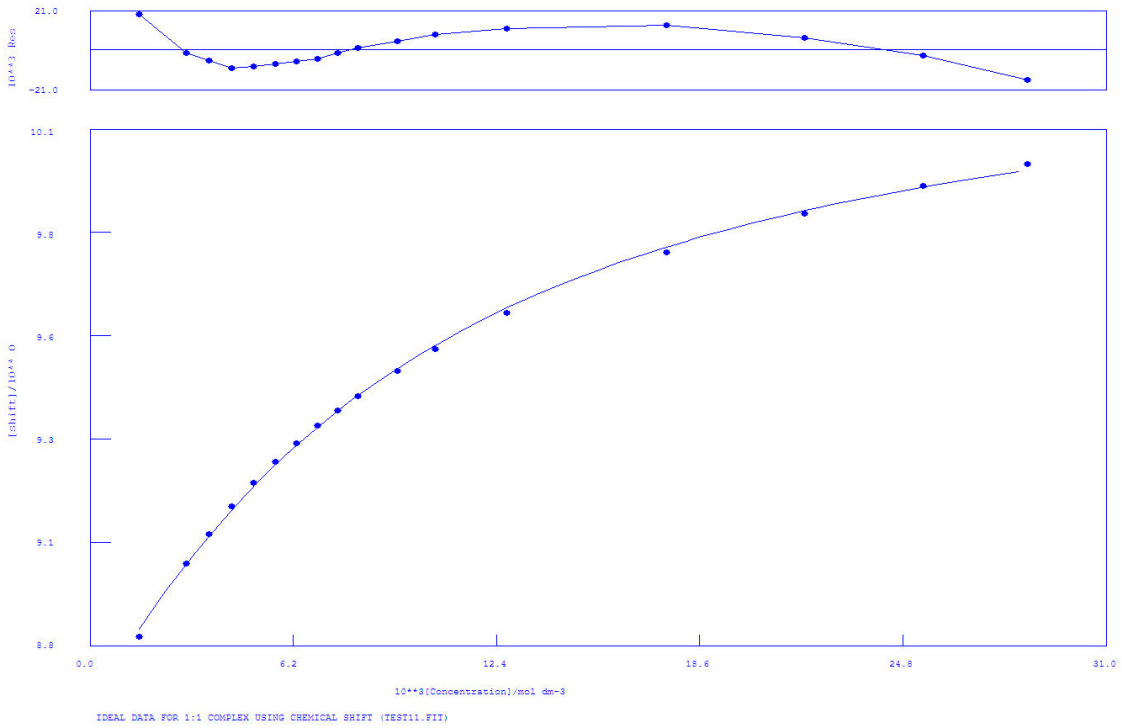

Calculations by WinEQNMR Version 1.20 by Michael J. Hynes
Program run at 12:08:55 on 01/05/2012

IDEAL DATA FOR 1:1 COMPLEX USING CHEMICAL SHIFT (TEST11.FIT)
Reaction: M + L = ML
FILE: TEST11.FIT
IDEAL DATA: K1 = 63.091; DELTA M = 20.0; DELTA ML = 120.0
File prepared by M. J. Hynes, October 22 2000

NO.	A	PARAMETER	DELTA	ERROR	CONDITION	DESCRIPTION
1	1	1.36759E+02	2.000E-01	6.352E+00	3.705E+01	K1
2	1	8.64369E+00	2.000E-01	1.102E-02	7.098E+00	SHIFT M
3	1	1.03948E+01	1.000E+00	2.188E-02	1.974E+01	SHIFT ML

0RMS ERROR = 9.92E-03 MAX ERROR = 1.91E-02 AT OBS.NO. 1
RESIDUALS SQUARED = 1.38E-03
RFACTOR = 0.0954 PERCENT

Figure 3.23 ^{1}H-NMR titration of **L^{3}** with TBAAcO in DMSO-d_6.

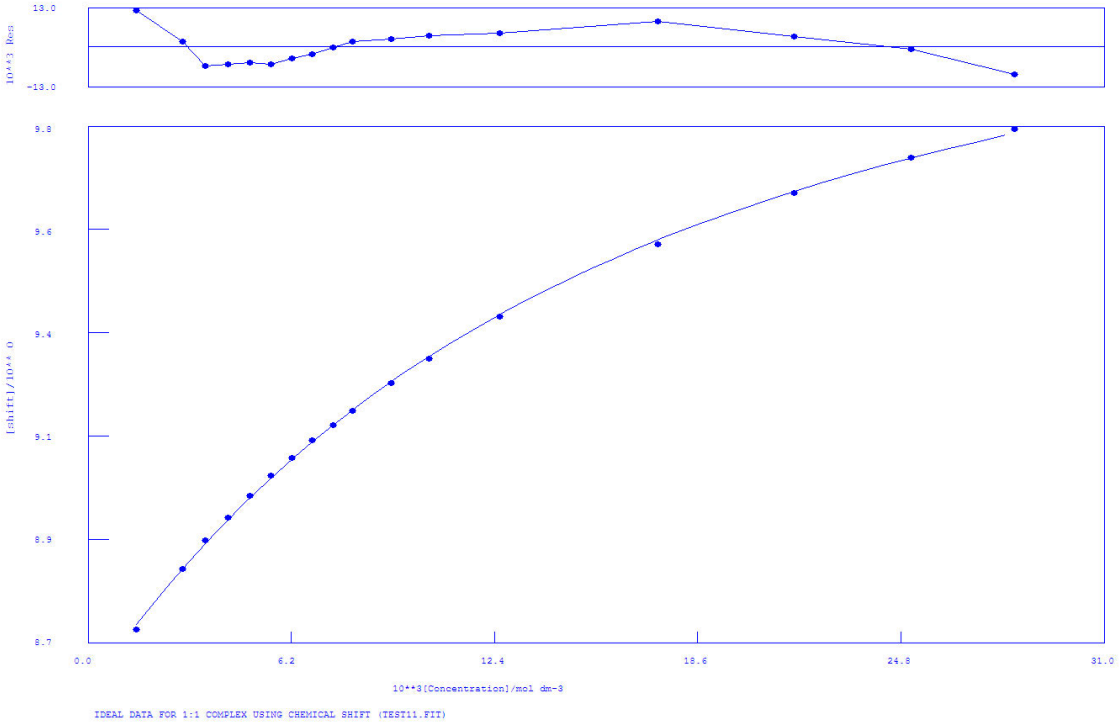

Calculations by WinEQNMR Version 1.20 by Michael J. Hynes
Program run at 12:14:41 on 01/05/2012

IDEAL DATA FOR 1:1 COMPLEX USING CHEMICAL SHIFT (TEST11.FIT)
Reaction: M + L = ML
FILE: TEST11.FIT
IDEAL DATA: K1 = 63.091; DELTA M = 20.0; DELTA ML = 120.0
File prepared by M. J. Hynes, October 22 2000

NO.	A	PARAMETER	DELTA	ERROR	CONDITION	DESCRIPTION
1	1	7.83725E+01	2.000E-01	2.803E+00	6.018E+01	K1
2	1	8.60057E+00	2.000E-01	6.112E-03	7.970E+00	SHIFT M
3	1	1.03937E+01	1.000E+00	2.247E-02	3.531E+01	SHIFT ML

0RMS ERROR = 6.02E-03 MAX ERROR = 1.20E-02 AT OBS.NO. 1
RESIDUALS SQUARED = 5.07E-04
RFACTOR = 0.0592 PERCENT

Figure 3.24 ^{1}H-NMR titration of **L^{3}** with TBABzO in DMSO-d_6.

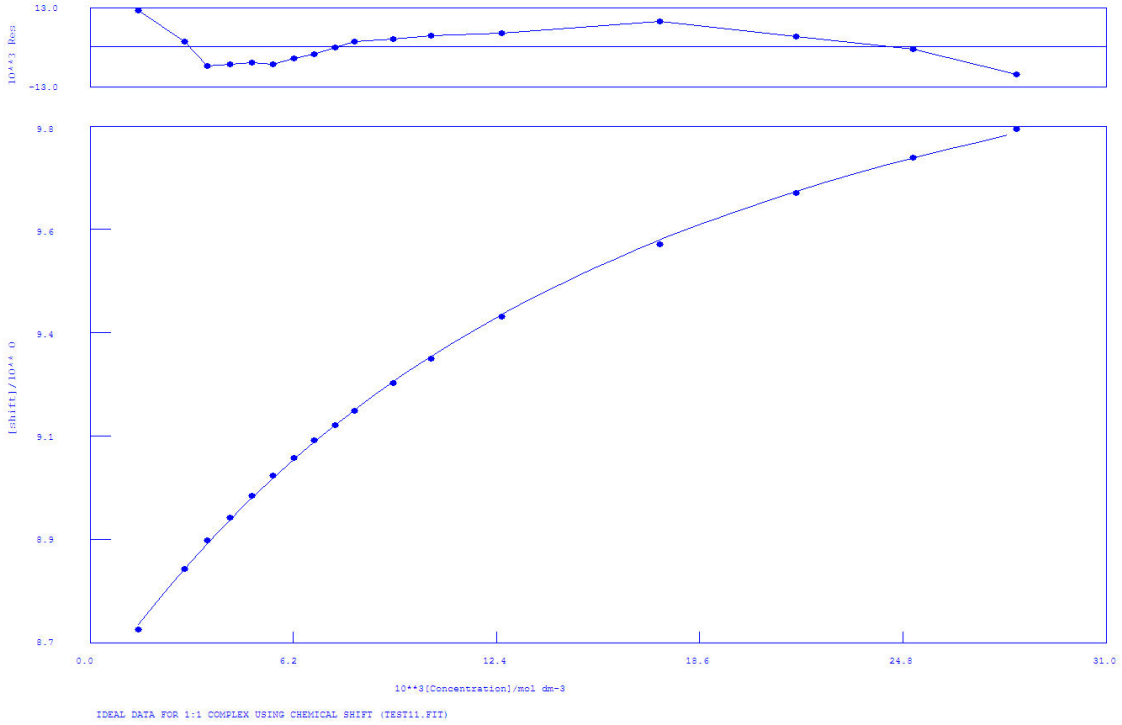

Calculations by WinEQNMR Version 1.20 by Michael J. Hynes
Program run at 15:30:21 on 01/04/2012

IDEAL DATA FOR 1:1 COMPLEX USING CHEMICAL SHIFT (TEST11.FIT)
Reaction: M + L = ML
FILE: TEST11.FIT
IDEAL DATA: K1 = 63.091; DELTA M = 20.0; DELTA ML = 120.0
File prepared by M. J. Hynes, October 22 2000

NO.	A	PARAMETER	DELTA	ERROR	CONDITION	DESCRIPTION
1	1	4.35285E+02	2.000E-01	1.209E+01	1.759E+01	K1
2	1	8.50083E+00	2.000E-01	8.853E-03	4.244E+00	SHIFT M
3	1	1.04192E+01	1.000E+00	9.400E-03	1.028E+01	SHIFT ML

0RMS ERROR = 7.52E-03 MAX ERROR = 1.86E-02 AT OBS.NO. 15
RESIDUALS SQUARED = 7.34E-04
RFACTOR = 0.0700 PERCENT

Figure 3.25 ^{1}H-NMR titration of **L^{3}** with $TBAH_2PO_4$ in DMSO-d_6.

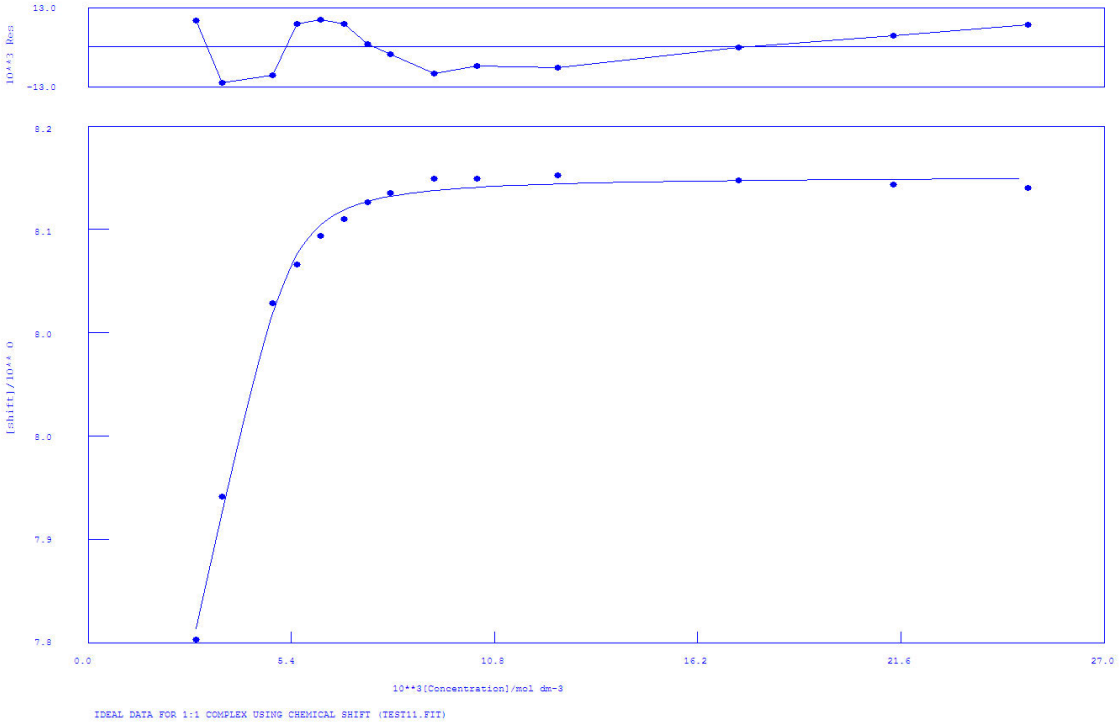

Calculations by WinEQNMR Version 1.20 by Michael J. Hynes
Program run at 15:22:35 on 01/04/2012

IDEAL DATA FOR 1:1 COMPLEX USING CHEMICAL SHIFT (TEST11.FIT)
Reaction: M + L = ML
FILE: TEST11.FIT
IDEAL DATA: K1 = 63.091; DELTA M = 20.0; DELTA ML = 120.0
File prepared by M. J. Hynes, October 22 2000

NO.	A	PARAMETER	DELTA	ERROR	CONDITION	DESCRIPTION
1	1	1.60759E+04	2.000E-01	2.052E+03	1.981E+00	K1
2	1	7.41311E+00	2.000E-01	1.563E-02	1.362E+00	SHIFT M
3	1	8.16089E+00	1.000E+00	3.130E-03	1.759E+00	SHIFT ML

0RMS ERROR = 8.15E-03 MAX ERROR = 1.16E-02 AT OBS.NO. 2
RESIDUALS SQUARED = 7.31E-04
RFACTOR = 0.0892 PERCENT

Figure 3.26 ^{1}H-NMR titration of **L^{3}** with $(TBA)_3HPpi$ in DMSO-d_6.

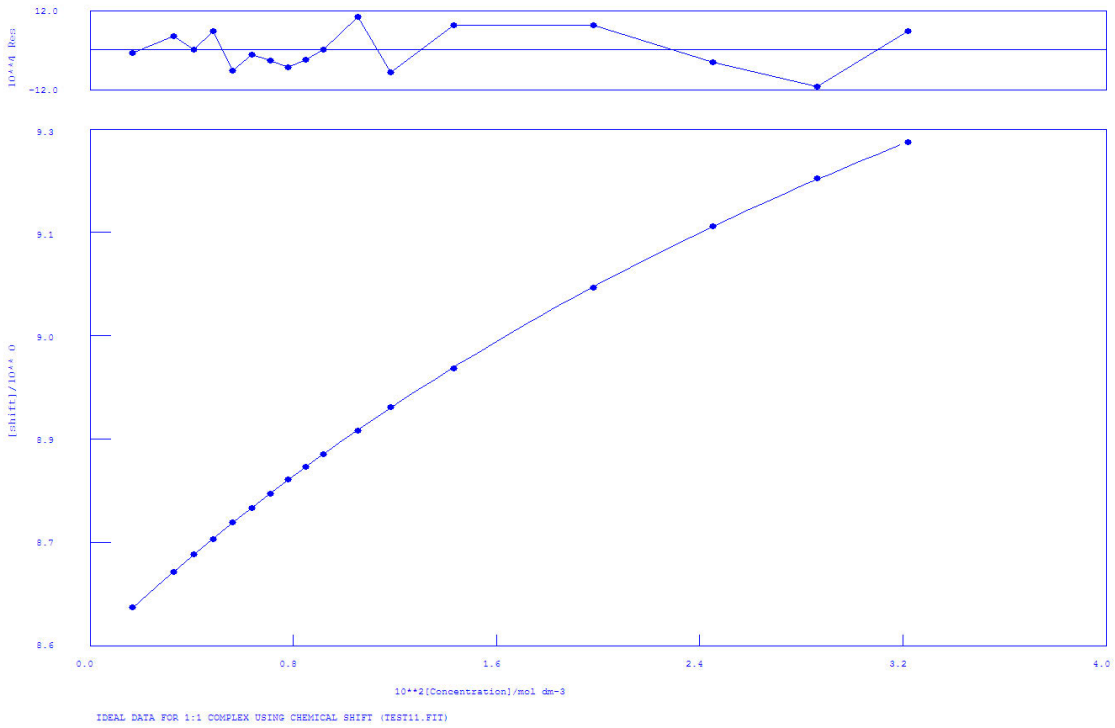

Calculations by WinEQNMR Version 1.20 by Michael J. Hynes
Program run at 13:56:31 on 01/23/2012

IDEAL DATA FOR 1:1 COMPLEX USING CHEMICAL SHIFT (TEST11.FIT)
Reaction: M + L = ML
FILE: TEST11.FIT
IDEAL DATA: K1 = 63.091; DELTA M = 20.0; DELTA ML = 120.0
File prepared by M. J. Hynes, October 22 2000

NO.	A	PARAMETER	DELTA	ERROR	CONDITION	DESCRIPTION
1	1	1.98147E+01	2.000E-01	1.999E-01	2.863E+02	K1
2	1	8.54750E+00	2.000E-01	5.498E-04	9.004E+00	SHIFT M
3	1	1.05114E+01	1.000E+00	1.200E-02	2.226E+02	SHIFT ML

0RMS ERROR = 6.37E-04 MAX ERROR = 1.11E-03 AT OBS.NO. 16
RESIDUALS SQUARED = 5.67E-06
RFACTOR = 0.0065 PERCENT

Figure 3.27 ^{1}H-NMR titration of **L^{3}** with $(TBA)_2Glu$ in DMSO-d_6.

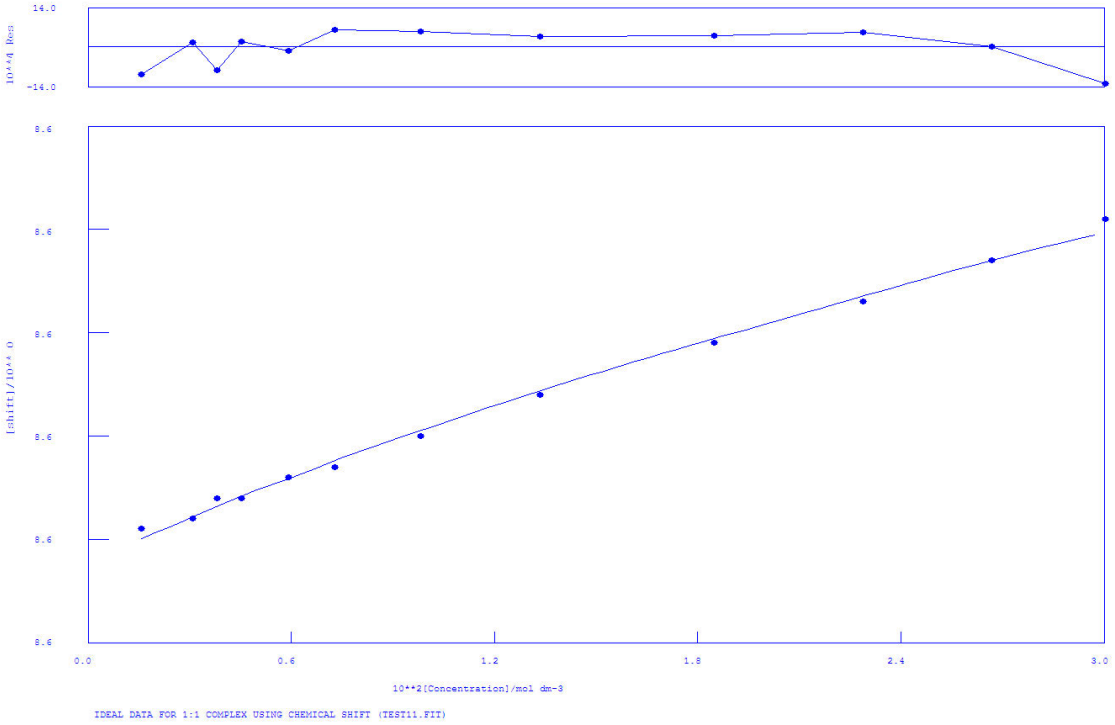

Calculations by WinEQNMR Version 1.20 by Michael J. Hynes
Program run at 14:07:16 on 01/23/2012

IDEAL DATA FOR 1:1 COMPLEX USING CHEMICAL SHIFT (TEST11.FIT)
Reaction: M + L = ML
FILE: TEST11.FIT
IDEAL DATA: K1 = 63.091; DELTA M = 20.0; DELTA ML = 120.0
File prepared by M. J. Hynes, October 22 2000

NO.	A	PARAMETER	DELTA	ERROR	CONDITION	DESCRIPTION
1	1	9.79880E+00	2.000E-01	1.173E+00	5.838E+01	K1
2	1	8.58775E+00	2.000E-01	3.937E-04	2.958E+00	SHIFT M
3	1	8.72901E+00	1.000E+00	1.238E-02	5.177E+01	SHIFT ML

0RMS ERROR = 7.17E-04 MAX ERROR = 1.30E-03 AT OBS.NO. 12
RESIDUALS SQUARED = 4.63E-06
RFACTOR = 0.0072 PERCENT

Figure 3.28 ^{1}H-NMR titration of **L^{3}** with $(TBA)_2Mal$ in DMSO-d_6.

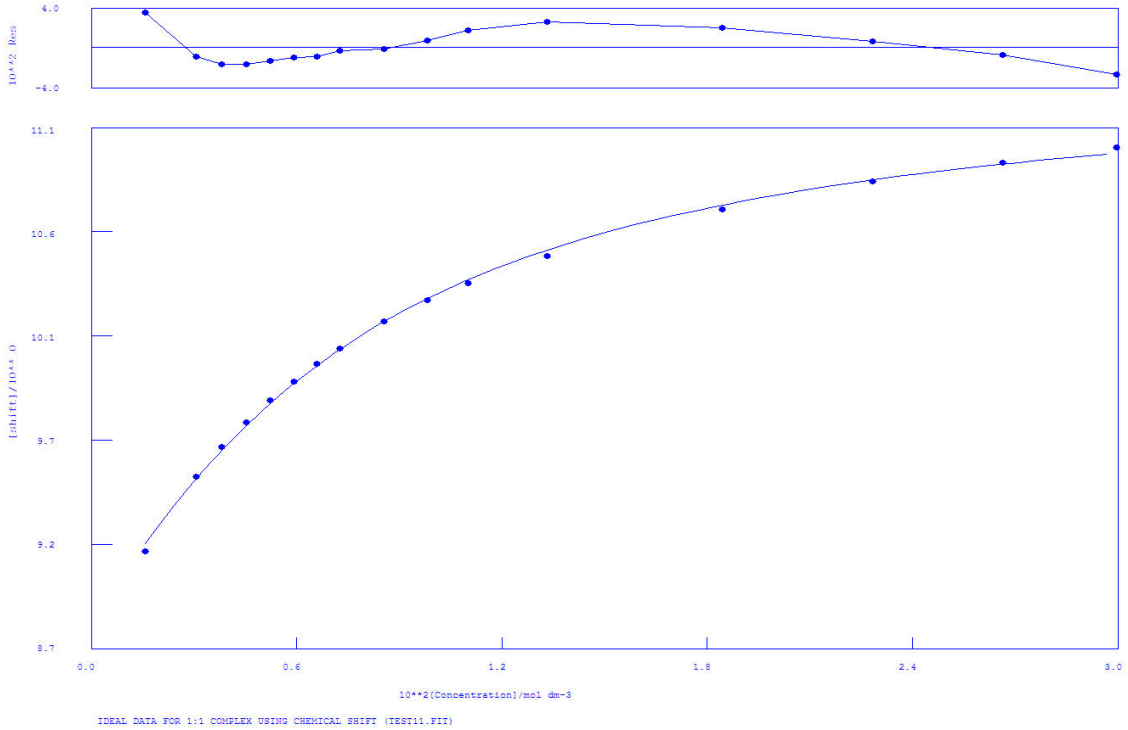

Calculations by WinEQNMR Version 1.20 by Michael J. Hynes
Program run at 15:47:29 on 06/06/2012

IDEAL DATA FOR 1:1 COMPLEX USING CHEMICAL SHIFT (TEST11.FIT)
Reaction: M + L = ML
FILE: TEST11.FIT
IDEAL DATA: K1 = 63.091; DELTA M = 20.0; DELTA ML = 120.0
File prepared by M. J. Hynes, October 22 2000

NO.	A	PARAMETER	DELTA	ERROR	CONDITION	DESCRIPTION
1	1	1.97486E+02	2.000E-01	1.029E+01	2.566E+01	K1
2	1	8.80900E+00	2.000E-01	2.233E-02	6.163E+00	SHIFT M
3	1	1.14063E+01	1.000E+00	2.981E-02	1.301E+01	SHIFT ML

0RMS ERROR = 1.86E-02 MAX ERROR = 3.52E-02 AT OBS.NO. 1
RESIDUALS SQUARED = 4.49E-03
RFACTOR = 0.1644 PERCENT

Figure 3.29 ^{1}H-NMR titration of **L^{4}** with TBAAcO in DMSO-d_6.

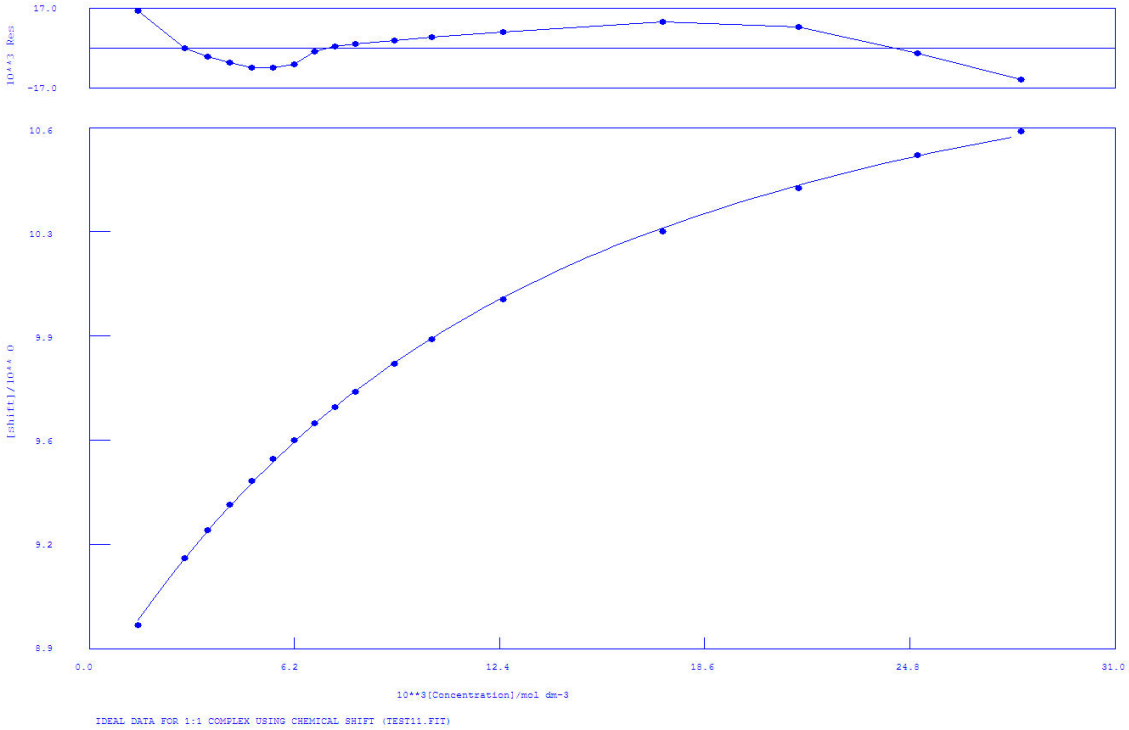

Calculations by WinEQNMR Version 1.20 by Michael J. Hynes
Program run at 16:08:11 on 06/06/2012

IDEAL DATA FOR 1:1 COMPLEX USING CHEMICAL SHIFT (TEST11.FIT)
Reaction: M + L = ML
FILE: TEST11.FIT
IDEAL DATA: K1 = 63.091; DELTA M = 20.0; DELTA ML = 120.0
File prepared by M. J. Hynes, October 22 2000

NO.	A	PARAMETER	DELTA	ERROR	CONDITION	DESCRIPTION
1	1	1.06438E+02	2.000E-01	3.285E+00	4.759E+01	K1
2	1	8.75456E+00	2.000E-01	8.965E-03	7.752E+00	SHIFT M
3	1	1.12730E+01	1.000E+00	2.354E-02	2.626E+01	SHIFT ML

0RMS ERROR = 8.32E-03 MAX ERROR = 1.59E-02 AT OBS.NO. 1
RESIDUALS SQUARED = 9.68E-04
RFACTOR = 0.0772 PERCENT

Figure 3.30 ^{1}H-NMR titration of **L^{4}** with TBABzO in DMSO-d_6.

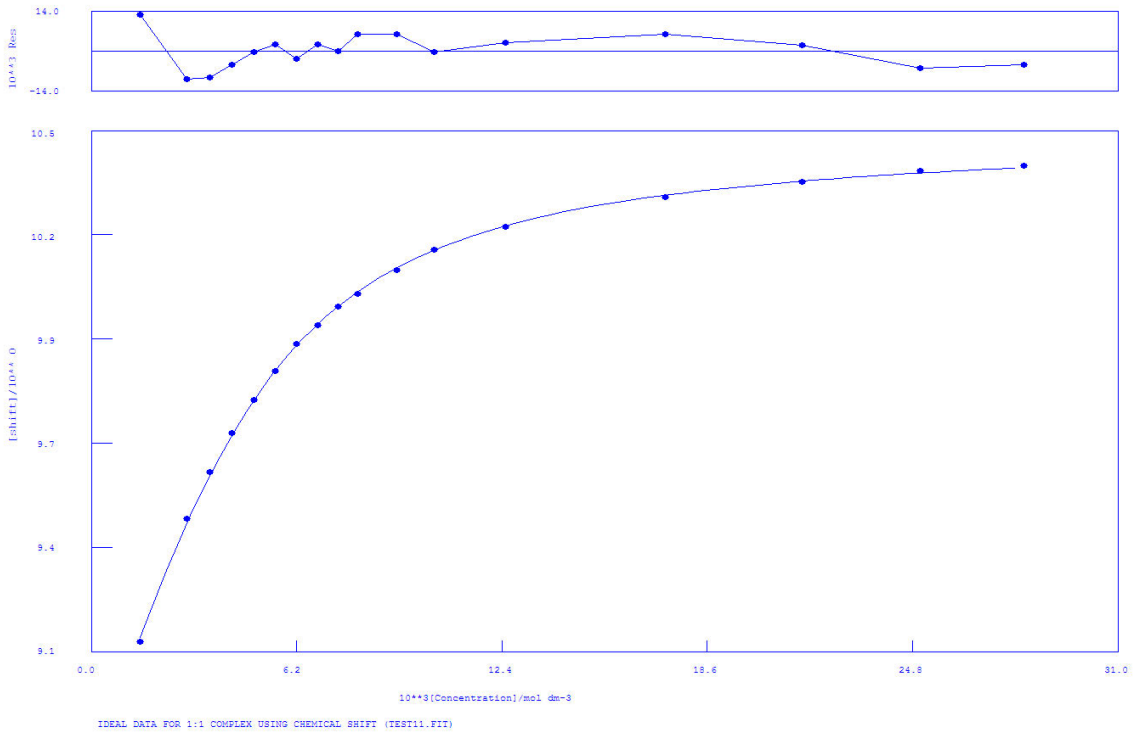

Calculations by WinEQNMR Version 1.20 by Michael J. Hynes
Program run at 15:59:57 on 06/06/2012

IDEAL DATA FOR 1:1 COMPLEX USING CHEMICAL SHIFT (TEST11.FIT)
Reaction: M + L = ML
FILE: TEST11.FIT
IDEAL DATA: K1 = 63.091; DELTA M = 20.0; DELTA ML = 120.0
File prepared by M. J. Hynes, October 22 2000

NO.	A	PARAMETER	DELTA	ERROR	CONDITION	DESCRIPTION
1	1	6.98292E+02	2.000E-01	1.614E+01	1.074E+01	K1
2	1	8.76393E+00	2.000E-01	7.809E-03	3.386E+00	SHIFT M
3	1	1.04988E+01	1.000E+00	5.360E-03	6.271E+00	SHIFT ML

0RMS ERROR = 6.38E-03 MAX ERROR = 1.28E-02 AT OBS.NO. 1
RESIDUALS SQUARED = 5.70E-04
RFACTOR = 0.0581 PERCENT

Figure 3.31 ^{1}H-NMR titration of **L^{4}** with $TBAH_2PO_4$ in DMSO-d_6.

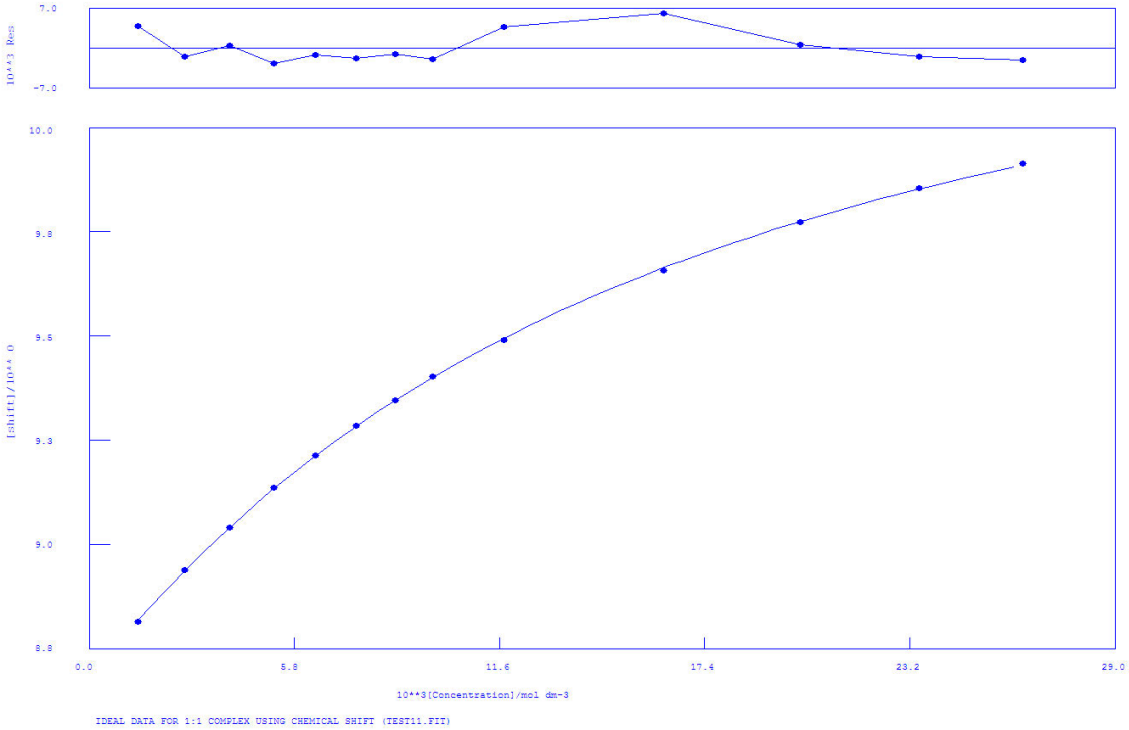

Calculations by WinEQNMR Version 1.20 by Michael J. Hynes
Program run at 16:21:44 on 06/06/2012

IDEAL DATA FOR 1:1 COMPLEX USING CHEMICAL SHIFT (TEST11.FIT)
Reaction: M + L = ML
FILE: TEST11.FIT
IDEAL DATA: K1 = 63.091; DELTA M = 20.0; DELTA ML = 120.0
File prepared by M. J. Hynes, October 22 2000

NO.	A	PARAMETER	DELTA	ERROR	CONDITION	DESCRIPTION
1	1	7.71037E+01	2.000E-01	1.590E+00	6.830E+01	K1
2	1	8.73194E+00	2.000E-01	3.174E-03	6.310E+00	SHIFT M
3	1	1.05761E+01	1.000E+00	1.407E-02	4.574E+01	SHIFT ML

0RMS ERROR = 3.02E-03 MAX ERROR = 5.99E-03 AT OBS.NO. 10
RESIDUALS SQUARED = 9.10E-05
RFACTOR = 0.0281 PERCENT

Figure 3.32 ^{1}H-NMR titration of **L^{4}** with $(TBA)_2Glu$ in DMSO-d_6.

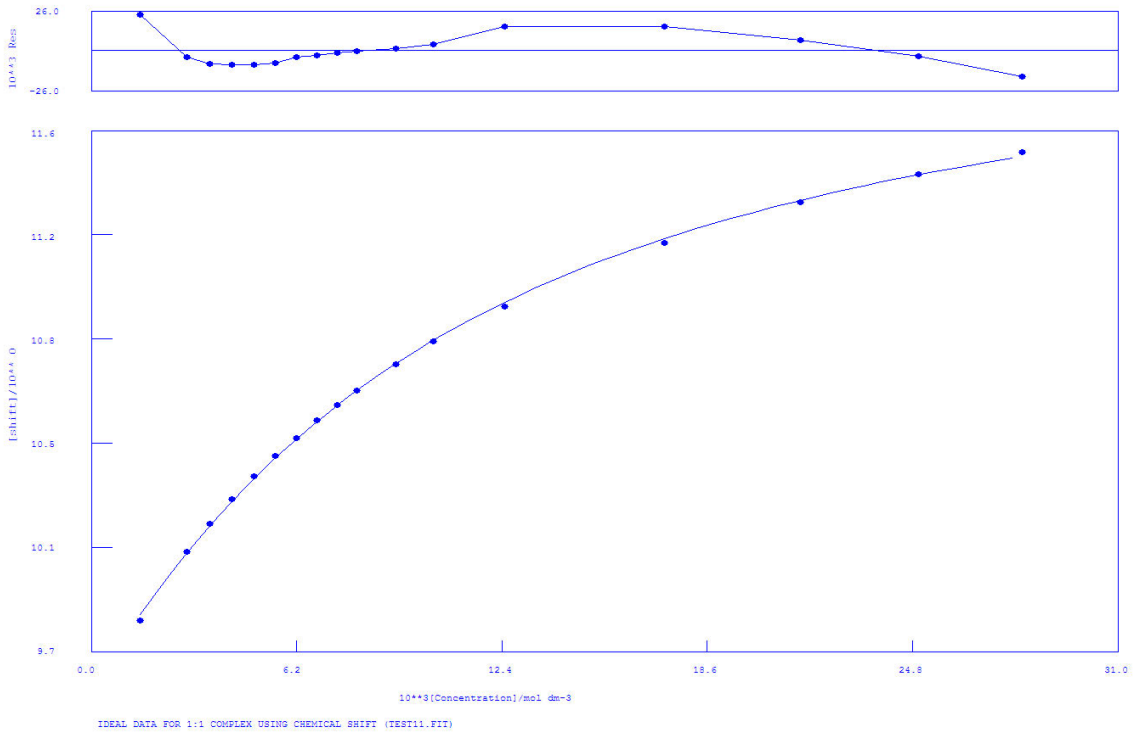

Calculations by WinEQNMR Version 1.20 by Michael J. Hynes
Program run at 14:48:56 on 06/06/2012

IDEAL DATA FOR 1:1 COMPLEX USING CHEMICAL SHIFT (TEST11.FIT)
Reaction: M + L = ML
FILE: TEST11.FIT
IDEAL DATA: K1 = 63.091; DELTA M = 20.0; DELTA ML = 120.0
File prepared by M. J. Hynes, October 22 2000

NO.	A	PARAMETER	DELTA	ERROR	CONDITION	DESCRIPTION
1	1	1.21073E+02	2.000E-01	4.592E+00	4.259E+01	K1
2	1	9.56785E+00	2.000E-01	1.224E-02	7.395E+00	SHIFT M
3	1	1.21602E+01	1.000E+00	2.839E-02	2.325E+01	SHIFT ML

0RMS ERROR = 1.12E-02 MAX ERROR = 2.33E-02 AT OBS.NO. 1
RESIDUALS SQUARED = 1.77E-03
RFACTOR = 0.0954 PERCENT

Figure 3.33 ^{1}H-NMR titration of **L^{5}** with TBAAcO in DMSO-d_6.

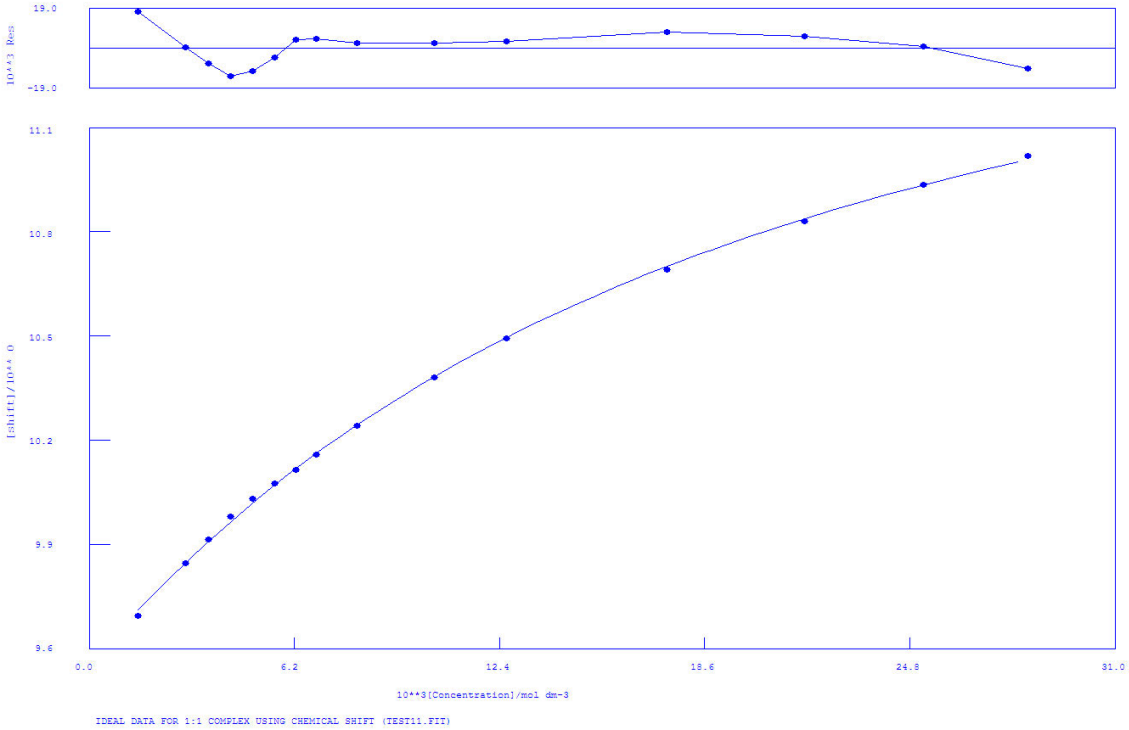

Calculations by WinEQNMR Version 1.20 by Michael J. Hynes
Program run at 15:03:17 on 06/06/2012

IDEAL DATA FOR 1:1 COMPLEX USING CHEMICAL SHIFT (TEST11.FIT)
Reaction: M + L = ML
FILE: TEST11.FIT
IDEAL DATA: K1 = 63.091; DELTA M = 20.0; DELTA ML = 120.0
File prepared by M. J. Hynes, October 22 2000

NO.	A	PARAMETER	DELTA	ERROR	CONDITION	DESCRIPTION
1	1	6.03580E+01	2.000E-01	3.150E+00	9.171E+01	K1
2	1	9.55363E+00	2.000E-01	9.247E-03	8.442E+00	SHIFT M
3	1	1.19574E+01	1.000E+00	4.975E-02	5.886E+01	SHIFT ML

0RMS ERROR = 8.78E-03 MAX ERROR = 1.72E-02 AT OBS.NO. 1
RESIDUALS SQUARED = 9.25E-04
RFACTOR = 0.0762 PERCENT

Figure 3.34 ^{1}H-NMR titration of **L^{5}** with TBABzO in DMSO-d_6.

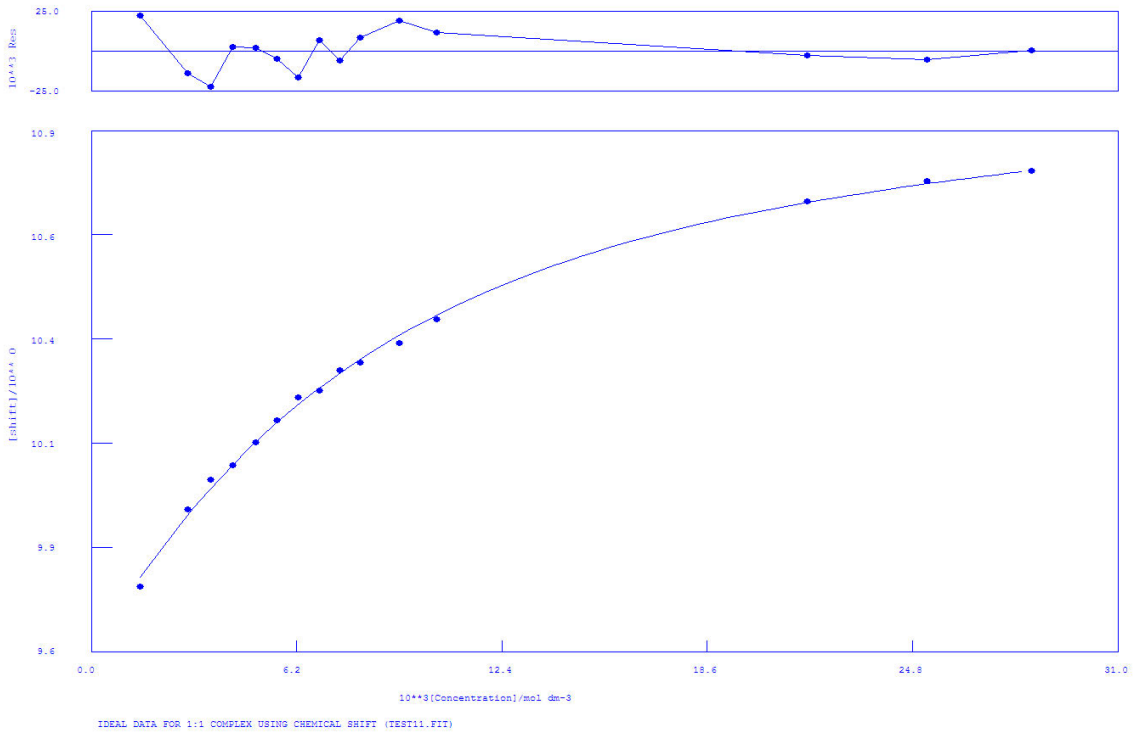

Calculations by WinEQNMR Version 1.20 by Michael J. Hynes
Program run at 14:36:47 on 06/06/2012

IDEAL DATA FOR 1:1 COMPLEX USING CHEMICAL SHIFT (TEST11.FIT)
Reaction: M + L = ML
FILE: TEST11.FIT
IDEAL DATA: K1 = 63.091; DELTA M = 20.0; DELTA ML = 120.0
File prepared by M. J. Hynes, October 22 2000

NO.	A	PARAMETER	DELTA	ERROR	CONDITION	DESCRIPTION
1	1	1.66748E+02	2.000E-01	1.195E+01	2.979E+01	K1
2	1	9.59614E+00	2.000E-01	1.690E-02	7.748E+00	SHIFT M
3	1	1.10940E+01	1.000E+00	2.570E-02	1.365E+01	SHIFT ML

0RMS ERROR = 1.35E-02 MAX ERROR = 2.25E-02 AT OBS.NO. 3
RESIDUALS SQUARED = 2.18E-03
RFACTOR = 0.1170 PERCENT

Figure 3.35 ^{1}H-NMR titration of **L^{5}** with $TBAH_2PO_4$ in DMSO-d_6.

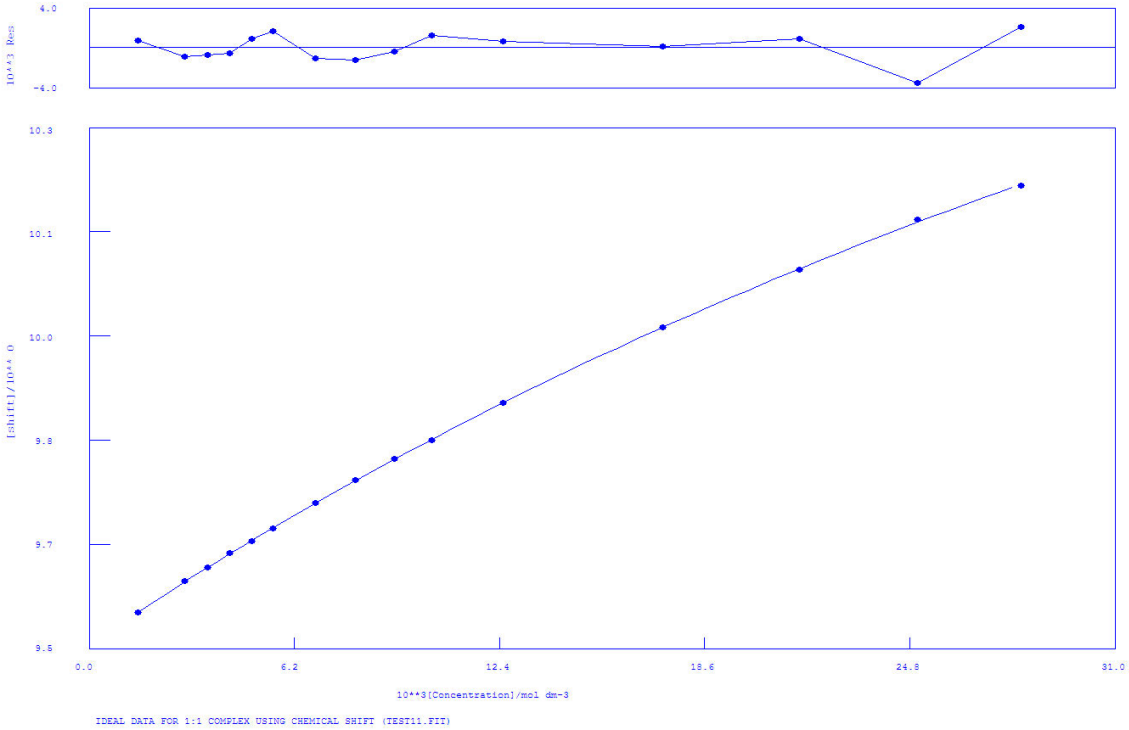

Calculations by WinEQNMR Version 1.20 by Michael J. Hynes
Program run at 15:26:34 on 06/06/2012

IDEAL DATA FOR 1:1 COMPLEX USING CHEMICAL SHIFT (TEST11.FIT)
Reaction: M + L = ML
FILE: TEST11.FIT
IDEAL DATA: K1 = 63.091; DELTA M = 20.0; DELTA ML = 120.0
File prepared by M. J. Hynes, October 22 2000

NO.	A	PARAMETER	DELTA	ERROR	CONDITION	DESCRIPTION
1	1	1.52949E+01	2.000E-01	4.882E-01	4.931E+02	K1
2	1	9.50565E+00	2.000E-01	1.295E-03	8.319E+00	SHIFT M
3	1	1.19438E+01	1.000E+00	5.325E-02	4.130E+02	SHIFT ML

0RMS ERROR = 1.53E-03 MAX ERROR = 3.52E-03 AT OBS.NO. 14
RESIDUALS SQUARED = 2.80E-05
RFACTOR = 0.0139 PERCENT

Figure 3.36 ^{1}H-NMR titration of **L^{5}** with $(TBA)_2Glu$ in DMSO-d_6.

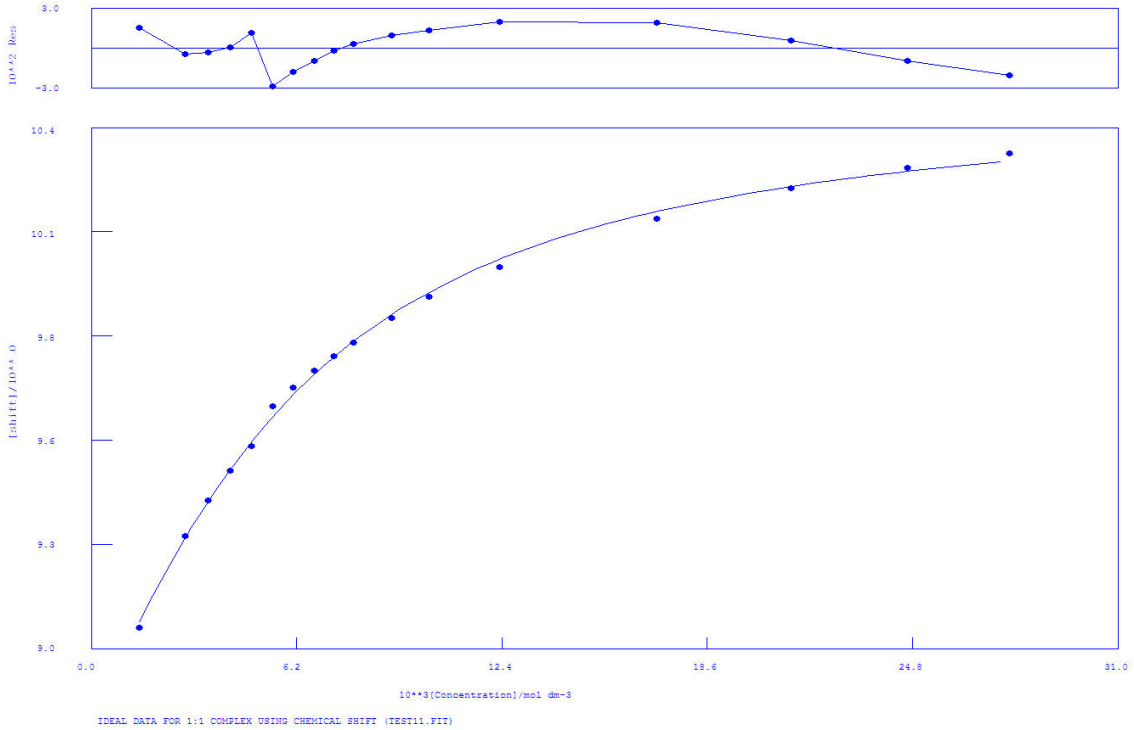

Calculations by WinEQNMR Version 1.20 by Michael J. Hynes
Program run at 11:44:14 on 02/08/2012

IDEAL DATA FOR 1:1 COMPLEX USING CHEMICAL SHIFT (TEST11.FIT)
Reaction: M + L = ML
FILE: TEST11.FIT
IDEAL DATA: K1 = 63.091; DELTA M = 20.0; DELTA ML = 120.0
File prepared by M. J. Hynes, October 22 2000

NO.	A	PARAMETER	DELTA	ERROR	CONDITION	DESCRIPTION
1	1	2.99470E+02	2.000E-01	1.765E+01	1.905E+01	K1
2	1	8.79504E+00	2.000E-01	1.701E-02	4.785E+00	SHIFT M
3	1	1.05260E+01	1.000E+00	1.959E-02	1.045E+01	SHIFT ML

0RMS ERROR = 1.52E-02 MAX ERROR = 2.90E-02 AT OBS.NO. 6
RESIDUALS SQUARED = 3.22E-03
RFACTOR = 0.1405 PERCENT

Figure 3.37 ^{1}H-NMR titration of **L^{6}** with TBAAcO in DMSO-d_6.

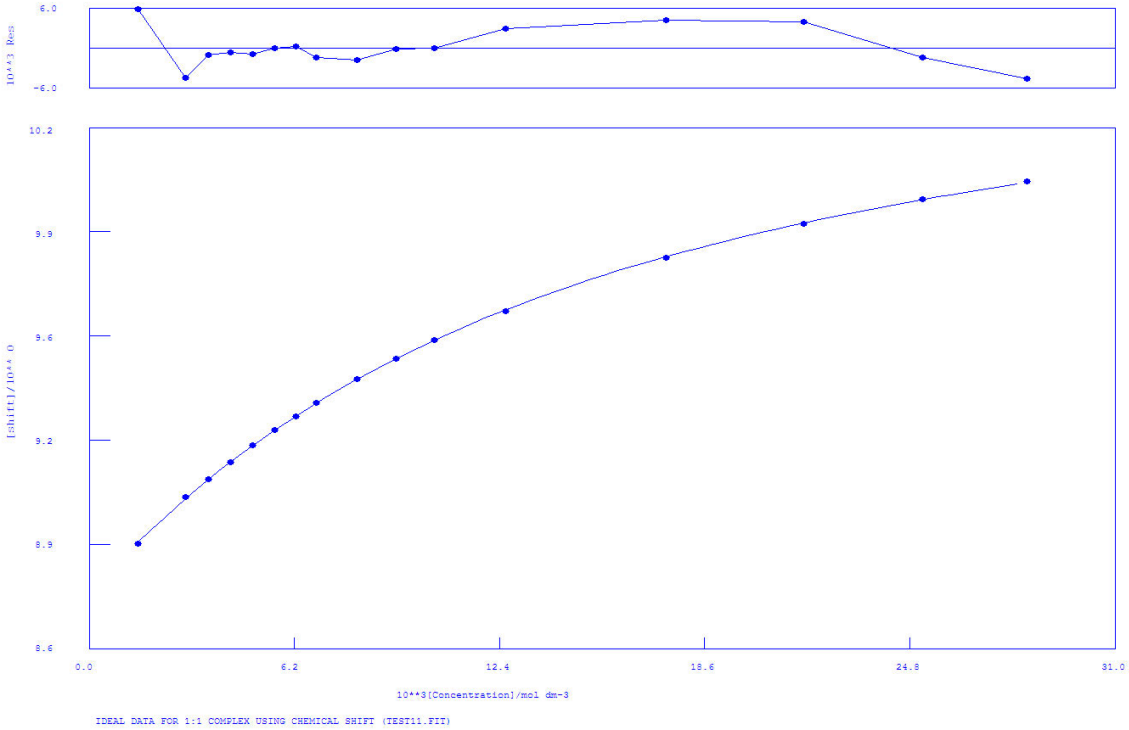

Calculations by WinEQNMR Version 1.20 by Michael J. Hynes
Program run at 17:06:57 on 03/01/2012

IDEAL DATA FOR 1:1 COMPLEX USING CHEMICAL SHIFT (TEST11.FIT)
Reaction: M + L = ML
FILE: TEST11.FIT
IDEAL DATA: K1 = 63.091; DELTA M = 20.0; DELTA ML = 120.0
File prepared by M. J. Hynes, October 22 2000

NO.	A	PARAMETER	DELTA	ERROR	CONDITION	DESCRIPTION
1	1	8.79467E+01	2.000E-01	1.500E+00	5.130E+01	K1
2	1	8.77283E+00	2.000E-01	3.254E-03	7.445E+00	SHIFT M
3	1	1.06041E+01	1.000E+00	1.029E-02	2.960E+01	SHIFT ML

0RMS ERROR = 3.12E-03 MAX ERROR = 5.76E-03 AT OBS.NO. 1
RESIDUALS SQUARED = 1.26E-04
RFACTOR = 0.0297 PERCENT

Figure 3.38 ^{1}H-NMR titration of **L^{6}** with TBABzO in DMSO-d_6.

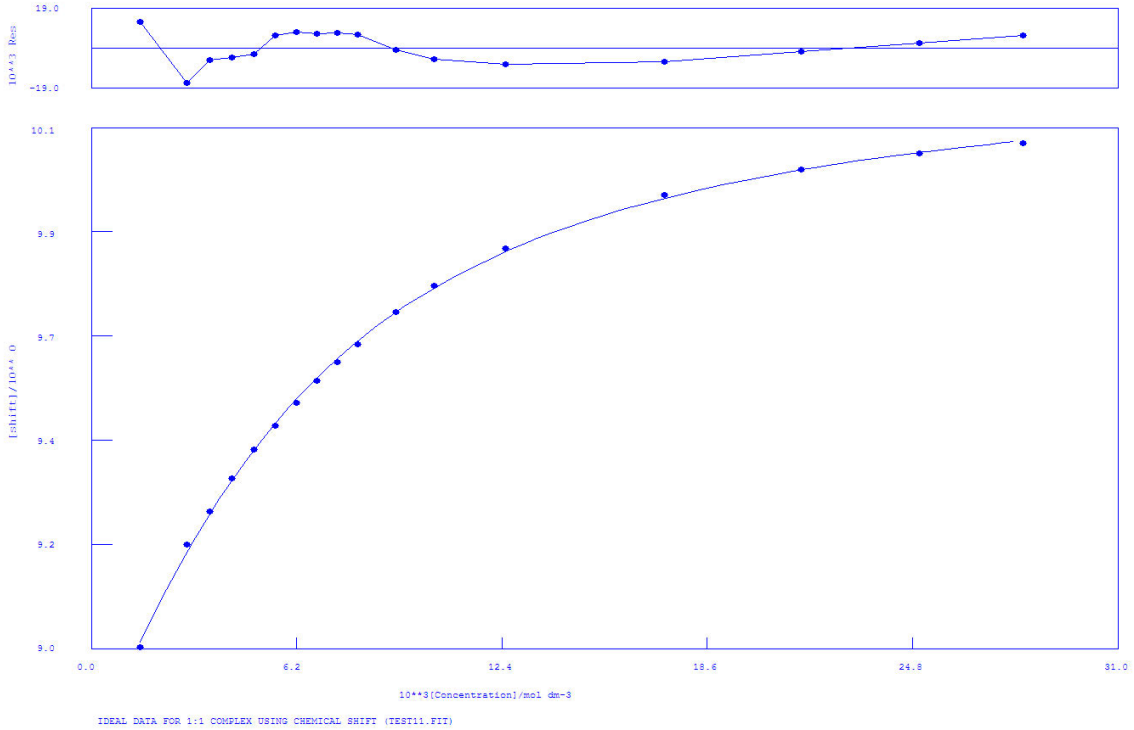

Calculations by WinEQNMR Version 1.20 by Michael J. Hynes
Program run at 12:10:49 on 02/08/2012

IDEAL DATA FOR 1:1 COMPLEX USING CHEMICAL SHIFT (TEST11.FIT)
Reaction: M + L = ML
FILE: TEST11.FIT
IDEAL DATA: K1 = 63.091; DELTA M = 20.0; DELTA ML = 120.0
File prepared by M. J. Hynes, October 22 2000

NO.	A	PARAMETER	DELTA	ERROR	CONDITION	DESCRIPTION
1	1	2.73005E+02	2.000E-01	1.018E+01	2.087E+01	K1
2	1	8.78206E+00	2.000E-01	9.409E-03	5.442E+00	SHIFT M
3	1	1.02701E+01	1.000E+00	1.072E-02	1.076E+01	SHIFT ML

0RMS ERROR = 8.03E-03 MAX ERROR = 1.69E-02 AT OBS.NO. 2
RESIDUALS SQUARED = 9.02E-04
RFACTOR = 0.0757 PERCENT

Figure 3.39 ^{1}H-NMR titration of **L^{6}** with $TBAH_2PO_4$ in DMSO-d_6.

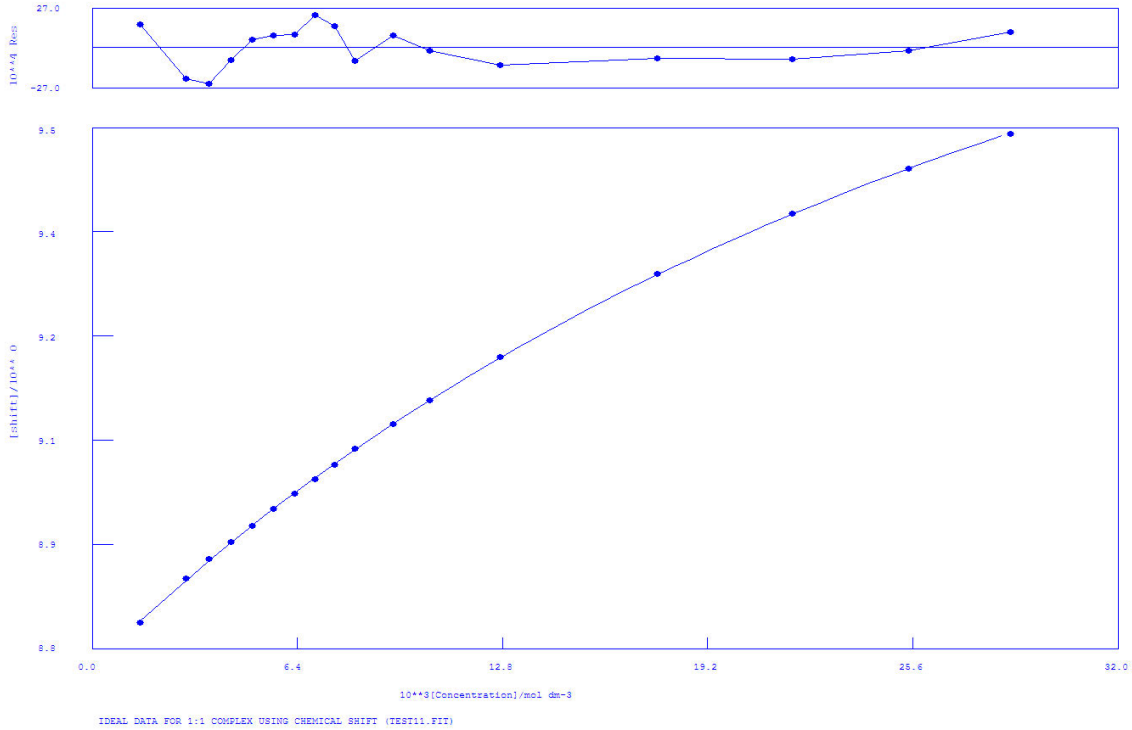

Calculations by WinEQNMR Version 1.20 by Michael J. Hynes
Program run at 16:06:56 on 03/01/2012

IDEAL DATA FOR 1:1 COMPLEX USING CHEMICAL SHIFT (TEST11.FIT)
Reaction: M + L = ML
FILE: TEST11.FIT
IDEAL DATA: K1 = 63.091; DELTA M = 20.0; DELTA ML = 120.0
File prepared by M. J. Hynes, October 22 2000

NO.	A	PARAMETER	DELTA	ERROR	CONDITION	DESCRIPTION
1	1	3.02974E+01	2.000E-01	5.495E-01	1.614E+02	K1
2	1	8.77531E+00	2.000E-01	1.252E-03	8.871E+00	SHIFT M
3	1	1.03904E+01	1.000E+00	1.555E-02	1.151E+02	SHIFT ML

0RMS ERROR = 1.40E-03 MAX ERROR = 2.43E-03 AT OBS.NO. 3
RESIDUALS SQUARED = 2.74E-05
RFACTOR = 0.0139 PERCENT

Figure 3.40 ^{1}H-NMR titration of **L^{6}** with $(TBA)_2Glu$ in DMSO-d_6.

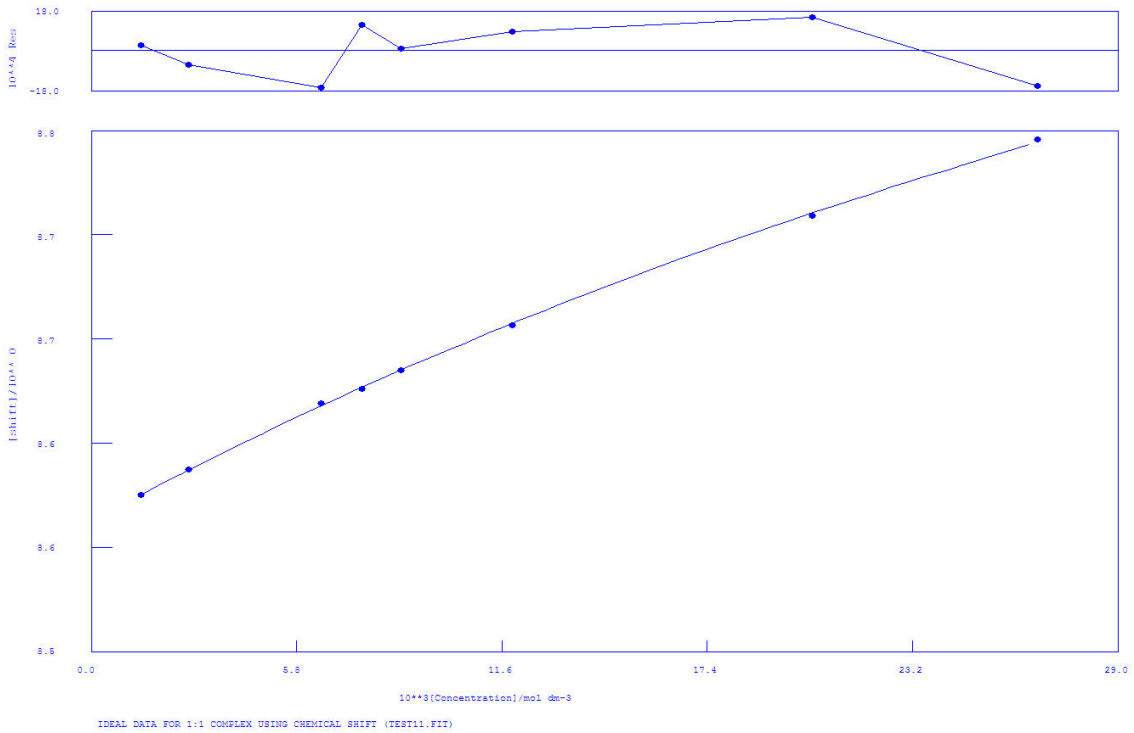

Calculations by WinEQNMR Version 1.20 by Michael J. Hynes
Program run at 13:22:08 on 07/25/2012

IDEAL DATA FOR 1:1 COMPLEX USING CHEMICAL SHIFT (TEST11.FIT)
Reaction: M + L = ML
FILE: TEST11.FIT
IDEAL DATA: K1 = 63.091; DELTA M = 20.0; DELTA ML = 120.0
File prepared by M. J. Hynes, October 22 2000

NO.	A	PARAMETER	DELTA	ERROR	CONDITION	DESCRIPTION
1	1	1.47071E+01	2.000E-01	1.452E+00	2.970E+02	K1
2	1	8.57506E+00	2.000E-01	1.292E-03	5.168E+00	SHIFT M
3	1	9.37610E+00	1.000E+00	5.472E-02	2.557E+02	SHIFT ML

0RMS ERROR = 1.42E-03 MAX ERROR = 1.65E-03 AT OBS.NO. 3
RESIDUALS SQUARED = 1.01E-05
RFACTOR = 0.0129 PERCENT

Figure 3.41 ^{1}H-NMR titration of **L^{3}** with TBAAcO in DMSO-d_6/0.5%H_2O.

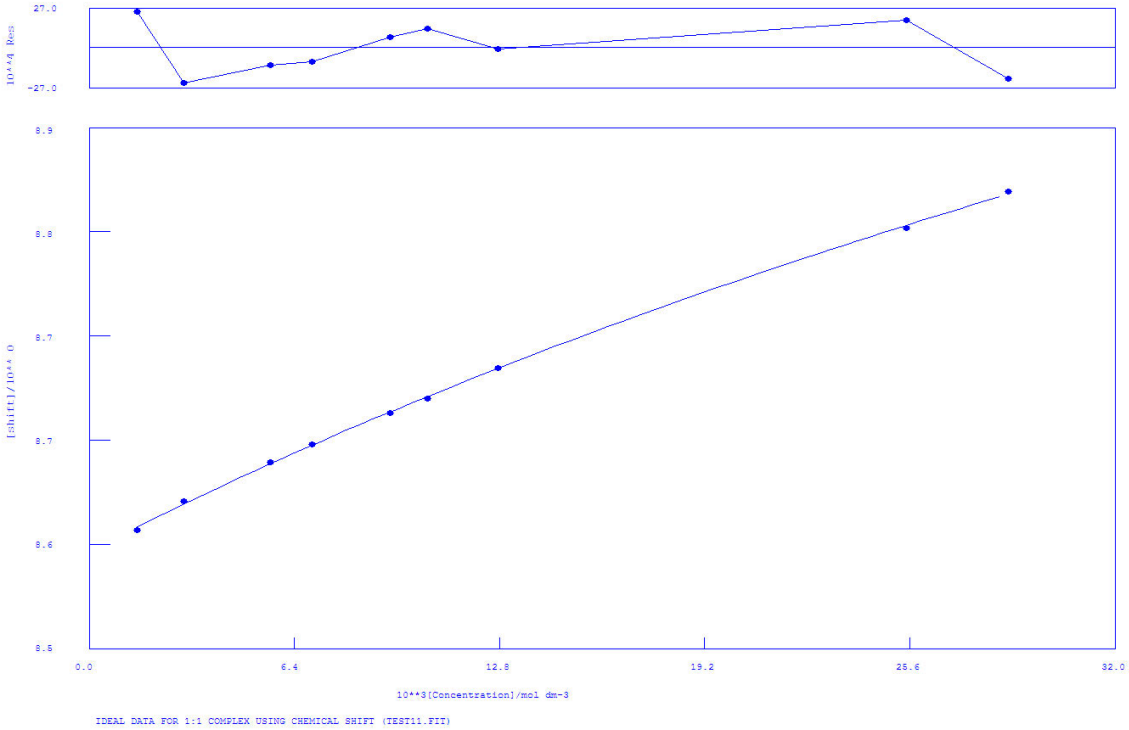

Calculations by WinEQNMR Version 1.20 by Michael J. Hynes
Program run at 13:29:07 on 07/25/2012

IDEAL DATA FOR 1:1 COMPLEX USING CHEMICAL SHIFT (TEST11.FIT)
Reaction: M + L = ML
FILE: TEST11.FIT
IDEAL DATA: K1 = 63.091; DELTA M = 20.0; DELTA ML = 120.0
File prepared by M. J. Hynes, October 22 2000

NO.	A	PARAMETER	DELTA	ERROR	CONDITION	DESCRIPTION
1	1	1.14006E+01	2.000E-01	1.607E+00	5.616E+02	K1
2	1	8.57504E+00	2.000E-01	2.008E-03	7.313E+00	SHIFT M
3	1	9.71930E+00	1.000E+00	1.117E-01	4.838E+02	SHIFT ML

0RMS ERROR = 1.99E-03 MAX ERROR = 2.45E-03 AT OBS.NO. 1
RESIDUALS SQUARED = 2.39E-05
RFACTOR = 0.0187 PERCENT

Figure 3.42 ^{1}H-NMR titration of **L^{3}** with TBABzO in DMSO-d_6/0.5%H_2O.

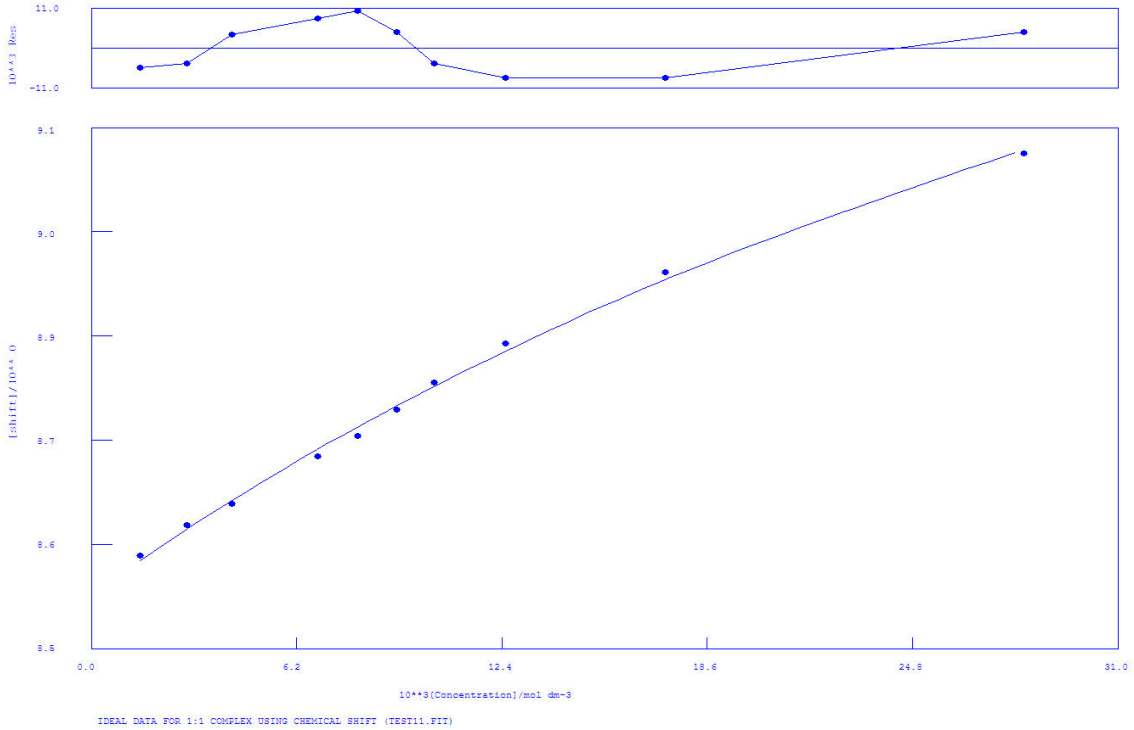

Calculations by WinEQNMR Version 1.20 by Michael J. Hynes
Program run at 13:34:19 on 07/25/2012

IDEAL DATA FOR 1:1 COMPLEX USING CHEMICAL SHIFT (TEST11.FIT)
Reaction: M + L = ML
FILE: TEST11.FIT
IDEAL DATA: K1 = 63.091; DELTA M = 20.0; DELTA ML = 120.0
File prepared by M. J. Hynes, October 22 2000

NO.	A	PARAMETER	DELTA	ERROR	CONDITION	DESCRIPTION
1	1	2.07454E+01	2.000E-01	4.325E+00	2.344E+02	K1
2	1	8.56248E+00	2.000E-01	7.751E-03	7.191E+00	SHIFT M
3	1	1.00055E+01	1.000E+00	1.895E-01	1.860E+02	SHIFT ML

0RMS ERROR = 7.80E-03 MAX ERROR = 1.02E-02 AT OBS.NO. 5
RESIDUALS SQUARED = 4.26E-04
RFACTOR = 0.0743 PERCENT

Figure 3.43 ^{1}H-NMR titration of **L^{3}** with $TBAH_2PO_4$ in DMSO-d_6/0.5%H_2O.

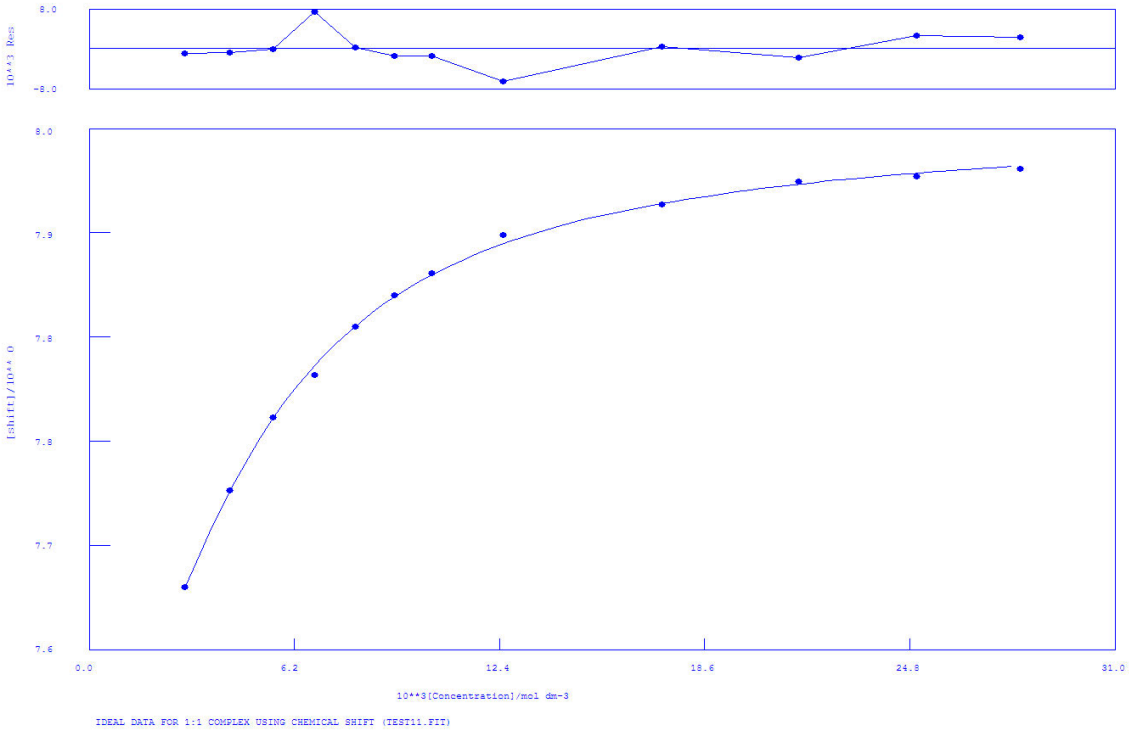

Calculations by WinEQNMR Version 1.20 by Michael J. Hynes
Program run at 17:52:28 on 06/21/2012

IDEAL DATA FOR 1:1 COMPLEX USING CHEMICAL SHIFT (TEST11.FIT)
Reaction: M + L = ML
FILE: TEST11.FIT
IDEAL DATA: K1 = 63.091; DELTA M = 20.0; DELTA ML = 120.0
File prepared by M. J. Hynes, October 22 2000

NO.	A	PARAMETER	DELTA	ERROR	CONDITION	DESCRIPTION
1	1	5.69754E+02	2.000E-01	3.132E+01	1.634E+01	K1
2	1	7.43388E+00	2.000E-01	8.033E-03	5.719E+00	SHIFT M
3	1	8.01066E+00	1.000E+00	3.742E-03	7.258E+00	SHIFT ML

0RMS ERROR = 3.64E-03 MAX ERROR = 7.45E-03 AT OBS.NO. 4
RESIDUALS SQUARED = 1.19E-04
RFACTOR = 0.0401 PERCENT

Figure 3.44 ^{1}H-NMR titration of **L^{3}** with $(TBA)_3HPpi$ in DMSO-d_6/0.5%H_2O.

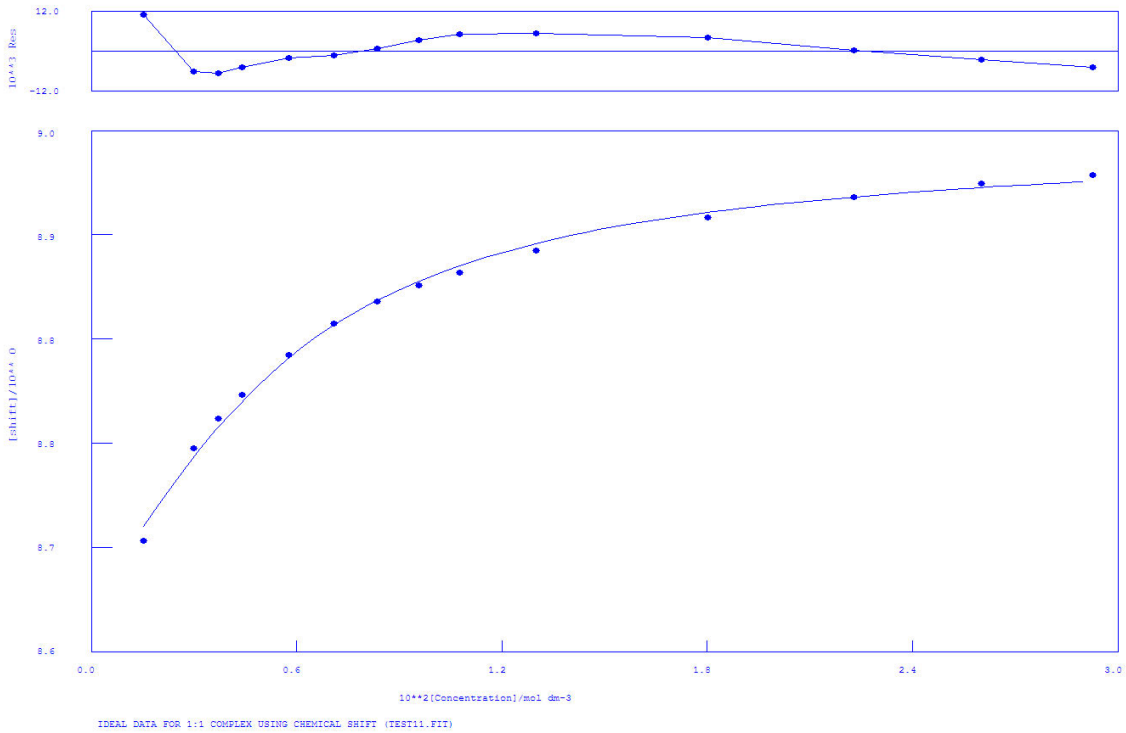

Calculations by WinEQNMR Version 1.20 by Michael J. Hynes
Program run at 17:41:55 on 06/06/2012

IDEAL DATA FOR 1:1 COMPLEX USING CHEMICAL SHIFT (TEST11.FIT)
Reaction: M + L = ML
FILE: TEST11.FIT
IDEAL DATA: K1 = 63.091; DELTA M = 20.0; DELTA ML = 120.0
File prepared by M. J. Hynes, October 22 2000

NO.	A	PARAMETER	DELTA	ERROR	CONDITION	DESCRIPTION
1	1	3.68944E+02	2.000E-01	3.693E+01	1.359E+01	K1
2	1	8.62850E+00	2.000E-01	6.646E-03	3.673E+00	SHIFT M
3	1	8.99647E+00	1.000E+00	6.268E-03	7.884E+00	SHIFT ML

0RMS ERROR = 5.57E-03 MAX ERROR = 1.08E-02 AT OBS.NO. 1
RESIDUALS SQUARED = 3.41E-04
RFACTOR = 0.0557 PERCENT

Figure 3.45 ^{1}H-NMR titration of **L^{3}** with NaAMP in DMSO-d_6.

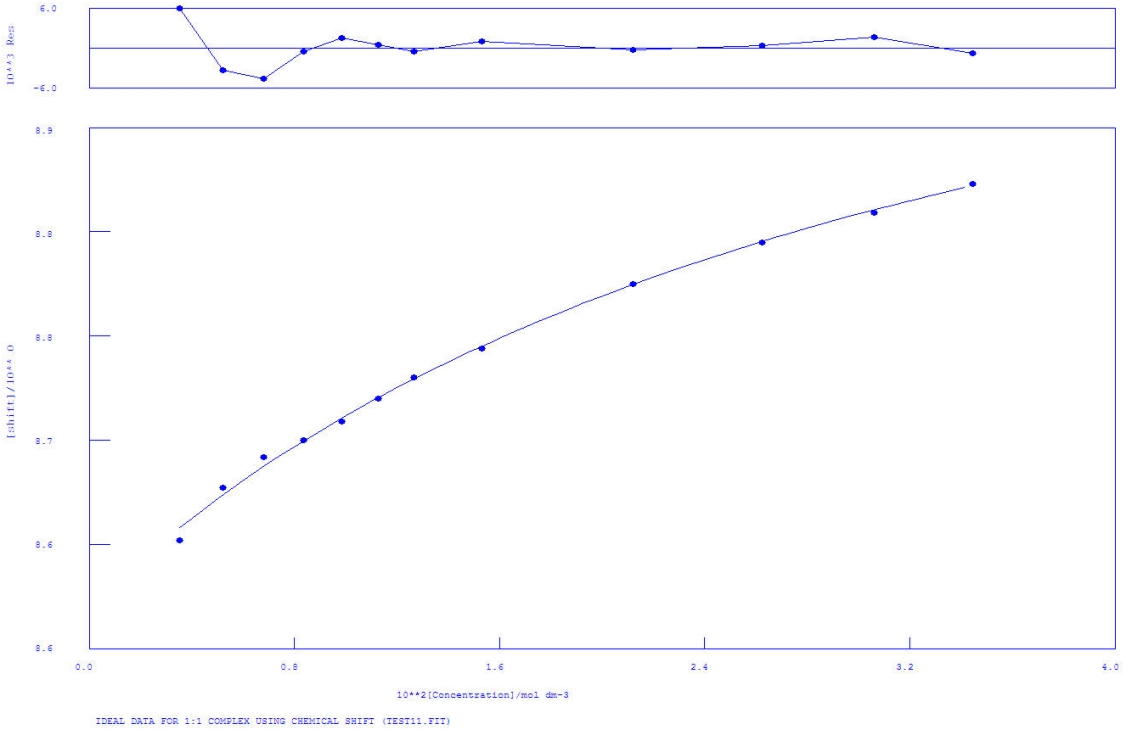

Calculations by WinEQNMR Version 1.20 by Michael J. Hynes
Program run at 18:02:50 on 06/21/2012

IDEAL DATA FOR 1:1 COMPLEX USING CHEMICAL SHIFT (TEST11.FIT)
Reaction: M + L = ML
FILE: TEST11.FIT
IDEAL DATA: K1 = 63.091; DELTA M = 20.0; DELTA ML = 120.0
File prepared by M. J. Hynes, October 22 2000

NO.	A	PARAMETER	DELTA	ERROR	CONDITION	DESCRIPTION
1	1	3.53294E+01	2.000E-01	5.083E+00	1.465E+02	K1
2	1	8.62097E+00	2.000E-01	3.994E-03	1.175E+01	SHIFT M
3	1	9.00015E+00	1.000E+00	2.445E-02	9.371E+01	SHIFT ML

0RMS ERROR = 2.88E-03 MAX ERROR = 5.89E-03 AT OBS.NO. 1
RESIDUALS SQUARED = 7.47E-05
RFACTOR = 0.0286 PERCENT

Figure 3.46 ^{1}H-NMR titration of **L^{3}** with NaAMP in DMSO-d_6/0.5%H_2O.

3.7.3 Crystallographic Data

Table 3.3. Crystal data and structure refinement details.

Identification code	**2012acc0042** (MAR94_4 BENZOATO)
Empirical formula	$C_{75}H_{107}N_7O_6$
	$C_{29}H_{25}N_5O_2$, 2($C_{16}H_{36}N$), 2($C_7H_5O_2$)
Formula weight	1202.68
Temperature	100(2) K
Wavelength	0.71075 Å
Crystal system	Monoclinic
Space group	$P2_1/n$
Unit cell dimensions	a = 8.623(3) Å
	b = 41.598(13) Å β = 100.518(5)°
	c = 19.413(6) Å
Volume	6846(4) Å^3
Z	4
Density (calculated)	1.167 Mg / m^3
Absorption coefficient	0.074 mm^{-1}
F(000)	2616
Crystal	Rod; Colourless
Crystal size	0.22 × 0.04 × 0.02 mm^3
θ range for data collection	2.94 – 25.03°
Index ranges	$-10 \le h \le 9$, $-49 \le k \le 44$, $-13 \le l \le 23$
Reflections collected	26420
Independent reflections	12037 [R_{int} = 0.0798]
Completeness to θ = 25.03°	99.5 %
Absorption correction	Semi–empirical from equivalents
Max. and min. transmission	0.9985 and 0.9840
Refinement method	Full-matrix least-squares on F^2
Data / restraints / parameters	12037 / 0 / 801
Goodness-of-fit on F^2	1.196
Final R indices [$F^2 > 2\sigma(F^2)$]	*R1* = 0.1018, *wR2* = 0.1504
R indices (all data)	*R1* = 0.1606, *wR2* = 0.1762
Largest diff. peak and hole	0.384 and –0.249 e Å^{-3}

Diffractometer: *Rigaku AFC12* goniometer equipped with an enhanced sensitivity (HG) *Saturn724+* detector mounted at the window of an *FR-E+ SuperBright* molybdenum rotating anode generator with HF *Varimax* optics (100µm focus). **Cell determination, Data collection, Data reduction and cell refinement & Absorption correction**: CrystalClear-SM Expert 2.0 r7 (Rigaku, 2011) , **Structure solution**: SHELXS97 (G. M. Sheldrick, Acta Cryst. (1990) A**46** 467–473). S**tructure refinement**: SHELXL97 (G. M. Sheldrick (1997), University of Göttingen, Germany). **Graphics:** CrystalMaker: a crystal and molecular structures program for Mac and Windows. CrystalMaker Software Ltd, Oxford, England (www.crystalmaker.com)

Table 3.4. Hydrogen bonds [Å and °].

D–H···*A*	*d*(*D*–H)	*d*(H···*A*)	*d*(*D*···*A*)	∠(*D*H*A*)
N1–H901···O3	0.88	1.94	2.816(4)	171.9
N2–H902···O4	0.88	1.95	2.809(4)	166.1
N4–H904···O5	0.88	1.96	2.831(4)	170.1
N5–H905···O6	0.88	1.91	2.760(4)	161.6

References

1. Sessler, J. L., Gale, P. & Cho, W.-S. *Anion Receptor Chemistry*. (Royal Society of Chemistry, 2006). doi:10.1039/9781847552471

2. Wenzel, M., Hiscock, J. R. & Gale, P. A. Anion receptor chemistry: highlights from 2010. *Chem. Soc. Rev.* **41,** 480–520 (2012).

3. Gale, P. A. & Gunnlaugsson, T. Preface: supramolecular chemistry of anionic species themed issue. *Chem. Soc. Rev.* **39,** 3595 (2010).

4. Wiskur, S. L., Ait-Haddou, H., Lavigne, J. J. & Anslyn, E. V. Teaching Old Indicators New Tricks. *Acc. Chem. Res.* **34,** 963–972 (2001).

5. Martínez-Máñez, R. & Sancenón, F. Fluorogenic and chromogenic chemosensors and reagents for anions. *Chem. Rev.* **103,** 4419–76 (2003).

6. Lee, H. N. *et al.* Pyrophosphate-selective fluorescent chemosensor at physiological pH: formation of a unique excimer upon addition of pyrophosphate. *J. Am. Chem. Soc.* **129,** 3828–9 (2007).

7. Mathews, C. P. . van H. K. E. in *Biochemistry* (The Benjamin/Cummings Publishing Co., Inc., 1990).

8. Xu, S. *et al.* A quantitative method to measure telomerase activity by bioluminescence connected with telomeric repeat amplification protocol. *Anal. Biochem.* **299,** 188–93 (2001).

9. Doherty, M., Belcher, C., Regan, M., Jones, A. & Ledingham, J. Association between synovial fluid levels of inorganic pyrophosphate and short term radiographic outcome of knee osteoarthritis. *Ann. Rheum. Dis.* **55,** 432–6 (1996).

10. Timms, a E., Zhang, Y., Russell, R. G. G. & Brown, M. a. Genetic studies of disorders of calcium crystal deposition. *Rheumatology (Oxford).* **41,** 725–9 (2002).

11. Kim, S. K., Lee, D. H., Hong, J.-I. & Yoon, J. Chemosensors for pyrophosphate. *Acc. Chem. Res.* **42,** 23–31 (2009).

12. Vance, D. H. & Czarnik, A. W. Real-Time Assay of Inorganic Pyrophosphatase Using a High-Affinity Chelation-Enhanced Fluorescence Chemosensor. *J. Am. Chem. Soc.* **116,** 9397–9398 (1994).

13. Cho, H. K., Lee, D. H. & Hong, J.-I. A fluorescent pyrophosphate sensor via excimer formation in water. *Chem. Commun. (Camb).* 1690–2 (2005). doi:10.1039/b417845a

14. Fabbrizzi, L., Marcotte, N., Stomeo, F. & Taglietti, A. Pyrophosphate detection in water by fluorescence competition assays: inducing selectivity through the choice of the indicator. *Angew. Chem. Int. Ed. Engl.* **41,** 3811–4 (2002).

15. McDonough, M. J., Reynolds, A. J., Lee, W. Y. G. & Jolliffe, K. A. Selective recognition of pyrophosphate in water using a backbone modified cyclic peptide receptor. *Chem. Commun. (Camb).* 2971–3 (2006). doi:10.1039/b606917g

16. Lee, D. H., Kim, S. Y. & Hong, J.-I. Quencher–fluorophore ensemble for detection of pyrophosphate in water. *Tetrahedron Lett.* **48,** 4477–4480 (2007).

17. Lee, D. H., Kim, S. Y. & Hong, J.-I. A fluorescent pyrophosphate sensor with high selectivity over ATP in water. *Angew. Chem. Int. Ed. Engl.* **43,** 4777–80 (2004).

18. Lee, J. H., Park, J., Lah, M. S., Chin, J. & Hong, J.-I. High-affinity pyrophosphate receptor by a synergistic effect between metal coordination and hydrogen bonding in water. *Org. Lett.* **9,** 3729–31 (2007).

19. Zhang, J. F. *et al.* Pyrophosphate-selective fluorescent chemosensor based on 1,8-naphthalimide-DPA-Zn(II) complex and its application for cell imaging. *Org. Lett.* **13,** 5294–7 (2011).

20. Nishizawa, S., Kato, Y. & Teramae, N. Fluorescence Sensing of Anions via Intramolecular Excimer Formation in a Pyrophosphate-Induced Self-Assembly of a Pyrene-Functionalized Guanidinium Receptor. *J. Am. Chem. Soc.* **121,** 9463–9464 (1999).

21. Sun, Y., Zhong, C., Gong, R. & Fu, E. A highly selective fluorescent probe for pyrophosphate in aqueous solution. *Org. Biomol. Chem.* **6,** 3044–7 (2008).

22. Kwon, J. Y. *et al.* Fluorescent GTP-sensing in aqueous solution of physiological pH. *J. Am. Chem. Soc.* **126,** 8892–3 (2004).

23. Yoon, J. *et al.* Highly effective fluorescent sensor for H2PO4(-). *J. Org. Chem.* **69,** 581–3 (2004).

24. Kim, S. K. *et al.* Fluorescent imidazolium receptors for the recognition of pyrophosphate. *Tetrahedron* **62,** 6065–6072 (2006).

25. Aldakov, D. & Anzenbacher, Jr, P. Dipyrrolyl quinoxalines with extended chromophores are efficient fluorimetric sensors for pyrophosphateElectronic supplementary information (ESI) available: experimental data. See http://www.rsc.org/suppdata/cc/b3/b301362f/. *Chem. Commun.* 1394 (2003). doi:10.1039/b301362f

26. Aldakov, D. & Anzenbacher, P. Sensing of aqueous phosphates by polymers with dual modes of signal transduction. *J. Am. Chem. Soc.* **126,** 4752–3 (2004).

27. Anzenbacher, P., Jursíková, K. & Sessler, J. L. Second Generation Calixpyrrole Anion Sensors. *J. Am. Chem. Soc.* **122,** 9350–9351 (2000).

28. Kwon, J. Y. *et al.* Unique hydrogen bonds between 9-anthracenyl hydrogen and anions. *J. Org. Chem.* **69,** 5155–7 (2004).

29. Gunnlaugsson, T., Davis, A. P., O'Brien, J. E. & Glynn, M. Synthesis and photophysical evaluation of charge neutral thiourea or urea based fluorescent PET sensors for bis-carboxylates and pyrophosphate. *Org. Biomol. Chem.* **3,** 48–56 (2005).

30. Nishizawa, S., Bühlmann, P., Iwao, M. & Umezawa, Y. Anion recognition by urea and thiourea groups: Remarkably simple neutral receptors for dihydrogenphosphate. *Tetrahedron Lett.* **36,** 6483–6486 (1995).

31. Nishizawa, S., Bühlmann, P., Xiao, K. P. & Umezawa, Y. Application of a bis-thiourea ionophore for an anion selective electrode with a remarkable sulfate selectivity. *Anal. Chim. Acta* **358,** 35–44 (1998).

32. Emgenbroich, M. *et al.* A phosphotyrosine-imprinted polymer receptor for the recognition of tyrosine phosphorylated peptides. *Chemistry* **14,** 9516–29 (2008).

33. Nolan, C. & Gunnlaugsson, T. Improved synthesis of a C3-symmetrical pyridinophane. *Tetrahedron Lett.* **49,** 1993–1996 (2008).

34. Hynes, M. J. EQNMR: a computer program for the calculation of stability constants from nuclear magnetic resonance chemical shift data. *J. Chem. Soc. Dalt. Trans.* 311 (1993). doi:10.1039/dt9930000311

35. Stewart, J. J. P. Optimization of parameters for semiempirical methods I. Method. *J. Comput. Chem.* **10,** 209–220 (1989).

36. Stewart, J. J. P. Optimization of parameters for semiempirical methods II. Applications. *J. Comput. Chem.* **10,** 221–264 (1989).

37. Duke, R. M., McCabe, T., Schmitt, W. & Gunnlaugsson, T. Recognition and sensing of biologically relevant anions in alcohol and mixed alcohol-aqueous solutions using charge neutral cleft-like glycol-derived pyridyl-amidothiourea receptors. *J. Org. Chem.* **77,** 3115–26 (2012).

38. Boiocchi, M. *et al.* Anion-induced urea deprotonation. *Chemistry* **11,** 3097–104 (2005).

39. Mei, M. & Wu, S. Fluorescent sensor for α,ω-dicarboxylate anions. *New J. Chem.* **25,** 471–475 (2001).

Chapter 4 : Bis-urea receptors as synthetic transmembrane anion transporters

Chapter 4: Bis-urea receptors as synthetic transmembrane anion transporters

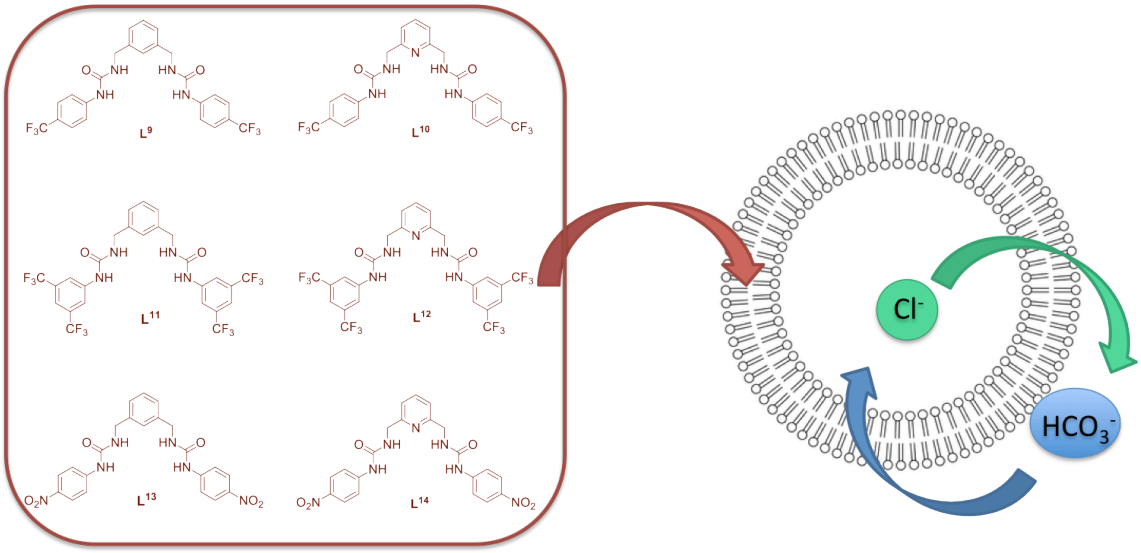

4.1 Introduction

Bis-urea synthetic motifs have been used extensively for anion recognition. As shown in previous chapter, Umezawa and co-workers reported that bis-ureas and thioureas (**136**-**138**) showed some affinity for $H_2PO_4^-$ (K_a = 820 M^{-1} for the urea derivative **136**) in DMSO-d_6.[1] The same group also studied the application of the phenyl-substituted thioureas as an ionophore for the fabrication of anion selective electrodes with remarkable sulfate selectivity.[2] More recently Sellergren and co-workers studied the recognition of tyrosine phosphorylated peptides by the vinylphenyl urea derivative of 1,3-bis(aminomethyl)benzene (**139**).[3]

We have recently reported the anion binding properties of a new family of bis-ureidic receptors based on 1,3-bis(aminomethyl)benzene and 2,6-bis(aminomethyl)pyridine (**L**^{3}-**L**^{8}) and the pyrophosphate optical sensing properties of 1,3-bis(aminomethyl)benzene (**L**^{5}) and 2,6-bis(aminomethyl)pyridine (**L**^{8}) discussed in Chapter 3.[4] We therefore decide to extend the family of bisureidic receptors and explore the anion transport properties of compounds **L**^{9}-**L**^{14}.

The development of synthetic transmembrane anion transporters is a rapidly expanding area of Supramolecular Chemistry.[5] The regulation of cellular anion concentrations is fundamental to many biological processes and a malfunction of anion transport is a cause of numerous diseases. Misregulation of chloride and bicarbonate transport is linked to various pathologies including Cystic Fibrosis.[6] Synthetic molecules that can facilitate the

transmembrane transport of chloride and bicarbonate may have applications in the treatment of this type of disease. [7,8,9,10]

4.2 Synthesis

The series of bis-ureidic compound **L[9]**-**L[14]** was synthesised similarly to the compounds **L[3]**-**L[8]** reported in the previous chapter. Compounds **L[9]**,**L[11]** and **L[13]** were synthesised starting by commercially available 1,3-bis(aminomethyl)benzene that reacted with the suitable isocyanate (4-(trifluoromethyl)phenyl isocyanate, 3,5-Bis(trifluoromethyl) phenyl isocyanate and 4-nitrophenyl isocyanate) in refluxing dichloromethane under nitrogen to give the three receptors in 70-97% yield.

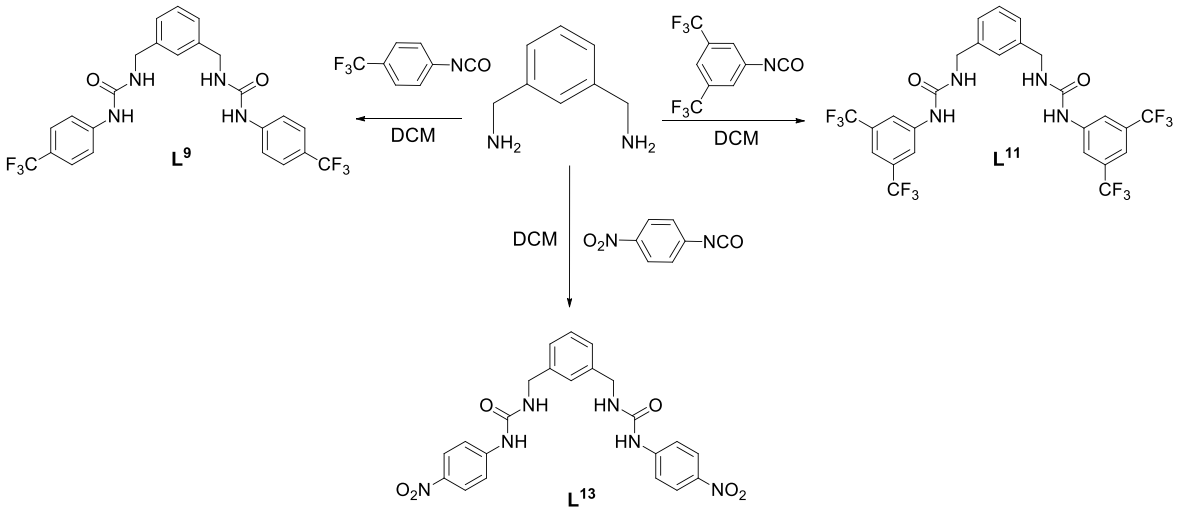

Scheme 4.1 Synthesis of **L[9]**, **L[11]** and **L[13]**

While, compounds **L[10]**, **L[12]** and **L[14]** were prepared by reaction of 2,6-Bis(aminomethyl)pyridine hydrochloridric salt, synthesised as shown in Scheme 4.1, with the suitable isocyanate (4-(trifluoromethyl)phenyl isocyanate, 3,5-Bis(trifluoromethyl) phenyl isocyanate and 4-nitrophenyl isocyanate) in refluxing dichloromethane in the presence of triethylamine under nitrogen to obtain the desired compounds in 52-74% yield.

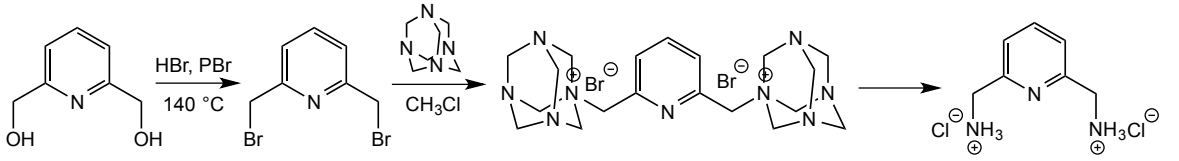

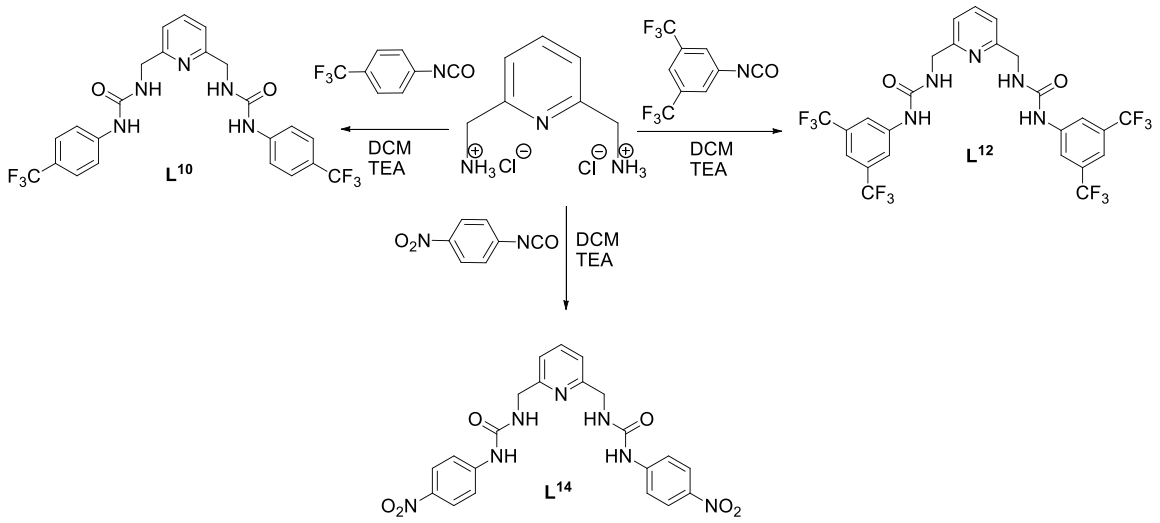

Scheme 4.2 Synthesis of **L**[10], **L**[12] and **L**[14]

4.3 Anion binding in solution

The ability of compounds **L**[9]-**L**[14] to bind anions (namely AcO^-, BzO^-, Cl^-, F^-, HCO_3^-, $H_2PO_4^-$, and NO_3^-) in solution was investigated using ^{1}H-NMR titration techniques in DMSO-d_6/0.5% H_2O (with the anions added as tetrabutylammonium (TBA) or tetraethylammonium (TEA) salts). Where possible the change in chemical shift of the most downfield NH signal was fitted to a 1:1 binding model using WinEQNMR software.[11] The results are summarised in Table 4.1. We observed that only compounds **L**[10] and **L**[12] demonstrated strong 1:1 binding with tetrabutylammonium fluoride ($K_a > 10^4$ M^{-1}) and moderate 1:1 binding with tetrabutylammonium dihydrogenphosphate. The other compounds had moderate affinity (or in the case of nitrate no interaction) for the anions studied.

Table 4.1 Stability constants K_a (M^{-1}) for compounds **L**[9]-**L**[14] with the tetrabutylammonium or tetraethylammonium salts of the anion considered in DMSO-d_6/0.5% water at 300 K. All errors estimated to be <10%

Compounds	AcO^-	BzO^-	Cl^-	F^-	HCO_3^-	$H_2PO_4^-$	NO_3^-
L[9]	152	124	32	deprot.	124	582	no interact.
L[10]	342	174	141	$>10^4$	793	1842	no interact.
L[11]	187	180	35	deprot.	506	592	no interact.
L[12]	357	183	168	$>10^4$	594	1730	no interact.
L[13]	242	172	44	deprot.	partial deprot.	475	no interact.

4.4 Solid state

Compounds **L^9-L^{14}** were crystallised by slow evaporation from different solvents and in presence of various anionic guests. Summary of the crystallization experiments, both successful and unsuccessful, are provided in *Table 4.7* in *section 4.7.2*. Interestingly only compounds **L^{11}** and **L^{12}** showed the tendency to form crystals suitable for X-ray investigation. A summary of the basic crystallographic data for the six structures obtained is reported in *Table 4.2*. A representation of the crystal packing for the six structures is reported in *Figure 4.1 a-f*. A more detailed table is reported in *section 4.7.2* (*Table 4.5*).

Table 4.2. Summary of basic crystallographic data.

	L^{11}DMSO	**$L^{11}AcO^-$(1:2)**	**$L^{11}CO_3^{2-}$ (2:1)**	**L^{12}MeOH**	**L^{12}**	**$L^{12}HPO_4^{2-}$(2:1) DMSO**
Formula	$C_{28}H_{24}F_{12}N_4O_3S$	$C_{62}H_{96}F_{12}N_6O_6$	$C_{89}H_{120}F_{24}N_{10}O_9S_2$	$C_{54}H_{50}F_{24}N_{10}O_8$	$C_{25}H_{17}F_{12}N_5O_2$	$C_{84}H_{113}F_{24}N_{12}O_9PS$
M.w.	724.57	1249.44	1994.06	1423.01	647.43	1953.90
Crystal syst.	monoclinic	monoclinic	orthorhombic	monoclinic	monoclinic	monoclinic
Space group	*C2/c*	*I2/a*	*Pbca*	*C12/c1*	*P2/c*	$P2_1/n$
a /Å	26.454(2)	19.05(8)	20.944(3)	26.22(2)	11.4364(9)	12.537(3)
b /Å	12.7445(9)	8.40(3)	24.898(3)	12.742(9)	12.8183(10)	32.566(7)
c /Å	8.9389(5)	42.23(18)	38.318(5)	8.976(7)	9.0313(7)	23.282(5)
α / º	90	90	90	90	90	90
β / º	94.842(3)	96.86(18)	90	96.795(14)	100.463(2)	97.648(4)
γ / º	90	90	90	90	90	90
V /Å^3	3002.93	6709.2	19981.4	2978(4)	1301.93	9421(4)
T (K)	100(2)	100(2)??	100(2)??	100(2)	100(2) ??	100(2)
Solvent	DMSO	EtOH/$MeNO_2$	DMSO	MeOH	DMSO	DMSO
Crystal shape	Blade	Plate	needle	Prism	Rod	Plate
Colour	colourless	colourless	colourless	colourless	colourless	colourless
Z	4	4	8	4	2	4

The analysis of the unit cell parameters suggests major differences in the set of structures isolated. The only exception consists of the two solvates **L^{11}DMSO** and **L^{12}MeOH** which show almost identical unit cell parameters.

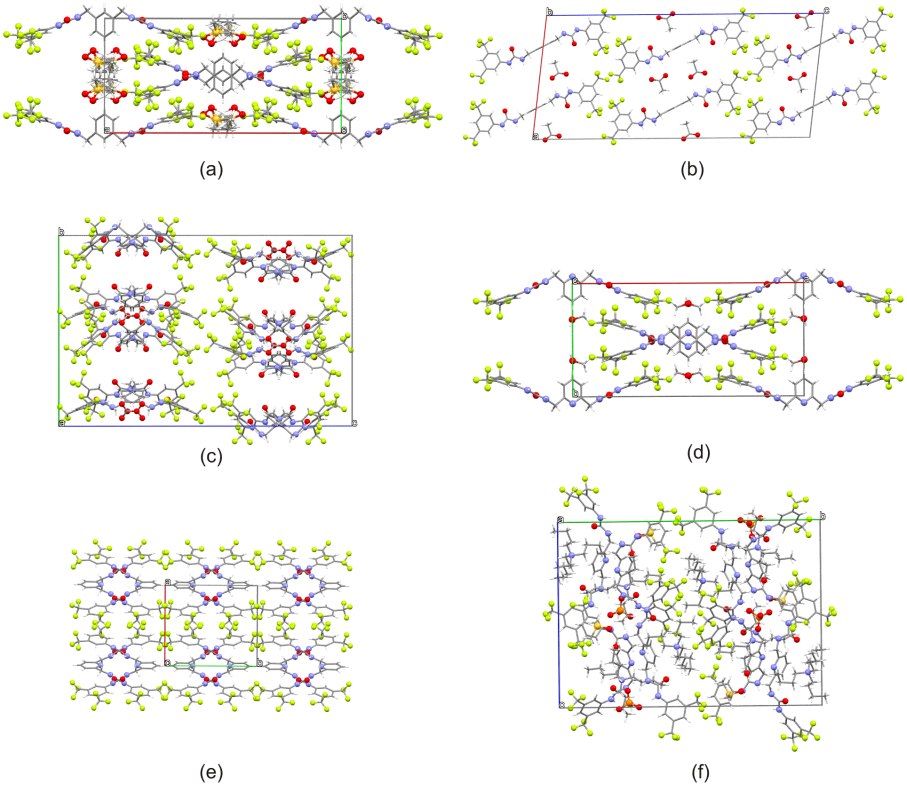

Figure 4.1. Crystal packing for the six structures: (a) **L^{11}DMSO**; (b) **$L^{11}AcO^{-}$(1:2)**; (c) **$L^{11}CO_3^{2-}$ (2:1)**; (d) **L^{12}MeOH**; (e) **L^{12}**; (f) **$L^{12}HPO_4^{2-}$(2:1) DMSO**

The majority of the structures crystallise in the monoclinic crystal system with the only exception of the structure **$L^{11}CO_3^{2-}$ (2:1)** which adopts an orthorhombic crystal system. The six structures show a wide variety of conformational choices, as represented in *Figure 4.2*. This is a clear indication of the high degree of flexibility of the two receptors **L^{11}** and **L^{12}** in solution.

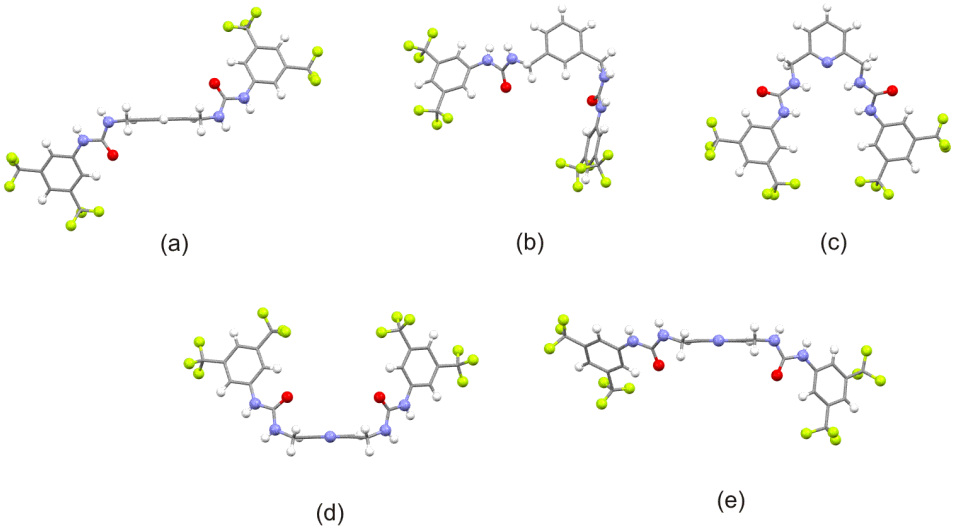

Figure 4.2. Representation of the main conformations typology (open and closed). a) open: **L^{11}DMSO**, **$L^{11}AcO^{-}$(1:2)** and **L^{12}MeOH**; b) closed **$L^{11}CO_3^{2-}$ (2:1)** (both independent units); c) closed: **L^{12}**; d)open: **$L^{12}HPO_4^{2-}$(2:1) DMSO** (independent unit 1); e) open: **$L^{12}HPO_4^{2-}$(2:1) DMSO** (independent unit 2). The molecules are oriented to best show the presence or absence of the cavity.

In particular in the three structures **$L^{11}CO_3^{2-}$ (2:1)**, **L^{12}**, and **$L^{12}HPO_4^{2-}$(2:1) DMSO**, the target molecule adopts a folded conformation (closed), with the ureidic functions differently oriented to form pseudo-cavities (*Figure 4.2b-e*). These are different for each structure and in the case of **$L^{12}HPO_4^{2-}$(2:1) DMSO**, the two independent molecules adopt different conformations.

Interestingly **L^{12}**, which crystallises without any anion or solvent molecules, adopts a classical conformation with a cavity, instead of adopting an open conformation, increasing the number of hydrogen bond donors and acceptors exposed, as observed for the remaining three structures **L^{11}DMSO**, **$L^{11}AcO^-$(1:2)** and **L^{12}MeOH** (*Figure 4.2a*). In these, the receptor units show an almost linear conformation (open), with the ureidic functions oriented approximately perpendicular to the plane of the benzene ring. This conformation is almost identical for the three structures, showing only small differences (*Figure 4.3*).

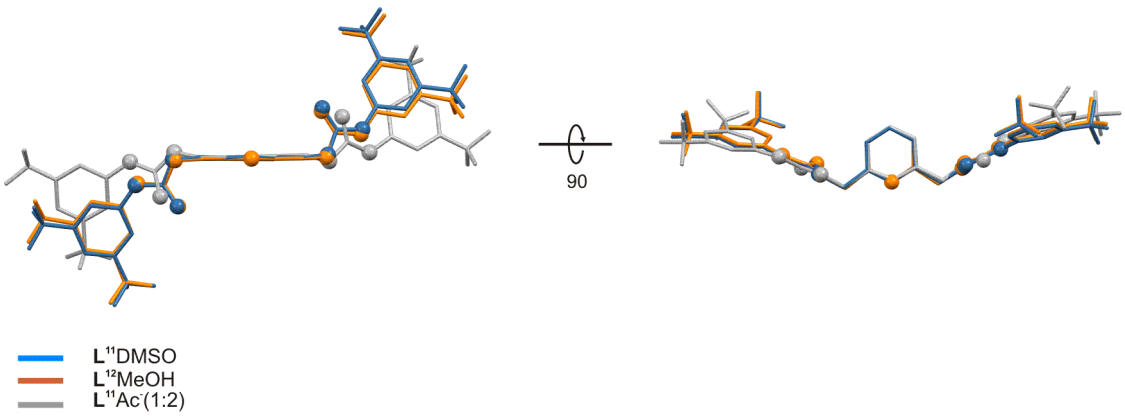

Figure 4.3. Differences in the open conformation for the three structures **L^{11}DMSO** (blue), **L^{12}MeOH** (orange) and **$L^{11}AcO^-$(1:2)** (grey). The structures are viewed along two perpendicular directions

The analysis of the crystal structures shows some interesting features. In the structures which do not contain ionic guests (**L^{11}DMSO**, **L^{12}MeOH** and **L^{12}**) adjacent molecules are connected each other via N-H···O hydrogen bonds between the ureidic NHs of one unit and the oxygens of the carbonyl group of another unit, and related by inversion symmetry to form infinite 1-D molecular arrangements (*Figure 4.4*) which propagates along the 001 direction (N-H···O distances are respectively 2.05 Å and 2.13 Å for **L^{11}DMSO**, 2.04 Å and 2.07 Å for **L^{12}MeOH** and 2.25 Å and 1.99Å for **L^{12}**). Note that the conformational differences together with the directionality of the hydrogen bonds involved have an important role in generating differences in the shape of the resulting molecular arrangements (*Figure 4.4a* and *b*).

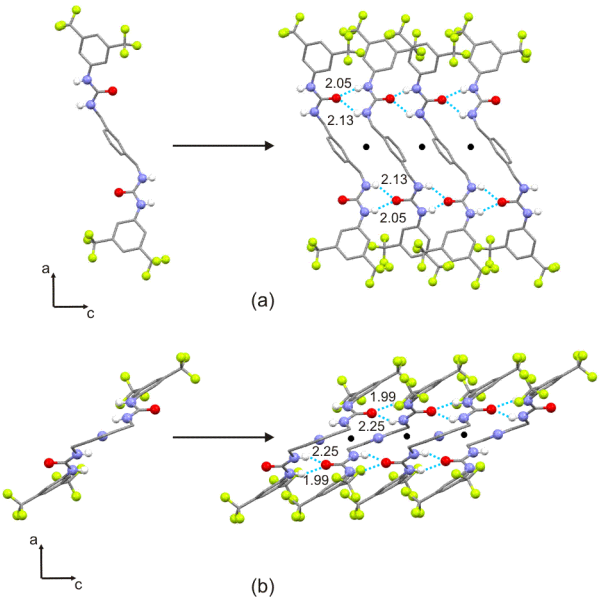

Figure 4.4. 1-D molecular arrangements viewed along the [*010*] direction: a) **L^{11}DMSO** reported as representative for the isostructural set **L^{11}DMSO**/ **L^{12}MeOH**; b) **L^{12}**. Relevant intermolecular interactions are indicated as blue dashed lines. Intermolecular distances are also reported and indicated in Å.

Interestingly, an analogous molecular arrangement can be also observed for the structure **$L^{11}AcO^{-}$(1:2)** in which the receptor molecules are not directly bonded to each other via N-H···O hydrogen bonds but bridged via AcO^{-} molecules (two acetate anions for each receptor molecule) (*Figure 4.5*) interacting via N-H···O and N-H···O^{-} hydrogen bonds. Unfortunately the quality of the data does not allow a reliable geometrical description (hydrogen bond distances and angles) of the molecular interactions involved)[5]. However it is interesting to note that in this specific case the receptor **L^{11}** instead to adopt a close conformation with a cavity able to accommodate the guest (AcO^{-}), prefers to bind two guest molecules, by adopts an open conformation resulting in a 1:2 stoichiometry.

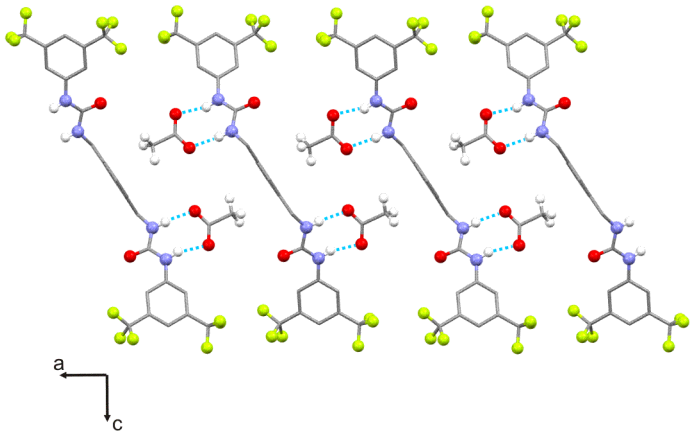

Figure 4.5. 1-D molecular arrangements in **$L^{11}AcO^{-}$(1:2)** structure viewed along the [*100*] direction. Possible intermolecular interactions are indicated as blue dashed lines

[5] The crystal did not produce good diffraction images, even using synchrotron radiation, resulting in the high R(int) and R-values.The poor quality of the data made impossible the identification of tetrabutylammonium. However there is enough information to prove the location of the atoms in space for the other components.

A different behaviour is observed for the last two crystal structures, **$L^{11}CO_3^{2-}$ (2:1)** and **$L^{12}HPO_4^{2-}$(2:1) DMSO**, in which the molecular features of the anionic guests and the different stoichiometry of the host-guest complexes generate some differences in the resulting crystal structures. In contrast to the approach taken so far to describe the crystal structures, in this case, it is advantageous to focus on the coordination of the anionic moiety and consider this as a building unit of particular molecular arrangements. The two structures **$L^{11}CO_3^{2-}$ (2:1)** and **$L^{12}HPO_4^{2-}$(2:1) DMSO** show some similar features. In the asymmetric unit of both structures there is one anion and two independent receptor units, resulting in a 2:1 stoichiometry. Each anion is coordinated by four receptor molecules *via* N-H···O and N-H···O^- hydrogen bonds (*Figure 4.6a* and *b*).

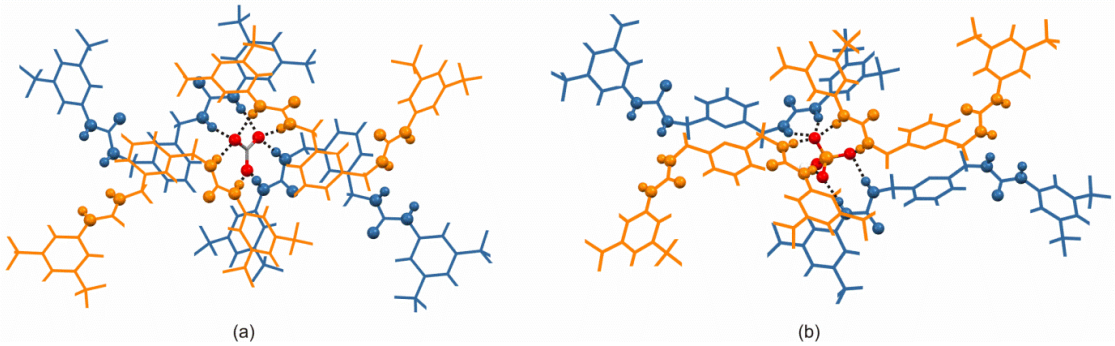

Figure 4.6. Coordination of the anionic moiety showed for: a) **$L^{11}CO_3^{2-}$ (2:1)**; b) **$L^{12}HPO_4^{2-}$(2:1) DMSO**. Solvent molecules (DMSO) and tetrabutylammonium (TBA) molecules are omitted for clarity. Crystallographically independent receptor units are respectively coloured in orange and blue. Intermolecular interactions are indicated as black dashed lines.

These units respectively develop along the [100] direction for **$L^{11}CO_3^{2-}$ (2:1)** and along the [101] direction for **$L^{12}HPO_4^{2-}$(2:1) DMSO** by glide symmetry (*Figure 4.7a* and *b*).

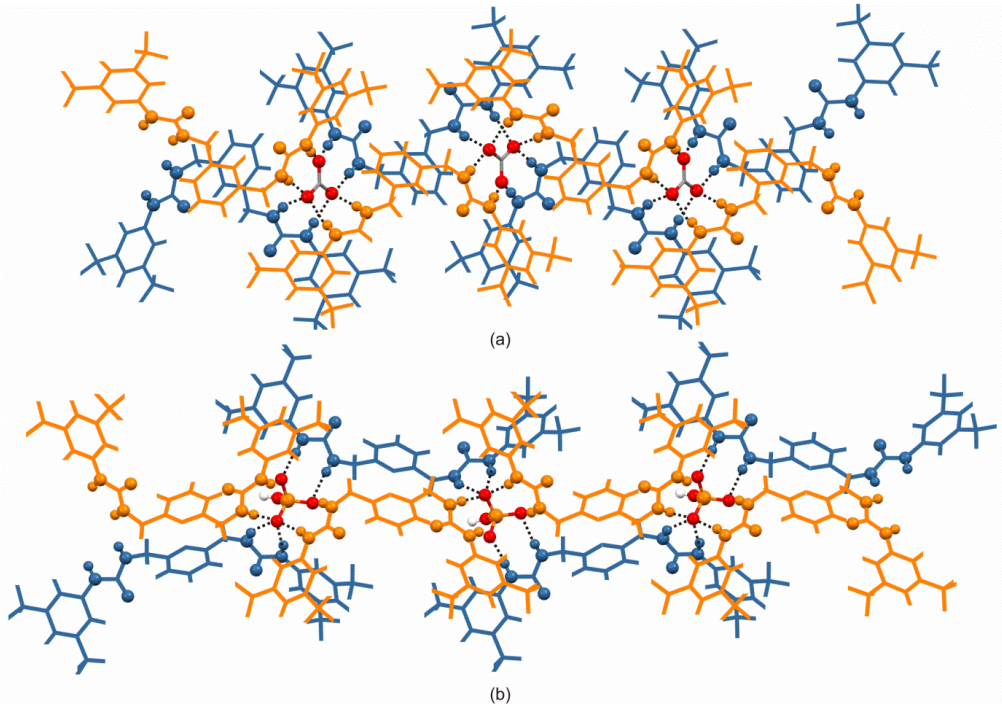

Figure 4.7. 1-D molecular arrangement showed for: a) **$L^{11}CO_3^{2-}$ (2:1)**; b) **$L^{12}HPO_4^{2-}$(2:1) DMSO**. Solvent molecules (DMSO) and tetrabutylammonium (TBA) molecules are omitted for clarity. Crystallographically independent receptor units are respectively coloured in orange and blue. Intermolecular interactions are indicated as black dashed lines.

4.5 Transport studies

4.5.1 Chloride/nitrate transport studies

The ability of compounds **L**^{9}-**L**^{14} to facilitate Cl^-/NO_3^- antiport was investigated as follows. A unilamellar 1-palmitoyl-2-oleoylphosphatidylcholine (POPC) vesicles of defined size (200 nm in diameter) were prepared containing 489 mM NaCl and suspended in 489 mM $NaNO_3$. All of the solutions were buffered to pH 7.2 with 5 mM sodium phosphate salts.[12,13] The compounds were added as solution in DMSO (2 mol% with respect to lipid) and the resulting chloride efflux from vesicles was monitored using a chloride selective electrode. After 300 s the vesicles were lysed by the addition of octaethylene glycol monodecyl ether solution (H_2O/DMSO 7:1 v/v) to calibrate 100 % chloride efflux. Full details of vesicle preparation and transport experiments may be found in the Appendix. The results are shown in *Figure 4.8*.

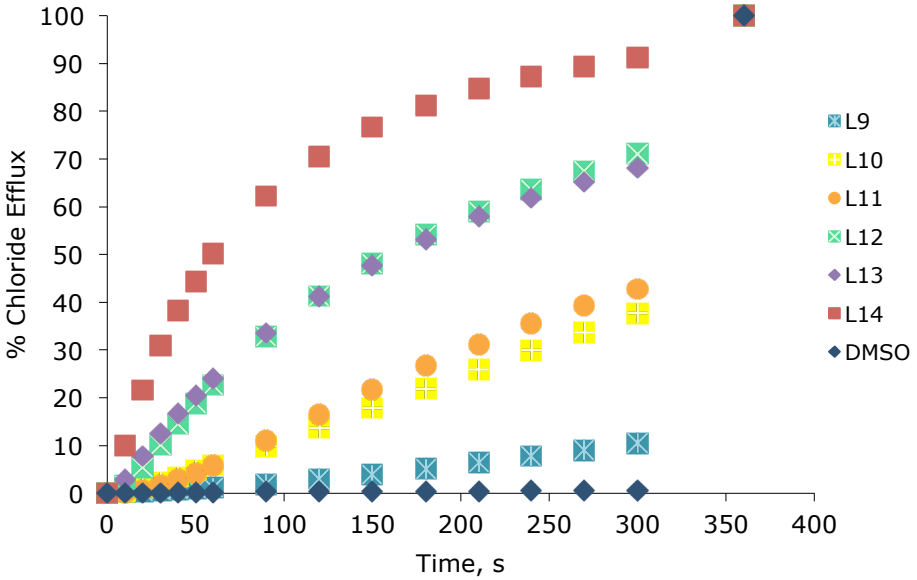

Figure 4.8 Chloride efflux promoted by a DMSO solution of compounds **L**^{9}–**L**^{14} (2% carrier to lipid) from unilamellar POPC vesicles loaded with 489 mM NaCl buffered to pH 7.2 with 5 mM sodium phosphate salts. The vesicles were dispersed in 489 mM $NaNO_3$ buffered to pH 7.2 with 5 mM sodium phosphate salts. At the end of the experiment detergent was added to lyse the vesicles and calibrate the ISE to 100% chloride efflux. Each point represents an average of three trials. DMSO was used as a control.

The results shows that compound **L**^{9}-**L**^{14} exhibit a range of chloride transport activity. Compound **L**^{9} displays poor transport activity while compound **L**^{14} is the most active transporter of the series. In *Figure 4.9* is shown the Cl^-/NO_3^- antiport promoted by different concentrations of compound **L**^{14}. The corresponding graphs for **L**^{10}-**L**^{13} may be found in *section 4.7.4* of this chapter.

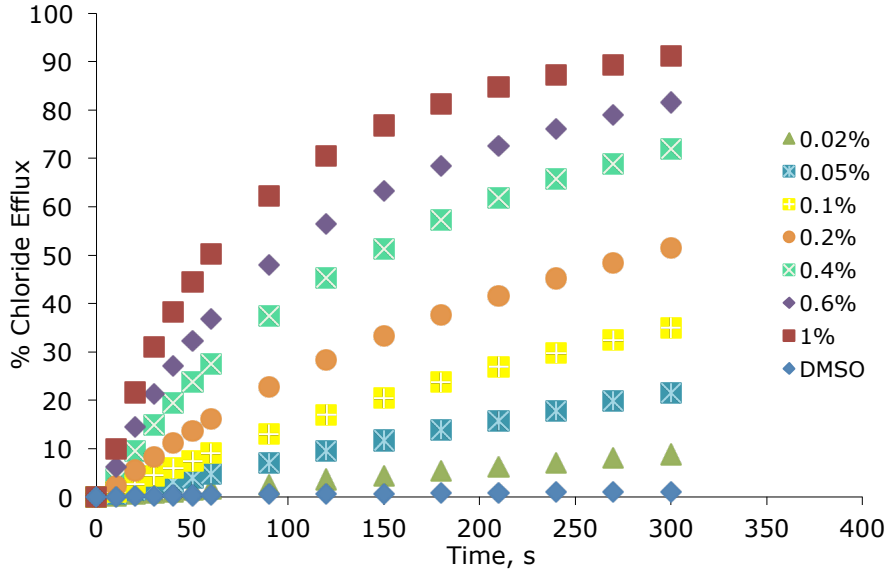

Figure 4.9 Chloride efflux promoted by various concentrations of **L**[14] (2% carrier to lipid) from unilamellar POPC vesicles loaded with 489 mM NaCl buffered to pH 7.2 with 5 mM sodium phosphate salts. The vesicles were dispersed in 489 mM $NaNO_3$ buffered to pH 7.2 with 5 mM sodium phosphate salts. At the end of the experiment detergent was added to lyse the vesicles and calibrate the ISE to 100% chloride efflux. Each point represents an average of three trials. DMSO was used as a control.

4.5.2 Chloride/bicarbonate transport studies

In these assays ion transport occurs by a passive process. To maintain charge balance, ion transport must occur by either a Cl^-/Na^+ or HCl symport or a Cl^-/NO_3^- antiport. To probe the mechanism of this process and test the ability of the compounds to function as chloride/bicarbonate antiporters, a more biologically significant process,[14,15] the experiments were repeated suspending vesicles containing sodium chloride (451 mM with 20 mM phosphate buffer at pH 7.2) in a solution of sodium sulfate (150 mM with 20mM phosphate buffer at pH 7.2). Sulfate is more hydrophilic than nitrate and posses a double negative charge, therefore is more challenging to transport across a hydrophobic membrane and usually chloride efflux is not observed when the external anion is sulfate.[16] Two minutes after addition of the transporter, a $NaHCO_3$ 'pulse' was added, such that the external concentration of bicarbonate was 40 mM, and the chloride started to efflux. This is attributed to a Cl^-/HCO_3^- antiport. The results are shown in *Figure 4.10*. In the first 120s under these conditions the majority of the compounds release only a limited amount of chloride. This dependence on the external anion suggests that the receptors transport chloride predominantly *via* exchange mechanism.

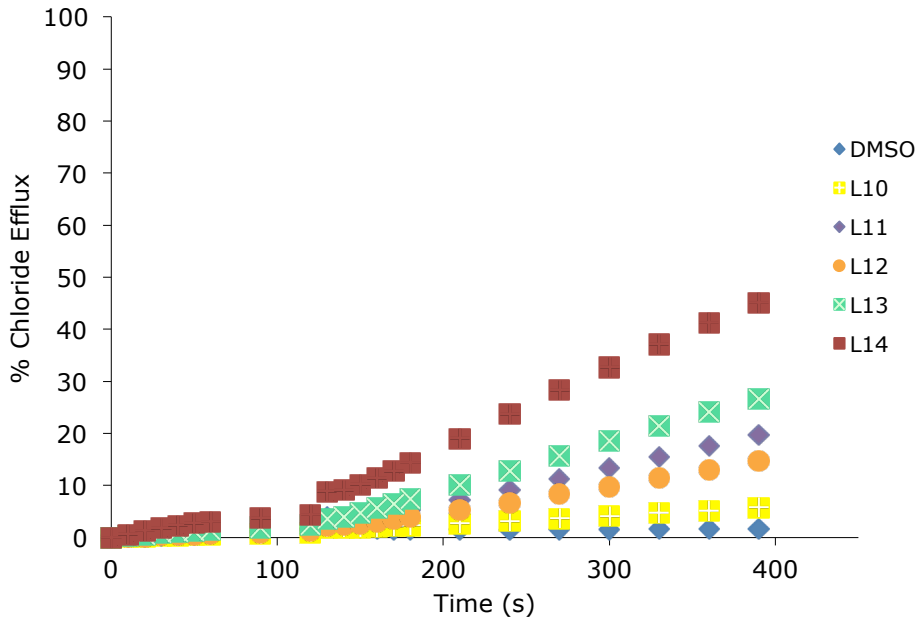

Figure 4.10 Chloride efflux promoted by a DMSO solution of compounds $\mathbf{L^{10}}$–$\mathbf{L^{14}}$ (2 mol% carrier to lipid) from unilamellar POPC vesicles loaded with 451 mM NaCl buffered to pH 7.2 with 20 mM sodium phosphate salts. The vesicles were dispersed in 150 mM Na_2SO_4 buffered to pH 7.2 with 20 mM sodium phosphate salts. At t 120 s a solution of sodium bicarbonate was added such that the external concentration of bicarbonate was 40 mM. At the end of the experiment, detergent was added to lyse the vesicles and calibrate the ISE to 100% chloride efflux. Each point represents an average of three trials. DMSO was used as a control.

These results show that the compound $\mathbf{L^{14}}$ is the most potent transport also for Cl^-/HCO_3^- exchange whilst, in this experimental condition $\mathbf{L^{10}}$ was found to be inactive. The Cl^-/HCO_3^- antiport promoted by different concentrations of compound $\mathbf{L^{14}}$ in *Figure 4.11* is shown. The corresponding graphs for $\mathbf{L^{11}}$-$\mathbf{L^{13}}$ may be found in *section 4.7.4*.

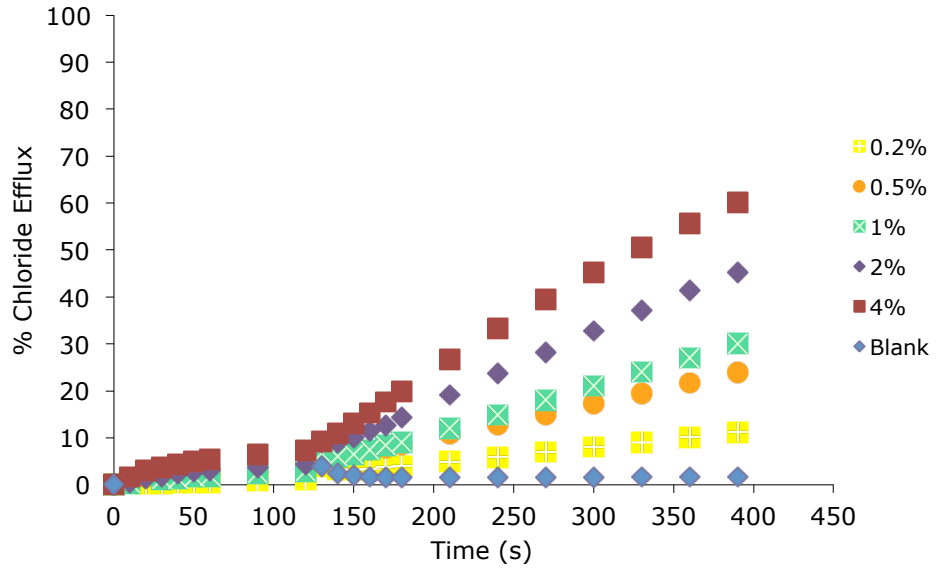

Figure 4.11 Chloride efflux promoted by various concentrations of $\mathbf{L^{14}}$ from unilamellar POPC vesicles loaded with 451 mM NaCl buffered to pH 7.2 with 20 mM sodium phosphate salts. The vesicles were dispersed in 150 mM Na_2SO_4 buffered to pH 7.2 with 20 mM sodium phosphate salts. At t. 120 s a solution of sodium bicarbonate was added such that the external concentration of bicarbonate was 40 mM. At the end of the experiment, detergent was added to lyse the vesicles and calibrate the ISE to 100% chloride efflux. Each point represents an average of three trials. DMSO was used as a control.

In order to quantify the transport activity of compounds **L[10]–L[14]** Hill analyses[17,18] for the chloride/nitrate and chloride/bicarbonate antiport assays were performed. Hill analysis enables to calculate $EC_{50,270s}$ value, which is a measure of transporter efficiency, defined as the required receptor concentration to mediate 50% of the total chloride efflux at 270s. This allows to compare the transport activity of the compounds. These values are summarised in *Table 4.3*, together with the Hill coefficients, which is commonly interpreted as an estimate of the number of transporter molecules required to transport a single anion and can provide supporting evidence for a mobile carrier mechanism.

Table 4.3 The EC_{50} is the concentration (mol% carrier to lipid) needed to obtain 50% efflux after 270s and n is the Hill coefficient that represents an estimate of the number of transporter molecules required to transport a single anion.

Compound	EC_{50} at 270s (Cl^-/NO_3^-)	n	EC_{50} at 270s (Cl^-/HCO_3^-)	n
L[10]	3.6	1.2	--	--
L[11]	2.8	1.6	7.9	0.9
L[12]	1.3	1.1	10.7	1
L[13]	1.0	0.9	6.8	0.8
L[14]	0.2	1.1	2.3	0.8

The $EC_{50,270s}$ values demonstrate that the most potent transporter is **L[14]** in both nitrate and bicarbonate antiport tests with a $EC_{50,270s}$ of 0.2 and 2.3 mol% (carrier to lipid) respectively.

The values of EC_{50} for Cl^-/HCO_3^- exchange process are higher than for Cl^-/NO_3^- antiport. This is commonly observed for two reasons: HCO_3^- is more hydrophilic than NO_3^- and is therefore expected to be more difficult to transport across a bilayer; and the nature of the Cl^-/HCO_3^- assay provides a smaller HCO_3^- gradient (40 mM external HCO_3^-) than the NO_3^- gradient present in the Cl^-/NO_3^- assay (489 mM external NO_3^-) thus there is a smaller electrochemical gradient to drive the transport process.

The Hill coefficient (n) values indicate that the transport process by each receptor is unimolecular, i.e. that each anion is transported by a single receptor. This offers an evidence of a mobile carrier process rather than the possible assembly of pores.

4.5.3 Mobility assays

In order to further investigate if the compounds were functioning as mobile carriers rather than channels, transport experiments were repeated in vesicles composed of POPC/cholesterol (7:3). Cholesterol decreases membrane fluidity and that would have a negative effect on the transport ability of a mobile carrier, which is largely dependent on diffusion within the membrane.[19] In the presence of cholesterol all compounds, except **L[11]**, show a decrease in transport activity in agreement with a mobile carrier mechanism. The graph for all compounds may be found in the *section 4.7.4* of this chapter.

To prove the carrier mechanism of compound **L[11]** a U-tube experiment was performed. In these experiments the membrane is replaced by a bulk organic phase separating two aqueous phases. Transport due to the formation of channels is impossible in this case because of the large dimensions of the organic phase.[20] The setup of the experiment involved a U-shaped glass tube filled with the organic phase of nitrobenzene containing 1 mM carrier. One arm of the tube was filled with an aqueous $NaNO_3$ solution (489 mM buffered to pH 7.2 with 5 mM sodium phosphate salts), while the other arm was filled with a NaCl solution (489 mM buffered to pH 7.2 with 5 mM sodium phosphate salts) and the chloride concentration of the $NaNO_3$ phase was monitored with an ISE (ion selective electrode) to quantify the transport through nitrobenzene. Full details of this experiment may be found in the appendix. For solubility reason the U tube assays for compound **L[11]** was inconclusive. However the Hill coefficient of this receptor is 1.0 and that may imply that a carrier mechanism is the most likely.

4.6 Conclusion

The work in this chapter demonstrates that the bis-urea scaffold reported in Chapter 3 can be readily modified to yield efficient anion carriers. A range of vesicle-based techniques has been used to fully investigate the transport mechanism. The vesicle studies indicate that the compounds function as mobile carriers that mediate the anion transport *via* anion exchange mechanism including chloride/nitrate and chloride/bicarbonate antiport. The results show that the compound **L[14]** possess the highest transport efficiency among the series with an $EC_{50,270s}$ of 0.2 and 2.3 mol% (carrier to lipid) for the nitrate and bicarbonate antiport respectively.
As anion receptors, we observed that only compounds **L[10]** and **L[12]** demonstrate strong 1:1 binding with TBA fluoride (K_a $>10^4$ M^{-1}) and moderate 1:1 binding with TBA dihydrogenphosphate.

4.7 Experimental

All reactions were performed in oven-dried glassware under a slight positive pressure of nitrogen. ^{1}H-NMR (400 MHz, 500MHz) and ^{13}C NMR (100 MHz, 125MHz) spectra were determined on a Varian INOVA-400 spectrometer, and Varian INOVA-500 spectrometer. Chemical shifts for ^{1}H NMR are reported in parts per million (ppm), calibrated to the residual solvent peak set, with coupling constants reported in Hertz (Hz). The following abbreviations are used for spin multiplicity: s = singlet, d = doublet, t = triplet, m = multiplet. Chemical shifts for ^{13}C NMR are reported in ppm, relative to the central line of a septet at δ = 39.52 ppm for deuterio-dimethylsulfoxide. Infrared (IR) spectra were

recorded on a NICOLET 5700 FT-IR spectrophotometer and reported in wavenumbers (cm^{-1}). Microanalytical data were obtained using a Fisons EA CHNS-O instrument (*T* = 1000 °C). Fluorescence spectra were recorded on a Cary Eclypse spectrofluorimeter. All solvents and starting materials were purchased from commercial sources where available. Proton NMR titrations were performed by adding aliquots of the putative anionic guest (as the TBA salt, 0.075 M) in a solution of the receptor (0.005M) in DMSO-d_6/0.5% water to a solution of the receptor (0.005M).
The synthesis of pyridine-2,6-diyldimethanaminium chloride has already been reported in literature.[21]

4.7.1 Synthetic procedure

Synthesis of 1,1'-(1,3-phenylenebis(methylene))bis(3-(4-(trifluoromethyl)phenyl)urea) L[9]

A solution of 4-(trifluoromethyl)phenyl isocyanate (0.550 g; 2.94 mmol) in 15 ml of DCM was added dropwise to a solution of m-xylylenediamine (0.200 g; 1.47 mmol) in 15 ml of DCM and was left stirring at reflux under N_2 atmosphere overnight. The precipitate thus formed was collected by filtration and dried under vacuum to give a white solid.
Yield: 97% (0.730 g; 1.43 mmol); M.p. 237°C; ^{1}H NMR (500 MHz, DMSO-d_6, 298K) δ_{CH} 4.3 (d, J=5 Hz, 4H); δ_{ArH} 6.78 (t, 2H, NH) 7.19 (d, J=10 Hz, 2H) 7.26 (s, 1H), 7.30 (t, J= Hz, 1H), 7.54 (d, J=10 Hz, 4H) 7.59 (d, J=10, 4H), 8.99 (s, 2H, NH); ^{13}C-NMR(100 MHz, DMSO-d_6, 298 K) δ_C 42.73; δ_{ArC} 117.29, 120. 90 (q, J= 100.8 Hz, CF_3), 125.66, 125. 85, 125. 88, 125.90, 128.31, 140. 16, 144.14, 154.82.

Synthesis of 1,1'-(pyridine-2,6-diylbis(methylene))bis(3-(4-(trifluoromethyl)phenyl)urea) L[10]

A solution of 4-(trifluoromethyl)phenyl isocyanate (0.426 g; 2.28 mmol) in 15 ml of DCM was added dropwise to a stirred suspension of pyridine-2.6-diyldimethanamine dihydrocloride (0.240g; 1.14 mmol) and TEA (1 ml) in 15 ml of DCM. After the addition of isocyanate a colourless solution was obtained. The reaction was refluxed under N_2 atmosphere overnight. The solvent was evaporated *in vacuo* and the solid obtained was washed with water and then filtered off, dried under reduced pressure and isolated as a white solid.
Yield: 70% (0.340g, 0.73 mmol); M.p. 234°C; ^{1}H NMR (500 MHz, DMSO-d_6, 298K) δ_{CH} 4.425 (d, J=5.5 Hz, 4H); δ_{ArH} 6.91 (t, NH, 2H); 7.23 (d, J=7.5 Hz, ArH, 2H); 7.56-7.63 (m, 4H); 7.76 (t, J= 8 Hz, ArH, 1H); 9.20 (s, NH, 2H); ^{13}C-NMR(125 MHz, DMSO-d_6, 298 K) δ_C 44.66; δ_{ArC} 117.30, 119.12, 121.10 (q, j=128 Hz, CF_3), 123.27, 125.96, 137.45, 144.14, 154.88; δ_{CO} 158.26. LMRS (ES^-) m/z: 510.0381 $[M\text{-}H^+]^-$.

Synthesis of 1,1'-(1,3-phenylenebis(methylene))bis(3-(3,5-bis(trifluoromethyl)phenyl) urea) L[11]

A solution of 3,5-Bis(trifluoromethyl)phenyl isocyanate (0.750 g; 2.94 mmol) in 15 ml of DCM was added dropwise to the solution of m-xylylenediamine (0.200g; 1.47 mmol) in 15 ml of DCM and was left stirring at reflux under N_2 atmosphere overnight. The precipitate thus formed was isolated by filtration, washed with MeOH and Et_2O and dried over vacuum.

Yield: 77% (0.730 g; 1.13 mmol); M.p. 245°C; ^{1}H NMR(500 MHz, DMSO-*d*$_6$, 298K) δ_{CH} 4.31 (d, J=6 Hz, 4H); δ_{ArH} 7.01 (t, J=6 Hz, NH, 2H); 7.18 (d, J=7.5 Hz, 2H); 7.25 (s, 1H); 7.30 (t, J=8 Hz, 1H); 7.50 (s, 2H); 8.07 (s, 4H); 9.35 (s, 2H); ^{13}C-NMR (125 MHz, DMSO-*d*$_6$, 298 K) δ_C 42.75, δ_{ArC} 113.41, 117.21, 123.33 (q, J=1080, CF_3), 125.59, 125.67, 128.28, 130.54 (q, J=128, CF_3), 140.11, δ_{CO} 154.83. LMRS (ES^-) m/z: 645.1481 $[M\text{-}H^+]^-$.

Synthesis of 1,1'-(pyridine-2,6-diylbis(methylene))bis(3-(3,5-bis(trifluoromethyl)phenyl) urea) L[12]

A solution of 3,5-Bis(trifluoromethyl)phenyl isocyanate (0.619 g; 2.43 mmol) in 15 ml of DCM was added dropwise to the suspension of pyridine-2.6-diyldimethanamine dihydrocloride and TEA (1 ml) in 15 ml of DCM(0.255g; 1.21 mmol). After the addition of isocyanate a colourless solution was obtained. The mixture was heated to reflux under N_2 and stirred overnight. The solvent was removed under reduced pressure to give a white solid, which was washed with water and then with DCM, filtered off and dried, over vacuum.

Yield: 74% (0.58 g; 0.89 mmol); M.p. >250°C; ^{1}H NMR (500 MHz, DMSO-*d*$_6$, 298K) δ_{CH} 4.43 (d, J=5.6 Hz, 4H); 7.10 (t, NH, 2H); 7.23 (d, J=8 Hz, 2H); 7.55 (s, 2H); 7.76 (t, J=8 Hz, 1H); 8.10 (s, 4H); 9.56 (s, NH, 2H); ^{13}C-NMR(125 MHz, DMSO-*d*$_6$, 298 K) δ_C 44.68, δ_{ArC} 113.60, 117.213, 119.04, 123.32 (q, J=1080, CF_3), 130.60 (q, J=129.5, CF_3), 137.53, 142.49, 154.8, δ_{CO} 158.15. LMRS (ES^-) m/z: 646.0661 $[M\text{-}H^+]^-$.

Synthesis of 1,1'-(1,3-phenylenebis(methylene))bis(3-(4-nitrophenyl)urea) L[13]

A solution of 4-nitrophenyl isocyanate (0.480 g; 2.94 mmol) in 15 ml of DCM was added to the solution of m-xylylenediamine (0.200g; 1.47 mmol) in 15 ml of DCM. After refluxing under stirring in N_2 atmosphere overnight, the precipitate was filtered off, washed with MeOH and dried over vacuum to give a yellow solid.

Yield: 88% (0.6 g; 1.29 mmol); M.p. 228°C; ^{1}H NMR (500 MHz, DMSO-*d*$_6$, 298K) δ_{CH} 4.32 (d, J=6 Hz, 4H); δ_{ArH} 6.93 (t, J=6 Hz, NH, 2H); 7.20 (d, J=7.5 Hz, 2H); 7.26 (s, 1H); 7.30 (t, J=8 Hz, 1H); 7.61 (d, J=9.5 Hz, 4H); 8.10 (d, J=9 Hz, 4H); 9.36 (s, NH, 2H); ^{13}C-NMR(125 MHz, DMSO-*d*$_6$, 298 K) δ_C 42.78; δ_{ArC} 116.88, 125.05, 125.72, 125.88, 128.37, 139.99, 140.43, 147.09; δ_{CO} 154.45

Synthesis of 1,1'-(pyridine-2,6-diylbis(methylene))bis(3-(4-nitrophenyl)urea) L[14]

A solution of 4-nitrophenyl isocyanate (0.312 g; 1.9 mmol) in 10 ml of DCM was added to the stirring suspension of pyridine-2.6-diyldimethanamine dihydrocloride (0.200g; 0.95

mmol) and TEA (1 ml) in 15 ml of DCM. After the addition of isocyanate a yellow solution was obtained. The mixture of reaction was allowed to stir for 24h under a N_2 atmosphere at room temperature. The solvent was removed via reduced pressure to give a yellow solid, which was washed with water and then with hot MeOH, filtered off and dried, under vacuum.

Yield: 52% (0.23 g; 0.49 mmol); ^{1}H NMR (400 MHz, DMSO-*d*$_6$, 298K) δ_{CH} 4.44 (d, J=8 Hz, 4H); δ_{ArH} 7.06 (t, J=8 Hz, NH, 2H); 7.24 (d, J=8 Hz, 2H); 7.65 (d, J=8 Hz, 4H); 7.77 (t, J=8 Hz, 1H); 8.14 (d, J=8 Hz, 4H); 9.57 (s, NH, 1H); ^{13}C-NMR(125 MHz, DMSO-d_6 , 298 K) δ_C 44.68; δ_{ArC} 116.93, 119.21, 125.13, 137.51, 140.53, 147.08, 154.52; δ_{CO} 158.02. LMRS (ES^-) m/z: 463.9218 $[M\text{-}H^+]^-$.

4.7.2 X-Ray crystallography

Table 4.4. Crystal data and structure refinement details.

	L^{11}DMSO	$L^{11}AcO^-$(1:2)	$L^{11}CO_3^{2-}$ (2:1)
Empirical formula	$C_{28}H_{24}F_{12}N_4O_3S$	$C_{62}H_{96}F_{12}N_6O_6$	$C_{89}H_{120}F_{24}N_{10}O_9S_2$
Formula weight	724.57	1249.44	1994.06
Crystal system	monoclinic	monoclinic	orthorhombic
Space group	*C*2/*c*	*I*2/*a*	*Pbca*
a /Å	26.454(2)	19.05(8)	20.944(3)
b /Å	12.7445(9)	8.40(3)	24.898(3)
c /Å	8.9389(5)	42.23(18)	38.318(5)
α / º	90	90	90
β / º	94.842(3)	96.86(18)	90
γ / º	90	90	90
V /Å^3	3002.93	6709.2	19981.4
T / K	100(2)	100(2)	100(2)
Crystal shape	Blade	Plate	needle
Crystal size / m^3	0.130 × 0.100 × 0.040 mm^3	0.070 x 0.030 x 0.005 mm^3	0.120 x 0.015 x 0.015 mm^3
Colour	colourless	colourless	colourless
Z	4	4	8
θ range for data collection	2.96 – 25.02°	2.826-24.207°	2.856 – 26.573°
Index ranges	$-38 \le h \le 18$, $0 \le k \le 39$, $0 \le l \le 8$	$-21 \le h \le 22$, $-9 \le k \le 9$, $-50 \le l \le 49$	$-27 \le h \le 22$, $-32 \le k \le 32$, $-49 \le l \le 49$
Reflections collected	2613	29767	181899
Independent reflections	2613 [R_{int} = 0.0000]	5984 [R_{int} = 0.3289]	22857 [R_{int}=0.0926]
Completeness	99.6 % (θ = 25.02°)	96.7 % (θ = 24.415°)	99.7 % (θ = 24.415°)
Absorption correction	Semi–empirical from equivalents	Semi–empirical from equivalents	Semi–empirical from equivalents
Max. and min. transmission	0.9982 and 0.9826	1.000 and 0.044	1.000 and 0.805
Refinement method	Full-matrix least-squares on F^2	Full-matrix least-squares on F^2	Full-matrix least-squares on F^2
Data / restraints / parameters	2613 / 0 / 208	5845 / 484 / 423	22857 / 1568 / 1422
Goodness-of-fit on F^2	1.164	1.531	1.079
Final *R* indices [$F^2 > 2\sigma(F^2)$]	*R1* = 0.0712, *wR2* = 0.1314	*R1* = 0.2412, *wR2* = 0.5376	*R1 = 0.0727,* *wR2 = 0.1646*
***R* indices (all data)**	*R1* = 0.0990, *wR2* = 0.1421	*R1* = 0.3232, *wR2* = 0.5848	*R1 = 0.054, wR2 = 0.1835*
Largest diff. peak and hole	0.486 and –0.507 e Å^{-3}	0.672 and –0.537 e Å^{-3}	0.757 and –0.557 e Å^{-3}

Table 4.5. Crystal data and structure refinement details.

	L^{12}MeOH	L^{12}	$L^{12}HPO_4^{2-}$(2:1) DMSO
Empirical formula	$C_{54}H_{50}F_{24}N_{10}O_8$	$C_{25}H_{17}F_{12}N_5O_2$	$C_{84}H_{113}F_{24}N_{12}O_9PS$
Formula weight	1423.01	647.43	1953.90
Crystal system	monoclinic	monoclinic	monoclinic
Space group	*C12/c1*	*P2/c*	$P2_1/n$
a /Å	26.22(2)	11.4364(9)	12.537(3)
b /Å	12.742(9)	12.8183(10)	32.566(7)
c /Å	8.976(7)	9.0313(7)	23.282(5)
α / º	90	90	90
β / º	96.795(14)	100.463(2)	97.648(4)
γ / º	90	90	90
V /Å^3	2978(4)	1301.93	9421(4)
T / K	100(2)	100(2) ??	100(2)
Crystal shape	Prism	Rod	Plate
Crystal size / m^3	0.21 x 0.11 x 0.08 mm^3	0.220 × 0.050 × 0.040 mm^3	0.181 × 0.07 × 0.02 mm^3
Colour	colourless	colourless	colourless
Z	4	2	4
θ range for data collection	2.823 – 30.169°	3.092 – 27.467°	2.923 – 25.028°
Index ranges	$-34 \le h \le 31$, $-17 \le k \le 17$, $-7 \le l \le 12$	$-14 \le h \le 14$, $-12 \le k \le 16$, $-11 \le l \le 9$	$-14 \le h \le 14$, $-38 \le k \le 38$, $-27 \le l \le 27$
Reflections collected	10415	9371	55527
Independent reflections	3902 [R_{int} = 0.0461]	2968 [R_{int} = 0.0261]	16593 [R_{int} = 0.1512]
Completeness	99.5 % (θ = 25.242°)	99.3 %	97.5 %
Absorption correction	Semi–empirical from equivalents	Semi–empirical from equivalents	Semi–empirical from equivalents
Max. and min. transmission	1.000 and 0.713	1.000 and 0.798	1.000 and 0.826
Refinement method	Full-matrix least-squares on F^2	Full-matrix least-squares on F^2	Full-matrix least-squares on F^2
Data / restraints / parameters	3902 / 0 / 220	2968 / 204 / 226	16593 / 27 / 1204
Goodness-of-fit on F^2	1.127	1.037	1.175
Final *R* indices [$F^2 > 2\sigma(F^2)$]	*R1* = 0.1118, *wR2* = 0.3206	*R1* = 0.0381, *wR2* = 0.0974	*R1* = 0.1274, *wR2* = 0.2989
***R* indices (all data)**	*R1* = 0.1289, *wR2* = 0.3410	*R1* = 0.0465, *wR2* = 0.1025	*R1* = 0.1408, *wR2* = 0.3087
Largest diff. peak and hole	0.821 and –0.639 e Å^{-3}	0.390 and –0.246 e Å^{-3}	3.184 and –0.781 e Å^{-3}

Table 4.6 Hydrogen bonds [Å and °].

Phase	*D*–H···*A*	*d*(*D*–H)	*d*(H···*A*)	*d*(*D*···*A*)	∠(*DHA*)
$L^{11}AcO^-$(1:2)	N1–H1A···O41	0.88	1.94	2.817(18)	171.4
	N2–H2···O42	0.88	1.99	2.789(16)	149.6
$L^{11}CO_3^{2-}$ (2:1)	N1–H1A···O201^{i}	0.88	1.95	2.822(3)	170.8
	N2–H2···O203^{i}	0.88	1.88	2.706(3)	154.8
	N3–H3A···O202	0.88	1.98	2.824(3)	159.8
	N4–H4A···O201	0.88	2.06	2.900(3)	158.9
	N31–H31A···O202	0.88	1.92	2.764(3)	161.0
	N32–H32···O203	0.88	1.94	2.805(3)	167.2
	N33–H33A···O201^{i}	0.88	2.04	2.915(3)	175.4
	N34–H34A···O202^{i}	0.88	2.00	2.817(3)	153.3
$L^{12}HPO_4^{2-}$(2:1)	N2–H2A···O103	0.88	2.21	3.004(6)	150.0
	N3–H3A···O103	0.88	2.00	2.846(6)	161.1
	N34–H34A···O104	0.88	1.99	2.812(6)	155.7
	N35–H35···O103	0.88	2.03	2.895(6)	166.8
	O101–H101···O201	0.84	1.91	2.675(6)	151.1
	O101–H101···S201	0.84	2.88	3.421(4)	124.1

Symmetry transformations used to generate equivalent atoms:
(i) x+1/2,y,–z+1/2

Table 4.7. Summary of the crystallization experiments in different solvents for the receptors **L**[9]-**L**[14]. Conditions yielding single crystals are indicated as (√). (●) indicates an unsuccessful experiment and (-) is used to indicate "not applied" experimental conditions.

Guest	Host	solvent						
		MeOH	EtOH	EtOH/$MeNO_2$	MeOH /$MeNO_2$	MeCN	$MeNO_2$	DMSO
L^9	-	-	-	-	-	-	-	●
L^9	AcO^-	-	-	-	-	●	-	●
L^9	BzO^-	-	-	-	-	√	-	●
L^9	Cl^-	-	-	-	-	-	-	●
L^9	F^-	-	-	-	-	-	-	●
L^9	HCO_3^-	-	-	-	-	-	-	●
L^9	$H_2PO_4^-$	-	-	-	-	-	-	●
L^{10}	AcO^-	-	-	-	-	-	-	●
L^{10}	BzO^-	-	-	-	-	-	-	●
L^{10}	Cl^-	-	-	-	-	-	-	●
L^{10}	F^-	-	-	-	-	-	-	●
L^{10}	HCO_3^-	-	-	-	-	-	-	●
L^{10}	$H_2PO_4^-$	-	-	-	-	-	-	●
L^{10}	HSO_4^-	-	-	-	-	-	-	√
L^{11}	-	-	-	-	-	-	-	√
L^{11}	AcO^-	●	●	√[b]	-	●	●	√[a]
L^{11}	BzO^-	●	●	●	-	●	●	●
L^{11}	$HPpi^{2-}$	●	●	●	-	●	●	●
L^{11}	$H_2PO_4^-$	-	-	-	-	-	-	●
L^{11}	HCO_3^-	-	-	-	-	-	-	√[c]
L^{11}	F^-	-	-	-	-	-	-	●
L^{11}	Cl^-	-	-	-	-	-	-	●
L^{12}	-	√[d]	-	-	-	-	-	√[e]
L^{12}	BzO^-	●	●	-	●	●	●	√
L^{12}	AcO^-	●	●	-	-	●	●	√
L^{12}	$HPpi^{2-}$	●	●	-	-	●	●	●
L^{12}	$H_2PO_4^-$	-	-	-	-	-	-	√[f]
L^{12}	HCO_3^-	-	-	-	-	-	-	●
L^{12}	F^-	-	-	-	-	-	-	√
L^{12}	Cl^-	-	-	-	-	-	-	●

Guest	Host	solvent						
		MeOH	**EtOH**	**EtOH/$MeNO_2$**	**MeOH /$MeNO_2$**	**MeCN**	**$MeNO_2$**	**DMSO**
L^{13}	AcO^-	●	-	-	-	●	●	●
L^{13}	BzO^-	●	-	-	-	●	●	●
L^{13}	Cl^-	●	-	-	-	●	●	●
L^{13}	HCO_3^-	-	-	-	-	●	√	●
L^{13}	$HPpi^{2-}$	●	-	-	-	●	●	●

[a] crystal structure of **L^{11} DMSO**
[b] crystal structure of **L^{11} AcO (1:2)**
[c] crystal structure of **L^{11} CO_3^{2-} (2:1)**
[d] crystal structure of **L^{12} MeOH**
[e] crystal structure of **L^{12}**
[f] crystal structure of **L^{12} HPO_4^{2-} (2:1) DMSO**

4.7.3 Proton NMR titration fitting

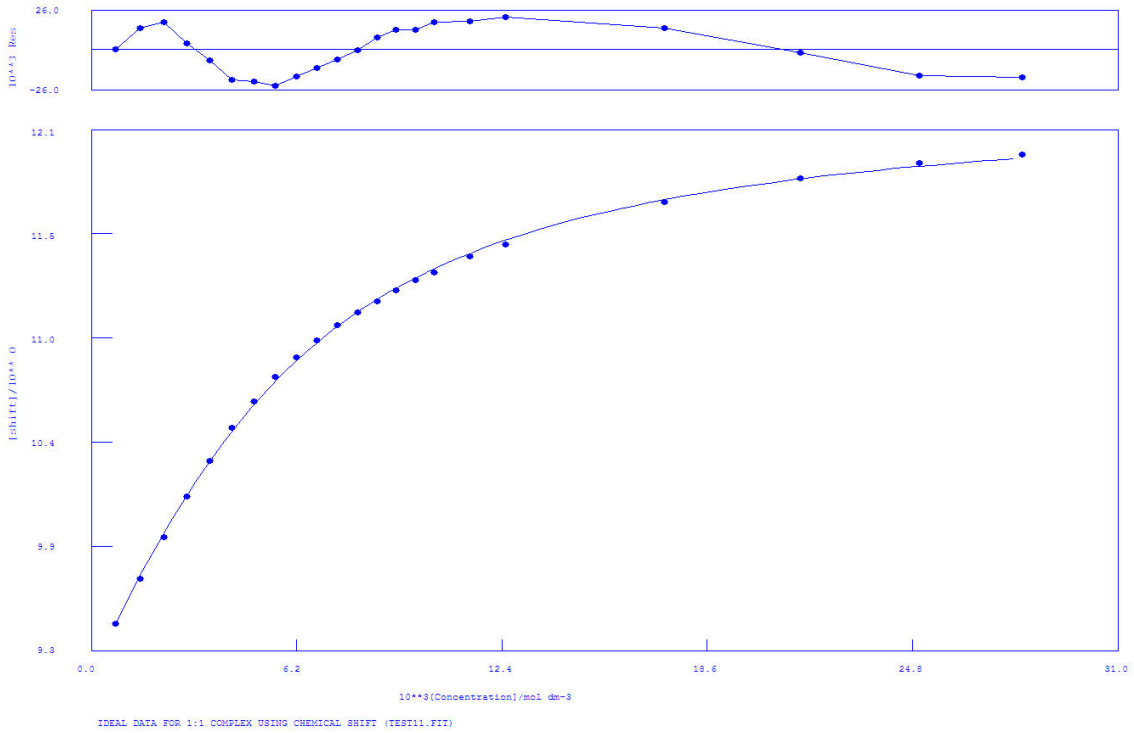

Calculations by WinEQNMR Version 1.20 by Michael J. Hynes
Program run at 17:44:44 on 09/19/2013
IDEAL DATA FOR 1:1 COMPLEX USING CHEMICAL SHIFT (TEST11.FIT)
Reaction: M + L = ML
FILE: TEST11.FIT
IDEAL DATA: K1 = 63.091; DELTA M = 20.0; DELTA ML = 120.0
File prepared by M. J. Hynes, October 22 2000

NO.	A	PARAMETER	DELTA	ERROR	CONDITION	DESCRIPTION
1	1	3.42611E+02	2.000E-01	9.574E+00	1.543E+01	K1
2	1	9.16612E+00	2.000E-01	1.227E-02	3.112E+00	SHIFT M
3	1	1.22897E+01	1.000E+00	1.779E-02	1.039E+01	SHIFT ML

Figure 4.12. ^{1}H-NMR of **L^{10}** with TBAAcO in DMSO-d_6/0.5%H_2O. The fitting has been obtained following the most downfield shifted NH proton.

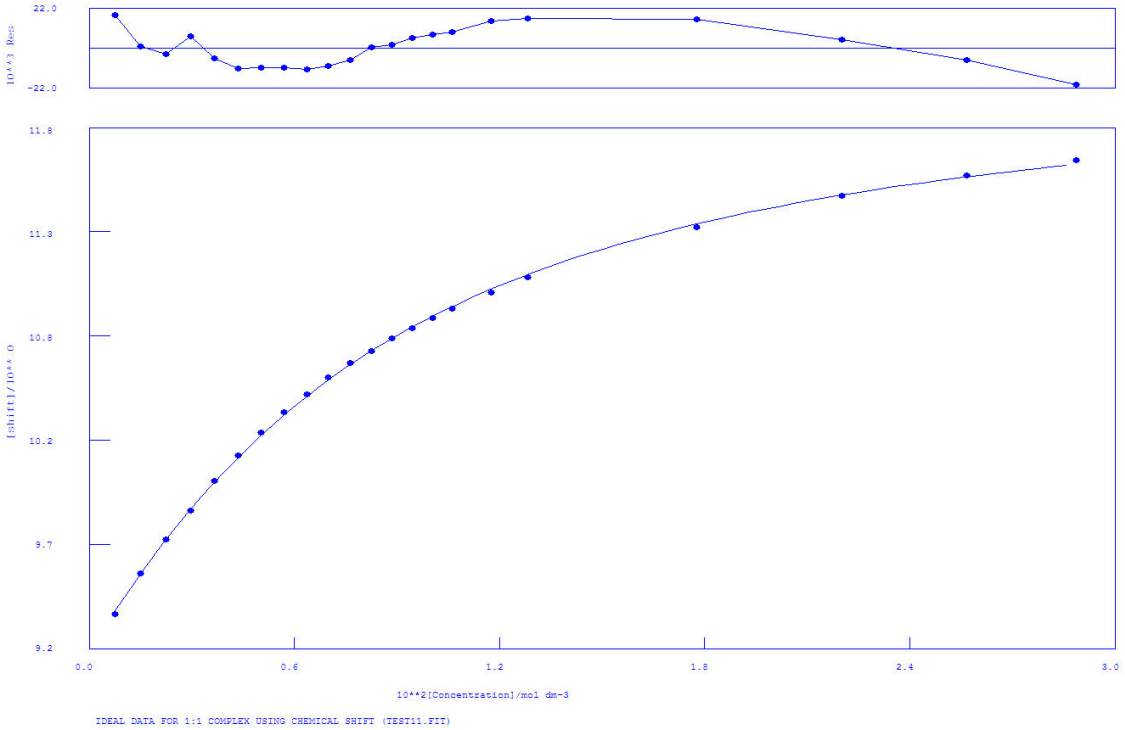

Calculations by WinEQNMR Version 1.20 by Michael J. Hynes
Program run at 15:23:20 on 01/09/2014

IDEAL DATA FOR 1:1 COMPLEX USING CHEMICAL SHIFT (TEST11.FIT)
Reaction: Sn + L = Sn(L)
FILE: TEST11.FIT (Measured shift is on 119Sn)
IDEAL DATA: K1 = 63.091; DELTA M = 20.0; DELTA ML = 120.0
File prepared by M. J. Hynes, October 22 2000

NO.	A	PARAMETER	DELTA	ERROR	CONDITION	DESCRIPTION
1	1	1.73966E+02	2.000E-01	3.942E+00	2.400E+01	K1
2	1	9.18417E+00	2.000E-01	8.745E-03	4.200E+00	SHIFT Sn
3	1	1.21793E+01	1.000E+00	1.842E-02	1.523E+01	SHIFT Sn(L)

Figure 4.13. ^{1}H-NMR of **L^{10}** with TBABzO in DMSO-d_6/0.5%H_2O. The fitting has been obtained following the most downfield shifted NH proton.

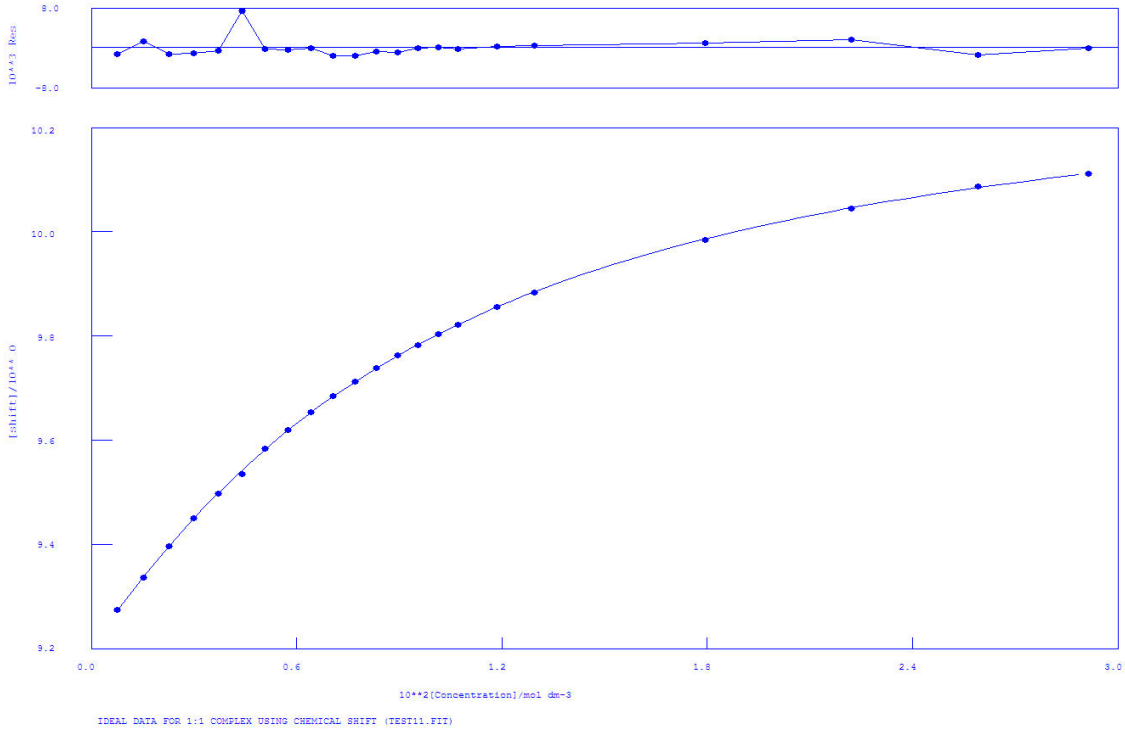

Calculations by WinEQNMR Version 1.20 by Michael J. Hynes
Program run at 15:31:04 on 01/09/2014

IDEAL DATA FOR 1:1 COMPLEX USING CHEMICAL SHIFT (TEST11.FIT)
Reaction: Sn + L = Sn(L)
FILE: TEST11.FIT (Measured shift is on 119Sn)
IDEAL DATA: K1 = 63.091; DELTA M = 20.0; DELTA ML = 120.0
File prepared by M. J. Hynes, October 22 2000

NO.	A	PARAMETER	DELTA	ERROR	CONDITION	DESCRIPTION
1	1	1.41834E+02	2.000E-01	1.508E+00	2.782E+01	K1
2	1	9.20194E+00	2.000E-01	1.469E-03	4.399E+00	SHIFT Sn
3	1	1.03656E+01	1.000E+00	3.696E-03	1.788E+01	SHIFT Sn(L)

Figure 4.14. ^{1}H-NMR of **L^{10}** with TBACl in DMSO-d_6/0.5%H_2O. The fitting has been obtained following the most downfield shifted NH proton.

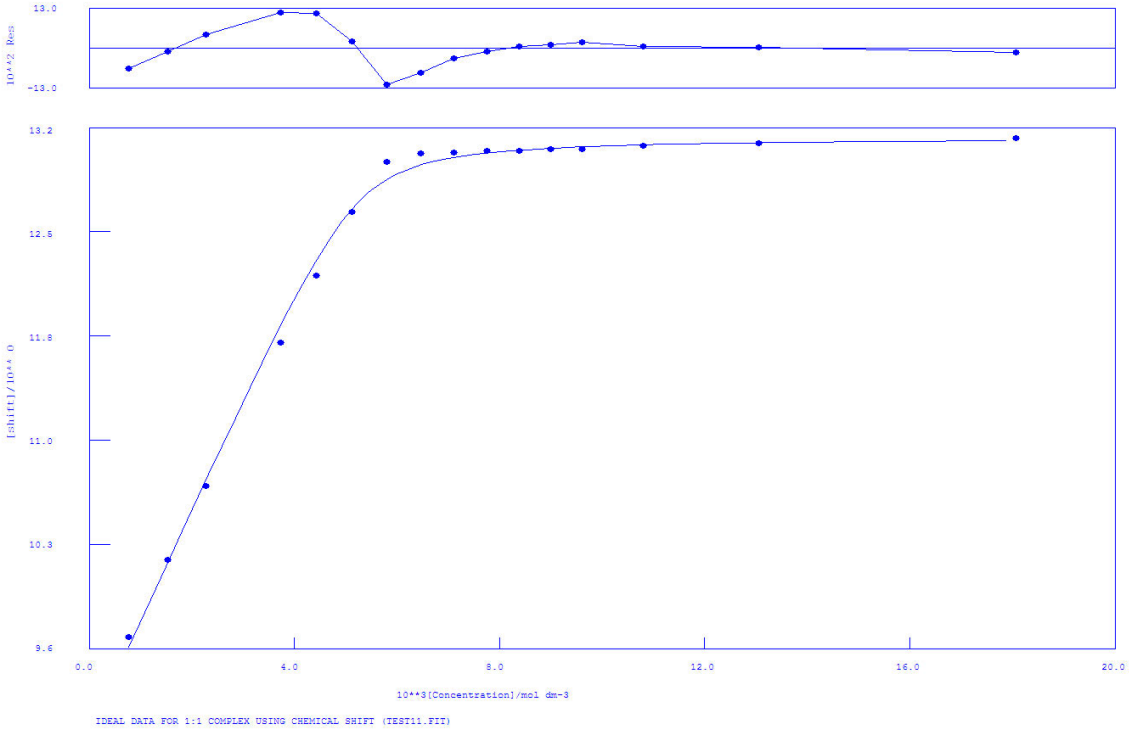

Calculations by WinEQNMR Version 1.20 by Michael J. Hynes
Program run at 10:37:50 on 06/28/2013

IDEAL DATA FOR 1:1 COMPLEX USING CHEMICAL SHIFT (TEST11.FIT)
Reaction: M + L = ML
FILE: TEST11.FIT
IDEAL DATA: K1 = 63.091; DELTA M = 20.0; DELTA ML = 120.0
File prepared by M. J. Hynes, October 22 2000

NO.	A	PARAMETER	DELTA	ERROR	CONDITION	DESCRIPTION
1	1	1.39502E+04	2.000E-01	3.049E+03	2.466E+00	K1
2	1	9.00793E+00	2.000E-01	5.287E-02	1.123E+00	SHIFT M
3	1	1.31304E+01	1.000E+00	2.986E-02	2.412E+00	SHIFT ML

Figure 4.15. ^{1}H-NMR of **L^{10}** with TBAF in DMSO-d_6/0.5%H_2O. The fitting has been obtained following the most downfield shifted NH proton.

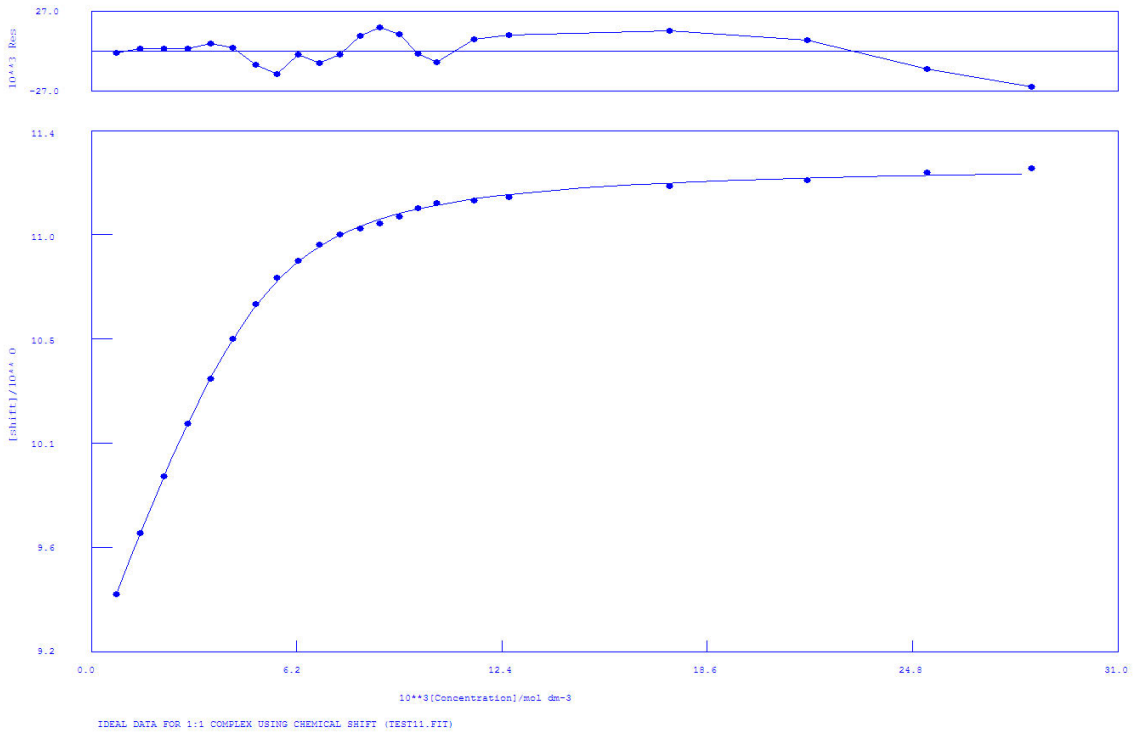

Calculations by WinEQNMR Version 1.20 by Michael J. Hynes
Program run at 18:20:22 on 09/19/2013

IDEAL DATA FOR 1:1 COMPLEX USING CHEMICAL SHIFT (TEST11.FIT)
Reaction: M + L = ML
FILE: TEST11.FIT
IDEAL DATA: K1 = 63.091; DELTA M = 20.0; DELTA ML = 120.0
File prepared by M. J. Hynes, October 22 2000

NO. A PARAMETER DELTA ERROR CONDITION DESCRIPTION
1 1 1.84167E+03 2.000E-01 6.193E+01 6.089E+00 K1
2 1 9.16573E+00 2.000E-01 8.302E-03 1.576E+00 SHIFT M
3 1 1.12642E+01 1.000E+00 6.453E-03 5.075E+00 SHIFT ML

Figure 4.16. ^{1}H-NMR of **L^{10}** with $TBAH_2PO_4$ in DMSO-d_6/0.5%H_2O. The fitting has been obtained following the most downfield shifted NH proton.

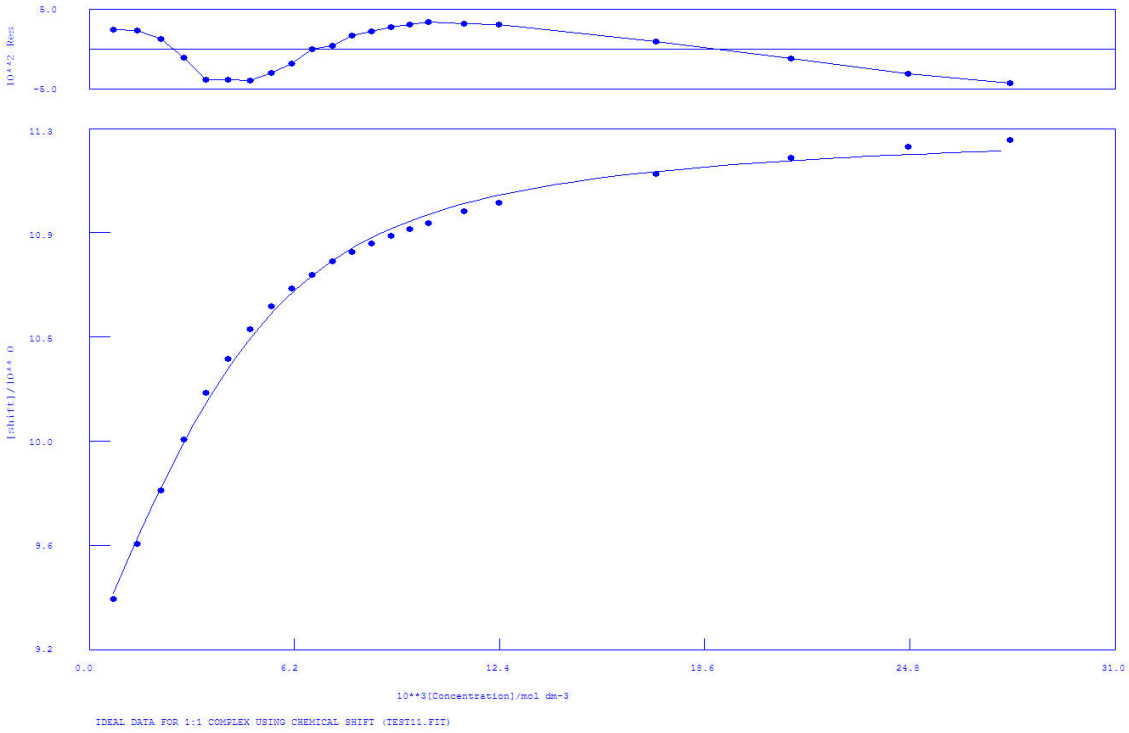

Calculations by WinEQNMR Version 1.20 by Michael J. Hynes
Program run at 14:59:12 on 06/26/2013
IDEAL DATA FOR 1:1 COMPLEX USING CHEMICAL SHIFT (TEST11.FIT)
Reaction: M + L = ML
FILE: TEST11.FIT
IDEAL DATA: K1 = 63.091; DELTA M = 20.0; DELTA ML = 120.0
File prepared by M. J. Hynes, October 22 2000

NO.	A	PARAMETER	DELTA	ERROR	CONDITION	DESCRIPTION
1	1	7.95574E+02	2.000E-01	5.900E+01	9.118E+00	K1
2	1	9.18599E+00	2.000E-01	2.241E-02	2.137E+00	SHIFT M
3	1	1.13205E+01	1.000E+00	2.248E-02	6.825E+00	SHIFT ML

Figure 4.17. ^{1}H-NMR of **L^{10}** with $TEAHCO_3$ in DMSO-d_6/0.5%H_2O. The fitting has been obtained following the most downfield shifted NH proton.

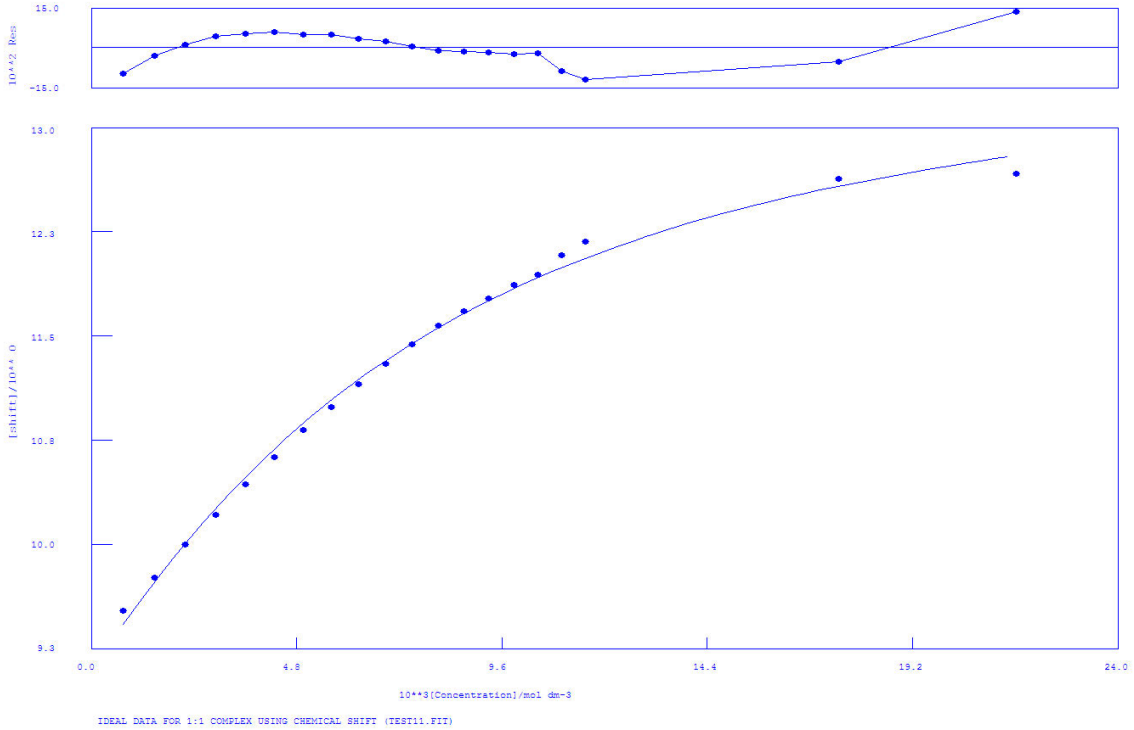

Calculations by WinEQNMR Version 1.20 by Michael J. Hynes
Program run at 15:59:14 on 01/09/2014

IDEAL DATA FOR 1:1 COMPLEX USING CHEMICAL SHIFT (TEST11.FIT)
Reaction: Sn + L = Sn(L)
FILE: TEST11.FIT (Measured shift is on 119Sn)
IDEAL DATA: K1 = 63.091; DELTA M = 20.0; DELTA ML = 120.0
File prepared by M. J. Hynes, October 22 2000

NO.	A	PARAMETER	DELTA	ERROR	CONDITION	DESCRIPTION
1	1	1.94560E+02	2.000E-01	2.241E+01	3.979E+01	K1
2	1	9.14315E+00	2.000E-01	5.102E-02	4.276E+00	SHIFT Sn
3	1	1.38697E+01	1.000E+00	1.556E-01	2.828E+01	SHIFT Sn(L)

Figure 4.18. ^{1}H-NMR of **L^{11}** with TBAAcO in DMSO-d_6/0.5%H_2O. The fitting has been obtained following the most downfield shifted NH proton.

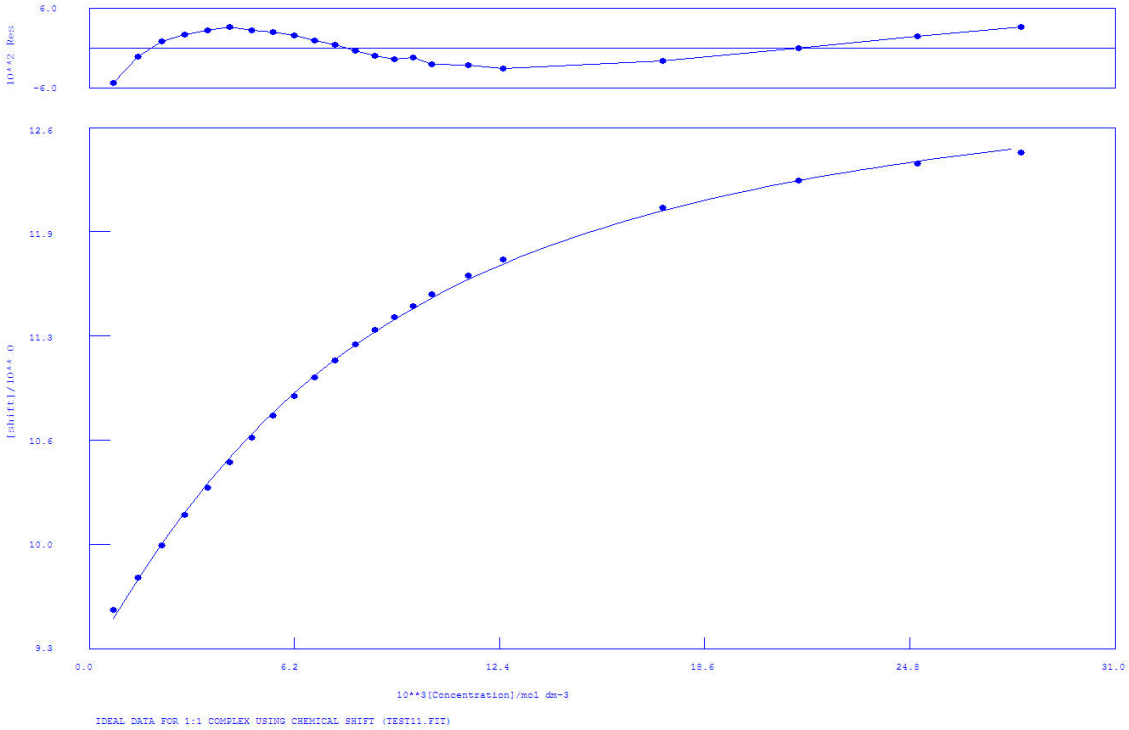

Calculations by WinEQNMR Version 1.20 by Michael J. Hynes
Program run at 16:01:51 on 01/09/2014

IDEAL DATA FOR 1:1 COMPLEX USING CHEMICAL SHIFT (TEST11.FIT)
Reaction: Sn + L = Sn(L)
FILE: TEST11.FIT (Measured shift is on 119Sn)
IDEAL DATA: K1 = 63.091; DELTA M = 20.0; DELTA ML = 120.0
File prepared by M. J. Hynes, October 22 2000

NO.	A	PARAMETER	DELTA	ERROR	CONDITION	DESCRIPTION
1	1	1.80886E+02	2.000E-01	6.609E+00	2.400E+01	K1
2	1	9.21685E+00	2.000E-01	1.874E-02	4.159E+00	SHIFT Sn
3	1	1.32149E+01	1.000E+00	3.983E-02	1.530E+01	SHIFT Sn(L)

Figure 4.19. ^{1}H-NMR of **L^{11}** with TBABzO in DMSO-d_6/0.5%H_2O. The fitting has been obtained following the most downfield shifted NH proton.

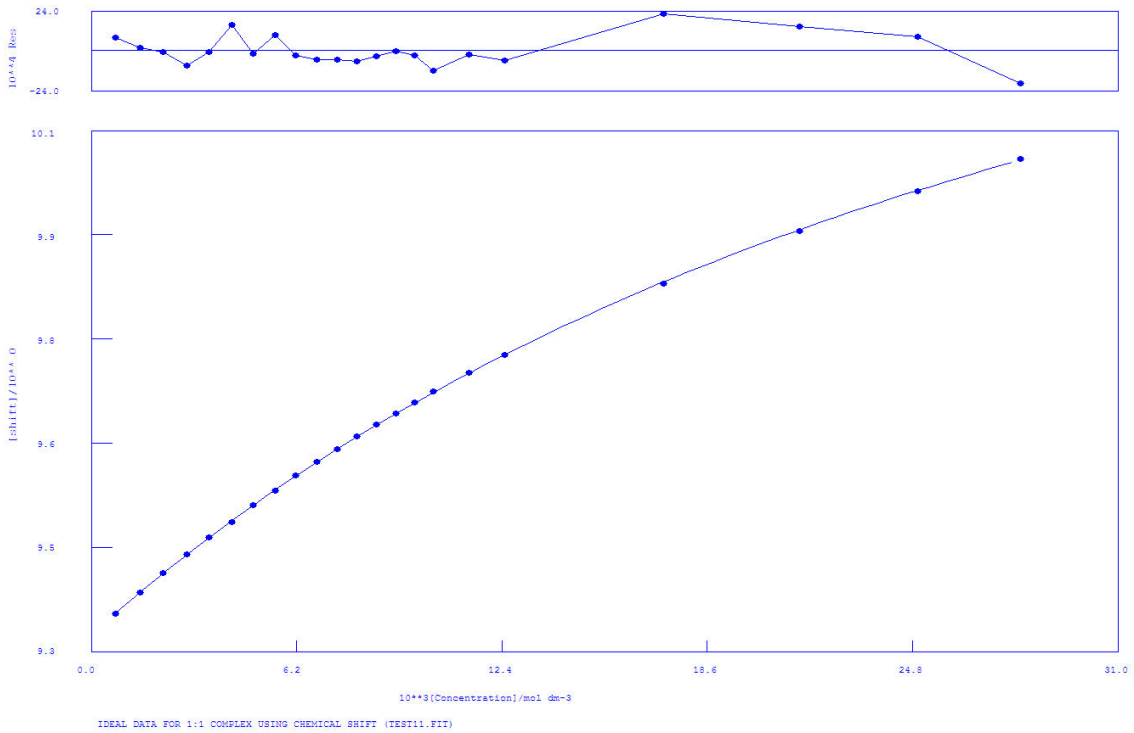

Calculations by WinEQNMR Version 1.20 by Michael J. Hynes
Program run at 16:04:11 on 01/09/2014

IDEAL DATA FOR 1:1 COMPLEX USING CHEMICAL SHIFT (TEST11.FIT)
Reaction: Sn + L = Sn(L)
FILE: TEST11.FIT (Measured shift is on 119Sn)
IDEAL DATA: K1 = 63.091; DELTA M = 20.0; DELTA ML = 120.0
File prepared by M. J. Hynes, October 22 2000

NO.	A	PARAMETER	DELTA	ERROR	CONDITION	DESCRIPTION
1	1	3.46683E+01	2.000E-01	3.688E-01	1.263E+02	K1
2	1	9.32563E+00	2.000E-01	6.642E-04	6.151E+00	SHIFT Sn
3	1	1.08721E+01	1.000E+00	8.872E-03	9.555E+01	SHIFT Sn(L)

Figure 4.20. ^{1}H-NMR of **L^{11}** with TBACl in DMSO-d_6/0.5%H_2O. The fitting has been obtained following the most downfield shifted NH proton.

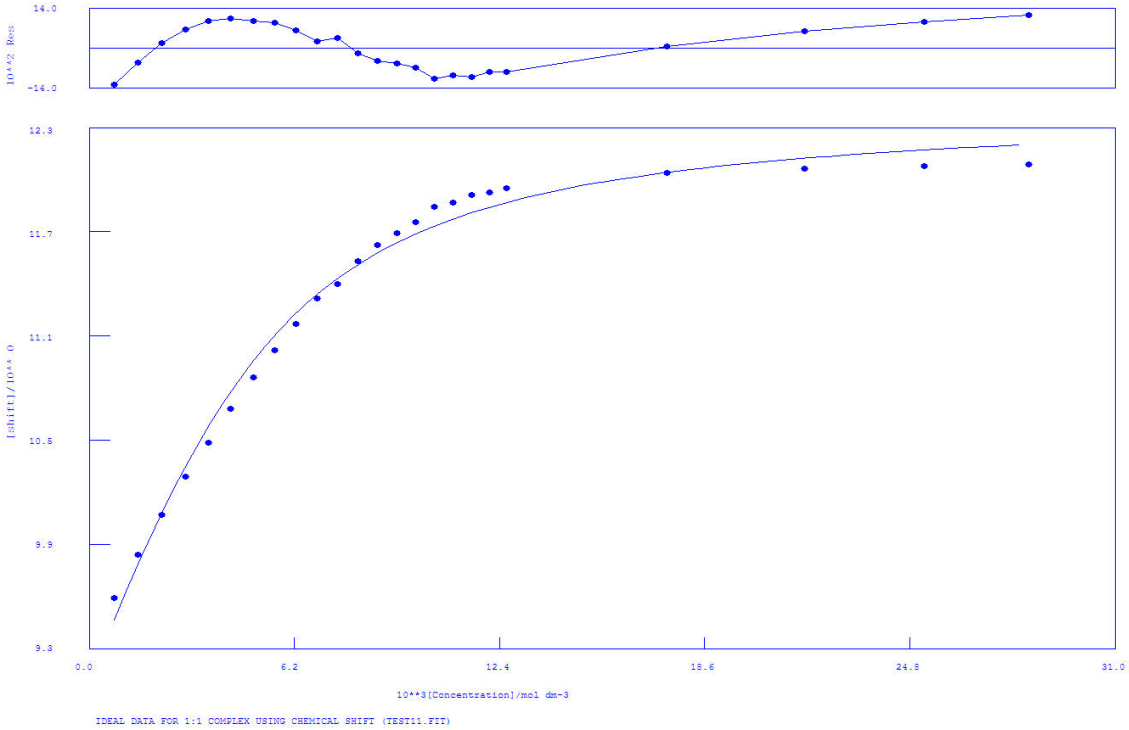

Calculations by WinEQNMR Version 1.20 by Michael J. Hynes
Program run at 16:06:56 on 01/09/2014

IDEAL DATA FOR 1:1 COMPLEX USING CHEMICAL SHIFT (TEST11.FIT)
Reaction: Sn + L = Sn(L)
FILE: TEST11.FIT (Measured shift is on 119Sn)
IDEAL DATA: K1 = 63.091; DELTA M = 20.0; DELTA ML = 120.0
File prepared by M. J. Hynes, October 22 2000

NO.	A	PARAMETER	DELTA	ERROR	CONDITION	DESCRIPTION
1	1	5.92470E+02	2.000E-01	7.931E+01	1.178E+01	K1
2	1	9.10526E+00	2.000E-01	6.554E-02	2.463E+00	SHIFT Sn
3	1	1.24211E+01	1.000E+00	7.136E-02	8.511E+00	SHIFT Sn(L)

Figure 4.21. ^{1}H-NMR of **L^{11}** with $TBAH_2PO_4$ in DMSO-d_6/0.5%H_2O. The fitting has been obtained following the most downfield shifted NH proton.

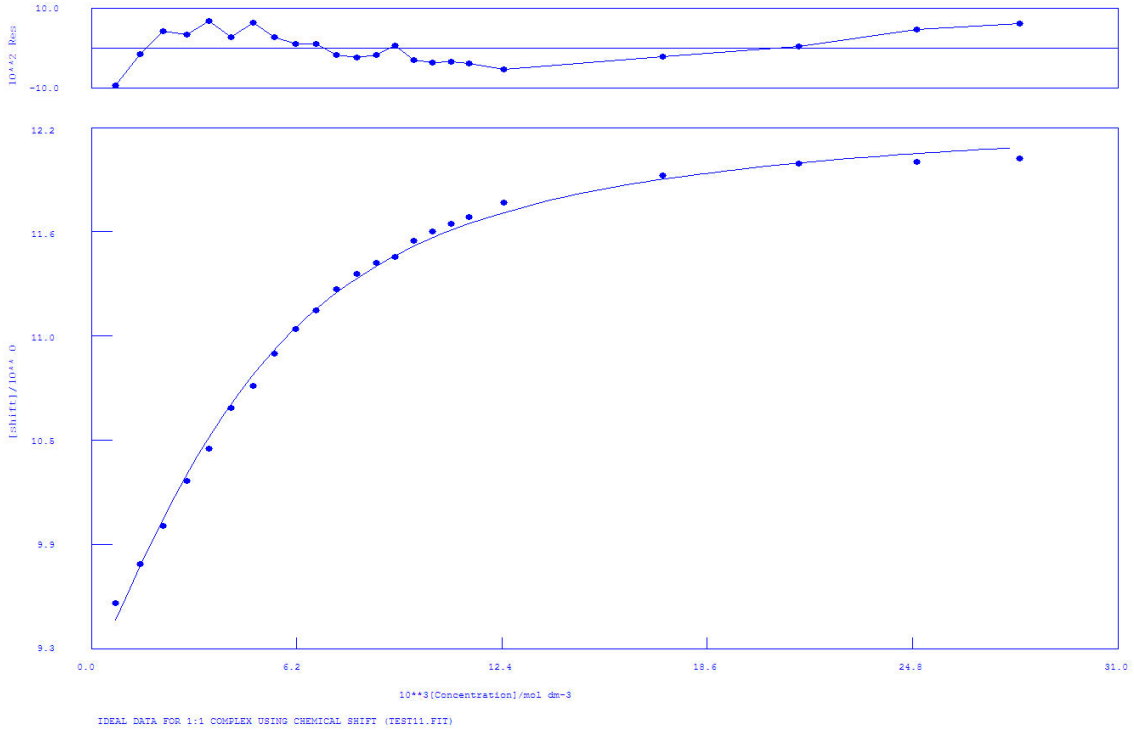

Calculations by WinEQNMR Version 1.20 by Michael J. Hynes
Program run at 16:10:12 on 01/09/2014

IDEAL DATA FOR 1:1 COMPLEX USING CHEMICAL SHIFT (TEST11.FIT)
Reaction: Sn + L = Sn(L)
FILE: TEST11.FIT (Measured shift is on 119Sn)
IDEAL DATA: K1 = 63.091; DELTA M = 20.0; DELTA ML = 120.0
File prepared by M. J. Hynes, October 22 2000

NO.	A	PARAMETER	DELTA	ERROR	CONDITION	DESCRIPTION
1	1	5.06561E+02	2.000E-01	3.641E+01	1.244E+01	K1
2	1	9.12879E+00	2.000E-01	3.376E-02	2.624E+00	SHIFT Sn
3	1	1.23375E+01	1.000E+00	4.004E-02	8.802E+00	SHIFT Sn(L)

Figure 4.22. ^{1}H-NMR of **L^{11}** with $TEAHCO_3$ in DMSO-d_6/0.5%H_2O. The fitting has been obtained following the most downfield shifted NH proton.

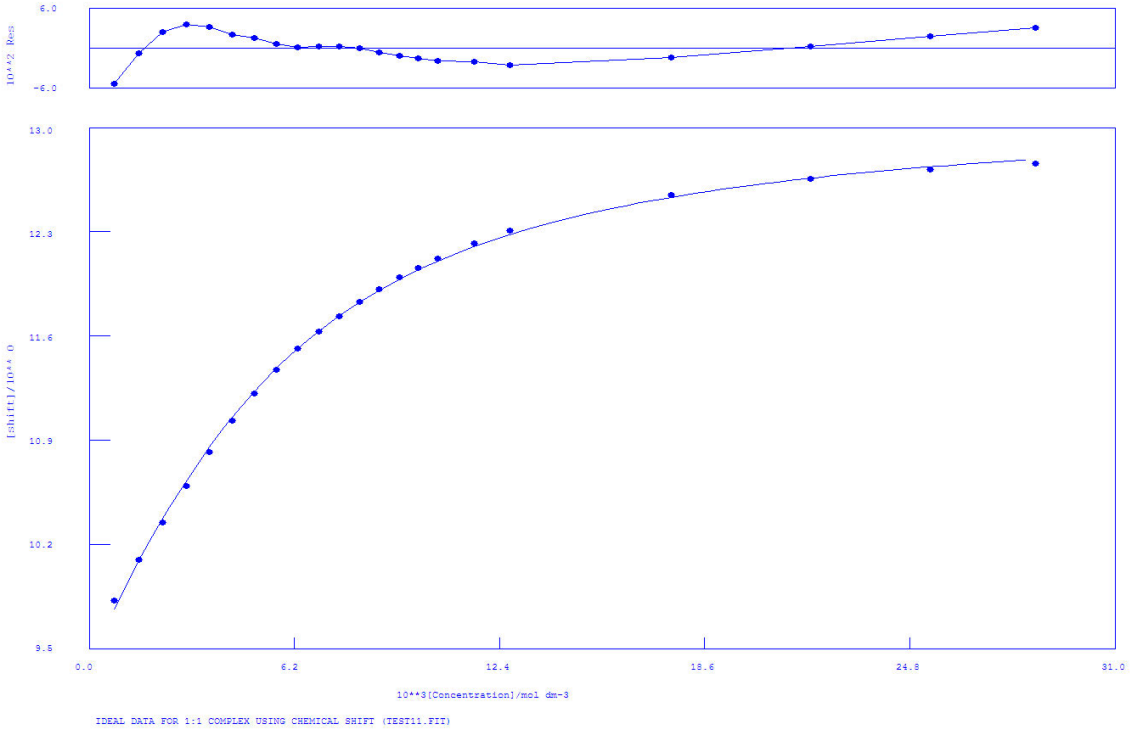

Calculations by WinEQNMR Version 1.20 by Michael J. Hynes
Program run at 16:12:44 on 01/09/2014

IDEAL DATA FOR 1:1 COMPLEX USING CHEMICAL SHIFT (TEST11.FIT)
Reaction: Sn + L = Sn(L)
FILE: TEST11.FIT (Measured shift is on 119Sn)
IDEAL DATA: K1 = 63.091; DELTA M = 20.0; DELTA ML = 120.0
File prepared by M. J. Hynes, October 22 2000

NO.	A	PARAMETER	DELTA	ERROR	CONDITION	DESCRIPTION
1	1	3.57372E+02	2.000E-01	1.146E+01	1.452E+01	K1
2	1	9.41181E+00	2.000E-01	1.806E-02	3.106E+00	SHIFT Sn
3	1	1.31764E+01	1.000E+00	2.416E-02	9.653E+00	SHIFT Sn(L)

Figure 4.23. ^{1}H-NMR of **L^{12}** with TBAAcO in DMSO-d_6/0.5%H_2O. The fitting has been obtained following the most downfield shifted NH proton.

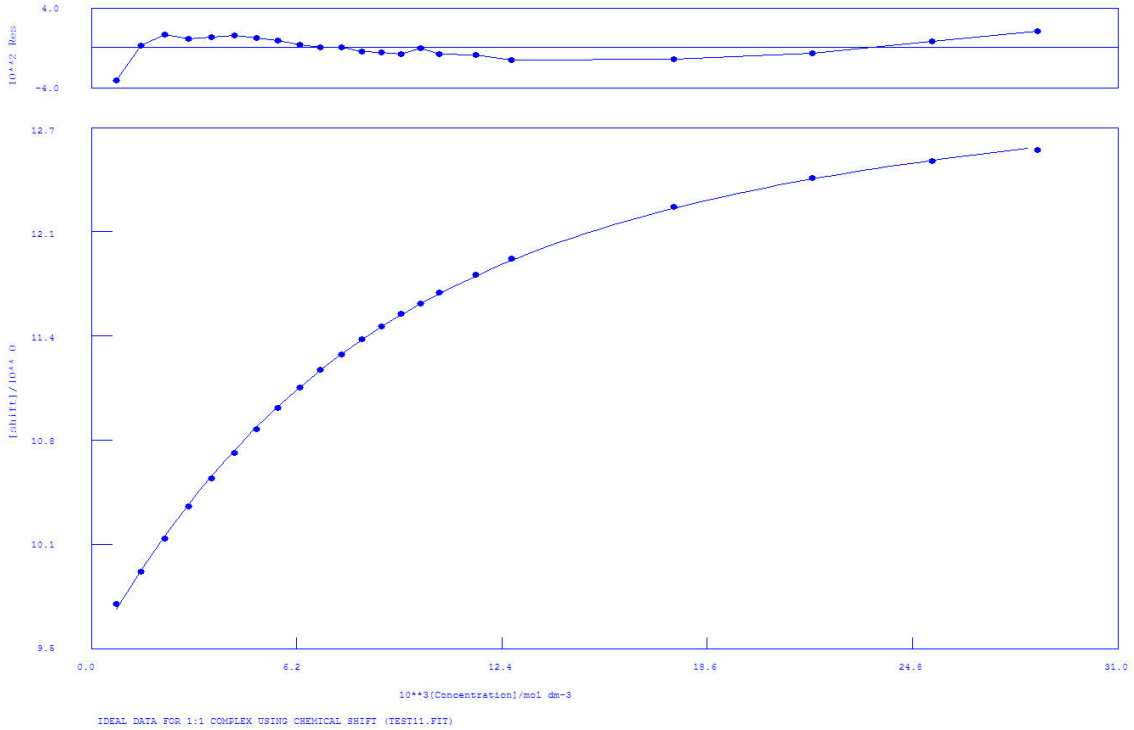

Calculations by WinEQNMR Version 1.20 by Michael J. Hynes
Program run at 16:15:21 on 01/09/2014

IDEAL DATA FOR 1:1 COMPLEX USING CHEMICAL SHIFT (TEST11.FIT)
Reaction: Sn + L = Sn(L)
FILE: TEST11.FIT (Measured shift is on 119Sn)
IDEAL DATA: K1 = 63.091; DELTA M = 20.0; DELTA ML = 120.0
File prepared by M. J. Hynes, October 22 2000

NO.	A	PARAMETER	DELTA	ERROR	CONDITION	DESCRIPTION
1	1	1.83482E+02	2.000E-01	3.375E+00	2.352E+01	K1
2	1	9.48041E+00	2.000E-01	8.831E-03	4.060E+00	SHIFT Sn
3	1	1.32699E+01	1.000E+00	1.864E-02	1.512E+01	SHIFT Sn(L)

Figure 4.24. ^{1}H-NMR of **L^{12}** with TBABzO in DMSO-d_6/0.5%H_2O. The fitting has been obtained following the most downfield shifted NH proton.

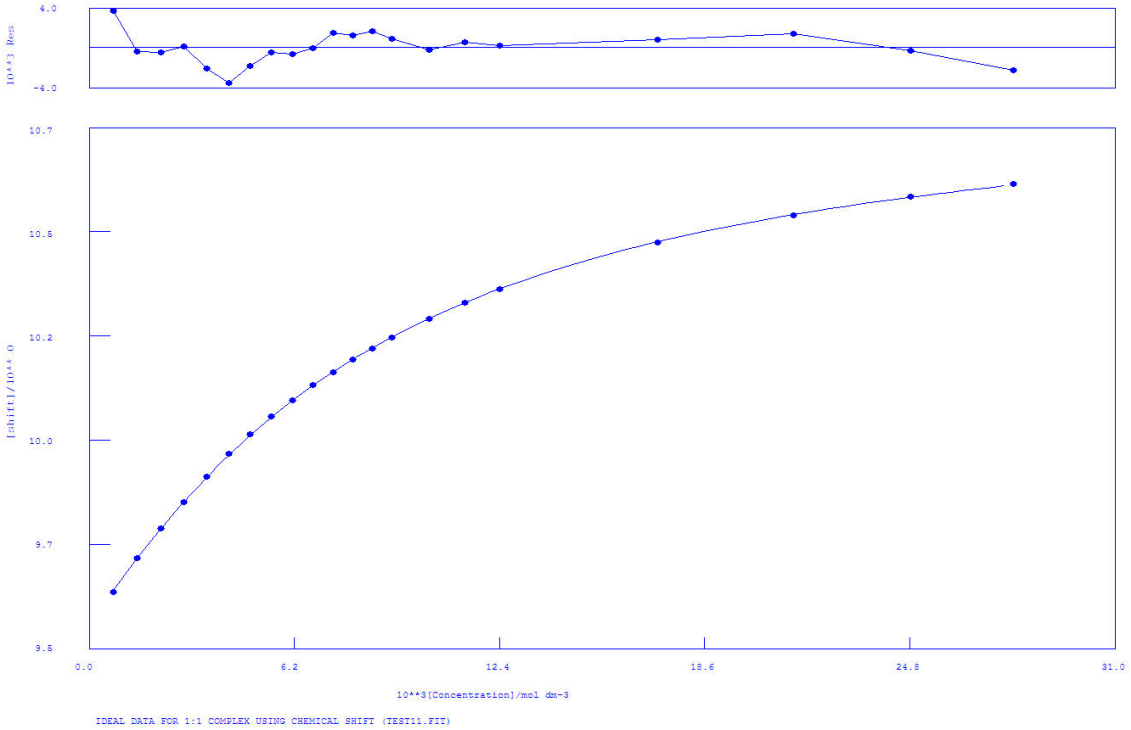

Calculations by WinEQNMR Version 1.20 by Michael J. Hynes
Program run at 16:18:20 on 01/09/2014

IDEAL DATA FOR 1:1 COMPLEX USING CHEMICAL SHIFT (TEST11.FIT)
Reaction: Sn + L = Sn(L)
FILE: TEST11.FIT (Measured shift is on 119Sn)
IDEAL DATA: K1 = 63.091; DELTA M = 20.0; DELTA ML = 120.0
File prepared by M. J. Hynes, October 22 2000

NO.	A	PARAMETER	DELTA	ERROR	CONDITION	DESCRIPTION
1	1	1.68534E+02	2.000E-01	1.382E+00	2.437E+01	K1
2	1	9.55125E+00	2.000E-01	1.273E-03	4.135E+00	SHIFT Sn
3	1	1.08181E+01	1.000E+00	2.902E-03	1.559E+01	SHIFT Sn(L)

Figure 4.25. ^{1}H-NMR of **L^{12}** with TBACl in DMSO-d_6/0.5%H_2O. The fitting has been obtained following the most downfield shifted NH proton.

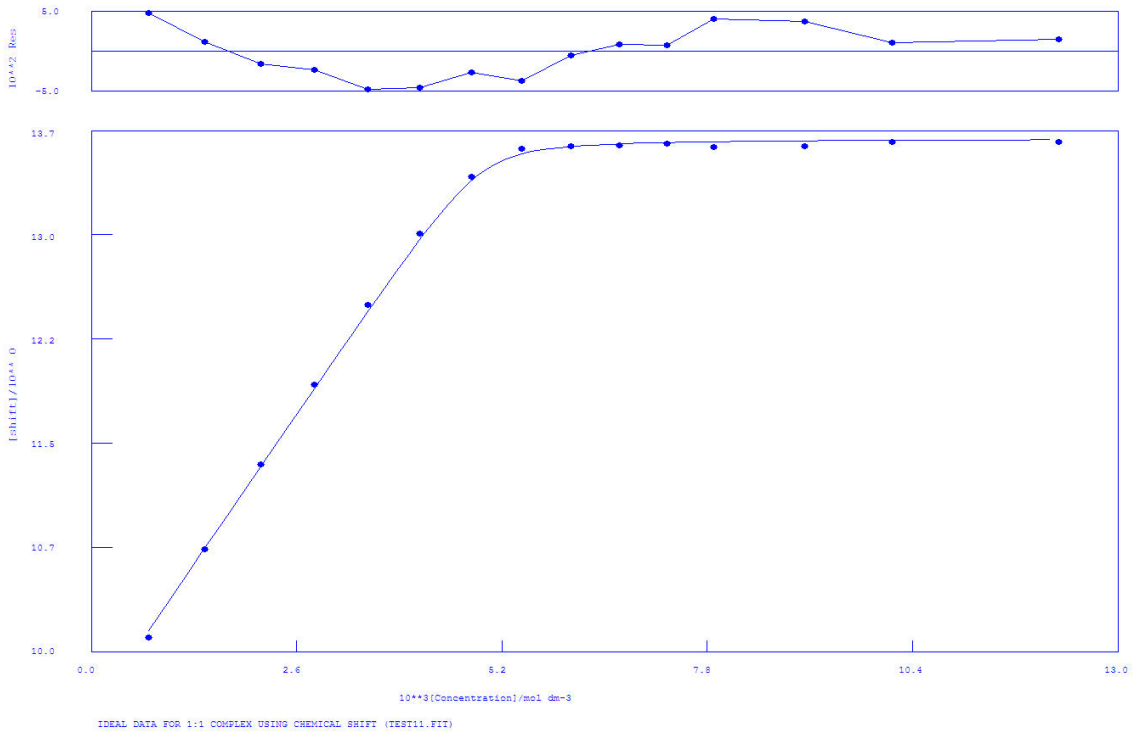

Calculations by WinEQNMR Version 1.20 by Michael J. Hynes
Program run at 11:30:16 on 09/19/2013

IDEAL DATA FOR 1:1 COMPLEX USING CHEMICAL SHIFT (TEST11.FIT)
Reaction: M + L = ML
FILE: TEST11.FIT
IDEAL DATA: K1 = 63.091; DELTA M = 20.0; DELTA ML = 120.0
File prepared by M. J. Hynes, October 22 2000

NO.	A	PARAMETER	DELTA	ERROR	CONDITION	DESCRIPTION
1	1	5.76469E+04	2.000E-01	5.039E+03	1.439E+00	K1
2	1	9.54863E+00	2.000E-01	2.644E-02	1.186E+00	SHIFT M
3	1	1.36427E+01	1.000E+00	1.284E-02	1.568E+00	SHIFT ML

Figure 4.26. ^{1}H-NMR of **L^{12}** with TBAF in DMSO-d_6/0.5%H_2O. The fitting has been obtained following the most downfield shifted NH proton.

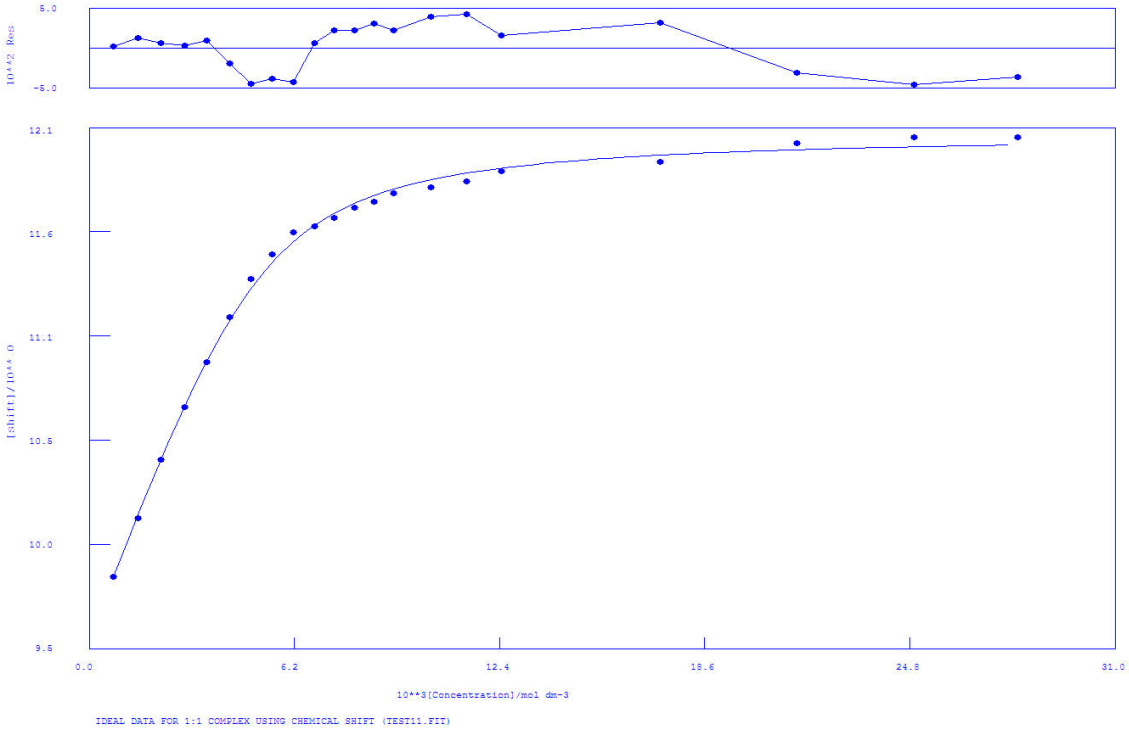

Calculations by WinEQNMR Version 1.20 by Michael J. Hynes
Program run at 11:44:37 on 09/19/2013
IDEAL DATA FOR 1:1 COMPLEX USING CHEMICAL SHIFT (TEST11.FIT)
Reaction: M + L = ML
FILE: TEST11.FIT
IDEAL DATA: K1 = 63.091; DELTA M = 20.0; DELTA ML = 120.0
File prepared by M. J. Hynes, October 22 2000

NO.	A	PARAMETER	DELTA	ERROR	CONDITION	DESCRIPTION
1	1	1.72815E+03	2.000E-01	1.383E+02	5.912E+00	K1
2	1	9.53498E+00	2.000E-01	2.411E-02	1.599E+00	SHIFT M
3	1	1.20740E+01	1.000E+00	1.939E-02	4.894E+00	SHIFT ML

Figure 4.27. ^{1}H-NMR of **L^{12}** with $TBAH_2PO_4$ in DMSO-d_6/0.5%H_2O. The fitting has been obtained following the most downfield shifted NH proton.

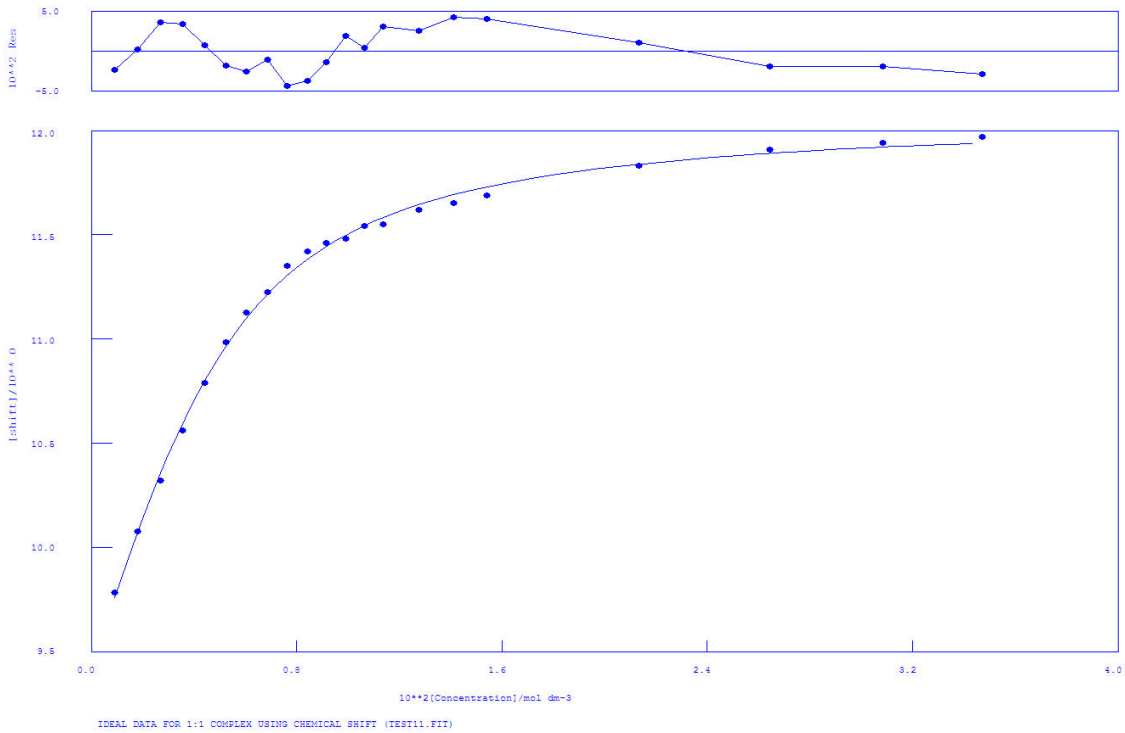

Calculations by WinEQNMR Version 1.20 by Michael J. Hynes
Program run at 11:52:07 on 09/19/2013
IDEAL DATA FOR 1:1 COMPLEX USING CHEMICAL SHIFT (TEST11.FIT)
Reaction: M + L = ML
FILE: TEST11.FIT
IDEAL DATA: K1 = 63.091; DELTA M = 20.0; DELTA ML = 120.0
File prepared by M. J. Hynes, October 22 2000

NO.	A	PARAMETER	DELTA	ERROR	CONDITION	DESCRIPTION
1	1	5.94298E+02	2.000E-01	3.296E+01	9.007E+00	K1
2	1	9.40172E+00	2.000E-01	2.580E-02	2.498E+00	SHIFT M
3	1	1.20809E+01	1.000E+00	2.124E-02	6.076E+00	SHIFT ML

Figure 4.28. ^{1}H-NMR of **L^{12}** with $TEAHCO_3$ in DMSO-d_6/0.5%H_2O. The fitting has been obtained following the most downfield shifted NH proton.

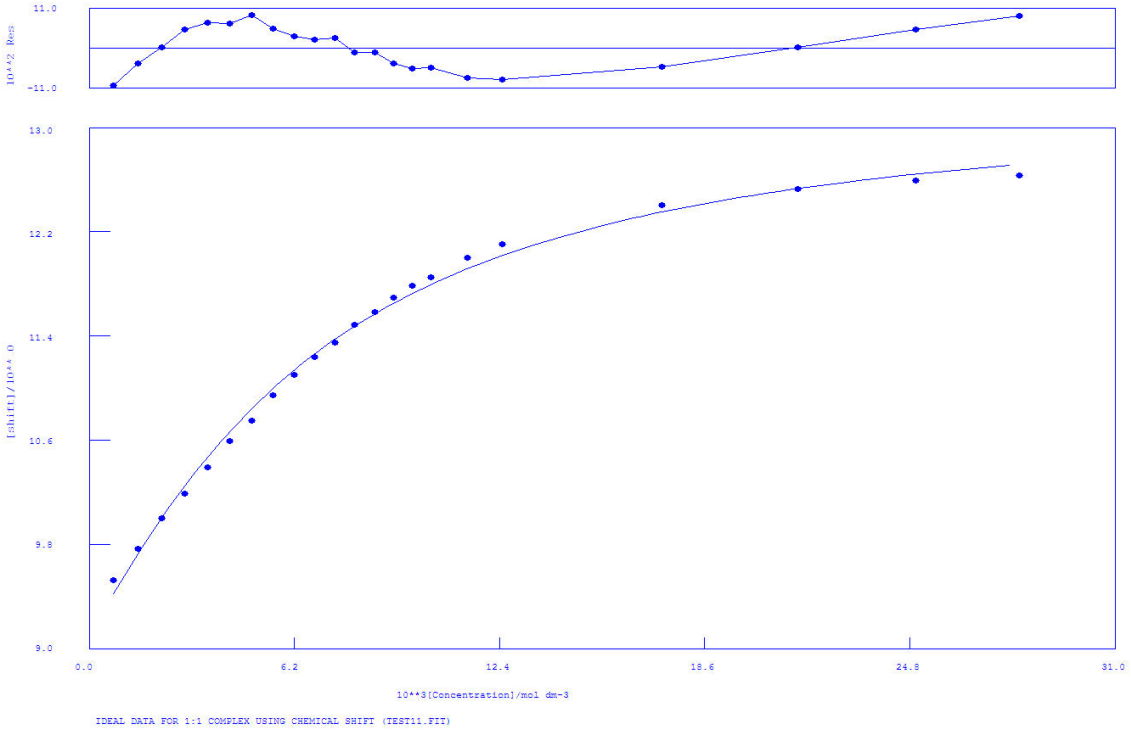

Calculations by WinEQNMR Version 1.20 by Michael J. Hynes
Program run at 13:11:10 on 09/16/2013

IDEAL DATA FOR 1:1 COMPLEX USING CHEMICAL SHIFT (TEST11.FIT)
Reaction: M + L = ML
FILE: TEST11.FIT
IDEAL DATA: K1 = 63.091; DELTA M = 20.0; DELTA ML = 120.0
File prepared by M. J. Hynes, October 22 2000

NO.	A	PARAMETER	DELTA	ERROR	CONDITION	DESCRIPTION
1	1	2.41661E+02	2.000E-01	2.004E+01	1.989E+01	K1
2	1	9.08094E+00	2.000E-01	4.968E-02	3.870E+00	SHIFT M
3	1	1.33459E+01	1.000E+00	8.387E-02	1.254E+01	SHIFT ML

Figure 4.29. ^{1}H-NMR of **L^{13}** with TBAAcO in DMSO-d_6/0.5%H_2O. The fitting has been obtained following the most downfield shifted NH proton.

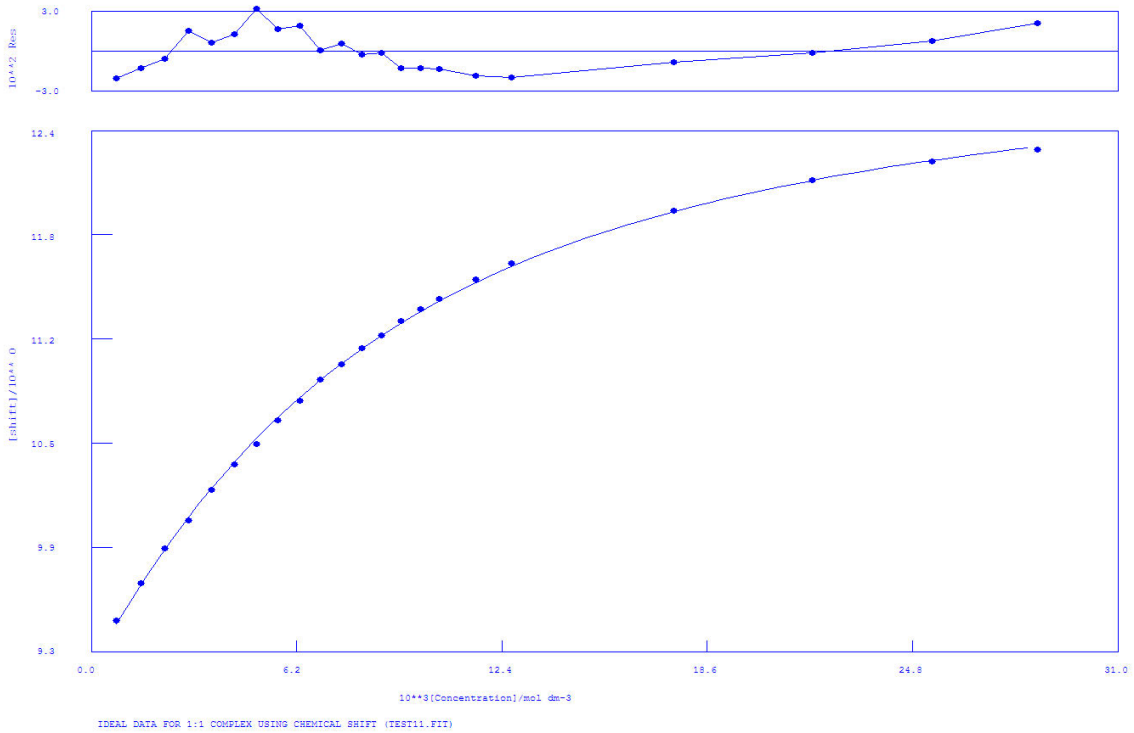

Calculations by WinEQNMR Version 1.20 by Michael J. Hynes
Program run at 15:35:14 on 01/09/2014

IDEAL DATA FOR 1:1 COMPLEX USING CHEMICAL SHIFT (TEST11.FIT)
Reaction: Sn + L = Sn(L)
FILE: TEST11.FIT (Measured shift is on 119Sn)
IDEAL DATA: K1 = 63.091; DELTA M = 20.0; DELTA ML = 120.0
File prepared by M. J. Hynes, October 22 2000

NO.	A	PARAMETER	DELTA	ERROR	CONDITION	DESCRIPTION
1	1	1.71752E+02	2.000E-01	4.191E+00	2.462E+01	K1
2	1	9.20606E+00	2.000E-01	1.180E-02	4.206E+00	SHIFT Sn
3	1	1.30398E+01	1.000E+00	2.579E-02	1.571E+01	SHIFT Sn(L)

Figure 4.30. ^{1}H-NMR of **L^{13}** with TBABzO in DMSO-d_6/0.5%H_2O. The fitting has been obtained following the most downfield shifted NH proton.

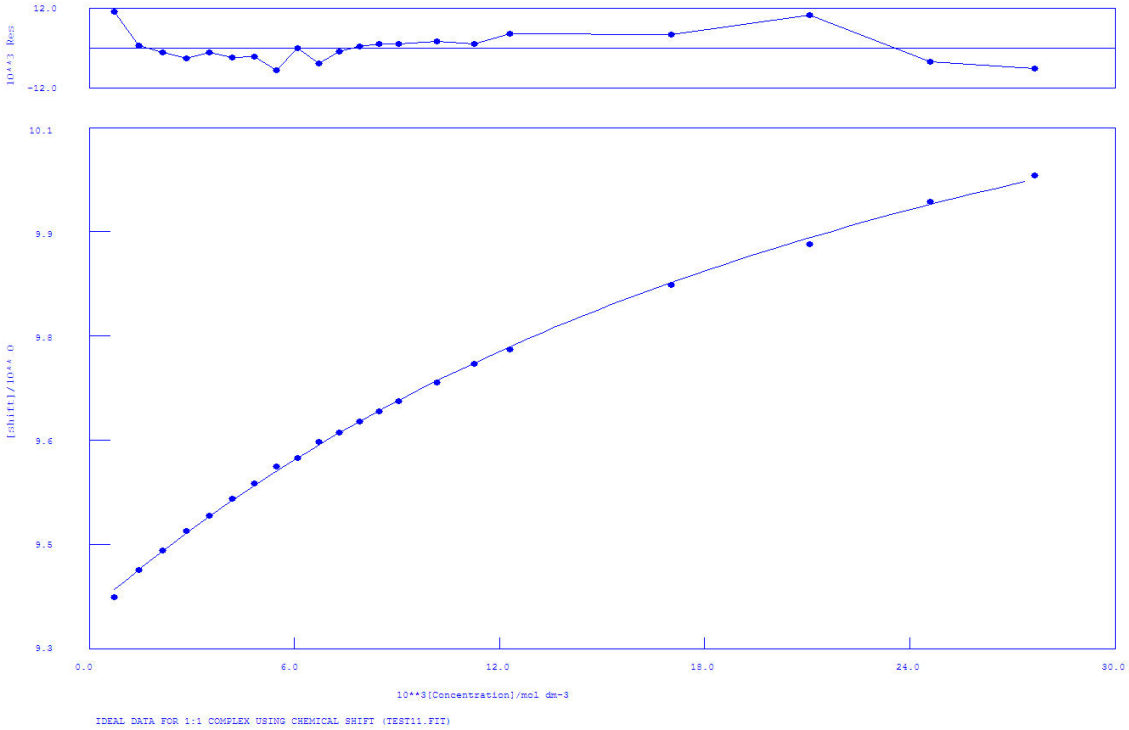

Calculations by WinEQNMR Version 1.20 by Michael J. Hynes
Program run at 15:39:07 on 01/09/2014

IDEAL DATA FOR 1:1 COMPLEX USING CHEMICAL SHIFT (TEST11.FIT)
Reaction: Sn + L = Sn(L)
FILE: TEST11.FIT (Measured shift is on 119Sn)
IDEAL DATA: K1 = 63.091; DELTA M = 20.0; DELTA ML = 120.0
File prepared by M. J. Hynes, October 22 2000

NO.	A	PARAMETER	DELTA	ERROR	CONDITION	DESCRIPTION
1	1	4.44922E+01	2.000E-01	2.233E+00	9.052E+01	K1
2	1	9.35733E+00	2.000E-01	3.252E-03	5.825E+00	SHIFT Sn
3	1	1.06151E+01	1.000E+00	3.110E-02	6.584E+01	SHIFT Sn(L)

Figure 4.31. ^{1}H-NMR of **L^{13}** with TBACl in DMSO-d_6/0.5%H_2O. The fitting has been obtained following the most downfield shifted NH proton.

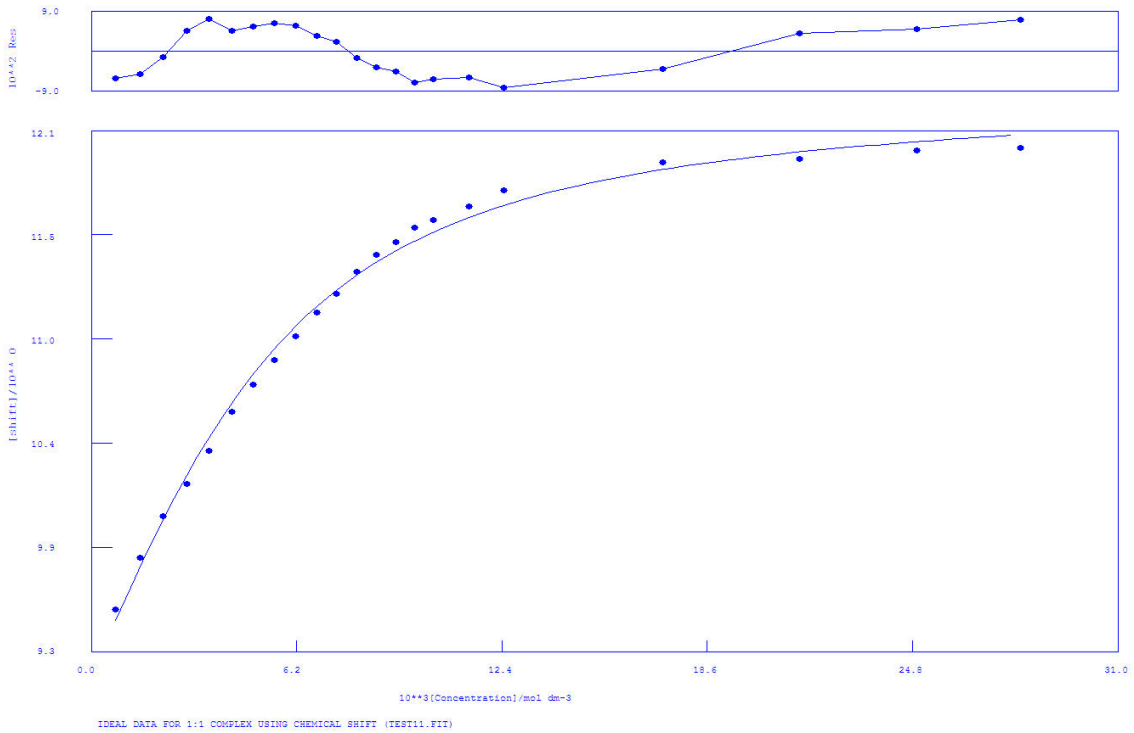

Calculations by WinEQNMR Version 1.20 by Michael J. Hynes
Program run at 15:40:30 on 01/09/2014

IDEAL DATA FOR 1:1 COMPLEX USING CHEMICAL SHIFT (TEST11.FIT)
Reaction: Sn + L = Sn(L)
FILE: TEST11.FIT (Measured shift is on 119Sn)
IDEAL DATA: K1 = 63.091; DELTA M = 20.0; DELTA ML = 120.0
File prepared by M. J. Hynes, October 22 2000

NO.	A	PARAMETER	DELTA	ERROR	CONDITION	DESCRIPTION
1	1	4.75339E+02	2.000E-01	4.375E+01	1.167E+01	K1
2	1	9.15035E+00	2.000E-01	4.421E-02	2.680E+00	SHIFT Sn
3	1	1.23385E+01	1.000E+00	5.279E-02	8.072E+00	SHIFT Sn(L)

Figure 4.32. ^{1}H-NMR of **L^{13}** with $TBAH_2PO_4$ in DMSO-d_6/0.5%H_2O. The fitting has been obtained following the most downfield shifted NH proton.

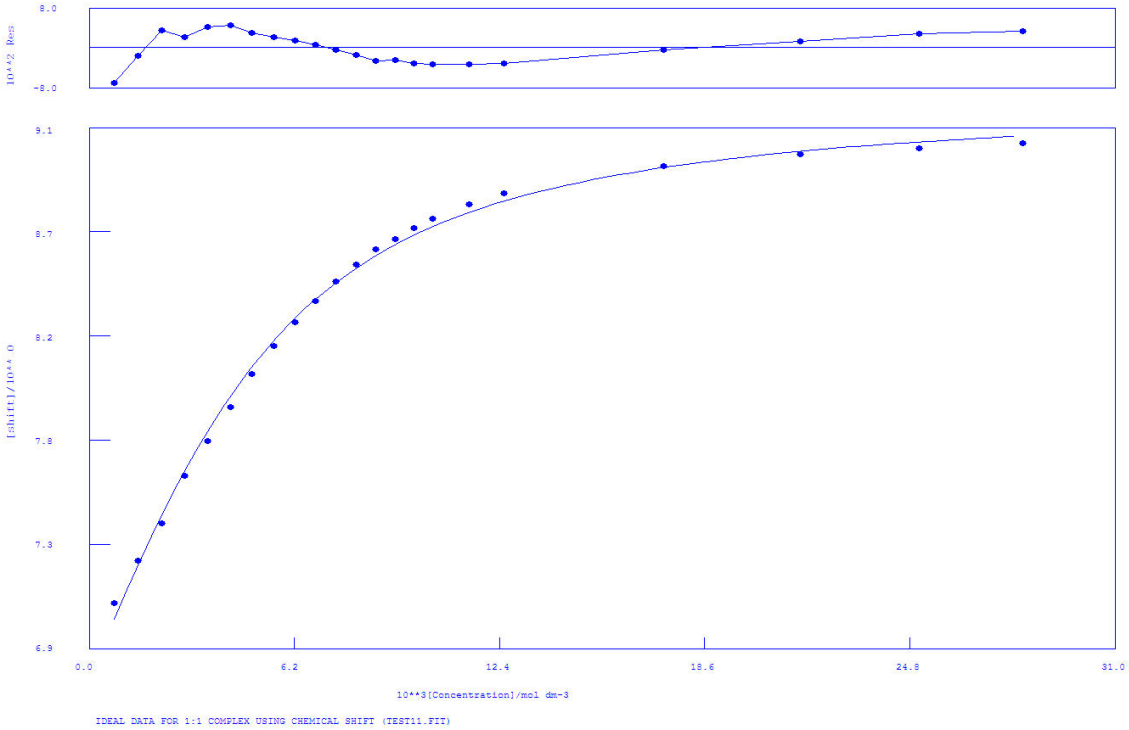

Calculations by WinEQNMR Version 1.20 by Michael J. Hynes
Program run at 17:42:22 on 03/25/2013
IDEAL DATA FOR 1:1 COMPLEX USING CHEMICAL SHIFT (TEST11.FIT)
Reaction: M + L = ML
FILE: TEST11.FIT
IDEAL DATA: K1 = 63.091; DELTA M = 20.0; DELTA ML = 120.0
File prepared by M. J. Hynes, October 22 2000

NO.	A	PARAMETER	DELTA	ERROR	CONDITION	DESCRIPTION
1	1	5.22724E+02	2.000E-01	3.653E+01	1.156E+01	K1
2	1	6.76960E+00	2.000E-01	2.518E-02	2.550E+00	SHIFT M
3	1	9.25140E+00	1.000E+00	2.967E-02	8.191E+00	SHIFT ML

Figure 4.33. ^{1}H-NMR of **L^{13}** with $TEAHCO_3$ in DMSO-d_6/0.5%H_2O. The fitting has been obtained following the most downfield shifted NH proton.

4.7.4 Anion Transport Studies

4.7.4.1 Experimental details

Preparation of Vesicles

A lipid film of 1-palmitoyl-2-oleoyl-sn-glycero-3-phosphocholine (POPC) and cholesterol (0% or 30%) was formed from a chloroform solution under reduced pressure and dried under vacuum for at least 2 hours. The lipid film was rehydrated by vortexing with an internal solution (489 mM NaCl, 5 mM phosphate buffer at pH 7.2). The lipid suspension was then subjected to nine freeze-thaw cycles and allowed to age for 30 min at room temperature before extruding 20 times through a 200 nm polycarbonate membrane. The resulting unilamellar vesicles were dialyzed against the external solution to remove unencapsulated NaCl salts. The vesicles were diluted to 5mL with the external solution to form a stock solution of lipid.

Samples for assay were prepared by diluting lipid stock solution to 5mL (using the external solution) to give a solution of 1mM lipid. Chloride efflux was monitored using a chloride selective electrode (Accumet). To initiate the experiment compounds were added as solutions in DMSO, to give a 1:50 compound to lipid ratio (2mol%). At the end of the experiment detergent (octaethylene glycol monododecyl ether) was added to allow the determination of 100% chloride efflux. Experiments were repeated in triplicate and all traces presented are the average of three trials. The chloride electrode was calibrated against sodium chloride solutions of known concentration.

Chloride Transport Assays

Unilamellar POPC vesicles containing NaCl, prepared as described above, were suspended in 489 mM $NaNO_3$ buffered to pH 7.2 with 5 mM sodium phosphate salts. The lipid concentration per sample was 1 mM. A DMSO solution of the carrier molecule (10 mM) was added to start the experiment and the chloride efflux was monitored using a chloride sensitive electrode. At 5 min, the vesicles were lysed with 50 µl of octaethylene glycol monododecyl ether and a total chloride reading was taken at 7 min.

Bicarbonate Transport Assay

Unilamellar POPC vesicles containing 451 mM NaCl solution buffered to pH 7.2 with 20 mM sodium phosphate salts, prepared as described above, were suspended in 150 mM Na_2SO_4 solution buffered to pH 7.2 with sodium phosphate salts. The lipid concentration per sample was 1 mM. A DMSO solution of the carrier molecule (10 mM) was added to start the experiment and chloride efflux was monitored using a chloride sensitive electrode. At 2 min, $NaHCO_3$ solution (1 M in 150 mM Na_2SO_4 buffered to pH 7.2 with 20 mM sodium phosphate salts) was added so that the outer solution contained 40 mM $NaHCO_3$. At 7 min, the vesicles were lysed with 50 µl of octaethylene glycol monododecyl ether and a total chloride reading was taken at 9 min.

4.7.4.2 Additional membrane transport studies

Cl^-/NO_3^- transport studies

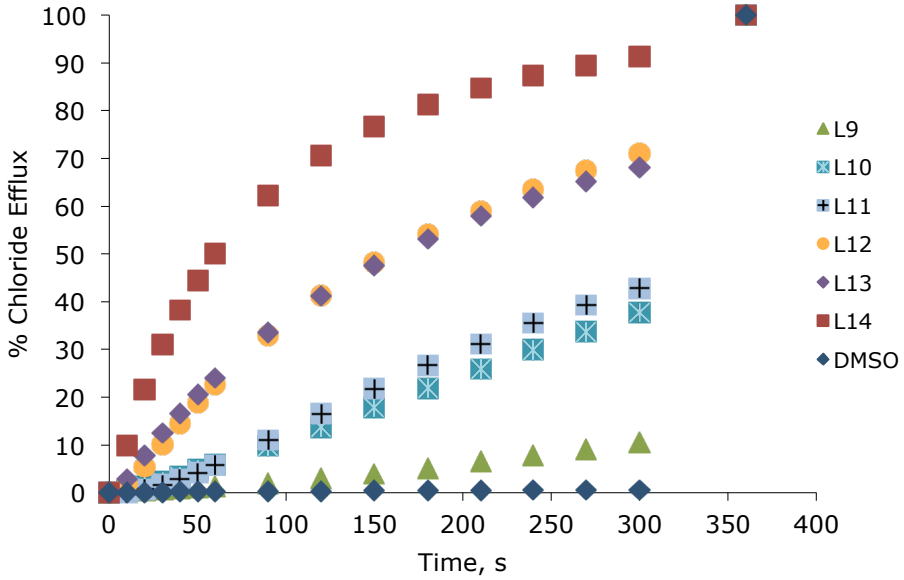

Figure 4.34 Chloride efflux promoted by a DMSO solution of compounds $\mathbf{L^9}$–$\mathbf{L^{14}}$ (2% carrier to lipid) from unilamellar POPC vesicles loaded with 489 mM NaCl buffered to pH 7.2 with 5 mM sodium phosphate salts. The vesicles were dispersed in 489 mM $NaNO_3$ buffered to pH 7.2 with 5 mM sodium phosphate salts. At the end of the experiment detergent was added to lyse the vesicles and calibrate the ISE to 100% chloride efflux. Each point represents an average of three trials. DMSO was used as a control.

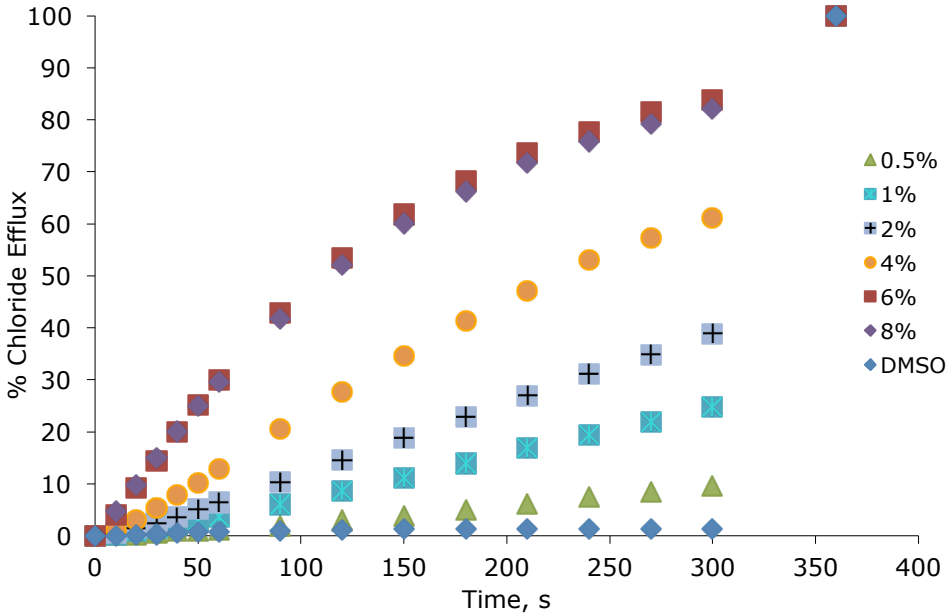

Figure 4.35 Chloride efflux promoted by various concentrations of **L**[10] (2% carrier to lipid) from unilamellar POPC vesicles loaded with 489 mM NaCl buffered to pH 7.2 with 5 mM sodium phosphate salts. The vesicles were dispersed in 489 mM $NaNO_3$ buffered to pH 7.2 with 5 mM sodium phosphate salts. At the end of the experiment detergent was added to lyse the vesicles and calibrate the ISE to 100% chloride efflux. Each point represents an average of three trials. DMSO was used as a control.

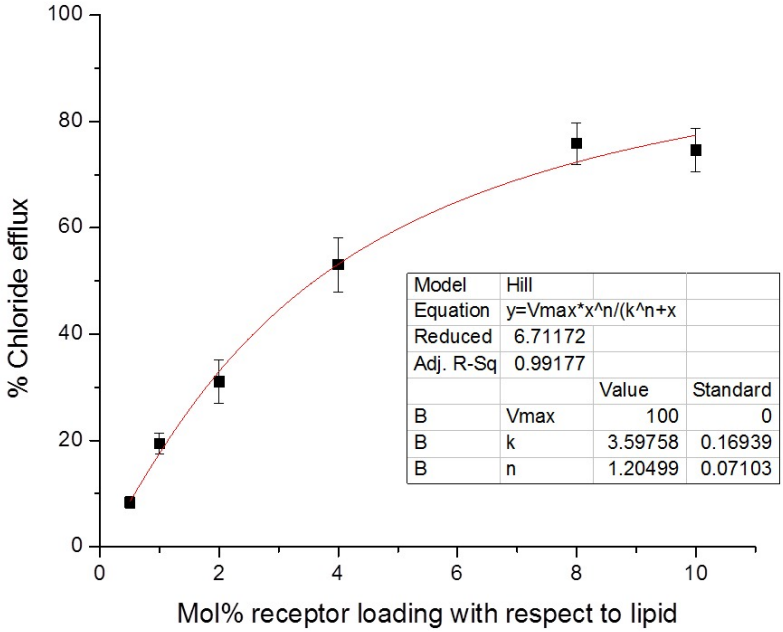

Figure 4.36 Hill plot of chloride efflux promoted by varying concentrations of compound **L**[10] from unilamellar POPC vesicles loaded with 489 mM NaCl buffered to pH 7.2 with 5mM sodium phosphate salts. The vesicles were dispersed in 489 mM $NaNO_3$ buffered at pH 7.2 with 5mM sodium phosphate salts. Each point represents an average of 3 trials.

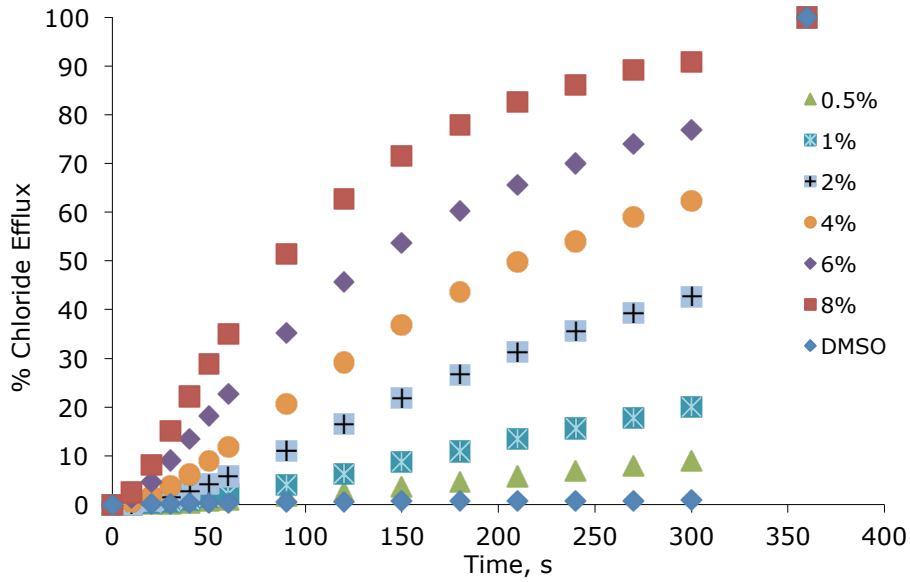

Figure 4.37 Chloride efflux promoted by various concentrations of **L**[11] (2% carrier to lipid) from unilamellar POPC vesicles loaded with 489 mM NaCl buffered to pH 7.2 with 5 mM sodium phosphate salts. The vesicles were dispersed in 489 mM $NaNO_3$ buffered to pH 7.2 with 5 mM sodium phosphate salts. At the end of the experiment detergent was added to lyse the vesicles and calibrate the ISE to 100% chloride efflux. Each point represents an average of three trials. DMSO was used as a control.

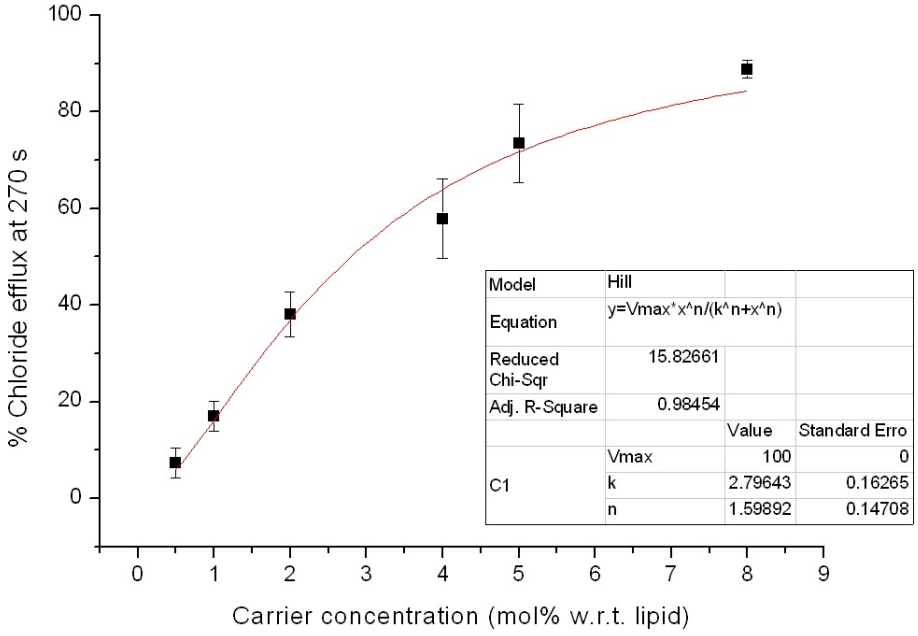

Figure 4.38 Hill plot of chloride efflux promoted by varying concentrations of compound **L**[11] from unilamellar POPC vesicles loaded with 489 mM NaCl buffered to pH 7.2 with 5mM sodium phosphate salts. The vesicles were dispersed in 489 mM $NaNO_3$ buffered at pH 7.2 with 5mM sodium phosphate salts. Each point represents an average of 3 trials.

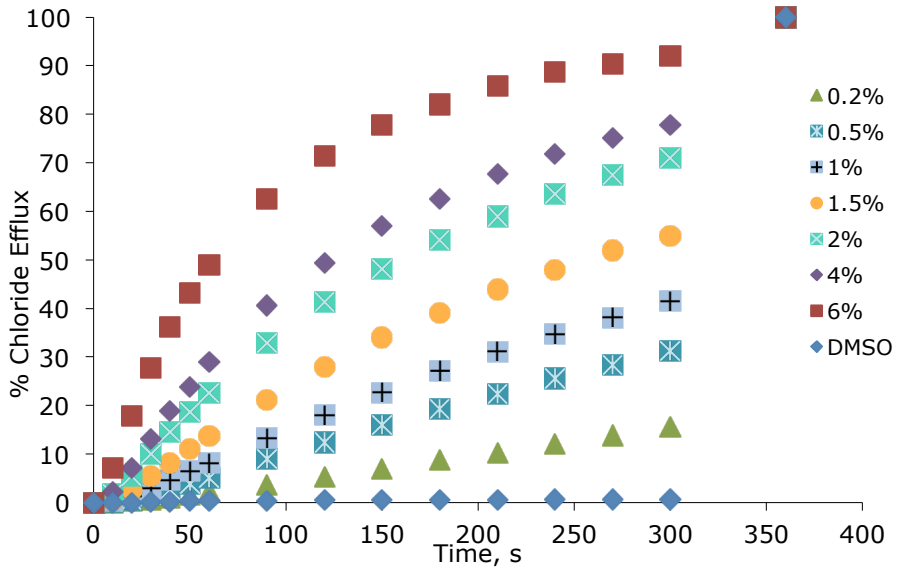

Figure 4.39 Chloride efflux promoted by various concentrations of **L**^{12} (2% carrier to lipid) from unilamellar POPC vesicles loaded with 489 mM NaCl buffered to pH 7.2 with 5 mM sodium phosphate salts. The vesicles were dispersed in 489 mM $NaNO_3$ buffered to pH 7.2 with 5 mM sodium phosphate salts. At the end of the experiment detergent was added to lyse the vesicles and calibrate the ISE to 100% chloride efflux. Each point represents an average of three trials. DMSO was used as a control.

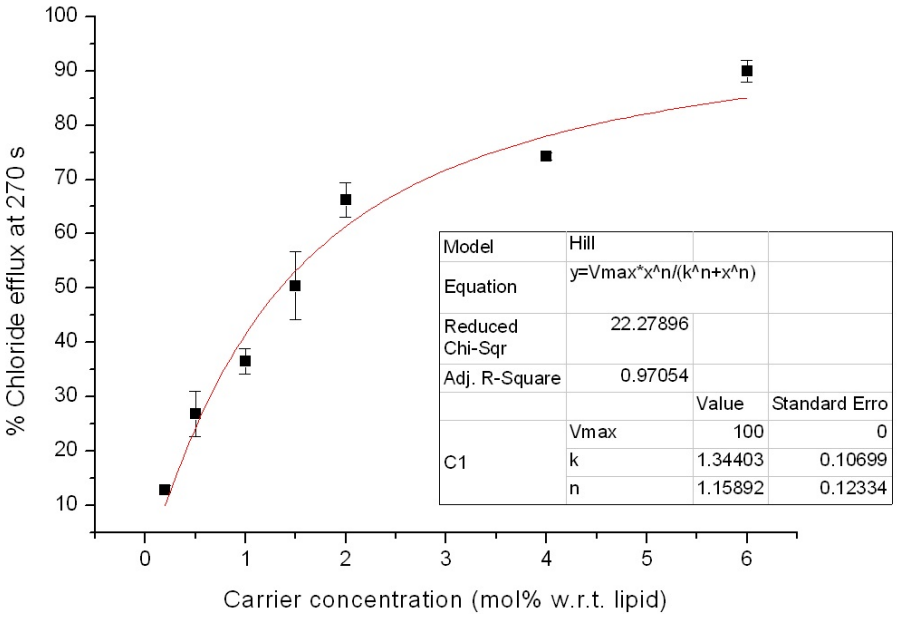

Figure 4.40 Hill plot of chloride efflux promoted by varying concentrations of compound **L**^{12} from unilamellar POPC vesicles loaded with 489 mM NaCl buffered to pH 7.2 with 5mM sodium phosphate salts. The vesicles were dispersed in 489 mM $NaNO_3$ buffered at pH 7.2 with 5mM sodium phosphate salts. Each point represents an average of 3 trials.

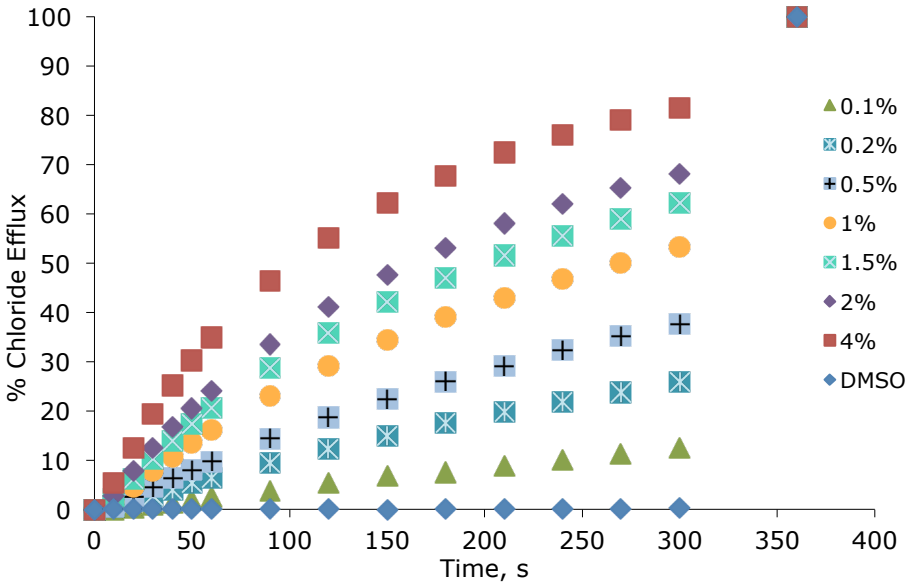

Figure 4.41 Chloride efflux promoted by various concentrations of **L**[13] (2% carrier to lipid) from unilamellar POPC vesicles loaded with 489 mM NaCl buffered to pH 7.2 with 5 mM sodium phosphate salts. The vesicles were dispersed in 489 mM $NaNO_3$ buffered to pH 7.2 with 5 mM sodium phosphate salts. At the end of the experiment detergent was added to lyse the vesicles and calibrate the ISE to 100% chloride efflux. Each point represents an average of three trials. DMSO was used as a control.

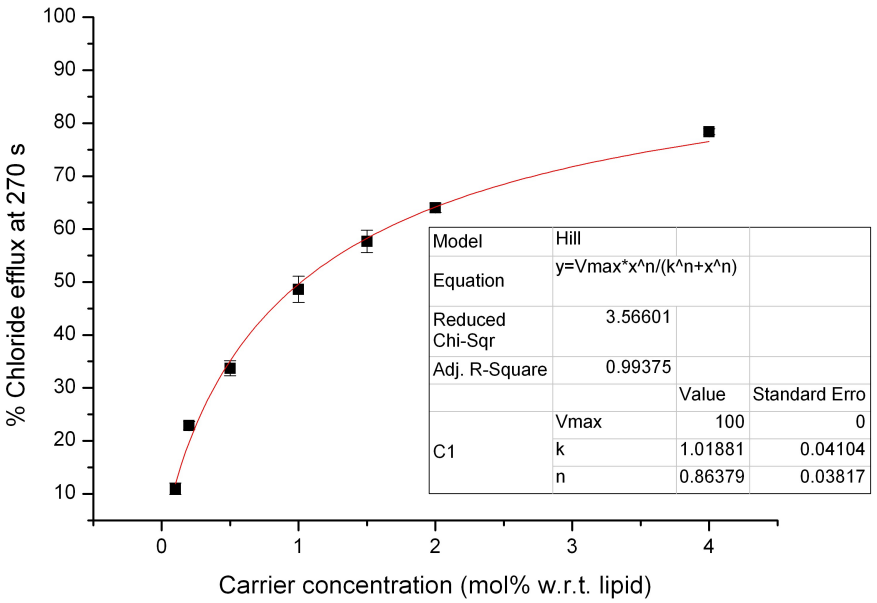

Figure 4.42 Hill plot of chloride efflux promoted by varying concentrations of compound **L**[12] from unilamellar POPC vesicles loaded with 489 mM NaCl buffered to pH 7.2 with 5mM sodium phosphate salts. The vesicles were dispersed in 489 mM $NaNO_3$ buffered at pH 7.2 with 5mM sodium phosphate salts. Each point represents an average of 3 trials.

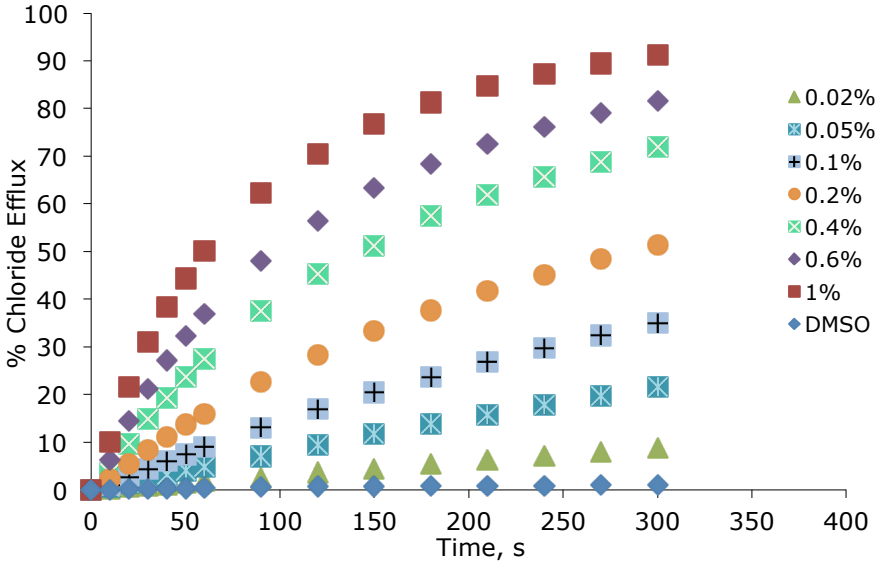

Figure 4.43 Chloride efflux promoted by various concentrations of **L**[14] from unilamellar POPC vesicles loaded with 489 mM NaCl buffered to pH 7.2 with 5 mM sodium phosphate salts. The vesicles were dispersed in 489 mM $NaNO_3$ buffered to pH 7.2 with 5 mM sodium phosphate salts. At the end of the experiment detergent was added to lyse the vesicles and calibrate the ISE to 100% chloride efflux. Each point represents an average of three trials. DMSO was used as a control.

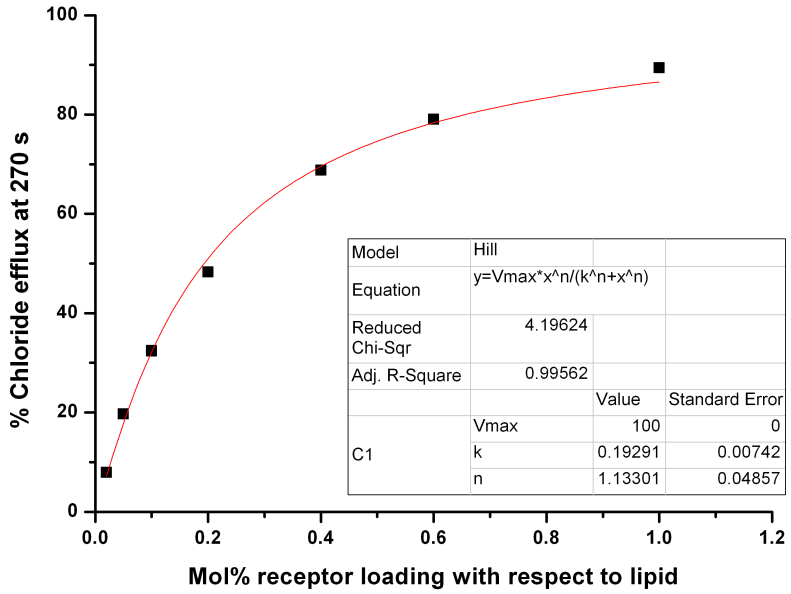

Figure 4.44 Hill plot of chloride efflux promoted by varying concentrations of compound **L**[12] from unilamellar POPC vesicles loaded with 489 mM NaCl buffered to pH 7.2 with 5mM sodium phosphate salts. The vesicles were dispersed in 489 mM $NaNO_3$ buffered at pH 7.2 with 5mM sodium phosphate salts. Each point represents an average of 3 trials.

Cl^-/HCO_3^- transport studies

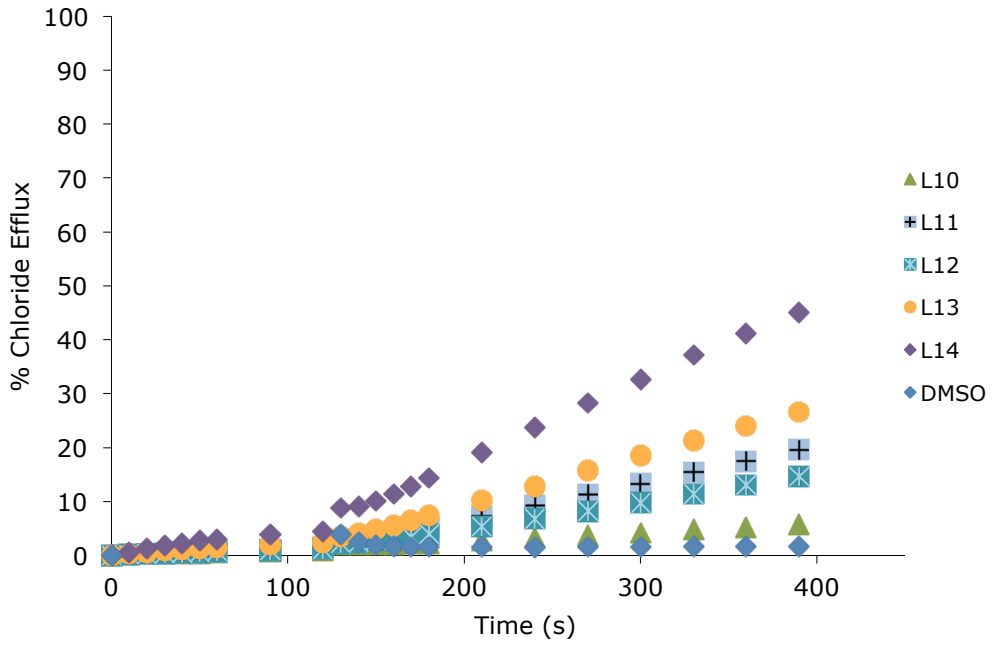

Figure 4.45 Chloride efflux promoted by a DMSO solution of compounds **L^9–L^{14}** (2 mol% carrier to lipid) from unilamellar POPC vesicles loaded with 451 mM NaCl buffered to pH 7.2 with 20 mM sodium phosphate salts. The vesicles were dispersed in 150 mM Na_2SO_4 buffered to pH 7.2 with 20 mM sodium phosphate salts. At t. 120 s a solution of sodium bicarbonate was added such that the external concentration of bicarbonate was 40 mM. At the end of the experiment, detergent was added to lyse the vesicles and calibrate the ISE to 100% chloride efflux. Each point represents an average of three trials. DMSO was used as a control.

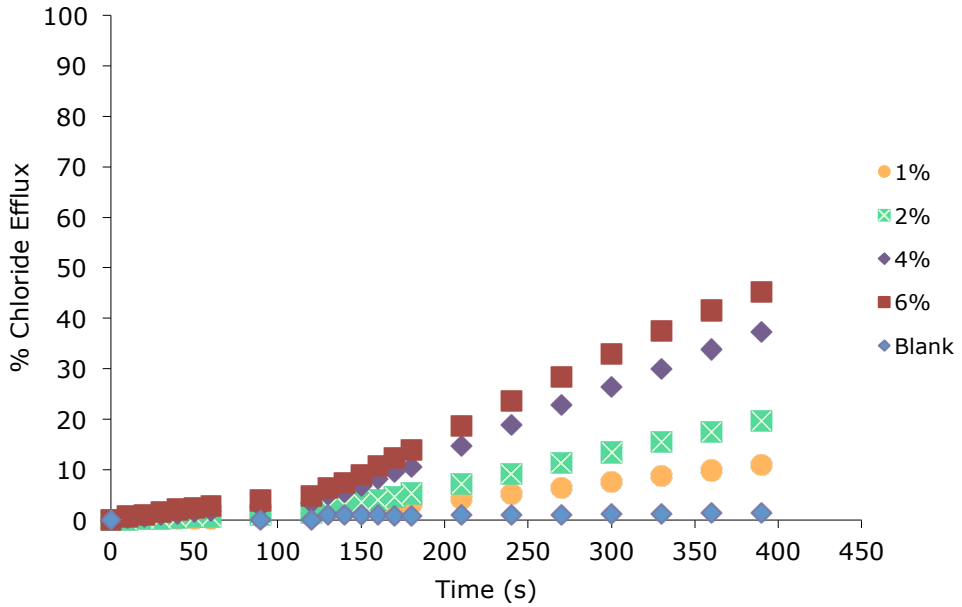

Figure 4.46 Chloride efflux promoted by various concentrations of **L**[11] from unilamellar POPC vesicles loaded with 451 mM NaCl buffered to pH 7.2 with 20 mM sodium phosphate salts. The vesicles were dispersed in 150 mM Na_2SO_4 buffered to pH 7.2 with 20 mM sodium phosphate salts. At t. 120 s a solution of sodium bicarbonate was added such that the external concentration of bicarbonate was 40 mM. At the end of the experiment, detergent was added to lyse the vesicles and calibrate the ISE to 100% chloride efflux. Each point represents an average of three trials. DMSO was used as a control.

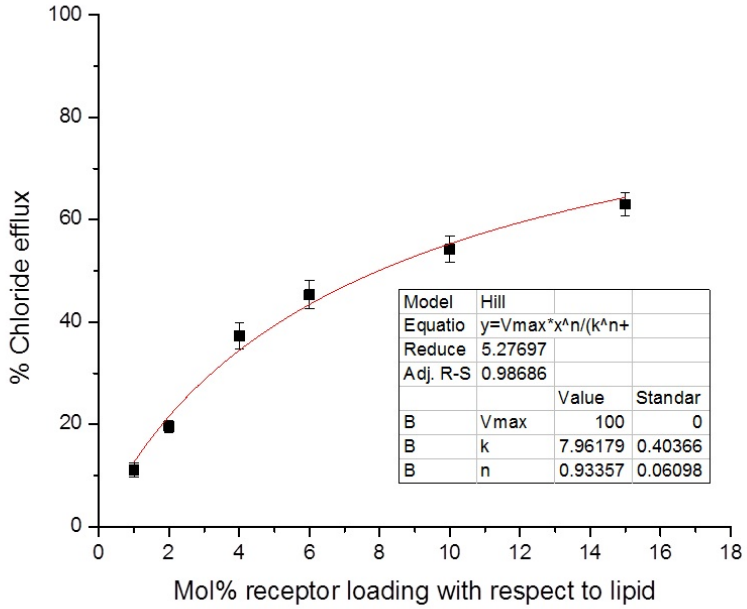

Figure 4.47 Hill plot of chloride efflux promoted varying concentrations of compound **L**[11] from unilamellar POPC vesicles loaded with 451mM NaCl buffered to pH 7.2 with 20mM sodium phosphate salts upon addition of a bicarbonate 'pulse', bringing the external concentration of bicarbonate to 40mM. The vesicles were dispersed in 150mM Na_2SO_4 buffered to pH 7.2 with 20mM sodium phosphate salts. Each point represents an average of 3 trials.

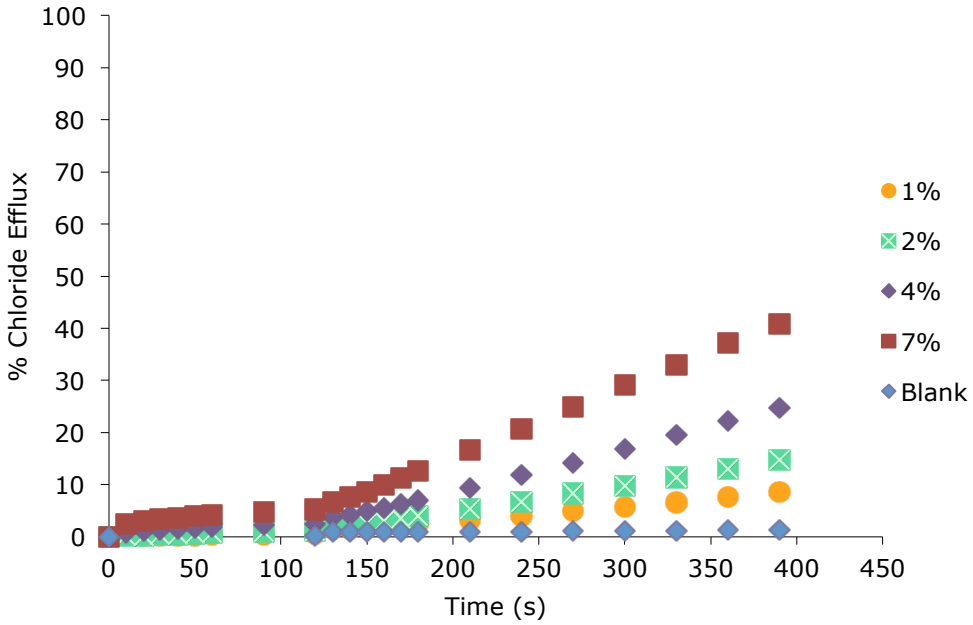

Figure 4.48 Chloride efflux promoted by various concentrations of **L**[12] from unilamellar POPC vesicles loaded with 451 mM NaCl buffered to pH 7.2 with 20 mM sodium phosphate salts. The vesicles were dispersed in 150 mM Na_2SO_4 buffered to pH 7.2 with 20 mM sodium phosphate salts. At t. 120 s a solution of sodium bicarbonate was added such that the external concentration of bicarbonate was 40 mM. At the end of the experiment, detergent was added to lyse the vesicles and calibrate the ISE to 100% chloride efflux. Each point represents an average of three trials. DMSO was used as a control.

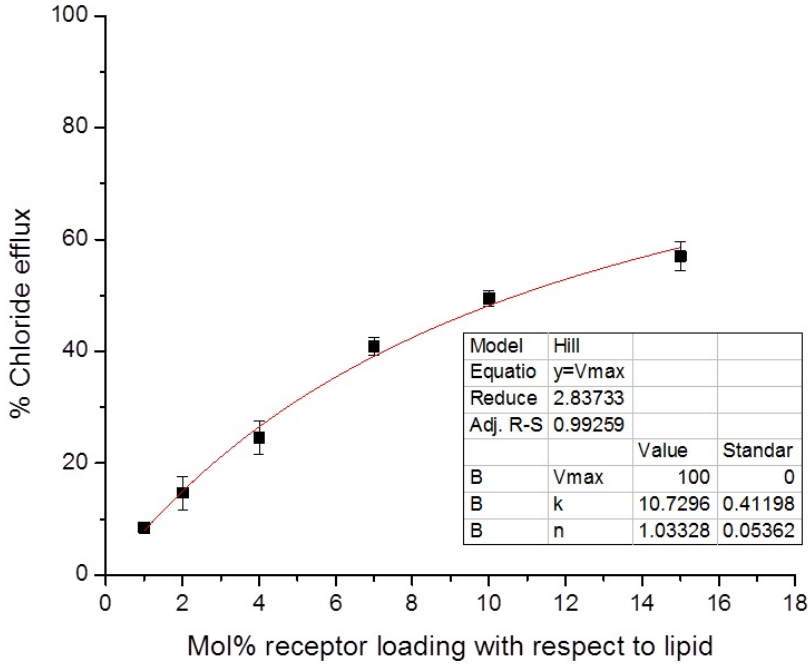

Figure 4.49 Hill plot of chloride efflux promoted varying concentrations of compound **L**[12] from unilamellar POPC vesicles loaded with 451mM NaCl buffered to pH 7.2 with 20mM sodium phosphate salts upon addition of a bicarbonate 'pulse', bringing the external concentration of bicarbonate to 40mM. The vesicles were dispersed in 150mM Na_2SO_4 buffered to pH 7.2 with 20mM sodium phosphate salts. Each point represents an average of 3 trials.

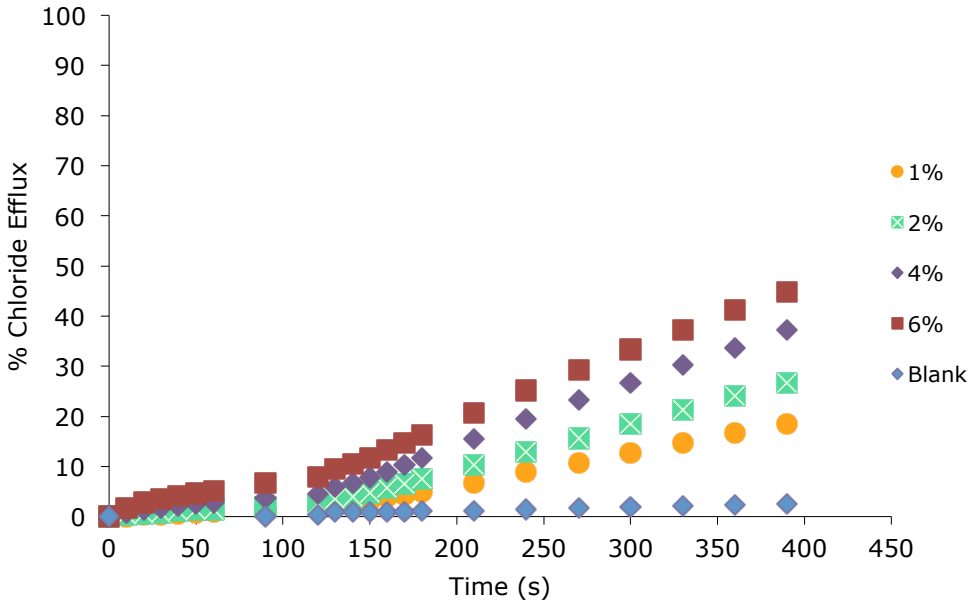

Figure 4.50 Chloride efflux promoted by various concentrations of **L**[13] from unilamellar POPC vesicles loaded with 451 mM NaCl buffered to pH 7.2 with 20 mM sodium phosphate salts. The vesicles were dispersed in 150 mM Na_2SO_4 buffered to pH 7.2 with 20 mM sodium phosphate salts. At t. 120 s a solution of sodium bicarbonate was added such that the external concentration of bicarbonate was 40 mM. At the end of the experiment, detergent was added to lyse the vesicles and calibrate the ISE to 100% chloride efflux. Each point represents an average of three trials. DMSO was used as a control.

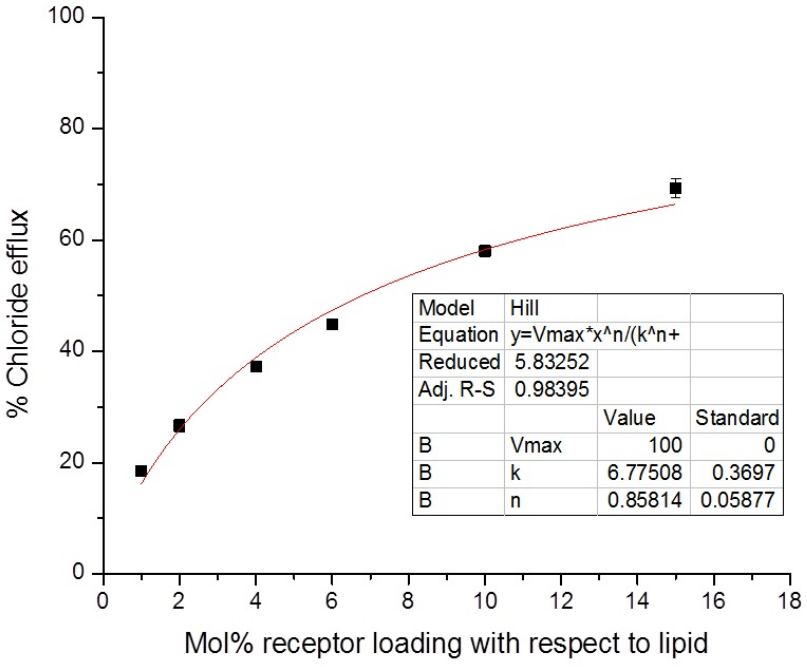

Figure 4.51 Hill plot of chloride efflux promoted varying concentrations of compound **L**[13] from unilamellar POPC vesicles loaded with 451mM NaCl buffered to pH 7.2 with 20mM sodium phosphate salts upon addition of a bicarbonate 'pulse', bringing the external concentration of bicarbonate to 40mM. The vesicles were dispersed in 150mM Na_2SO_4 buffered to pH 7.2 with 20mM sodium phosphate salts. Each point represents an average of 3 trials.

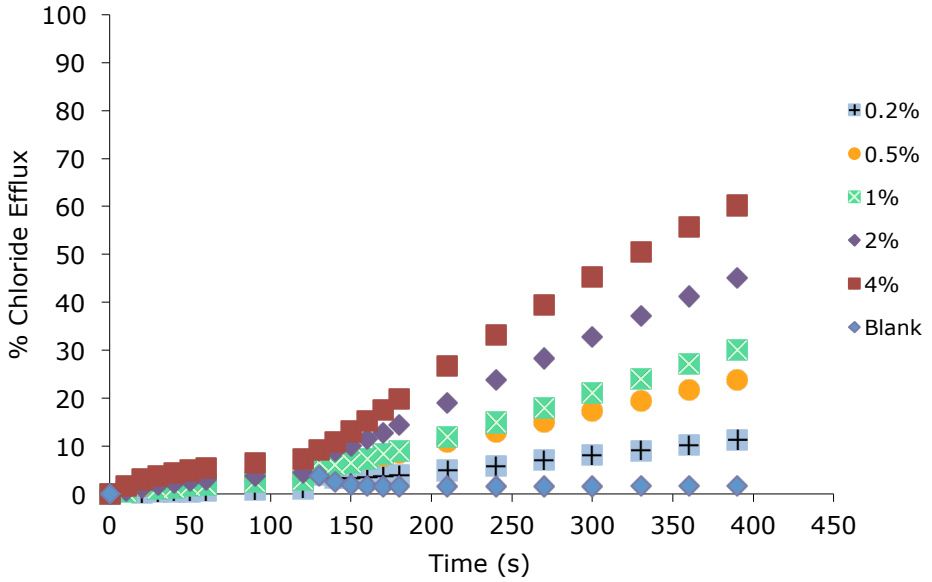

Figure 4.52 Chloride efflux promoted by various concentrations of **L**[14] (2 mol% carrier to lipid) from unilamellar POPC vesicles loaded with 451 mM NaCl buffered to pH 7.2 with 20 mM sodium phosphate salts. The vesicles were dispersed in 150 mM Na_2SO_4 buffered to pH 7.2 with 20 mM sodium phosphate salts. At t. 120 s a solution of sodium bicarbonate was added such that the external concentration of bicarbonate was 40 mM. At the end of the experiment, detergent was added to lyse the vesicles and calibrate the ISE to 100% chloride efflux. Each point represents an average of three trials. DMSO was used as a control.

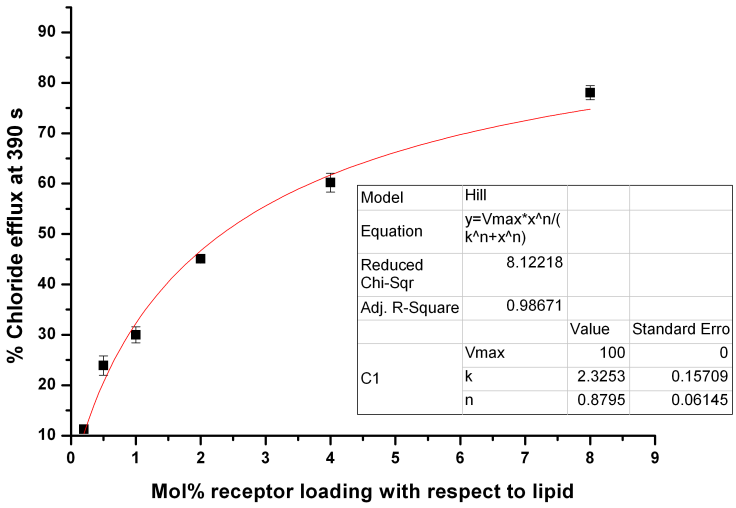

Figure 4.53 Hill plot of chloride efflux promoted varying concentrations of compound **L**[14] from unilamellar POPC vesicles loaded with 451mM NaCl buffered to pH 7.2 with 20mM sodium phosphate salts upon addition of a bicarbonate 'pulse', bringing the external concentration of bicarbonate to 40mM. The vesicles were dispersed in 150mM Na_2SO_4 buffered to pH 7.2 with 20mM sodium phosphate salts. Each point represents an average of 3 trials.

Cholesterol assays

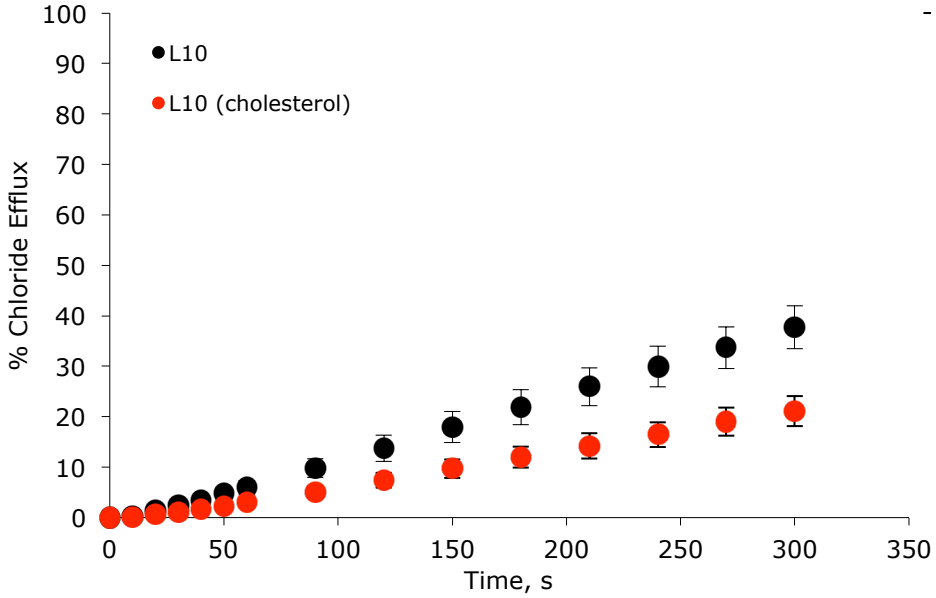

Figure 5.54 Chloride efflux promoted by a DMSO solution of compound **L**[10] (2mol% carrier to lipid) from unilamellar vesicles comprising of either POPC or POPC/cholesterol (7:3 molar ratio), loaded with 489 mM NaCl buffered to pH 7.2 with 5mM sodium phosphate salts. The vesicles were dispersed in 489mM $NaNO_3$ buffered to pH 7.2 with 5mM sodium phosphate salts. At the end of the experiment detergent was added to lyse the vesicles and calibrate the ISE to 100% chloride efflux. Each point represents an average of three trials. DMSO was used as a control.

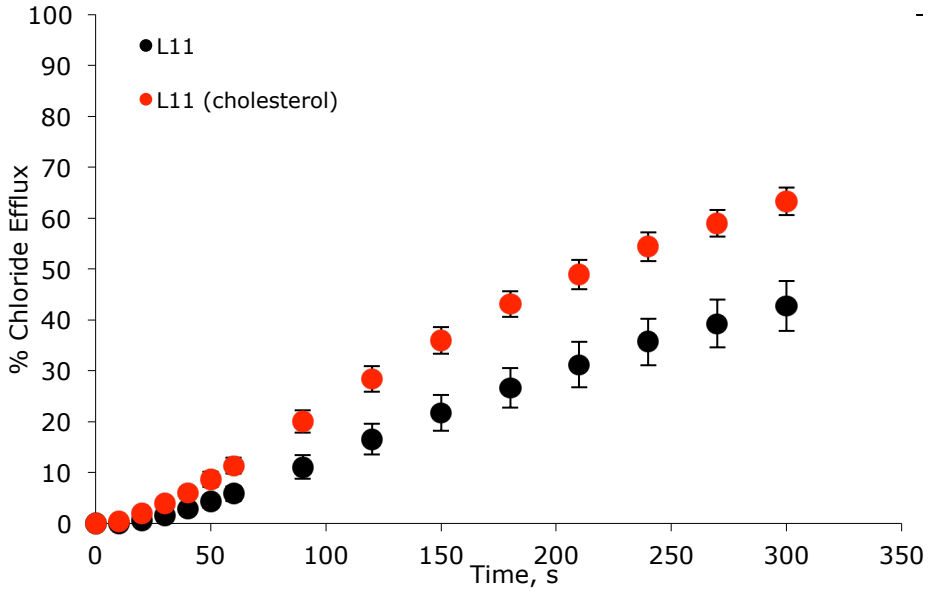

Figure 5.55 Chloride efflux promoted by a DMSO solution of compound **L**[11] (2mol% carrier to lipid) from unilamellar vesicles comprising of either POPC or POPC/cholesterol (7:3 molar ratio), loaded with 489 mM NaCl buffered to pH 7.2 with 5mM sodium phosphate salts. The vesicles were dispersed in 489mM $NaNO_3$ buffered to pH 7.2 with 5mM sodium phosphate salts. At the end of the experiment detergent was added to lyse the vesicles and calibrate the ISE to 100% chloride efflux. Each point represents an average of three trials. DMSO was used as a control.

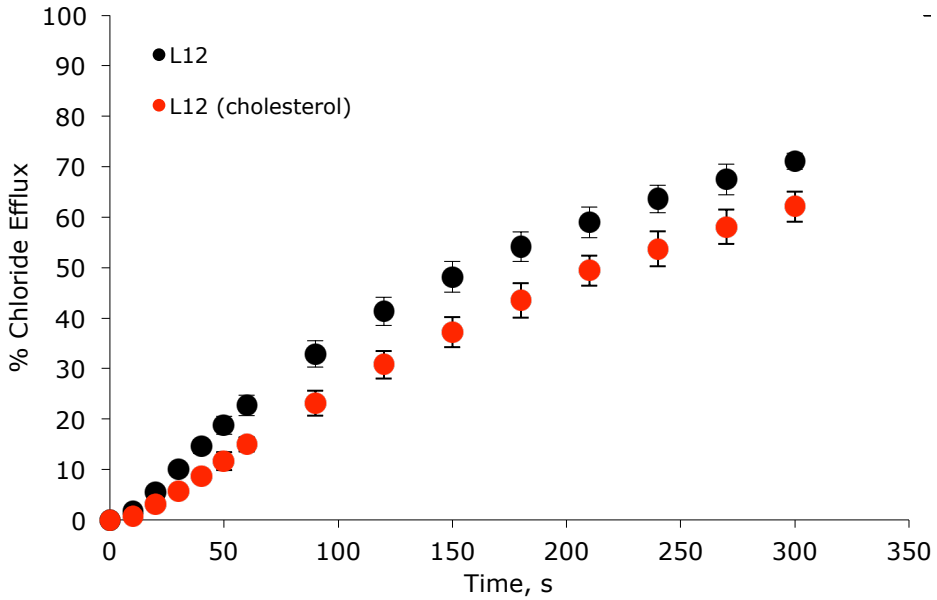

Figure 5.56 Chloride efflux promoted by a DMSO solution of compound **L**[12] (2mol% carrier to lipid) from unilamellar vesicles comprising of either POPC or POPC/cholesterol (7:3 molar ratio), loaded with 489mM NaCl buffered to pH 7.2 with 5mM sodium phosphate salts. The vesicles were dispersed in 489mM $NaNO_3$ buffered to pH 7.2 with 5mM sodium phosphate salts. At the end of the experiment detergent was added to lyse the vesicles and calibrate the ISE to 100% chloride efflux. Each point represents an average of three trials. DMSO was used as a control.

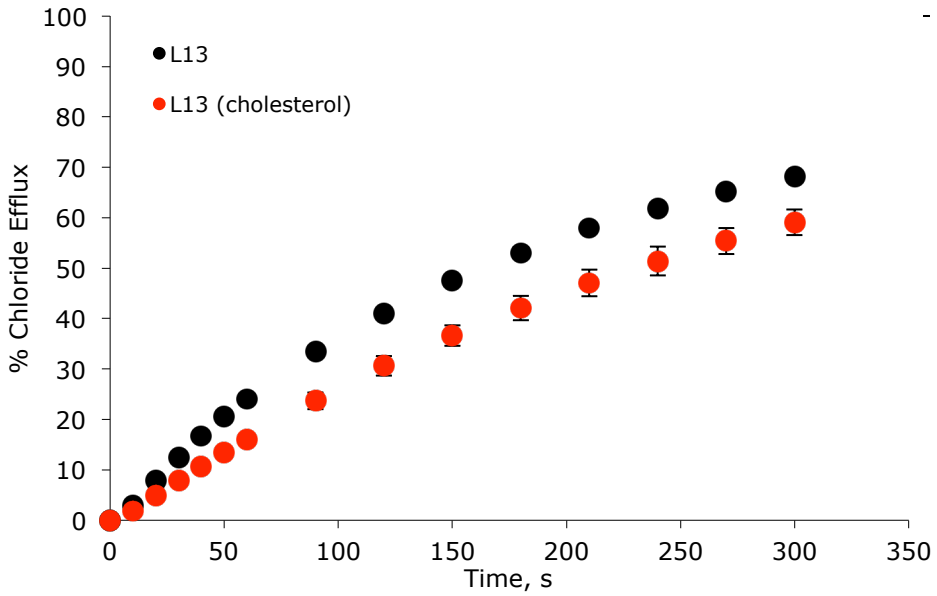

Figure 5.57 Chloride efflux promoted by a DMSO solution of compound **L**[13] (2mol% carrier to lipid) from unilamellar vesicles comprising of either POPC or POPC/cholesterol (7:3 molar ratio), loaded with 489mM NaCl buffered to pH 7.2 with 5mM sodium phosphate salts. The vesicles were dispersed in 489mM $NaNO_3$ buffered to pH 7.2 with 5mM sodium phosphate salts. At the end of the experiment detergent was added to lyse the vesicles and calibrate the ISE to 100% chloride efflux. Each point represents an average of three trials. DMSO was used as a control.

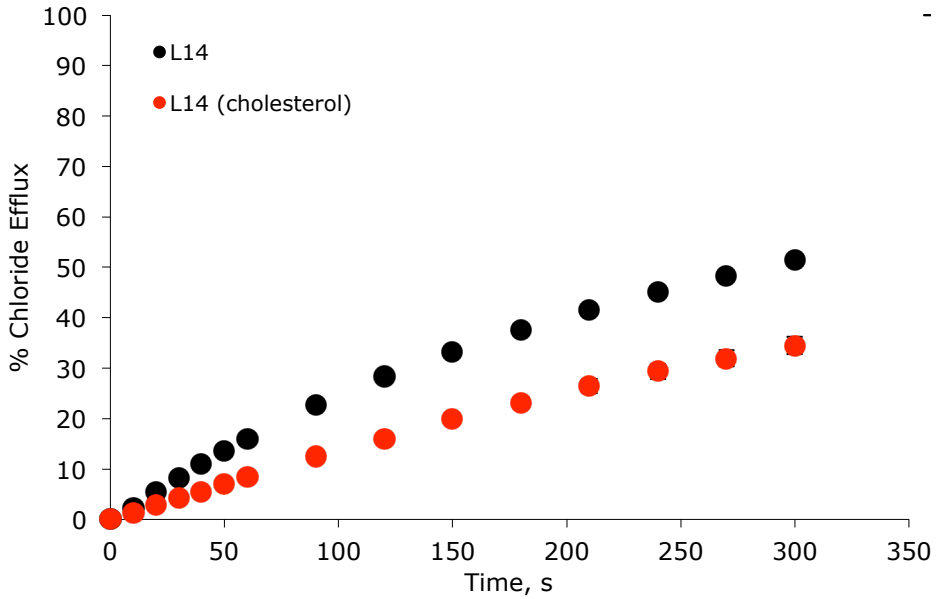

Figure 5.58. Chloride efflux promoted by a DMSO solution of compound **L**^{14} (0.2mol% carrier to lipid) from unilamellar vesicles comprising of either POPC or POPC/cholesterol (7:3 molar ratio), loaded with 489mM NaCl buffered to pH 7.2 with 5mM sodium phosphate salts. The vesicles were dispersed in 489mM $NaNO_3$ buffered to pH 7.2 with 5mM sodium phosphate salts. At the end of the experiment detergent was added to lyse the vesicles and calibrate the ISE to 100% chloride efflux. Each point represents an average of three trials. DMSO was used as a control.

References

1. Nishizawa, S., Bühlmann, P., Iwao, M. & Umezawa, Y. Anion recognition by urea and thiourea groups: Remarkably simple neutral receptors for dihydrogenphosphate. *Tetrahedron Lett.* **36,** 6483–6486 (1995).

2. Nishizawa, S., Bühlmann, P., Xiao, K. P. & Umezawa, Y. Application of a bis-thiourea ionophore for an anion selective electrode with a remarkable sulfate selectivity. *Anal. Chim. Acta* **358,** 35–44 (1998).

3. Emgenbroich, M. *et al.* A phosphotyrosine-imprinted polymer receptor for the recognition of tyrosine phosphorylated peptides. *Chemistry* **14,** 9516–29 (2008).

4. Caltagirone, C. *et al.* A new family of bis-ureidic receptors for pyrophosphate optical sensing. *Org. Biomol. Chem.* **11,** 2445–51 (2013).

5. Busschaert, N. & Gale, P. a. Small-molecule lipid-bilayer anion transporters for biological applications. *Angew. Chem. Int. Ed. Engl.* **52,** 1374–82 (2013).

6. Ashcroft, F. M. *Ion Channels and Disease: Channelopathies*. (2000).

7. Davis, J. T., Okunola, O. & Quesada, R. Recent advances in the transmembrane transport of anions. *Chem. Soc. Rev.* **39,** 3843–62 (2010).

8. Davis, A. P., Sheppard, D. N. & Smith, B. D. Development of synthetic membrane transporters for anions. *Chem. Soc. Rev.* **36,** 348–57 (2007).

9. Matile, S., Vargas Jentzsch, A., Montenegro, J. & Fin, A. Recent synthetic transport systems. *Chem. Soc. Rev.* **40,** 2453–74 (2011).

10. Haynes, C. J. E. & Gale, P. A. Transmembrane anion transport by synthetic systems. *Chem. Commun. (Camb).* **47,** 8203–9 (2011).

11. Hynes, M. J. EQNMR: a computer program for the calculation of stability constants from nuclear magnetic resonance chemical shift data. *J. Chem. Soc. Dalt. Trans.* 311 (1993). doi:10.1039/dt9930000311

12. Smith, B. D. & Lambert, T. N. Molecular ferries: membrane carriers that promote phospholipid flip-flop and chloride transport. *Chem. Commun.* 2261 (2003). doi:10.1039/b303359g

13. Koulov, A. V *et al.* Chloride transport across vesicle and cell membranes by steroid-based receptors. *Angew. Chem. Int. Ed. Engl.* **42,** 4931–3 (2003).

14. Cleland, W. W., Andrews, T. J., Gutteridge, S., Hartman, F. C. & Lorimer, G. H. Mechanism of Rubisco: The Carbamate as General Base. *Chem. Rev.* **98,** 549–562 (1998).

15. Cordat, E. & Casey, J. R. Bicarbonate transport in cell physiology and disease. *Biochem. J.* **417,** 423–39 (2009).

16. Marcus, Y. Thermodynamics of solvation of ions. Part 5.?Gibbs free energy of hydration at 298.15 K. *J. Chem. Soc. Faraday Trans.* **87,** 2995 (1991).

17. Hill, A. V. The Combinations of Haemoglobin with Oxygen and with Carbon Monoxide. I. *Biochem. J.* **7,** 471 (1913).

18. Bhosale, S. & Matile, S. A Simple Method to Identify Supramolecules in Action: Hill Coefficients for Exergonic Self-Assembly. *Chirality* **18,** 849–856 (2006).

19. Kirby, C., Clarke, J. & Gregoriadis, G. Effect of the cholesterol content of small unilamellar liposomes on their stability in vivo and in vitro. *Biochem. J.* **186,** 591–8 (1980).

20. Murillo, O. *et al.* Synthetic Transmembrane Channels: Functional Characterization Using Solubility Calculations, Transport Studies, and Substituent Effects. *J. Am. Chem. Soc.* **119,** 5540–5549 (1997).

21. Nolan, C. & Gunnlaugsson, T. Improved synthesis of a C3-symmetrical pyridinophane. *Tetrahedron Lett.* **49,** 1993–1996 (2008).

Chapter 5: Trisureas as transmembrane transporters for chloride and bicarbonate

Chapter 5: Trisureas as transmembrane transporters for chloride and bicarbonate

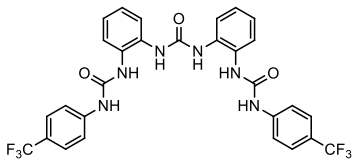

L[15]

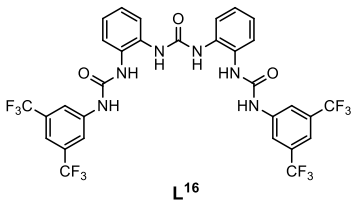

L[16]

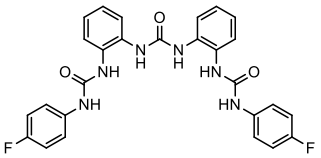

L[17]

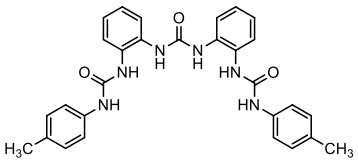

L[18]

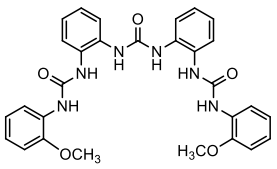

L[19]

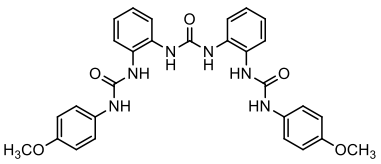

L[20]

5.1 Introduction

Transmembrane transport of anions across lipid bilayers is an important biological process that is normally regulated by complex membrane spanning proteins (ion channels). A range of diseases, known as "channelopathies", including the most commonly cystic fibrosis, are caused by malfunctioning ion channels.[1] There is currently strong interest in the design of synthetic membrane transporters for anion that can act as potential future therapeutic substitutes for these malfunctioning proteins.[2,3,4,5]

Gale and co worker have recently reported a series of ortho-phenylenediamine-based bis-ureas **140**-**147**.[6] These compound are highly effective anion transporters that function by an anion antiport and in some case a HCl symport with a carrier mechanism. Addition of electron withdrawing groups to either the central core or the peripheral phenyl groups yielded potent anion transporters. Transporter activity was observed to increase with increasing electron withdrawing strength of the substituent with the trend H < F ≈ Cl< CF_3 < CN < NO_2. Indeed, para-nitro functionalised compound **145** displays very high transport activity, facilitating chloride efflux at concentrations as low as 1:1000000 transporter to lipid molar ratio.

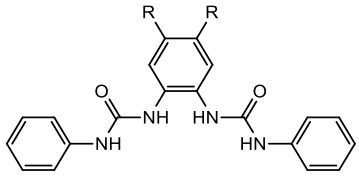

140 R = H
141 R = F
142 R = Cl

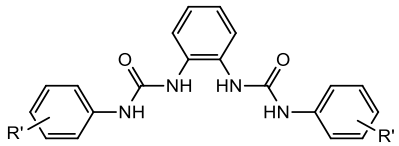

143 R' = *p*-CN
144 R' = *p*-CF_3
145 R' = *p*-NO_2
146 R' = *m*-NO_2
147 R' = *o*-NO_2

Molecules developed from this scaffold have found extensive use in the field of anion complexation. The same group have previously reported that ortho-phenylenediamine-based bisureas function as selective carboxylate complexation agents (see Introduction *section 1.3.2*),[7,8] whilst the analogous 4,5-dimethyl-1,2-phenylenediamine scaffold has been used to construct colorimetric anion sensors.[9] These motifs can be extended with additional hydrogen bond donor groups to yield receptors with enhanced anion affinity. In 2010 Wu and his group have studied the sulfate binding properties of a tris- and tetra-ureas **148**-**151**.[10] Binding studies were investigated by proton NMR titration in DMSO-d_6/0.5% water. Both trisureas and tetraureas showed high affinity for sulfate in a 1:1 stoichiometry, stronger in the case of trisureas due to their fully complementary conformation with sulfate. However, increasing the amounts of water to 25% (v/v) **148** and **149** showed a decreased binding properties, while receptor **150** is more water-tolerant and in DMSO-d_6/25% water its chelate effect and hydrophobic effect exceeded its inferiority in conformational complementarity, which results in the stronger binding with sulfate.

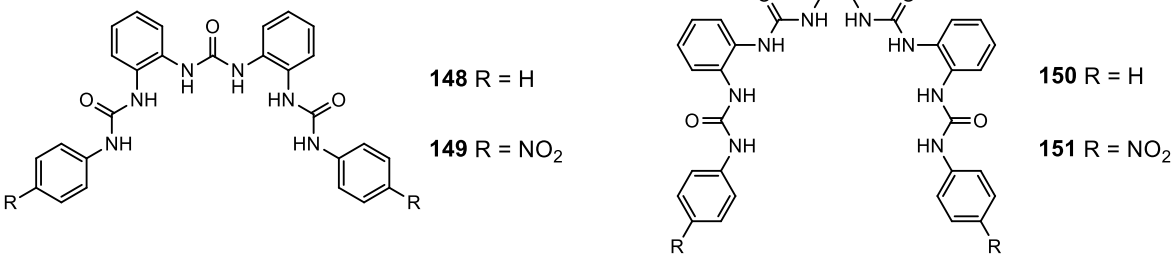

Inspired by the high transport activity exhibited by the ortho-phenylenediamine-based bis-ureas, a series of new trisureas **L**^{15}-**L**^{20} were synthesised and their transmembrane transport properties were investigated. The anion binding properties of this series of compounds were determined using ^{1}H-NMR titration techniques in DMSO-d$_6$/0.5% H_2O mixtures. Anion transport was studied using a combination of ion selective electrode assays and fluorescence techniques in phospholipid vesicles.

5.2 Synthesis

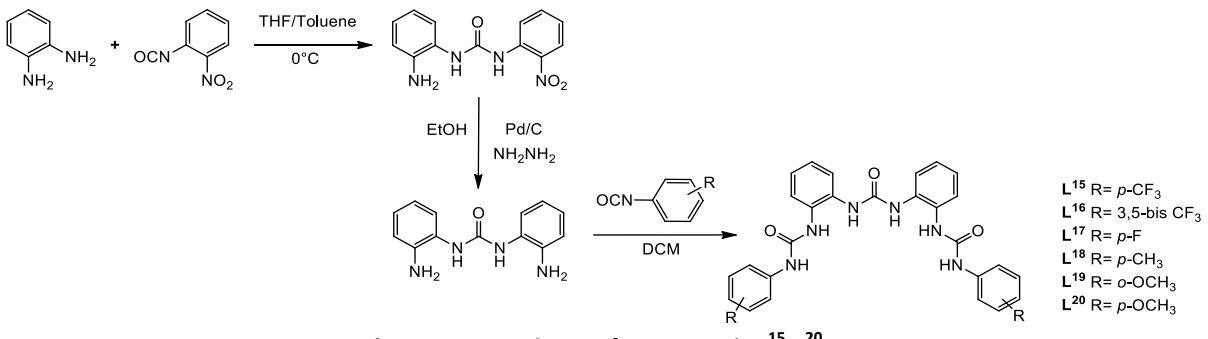

Scheme 5.1. Synthesis of compounds **L**^{15}-**L**^{20}.

The compounds **L^{15}-L^{20}** were synthesized as shown on *Scheme 5.1*. Firstly 1,3-Bis(2 aminophenyl)urea was prepared by reaction of *o*-phenylenediamine with o-nitro-phenylisocyanate in a mixed solvent THF/Toluene at 0°C and subsequent reduction of the 1-(2-nitrophenyl)-3-(2-amino phenyl)urea obtained by hydrazine hydrate/palladium on carbon. 1,3-Bis(2 aminophenyl)urea was reacted with the appropriate isocyanate (4-(Trifluoromethyl)phenyl isocyanate; 3,5-Bis(Trifluoromethyl)phenyl isocyanate; 4-Fluorophenyl isocyanate; p-Tolyl isocyanate; 2-Methoxyphenyl isocyanate; 4-Methoxyphenyl isocyanate) in refluxing DCM under N_2 atmosphere to obtain **L^{15}-L^{20}** in 60-90% yield.

5.3 Anion binding in solution

The ability of compounds **L^{15}-L^{20}** to bind anions in solution was investigated using ^{1}H-NMR titration techniques in DMSO-d_6/0.5% water (with the anions added as tetrabutylammonium (TBA) or tetraethylammonium (TEA) salts). The binding studies were performed for anions relevant in biological systems and in transmembrane transport assays. Where possible the change in chemical shift of the most downfield NH signal was fitted to a 1:1 binding model using WinEQNMR software.[11] As shown in *Table 5.1* no significant interactions were observed between **L^{15}-L^{20}** and the anions taken into account.

Table 5.1 Stability constants K_a (M^{-1}) for compounds **L^{15}-L^{20}** with the tetrabutylammonium or tetraethylammonium salts of the anion considered in DMSO-d_6/0.5% water at 300 K. All errors estimated to be <10%

compounds	Cl^-	HCO_3^-	NO_3^-
L^{15}	261	deprot	no interaction
L^{16}	226	deprot	no interaction
L^{17}	205	203	no interaction
L^{18}	226	220	no interaction
L^{19}	28	802	no interaction
L^{20}	225	239	no interaction

5.4 Transport studies

5.4.1 Chloride/nitrate transport studies

Initially, the Cl^-/NO_3^- antiport activity of **L^{15}-L^{20}** was investigated. A solution of each receptor in DMSO was added to a suspension of unilamellar POPC vesicles containing NaCl (489 mM NaCl buffered to pH 7.2 with 5 mM sodium phosphate salts) suspended in $NaNO_3$ (489 mM NaCl buffered to pH 7.2 with 5 mM sodium phosphate salts) and the resulting chloride efflux from vesicles was monitored using a chloride selective electrode

(Full details of vesicle preparation and transport experiments may be found in the Appendix). The results are shown in *Figure 5.1*.

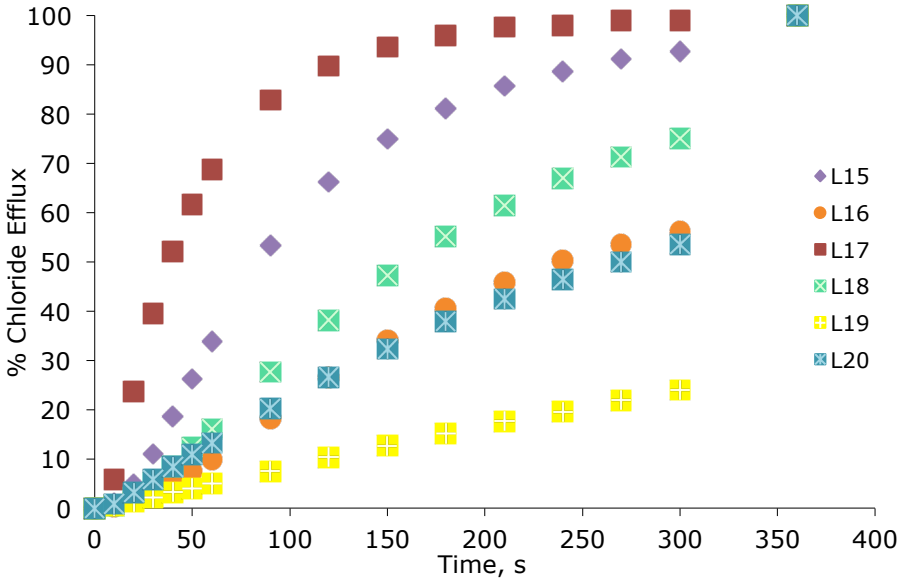

Figure 5.1 Chloride efflux promoted by a DMSO solution of compounds 1–6 (2 mol% carrier to lipid) from unilamellar POPC vesicles loaded with 489 mM NaCl buffered to pH 7.2 with 5 mM sodium phosphate salts. The vesicles were dispersed in 489 mM $NaNO_3$ buffered to pH 7.2 with 5 mM sodium phosphate salts. At the end of the experiment detergent was added to lyse the vesicles and calibrate the ISE to 100% chloride efflux. Each point represents an average of three trials. DMSO was used as a control.

The data in *Figure 5.1* indicates that the maximum activity under these conditions was observed for compound $\mathbf{L^{17}}$. However at lower carrier concentrations it becomes apparent that receptors $\mathbf{L^{15}}$ is more potent. For example, the chloride efflux mediated by each receptor at a concentration of 0.2 mol% (with respect to the lipid) is shown in *Figure 5.2*.

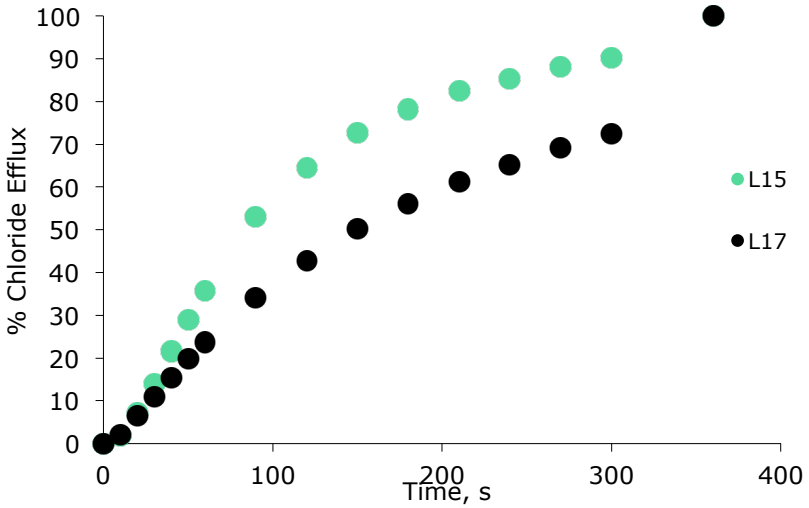

Figure 5.2 Chloride efflux mediate by compounds $\mathbf{L^{15}}$ and $\mathbf{L^{17}}$ (0.2 mol% carrier to lipid) from unilamellar POPC vesicles loaded with 489 mM NaCl buffered to pH 7.2 with 5 mM sodium phosphate salts. The vesicles were dispersed in 489 mM $NaNO_3$ buffered to pH 7.2 with 5 mM sodium phosphate salts. At the end of the experiment, the vesicles were lysed to calibrate the ISE to 100% chloride efflux. Each point represents an average of three trials.

This result clearly indicates that receptor **L**^{15} is a more efficient carrier at lower concentrations than **L**^{17}. This highlights that testing at a single concentration is not sufficient to fully examine the relative efficiencies of the carriers.

The full Hill analysis of Cl^-/NO_3^- antiport activity for receptor **L**^{15} was investigated. The results are shown in *Figure 5.3*. It was found that this compound is the most active transporter of the series, as confirmed by the EC_{50} value (*Table 5.2*). The corresponding graphs for **L**^{16}-**L**^{20} may be found in *section 5.6.3*.

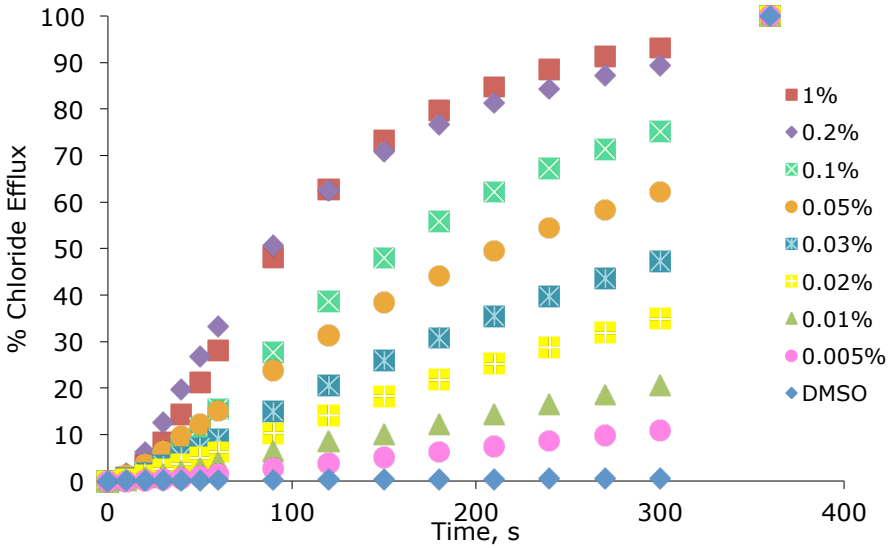

Figure 5.3 Chloride efflux promoted by a various concentration of compounds **L**^{15} from unilamellar POPC vesicles loaded with 489 mM NaCl buffered to pH 7.2 with 5 mM sodium phosphate salts. The vesicles were dispersed in 489 mM $NaNO_3$ buffered to pH 7.2 with 5 mM sodium phosphate salts. At the end of the experiment detergent was added to lyse the vesicles and calibrate the ISE to 100% chloride efflux. Each point represents an average of three trials. DMSO was used as a control.

Transport of ions by simple synthetic molecules usually only occurs via passive transport mechanisms in which the charge balance across the membrane is maintained. This can be achieved by either a symport mechanism, where both an anion and a cation are transported, or by an antiport mechanism, where two anions are transported across the membrane in opposite directions.[12,5,4] Therefore, the chloride efflux shown in *Figure 5.1* could be the result of Na^+/Cl^- or H^+/Cl^- symport or Cl^-/NO_3^- antiport. In order to understand the mechanism of transport a further assays were performed.

5.4.2 Chloride/bicarbonate transport studies

The ability of compound to function as Cl^-/HCO_3^- antiporters was also investigated, because this is a more biologically relevant process,[13,14] that has been linked to a number of pathologies.[15,16,17,18] The transport assays were repeated suspending POPC vesicle loaded with NaCl (451 mM with 20 mM phosphate buffer at pH 7.2) in a solution of Na_2SO_4 (150 mM with 20mM phosphate buffer at pH 7.2). Compounds **L**^{15}-**L**^{20} were added as solutions in DMSO. After 120s a solution of NaHCO3 was added (such that the external concentration of bicarbonate was 40 mM). The external sulfate, as explain in the previous chapter, is more challenging to transport through a lipid bilayer due to its higher hydrophilicity. Consequently, chloride efflux observed in the first two minutes of the assay (before the bicarbonate 'pulse') is not expected to be the result of an anion antiport mechanism. Upon addition of the 'bicarbonate pulse' a chloride/bicarbonate antiport mechanism becomes possible and an increase in transport activity was observed for compounds **L**^{15}-**L**^{20} at this point (*Figure 5.4*) in according with an antiport mechanism.

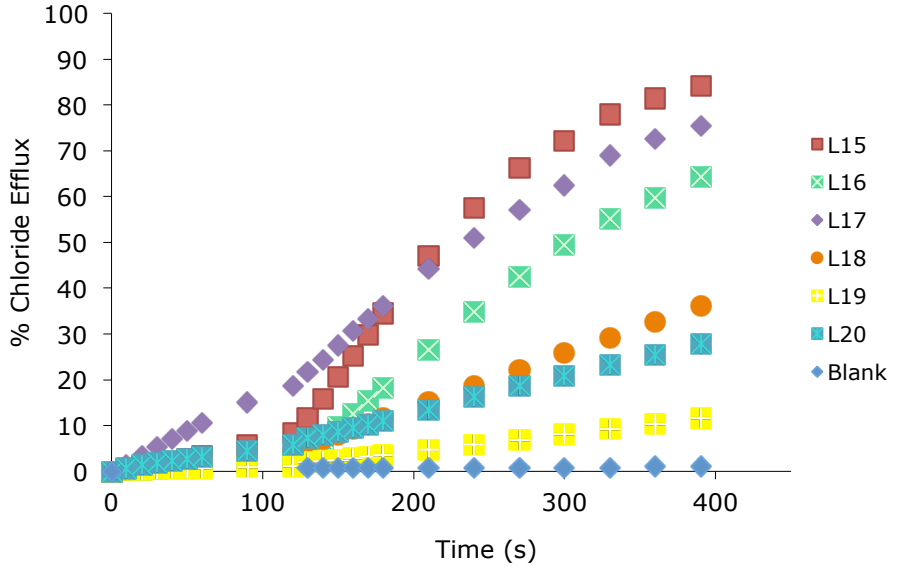

Figure 5.4 Chloride efflux promoted by a DMSO solution of compounds 1–6 (2 mol% carrier to lipid) from unilamellar POPC vesicles loaded with 451 mM NaCl buffered to pH 7.2 with 20 mM sodium phosphate salts. The vesicles were dispersed in 150 mM Na_2SO_4 buffered to pH 7.2 with 20 mM sodium phosphate salts. At t ¼ 120 s a solution of sodium bicarbonate was added such that the external concentration of bicarbonate was 40 mM. At the end of the experiment, detergent was added to lyse the vesicles and calibrate the ISE to 100% chloride efflux. Each point represents an average of three trials. DMSO was used as a control.

Again, receptor **L**^{15} is also the most active carrier for Cl^-/HCO_3^- antiport. In *Figure 5.5* is shown the Cl^-/HCO_3^- antiport promoted by different concentrations of compound **L**^{15}. The corresponding graphs for **L**^{16}-**L**^{20} may be found in *section 5.6.3*.

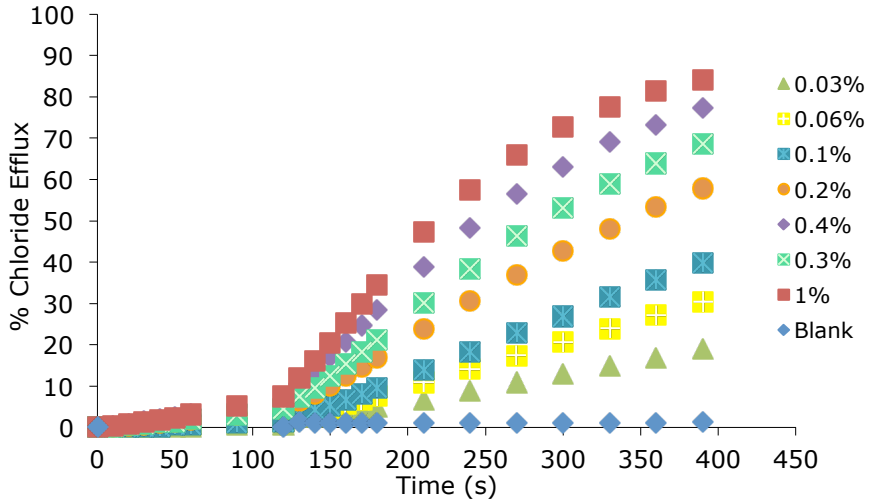

Figure 5.5 Chloride efflux promoted by various concentrations of **L**^{15} from unilamellar POPC vesicles loaded with 451 mM NaCl buffered to pH 7.2 with 20 mM sodium phosphate salts. The vesicles were dispersed in 150 mM Na_2SO_4 buffered to pH 7.2 with 20 mM sodium phosphate salts. At t. 120 s a solution of $NaHCO_3$ was added such that the external concentration of HCO_3^- was 40 mM. At the end of the experiment, the vesicles were lysed and calibrate the ISE to 100% chloride efflux. Each point represents an average of three trials. DMSO was used as a control.

To quantify the transport abilities of **L**^{15}-**L**^{20} a series of Hill analysis for the chloride efflux in both the nitrate and bicarbonate antiport tests was performed. In *Table 5.2* are reported the $EC_{50,270s}$ values (defined as the concentration of transporter required to achieve 50% chloride release 270 s after the addition of carrier or after the addition of bicarbonate) and the Hill coefficient (the number of transporter molecules required to transport a single ion). The low EC50 values of compound **L**^{15} confirmed that it is the most efficient in both experiments, in facts is able to mediate the Cl^-/NO_3^- antiport at a loading of 0.039 mol% (carrier to lipid) and the Cl^-/HCO_3^- antiport at a loading of 0.14 mol% (carrier to lipid).

The Hill coefficient indicates that each anion is transported by a single receptor, this suggests that all compounds function as a mobile carrier.

Table 5.2 The EC_{50} for the Cl^-/NO_3^- and Cl^-/HCO_3^- antiport by compounds **L**^{15}-**L**^{20} and the Hill coefficient (n) calculated by the Hill analysis.

compounds	EC_{50} at 270s (Cl^-/NO_3^-)	n	EC_{50} at 270s (Cl^-/HCO_3^-)	n
L^{15}	0.039	1.07	0.14	0.98
L^{16}	0.066	0.88	0.25	0.97
L^{17}	0.10	1.39	0.76	0.80
L^{18}	0.6	0.96	4.27	0.88
L^{19}	4.98	1.29	21.93	0.86
L^{20}	1.96	0.88	8.43	0.84

5.4.3 Mechanism of transport

Low levels of chloride efflux were observed for some of the compounds in the two minutes before the bicarbonate pulse in the Cl^-/HCO_3^- assay.

To examine the possibility of sodium/chloride co-transport, the Cl^-/NO_3^- transport assays were repeated using vesicles containing caesium chloride (489 mM NaCl buffered to pH 7.2 with 5 mM sodium phosphate salts) instead of sodium chloride, suspended in an isotonic sodium nitrate solution. In the event of NaCl co-transport we would expect the rate of chloride release to be lower in the presence of CsCl. As shown in *Figure 5.6* the release of chloride is dependent on the nature of metal cation and it is reduced when the internal solution was replaced by CsCl, implying that these molecules can facilitate NaCl symport in addition to Cl^-/NO_3^- or HCO_3^- antiport (see *section 5.6.3* for comparative plots).

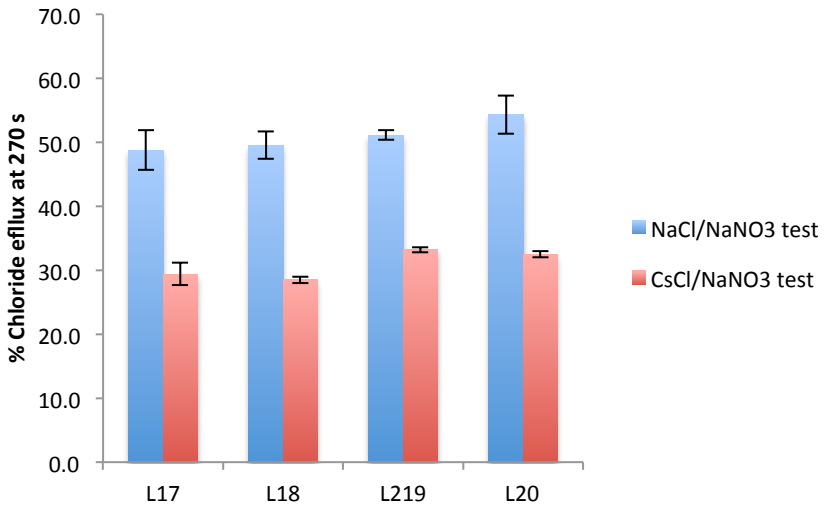

Figure 5.6 Chloride efflux promoted by a DMSO solution of compounds $\mathbf{L^{17}}$-$\mathbf{L^{20}}$ from unilamellar POPC vesicles loaded with either 489mM NaCl (red) or 489mM CsCl (blue) buffered to pH 7.2 with 5mM sodium phosphate salts. The vesicles were dispersed in 489mM $NaNO_3$ buffered to pH 7.2 with 5mM sodium phosphate salts. At the end of the experiment detergent was added to lyse the vesicles and calibrate the ISE to 100% chloride efflux. Each point represents an average of three trials. DMSO was used as a control.

Furthermore, a series of fluorescence assays were performed to test the possibility of HCl symport or Cl^-/SO_4^{2-} antiport. To investigate the transport of sulfate, unilamellar POPC vesicles were prepared containing 100 mM NaCl and 2 mM buffered to pH 7.2 with 20 mM phosphate salts that were suspended in an isotonic solution of NaCl. Lucigenin was used to monitor the internal chloride concentration, since the fluorescence of this dye is quenched by halide ions.[19] A solution of sodium sulfate was added such that the external concentration of sulfate was 40 mM, and after one minute compounds $\mathbf{L^{15}}$-$\mathbf{L^{20}}$ were added as solutions in methanol (2 mol% carrier to lipid). No evidence of sulfate transport was observed using this assay.

To investigate the HCl transport, we prepared POPC vesicles loaded with NaCl (489 mM) and 1 mM of the pH-sensitive dye 8-hydroxy-1,3,6-pyrenetrisulfonate (HPTS).[20,21] The vesicles were suspended in a Na_2SO_4 solution and upon addition of the carriers the fluorescence was measured. At the end of the experiment the vesicles were lysed with

detergent. No change in intravesicular pH was observed, implying that these compounds are not able to facilitate HCl transport.
Therefore, the chloride efflux observed in the first 120s in the bicarbonate test is attributed to a NaCl co-transport.

5.4.4 Mobility assays

The transport mechanism of these systems was probed repeating the ion selective electrode (ISE) assays with POPC vesicles containing 30% cholesterol. The vesicles were prepared containing sodium chloride (489 mM with 5 mM phosphate buffer at pH 7.2) and suspended in a solution of sodium nitrate (489 mM with 5 mM phosphate buffer at pH 7.2). By comparing the chloride efflux observed in this assay with that observed in the absence of cholesterol we can deduce if these molecules are mobile carriers. Cholesterol decreases membrane fluidity and thus transport that relies on a diffusion mechanism (i.e. mobile carrier), is expected to be slower in the presence of cholesterol.[22] Compounds **L**^{15}-**L**^{20} all showed reduced chloride efflux in the cholesterol containing vesicles except **L**^{16}. The cholesterol analysis for compound **L**^{15} is shown below as an example of this procedure, all other graphs may be found in *section 5.6.3*.

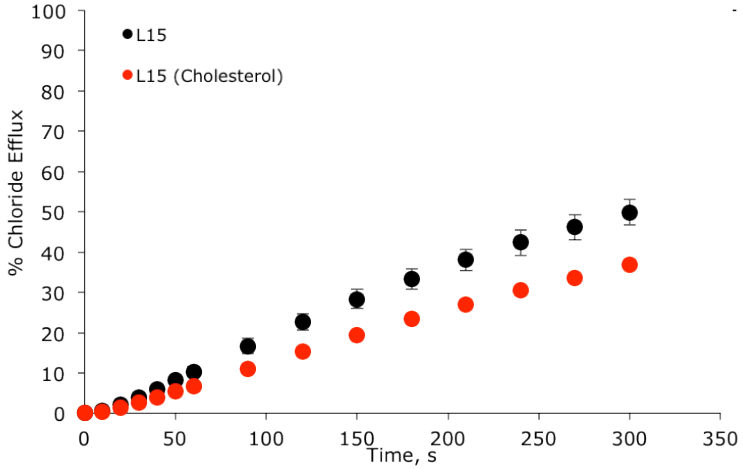

Figure 5.7. Chloride efflux promoted by a DMSO solution of compound **L**^{15} (0.03 mol% carrier to lipid) from unilamellar vesicles comprising of either POPC or POPC/cholesterol (7:3 molar ratio), loaded with 489mM NaCl buffered to pH 7.2 with 5mM sodium phosphate salts. The vesicles were dispersed in 489mM $NaNO_3$ buffered to pH 7.2 with 5mM sodium phosphate salts. At the end of the experiment detergent was added to lyse the vesicles and calibrate the ISE to 100% chloride efflux. Each point represents an average of three trials. DMSO was used as a control.

To prove the carrier mechanism of compound **L**^{16} a U-tube experiment was performed. A membrane is modelled by two aqueous phases separated by a nitrobenzene organic phase. The source phase was loaded with sodium chloride (489 mM buffered to pH 7.2 with 5 mM sodium phosphate salts) and the receiving phase was loaded with sodium nitrate (489 mM buffered to pH 7.2 with 5 mM sodium phosphate salts). The carrier (1 mM) was dissolved in the nitrobenzene phase and chloride transport into the receiving phase was monitored using an ion selective electrode. The separation of the two aqueous

phases rules out the possibility of channel formation.[23] No change in chloride concentration was observed in the absence of carrier, but an increase in chloride concentration could be detected when carrier was present, indicating that these compounds can act as mobile carriers.

5.5 Conclusion

The work in this chapter demonstrates that these simple tris-urea receptors show high transmembrane transport activity. A series of vesicle studies using ion-selective electrodes and fluorescent dyes indicate that compounds **L^{15}-L^{20}** function as mobile carriers that can mediate the transport of anions predominantly *via* an anion exchange mechanism, including chloride/nitrate and chloride/bicarbonate and a small amount of NaCl symport can also occur. The tris-urea **L^{15}** was found to be a remarkably potent anion carrier at low concentration ($EC_{50,270}$ 0.039 mol% and 0.14 mol% with respect to lipid for nitrate and bicarbonate antiport respectively). The development of anion carriers which function at low concentrations is an important target because the purpose of this research is to produce carriers with potential application as drugs for the treatment of various diseases, such as cystic fibrosis. High potency is a desirable requirement in the synthesis of new pharmaceuticals as it allows the administration of lower concentrations and potentially reduces the risk of other harmful side effects.

5.6 Experimental

All reactions were performed in oven-dried glassware under a slight positive pressure of nitrogen. ^{1}H-NMR (400 MHz, 500MHz) and ^{13}C NMR (100 MHz, 125MHz) spectra were determined on a Varian INOVA-400 spectrometer, and Varian INOVA-500 spectrometer. Chemical shifts for ^{1}H-NMR are reported in parts per million (ppm), calibrated to the residual solvent peak set, with coupling constants reported in Hertz (Hz). The following abbreviations are used for spin multiplicity: s = singlet, d = doublet, t = triplet, m = multiplet. Chemical shifts for ^{13}C NMR are reported in ppm, relative to the central line of a septet at δ = 39.52 ppm for deuterio-dimethylsulfoxide. Infrared (IR) spectra were recorded on a NICOLET 5700 FT-IR spectrophotometer and reported in wavenumbers (cm^{-1}). Microanalytical data were obtained using a Fisons EA CHNS-O instrument (*T* = 1000 °C). Fluorescence spectra were recorded on a Cary Eclypse spectrofluorimeter. All solvents and starting materials were purchased from commercial sources where available. Proton NMR titrations were performed by adding aliquots of the putative anionic guest (as the TBA salt, 0.075 M) in a solution of the receptor (0.005M) in DMSO-d_6/0.5% water to a solution of the receptor (0.005M).

5.6.1 Synthetic procedure

Synthesis of 1,3bis(2(3(4(trifluoromethyl)phenyl)ureido)phenyl)urea L[15]

A solution of p-trifluorophenyl isocyanate (0.534 mmol, 0.1 g) and amine (0.267 mmol, 0.078g) in 30 ml of DCM was refluxed under N_2 atmosphere for 6h. The precipitate obtained was filtered off and dried under vacuum to give a white solid.

Yield 91% (0.150 g, 0.243 mmol); M.p. >250°C; ^{1}H-NMR (400 MHz, DMSO-d_6, 298 K): δ_{CH} 7.06-7.17 (m, 4H), 7.52-7.7 (m, 12H), 8.19 (s, NH, 2H), 8.47 (s, NH, 2H), 9.54 (s, 2H, NH). ^{13}C-NMR (100 MHz, DMSO-d_6, 298 K) δ_C 117.80, 121.50, 121.82, 124.23, 124.30, 124.37, 126.03, 131.12, 131.30, 143.61; δ_{CO} 152.95, 154.15. LRMS (ES^-) m/z: 615.0154 $[M\text{-}H^+]^-$.

Synthesis of 1,3-bis(2-(3-(3,5-bis(trifluoromethyl)phenyl)ureido)phenyl) urea L[16]

To a solution of 3,5-Bis(trifluoromethyl)phenyl isocyanate (1.44 mmol; 0.367 g) in 10 ml of DCM was added a suspension of amine (0.413 mmol; 0.1 g) in 20 ml of DCM. The mixture of reaction was left stirring at reflux under N_2 atmosphere overnight. The precipitate formed was collect by filtration washed with DCM and with hot MeOH and than dried over vacuum to give a white solid.

Yield 81% (0.332 mmol; 0.25 g); M.p. >250°C; ^{1}H-NMR (400 MHz, DMSO-d_6, 298 K): δ_{ArH} 7.12 (4H), 7.52 (d, 2H), 7.56 (s, 2H), 7.60 (d, 2H), 8.06 (s, 4H), 8.35 (s, 2H,NH), 8.49 (s, 2H,NH), 9.84 (s, 2H,NH). ^{13}C-NMR (100 MHz, DMSO-d_6, 298 K) δ_C 114.11, 117.57, 121.90, 124.42, 124.48, 124.54, 124.61, 130.14, 130.47, 130.79, 131.12, 131.31, 142.01; δ_{CO} 152.99, 154.35. LRMS (ES^-) m/z: 751.0983 $[M\text{-}H^+]^-$.

Synthesis of 1,3-bis(2-(3-(4-fluorophenyl)ureido)phenyl)urea L[17]

To a solution of 4-Fluorophenyl isocyanate (1.24 mmol; 0.170 g) in 15 ml of DCM was added a suspension of amine (0.413 mmol; 0.1 g) in 15 ml of DCM. The mixture of reaction was left stirring at reflux under N_2 atmosphere overnight. The resulting precipitate was filtered off washed several times with DCM and with hot THF and than dried over vacuum to give a white solid.

Yield 70.3 % (0.29 mmol; 0.150 g); M.p. >250°C; ^{1}H-NMR (400 MHz, DMSO-d_6, 298 K): δ_{ArH} 7.05-7.15 (m, 8H), 7.40-7.50 (m, 4H), 7.50-7.62 (m, 4H), 8.07 (s, 2H, NH), 8.46 (s, 2H, NH), 9.14 (s, 2H, NH). ^{13}C-NMR (100 MHz, DMSO-d_6, 298 K) δ_C 115.11, 115.33, 119.82, 119.90, 124.09 (ArCF), 131.10, 131.47, 136.18, 153.23, 154.14; δ_{CO} 156.08, 158.45.

LRMS (ES^-) m/z: 515.1141 $[M\text{-}H^+]^-$.

Synthesis of 1,3-bis(2-(3-(p-tolyl)ureido)phenyl)urea L[18]

A suspension of amine (0.413 mmol; 0.1 g) in 20 ml of DCM was added to a solution of 4-Methylphenyl isocyanate (1.44 mmol; 0.192 g) in 10 ml of DCM. The mixture of reaction was left stirring at reflux under N_2 atmosphere overnight. The precipitate obtained was collect by filtration washed several times with DCM and with hot THF and than dried over vacuum to give a white solid.

Yield 63.3% (0.26 mmol; 0.133 g); M.p. >250°C; ^{1}H-NMR (400 MHz, DMSO-d_6, 298 K): δ_{ArH} 7.00-7.11 (m, 8H), 7.32 (d, J=5 Hz, 4H), 8.01 (s, 2H, NH), 8.43 (s, 2H, NH), 8.96 (s, 2H, NH). ^{13}C-NMR (100 MHz, DMSO-d_6, 298 K) δ_C 20.34; δ_{Ar} 118.27, 123.73, 123.90, 124.07, 124.19, 129.14, 130.53, 130.98, 131.56, 137.23; δ_{CO} 153.18, 154.10.

LRMS (ES^-) m/z: 507.0681 $[M\text{-}H^+]^-$.

Synthesis 1,3-bis(2-(3-(2-methoxyphenyl)ureido)phenyl)urea L[19]

A suspension of 2-Methoxyphenyl isocyanate (1.44 mmol, 0.215 g) and amine (0.413 mmol, 0.1g) in 25 ml of DCM was refluxed under N_2 atmosphere overnight. The precipitate obtained was filtered off and dried under vacuum to give a white solid.

Yield 62.7% (0.26 mmol; 0.140 g); M.p. 181°C; ^{1}H-NMR (500 MHz, DMSO-d_6, 298 K): δ_{CH} 3.83; δ_{ArH} 6.82-7.10 (m, 10H); 7.55 (d, J=10, 2H) 7.68 (d, J=5, 2H), 8.10 (d, J=10, 2H), 8.42 (s, 2H, NH), 8.50 (s, 2H, NH), 8.70 (s, 2H, NH). ^{13}C-NMR (100 MHz, DMSO-d_6, 298 K) δ_C 55.65, δ_{ArC} 110.68, 118.59, 120.47, 121.76, 123.41, 123.44, 123.92, 124.14, 128.74, 130.51, 131.71, 147.70; δ_{CO} 153.27, 153.57. LRMS (ES^-) m/z: 539.1984 $[M\text{-}H^+]^-$.

Synthesis of 1,3-bis(2-(3-(4-methoxyphenyl)ureido)phenyl)urea L[20]

To a solution of 4-Methoxyphenyl isocyanate (1.44 mmol, 0.215 g) in 10 ml of DCM was added a suspension of amine (0.413 mmol; 0.1 g) in 15 ml of DCM. The mixture of reaction was left stirring at reflux under N_2 atmosphere overnight. The precipitate formed was filtered off washed several times with DCM and dried over vacuum to give a white solid.

Yield 67.2% (0.28 mmol; 0.150 g); M.p. 205°C; ^{1}H-NMR (500 MHz, DMSO-d_6, 298 K): δ_{CH} 3.70; δ_{ArH} 6.84 (d, J=10 Hz, 4H), 7.00-7.11 (m, 4H), 7.34 (d, J=5, 4H), 7.54 (d, J=5, 4H), 7.60 (d, J=10, 4H), 7.98 (s, 2H, NH), 8.43 (s, 2H, NH), 8.89 (s, 2H, NH). ^{13}C-NMR (100 MHz, DMSO-d_6, 298 K) δ_C 55.14; δ_{ArC} 113.96, 119.97, 123.64, 123.83, 124.11, 124.26, 130.91, 131.74, 132.84, 153.32; δ_{CO} 154.14, 154.40. LRMS (ES^-) m/z: 539.3063 $[M\text{-}H^+]^-$.

5.6.2 Proton NMR titration fitting

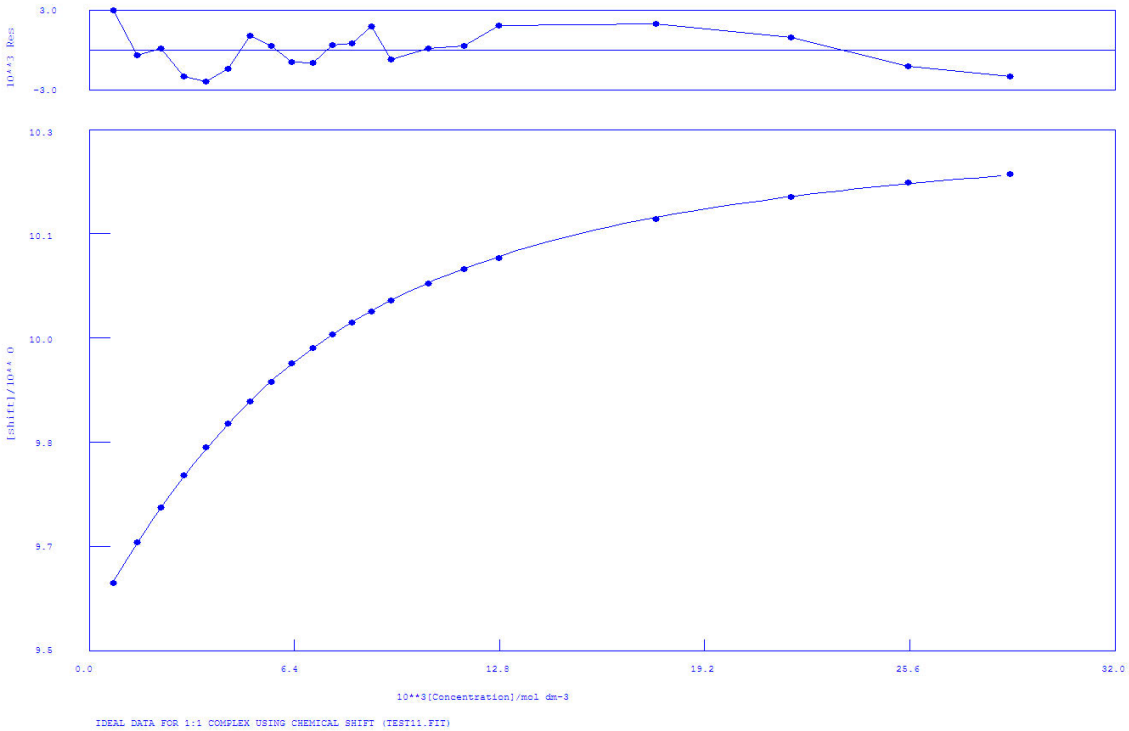

Calculations by WinEQNMR Version 1.20 by Michael J. Hynes
Program run at 17:48:04 on 01/09/2014

IDEAL DATA FOR 1:1 COMPLEX USING CHEMICAL SHIFT (TEST11.FIT)
Reaction: M + L = ML
FILE: TEST11.FIT
IDEAL DATA: K1 = 63.091; DELTA M = 20.0; DELTA ML = 120.0
File prepared by M. J. Hynes, October 22 2000

NO.	A	PARAMETER	DELTA	ERROR	CONDITION	DESCRIPTION
1	1	2.61563E+02	2.000E-01	2.742E+00	1.681E+01	K1
2	1	9.54024E+00	2.000E-01	1.182E-03	3.397E+00	SHIFT M
3	1	1.03369E+01	1.000E+00	1.915E-03	1.098E+01	SHIFT ML

Figure 5.8. ^{1}H-NMR of **L^{15}** with TBACl in DMSO-d_6/0.5%H_2O. The fitting has been obtained following the most downfield shifted NH proton.

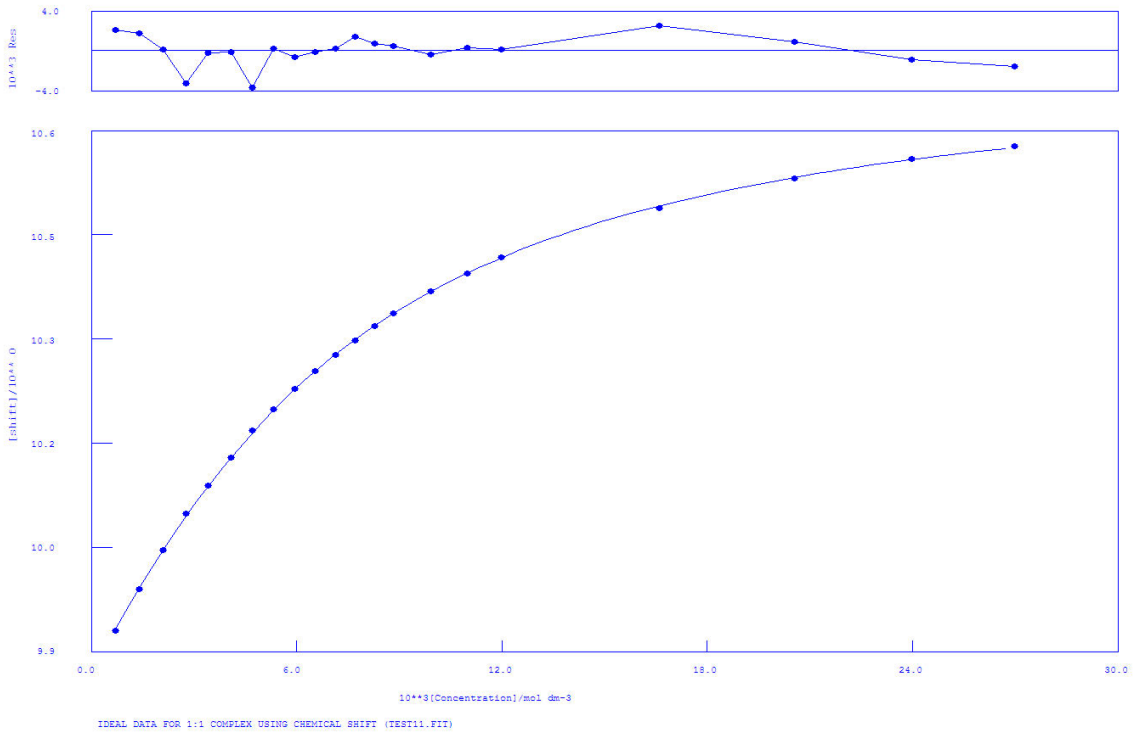

Calculations by WinEQNMR Version 1.20 by Michael J. Hynes
Program run at 19:42:53 on 02/06/2014

IDEAL DATA FOR 1:1 COMPLEX USING CHEMICAL SHIFT (TEST11.FIT)
Reaction: M + L = ML
FILE: TEST11.FIT
IDEAL DATA: K1 = 63.091; DELTA M = 20.0; DELTA ML = 120.0
File prepared by M. J. Hynes, October 22 2000

NO.	A	PARAMETER	DELTA	ERROR	CONDITION	DESCRIPTION
1	1	2.26310E+02	2.000E-01	1.869E+00	1.058E+01	K1
2	1	9.86912E+00	2.000E-01	1.118E-03	3.123E+00	SHIFT M
3	1	1.07138E+01	1.000E+00	1.704E-03	6.852E+00	SHIFT ML

Figure 5.9. ^{1}H-NMR of **L**^{16} with $TEAHCO_3$ in DMSO-d_6/0.5%H_2O. The fitting has been obtained following the most downfield shifted NH proton.

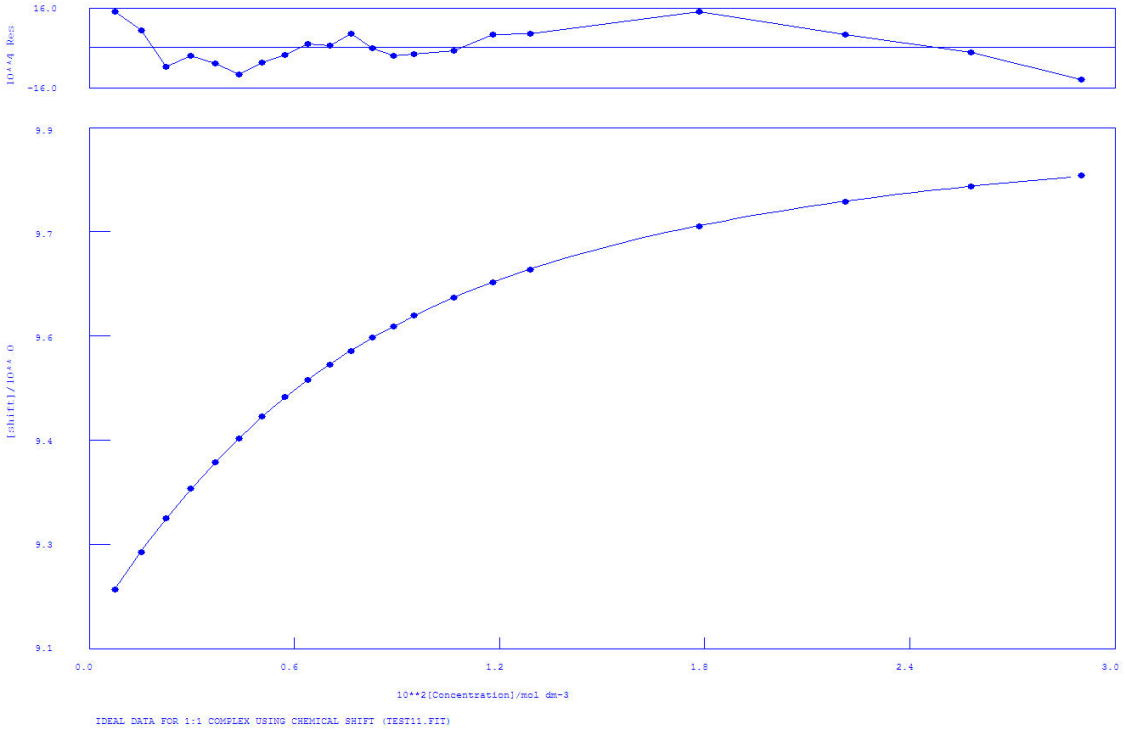

Calculations by WinEQNMR Version 1.20 by Michael J. Hynes
Program run at 16:24:27 on 01/09/2014

IDEAL DATA FOR 1:1 COMPLEX USING CHEMICAL SHIFT (TEST11.FIT)
Reaction: M + L = ML
FILE: TEST11.FIT
IDEAL DATA: K1 = 63.091; DELTA M = 20.0; DELTA ML = 120.0
File prepared by M. J. Hynes, October 22 2000

NO.	A	PARAMETER	DELTA	ERROR	CONDITION	DESCRIPTION
1	1	2.04939E+02	2.000E-01	9.658E-01	1.576E+01	K1
2	1	9.13029E+00	2.000E-01	5.327E-04	3.125E+00	SHIFT M
3	1	9.96097E+00	1.000E+00	1.013E-03	1.091E+01	SHIFT ML

Figure 5.10. ^{1}H-NMR of **L^{17}** with TBACl in DMSO-d_6/0.5%H_2O. The fitting has been obtained following the most downfield shifted NH proton.

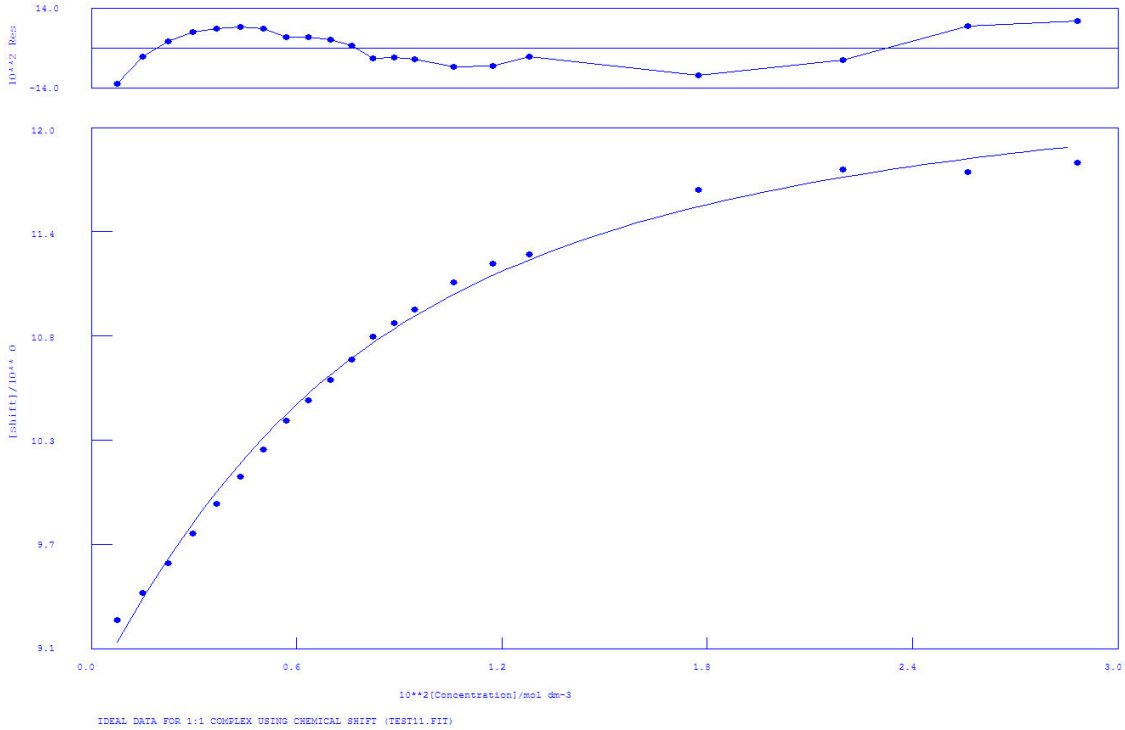

Calculations by WinEQNMR Version 1.20 by Michael J. Hynes
Program run at 16:36:29 on 01/09/2014

IDEAL DATA FOR 1:1 COMPLEX USING CHEMICAL SHIFT (TEST11.FIT)
Reaction: M + L = ML
FILE: TEST11.FIT
IDEAL DATA: K1 = 63.091; DELTA M = 20.0; DELTA ML = 120.0
File prepared by M. J. Hynes, October 22 2000

NO.	A	PARAMETER	DELTA	ERROR	CONDITION	DESCRIPTION
1	1	2.02716E+02	2.000E-01	2.129E+01	2.067E+01	K1
2	1	8.86368E+00	2.000E-01	5.171E-02	3.945E+00	SHIFT M
3	1	1.25001E+01	1.000E+00	9.678E-02	1.301E+01	SHIFT ML

Figure 5.11. ^{1}H-NMR of **L^{17}** with $TEAHCO_3$ in DMSO-d_6/0.5%H_2O. The fitting has been obtained following the most downfield shifted NH proton.

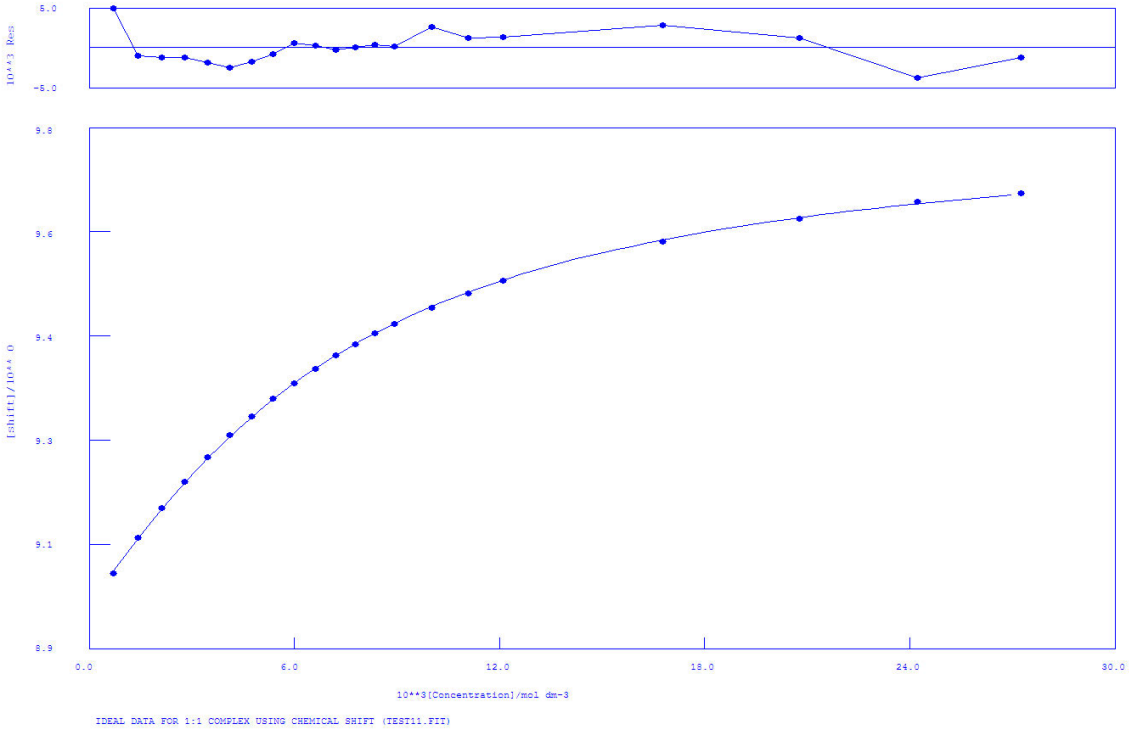

Calculations by WinEQNMR Version 1.20 by Michael J. Hynes
Program run at 16:56:34 on 01/09/2014

IDEAL DATA FOR 1:1 COMPLEX USING CHEMICAL SHIFT (TEST11.FIT)
Reaction: M + L = ML
FILE: TEST11.FIT
IDEAL DATA: K1 = 63.091; DELTA M = 20.0; DELTA ML = 120.0
File prepared by M. J. Hynes, October 22 2000

NO.	A	PARAMETER	DELTA	ERROR	CONDITION	DESCRIPTION
1	1	2.26371E+02	2.000E-01	3.075E+00	1.713E+01	K1
2	1	8.97249E+00	2.000E-01	1.541E-03	3.524E+00	SHIFT M
3	1	9.82067E+00	1.000E+00	2.807E-03	1.107E+01	SHIFT ML

Figure 5.12. ^{1}H-NMR of **L^{18}** with TBACl in DMSO-d_6/0.5%H_2O. The fitting has been obtained following the most downfield shifted NH proton.

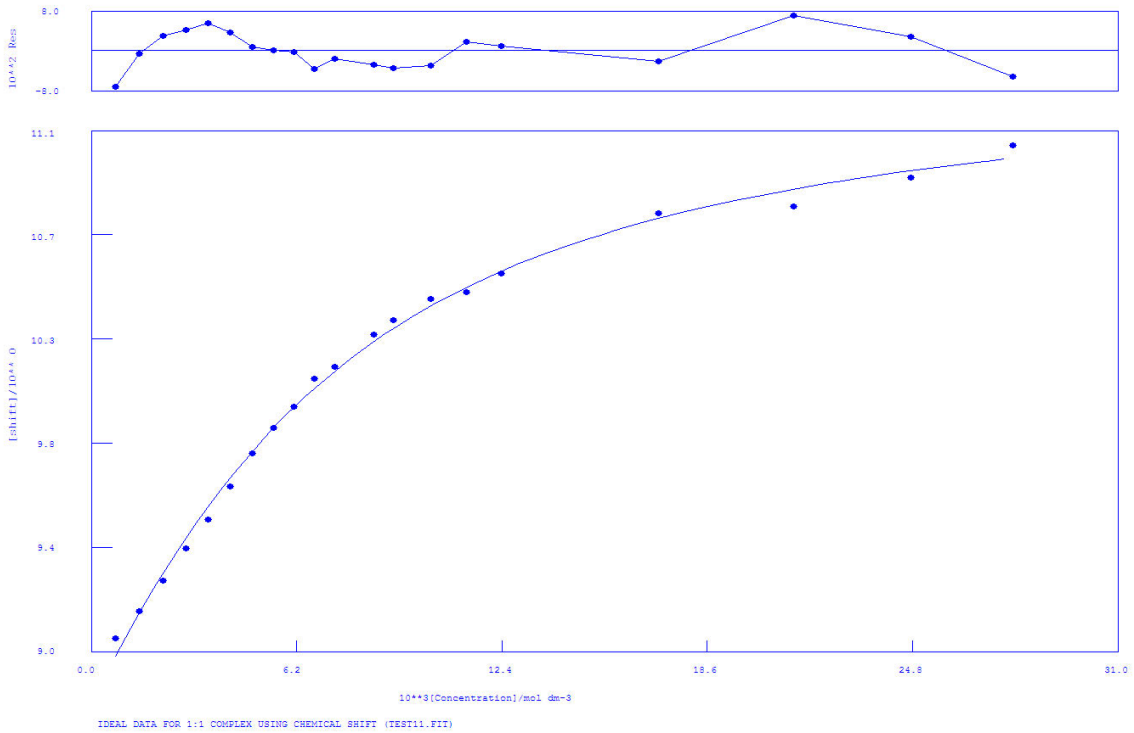

Calculations by WinEQNMR Version 1.20 by Michael J. Hynes
Program run at 17:04:09 on 01/09/2014

IDEAL DATA FOR 1:1 COMPLEX USING CHEMICAL SHIFT (TEST11.FIT)
Reaction: M + L = ML
FILE: TEST11.FIT
IDEAL DATA: K1 = 63.091; DELTA M = 20.0; DELTA ML = 120.0
File prepared by M. J. Hynes, October 22 2000

NO.	A	PARAMETER	DELTA	ERROR	CONDITION	DESCRIPTION
1	1	2.20888E+02	2.000E-01	1.984E+01	1.954E+01	K1
2	1	8.78946E+00	2.000E-01	3.013E-02	3.647E+00	SHIFT M
3	1	1.14096E+01	1.000E+00	5.761E-02	1.260E+01	SHIFT ML

Figure 5.13. ^{1}H-NMR of **L^{18}** with $TEAHCO_3$ in DMSO-d_6/0.5%H_2O. The fitting has been obtained following the most downfield shifted NH proton.

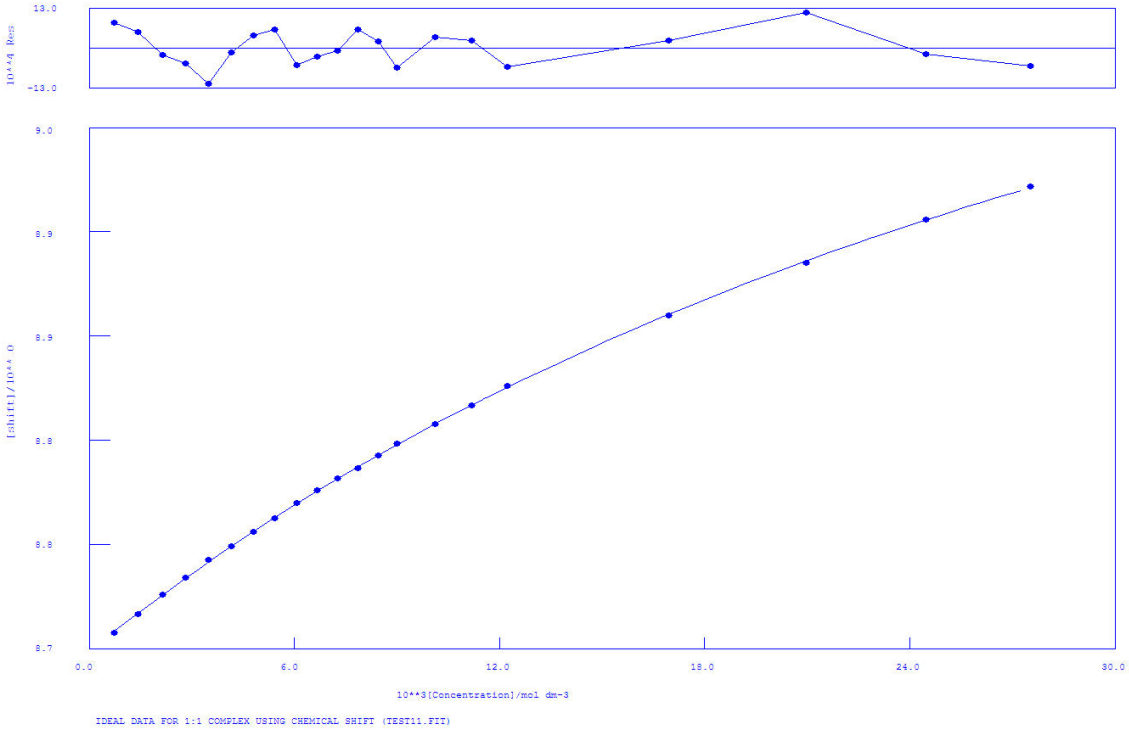

Calculations by WinEQNMR Version 1.20 by Michael J. Hynes
Program run at 17:10:32 on 01/09/2014

IDEAL DATA FOR 1:1 COMPLEX USING CHEMICAL SHIFT (TEST11.FIT)
Reaction: M + L = ML
FILE: TEST11.FIT
IDEAL DATA: K1 = 63.091; DELTA M = 20.0; DELTA ML = 120.0
File prepared by M. J. Hynes, October 22 2000

NO.	A	PARAMETER	DELTA	ERROR	CONDITION	DESCRIPTION
1	1	2.80113E+01	2.000E-01	5.287E-01	1.527E+02	K1
2	1	8.69857E+00	2.000E-01	3.825E-04	5.741E+00	SHIFT M
3	1	9.33840E+00	1.000E+00	7.126E-03	1.205E+02	SHIFT ML

Figure 5.14. ^{1}H-NMR of **L^{19}** with TBACl in DMSO-d_6/0.5%H_2O. The fitting has been obtained following the most downfield shifted NH proton.

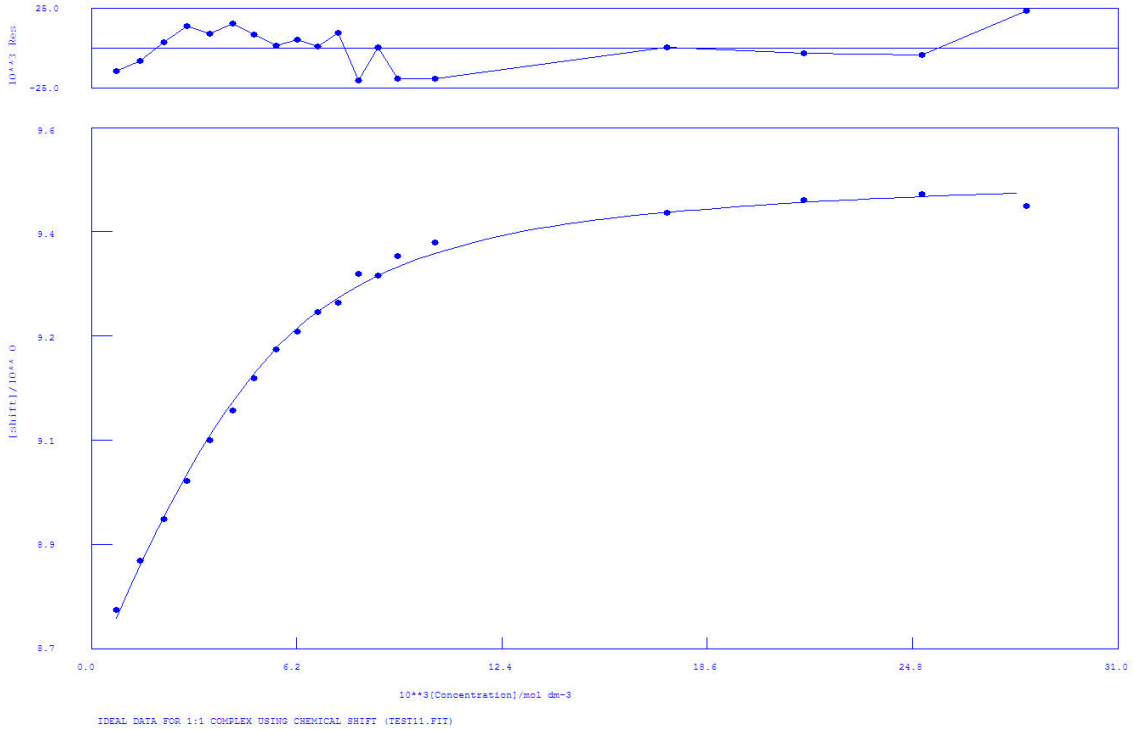

Calculations by WinEQNMR Version 1.20 by Michael J. Hynes
Program run at 17:21:46 on 01/09/2014

IDEAL DATA FOR 1:1 COMPLEX USING CHEMICAL SHIFT (TEST11.FIT)
Reaction: M + L = ML
FILE: TEST11.FIT
IDEAL DATA: K1 = 63.091; DELTA M = 20.0; DELTA ML = 120.0
File prepared by M. J. Hynes, October 22 2000

NO.	A	PARAMETER	DELTA	ERROR	CONDITION	DESCRIPTION
1	1	8.01729E+02	2.000E-01	6.472E+01	7.721E+00	K1
2	1	8.65338E+00	2.000E-01	9.999E-03	2.041E+00	SHIFT M
3	1	9.53084E+00	1.000E+00	1.042E-02	5.862E+00	SHIFT ML

Figure 5.15. ^{1}H-NMR of **L^{19}** with $TEAHCO_3$ in DMSO-d_6/0.5%H_2O. The fitting has been obtained following the most downfield shifted NH proton.

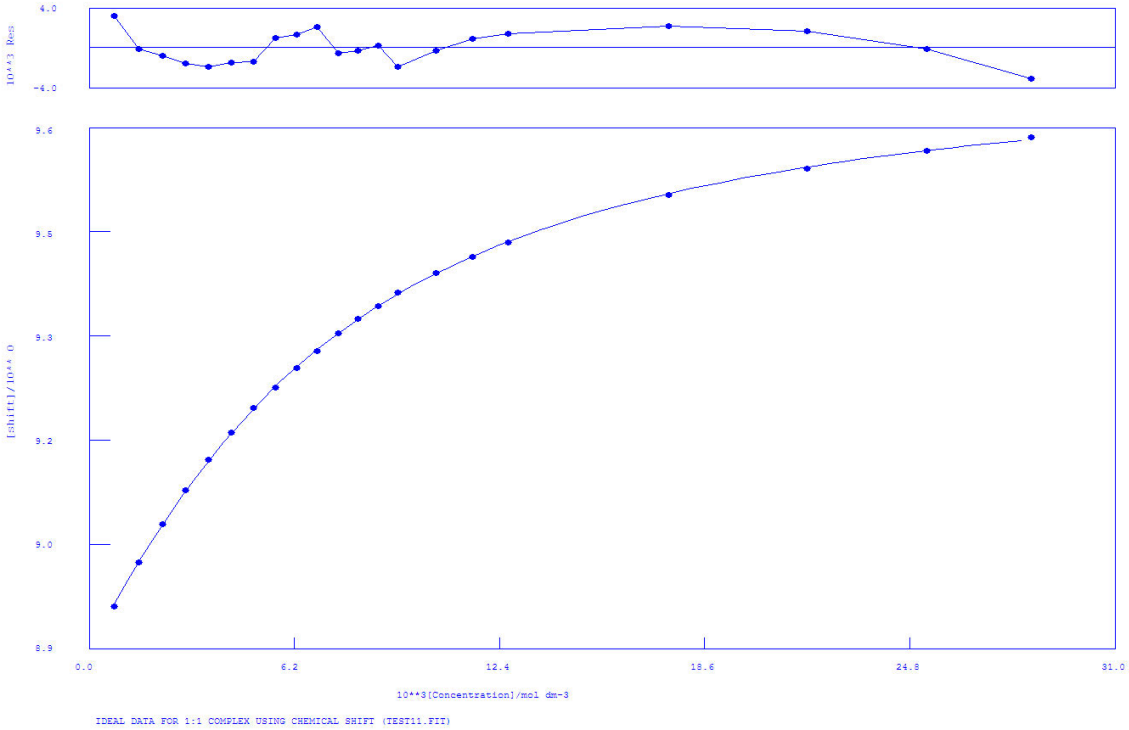

Calculations by WinEQNMR Version 1.20 by Michael J. Hynes
Program run at 17:37:12 on 01/09/2014

IDEAL DATA FOR 1:1 COMPLEX USING CHEMICAL SHIFT (TEST11.FIT)
Reaction: M + L = ML
FILE: TEST11.FIT
IDEAL DATA: K1 = 63.091; DELTA M = 20.0; DELTA ML = 120.0
File prepared by M. J. Hynes, October 22 2000

NO.	A	PARAMETER	DELTA	ERROR	CONDITION	DESCRIPTION
1	1	2.25143E+02	2.000E-01	2.507E+00	1.560E+01	K1
2	1	8.89882E+00	2.000E-01	1.286E-03	3.501E+00	SHIFT M
3	1	9.70864E+00	1.000E+00	2.144E-03	9.930E+00	SHIFT ML

Figure 5.16. ^{1}H-NMR of **L^{20}** with TBACl in DMSO-d_6/0.5%H_2O. The fitting has been obtained following the most downfield shifted NH proton.

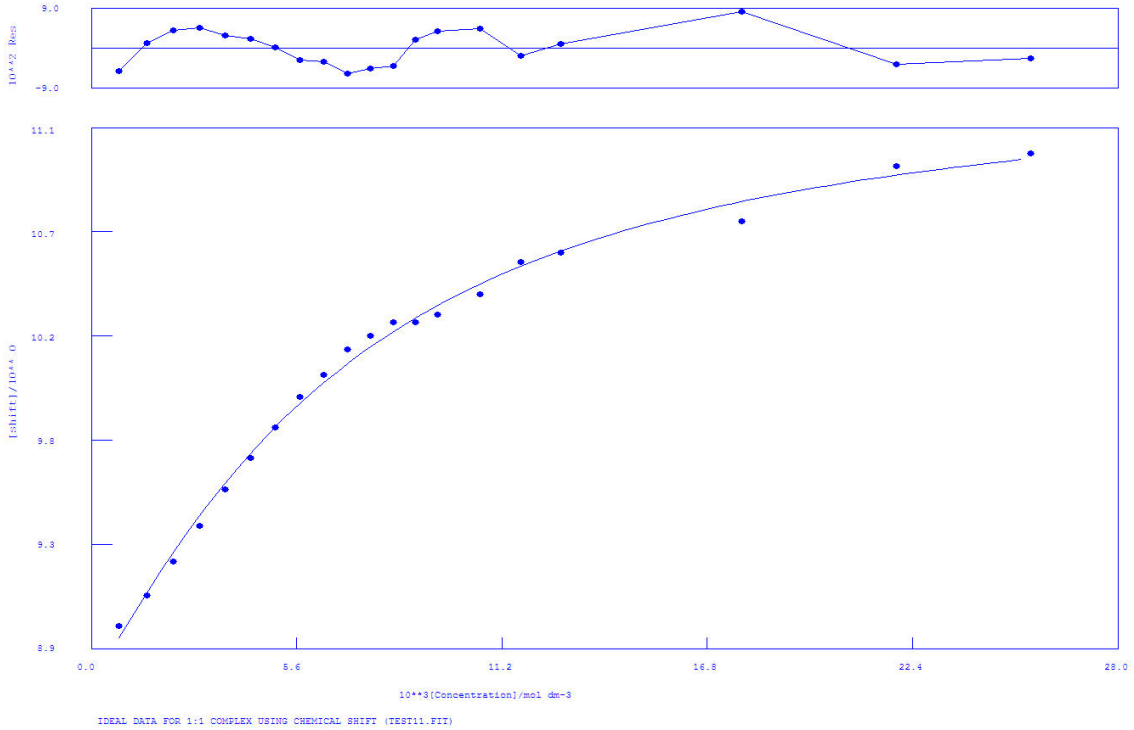

Calculations by WinEQNMR Version 1.20 by Michael J. Hynes
Program run at 17:42:08 on 01/09/2014

IDEAL DATA FOR 1:1 COMPLEX USING CHEMICAL SHIFT (TEST11.FIT)
Reaction: M + L = ML
FILE: TEST11.FIT
IDEAL DATA: K1 = 63.091; DELTA M = 20.0; DELTA ML = 120.0
File prepared by M. J. Hynes, October 22 2000

NO.	A	PARAMETER	DELTA	ERROR	CONDITION	DESCRIPTION
1	1	2.39579E+02	2.000E-01	2.332E+01	2.334E+01	K1
2	1	8.73131E+00	2.000E-01	3.287E-02	3.760E+00	SHIFT M
3	1	1.14046E+01	1.000E+00	6.816E-02	1.561E+01	SHIFT ML

Figure 5.17. ^{1}H-NMR of **L^{20}** with $TEAHCO_3$ in DMSO-d_6/0.5%H_2O. The fitting has been obtained following the most downfield shifted NH proton.

5.6.3 Anion Transport Studies

5.6.3.1 Experimental details

Preparation of Vesicles

A lipid film of 1-palmitoyl-2-oleoyl-sn-glycero-3-phosphocholine (POPC) and cholesterol (0% or 30%) was formed from a chloroform solution under reduced pressure and dried under vacuum for at least 2 hours. The lipid film was rehydrated by vortexing with an internal solution (489 mM NaCl, 5 mM phosphate buffer at pH 7.2). The lipid suspension was then subjected to nine freeze-thaw cycles and allowed to age for 30 min at room temperature before extruding 20 times through a 200 nm polycarbonate membrane. The resulting unilamellar vesicles were dialyzed against the external solution to remove unencapsulated NaCl salts. The vesicles were diluted to 5mL with the external solution to form a stock solution of lipid.

Samples for assay were prepared by diluting lipid stock solution to 5mL (using the external solution) to give a solution of 1mM lipid. Chloride efflux was monitored using a chloride selective electrode (Accumet). To initiate the experiment compounds were added as solutions in DMSO, to give a 1:50 compound to lipid ratio (2mol%). At the end of the experiment detergent (octaethylene glycol monododecyl ether) was added to allow the determination of 100% chloride efflux. Experiments were repeated in triplicate and all traces presented are the average of three trials. The chloride electrode was calibrated against sodium chloride solutions of known concentration.

Chloride Transport Assays

Unilamellar POPC vesicles containing NaCl, prepared as described above, were suspended in 489 mM $NaNO_3$ buffered to pH 7.2 with 5 mM sodium phosphate salts. The lipid concentration per sample was 1 mM. A DMSO solution of the carrier molecule (10 mM) was added to start the experiment and the chloride efflux was monitored using a chloride sensitive electrode. At 5 min, the vesicles were lysed with 50 µl of octaethylene glycol monododecyl ether and a total chloride reading was taken at 7 min.

Bicarbonate Transport Assay

Unilamellar POPC vesicles containing 451 mM NaCl solution buffered to pH 7.2 with 20 mM sodium phosphate salts, prepared as described above, were suspended in 150 mM Na_2SO_4 solution buffered to pH 7.2 with sodium phosphate salts. The lipid concentration per sample was 1 mM. A DMSO solution of the carrier molecule (10 mM) was added to start the experiment and chloride efflux was monitored using a chloride sensitive electrode. At 2 min, $NaHCO_3$ solution (1 M in 150 mM Na_2SO_4 buffered to pH 7.2 with 20 mM sodium phosphate salts) was added so that the outer solution contained 40 mM $NaHCO_3$. At 7 min, the vesicles were lysed with 50 µl of octaethylene glycol monododecyl ether and a total chloride reading was taken at 9 min.

5.6.3.2 Additional membrane transport studies

Cl^-/NO_3^- antiport studies

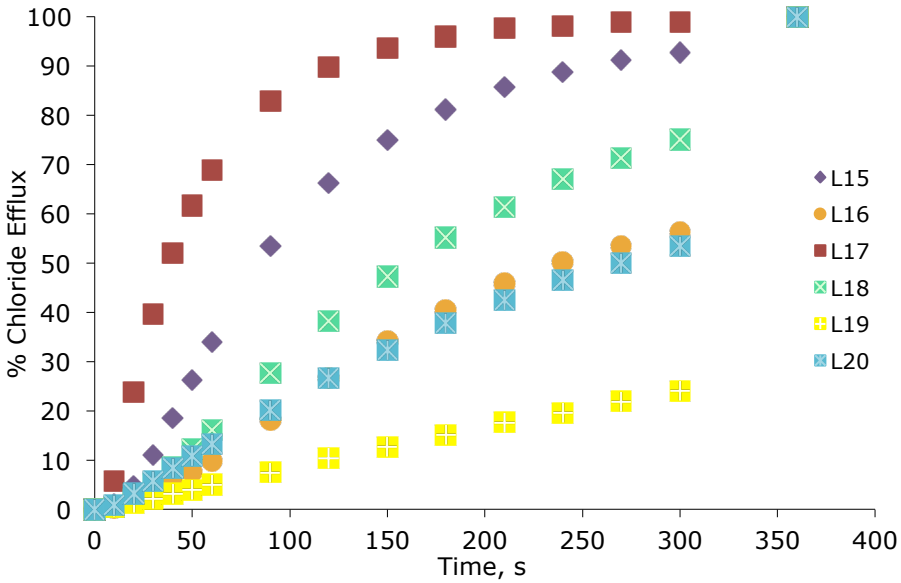

Figure 5.18 Chloride efflux promoted by a DMSO solution of compounds 1–6 (2 mol% carrier to lipid) from unilamellar POPC vesicles loaded with 489 mM NaCl buffered to pH 7.2 with 5 mM sodium phosphate salts. The vesicles were dispersed in 489 mM $NaNO_3$ buffered to pH 7.2 with 5 mM sodium phosphate salts. At the end of the experiment detergent was added to lyse the vesicles and calibrate the ISE to 100% chloride efflux. Each point represents an average of three trials. DMSO was used as a control.

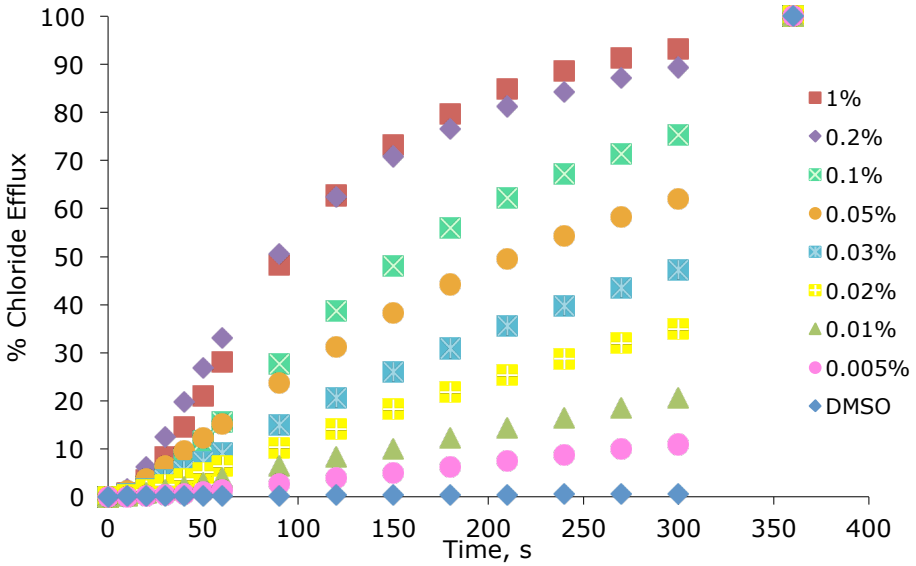

Figure 5.19 Chloride efflux promoted by a various concentration of compounds **L**[15] from unilamellar POPC vesicles loaded with 489 mM NaCl buffered to pH 7.2 with 5 mM sodium phosphate salts. The vesicles were dispersed in 489 mM $NaNO_3$ buffered to pH 7.2 with 5 mM sodium phosphate salts. At the end of the experiment detergent was added to lyse the vesicles and calibrate the ISE to 100% chloride efflux. Each point represents an average of three trials. DMSO was used as a control.

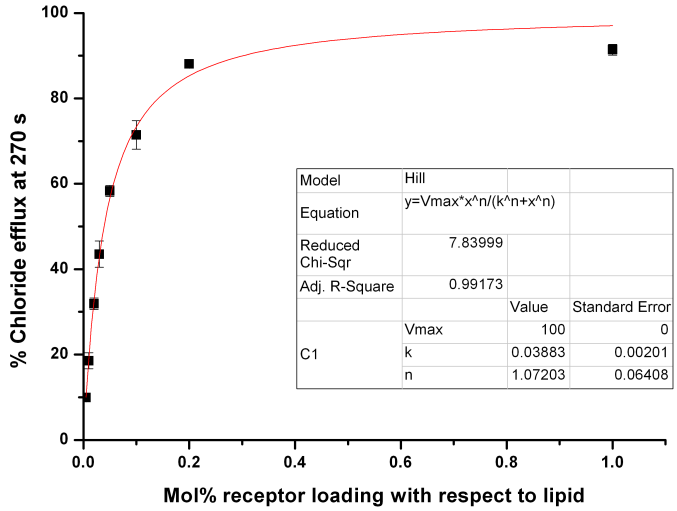

Figure 5.20 Hill plot of chloride efflux promoted by varying concentrations of compound **L**[15] from unilamellar POPC vesicles loaded with 489 mM NaCl buffered to pH 7.2 with 5mM sodium phosphate salts. The vesicles were dispersed in 489 mM $NaNO_3$ buffered at pH 7.2 with 5mM sodium phosphate salts. Each point represents an average of 3 trials.

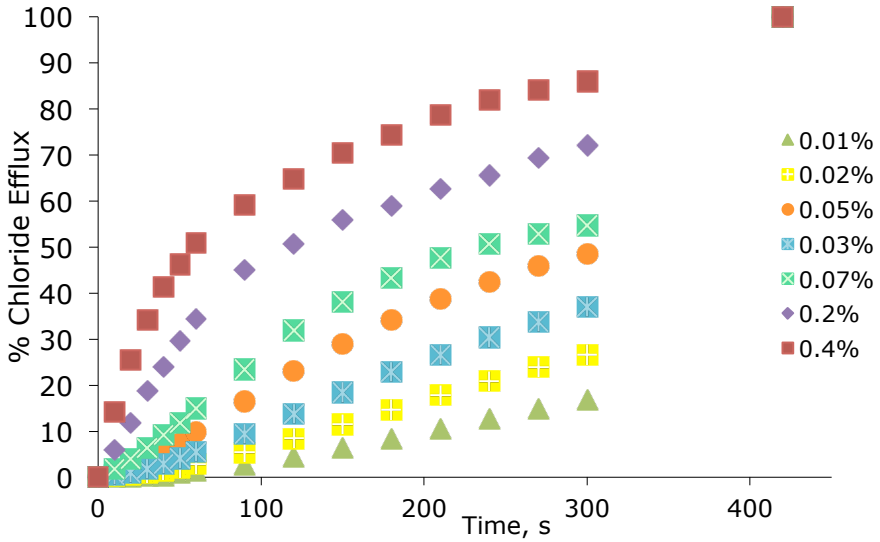

Figure 5.21 Chloride efflux promoted by a various concentration of compounds **L**[16] from unilamellar POPC vesicles loaded with 489 mM NaCl buffered to pH 7.2 with 5 mM sodium phosphate salts. The vesicles were dispersed in 489 mM $NaNO_3$ buffered to pH 7.2 with 5 mM sodium phosphate salts. At the end of the experiment detergent was added to lyse the vesicles and calibrate the ISE to 100% chloride efflux. Each point represents an average of three trials. DMSO was used as a control.

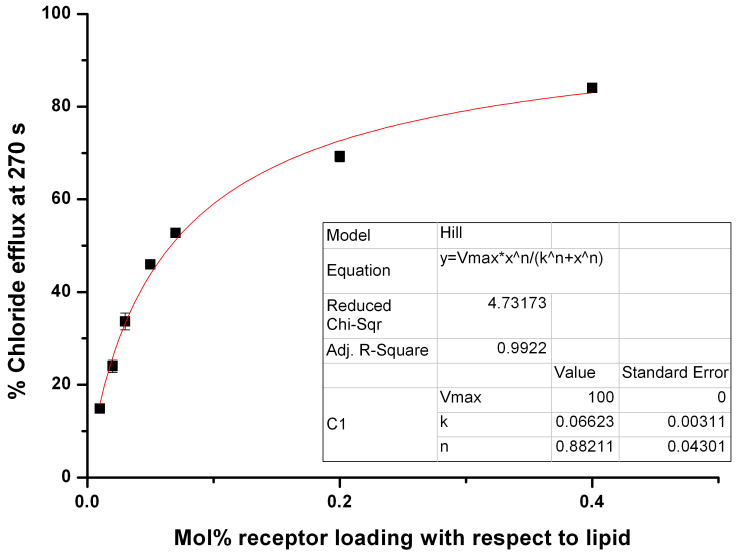

Figure 5.22 Hill plot of chloride efflux promoted by varying concentrations of compound **L**[16] from unilamellar POPC vesicles loaded with 489 mM NaCl buffered to pH 7.2 with 5mM sodium phosphate salts. The vesicles were dispersed in 489 mM $NaNO_3$ buffered at pH 7.2 with 5mM sodium phosphate salts. Each point represents an average of 3 trials.

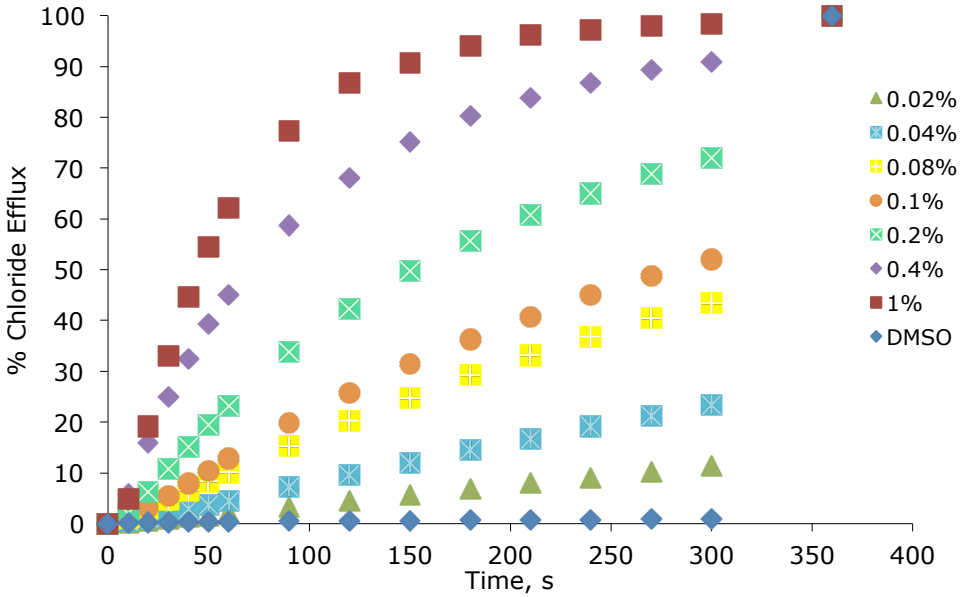

Figure 5.23 Chloride efflux promoted by a various concentration of compounds **L**[17] from unilamellar POPC vesicles loaded with 489 mM NaCl buffered to pH 7.2 with 5 mM sodium phosphate salts. The vesicles were dispersed in 489 mM $NaNO_3$ buffered to pH 7.2 with 5 mM sodium phosphate salts. At the end of the experiment detergent was added to lyse the vesicles and calibrate the ISE to 100% chloride efflux. Each point represents an average of three trials. DMSO was used as a control.

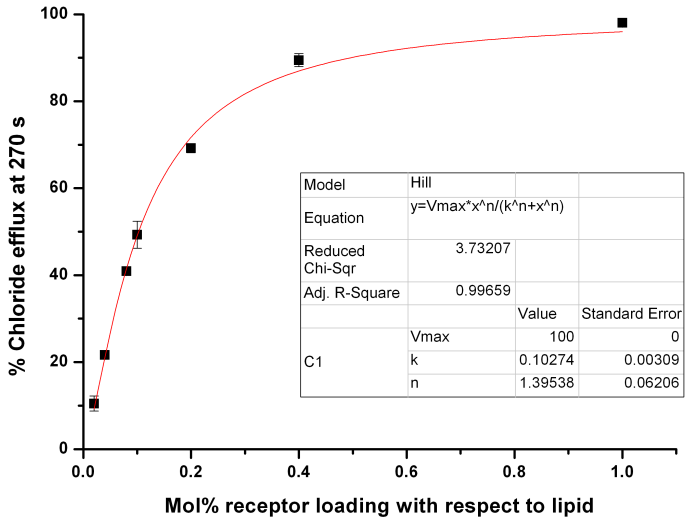

Figure 5.24 Hill plot of chloride efflux promoted by varying concentrations of compound **L**[17] from unilamellar POPC vesicles loaded with 489 mM NaCl buffered to pH 7.2 with 5mM sodium phosphate salts. The vesicles were dispersed in 489 mM $NaNO_3$ buffered at pH 7.2 with 5mM sodium phosphate salts. Each point represents an average of 3 trials.

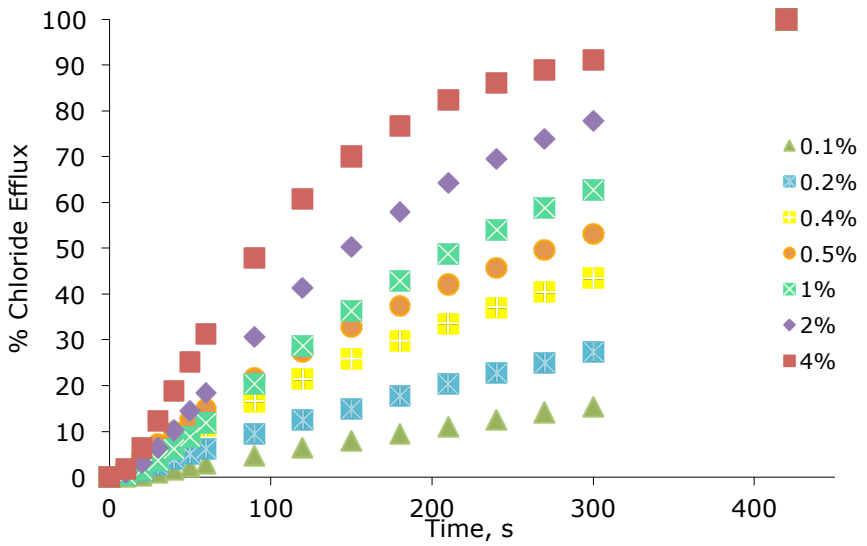

Figure 5.25 Chloride efflux promoted by a various concentration of compounds **L**[18] from unilamellar POPC vesicles loaded with 489 mM NaCl buffered to pH 7.2 with 5 mM sodium phosphate salts. The vesicles were dispersed in 489 mM $NaNO_3$ buffered to pH 7.2 with 5 mM sodium phosphate salts. At the end of the experiment detergent was added to lyse the vesicles and calibrate the ISE to 100% chloride efflux. Each point represents an average of three trials. DMSO was used as a control.

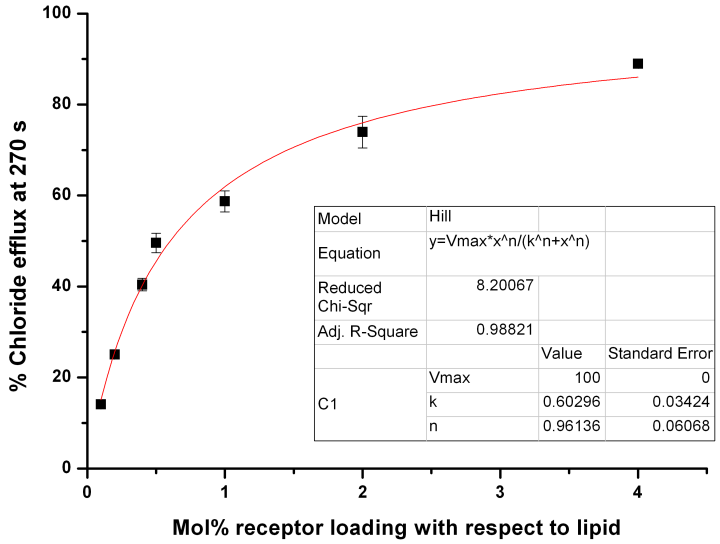

Figure 5.26 Hill plot of chloride efflux promoted by varying concentrations of compound **L**[18] from unilamellar POPC vesicles loaded with 489 mM NaCl buffered to pH 7.2 with 5mM sodium phosphate salts. The vesicles were dispersed in 489 mM $NaNO_3$ buffered at pH 7.2 with 5mM sodium phosphate salts. Each point represents an average of 3 trials.

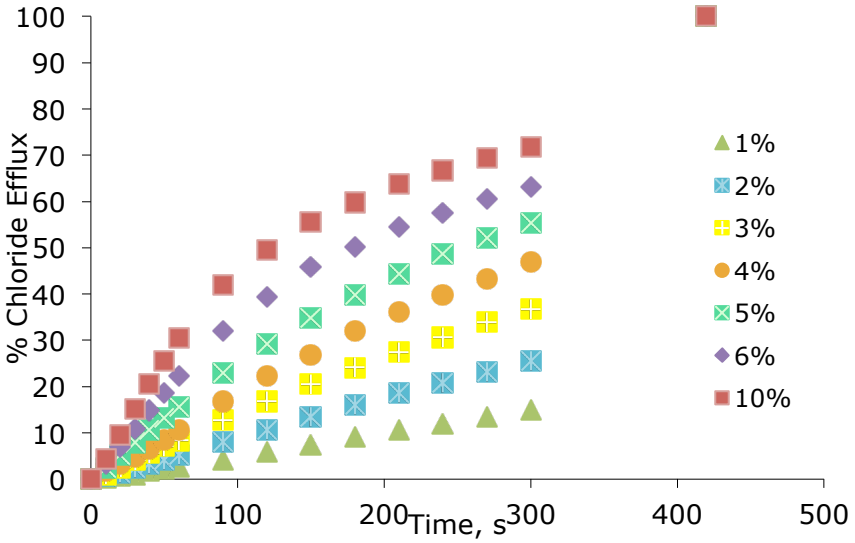

Figure 5.27 Chloride efflux promoted by a various concentration of compounds **L**[19] from unilamellar POPC vesicles loaded with 489 mM NaCl buffered to pH 7.2 with 5 mM sodium phosphate salts. The vesicles were dispersed in 489 mM $NaNO_3$ buffered to pH 7.2 with 5 mM sodium phosphate salts. At the end of the experiment detergent was added to lyse the vesicles and calibrate the ISE to 100% chloride efflux. Each point represents an average of three trials. DMSO was used as a control.

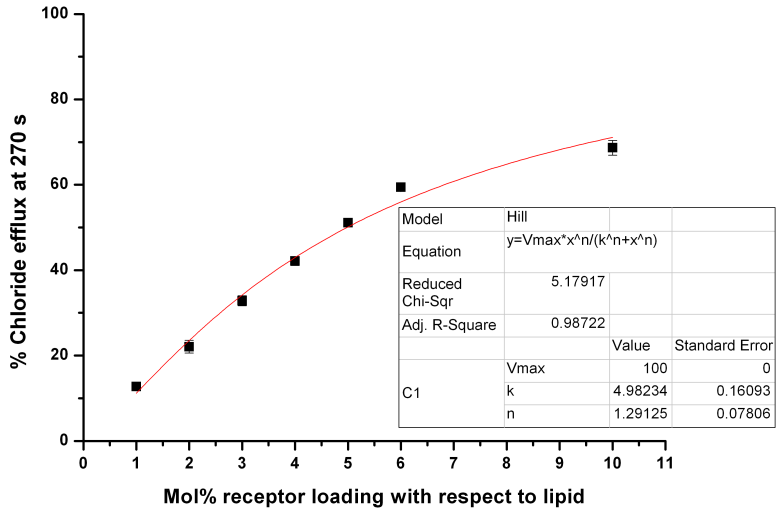

Figure 5.28 Hill plot of chloride efflux promoted by varying concentrations of compound **L**[19] from unilamellar POPC vesicles loaded with 489 mM NaCl buffered to pH 7.2 with 5mM sodium phosphate salts. The vesicles were dispersed in 489 mM $NaNO_3$ buffered at pH 7.2 with 5mM sodium phosphate salts. Each point represents an average of 3 trials.

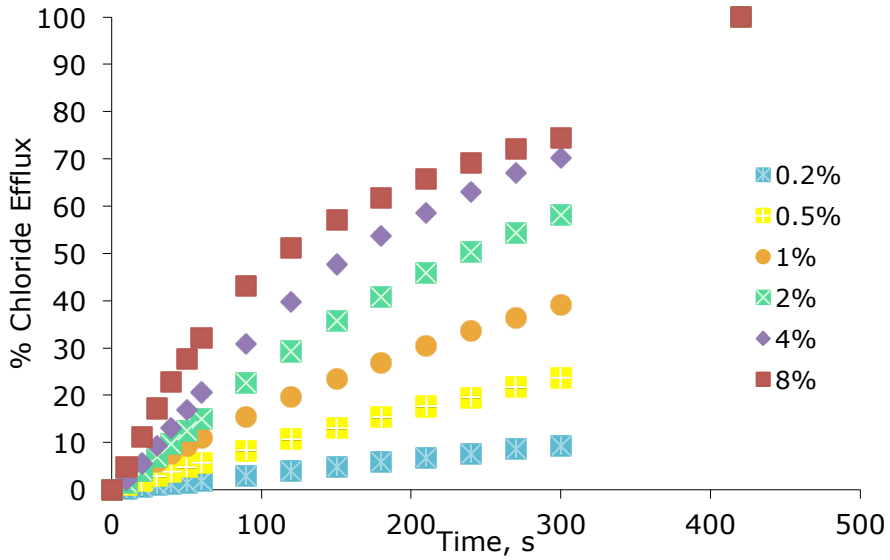

Figure 5.29 Chloride efflux promoted by a various concentration of compounds **L**^{20} from unilamellar POPC vesicles loaded with 489 mM NaCl buffered to pH 7.2 with 5 mM sodium phosphate salts. The vesicles were dispersed in 489 mM $NaNO_3$ buffered to pH 7.2 with 5 mM sodium phosphate salts. At the end of the experiment detergent was added to lyse the vesicles and calibrate the ISE to 100% chloride efflux. Each point represents an average of three trials. DMSO was used as a control.

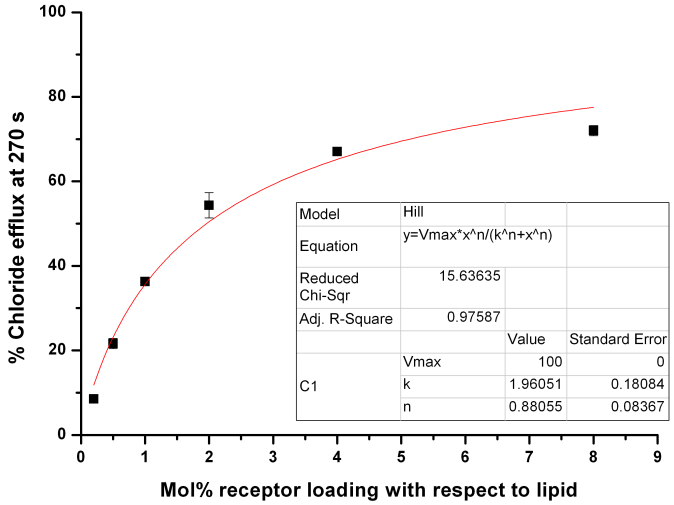

Figure 5.30 Hill plot of chloride efflux promoted by varying concentrations of compound **L**^{20} from unilamellar POPC vesicles loaded with 489 mM NaCl buffered to pH 7.2 with 5mM sodium phosphate salts. The vesicles were dispersed in 489 mM $NaNO_3$ buffered at pH 7.2 with 5mM sodium phosphate salts. Each point represents an average of 3 trials.

Cl^-/HCO_3^- antiport studies

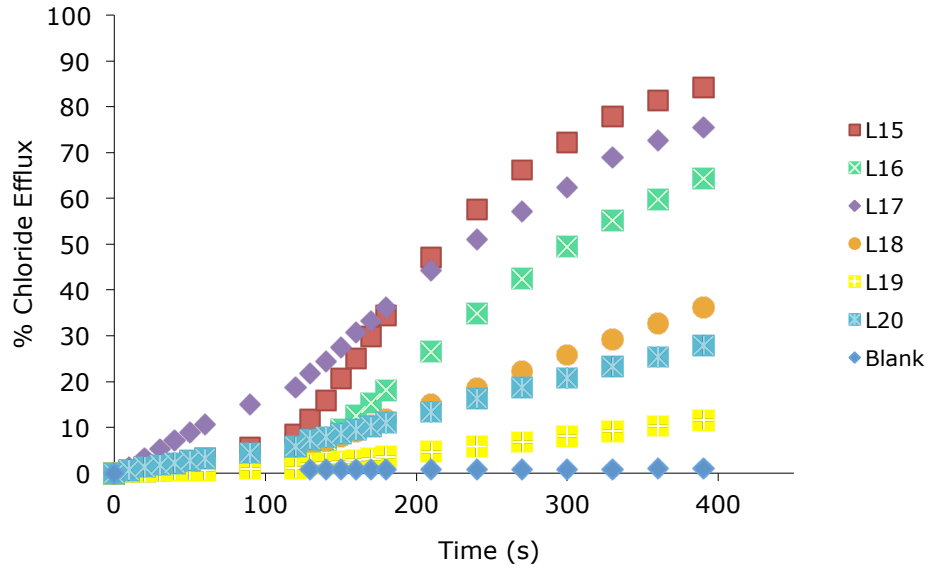

Figure 5.31 Chloride efflux promoted by a DMSO solution of compounds 1–6 (2 mol% carrier to lipid) from unilamellar POPC vesicles loaded with 451 mM NaCl buffered to pH 7.2 with 20 mM sodium phosphate salts. The vesicles were dispersed in 150 mM Na_2SO_4 buffered to pH 7.2 with 20 mM sodium phosphate salts. At t ¼ 120 s a solution of sodium bicarbonate was added such that the external concentration of bicarbonate was 40 mM. At the end of the experiment, detergent was added to lyse the vesicles and calibrate the ISE to 100% chloride efflux. Each point represents an average of three trials. DMSO was used as a control.

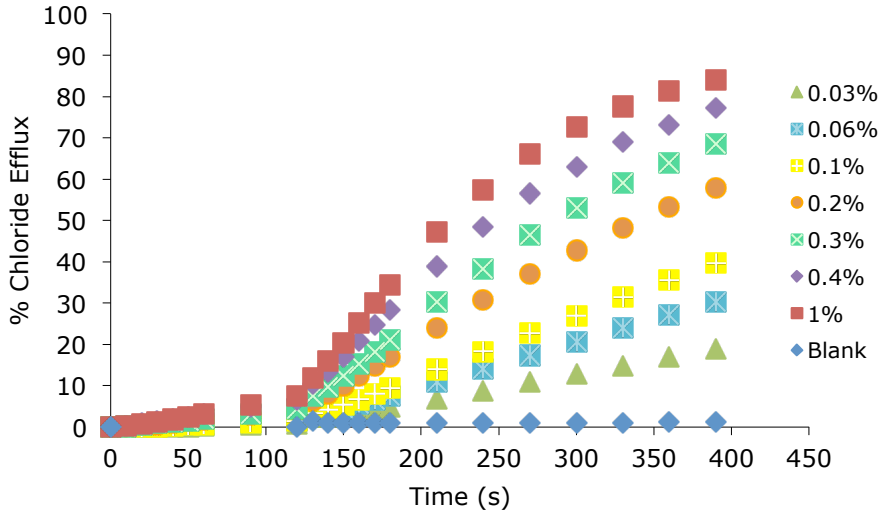

Figure 5.32 Chloride efflux promoted by various concentrations of **L**[15] from unilamellar POPC vesicles loaded with 451 mM NaCl buffered to pH 7.2 with 20 mM sodium phosphate salts. The vesicles were dispersed in 150 mM Na_2SO_4 buffered to pH 7.2 with 20 mM sodium phosphate salts. At t. 120 s a solution of sodium bicarbonate was added such that the external concentration of bicarbonate was 40 mM. At the end of the experiment, detergent was added to lyse the vesicles and calibrate the ISE to 100% chloride efflux. Each point represents an average of three trials. DMSO was used as a control.

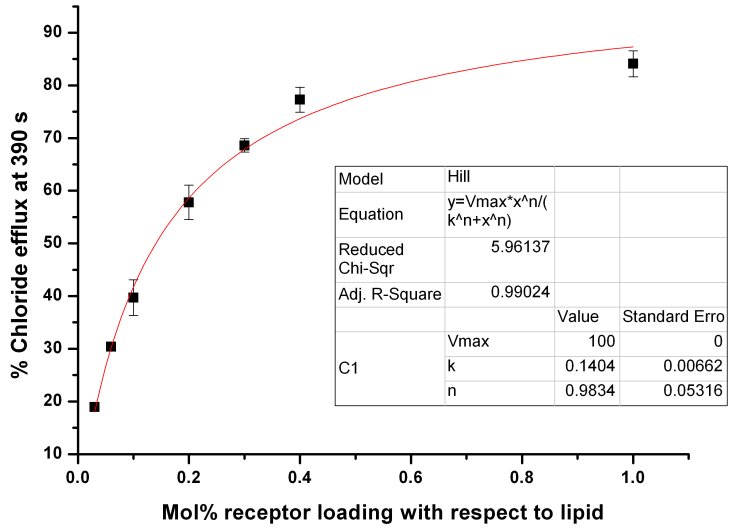

Figure 5.33 Hill plot of chloride efflux promoted varying concentrations of compound **L**[15] from unilamellar POPC vesicles loaded with 451mM NaCl buffered to pH 7.2 with 20mM sodium phosphate salts upon addition of a bicarbonate 'pulse', bringing the external concentration of bicarbonate to 40mM. The vesicles were dispersed in 150mM Na_2SO_4 buffered to pH 7.2 with 20mM sodium phosphate salts. Each point represents an average of 3 trials.

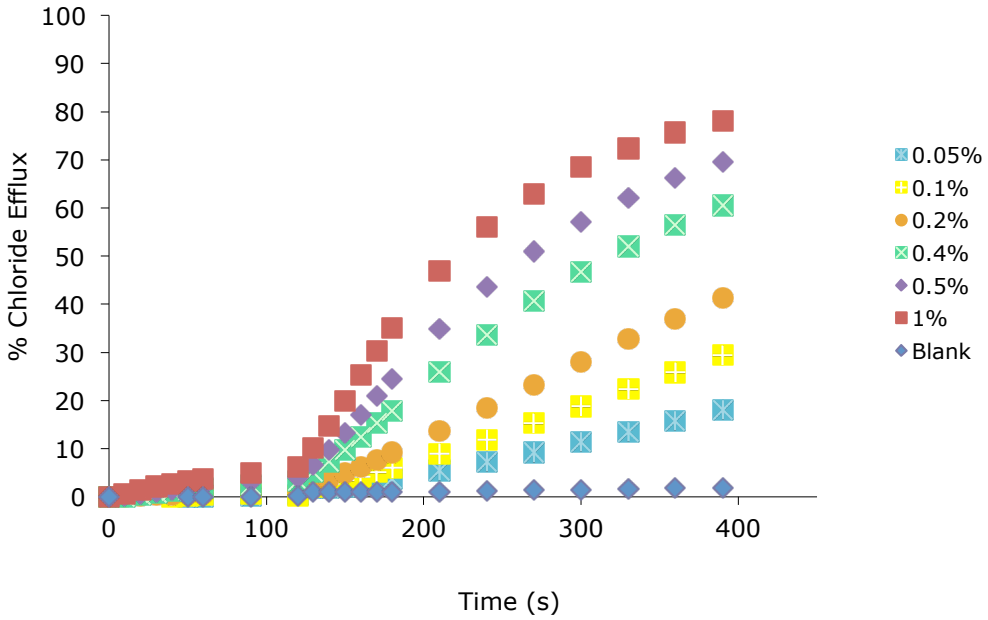

Figure 5.34 Chloride efflux promoted by various concentrations of **L**[16] from unilamellar POPC vesicles loaded with 451 mM NaCl buffered to pH 7.2 with 20 mM sodium phosphate salts. The vesicles were dispersed in 150 mM Na_2SO_4 buffered to pH 7.2 with 20 mM sodium phosphate salts. At t. 120 s a solution of sodium bicarbonate was added such that the external concentration of bicarbonate was 40 mM. At the end of the experiment, detergent was added to lyse the vesicles and calibrate the ISE to 100% chloride efflux. Each point represents an average of three trials. DMSO was used as a control.

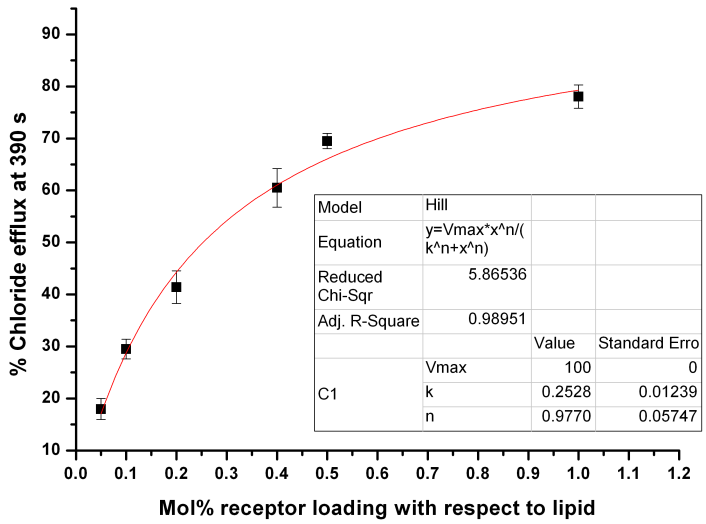

Figure 5.35 Hill plot of chloride efflux promoted varying concentrations of compound **L**[16] from unilamellar POPC vesicles loaded with 451mM NaCl buffered to pH 7.2 with 20mM sodium phosphate salts upon addition of a bicarbonate 'pulse', bringing the external concentration of bicarbonate to 40mM. The vesicles were dispersed in 150mM Na_2SO_4 buffered to pH 7.2 with 20mM sodium phosphate salts. Each point represents an average of 3 trials.

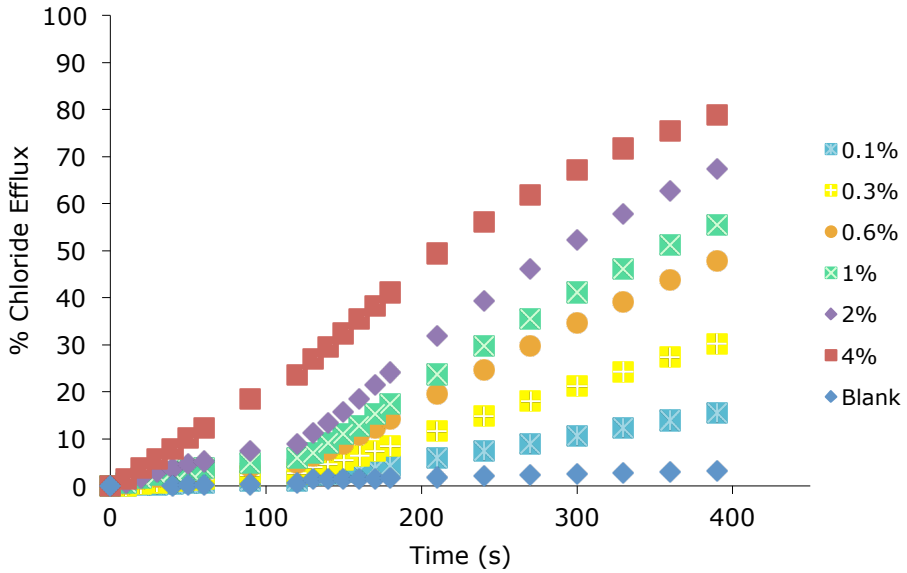

Figure 5.36 Chloride efflux promoted by various concentrations of **L**[17] from unilamellar POPC vesicles loaded with 451 mM NaCl buffered to pH 7.2 with 20 mM sodium phosphate salts. The vesicles were dispersed in 150 mM Na_2SO_4 buffered to pH 7.2 with 20 mM sodium phosphate salts. At t. 120 s a solution of sodium bicarbonate was added such that the external concentration of bicarbonate was 40 mM. At the end of the experiment, detergent was added to lyse the vesicles and calibrate the ISE to 100% chloride efflux. Each point represents an average of three trials. DMSO was used as a control.

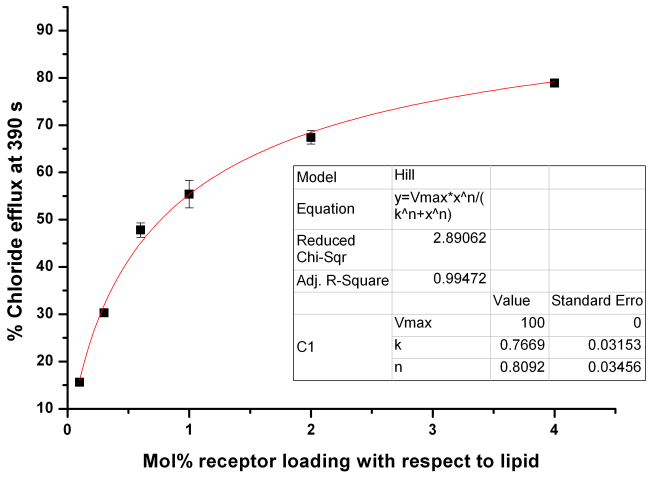

Figure 5.37 Hill plot of chloride efflux promoted varying concentrations of compound **L**[17] from unilamellar POPC vesicles loaded with 451mM NaCl buffered to pH 7.2 with 20mM sodium phosphate salts upon addition of a bicarbonate 'pulse', bringing the external concentration of bicarbonate to 40mM. The vesicles were dispersed in 150mM Na_2SO_4 buffered to pH 7.2 with 20mM sodium phosphate salts. Each point represents an average of 3 trials.

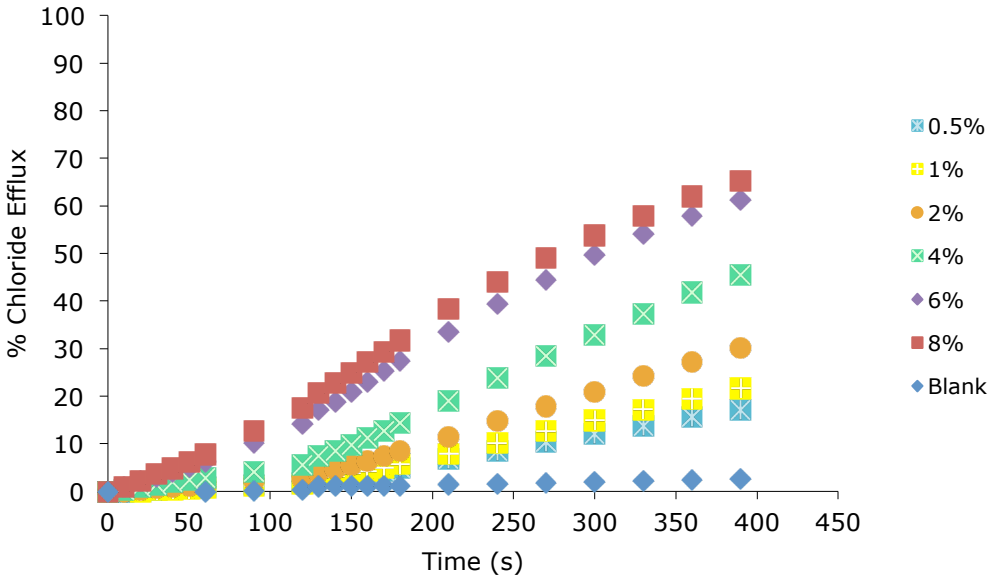

Figure 5.38 Chloride efflux promoted by various concentrations of **L**[18] from unilamellar POPC vesicles loaded with 451 mM NaCl buffered to pH 7.2 with 20 mM sodium phosphate salts. The vesicles were dispersed in 150 mM Na_2SO_4 buffered to pH 7.2 with 20 mM sodium phosphate salts. At t. 120 s a solution of sodium bicarbonate was added such that the external concentration of bicarbonate was 40 mM. At the end of the experiment, detergent was added to lyse the vesicles and calibrate the ISE to 100% chloride efflux. Each point represents an average of three trials. DMSO was used as a control.

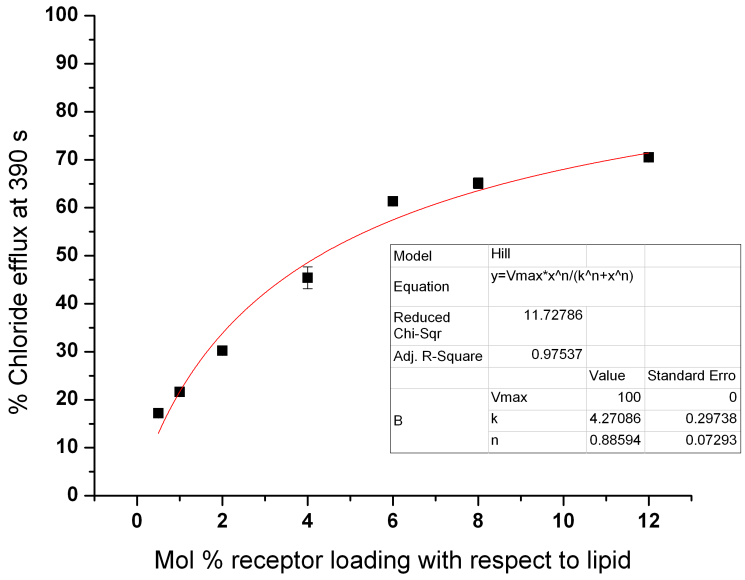

Figure 5.39 Hill plot of chloride efflux promoted varying concentrations of compound **L**[18] from unilamellar POPC vesicles loaded with 451mM NaCl buffered to pH 7.2 with 20mM sodium phosphate salts upon addition of a bicarbonate 'pulse', bringing the external concentration of bicarbonate to 40mM. The vesicles were dispersed in 150mM Na_2SO_4 buffered to pH 7.2 with 20mM sodium phosphate salts. Each point represents an average of 3 trials.

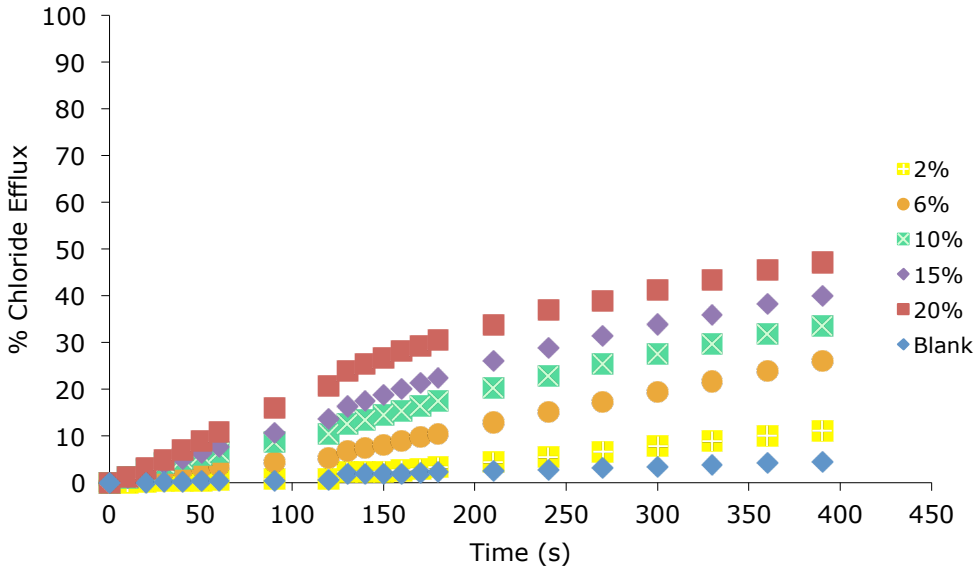

Figure 5.40 Chloride efflux promoted by various concentrations of **L**[19] from unilamellar POPC vesicles loaded with 451 mM NaCl buffered to pH 7.2 with 20 mM sodium phosphate salts. The vesicles were dispersed in 150 mM Na_2SO_4 buffered to pH 7.2 with 20 mM sodium phosphate salts. At t. 120 s a solution of sodium bicarbonate was added such that the external concentration of bicarbonate was 40 mM. At the end of the experiment, detergent was added to lyse the vesicles and calibrate the ISE to 100% chloride efflux. Each point represents an average of three trials. DMSO was used as a control.

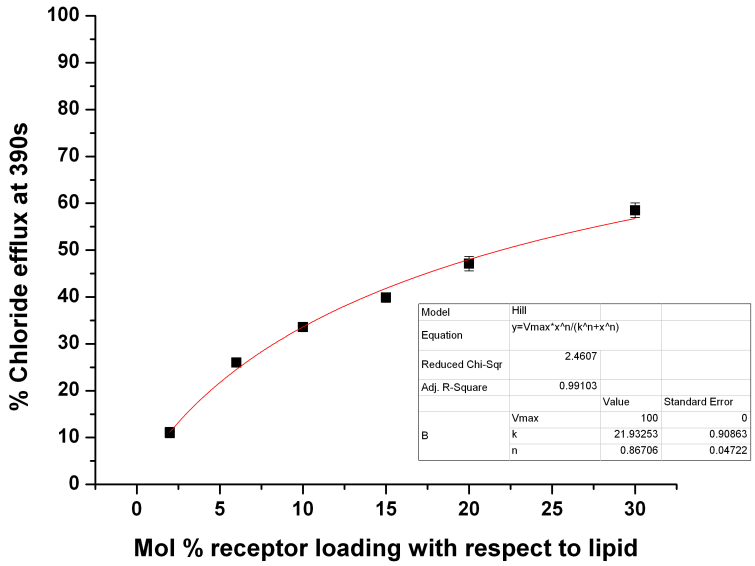

Figure 5.41 Hill plot of chloride efflux promoted varying concentrations of compound **L**[19] from unilamellar POPC vesicles loaded with 451mM NaCl buffered to pH 7.2 with 20mM sodium phosphate salts upon addition of a bicarbonate 'pulse', bringing the external concentration of bicarbonate to 40mM. The vesicles were dispersed in 150mM Na_2SO_4 buffered to pH 7.2 with 20mM sodium phosphate salts. Each point represents an average of 3 trials.

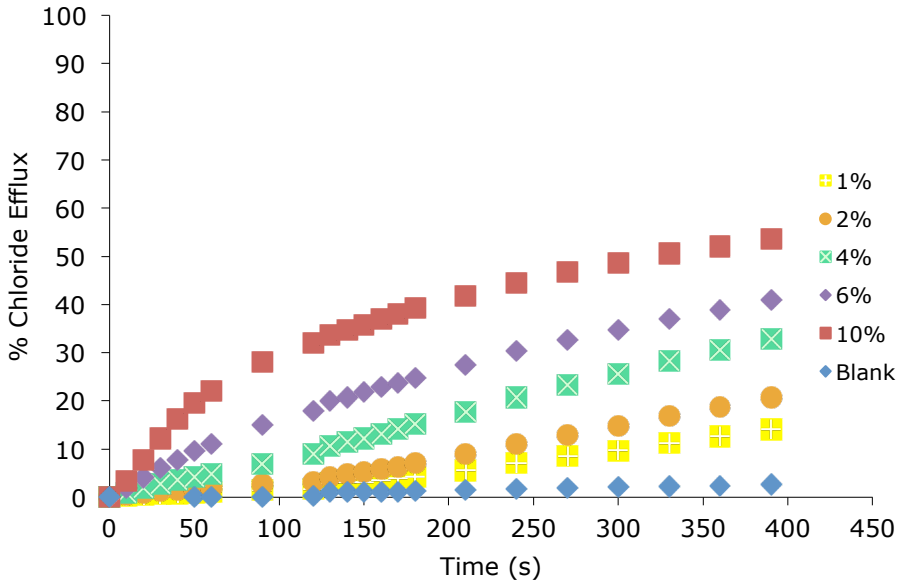

Figure 5.42 Chloride efflux promoted by various concentrations of $\mathbf{L^{20}}$ from unilamellar POPC vesicles loaded with 451 mM NaCl buffered to pH 7.2 with 20 mM sodium phosphate salts. The vesicles were dispersed in 150 mM Na_2SO_4 buffered to pH 7.2 with 20 mM sodium phosphate salts. At t. 120 s a solution of sodium bicarbonate was added such that the external concentration of bicarbonate was 40 mM. At the end of the experiment, detergent was added to lyse the vesicles and calibrate the ISE to 100% chloride efflux. Each point represents an average of three trials. DMSO was used as a control.

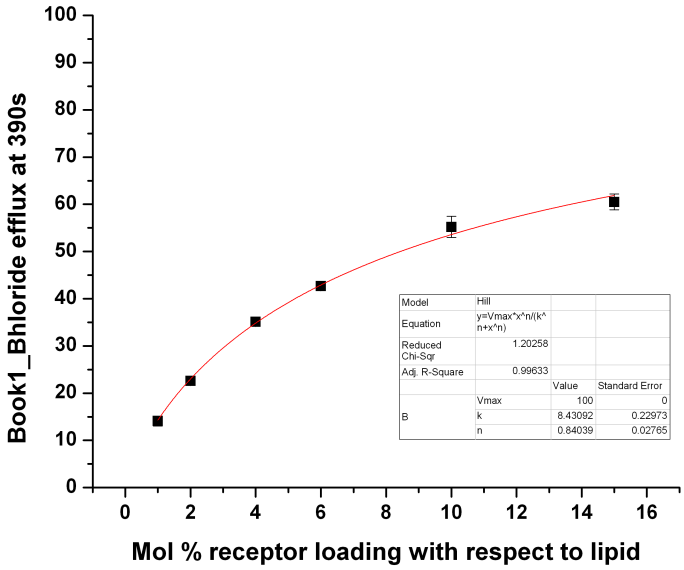

Figure 5.43 Hill plot of chloride efflux promoted varying concentrations of compound $\mathbf{L^{20}}$ from unilamellar POPC vesicles loaded with 451mM NaCl buffered to pH 7.2 with 20mM sodium phosphate salts upon addition of a bicarbonate 'pulse', bringing the external concentration of bicarbonate to 40mM. The vesicles were dispersed in 150mM Na_2SO_4 buffered to pH 7.2 with 20mM sodium phosphate salts. Each point represents an average of 3 trials.

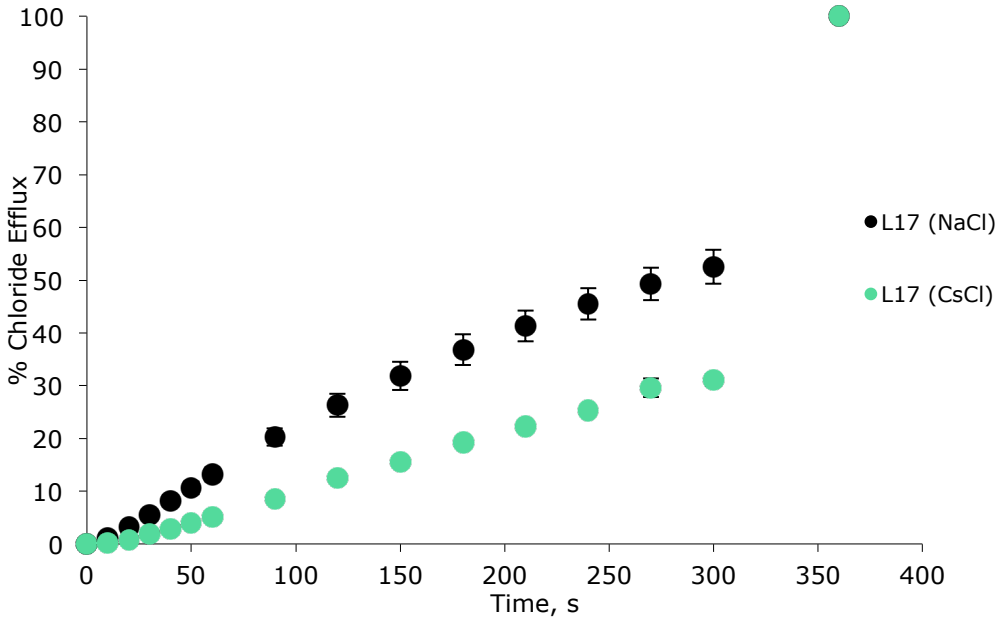

Figure 5.44 Chloride efflux promoted by a DMSO solution of compound **L**[17] (0.1 mol% carrier to lipid) from unilamellar POPC vesicles loaded with either 489mM NaCl or 489mM CsCl buffered to pH 7.2 with 5mM sodium phosphate salts. The vesicles were dispersed in 489mM $NaNO_3$ buffered to pH 7.2 with 5mM sodium phosphate salts. At the end of the experiment detergent was added to lyse the vesicles and calibrate the ISE to 100% chloride efflux. Each point represents an average of three trials. DMSO was used as a control.

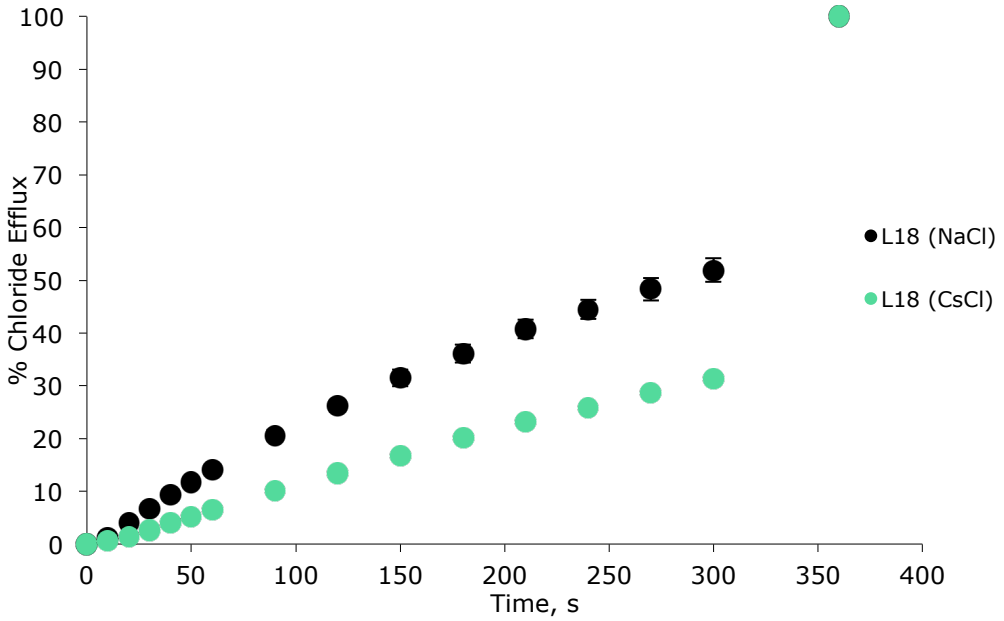

Figure 5.45 Chloride efflux promoted by a DMSO solution of compound **L**[18] (0.5 mol% carrier to lipid) from unilamellar POPC vesicles loaded with either 489mM NaCl or 489mM CsCl buffered to pH 7.2 with 5mM sodium phosphate salts. The vesicles were dispersed in 489mM $NaNO_3$ buffered to pH 7.2 with 5mM sodium phosphate salts. At the end of the experiment detergent was added to lyse the vesicles and calibrate the ISE to 100% chloride efflux. Each point represents an average of three trials. DMSO was used as a control.

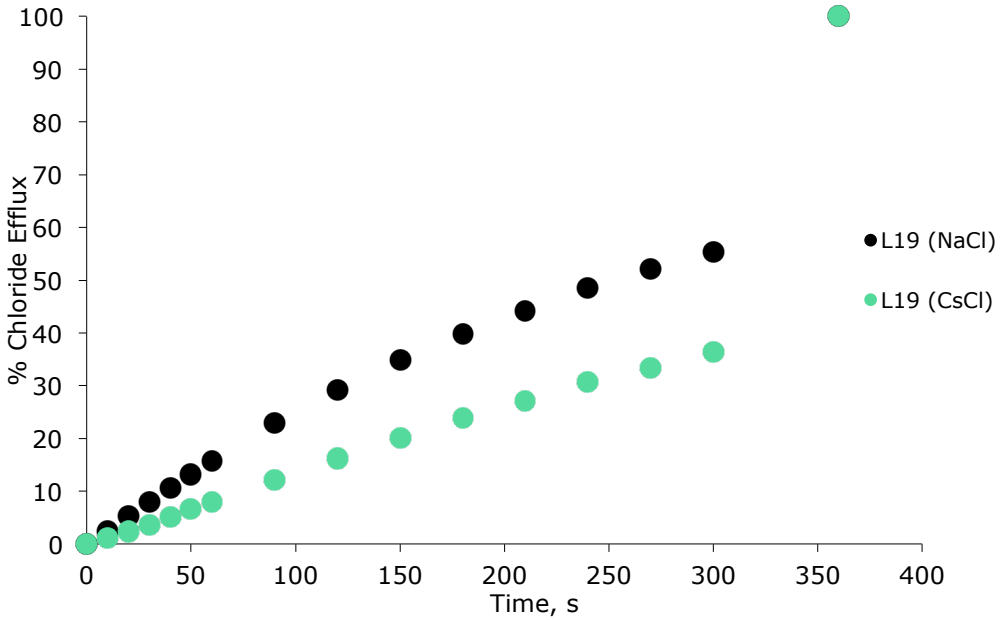

Figure 5.46 Chloride efflux promoted by a DMSO solution of compound **L**[19] (5 mol% carrier to lipid) from unilamellar POPC vesicles loaded with either 489mM NaCl or 489mM CsCl buffered to pH 7.2 with 5mM sodium phosphate salts. The vesicles were dispersed in 489mM $NaNO_3$ buffered to pH 7.2 with 5mM sodium phosphate salts. At the end of the experiment detergent was added to lyse the vesicles and calibrate the ISE to 100% chloride efflux. Each point represents an average of three trials. DMSO was used as a control.

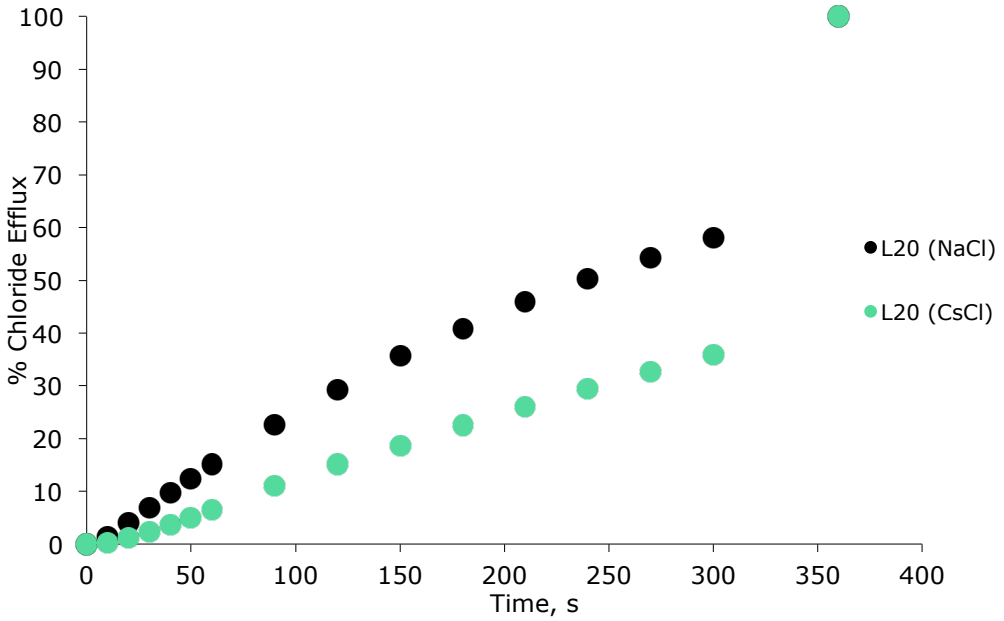

Figure 5.47 Chloride efflux promoted by a DMSO solution of compound **L**[20] (2 mol% carrier to lipid) from unilamellar POPC vesicles loaded with either 489mM NaCl or 489mM CsCl buffered to pH 7.2 with 5mM sodium phosphate salts. The vesicles were dispersed in 489mM $NaNO_3$ buffered to pH 7.2 with 5mM sodium phosphate salts. At the end of the experiment detergent was added to lyse the vesicles and calibrate the ISE to 100% chloride efflux. Each point represents an average of three trials. DMSO was used as a control.

Cholesterol assays

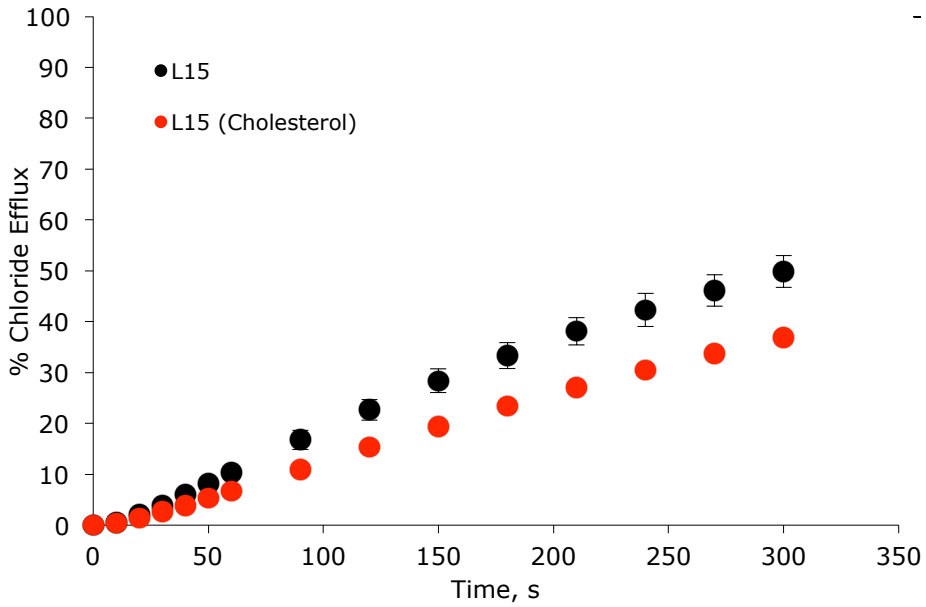

Figure 5.48 Chloride efflux promoted by a DMSO solution of compound **L**[15] (0.03 mol% carrier to lipid) from unilamellar vesicles comprising of either POPC or POPC/cholesterol (7:3 molar ratio), loaded with 489mM NaCl buffered to pH 7.2 with 5mM sodium phosphate salts. The vesicles were dispersed in 489mM $NaNO_3$ buffered to pH 7.2 with 5mM sodium phosphate salts. At the end of the experiment detergent was added to lyse the vesicles and calibrate the ISE to 100% chloride efflux. Each point represents an average of three trials. DMSO was used as a control.

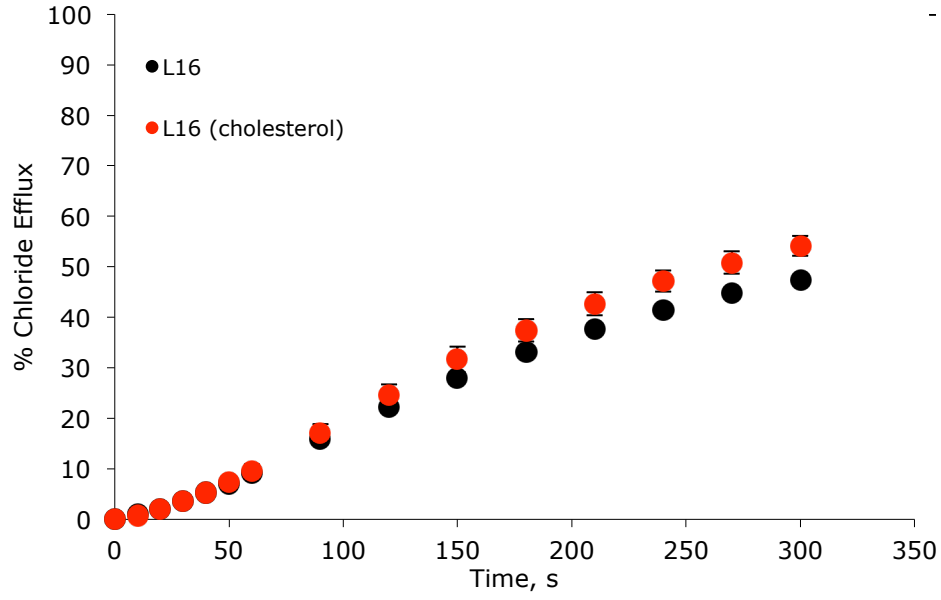

Figure 5.49 Chloride efflux promoted by a DMSO solution of compound **L**[16] (0.05 mol% carrier to lipid) from unilamellar vesicles comprising of either POPC or POPC/cholesterol (7:3 molar ratio), loaded with 489mM NaCl buffered to pH 7.2 with 5mM sodium phosphate salts. The vesicles were dispersed in 489mM $NaNO_3$ buffered to pH 7.2 with 5mM sodium phosphate salts. At the end of the experiment detergent was added to lyse the vesicles and calibrate the ISE to 100% chloride efflux. Each point represents an average of three trials. DMSO was used as a control.

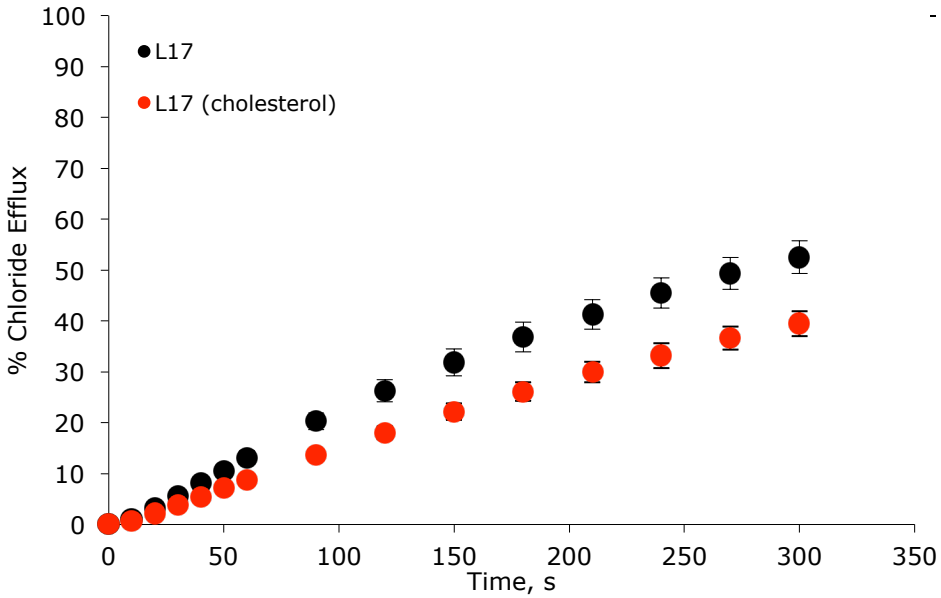

Figure 5.50. Chloride efflux promoted by a DMSO solution of compound **L**[17] (0.1 mol% carrier to lipid) from unilamellar vesicles comprising of either POPC or POPC/cholesterol (7:3 molar ratio), loaded with 489mM NaCl buffered to pH 7.2 with 5mM sodium phosphate salts. The vesicles were dispersed in 489mM $NaNO_3$ buffered to pH 7.2 with 5mM sodium phosphate salts. At the end of the experiment detergent was added to lyse the vesicles and calibrate the ISE to 100% chloride efflux. Each point represents an average of three trials. DMSO was used as a control.

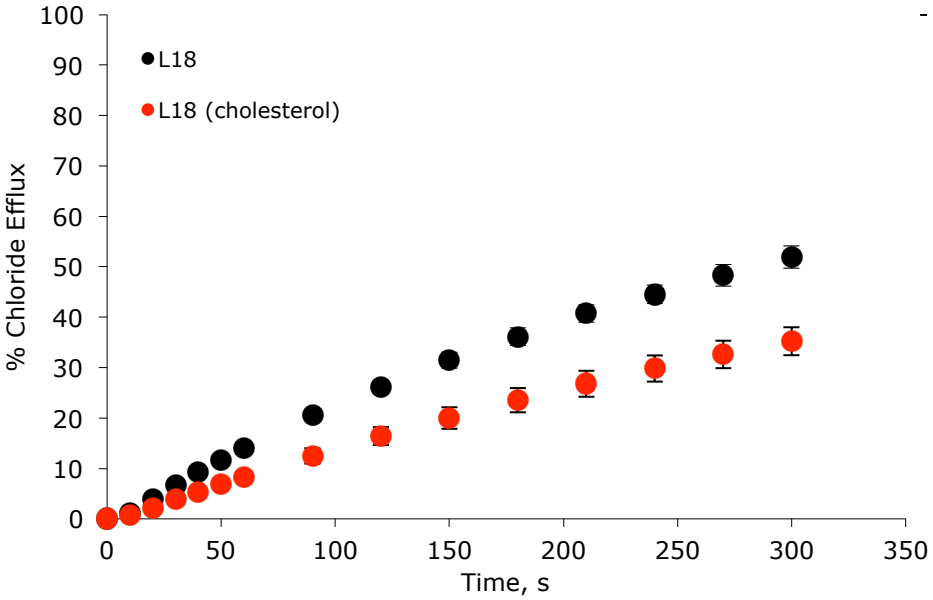

Figure 5.51 Chloride efflux promoted by a DMSO solution of compound **L**[18] (0.5 mol% carrier to lipid) from unilamellar vesicles comprising of either POPC or POPC/cholesterol (7:3 molar ratio), loaded with 489mM NaCl buffered to pH 7.2 with 5mM sodium phosphate salts. The vesicles were dispersed in 489mM $NaNO_3$ buffered to pH 7.2 with 5mM sodium phosphate salts. At the end of the experiment detergent was added to lyse the vesicles and calibrate the ISE to 100% chloride efflux. Each point represents an average of three trials. DMSO was used as a control.

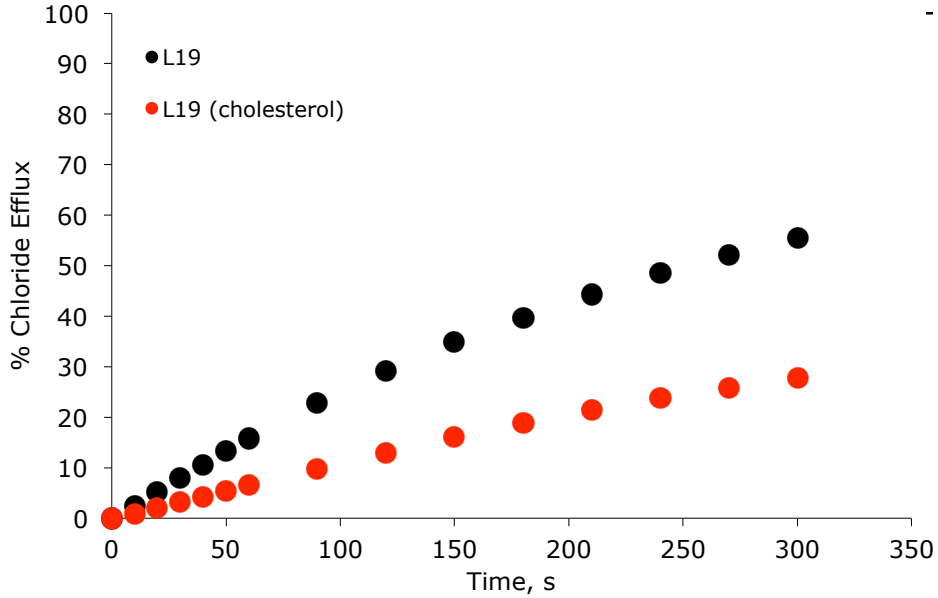

Figure 5.52 Chloride efflux promoted by a DMSO solution of compound **L**[19] (5 mol% carrier to lipid) from unilamellar vesicles comprising of either POPC or POPC/cholesterol (7:3 molar ratio), loaded with 489mM NaCl buffered to pH 7.2 with 5mM sodium phosphate salts. The vesicles were dispersed in 489mM $NaNO_3$ buffered to pH 7.2 with 5mM sodium phosphate salts. At the end of the experiment detergent was added to lyse the vesicles and calibrate the ISE to 100% chloride efflux. Each point represents an average of three trials. DMSO was used as a control.

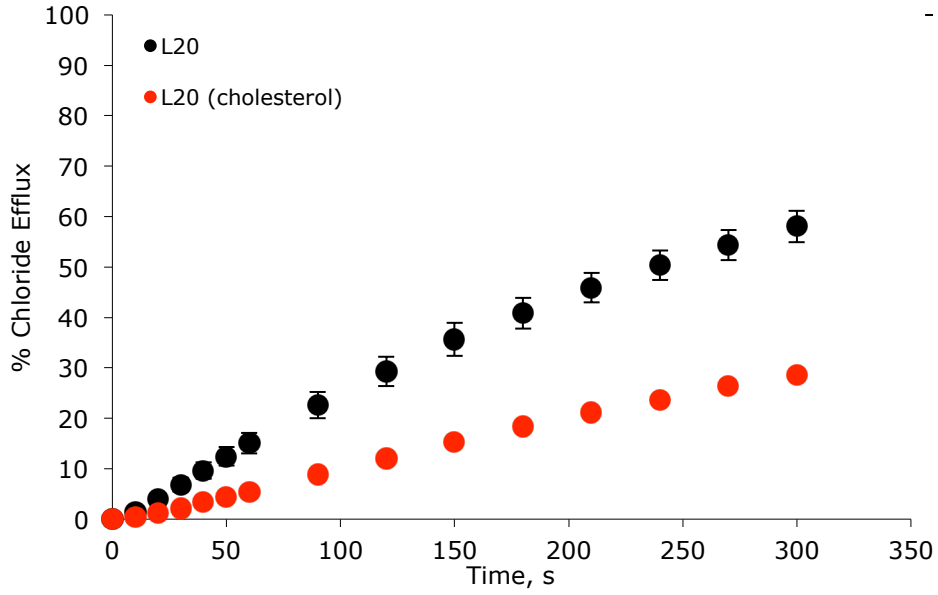

Figure 5.53 Chloride efflux promoted by a DMSO solution of compound **L**[20] (2 mol% carrier to lipid) from unilamellar vesicles comprising of either POPC or POPC/cholesterol (7:3 molar ratio), loaded with 489mM NaCl buffered to pH 7.2 with 5mM sodium phosphate salts. The vesicles were dispersed in 489mM $NaNO_3$ buffered to pH 7.2 with 5mM sodium phosphate salts. At the end of the experiment detergent was added to lyse the vesicles and calibrate the ISE to 100% chloride efflux. Each point represents an average of three trials. DMSO was used as a control.

References

1. Ashcroft, F. M. *Ion Channels and Disease: Channelopathies*. (2000).

2. Brotherhood, P. R. & Davis, A. P. Steroid-based anion receptors and transporters. *Chem. Soc. Rev.* **39,** 3633–47 (2010).

3. Gokel, G. W. & Barkey, N. Transport of chloride ion through phospholipid bilayers mediated by synthetic ionophores. *New J. Chem.* **33,** 947 (2009).

4. Davis, A. P., Sheppard, D. N. & Smith, B. D. Development of synthetic membrane transporters for anions. *Chem. Soc. Rev.* **36,** 348–57 (2007).

5. Gale, P. A. From anion receptors to transporters. *Acc. Chem. Res.* **44,** 216–26 (2011).

6. Moore, S., Haynes, C. & González, J. Chloride, carboxylate and carbonate transport by ortho-phenylenediamine-based bisureas. *Chem. …* **4,** 103 (2013).

7. Brooks, S. J., Gale, P. A. & Light, M. E. Carboxylate complexation by 1,1'-(1,2-phenylene)bis(3-phenylurea) in solution and the solid state. *Chem. Commun. (Camb).* 4696–8 (2005).

8. Brooks, S. J., Edwards, P. R., Gale, P. A. & Light, M. E. Carboxylate complexation by a family of easy-to-make ortho-phenylenediamine based bis-ureas: studies in solution and the solid state. *New J. Chem.* **30,** 65 (2006).

9. Kim, Y.-J. *et al.* Urea/thiourea-based colorimetric chemosensors for the biologically important ions: efficient and simple sensors. *Tetrahedron* **62,** 9635–9640 (2006).

10. Jia, C., Wu, B., Li, S., Huang, X. & Yang, X.-J. Tetraureas versus triureas in sulfate binding. *Org. Lett.* **12,** 5612–5 (2010).

11. Hynes, M. J. EQNMR: a computer program for the calculation of stability constants from nuclear magnetic resonance chemical shift data. *J. Chem. Soc. Dalt. Trans.* 311 (1993).

12. Davis, J. T., Okunola, O. & Quesada, R. Recent advances in the transmembrane transport of anions. *Chem. Soc. Rev.* **39,** 3843–62 (2010).

13. Cleland, W. W., Andrews, T. J., Gutteridge, S., Hartman, F. C. & Lorimer, G. H. Mechanism of Rubisco: The Carbamate as General Base. *Chem. Rev.* **98,** 549–562 (1998).

14. Cordat, E. & Casey, J. R. Bicarbonate transport in cell physiology and disease. *Biochem. J.* **417,** 423–39 (2009).

15. Rousselle, A.-V. & Heymann, D. Osteoclastic acidification pathways during bone resorption. *Bone* **30,** 533–540 (2002).

16. Vaughan-Jones, R. D., Spitzer, K. W. & Swietach, P. Intracellular pH regulation in heart. *J. Mol. Cell. Cardiol.* **46,** 318–31 (2009).

17. Higgins, C. Cystic fibrosis. Chloride channels revisited. *Nature* **358,** 536 (1992).

18. Choi, J. Y. *et al.* Aberrant CFTR-dependent HCO3- transport in mutations associated with cystic fibrosis. *Nature* **410,** 94–7 (2001).

19. Biwersi, J., Tulk, B. & Verkman, A. S. Long-wavelength chloride-sensitive fluorescent indicators. *Anal. Biochem.* **219,** 139–43 (1994).

20. Clement, N. R. & Gould, J. M. Pyranine (8-hydroxy-1,3,6-pyrenetrisulfonate) as a probe of internal aqueous hydrogen ion concentration in phospholipid vesicles. *Biochemistry* **20,** 1534–1538 (1981).

21. Kano, K. & Fendler, J. H. Pyranine as a sensitive pH probe for liposome interiors and surfaces. pH gradients across phospholipid vesicles. *Biochim. Biophys. Acta* **509,** 289–99 (1978).

22. Kirby, C., Clarke, J. & Gregoriadis, G. Effect of the cholesterol content of small unilamellar liposomes on their stability in vivo and in vitro. *Biochem. J.* **186,** 591–8 (1980).

23. Murillo, O. *et al.* Synthetic Transmembrane Channels: Functional Characterization Using Solubility Calculations, Transport Studies, and Substituent Effects. *J. Am. Chem. Soc.* **119,** 5540–5549 (1997).

Appendix

A.1 Anion transport studies using vesicles

Vesicles

Laboratory made unilamellar vesicles are able to function as a simple model of cell membrane allowing for reproducible experiments to assess the transport capabilities of neutral synthetic small molecule anion transporters. The Vesicles are prepared by the hydration of a thin film of phospholipid, followed by numerous freeze-thaw cycles and extrusion through a polycarbonate membrane. The preparation of the vesicles used in this work is versatile, allowing for careful control of the intra- and extra-vesicular solutions. There is a criteria that the intra- and extra-vesicular solutions should be isotonic, as transmembrane osmotic imbalances can result in membrane rupture. Solutions are buffered to prevent the build up of undesirable pH gradients. However, it is possible to vary the salt composition of the intra- and extra-vesicular solution within these limits. By systematically varying these salt compositions, it is possible not only to observe anion transport but also to understand important mechanistic insight into the process.

Choice of phospholipid

There are a number of different phospholipids commonly utilized for transport experiments. Phosphotidylcholines are a major component of cell membranes so are a good class of lipid for use in synthetic vesicles, which aim to model cell membranes. 1-Palmitoyl-2-oleoylphosphatidylcholine (POPC) is commonly used for transport studies, has been used by Gale and co-workers in all publications to date, and as such has been used for all vesicle-based assays within this thesis. The structure of POPC is shown in *Figure A.1*.

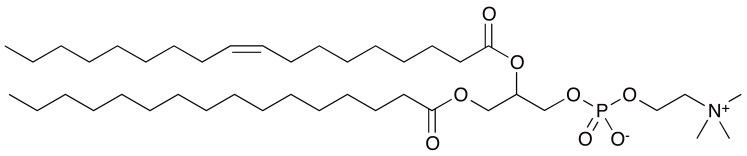

Figure A.1: Structure of POPC

Monitoring the movement of anions

It is possible to observe the transport of various anions by a number of methods. In this work, the transport of chloride has been monitored using exclusively a chloride selective electrode (ISE The internal chloride concentration cannot be detected by the ISE and hence any changes in electrode potential can be attributed to the efflux of chloride from the vesicles, facilitated by an anion transporter. Lysing the vesicles with a chloride free

detergent gives a 100 % chloride efflux reading and allows the system to be calibrated against chloride solutions of known concentrations.

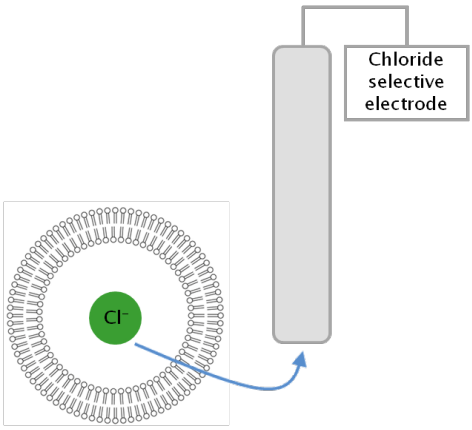

Figure A.2: Monitoring chloride efflux from phospholipid vesicles using ISE.

Alternatively, a number of fluorescent probes may encapsulated within the vesicles and utilized to track the movement of anions. The structures of some commonly used dyes are shown in *Figure 3*. Halide sensitive dyes such as lucigenin may be used to monitor changes in the intra-vesicular chloride concentration as its fluorescence is quenched by chloride.[1,2] 8-Hydroxypyrene-1,3,6-trisulfonate (HPTS, also known as pyranine) is a pH sensitive dye, which has been used to great effect in monitoring the changes in intravesicular pH associated with H^+/Cl^- co-transport.[3] Protonated and deprotonated forms of HPTS have different excitation wavelengths (403 and 460 nm), but both species emit at the same wavelength (510 nm). Thus, one can determine intravesicular pH by measuring the ratio of the protonated to the deprotonated dye. As this technique is independent of the nature of the anion, it has also been utilized to demonstrate the co-transport of anions other than chloride with protons. Safranin-O is a potential sensitive dye that may be used to identify changes in the membrane potential induced by the transport of ions.[4] Safranin O is able to increase its fluorescence upon creation of a membrane potential due to an imbalanced efflux of chloride from the vesicle associated with Cl^- uniport.

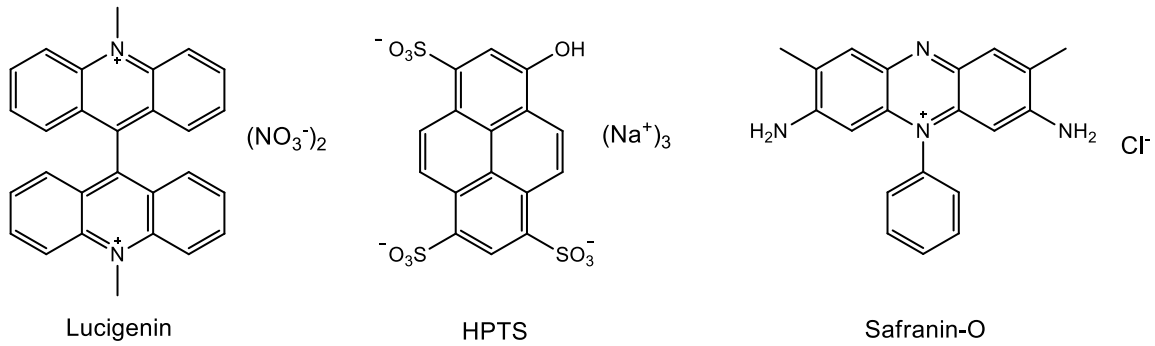

Figure A.3. The structure of various fluorescent dyes that can be used to track the movement of ions in vesicle studies.

Mechanism of transport

Variation of the intra- and extra- vesicular salt solutions can distinguish between and characterise an antiport or symport mechanism. An initial test for chloride antiport processes uses vesicles containing NaCl suspended in $NaNO_3$. When an active transporter is added, the observed chloride efflux can be the product of different transport mechanisms including H^+/Cl^- symport, Na^+/Cl^- symport or Cl^-/NO_3^- antiport. Anion antiport mechanisms are dependent on the nature of both the intra- and extra-vesicular anion as both are involved in the transport process. Substituting the external anion from NO_3^- to SO_4^{2-} should inhibit an antiport mechanism, as SO_4^{2-} is divalent and highly hydrophilic, and is very difficult for this anion to be transported across POPC membranes.[5,6,7] In fact there are only a select few receptors known to date which can act as sulfate transporters.[8] If chloride efflux is inhibited under these conditions then the symport processes can be ruled out and an antiport mechanism must be the route of anion transport. Once a Cl^-/NO_3^- antiport mechanism is proved, it is then desirable to establish if the carrier is able to facilitate the antiport of Cl^- and HCO_3^- due to the greater biological relevance of this process. This is investigated using vesicles containing NaCl suspended in Na_2SO_4. The receptor is added and, as the receptor is an antiporter, no chloride efflux should be observed. A pulse of $NaHCO_3$ is then added, and any resulting chloride efflux may be attributed to a Cl^-/HCO_3^- antiport process. Alternatively, if the carrier is able to facilitate M^+/Cl^- symport, the transport will not be dependent on the nature of the extra-vesicular anion. It will however be dependent on the nature of the intra-vesicular cation. Using vesicles suspended in Na_2SO_4 to rule out any antiport activity, the alkali metal cation in the intra-vesicular MCl solution can be varied to establish the preferred cation for the symport process. Meanwhile, a H^+/Cl^- symport process can be evaluated by varying the relative starting pH of the intra- and extra-vesicular solutions. For example, for a solution of vesicles containing NaCl suspended in Na_2SO_4, H^+/Cl^- efflux should be encouraged if the intra-vesicular solution is more acidic than the external solution, and inhibited if the opposite pH gradient is applied.

Mobility assays

The inclusion of cholesterol within a lipid membrane is known to reduce membrane fluidity.[9] Small synthetic molecules operating as mobile carries do so under diffusion controlled conditions, and so if the membrane is made more viscous it becomes more difficult for mobile carries to move around inside the membrane and hence a reduction in transport activity is observed. On the other hand, some molecules which can span the distance of the membrane or aggregate together to form channels may function via a channel transport mechanism, in which case the increased viscosity of the membrane should have little or no effect on the transporters activity rate.

U-tubes provide a very simplistic model for transport across biological membranes. They consist of two aqueous phases separated by a water immiscible organic phase containing a transporter molecule. The aqueous phases represent the intra- and extra- cellular environments and the organic phase represents the lipophilic membrane environment. The movement of anions across the bulk organic phase can be monitored by recording changes in the ion concentration of the aqueous phases. If transport of anions from one aqueous phase, through the organic phase, to the other aqueous phase occurs then it can be concluded that the transporter functions as a mobile carrier. This is in view of the fact that the large volume and hence distance separation of the two aqueous phases ensures that channel formation is not feasible, hence channel transport mechanisms cannot occur.

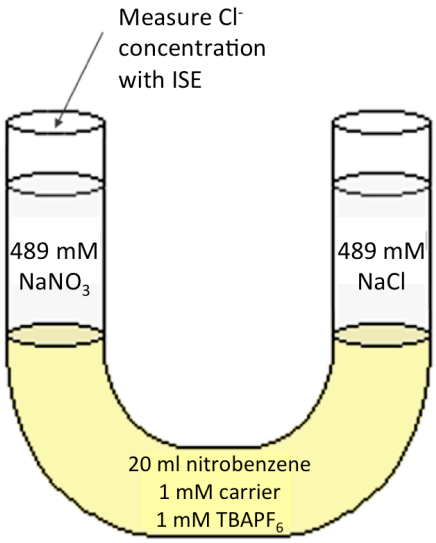

Figure A.4. U-Tube test experiment

Hill plots

The Hill equation was first introduced by A. V. Hill in 1910 to describe the cooperativity of oxygen binding to haemoglobin.[10] More specifically, the equation described the relationship between the concentration of a substrate (in this case oxygen), and an observed effect (the % of saturated haemoglobin binding sites). Since then, the Hill equation has been applied to a wide range of systems.[11] It has been often utilized in pharmacodynamics to describe the relationship between drug concentration (C) and observed drug effect (E).[12,13] A form of the Hill equation that is useful in this context is shown below (Equation 1.1), where EC_{50} is the drug concentration for which 50 % of maximum effect is obtained and n is the Hill coefficient of sigmoidality. The Hill

coefficient has been interpreted to represent the number of ligand binding patterns required to mediate the observed effect.

$$E = EmaxCn / (EC50n + Cn)$$

Equation A.1 A form of the Hill equation frequently applied to pharmadynamics.

The Hill equation can been applied to ion transport systems by examining the effect of varying the concentration of transporter (C) on the observed ion flux (E). In this way, a value of EC_{50} can be calculated and used to quantify transport activity, the lower the value of EC_{50}, the more potent the transporter. Calculation of the Hill coefficient can provide mechanistic insight into the transport process, representing the number of transporter molecules required to transport a single ion; either as an aggregate mobile carrier complex, or as a self-assembled channel species. However, Matile reports that the use of the Hill coefficient to study supramolecular self assembly is not always straightforward.[14] The formation of highly stable assemblies may give a Hill coefficient of 1, presumably because the assembly "behaves" as a single entity and can be misinterpreted as a monomer. It has also been suggested that the Hill analysis is only compatible with endergonic self-assembly, thus inconsistencies may arise if the assembly is exergonic.

A.2 Experimental procedures to assess anion transport

The vesicles used in all of the following studies were prepared according to literature procedures.[15],[16] To prevent the vesicle membranes from bursting the ionic strength of the intra-vesicular and extra-vesicular solutions were made to be isotonic. All solutions were buffered to pH 7.2 with 5 mM or 20 mM (in the case of the HCO_3^- assays) sodium phosphate salts unless otherwise stated. The ionic strength of the solutions was controlled at 500 mM with the desired internal salt (most commonly NaCl) or external salt (most commonly $NaNO_3$ or Na_2SO_4) as applicable.

Vesicle preparation

POPC was dissolved in chloroform (approximately 29 mg mL^{-1}). A known volume of the POPC solution was transferred to a RBF (round bottom flask) and the chloroform removed *in vacuo*. The resultant thin film was dried under high vacuum for 4-24 hrs. The POPC was suspended in internal solution. The suspension was vortexed using a lab dancer to ensure that all POPC was removed from the sides of the flask. The volume of internal solution required to suspend the POPC is identical to that of the initial chloroform

solution. The suspension was subjected to nine freeze-thaw cycles using liquid nitrogen and room temperature water alternately, after which the suspension was left to equilibrate to room temperature for thirty minutes. The resultant vesicles were extruded 25 times through a 200 nm polycarbonate membrane to generate vesicles of uniform size. The vesicles were dialysed in the external solution for 2-18 hrs to remove any unencapsulated "internal salts". The vesicle suspension was then diluted to a concentration of 1 mM using the external solution.

Cl^-/NO_3^- antiport assays

Unilamellar POPC vesicles were loaded with aqueous internal solution containing 489 mM NaCl buffered to pH 7.2 with 5 mM sodium phosphate salts. The vesicles were dispersed in an aqueous external solution containing 489 mM $NaNO_3$ buffered to pH 7.2 with 5 mM sodium phosphate salts. The receptor was loaded as a DMSO solution at 0 s. After 300 s, octaethylene glycol monododecyl ether detergent was added to lyse the vesicles (2.32 mM in 7:1 H_2O:DMSO v/v) and calibrate the chloride selective electrode to 100 % chloride efflux at 420 s. All endpoint values are taken as of 270 s. Chloride concentrations were monitored using an Accumet solid-state combination chloride selective electrode. The lipid concentration per sample was 1 mM.

Cl^-/HCO_3^- antiport assays

Unilamellar POPC vesicles were loaded with aqueous internal solution containing 451 mM NaCl buffered to pH 7.2 with 20 mM sodium phosphate salts. The vesicles were dispersed in an aqueous external solution containing 150 mM Na_2SO_4 buffered to pH 7.2 with 20 mM sodium phosphate salts. The lipid concentration per sample was 1 mM. The receptor was loaded as a DMSO solution at 0 s to start the experiment and chloride efflux was monitored using a chloride sensitive electrode. At 120 s a solution of $NaHCO_3$ (1 M in 150 mM Na_2SO_4 buffered to pH 7.2 with 20 mM sodium phosphate salts) was added such that the external concentration of bicarbonate was 40 mM. After 420 s, 50 µl of octaethylene glycol monododecyl ether detergent were added to lyse the vesicles and a total chloride reading was taken at 540 s. The initial value was set at 0 % chloride efflux and the final chloride reading (at 9 minutes) was set as 100 % chloride efflux. All other data points were calibrated to these points. All endpoint values are taken as of 390 s.

HPTS assays (HCl co-transport)

A lipid film of POPC was formed from a chloroform solution under reduced pressure and dried under vacuum for at least 6 hours. The lipid film was rehydrated by vortexing with a

NaCl solution (1mM HPTS, 489 mM NaCl, 5 mM phosphate buffer at pH 7.2). The lipid suspension was then subjected to nine freeze-thaw cycles and allowed to age for 30 min at room temperature before extruding 25 times through a 200 nm polycarbonate membrane. The unincorporated HPTS was removed by size exclusion chromatography on a Sephadex G-25 column using a sodium sulfate solution as eluent (162 mM Na_2SO_4, 5 mM phosphate buffer at pH 7.2). Unilamellar POPC vesicles containing NaCl and HPTS, prepared as described above, were suspended in a Na_2SO_4 solution buffered to pH 7.2 with sodium phosphate salts. The lipid concentration per sample was 1 mM. A DMSO solution of the carrier molecule (10 mM) was added to start the experiment. The fluorescence of intravesicular HPTS was monitored by excitation at both 403 nm and 460 nm and recording the emission at 510 nm. After 300 s the vesicles were lysed with 30 µl of octaethylene glycol monododecyl ether detergent (0.232 mM in 7:1 water:DMSO v/v). The internal pH was obtained by fitting the data to the following equation:

$$ph = -\frac{1}{1.796} \cdot \ln\left(\frac{4.2055}{\frac{I_{460nm}}{I_{403nm}} - 1}\right) + 7.6142$$

Lucigenin assays (Cl^-/SO_4^{2-} antiport)

A lipid film of POPC was formed from a chloroform solution under reduced pressure and dried under vacuum for at least 6 hours. The lipid film was rehydrated by vortexing with a NaCl solution (2 mM lucigenin, 100 mM NaCl, 20 mM phosphate buffer at pH 7.2). The lipid suspension was then subjected to nine freeze-thaw cycles and allowed to age for 30 min at room temperature before extruding 25 times through a 200 nm polycarbonate membrane. The unincorporated lucigenin was removed by size exclusion chromatography on a Sephadex G-25 column using a sodium chloride solution as eluent (100 mM NaCl, 20 mM phosphate buffer at pH 7.2). Unilamellar POPC vesicles containing NaCl and lucigenin, prepared as described above, were suspended in a NaCl solution buffered to pH 7.2 with sodium phosphate salts. The lipid concentration per sample was 0.5 mM. The internal chloride concentration could be monitored by the fluorescence of intravesicular lucigenin after excitation at 372 nm and recording the emission at 503 nm. At t = 30 s, a stock salt solution was added so that the outer concentration contained 40 mM of the new salt (stock solutions: 1 M $NaNO_3$, 1 M NaCl or 0.5 M Na_2SO_4). After 60 s, a methanol solution of the carrier molecule was added to start ion transport. After 240 s the vesicles were lysed with 30 µl of octaethylene glycol monododecyl ether (0.232 mM in 7:1 water:DMSO v/v).

Hill analysis

Hill plot analysis was carried out using the above transport conditions, where each receptor is tested at multiple concentrations. Each point was taken at 270 s for Cl^-/NO^- transport and 390 s for Cl^-/HCO^- transport, and each represents the average of three runs.

Test for Cl^-/NO^- antiport with cholesterol added to the membrane

To the POPC thin film was added a solution of cholesterol in chloroform to result in a 7:3 lipid:cholesterol molar ratio. The chloroform was again removed *in vacuo* and the resultant thin film dried under high vacuum for 4-24 hrs. The remaining vesicle preparation steps and experiment were run identical to that of the Cl^-/NO^- antiport experiment.

U-tube experiments

A nitrobenzene solution (20 mL) of 1 mM tetrabutylammonium hexafluorophosphate was loaded with 1 mM receptor and placed in a U-tube. To one side of the U-tube was added 10 mL of aqueous solution containing 489 mM NaCl buffered to pH 7.2 with 5 mM sodium phosphate salts, and to the other side of the U-tube was added 10 mL of aqueous solution containing 489 mM $NaNO_3$ buffered to pH 7.2 with 5 mM sodium phosphate salts. The experiments were stirred and the chloride concentration of the $NaNO_3$ solution was monitored using an Accumet solid-state combination chloride selective electrode.

References

1. McNally, B. A., Koulov, A. V, Smith, B. D., Joos, J.-B. & Davis, A. P. A fluorescent assay for chloride transport; identification of a synthetic anionophore with improved activity. *Chem. Commun. (Camb).* 1087–9 (2005). doi:10.1039/b414589e

2. Jiang, J. *et al.* Pleural surface fluorescence measurement of Na+ and Cl- transport across the air space-capillary barrier. *J. Appl. Physiol.* **94,** 343–52 (2003).

3. Kano, K. & Fendler, J. H. Pyranine as a sensitive pH probe for liposome interiors and surfaces. pH gradients across phospholipid vesicles. *Biochim. Biophys. Acta* **509,** 289–99 (1978).

4. Sakai, N., Houdebert, D. & Matile, S. Voltage-Dependent Formation of Anion Channels by Synthetic Rigid-Rod Push-Pull ß-Barrels. *Chem. - A Eur. J.* **9,** 223–232 (2003).

5. Bergstroem, P. A., Lindgren, J. & Kristiansson, O. An IR study of the hydration of perchlorate, nitrate, iodide, bromide, chloride and sulfate anions in aqueous solution. *J. Phys. Chem.* **95,** 8575–8580 (1991).

6. Cannon, W. R., Pettitt, B. M. & McCammon, J. A. Sulfate Anion in Water: Model Structural, Thermodynamic, and Dynamic Properties. *J. Phys. Chem.* **98,** 6225–6230 (1994).

7. Marcus, Y. Thermodynamics of solvation of ions. Part 5.?Gibbs free energy of hydration at 298.15 K. *J. Chem. Soc. Faraday Trans.* **87,** 2995 (1991).

8. Busschaert, N. *et al.* Tripodal transmembrane transporters for bicarbonate. *Chem. Commun. (Camb).* **46,** 6252–4 (2010).

9. Subczynski, W. K., Wisniewska, A., Yin, J. J., Hyde, J. S. & Kusumi, A. Hydrophobic barriers of lipid bilayer membranes formed by reduction of water penetration by alkyl chain unsaturation and cholesterol. *Biochemistry* **33,** 7670–81 (1994).

10. Hill, A. V. The possible effects of the aggregation of the molecules of haemoglobin on its dissociation curve. *J. Physiol.* **40,** (1910).

11. Goutelle, S. *et al.* The Hill equation: a review of its capabilities in pharmacological modelling. *Fundam. Clin. Pharmacol.* **22,** 633–48 (2008).

12. N H Holford, L. B. S. Pharmacokinetic and pharmacodynamic modeling in vivo. *Crit. Rev. Bioeng.* **5,** 273 – 322 (1981).

13. Holford, N. Holford NHG and Sheiner LB "Understanding the Dose-Effect Relationship-Clinical Application of Pharmacokinetic-Pharmacodynamic Models", Clin Pharmacokin 6:429-453 (1981)-The Backstory. *AAPS J.* **13,** 662–4 (2011).

14. Perez-Velasco, A., Gorteau, V. & Matile, S. Rigid oligoperylenediimide rods: anion-pi slides with photosynthetic activity. *Angew. Chem. Int. Ed. Engl.* **47,** 921–3 (2008).

15. MacDonald, R. C. *et al.* Small-volume extrusion apparatus for preparation of large, unilamellar vesicles. *Biochim. Biophys. Acta - Biomembr.* **1061,** 297–303 (1991).

16. Torchilin, V. P. & Weissig, V. *Liposomes: A Practical Approach*. (Oxford University Press, 2003).